

Evaluating the Potential of an Intersection Driver Assistance System to Prevent U.S. Intersection Crashes

John Michael Scanlon III

Dissertation submitted to the faculty of the
Virginia Polytechnic Institute and State University
in partial fulfillment of the requirements for the degree of

Doctor of Philosophy

In

Biomedical Engineering

Hampton C. Gabler, Chair
Zachary R. Doerzaph
Andrew R. Kemper
Steven Rowson
Ashley A. Weaver

March 24, 2017
Blacksburg, Virginia

Keywords: Intersection Advanced Driver Assistance Systems, Active Safety, Benefits Estimates, Driver Behavior, Event Data Recorders, Naturalistic Driving, Crash, Injury Biomechanics

©Copyright 2017, John Michael Scanlon III

Evaluating the Potential of an Intersection Driver Assistance System to Prevent U.S. Intersection Crashes

John Michael Scanlon III

ABSTRACT

Intersection crashes are among the most frequent and lethal crash modes in the United States. Intersection Advanced Driver Assistance Systems (I-ADAS) are an emerging active safety technology which aims to help drivers safely navigate through intersections. One primary function of I-ADAS is to detect oncoming vehicles and in the event of an imminent collision can (a) alert the driver and/or (b) autonomously evade the crash. Another function of I-ADAS may be to detect and prevent imminent traffic signal violations (i.e. running a red light or stop sign) earlier in the intersection approach, while the driver still has time to yield for the traffic control device.

This dissertation evaluated the capacity of I-ADAS to prevent U.S. intersection crashes and mitigate associated injuries. I-ADAS was estimated to have the potential to prevent up to 64% of crashes and 79% of vehicles with a seriously injured driver. However, I-ADAS effectiveness was found to be highly dependent on driver behavior, system design, and intersection/roadway characteristics. To generate this result, several studies were performed. First, driver behavior at intersections was examined, including typical, non-crash intersection approach and traversal patterns, the acceleration patterns of drivers prior to real-world crashes, and the frequency, timing, and magnitude of any crash avoidance actions. Second, two large simulation case sets of intersection crashes were generated from U.S. national crash databases. Third, the developed simulation case sets were used to examine I-ADAS performance in real-world crash scenarios. This included examining the capacity of a stop sign violation detection algorithm, investigating the sensor detection needs of I-ADAS technology, and quantifying the proportion of crashes and seriously injuries that are potentially preventable by this crash avoidance technology.

Evaluating the Potential of an Intersection Driver Assistance System to Prevent U.S. Intersection Crashes

John Michael Scanlon III

GENERAL AUDIENCE ABSTRACT

Intersection crashes account for over 5,000 fatalities each year in the U.S., which places them among the most lethal crash modes. Highly automated vehicles are a rapidly emerging technology, which has the potential to greatly reduce all traffic fatalities. This work evaluated the capacity of intersection advanced driver assistance systems (I-ADAS) to prevent U.S. intersection crashes and mitigate associated injuries. I-ADAS is an emerging technology used by highly automated vehicles to help drivers safely navigate intersections. This technology utilizes onboard sensors to detect oncoming vehicles. If an imminent crash is detected, I-ADAS can respond by (a) warning the driver and/or (b) autonomously braking. Another function of I-ADAS may be to prevent intersection violations altogether, such as running a red light or a stop sign. Preventing and/or mitigating crashes and injuries that occur in intersection crashes are among the highest priority for designers, evaluators, and regulatory agencies.

This dissertation has three main components. The first aim of this research was to describe how individuals drive through intersections. This included examining how drivers approach, traverse, and take crash avoidance actions at intersections. The second aim was to develop a dataset of intersection crashes that could be used to examine I-ADAS effectiveness. This was completed by extracting crashes that occurred throughout the U.S., and reconstructing vehicle positions before and after impact. The third aim was to use the extracted dataset of intersection crashes, and consider a scenario where one of the vehicles had been equipped with I-ADAS. Estimates of I-ADAS effectiveness were then generated based on these results.

Acknowledgement

This research was funded by the Toyota Collaborative Safety Research Center (CSRC) and
Toyota Motor Corporation

First, I want to thank my family for their love and support. Thank you Liz. You has been with me every step of the way. You make me the best person that I can be. Thank you especially for your patience these last few years. Now, we get to take our next steps together. To Mom, Dad, Mimi, Papa, Grandpapa, Katie, and Ellie, thank you for supporting me throughout this entire process. Whether it be career advice, moral support, or just showing a general interest in my work, I could not have done this without you. My Mom and Dad have gone through great lengths to make sure that I am happy and comfortable, and I am eternally grateful.

Second, a special thanks to my advisor, Dr. Gabler. I thought that I was facing a difficult decision when I needed to choose whether or not to pursue a Ph.D. I was very wrong. I have grown immensely as a researcher and as a leader. Working for you has been one of the best decisions of my life.

Third, my special thanks to Katsuhiko Iwazaki and Rini Sherony of Toyota for sharing technical insights and expertise throughout the project. I am fortunate to have had the opportunity to work on such an interesting research topic. I would like to thank the members of my defense committee, including Dr. Zach Doerzaph, Dr. Andrew Kemper, Dr. Steve Rowson, and Dr. Ashley Weaver. Your expertise has greatly strengthened this work. I also want to thank my Master's advisor Dr.

Michael Madigan. You took a chance on hiring me when I was an undergraduate. Without your guidance, I do not see how any of this would have been possible.

Fourth, many of my lab group members have contributed to this work. I would like to acknowledge Dr. Kristofer Kusano for his mentorship and guidance during the early stages of this project. Having had your expertise readily available early on greatly accelerated the progress of this work. I would like to acknowledge Dr. Ada Tsoi for her gracious assistance in interpreting EDR data. I want to thank Alex Noble for her assistance in analyzing naturalistic data. Your early insights were very helpful in shaping the direction of this work. I would also like to acknowledge David Holmes, Stephen Hunter, Daniel Gutierrez, Kaitlyn Wheeler, Stephani Martinelli, Kristin Dunford, Kay Battogtokh, Elizabeth Mack, Robert Vasinko, Daniel Surinach, Dong Gyu Lee, Dillon Richardson, Kevin Ota, and Arnab Gupta (a.k.a. The Army) for their assistance in data collection. I want to also thank the rest of my lab members for providing their insights: Dr. Nicholas Johnson, Dr. Jackey Chen, Whitney Tatem, Grace Wusk, and Max Bareiss.

Lastly, I have made a lot of great friends while working in the CIB. To Zach, Nora, Allie, Dev, and Jackey, I was not expecting to have such a close-knit group of friends when I started graduate school. Thank you for making every day fun! I also need to give a shout out to everyone on team SBEST. I have had an absolute blast playing intramural sports.

Table of Contents

1.	Introduction.....	1
1.1	Motivation	1
1.2	I-ADAS Target Population.....	6
1.3	Strategies for Predictive Evaluation of Active Safety Systems	11
1.4	Overall Objective and Research Questions	15
1.5	Overview of Chapters.....	16
2.	Data Sources	18
2.1	Introduction	18
2.2	NMVCCS.....	18
2.3	NASS/CDS (w/ Event Data Recorders).....	20
2.4	100-Car Naturalistic Driving Study	22
3.	Intersection Approach and Traversal Patterns during Normal Driving	26
3.1	Introduction	26
3.2	Methods.....	27
3.3	Results/Discussion	34
3.4	Limitations	75
3.5	Conclusions	75
4.	Using Event Data Recorders to Model Driver Acceleration Behavior prior to Real-World Intersection Crashes	76
4.1	Introduction	76
4.2	Methods.....	80
4.3	Results	89
4.4	Discussion	99
4.5	Validating the Composition of the EDR Dataset	101
4.6	Limitations	107
4.7	Conclusions	107
5.	Analysis of Driver Evasive Maneuvering prior to Real-World Intersection Crashes	108
5.1	Introduction	108
5.2	Methods.....	109
5.3	Results	124
5.4	Discussion	139
5.5	Limitations	142
5.6	Conclusions.....	145
6.	Estimating Pre-crash Driver Actions for Travelling Through Drivers	147
6.1	Introduction	147
6.2	Methods.....	150
6.3	Results and Discussion.....	158
6.4	Evaluating the Traversal Speed Model	167
6.5	Conclusions	169
7.	Reconstructing the Pre-Crash Trajectories of Vehicles involved in Intersection Crashes ..	170
7.1	Reconstruction Strategy	170
7.2	Data Sources.....	173
7.3	Path Reconstructions	176
7.4	Speed Reconstructions	182

7.5	Overview of NMVCCS Dataset.....	203
8.	Predicting Crash-Relevant Violations at Stop Sign-Controlled Intersections for the Development of an Intersection Driver Assistance System.....	212
8.1	Introduction	212
8.2	Methods.....	214
8.3	Results	222
8.4	Discussion	229
8.5	Limitations	230
8.6	Conclusions	231
9.	Evaluating the Sensor Detection Capabilities of I-ADAS for Preventing Left Turn Across Path Opposite Direction Crashes	232
9.1	Introduction	232
9.2	Methods.....	236
9.3	Results and Discussions	240
9.4	Limitations	249
9.5	Conclusions	250
10.	Evaluating the Sensor Detection Capabilities of I-ADAS for Preventing Cross Traffic Intersection Crashes	251
10.1	Introduction	251
10.2	Methods	255
10.3	Results and Discussions.....	259
10.4	Limitations.....	285
10.5	Conclusions	287
11.	Crash and Safety Benefits of I-ADAS for SCP and LTAP/LD crashes in the U.S. Vehicle Fleet 288	
11.1	Introduction	288
11.2	Methods	292
11.3	Results and Discussion.....	306
11.4	Limitations.....	332
11.5	Conclusions	334
12.	Conclusions.....	335
13.	Current and Anticipated Contributions to Literature	373
	References.....	375
	Appendix.....	396
A.1	Extracting Speed Limit Data from Shape Files.....	396
A.2	MARS Model Outputs for Intersection approach and traversal models	398
A.3	Path Reconstruction protocol	407
A.4	PC-Crash Reconstruction Protocol.....	421
A.5	Case Viewer Program.....	431
A.6	Easy Street Draw Program	432

List of Figures

Figure 1. A general depiction of how I-ADAS might prevent intersection crashes.	2
Figure 2. Tabulations of the most common intersection crash modes in the U.S. crash population. Tabulations are shown for all police-reported intersection crashes and all fatal intersection crashes.	7
Figure 3. Tabulation of TCD present for the three most common intersection crash modes.	8
Figure 4. Critical reasons that led to intersection crashes.	10
Figure 5. Box plots of vehicle speed versus distance from the beginning of the intersection traversal phase. Two pre-crash movements are shown, including rolling stopped and completely stopped. Every deceleration and acceleration phase were shifted in order to have the driver reach their minimum velocity at $d=0$	36
Figure 6. A summary of acceleration magnitudes during the intersection approach and traversal phase. The bars represent the 95% confident interval about the mean. A * was used to indicate significant differences ($p<0.05$) between the two stopping categories. The graph depicts least squares means with confidence intervals that were generated from the mixed effects ANOVA.	41
Figure 7. A cumulative distribution plot of minimum speeds for driver's that came to a complete stop at a stop sign-controlled intersection.	42
Figure 8. Cumulative distribution plots of the location where the driver began accelerating into the intersection relative to the point of intersection entry.	44
Figure 9. Approach and traversal kinematics by traffic control device and stopping behavior. ..	46
Figure 10. Approach and traversal vehicle kinematics by stopping behavior and turning behavior.	48
Figure 11. Median (50 th percentile) intersection approach and traversal kinematics by turning behavior, stopping behavior, and speed limit. Only signalized intersection approaches are shown in this graphic.	52
Figure 12. Example approach kinematics models generated for stopped vehicles. Several variations of this model are shown by speed limit and stopping behavior. The driver was assumed to be non-turning, not young or senior, a male, and approaching a stop sign controlled intersection.	58
Figure 13. Example Traversal kinematics model outputs generated for stopped vehicles. Several variations of this model are shown by speed limit and stopping behavior. The driver was assumed to be non-turning, not young or senior, a male, and traversing through a stop sign controlled intersection.	59
Figure 14. Intersection approach and traversal kinematics for travelling through drivers at signalized intersection. The graphs are separated by turning behavior. The location where distance = 0 represents the location where the traffic signal was last visible.	61
Figure 15. Median traversal kinematics by speed limit for non-turning and left-turning drivers approaching signalized intersections.	64
Figure 16. Example trajectories of the approach phase for non-turning drivers travelling through an intersection. Trajectories are for an adult male.	69
Figure 17. Example trajectories of the traversal phase for non-turning drivers travelling through an intersection. Trajectories are for an adult male.	70
Figure 18. Example trajectories of the approach phase for left-turning drivers travelling through an intersection. Trajectories are for an adult male.	71

Figure 19. Example trajectories of the traversal phase for left-turning drivers travelling through an intersection. Trajectories are for an adult male.	72
Figure 20. Example trajectories (acceleration versus distance) of the approach phase for left-turning drivers travelling through an intersection. Trajectories are for an adult male.	74
Figure 21. An EDR-recorded speed profile of a vehicle involved in a SCP intersection crash (NASS/CDS 2013-76-166) with the scene diagram prepared by the investigator of the crash....	79
Figure 22. Extracting intersection traversal acceleration. The first step in this process required the removal of all EDR-recorded time points where evasive braking was indicated. The second step in the process required the extraction of the acceleration portion of the EDR record.	81
Figure 23. Example acceleration profiles of previously developed models.	83
Figure 24. Simulated speeds versus EDR-recorded speed for every data point used in this study. Results were generated using the leave-one-out cross-validation method. Three previously generated models are shown in the figure, including the Bham two-phase, Wang linear-decreasing, and Wang quadratic-decreasing models. The Scanlon linear-decreasing and quadratic-decreasing models generated in this study are additionally presented in the figure. Data points are sized based on their NASS case weight.	94
Figure 25. Comparing model predicted speed with recorded speed. These results were generated using the most basic cross-validation method.	96
Figure 26. Simulated distance versus time trajectories for a vehicle accelerating from rest. Each acceleration trace corresponds to one of the models evaluated in this study.....	98
Figure 27. Comparing driver ages between the datasets.....	104
Figure 28. Comparing driver gender between the datasets.....	105
Figure 29. Comparing vehicle body types between the datasets.	106
Figure 30. Comparing roadway speed limits between the datasets.	106
Figure 31. Example EDR (NASS/CDS 2013-74-106) recorded vehicle indicated speed profiles (sampled at 10 Hz). The subject vehicle (indicated by blue arrow) turned left while travelling through an intersection without yielding. The driver was then struck by a straight crossing vehicle travelling from the opposite direction. The subject vehicle did not take any evasive braking action. Based on a spike in yaw rate just before impact, which is not depicted, the driver likely attempted an evasive steering maneuver to the left just before impact. The image depicts a left turn across path/ opposite direction (LTAP/OD) intersection crash.	111
Figure 32. Example EDR (NASS/CDS 2013-78-145) recorded vehicle indicated speed profiles (sampled at 10 Hz). The subject vehicle (indicated by blue arrow) travelled straight through an intersection without yielding. The driver then struck a left turning vehicle. The subject vehicle performed an evasive braking and evasive steering maneuver in the last second (braking = 0.6 seconds, steering = 0.7 seconds) before impact. The image depicts a left turn across path/ opposite direction (LTAP/OD) intersection crash.	112
Figure 33. Example EDR (NASS/CDS 2013-76-166) recorded vehicle indicated speed profiles (sampled at 10 Hz). The subject vehicle (indicated by blue arrow) performed a complete stop, and then accelerated straight through an intersection. The driver then struck a vehicle that has the right-of-way. An evasive braking and steering maneuver were performed in the last second (braking = 0.2 seconds, steering = 0.5 seconds) before impact. The image depicts a straight cross path (SCP) intersection crash.....	113
Figure 34. Example EDR (NASS/CDS 2011-43-163) recorded vehicle indicated speed profiles (sampled at 10 Hz). The subject vehicle (indicated by blue arrow) performed a rolling stop at 3 mph, and then accelerated straight across the intersection. The driver was then struck by a	

vehicle approaching from his left. The driver did not perform a steering or braking evasive maneuver. The image depicts a straight crossing path (SCP) intersection crash.....	114
Figure 35. Comparison of the EDR time coordinate system and the actual time coordinate system.	119
Figure 36. The figure depicts an example EDR braking time series. All of the data points are plotted on the actual time coordinate system. The actual points and timing of the EDR sampled time points are shown in the first graph. The remaining three graphs show how each manufacturer EDR would timestamp the sampled data points.....	122
Figure 37. Weighted cumulative distributions of evasive braking time points. All EDR modules with evasive braking were considered. Due to uncertainty in the time at which the evasive maneuver began, minimum and maximum possible time points are provided.....	132
Figure 38. Weighted cumulative distributions of evasive braking time points. Only modules that recorded pre-crash braking at 2 Hz or higher were considered. Due to uncertainty in the time at which the evasive maneuver began, minimum and maximum possible time points are provided.	133
Figure 39. Weighted cumulative distributions of evasive steering time points. Due to uncertainty in the time at which the evasive maneuver began, minimum and maximum possible time points are provided.	134
Figure 40. Weighted cumulative distribution of maximum evasive braking decelerations.	135
Figure 41. Weighted cumulative distribution of maximum evasive vehicle yaw rate.....	138
Figure 42. Impact speed as a function of traversal speed presented by turning behavior and evasive maneuvering.....	159
Figure 43. Model predicted speed versus vehicle speed recorded by the EDR for straight crossing drivers.	168
Figure 44. Model predicted speed versus vehicle recorded by the EDR for left turning drivers.	168
Figure 45. The downloaded EDRs for a SCP intersection crash (NASS/CDS 2013-76-166). The vehicle indicated in green stopped at a stop sign then accelerated into the intersection as indicated by the EDR download extracted from the vehicle. The vehicle indicated in orange did not have a traffic control device, and was travelling at approximately 20 mph for the 5-seconds prior to impact as indicated by the EDR download.	171
Figure 46. The scene diagram for NASS/CDS case 2014-4-55. The EDR speed profile records are additionally included for both vehicles. The left turning vehicle (red) slowed down throughout the intersection approach and left turn. The straight crossing vehicle (green) maintained a relatively constant speed approximately 15 mph higher than the posted speed limit (speed limit = 45 mph).....	171
Figure 47. Seven pre-crash movement categories that were used to reconstruct vehicle paths.	178
Figure 48. Examples for how intersection boundary lines were drawn. The scene diagram on the top was taken from NMVCCS case 2007-74-62. The scene diagram on the bottom comes from NMVCCS case 2006-03-043.	181
Figure 49. An example case for accounting for uncertainty in sample time step using a 1-Hz EDR. The top-figure shows a typical GM EDR recording of vehicle speed. Time zero represents impact. The last EDR-recorded vehicle speed (labeled as 1) was recorded at some point within 1-second prior to impact. In the middle figure, due to uncertainty in when the last EDR-recorded vehicle speed was recorded, the time series was shifted by one-half the sample time (0.5 s). In the bottom figure, impact speed was determined through linear extrapolation.....	183

Figure 50. The four main components of pre-intersection crash vehicle kinematics.	185
Figure 51. A depiction of point of impact and contact plane using PC-Crash (Figure taken from PC-Crash user manual [213])......	187
Figure 52. A depiction of the PC-Crash reconstruction protocol.	188
Figure 53. A depiction of point of impact and contact plane using PC-Crash (Figure taken from PC-Crash user manual [213])......	192
Figure 54. Overview of approach for determining “most-likely” kinematics of drivers that completely or rolling stopped prior to entering the intersection.	195
Figure 55. The intersection approach phase is highlighted among the four main components of pre-intersection crash vehicle kinematics.	196
Figure 56. The intersection traversal phase is highlighted among the four main components of pre-intersection crash vehicle kinematics.	197
Figure 57. Example travelling through profile for non-turning vehicle.	198
Figure 58. Example travelling through profile for vehicle turning left.	198
Figure 59. Steps that will be used to reconstruct the kinematics of travelling through vehicles.	199
Figure 60. The evasive actions phase is highlighted among the four main components of pre-intersection crash vehicle kinematics.....	200
Figure 61. The traversal phase is highlighted among the four main components of pre-intersection crash vehicle kinematics.....	201
Figure 62. The approach phase of the pre-crash action is highlighted.	201
Figure 63. Example trajectories (acceleration versus distance) of the approach phase for left-turning drivers travelling through an intersection. Trajectories are for an adult male.	202
Figure 64. Crashes within this study’s simulation case set by traffic control devices.....	204
Figure 65. Original set of cases extracted crashes broken down by traffic control devices.	205
Figure 66. The distribution of speed limits for the simulation case set used in this study.	206
Figure 67. The distribution of speed limits for the original set of extracted crashes prior to exclusion.	207
Figure 68. The pre-crash movements for all vehicles extracted from valid NMVCCS SCP crashes.....	210
Figure 69. The flowchart depicts this study’s overall strategy.	216
Figure 70. The figure provides graphical depictions of the braking deceleration magnitude that is required to stop the vehicle given vehicle kinematics at the earliest violation detection time point. Each data point on the graph depicts a unique speed and distance from intersection entry at the earliest violation detection time point. Lines are additionally shown to indicate corresponding RDP values. The graph on the left shows lines representing RDP at the time that the violation was detected, i.e. before a PRT. The graph on the right shows lines representing RDP after a 1.0 s PRT. Each row of graphs corresponds to the results of each unique violation detection algorithm.	228
Figure 71. A depiction of an LTAP/OD crash scenario. The blue (left turning) vehicle is equipped with hypothetical forward and side facing sensors.	232
Figure 72. A depiction of sensor orientation, maximum range, and field of view for detecting oncoming vehicles.	234
Figure 73. The scene diagram for NASS/CDS case 2014-4-55. The EDR speed profile records are additionally included for both vehicles. The left turning vehicle (red) slowed down throughout the intersection approach and left turn. The straight crossing vehicle (green)	

maintained a relatively constant speed approximately 15 mph higher than the posted speed limit (speed limit = 45 mph).....	235
Figure 74. The opportunities for earliest vehicle detection given sight obstructions. The worst-case earliest detection opportunity represents a scenario where (a) the left turning vehicle has begun initiating a left turn and (b) line-of-sight was obstructed by a queue of vehicles.....	238
Figure 75. Detection distance and angle measurements used to describe the relative positions of the two vehicles.....	238
Figure 76. Interval between detection and impact under best-case and worst-case scenarios. ..	240
Figure 77. Detection distance between the front-center of the vehicles at the best-case and worst-case earliest detection opportunities.	244
Figure 78. Detection angle between the front-center of the vehicles for the left turning vehicle at the best-case and worst-case earliest detection opportunities.....	244
Figure 79. Detection azimuth between the front-center of the vehicles for the straight crossing vehicle at best-case and worst-case earliest detection opportunities.	245
Figure 80. Convention used to describe relative location of oncoming vehicle (blue vehicle) with respect to the equipped vehicle (red vehicle).....	246
Figure 81. The position of the straight crossing vehicle (oncoming) from the perspective of the left turning vehicle (equipped). The red dot indicates the best-case detection opportunity, while the blue dot represents the worst-case detection opportunity. The trace terminates at the point of impact. Three sensor beams are considered with the assumption that the sensor was oriented in the direction of the vehicle heading.	247
Figure 82. The position of the left turning vehicle (oncoming) from the perspective of the straight crossing vehicle (equipped). The red dot indicates the best-case detection opportunity, while the blue dot represents the worst-case detection opportunity. The trace terminates at the point of impact. Three sensor beams are considered with the assumption that the sensor was oriented in the direction of the vehicle heading.	248
Figure 83. A depiction of SCP and LTAP/LD intersection crash modes.	252
Figure 84. A depiction of sensor orientation, range, and azimuth for detecting an oncoming vehicle.	253
Figure 85. Examples for how intersection boundary lines were drawn. The scene diagram on the left was taken from NMVCCS case 2007-74-62. The scene diagram on the right comes from NMVCCS case 2006-03-043.	256
Figure 86. A graphical representation of range and azimuth. The Red vehicle represents the vehicle from which range and azimuth are computed.	256
Figure 87. A depiction of sensor orientation, range, and azimuth for detecting an oncoming vehicle.	257
Figure 88. The figure on the left shows a sensor-equipped red vehicle whose front-facing radar beam does not detect an approaching blue vehicle. The figure on the right depicts a side-facing radar beam that does detect an oncoming blue vehicle.....	258
Figure 89. A cumulative distribution plot of range for the first vehicle to enter the intersection	261
Figure 90. A cumulative distribution plot of azimuth at the earliest detection opportunity from the perspective of the entering vehicle.....	262
Figure 91. A cumulative distribution plot of azimuth at the earliest detection opportunity from the perspective of the oncoming vehicle.....	263

Figure 92. A cumulative distribution of detection distance requirements by intersection group.	265
Figure 93. A cumulative distribution plot of detection angle for the entering vehicle at the earliest detection opportunity. Results are shown by crash mode.	266
Figure 94. A cumulative distribution plot of detection angle for the oncoming vehicle at the earliest detection opportunity. Results are shown by crash mode.	267
Figure 95. Cumulative distribution plots of detection distance at the earliest detection opportunity by whether at least one of the vehicles stopped.	269
Figure 96. Cumulative distribution plots of detection angle at the earliest detection opportunity for the first vehicle to enter the intersection. The results are shown by whether at least one of the vehicles stopped.	270
Figure 97. Cumulative distribution plots of detection angle at the earliest detection opportunity for the oncoming vehicle. The results are shown by whether at least one of the vehicles stopped.	271
Figure 98. A cumulative distribution plot of elapsed time to collision following the earliest detection opportunity.	272
Figure 99. A cumulative distribution plot of time to collision following the earliest detection opportunity. Results are shown by the intersection crash mode.	273
Figure 100. A cumulative distribution plot of time to collision following the earliest detection opportunity. Results are shown by the stopping behavior of the vehicles.	274
Figure 101. The proportion of oncoming vehicles detected at the earliest detection opportunity are shown. The perspective of the entering vehicle is depicted.	277
Figure 102. The proportion of entering vehicles detected at the earliest detection opportunity are shown. The perspective of the oncoming vehicle is depicted.	278
Figure 103. Detection distance requirements at the time point when the first vehicle crosses over the intersection boundary line. Estimates were generated for the EDR dataset and the NMVCCS dataset.	280
Figure 104. Detection angle requirements at the time point when the first vehicle crosses over the intersection boundary line. The perspective of the first vehicle to enter the intersection (entering vehicle) is considered. Estimates were generated for the EDR dataset and the NMVCCS dataset.	281
Figure 105. Detection angle requirements at the time point when the first vehicle crosses over the intersection boundary line. The perspective of the vehicle approaching the intersection when the entering vehicle crosses the boundary line. Estimates were generated for the EDR dataset and the NMVCCS dataset.	282
Figure 106. A cumulative distribution plot of the time-to-collision at the time point when the first vehicle first crosses the intersection boundary line. Estimates were generated for the EDR dataset and the NMVCCS dataset.	283
Figure 107. Scenarios being considered in the current benefits study.	290
Figure 108. Outline of study methods.	292
Figure 109. Overview of the approach for modeling I-ADAS in the current study.	294
Figure 110. Depiction of how TTC can be estimated from the kinematics of the I-ADAS equipped vehicle.	296
Figure 111. Reaction time values provided from the Monash group for cross-traffic crashes.	297
Figure 112. Example injury risk curves generated during the current study. Benefits Estimates Calculation	303

Figure 113. Proportion of CT crashes within the simulation case set that (a) were avoided, (b) had modified impact conditions, or (c) had unchanged impact conditions. All 30 variations of I-ADAS considered in this study are shown.	308
Figure 114. The proportion of seriously injured drivers potentially preventable if an I-ADAS had been equipped on one of the vehicles. All CT crashes are shown. The contribution of completely avoided crashes and crashes with modified impact conditions are shown.	309
Figure 115. The proportion of crashes potentially preventable for an I-ADAS with no latency time. Results are shown by intersection crash mode.	313
Figure 116. The proportion of crashes potentially preventable by whether one of the vehicles stopped or slowed prior to entering the intersection. Results are presented only for a system without computational latency time.	315
Figure 117. The proportion of crashes potentially preventable by driver reaction time or being AEB-equipped. Results are presented only for a system without computational latency time. .	317
Figure 118. Example of a case where disbenefits could potentially result for the I-ADAS-equipped driver. Here, the I-ADAS-equipped vehicle applies brakes and slows from 40 to 35 kph.	319
Figure 119. Example of a case where disbenefits could potentially result for the non-equipped driver. Here, the I-ADAS-equipped vehicle applies brakes and slows from 40 to 35 kph.	319
Figure 120. Proportion of all CT crashes with disbenefits in I-ADAS activation.	320
Figure 121. Proportion of CT crashes with modified impact conditions that resulted in MAIS3+ injury risk.	321
Figure 122. The proportion of added MAIS3+ injuries compared to original number of MAIS3+ injuries.	322
Figure 123. Changes in impact location before and after an I-ADAS intervention. Only crashes that were shown to have negative injury consequences were considered. Two hypothetical I-ADAS types are depicted.	324
Figure 124. Changes in delta-v before and after an I-ADAS intervention. Only crashes that were shown to have negative injury consequences were considered. Two hypothetical I-ADAS warning algorithms are depicted.	326
Figure 125. Potential proportion of CT intersection crashes potentially preventable if I-ADAS was equipped on all vehicles throughout the entire vehicle fleet.	330
Figure 126. Proportion of potentially prevented vehicles with MAIS3+ drivers if I-ADAS was equipped on all vehicles throughout the entire vehicle fleet.	331
Figure 127. Tabulations of the most common intersection crash modes in the U.S. crash population. Tabulations are shown for all police-reported intersection crashes and all fatal intersection crashes.	335
Figure 128. The four main components of pre-intersection crash vehicle kinematics.	336
Figure 129. Box plots of vehicle speed versus distance from the beginning of the intersection traversal phase. Two pre-crash movements are shown, including rolling stopped and completely stopped. Every deceleration and acceleration phase were shifted in order to have the driver reach their minimum velocity at $d=0$	337
Figure 130. Intersection approach and traversal kinematics for travelling through drivers at signalized intersection. The graphs are separated by turning behavior. The location where distance = 0 represents the location where the traffic signal was last visible.	338
Figure 131. Example approach kinematics models generated for stopped vehicles. Several variations of this model are shown by speed limit and stopping behavior. The driver was	

assumed to be non-turning, not young or senior, a male, and approaching a stop sign controlled intersection.....	339
Figure 132. Simulated distance versus time trajectories for a vehicle accelerating from rest. Each acceleration trace corresponds to one of the models evaluated in this study.....	341
Figure 133. Example travelling through profile for non-turning vehicle.	342
Figure 134. Example travelling through profile for vehicle turning left.	342
Figure 135. Evasive braking probability based on impact speed relative to the posted speed limit for a straight crossing driver.	344
Figure 136. Evasive braking likelihood based on impact speed for a left turning travelling through vehicle.....	344
Figure 137. Most likely traversal speed based on impact speed relative to the posted speed limit and whether evasive braking was performed for a straight crossing driver. This equation form was generated for a senior driver travelling on a 35 mph road that was impacted in the near-side.	345
Figure 138. Most likely traversal speed based on impact speed limit and whether evasive braking was performed for a straight crossing driver. This equation form was generated for a senior driver that was impacted on the near-side.....	345
Figure 139. Example trajectories (acceleration versus distance) of the approach phase for left-turning drivers travelling through an intersection. Trajectories are for an adult male.	347
Figure 140. Reaction time values provided from the Monash group for cross-traffic crashes...	348
Figure 141. The opportunities for earliest vehicle detection given sight obstructions. The worst-case earliest detection opportunity represents a scenario where (a) the left turning vehicle has begun initiating a left turn and (b) line-of-sight was obstructed by a queue of vehicles.	355
Figure 142. Interval between detection and impact under best-case and worst-case scenarios.	356
Figure 143. A graphical representation of range and azimuth. The Red vehicle represents the vehicle from which range and azimuth are computed.	359
Figure 144. A cumulative distribution plot of elapsed time to collision following the earliest detection opportunity.	361
Figure 145. Outline of Benefits Study Approach.	362
Figure 146. Approach for modeling I-ADAS reaction.	364
Figure 147. Proportion of CT crashes within the simulation case set that (a) were avoided, (b) had modified impact conditions, or (c) had unchanged impact conditions. All 30 variations of I-ADAS considered in this study are shown.	366
Figure 148. The proportion of seriously injured drivers potentially preventable if an I-ADAS had been equipped on one of the vehicles. All CT crashes are shown. The contribution of completely avoided crashes and crashes with modified impact conditions are shown.	367
Figure 149. Potential proportion of CT intersection crashes potentially preventable if I-ADAS was equipped on all vehicles throughout the entire vehicle fleet.	369
Figure 150. Proportion of potentially prevented vehicles with MAIS3+ drivers if I-ADAS was equipped on all vehicles throughout the entire vehicle fleet.....	370
Figure 151. Proportion of all CT crashes with disbenefits in I-ADAS activation.....	371
Figure 152. Example of a case where disbenefits could potentially result for the I-ADAS-equipped driver. Here, the I-ADAS-equipped vehicle applies brakes and slows from 40 to 35 kph.....	372

List of Tables

Table 1. Grouping Method for Signalized Intersections.....	29
Table 2. Excluded Intersection Traversals.....	34
Table 3. Case counts by stopping behavior, turning behavior, and traffic control device. The * was used to indicate traversal events that were excluded from this study's analyses.	35
Table 4. A summary of the results from the statistical analysis on the influence of several potentially important predictor variables on driver approach and traversal kinematics. A * was used to indicate statistical significance ($p < 0.05$). A + was used to indicate when a variable was nearly significant ($0.05 > p > 0.10$).	39
Table 5. Tabulations showing the results from the Tukey's Post Hoc Analysis examining which levels of the traffic control device x turning intent interaction effect were statistically significant at predicting maximum vehicle deceleration. Factor levels that do not share a common letter were found to be different from one another.	50
Table 6. A list of the different predictor variable combinations used in this study for the approach phase model of drivers that came to a complete stop.	57
Table 7. A list of the different predictor variable combinations used in this study for the traversal phase model of drivers that came to a complete stop.	57
Table 8. A summary of the results from the statistical analysis on the influence of several potentially important predictor variables on driver approach and traversal kinematics. A * was used to indicate statistical significance ($p < 0.05$). A + was used to indicate when a variable was nearly significant ($0.10 > p > 0.05$).	63
Table 9. A list of the different predictor variable combinations used in this study for the approach phase model of non-turning drivers that travelled straight through the intersection.	69
Table 10. A list of the different predictor variable combinations used in this study for the approach phase model of non-turning drivers that travelled straight through the intersection. ...	70
Table 11. A list of the different predictor variable combinations used in this study for the approach phase model of left-turning drivers that travelled through the intersection.	71
Table 12. A list of the different predictor variable combinations used in this study for the approach phase model of non-turning drivers that travelled straight through the intersection. ...	72
Table 13. A list of the different predictor variable combinations used in this study for the approach phase model left-turning drivers that travelled through the intersection. This model uses an acceleration versus distance relationship.	74
Table 14. Regression model equations developed by Wang et al. [131].	85
Table 15. Breakdown of included cases by crash mode.	89
Table 16. Count of EDR modules by specifications.	90
Table 17. Least -squares means of trajectory error and mean differences between the various models.	92
Table 18. Overall Error scores for the various models and crash modes.	93
Table 19. Overall Error scores for the various models generated using the Basic Cross-Validation method.....	95
Table 20. Equations for overall pre-crash model fits.....	97
Table 21. Dataset composition used in the study to develop models of driver acceleration prior to real-world crashes.	103
Table 22. Pre-crash movement categories	115

Table 23. Minimum and maximum possible time offset uncertainty for EDRs of all four vehicle manufacturers included in this study. The table only shows the time offset uncertainty for a 1-Hz EDR.....	120
Table 24. Minimum and maximum discretization error given EDR pre-crash sampling rate....	121
Table 25. Earliest and latest possible initial braking time point for an example case. The case assumes that an EDR that collects pre-crash data at 1-Hz was used. Vehicle braking began at 1.75 s prior to impact.	123
Table 26. Counts of EDRs containing vehicle speed and braking extracted are tabulated by crash mode. Tabulations with NASS/CDS case weights are additionally shown.....	125
Table 27. Counts of EDRs containing vehicle speed, braking, and yaw rate extracted are tabulated by crash mode. Tabulations with NASS/CDS case weights are additionally shown..	126
Table 28. A summary of evasive maneuvering by maneuver type.	127
Table 29. Composition of Evasive Braking Dataset.	129
Table 30. Results from the Wald test used to examine factors that significantly influence likelihood of taking evasive action. A * was used to identify parameters found to be statistically significant. A + was used to identify variables that were just above the established alpha level (0.05).....	130
Table 31. Frequency counts of evasive steering direction by crash configuration. The red car in the depicted scenes represent the EDR-equipped vehicle, while the blue car represents the other vehicle.....	137
Table 32. Pre-crash movement categories	151
Table 33. Parameters for the straight crossing evasive braking model. Reference parameters do not have coefficients are indicated by “---“	162
Table 34. Parameters for left turning evasive braking model. Reference parameters do not have coefficients are indicated by “---“	162
Table 35. Summary of model performance versus NASS/CDS investigator.	163
Table 36. Accuracy of NASS/CDS investigator coded avoidance maneuver determined using EDR-recorded avoidance maneuver.	164
Table 37. Accuracy of evasive braking likelihood model determined using leave-one-out cross-validation.....	165
Table 38. Results from the leave-one-out cross-validation analysis of the evasive prediction model. Several probability thresholds are considered. Both the straight crossing and left turning models are shown.....	165
Table 39. Model parameters and statistical result for the straight crossing traversal speed linear regression model. Reference parameters do not have coefficients are indicated by “---“.....	166
Table 40. Model parameters and statistical result for the left turning traversal speed linear regression model. Reference parameters do not have coefficients are indicated by “---“.....	166
Table 41. Total number of crashes included in the final simulation case set.	173
Table 42. Table for matching coded NMCCS road conditions within inputted PC-Crash surface conditions.....	191
Table 43. Summary of pre-crash movements observed in this study.	208
Table 44. Model coefficients, the area under the ROC curve (AUC) with 95% confidence intervals, and Wald χ^2 test results for overall dataset regressions. Regression models are generated for distances from intersection entry ranging from 10 m to 50 m prior to intersection entry in 2.5 m increments. Several distances along the intersection approach are considered. The violation detection probability thresholds for three false positive proportions (FPP) are presented.	

In this study, the early, intermediate, and delayed detection algorithms were developed by selecting violation detection probability thresholds that resulted in FPP values of 5%, 1%, and 0.5%, respectively. 224

Table 45. Results from the cross-validation evaluation of the models at several distances along the intersection approach prior to intersection entry are shown. 226

Table 46. A tabulation of violations where braking capacity exceeded braking demand is shown. Results from all three detection algorithms are presented. Three maximum braking capacity values were considered that are dependent on road surface conditions. RDP before and after an elapsed reaction time were considered. 227

Table 47. Sensor specifications that were examined in the current study. 239

Table 48. Sensor combinations modeled in this study. 257

Table 49. Parameters for logistic regression function used to predict driver MAIS3+ injuries. A Wald-test was also performed for each of the predictor variables in order to show significant predictors. * was used to show statistical significance (p -value < 0.05). + was used to indicate a near-significant correlation ($0.05 < p$ -value < 0.10). 303

Table 50. Equations for overall pre-crash model fits. 340

Table 51. Sensor combinations modeled in this study. 359

Table A1. Printout for model for the approach phase of drivers that came to a rolling or complete stop. 399

Table A2. Printout of model for the traversal phase of drivers that came to a rolling or complete stop. 400

Table A3. Printout of velocity versus distance model for approach phase of drivers that took a left turn while travelling through a signalized intersection. 401

Table A4. Printout of velocity versus distance model for traversal phase of drivers that took a left turn while travelling through a signalized intersection. 402

Table A5. Printout of velocity versus distance model for approach phase of non-turning drivers travelling through a signalized intersection. 403

Table A6. Printout of velocity versus distance model for the traversal phase of non-turning drivers travelling through a signalized intersection. 404

Table A7. Printout of acceleration versus distance model for approach phase of left-turning drivers travelling through a signalized intersection. 405

List of Acronyms and Abbreviations

ABS	Anti-lock Braking System
AEB	Automated Emergency Braking
AIS	Abbreviated Injury Scale
AUC	Area under the ROC Curve
CAMP	Crash Avoidance Metrics Partnership
CAN	Controller Area Network
CVS	Canadian Vehicle Specifications
EDR	Event Data Recorder
ESC	Electronic Stability Control
ESD	Easy Street Draw
FARS	Fatality Analysis Reporting System
FCW	Frontal Crash Warning
GM	General Motors
GPS	Global Positioning Systems
I-ADAS	Intersection Advanced Driver Assistance Systems
IIHS	Insurance Institute for Highway Safety
LDW	Lane Departure Warning
LKA	Lane Keeping Assist
LTAP/LD	Left Turn Across Path / Lateral Direction
LTAP/OD	Left Turn Across Path / Opposite Direction
LTIP	Left Turn Into Path
MAIS	Maximum Abbreviated Injury Scale
MARS	Multiple Adaptive Regression Splines
MY	Model Year
NASS/CDS	National Automotive Sampling System / Crashworthiness Data System
NASS/GES	National Automotive Sampling System General Estimates System

NCAP	New Car Assessment Program
NDS	Naturalistic Driving Study
NHTSA	National Highway Traffic Safety Administration
NMVCCS	National Motor Vehicle Crash Causation Survey
PRT	Perception-Reaction Time
RDP	Required Deceleration Parameter
ROC	Receiver Operating Characteristic
RTIP	Right Turn Into Path
SCP	Straight Crossing Path
SHL	Specific Longitudinal Location
TCD	Traffic Control Device
TTC	Time-to-Collision
TTI	Time-to-Intersection
USDOT	U.S. Department of Transportation
V2I	Vehicle-to-Infrastructure
V2V	Vehicle-to-Vehicle
VDOT	Virginia Department of Transportation
VTTI	Virginia Tech Transportation Institute

1. Introduction

1.1 *Motivation*

Intersection crashes are among the most frequent and lethal crash modes in the United States. Each year these crashes account for one-fourth of all crashes and one-sixth of all fatal crashes [1, 2]. In 2015 alone, there were 1.26 million police-reported intersection crashes in the United States. In these police-reported crashes, there were 5,707 fatalities from 5,251 fatal crashes [3].

Due to the frequent and often lethal nature of this collision type, intersection crashes in the United States account for significant economic costs. These expenses can be inflicted through a number of modalities, including property damage and medical expenditures. Previous work estimates the annual costs of all police-reported crashes in the United States to total approximately 300 billion dollars. Intersection-related account for approximately one-third of these costs (97 billion dollars) [4].

Intersection Advanced Driver Assistance Systems (I-ADAS) are emerging vehicle-based active safety systems that aim to help drivers safely navigate intersections. The primary function of this technology is to detect oncoming vehicles using onboard sensors and alert the driver or take autonomous evasive action (e.g., via braking or steering) if it is unsafe to traverse the intersection. A potential secondary function of this technology may be to detect an intersection violation (i.e. running a red light or stop sign) earlier in the intersection approach, while the driver still has time to yield for the traffic control device. Figure 1 gives a general depiction of how this proposed I-ADAS function might prevent intersection crashes.

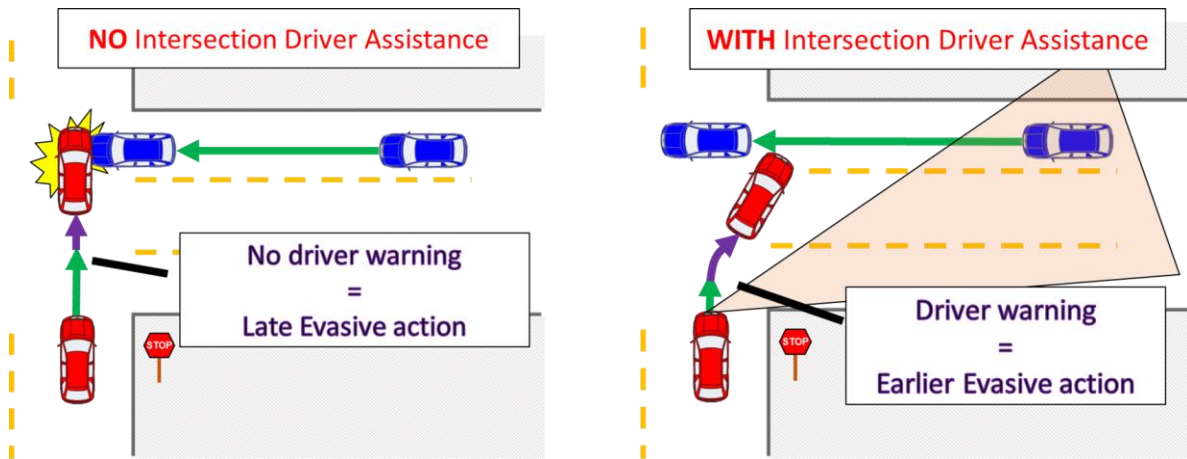


Figure 1. A general depiction of how I-ADAS might prevent intersection crashes.

Automakers and regulatory agencies are pursuing “Vision Zero”, which is the ambitious goal of eliminating all roadway fatalities [5, 6]. There are many types of vehicle-based safety technologies that aim to prevent crashes and injuries. These systems can be broken down into two main categories. Passive safety technologies seek to prevent and mitigate injuries by either (a) lowering impact severity or (b) providing in-vehicle protection for the occupant. Although these technologies can be very effective at preventing injuries [7-10], they are unlikely to completely prevent all injuries. Additionally, these passive safety technologies do not solve the problem of property damage. Some common passive safety technologies include:

- Seatbelts
- Airbags
- Knee bolsters
- Headrests
- Crumple zones
- Laminated windshields
- Structural reinforcements
- Padded interior

The past few decades have seen a strong push for vehicle-based driver assistance systems to be developed. Vehicle-based active safety systems aim to prevent crashes altogether or when

prevention is not possible to mitigate injury consequences by reducing impact severity. Crash avoidance systems have been and are being developed to target the most frequent and most harmful crash modes. Most current crash avoidance systems focus on passenger vehicle crashes, but a large amount of research and design has focused on vulnerable crash populations, such as pedestrians, bicyclists, and motorcycle users [11-21]. Although eliminating all crashes would be the ideal scenario, active safety technologies are unlikely to completely prevent all crashes anytime in the near future. Some common active safety technologies include:

- Antilock Brakes (ABS)
- Electronic Stability Control (ESC)
- Backup cameras
- Blind Spot Monitors
- Frontal Crash Warning (FCW)
- Automated Emergency Braking (AEB)
- Lane Departure Warning (LDW)
- Lane Keeping Assist (LKA)
- Intersection Advanced Driver Assistance Systems (I-ADAS)

There is a need to evaluate the potential effectiveness of these systems to justify their implementation. Assessing the crash prevention capability of any crash avoidance technology is important for designers, the consumer, and regulatory agencies. Until the system is widely deployed, evaluating I-ADAS using retrospective analysis is not practical. A method is needed to forecast these benefits.

In general, the evaluations of active safety systems need to be relevant for the real-world crashes which they aim to prevent. For example, the NCAP LDW confirmation test is run exclusively with the equipped vehicle travelling at 45 mph. Although previous studies have determined the average departure velocity to be near 45 mph for U.S. road departure crashes [22-25], these crashes can

occur at a wide range of departure velocities. Specifically, approximately one-fourth of departure velocities fall below 30-mph.

Automakers considering I-ADAS are interested in how effective the technology will be in the U.S. vehicle fleet. Developing and deploying this technology is very costly. Effectiveness evaluations not only provide motivation for the technology but also help set design priorities. For example, one area of interest for designers is driver behavior during “normal” driving scenarios. This includes analyzing how drivers typically approach intersections, traverse intersections, and perform crash avoidance maneuvers. Another important area of interest for designers is to quantify how design specifications will influence the performance of these systems in real-world settings. This includes examining various timings for I-ADAS and required sensor specifications to detect oncoming vehicles.

Regulatory agencies should also consider how I-ADAS might function within the vehicle fleet. The National Highway Traffic Safety Administration (NHTSA) is a part of the U.S. Department of Transportation and sets U.S. motor vehicle standards. Standards mandating active safety technology are slowly being implemented in the U.S. fleet as effectiveness data becomes available. In 2007, standards were set forth requiring that 100% of model year (MY) 2012 vehicles be equipped with ESC and ABS [26]. More recently, NHTSA, the Insurance Institute for Highway Safety (IIHS), and 20 automakers have announced a commitment to make AEB a standard feature on cars by MY 2022 [27].

Consumers are, of course, a critical party to consider during the development of I-ADAS. Demand for the product is essential for its success in the market. As such, consumers must be informed of the potential benefits of I-ADAS. Two important avenues for informing consumers in

the U.S. about the crash and injury prevention capabilities of new vehicles are the NHTSA New Car Assessment Program (NCAP) and the IIHS safety ratings. Both NCAP and IIHS safety ratings evaluate vehicle crashworthiness and the performance of any equipped crash avoidance technologies. As part of the U.S. NCAP, NHTSA runs “confirmation” tests which check for the presence of FCW and LDW [28, 29]. In order to pass both tests, alerts must be delivered to the driver before some time point threshold. However, neither of these tests consider whether any autonomous evasive action was performed by the vehicle (i.e. whether the vehicle was equipped with AEB or LKA). The IIHS safety tests check for the presence of FCW and AEB [30]. IIHS uses the NHTSA requirement that the warning must be delivered before some time point and awards extra points if the AEB system is able to successfully decrease impact speeds beyond some thresholds. Inconsistencies between the NHTSA and IIHS tests further highlight the need to provide compelling evidence for the effectiveness of active safety technologies.

In December 2015, NHTSA set forth a proposed framework of testing procedures for a future intersection collision avoidance system that uses vehicle-to-vehicle (V2V) communications [31]. They propose to evaluate these V2V crash avoidance systems in five crossing path intersection crash scenarios that are all depicted in Figure 2:

- (1) straight crossing path (SCP)
- (2) right turn into path (RTIP)
- (3) left turn into path (LTIP)
- (4) left turn across the path an approaching vehicle from the lateral direction (LTAP/LD)
- (5) left turn across the path an approaching vehicle from the opposite direction (LTAP/OD)

The purpose of the test is to evaluate and document the range that the system can detect oncoming vehicles, the timeliness of the collision alert, and any automated crash avoidance action the system may take. For each of the five crash scenarios, two tests will be performed, including one where both vehicles are moving and a second where the equipped vehicle stops then accelerates into the intersection. Additionally, these systems will be evaluated based on their tendency to deliver false alarms. These false-alarm tests will be performed by having the approaching vehicle stop or turn prior to crossing the path of the equipped vehicle, i.e. the oncoming vehicle never posed a threat. In light of these proposed future tests, there is a need to examine the important factors dictating the effectiveness of these systems, such as the pre-crash speeds of vehicles prior to impact, the stopping behaviors of the vehicles, and the acceleration rate of vehicles as they traverse the intersection. Although the test plans to only evaluate a V2V collision avoidance system, there is potential for the procedures to be adapted for an I-ADAS.

Outside of the U.S., EuroNCAP, which is the European vehicle assessment program and is backed by several governments, continuously develops test protocols and evaluates vehicle safety performance. A large part of this evaluation, of course, is the testing of vehicle active safety systems. In March 2015, EuroNCAP published their most recent “2020 Roadmap” of test procedures that they hope to have installed by the year 2020 [32]. Intersection assist has been proposed to have a test procedure developed by 2019 and adopted by the year 2020.

1.2 I-ADAS Target Population

There are several common variants of intersection crashes within the U.S. crash population. Previous work has aimed to tabulate the frequency of these crash modes for (a) all police-reported intersection crashes and (b) all fatal intersection crashes in the U.S. [2]. Only vehicle-to-vehicle,

crossing path crashes were considered. Tabulations were made by analyzing case years 2011 and 2012 of the National Automotive Sampling System General Estimates System (NASS/GES) [33] and the Fatality Analysis Reporting System (FARS) [3]. These tabulations can be seen in Figure 2.

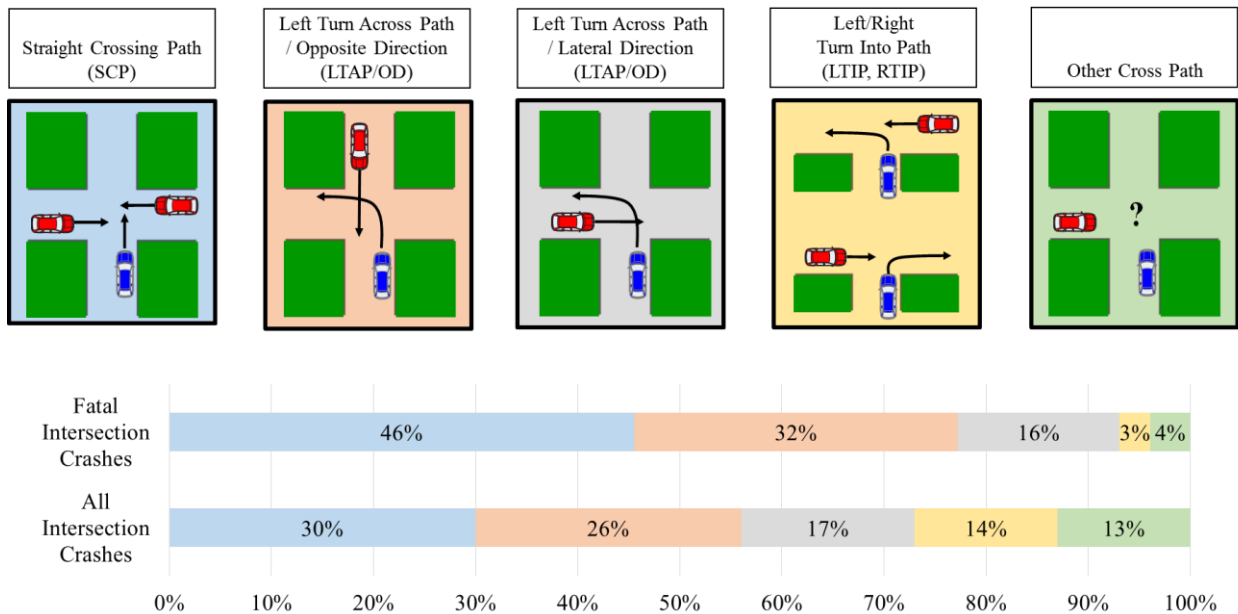


Figure 2. Tabulations of the most common intersection crash modes in the U.S. crash population. Tabulations are shown for all police-reported intersection crashes and all fatal intersection crashes.

The three most common intersection crash modes in the U.S. were straight crossing path (SCP), left turn across path / opposite direction (LTAP/OD), and left turn across path / lateral direction (LTAP/LD), which together accounted for 73% of all intersection crashes and 93% of fatal intersection crashes [2]. Accordingly, I-ADAS is expected to have the greatest impact on reducing crashes, injuries, and fatalities if focused on these most common modes.

The traffic control devices (TCD) typically present at intersection crashes vary by the intersection crash mode. To investigate this dependency, the National Motor Vehicle Crash

Causation Survey (NMVCCS) was used to tabulate TCD by the three most common intersection crash modes, which can be seen in Figure 3. The NMVCCS dataset is a U.S. national crash database and is described in detail in Chapter 2.

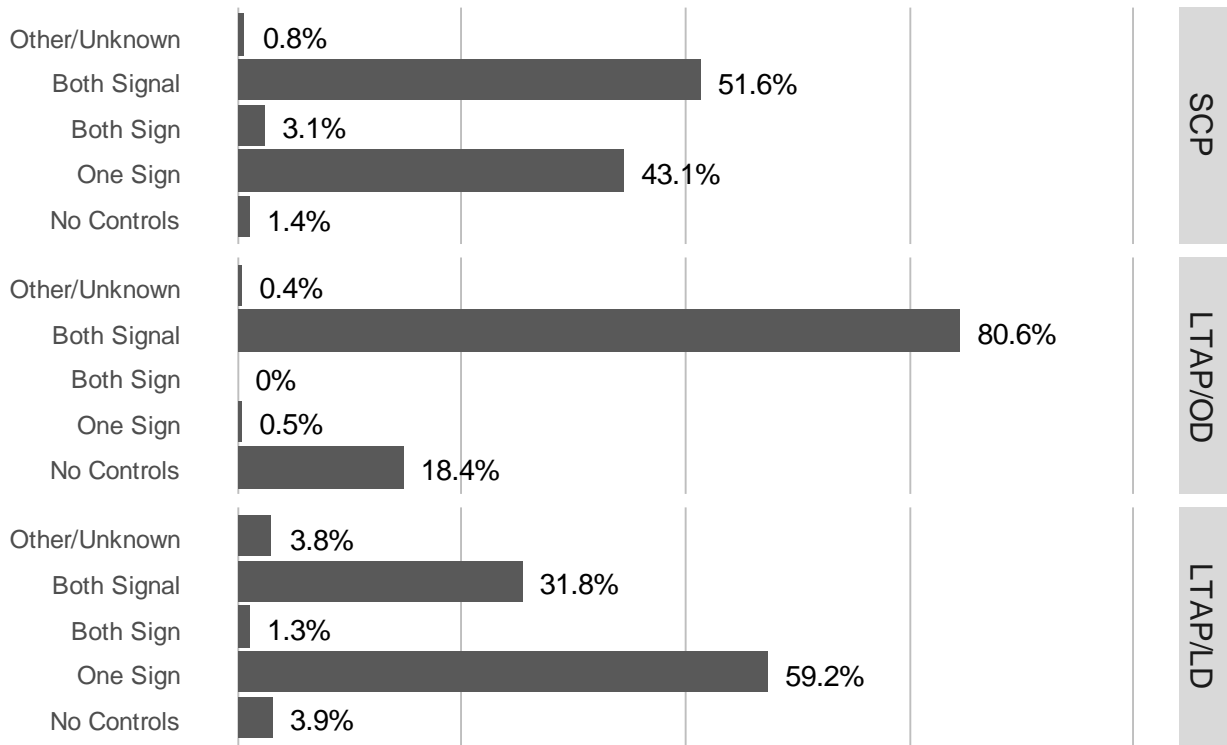


Figure 3. Tabulation of TCD present for the three most common intersection crash modes.

SCP crashes occur most frequently (52%) at signalized intersections. A majority of these crashes occurring at signalized intersections happened when one of the drivers entered the intersection on a red light. Two-way stop-sign controlled intersections were the second most common (43%) TCD present during SCP crashes in the U.S. For these crashes, one driver had the right of way, while the other driver failed to stop and wait at the stop sign for the oncoming vehicle to pass.

LTAP/OD crashes nearly always (99%) occurred when either (a) both vehicles had a signal or (b) neither vehicle had a TCD on their approach. These crashes occurred when one driver

attempted to make a left turn and either (a) failed to detect the oncoming vehicle or (b) misjudged the gap required to successfully perform the left turn. For these crashes, the left turning vehicle is almost always (94%) the violating vehicle (i.e., did not have right-of-way). An example of when the left turning vehicle would have had the right of way would be a case where the straight travelling vehicle entered the intersection on a red light and the left turning driver had a protected left turn green arrow.

LTAP/LD crashes most often (60%) occurred at two-way stop-sign controlled intersections. Using the 210 LTAP/LD crashes within the NMVCCS dataset that occurred at two-way stop-sign controlled intersections, the left turning vehicle pulled out from the stop sign for 100% of the crashes. Signalized intersections were the second most common (32%) type of TCD present during LTAP/LD crashes. These crashes almost always occur when at least one of the vehicles ran a red light (78% of the time the straight crossing vehicle runs the red light).

The critical reasons for real-world intersection crashes are important to consider for the development of I-ADAS. The critical reason describes the immediate reason for the crash having occurred. Figure 4 tabulates common critical reasons observed for the three most common intersection crash modes. These tabulations were generated using the NMVCCS database, which contains detailed events of the preceding events that led to the initial crash.

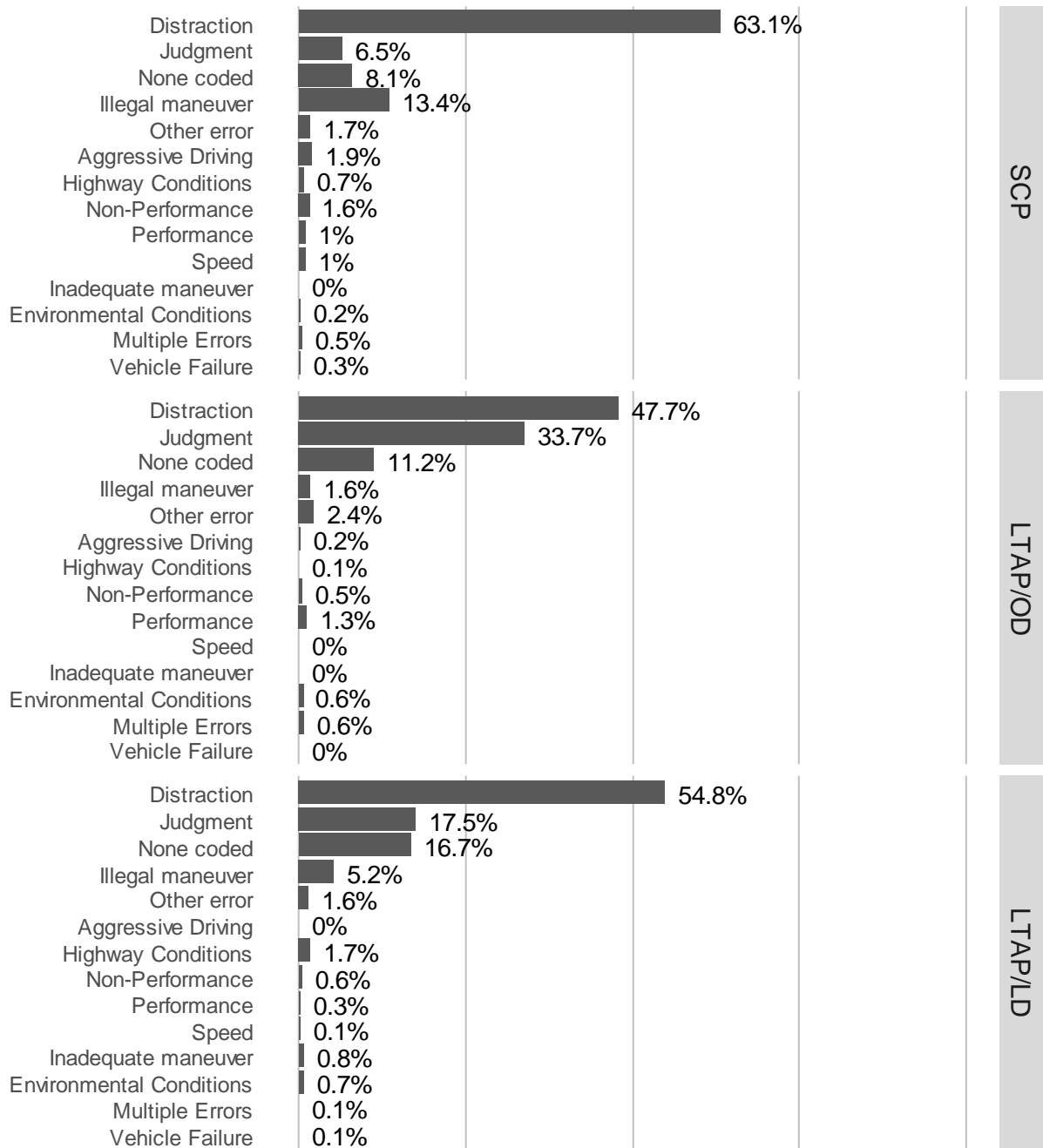


Figure 4. Critical reasons that led to intersection crashes.

Distraction and judgement errors were the most common errors observed in all three intersection crash modes accounting for 67% of SCP crashes, 81% of LTAP/OD crashes, and 72% of LTAP/LD crashes. This is a promising indication for I-ADAS, because these drivers may benefit from a system that can alert of an impending crash. It should be noted that NMVCCS was

compiled from 2005-2007. The widespread adoption of cell phones after this time period may lead to a higher proportion of distracted driving crashes in the current crash population. Distracted driving due to phone use is a widely known contributor to crash risk [34-37].

1.3 Strategies for Predictive Evaluation of Active Safety Systems

Predictive evaluation strategies were used in this dissertation work to examine how effective an I-ADAS might be in the U.S. vehicle fleet. Two main approaches were utilized. First, typical driver behavior was examined during normal driving and prior to real-world intersection crashes. Second, real-world intersection crashes were reconstructed and then simulated as if one of the involved vehicle was equipped with an I-ADAS.

Examining Normal Driving Behavior

There is a need to examine and develop representative models of normal driver behavior during intersection approach and traversals. First, the design of I-ADAS should account for how drivers typically approach and traverse intersections. Accounting for this “normal” driving behavior will help inform designers of important I-ADAS specifications (e.g. activation timing, sensor detection requirements). Tuning systems based on normal driving behavior will help to not only ensure system effectiveness but also limit false-positive activation. Second, a large part of this dissertation work was dedicated to developing models for estimating the number of crashes and injuries that could be prevented if every vehicle in the U.S. vehicle fleet was equipped with I-ADAS. As a part of this effort, intersection approach and traversal models were crucial for reconstructing real-world intersection crashes.

Examining Real-World Pre-Crash Driver Behavior

Little has been published on the detailed kinematics of drivers prior to real world intersection crashes. One method for obtaining this pre-crash vehicle data is through the use of Event Data Recorders, or EDRs. EDRs are the “black boxes” that are now in 96% of new U.S. passenger vehicles [38]. In the event of a triggering event, such as an airbag deployment, the EDR will immediately store the pre-event information (up to 5 seconds prior to the event). Several pre-crash data elements can be recorded by these event data recorders, including vehicle speed, accelerator application, brake application, yaw rate, and steering wheel angle. The sampling rate, resolution, and data elements recorded by these EDRs are dependent on the type of EDR module. The type of EDR module varies by vehicle make, model, and year.

This study utilized EDRs to study pre-crash driver behavior. Both driver action and vehicle kinematics will influence the performance of I-ADAS, because these factors directly affect the available time for the system to respond. Specifically, these systems must accommodate how drivers currently navigate through intersections (i.e., speeds and acceleration patterns of drivers) prior to real-world crashes. Lastly, proposed I-ADAS systems should seek to improve upon the frequency and timing of current driver evasive actions.

Evaluating I-ADAS by Simulating Real-World Intersection Crashes

One promising method for evaluating the effectiveness of a future crash avoidance system is through the retrospective simulation of real-world crashes. This method involves extracting a set of real-world crashes, reconstructing the crashes to determine pre-crash vehicle kinematics, and then simulating the scenario as though the vehicles were equipped with the proposed technology.

This type of predictive analysis has been implemented for a number of previously emerging crash avoidance technologies, including FCW/AEB [39-43] and LDW/LKA [22, 43-49].

Two technologies that have been evaluated at length using this technique are LDW and LKA [43-61]. These technologies help to prevent crashes resulting from an initial lane departure, such as road departure crashes. Accounting for around one-third of U.S. roadway fatalities, road departure crashes are the most lethal crash mode in the U.S. [3]. These fatalities are primarily a result of striking rigid roadside objects, such as trees, poles, or barriers [62-76]. Previous studies have aimed to predict the potential reduction in the number of road departure crashes if these systems were equipped throughout the entire vehicle fleet. Additionally, researchers have varied components of the warning being delivered to the driver [77, 78], varied the timing of the warning [23, 79], considered methods to reduce driver annoyance to LDW alarms [80], examined how the driver will adapt to these systems [81], and examined how roadway infrastructure influences the effectiveness of the technology [22].

This dissertation work evaluated I-ADAS using the retrospective simulation of real-world intersection crashes. The following paragraphs detail several research topics explored in this dissertation work using this method.

The performance of an I-ADAS will depend on the ability of the onboard sensors used to detect an imminent collision early enough for an I-ADAS to respond in a timely manner. There are only a few vehicles [82-84] commercially available that are equipped with these systems. Existing I-ADAS technologies are intended primarily for an LTAP/OD crash, and solely utilize a forward-facing radar sensor. Other crash modes, such as SCP and LTAP/LD, where vehicles are approaching one another from lateral directions, were hypothesized to require an entirely different

set of sensor specifications. Specifically, side-facing sensors were expected to be more appropriate given pre-crash approach directions. One effective method for evaluating the requirements of this technology was to simulate real-world crashes as they actually occurred, but include hypothetical I-ADAS sensors in order to investigate their potential vehicle detection capability in a real-world crash scenario. Important sensor specifications can additionally be varied in order to examine their influence on detection capability.

The primary function of I-ADAS will be to detect oncoming vehicles using on-board sensors and alert or take autonomous action if a crash is imminent. However, this strategy will be less effective when vehicles fail to yield prior to entering the intersection due to less time available to detect and avoid an imminent crash. An alternative method is to warn the driver or autonomously stop the vehicle during the intersection approach if an intersection violation is imminent. One strategy for evaluating a future violation detection algorithm in the vehicle fleet is by using a dataset composed of violations and non-violations, and then developing a classification model, such as using machine learning or logistic regression, to predict whether a violation is likely to occur. This procedure has been implemented in several previous studies for red light runners during signalized intersection approaches [85-89]. However, there are a limited number of predictive models for stop sign running. This may be due to the fact that running stop signs at excessive speeds is uncommon in the U.S. Previous work has indicated that drivers cross over the stop bar at a speed greater than 15 mph 0.6% of the time and at a speed greater than 20 mph a mere 0.2% of the time [85, 86, 90]. Although stop sign running at these high speeds is uncommon during normal driving scenarios, this behavior is very common in real-world crash scenarios. In fact, for straight crossing path (SCP) intersection crashes in the U.S., approximately one-third [91, 92] of stop sign-controlled crashes involved a vehicle travelling through the intersection without

stopping. A promising method for obtaining this violation data is through coupling typical driver behavior (100-Car Naturalistic Driving Study) and violations from Event Data Recorders downloaded from real-world crashes.

There is a need to quantify the number of crashes and injuries that can be prevented in the U.S. by I-ADAS. Additionally, it is important to recognize how I-ADAS design, intersection characteristics, and driver behavior will influence these estimates. Each of these factors will influence (a) whether the system can detect an imminent threat and (b) whether the driver can respond in a timely manner. For crashes where the driver is unable to successfully evade the crash, there is a need to examine whether changing the impact configuration would have negative injury consequences.

1.4 Overall Objective and Research Questions

The overall objective of this thesis was to evaluate the ability of I-ADAS to prevent U.S. intersection crashes and mitigate associated injuries. To accomplish this objective, several studies were first performed to examine how drivers typically traverse intersections during normal driving and prior to real-world crashes. The general research question of interest for these studies were: How will current driver behavior influence the effectiveness of I-ADAS? The second set of studies reconstructed real-world crashes then simulate the crashes as if either vehicle was equipped with I-ADAS. The first main research question of interest from these studies was: what proportion of intersection crashes and associated injuries could be prevented by an I-ADAS? The second research question was: How will I-ADAS design influence the effectiveness of these systems?

1.5 *Overview of Chapters*

The subsequent chapters describe the data sources that were used, the pre-crash driver analyses that were performed, the simulation case sets that were generated, and the predictive I-ADAS evaluations that were implemented.

Chapter 2 details the datasets that were used in this study. Each of the studies in the proposed thesis utilized at least one of these data sources. The chapter details the contents of each data source, the population from which it is derived, and how it was used in light of proposed research questions. After the data source chapter, the manuscript is divided into three sections.

Section 1 is divided into Chapters 3, 4, and 5 and aimed to describe typical pre-crash driver behavior. Chapter 3 analyzes typical intersection approach and traversal vehicle kinematics. The objective of this study was to generate vehicle kinematics models as drivers approach and traverse intersections. Additionally, factors influencing driver behavior at intersections are explored. Chapter 4 presents an analysis of pre-crash vehicle acceleration patterns as drivers traverse intersections. The objective of this study was to evaluate the accuracy of previously generated acceleration models with this pre-crash data and to develop improved acceleration models that are more representative of this pre-crash data. Chapter 5 describes an analysis of typical crash avoidance actions taken by drivers prior to intersection crashes. The objective of this study was to examine the frequency, timing, magnitude, and direction of driver evasive actions.

Section 2 is comprised solely of Chapters 6 and 7, and aimed to develop a simulation case set of reconstructed real-world crashes. Chapter 6 presents the development of models for estimating pre-crash actions. These models were instrumental in reconstructing pre-crash vehicle kinematics. Two models are presented: (1) a model for estimating likelihood of an evasive braking maneuver

having occurred based on impact speed and (2) a model for estimating intersection traversal speeds from impact speeds and whether evasive braking occurred. Chapter 7 presents work completed that generated simulation case sets to be used for evaluating I-ADAS. The simulation case sets consists of (1) extracted intersection crashes from U.S. national crash databases, (2) reconstructed pre-crash paths, and (3) reconstructed pre-crash vehicle kinematics. The first simulation case set, the EDR dataset, utilizes crashes where event data recorder (EDR) pre-crash data were extracted from both vehicles involved. The second simulation case set, the NMVCCS dataset, uses a larger dataset of intersection crashes where on-scene investigators provided a detailed account of the events leading up to the crash.

Section 3 is comprised of Chapters 8 through 11. Each chapter describes a separate study for evaluating I-ADAS within the U.S. vehicle fleet. Chapter 8 details a study for developing and evaluating an I-ADAS that warns drivers or takes autonomous evasive braking action if the driver is about to inadvertently run through a stop sign. The objective of this study was to determine how often drivers would be alerted, when drivers would be alerted, and if the driver could bring the vehicle to a stop given vehicle kinematics and the timing of the warning. Chapter 9 and Chapter 10 evaluated the sensor detection needs for I-ADAS in LTAP/OD and cross-traffic (SCP and LTAP/LD) crashes, respectively. The objective of these studies were to determine the detection distances and angles between vehicles at the earliest detection opportunity, the time-to-collision at the earliest detection opportunity, and the proportion of oncoming vehicles that could be detected given various sensor specifications. Chapter 11 generates estimates for how effective I-ADAS will be at preventing and mitigating crashes. The objective of this study was to estimate the proportion of crashes and vehicles with seriously injured drivers in the U.S. fleet that could be prevented if one of, or both, of the vehicles in SCP and LTAP/LD crashes were equipped with I-ADAS.

2. Data Sources

2.1 *Introduction*

A collection of different data sources were utilized to complete the studies described in this manuscript. These data sources include the National Motor Vehicle Crash Causation Survey (NMVCCS), National Automotive Sampling System / Crashworthiness Data System (NASS/CDS), and the 100-Car Naturalistic Driving Study (NDS). Each data source contains unique information and focuses on different populations of driving behavior. The following sections summarize the contents of each data source, the population from which it is derived, and how it was be used to advance the goals of this study (i.e. evaluating the potential of I-ADAS to prevent U.S. intersection crashes).

2.2 *NMVCCS*

The National Motor Vehicle Crash Causation Survey (NMVCCS) is a nationally representative crash database compiled by the National Highway Traffic Safety Administration (NHTSA). NMVCCS was a special study conducted for 2.5 years between July 2005 and December 2007 [93]. For a case to be included in the database, the NMVCCS crash investigator must have been present on the scene of the crash before it was cleared by emergency responders. There were several other requirements for inclusion in NMVCCS, including (1) the crash must have had a completed police accident report, (2) the crash must have occurred between 6 AM and midnight, and (3) the EMS must have been dispatched.

This allowed the investigators to prepare detailed scene diagrams and conduct interviews with witnesses, involved occupants, and first responders. Data from this crash database is publicly

available for download from the National Highway Traffic Safety Administration (NHTSA, <ftp://ftp.nhtsa.dot.gov/>).

NMVCCS (as well as NASS/CDS) used a complex sampling scheme in order to generate nationally representative estimates that represent the entire U.S. crash population [94]. Three stages of sampling were used to select crashes for inclusion in the database. First, the U.S. was divided into primary sampling units, or PSUs. This was done by dividing up the country into 1,195 areas based on whether the area is “central city, a county surrounding a central city, an entire county or a group of contiguous counties”. PSU’s were then divided into 12 strata based on geographic region and type, such as urban vs. rural areas. A total of 24 PSUs were then selected from these 12 strata, where each strata represents an approximately equal proportion of crashes. Second, police jurisdictions were selected from each of the PSU’s. It is impractical and expensive to sample all crashes within a PSU. As an alternative, a sample of jurisdictions within each PSU were selected from which to draw crashes. Third, crashes were selected from each of the jurisdictions. Crashes were classified based on vehicle type, occupant injuries, vehicle towing, and vehicle model years. Each crash was then assigned a national weighting factor (“RATWGT” variable) that adjusts for crash severity and location. This study used these national weighting factors in order to make nationally representative estimates.

The NMVCCS dataset was generated in response to the emergence of crash avoidance systems in the U.S. [95]. Because crash investigators arrived on scene prior to vehicles being cleared, extensive vital information was available for the investigators to determine the critical factors that led to the crash, such as roadway design (e.g. sightline restrictions, traffic control device failure) and driver behavior (surveillance, yielding at intersections, aggressiveness).

The breadth of information available in NMVCCS was used to generate a simulation case set of SCP, LTAP/LD, and LTAP/OD intersection crashes in the United States. The information provided in the NMVCCS investigations allowed for each crash to be reconstructed. Simulations as if each vehicle was equipped with I-ADAS were then performed for each crash (1) to evaluate sensor detection performance and (2) to estimate the crash and injury prevention capabilities.

2.3 NASS/CDS (w/ *Event Data Recorders*)

The National Automotive Sampling System / Crashworthiness Data System (NASS/CDS) is also a nationally representative crash database. This dataset is compiled annually with 4,000-5,000 new crashes that occurred at various locations throughout the United States. For a crash to be included in this database, at least one vehicle involved must have been towed away from the scene due to damage. Like NMVCCS, NASS/CDS case includes a national weighting factor which, when applied, allows for the generation of nationally representative estimates [94]. These national weighting factors were used throughout the proposed studies.

Each NASS/CDS case contains information regarding the occupants, vehicles, and environment at the time of the crash. However, unlike NMVCCS, investigators were not required to have arrived at the scene prior to it being cleared. Consequently, NASS/CDS lacks much of the detailed accounts regarding the events leading up to the crash. However, NASS/CDS contains three pieces of information not regularly available in the NMVCCS database. First, detailed medical records are provided for each occupant involved. Second, a large dataset of event data recorder (EDR) downloads are available that contain records of the vehicle's pre-crash kinematics just prior to impact. As previously described, several pre-crash data elements can be recorded by these event data recorders, including vehicle speed, accelerator application, brake application, yaw rate, and

steering wheel angle [96]. Although NMVCCS investigators did collect EDR data when available, most vehicles were not equipped with EDRs, and the NMVCCS dataset does not contain as many crashes. Third, NASS/CDS contains delta-v estimates for each vehicle in each crash.

Several criteria are required for an EDR module to be included for analysis in the proposed studies. First, these studies will only include EDRs either for crashes which deployed the airbags, or non-deployment crashes with a recorded delta-v of at least 5 mph. EDRs may overwrite non-deployment events by later events in some cases, but the data from airbag deployment events are locked into the EDR module. A non-deployment event of at least a 5-mph delta-v will result in substantial damage to the vehicle which would be unlikely to be associated with any event other than the NASS/CDS case. These criteria help ensure that the event being analyzed corresponds to the crash described in NASS/CDS. Second, the first event listed in the NASS/CDS database (vehicle-to-vehicle impact in intersection crashes) must have also been the most severe impact (highest delta-v) experienced by the vehicle, as indicated by the crash investigator (“accseq1” variable in NASS/CDS). This helped to ensure that the airbag deployment or airbag algorithm wake up associated with the non-deployment was due to this first vehicle-to-vehicle impact. When analyzing all SCP crashes in NASS/CDS, the first event was found to be the most severe event for 97% of intersection crashes. Third, the EDR module must have successfully recorded pre-crash vehicle indicated speed and pre-crash brake application. The complete file recorded flag was checked for each EDR to ensure the event was fully recorded. This flag was not available for some of the older Chrysler EDR modules, but these EDRs contained time series flags that indicated successful recording of pre-crash variables for each recorded time point. Lastly, crashes with case weightings greater than 5,000 were excluded to excluded to limit skewing of the results [97].

The proposed studies looked to analyze and develop models from the NASS/CDS (1) EDR pre-crash data and (2) injury data. The EDR pre-crash data helped to describe and explain typical pre-crash driving behaviors. The injury data was used to explore occupant injury risk given varying crash configurations and severities.

2.4 100-Car Naturalistic Driving Study

The 100-Car Naturalistic Driving Study (NDS) [98] was performed by the Virginia Tech Transportation Institute from 2001 to 2004, and consisted of approximately 1.2 million vehicle miles driven by 108 primary drivers. Each vehicle was instrumented with a variety of measurement devices, including cameras, inertial measurement systems, GPS, and data collected by the Controller Area Network (CAN). Study participants lived and primarily drove within the Washington, DC and Northern Virginia metropolitan areas.

A previously extracted subset of intersection traversal events identified as part of the CICAS-V study [99] was used. This dataset of approximately 95,000 intersection traversals were found using GPS coordinates from (1) a list of intersections provided by the Virginia Department of Transportation (VDOT) as having elevated crash frequencies and (2) intersections frequently traversed by study participants. Each intersection approach was manually reviewed by a team of reductionists at VTTI to verify the event was correctly identified from the GPS trace, to determine the driver's turning behavior, and to determine last visible light phase. During this study, data reductionists manually reviewed video from each event and recorded the approximate time point where the vehicle entered the intersection. For stop sign traversals, the point of intersection entry was the location where the stop bar was last visible. For signalized intersection traversals, the intersection entry location was the instance where the traffic light was last visible.

The 100-Car study provided a large, unique data source of “typical” driver behavior during intersection traversals. Models were developed from this data source that aimed to describe typical intersection approach and traversal kinematics and predict imminent traffic violations.

Virginia GIS Data

Speed limit information is not available from the 100-car dataset. However, GPS coordinates taken from the 100-car vehicles can be used to determine these speed limits. This study used map data provided by Loudon, Fairfax, and Arlington counties in the Northern Virginia Area to supplement the 100-Car data with speed limit information. This roadmap data was provided to the Virginia Tech research group in the form of “shapefiles”, which store roadway information as a collection of positional data points with other information, such as speed limit, road type, county, and route name also available. This study only used speed limit information.

Two GPS coordinates were used for each traversal event, i.e. the speed limit on the roadway when approaching the intersection and the speed limit on the roadway after leaving the intersection. A GPS coordinate 75 m before and after the driver entered the intersection was used to determine these two speed limits. In the simulation case set of SCP crashes developed in Chapter 6, the maximum distance travelled into the intersection prior to being impacted was found to be around 40 m. ArcMap (an ArcGIS program [100]) was then used to link these coordinates to the information in the Virginia GIS shapefile using the join function. The join function matches each set of GPS coordinates to the nearest roadway. The speed limit from this nearest roadway was extracted, along with the distance from the GPS coordinate to the location of the nearest roadway. A 30-m threshold from the coordinate to the nearest road was used to confirm that the nearest roadway was the same roadway as that being traversed by the driver. This large distance

threshold was selected because of error associated with matching GPS coordinates with shape file roadways. This error has two sources: (1) error in the GPS position and (2) representation of roadways as a line segment (i.e., zero-width roadways). The research protocol used by the researchers for performing this analysis can be found in the Appendix (Chapter 0).

Section 1:
Analyzing Driver Behavior at Intersections

3. Intersection Approach and Traversal Patterns during Normal Driving

3.1 Introduction

This study looked to analyze normal driving behavior during intersection approach and traversals. Characterizing and quantifying driver behavior is an important aspect of evaluating crash avoidance technologies [101-115]. A number of factors motivated this analysis. First, I-ADAS should be designed based on and evaluated under conditions of how drivers typically traverse intersections. Second, examining factors that influence driver behavior can help in developing path prediction algorithms and system timings. Third, simulating intersection behavior, such as in the benefits study performed in this dissertation work, relies on intersection approach and traversal models.

The objective of this study was to generate vehicle kinematics models as drivers approach and traverse intersections. These models were essential for developing the simulation case set that has been used in the benefits analysis and sensor detection requirements study. The overall benefits project reconstructs pre-crash intersection approach and traversals as a function of the known pre-crash movement of the driver (completely stopped, rolling stopped, and travelling through), the traffic control device (TCD) at the intersection (signalized or stop sign-controlled), the turning behavior of the driver (left-turning, straight through), driver characteristics (age, gender), roadway characteristics (speed limit), and impact speed.

As a part of this model development, I was also interested in exploring how various factors influence driver approach and traversal behavior. Several research questions were posed in an effort to address these relationships, including:

1. How are vehicle kinematics influenced by whether the driver comes to a complete stop or rolling stop?
2. How does the traffic control device influence vehicle kinematics?
3. How does turning behavior affect intersection approach and traversal kinematics?
4. How does roadway speed limit affect intersection approach and traversal kinematics?
5. How do driver demographics influence approach and traversal kinematics for stopped vehicles?

3.2 *Methods*

Data Source

This study used data collected as a part of the 100-Car Naturalistic Driving Study. Chapter 2 details this data source. As previously discussed, a large compilation of previously identified intersection approaches and traversals were used to perform this study's analysis.

Several exclusion criteria were used to select cases for this study's analysis. First, some case files provided by VTTI did not contain any time series data and were excluded. Second, some traversal events provided by VTTI were not present within the 100-car data pool. Third, some approach and traversal time series data were incomplete. Occasionally this data was invalid for some vehicles due to a malfunctioning of either the sensor or the CAN bus. Vehicle speed sampling failure is apparent when sampled speeds and braking are continuously recorded with a zero value. If more than 90% of the data was invalid, the case was excluded. Fourth, traversals where speed limit data could not be obtained were excluded. Speed limit data was only available if GPS data was available for that case and if the roadway information was available. Some GPS data were not provided to the research group. Occasionally, the GPS data were invalid. Additionally, only GPS

data from the Northern Virginia area were considered in this study. Fifth, only straight crossing and left turning traversals were of interest in this study. Other movements, such as right turns and U-turns, were excluded. Sixth, only events where the vehicle was not stopped in a queue was of interest in this study. Extracting only lead vehicle events helped to ensure that the driver behavior was not being influenced by another lead vehicle. Cases in which the data reductionist indicated that the vehicle was stopped behind a lead vehicle were excluded from this study's analysis.

Extracting Approach/Traversal Events

For every event, the speed profile of the intersection approach and traversal phase was extracted. The intersection entry time point provided by VTTI was first selected as a reference point for identifying the transition between the approach and traversal phase. For stop sign traversals, the point of intersection entry was the location where the stop bar was last visible. For signalized intersection traversals, the intersection entry location was the instance where the traffic light was last visible.

Each event was classified into one of three categories based on the movements of the driver. These categories were completely stopped, rolling stopped, or travelling through. Completely stopped and rolling stopped pre-crash movement behavior, respectively, is when a driver slows for an intersection and either (a) comes to rest or (b) comes to a low-speed ("rolls") prior to accelerating into the intersection. Travelling through driving behavior depends on the turning intention of the driver. For straight crossing drivers, a travelling through driver tends to maintain some speed throughout the intersection approach and traversal. Occasionally, drivers will accelerate as they attempt to "beat the yellow" signal phase change [116]. For left-turning drivers,

drivers tend to slow as they approach and enter the intersection [116-118]. These drivers then accelerate as they leave the intersection [118].

The minimum vehicle speed as the driver approached and began traversing the intersection was used to define the movement category. For stop sign events, the minimum speed search window extended from 25 m before intersection entry to 25 m after intersection entry. For signalized intersection events, the minimum speed search window extended from 75 m before intersection entry to 25 m after intersection entry. As will be discussed in the results, depending on the queue at the signalized intersection, drivers occasionally stop at larger distances from the intersection than a driver at a stop sign-controlled intersection. Using this minimum speed within this search window, the traffic control device, and the turning behavior of the driver, the movement category of the event was determined. Detailed descriptions of the vehicle kinematics classifications can be found in Table 1.

Table 1. Grouping Method for Signalized Intersections

Movement Group	Traffic Control Device	Turning Behavior	Minimum Speed Threshold
Complete Stop	All	All	Minimum Speed \leq 2.8 mph (1.2 m/s) *typical walking speed [119]
Rolling Stop	Stop Sign	All	2.8 mph < Minimum Speed \leq 20 mph
	Traffic Light	Straight	2.8 mph < Minimum Speed \leq 20 mph
		left	2.8 mph < Minimum Speed \leq 10 mph
Traveling Through	All	All	All remaining events

Different minimum speed thresholds for distinguishing between travelling through and rolling stopped drivers were selected depending on the traffic control device present at the intersection and turn intent. At stop sign-controlled intersections, drivers must stop for the stop sign, but frequently will “roll” through the sign. In our dataset, drivers that crossed into the intersections at speeds less than 20 mph tended to slow prior to entering the intersection. Conversely, although rare, drivers that entered the intersection at speeds greater than 20 mph maintain a relatively constant speed. The latter behavior was classified as “travelling through”. At signalized intersections, drivers must stop on red lights. Occasionally, a phase change occurs during the intersection approach, and the driver will then begin to accelerate into the intersection prior to coming to a complete stop. This behavior was labeled as a “rolling stop”. A similar (20 mph) rolling stop speed threshold that was used for stop sign-controlled intersections was also used for Straight crossing drivers at signalized intersections. Left turning, travelling through drivers at signalized intersections almost always slow down prior to entering the intersection in order to safely complete the left turn. To avoid mislabeling this slowing as a rolling stop, an even lower minimum speed threshold was used for left turning drivers.

For stopped drivers (complete or rolling), the minimum speed point was referred to as the “traversal start location”, and represents the location where the driver transitioned from a deceleration approach phase to a traversal acceleration. Occasionally, the driver will “double-stop” prior to entering the intersection. This could occur, for example, if the driver has to move forward in order to see around parked vehicles on the roadway. For cases with multiple “dips” in the velocity profile, the first dip was considered to be the end of the approach phase, and the last dip was considered to be the beginning of the traversal phase. Additionally, as discussed later in the

results, it should be noted that this minimum speed location relative to the intersection is dependent on the driving context, such as the traffic control device and the turning behavior of the driver.

For travelling through drivers, the intersection entry time point was used to distinguish between approach and traversal phase. As will be shown in the results, travelling through drivers do not typically experience a clear dip in vehicle velocity during the approach and traversal. Left turning, travelling through drivers almost always slow prior to entering the intersection, but often maintain this slower speed as they execute their left turn.

Statistical Analysis of Vehicle Kinematics Features

There is often considerable variability in driver behavior during intersection traversal events. One aim of this study is to quantify the influence of several factors on driver behavior in order to help limit this variability.

A mixed-effects analysis of variance (ANOVA) with planned contrasts was used to investigate the influence of several predictor variables. All statistical analyses were run using the “lme4” package [120] in the R-Programming language [121]. Each driver unique identification number was used as a random effect that influenced the model intercept. Several predictor variables were examined in this study, including stopping behavior, traffic control device, turning behavior, speed limit during the approach, speed limit during the traversal, driver age, and driver gender. Several potential interaction effects between the variables were additionally examined. A number of kinematics features were examined as dependent variables. These dependent variables included, the elapsed time during the last 30 m of the intersection approach, average approach deceleration, maximum approach deceleration, and vehicle speed at traversal start, the elapsed time during the first 30 m of the intersection traversal, average traversal acceleration, and maximum traversal

acceleration. The predictor variables considered for a given model depended on the subset of the data being analyzed, the research question being addressed, and the dependent variable being analyzed. Each statistical model developed in this study is detailed in the appropriate section of the results.

Three driver age groups were examined, including young (18-20 y.o.), adult (21-60 y.o.), and senior (61+ y.o.). In the event of driver age being indicated as a significant predictor variable, post hoc pair-wise comparisons between the driver groups were performed using Tukey's Honest Significant difference (HSD) test. All pairwise comparisons and least squares means estimates were generated using the "lsmeans" package [122].

Developing Driver Behavior Models

This study used a non-parametric regression technique, Multivariate Adaptive Regression Splines (MARS) to develop all driver models. All models were built using the ARESLab toolbox [123] in Matlab. The MARS technique has some advantages over traditional regression methods. First, the developed models account for non-linear and linear trends and intersections between variables. Second, the models can handle the modeling of both continuous and non-continuous data.

In order to avoid overfitting, the MARS approach builds the regression model first through a forward selection phase, where predictor variables and interaction effects are iteratively added. This is then followed by a backwards deletion phase, during which a Generalized Cross-Validation (GCV) score is generated after each deletion. GCV is a measure of the model's predictive error. At the end of this process, the model with the lowest GCV is selected.

The final models developed in this study were in the form of several piecewise-cubic splines. The model created using the MARS technique is expressed in the form shown in Equation 1, where α_i values are coefficients that can be considered weights that represent the “importance” of the variable, and BF_i is the basis function which explains the relation between the independent variable, indexed by i , and the dependent variable, $f(x)$.

$$f(x) = \alpha_0 BF_0 + \sum_{i=1}^n \alpha_i BF_i \quad \text{Equation 1.}$$

Three models were developed in this study, including a model for stopped (complete/rolling) drivers, a model for travelling through left turn drivers, and a model for travelling through straight crossing drivers. The predictor variables considered were dependent on the model being developed. The components of each model are discussed in the results section. Additionally, a discussion is provided on how these models will be used for reconstructing vehicle trajectories in the simulation case set to be developed in Chapter 6.

3.3 Results/Discussion

Dataset Summary

A total of 96,429 previously identified intersection traversal events were available. From these events, several inclusion criteria were used to select candidate cases. A summary of the excluded cases can be found in Table 2. The final dataset consisted of 41,479 intersection traversal events.

Table 2. Excluded Intersection Traversals

Reason for Exclusion	Number of Traversals Excluded
Case file empty or not provided	4,845
Invalid Brake Data	12,199
Invalid Speed Data	16,725
Event Occurred too near beginning or end of trip	2,125
Not Left Turning or Straight Crossing	9,711
GPS or Roadway Speed Limit Data Not Available	5,490
Stopped behind a lead vehicle	3,855
Total Excluded	61,504

A summary of the dataset composition used in this study can be found in Table 3. Traversal counts for complete stop and traveling through traversals are provided by turning behavior and traffic control device. As discussed later in the results, travelling through events at stop signs (a traffic violation) were excluded from this study's analyses due to their infrequency during normal driving.

Table 3. Case counts by stopping behavior, turning behavior, and traffic control device. The * was used to indicate traversal events that were excluded from this study's analyses.

Completely Stopped		Traffic Control Device	
		Signalized	Stop Sign
Turning Behavior	Left	1,938	46
	Straight	9,061	56
Rolling Stopped		Traffic Control Device	
		Signalized	Stop Sign
Turning Behavior	Left	261	119
	Straight	1,080	285
Travelling Through		Traffic Control Device	
		Signalized	Stop Sign
Turning Behavior	Left	1,132	0*
	Straight	27,493	8*

Complete and Rolling Stopped Drivers

Overview of Stopped Drivers

Prior to any model development or statistical analysis, each stopping movement category was broadly analyzed without controlling for turning behavior, traffic control device, speed limit, or driver characteristics in order to investigate the overall variability of driver kinematics. Figure 5 shows sequential boxplots of vehicle velocity as drivers are transitioning from a deceleration phase during the intersection approach to an acceleration phase during the intersection traversal.

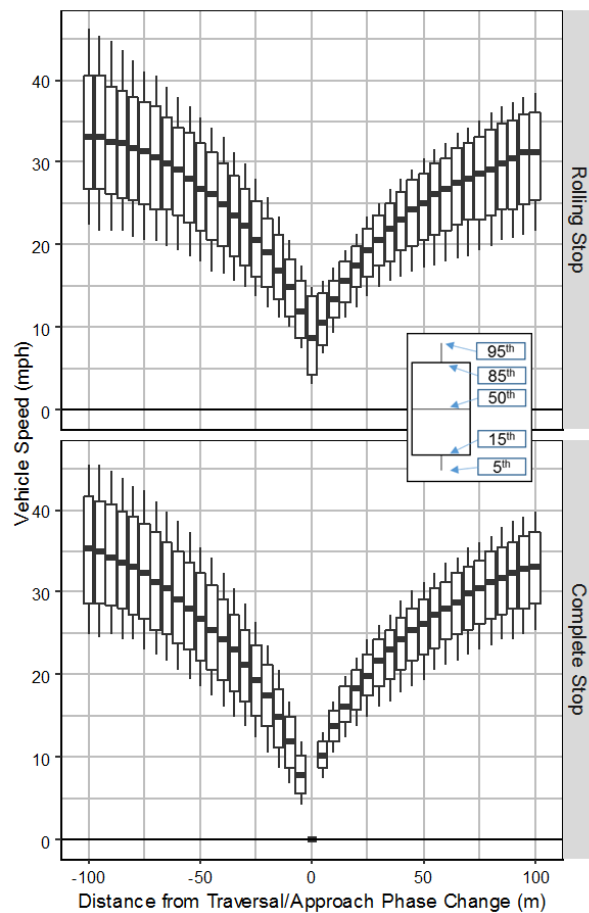


Figure 5. Box plots of vehicle speed versus distance from the beginning of the intersection traversal phase. Two pre-crash movements are shown, including rolling stopped and completely stopped. Every deceleration and acceleration phase were shifted in order to have the driver reach their minimum velocity at $d=0$.

There are several important trends that can be observed from these broad overview plots. First, there is considerable variability in vehicle speed at 75m before and after beginning the traversal phase for both the rolling and completely stopped drivers. At 75 m before beginning the intersection traversal, 95% of vehicle speed values fell between approximately 25 mph and 45 mph. At 75 m into the intersection traversal, 95% of speed values fell between approximately 20 mph and 35 mph. This result, in itself, provides motivation for attempting to limit variability by accounting for additional covariates.

A second notable observation that can be made is the speeds 75 m into the intersection traversal are, in general, higher than vehicle speeds 75 m before the beginning of the intersection traversal. This result suggests that, in general, acceleration rates during the intersection traversal phase may be a lower magnitude than deceleration rates during the intersection approach.

Statistical Analysis to Explore Factors Influencing Driver Behavior for Stopped Drivers

The influence of several predictor variables on vehicle kinematics metrics was explored using a mixed effects ANOVA. A full summary of the results from this analysis can be found in Table 4. The vehicle kinematics metrics included average traversal acceleration, maximum traversal acceleration, minimum velocity (rolling stopped vehicles only), average approach deceleration, and maximum approach deceleration. The predictor variables were stopping behavior (e.g., complete vs. rolling stop), turning behavior (straight vs. left turn), roadway speed limit, traffic control device (stop sign vs. signalized), driver age group, and driver gender. Two interaction effects were included, including an interaction between driver age and gender and an interaction between turning behavior and the traffic control device.

All of the predictor variables examined in this study were found to be significantly correlated with some aspect of intersection approach and traversal kinematics. The influence of each predictor variable is discussed independently in each of the following sections.

Table 4. A summary of the results from the statistical analysis on the influence of several potentially important predictor variables on driver approach and traversal kinematics. A * was used to indicate statistical significance ($p < 0.05$). A + was used to indicate when a variable was nearly significant ($0.05 > p > 0.10$).

Dependent Variable	Parameter Group	p-value
Average Approach Deceleration	Stopping Behavior	<0.001*
	Speed Limit	<0.001*
	Turning Behavior	0.068+
	Traffic Control Device	0.777
	Driver Age	0.434
	Driver Gender	0.738
	Turn x Traffic Control Device	0.469
	Age x Gender	0.102
Maximum Approach Deceleration	Stopping Behavior	<0.001*
	Speed Limit	<0.001*
	Turning Behavior	<0.001*
	Traffic Control Device	<0.001*
	Driver Age	0.073+
	Driver Gender	0.772
	Turn x Traffic Control Device	0.001 [†]
	Age x Gender	0.046*
Late Approach phase Elapsed Time: 30 m – to – Traversal start	Stopping Behavior	<0.001*
	Speed Limit	0.068+
	Turning Behavior	<0.001*
	Traffic Control Device	0.005*
	Driver Age	0.067 [†]
	Driver Gender	0.246
	Turn x Traffic Control Device	0.224
	Age x Gender	0.272
Minimum Speed	Stopping Behavior	--
	Speed Limit	0.733
	Turning Behavior	<0.001*
	Traffic Control Device	0.013*
	Driver Age	0.064 [†]
	Driver Gender	0.616
	Turn x Traffic Control Device	0.002*
	Age x Gender	0.802
Average Traversal Acceleration	Stopping Behavior	<0.001*
	Speed Limit	<0.001*
	Turning Behavior	0.235
	Traffic Control Device	0.006*
	Driver Age	0.003*
	Driver Gender	0.757
	Turn x Traffic Control Device	0.196
	Age x Gender	0.383
Maximum Traversal Acceleration	Stopping Behavior	<0.001*
	Speed Limit	<0.001*
	Turning Behavior	<0.001*
	Traffic Control Device	0.281
	Driver Age	0.209
	Driver Gender	0.834
	Turn x Traffic Control Device	<0.001*
	Age x Gender	0.535
Early Traversal phase Elapsed Time: Traversal start – to – 30 m	Stopping Behavior	<0.001*
	Speed Limit	<0.001*
	Turning Behavior	<0.001*
	Traffic Control Device	<0.001*
	Driver Age	0.338
	Driver Gender	0.873
	Turn x Traffic Control Device	0.520
	Age x Gender	0.556

How are vehicle kinematics influenced by whether the driver comes to a complete stop or rolling stop?

Whether a driver comes to a complete stop or a rolling stop prior to accelerating through the intersection will directly influence the available time for an I-ADAS to detect and respond to an imminent crash. Specifically, I-ADAS, in general, has a smaller time window if the driver does not come to rest prior to accelerating through the intersection. Accordingly, this stopping behavior is an important factor to consider when assessing the potential safety benefits of an I-ADAS system in the vehicle fleet. The mixed-effects ANOVA revealed stopping behavior to be correlated with every kinematics feature analyzed.

Differences were observed in the acceleration magnitudes of the two movement types. A summary of these differences in acceleration can be seen in Figure 6. During the deceleration phase, drivers that came to a complete stop tended to decelerate at higher magnitudes than drivers that came to rolling stops. Likewise for the acceleration phase, drivers tended to accelerate at higher magnitudes when they came to a complete stop. With regards to the deceleration phase, the rolling stopped drivers are likely coasting (no brake application) toward the end of the deceleration phase, which led to lower deceleration magnitudes. With regards to the acceleration phase, this finding may suggest that drivers tend to accelerate at higher rates while at lower speeds. This finding has been previously observed in studies analyzing both normal driving [124-128] and during the analysis of pre-crash data using EDR data presented in Chapter 4. These differences by stopping movements are further explored in the following sections.

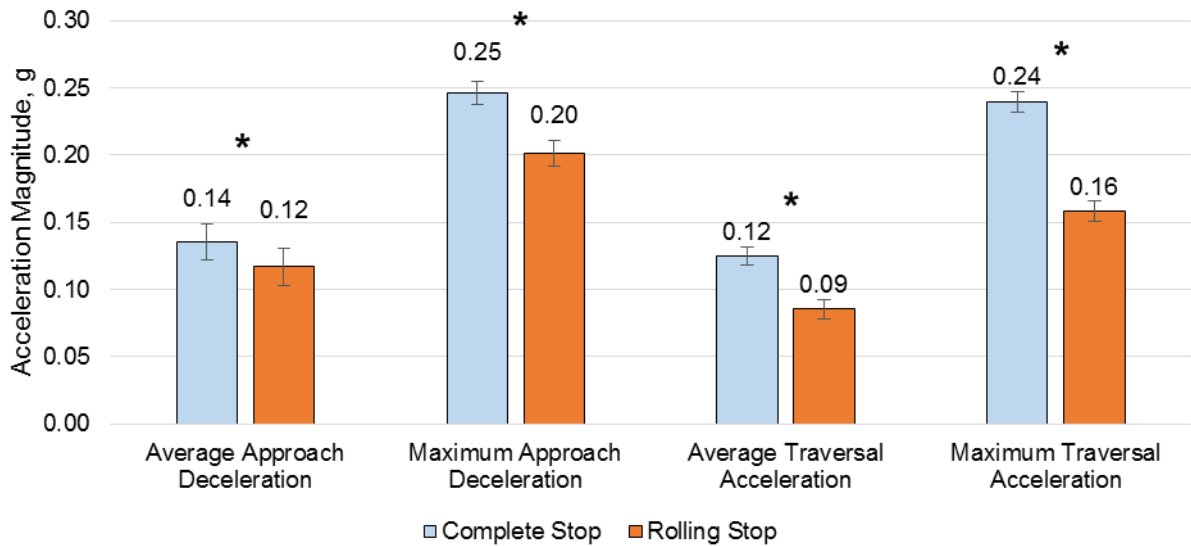


Figure 6. A summary of acceleration magnitudes during the intersection approach and traversal phase. The bars represent the 95% confident interval about the mean. A * was used to indicate significant differences ($p < 0.05$) between the two stopping categories. The graph depicts least squares means with confidence intervals that were generated from the mixed effects ANOVA.

Drivers that perform rolling stops traversed through the intersection much more quickly than drivers that came to a complete stop. During the late approach phase, it took completely stopped drivers an average of 7.1 s to travel the final 30 m compared to only 4.6 s for rolling stopped drivers. Likewise for the traversal phase, it takes a completely stopped driver an average of 5.7 s to travel 30 m from traversal start, whereas it take a rolling stopped driver only 5.1 s.

The difference in traversal time has important implications for I-ADAS. A typical reaction time for a driver in an cross traffic intersection crash is around 1.3 s [129]. Considering that a typical average evasive braking magnitude is around 0.5 g [130], 0.5 s of additional time for a driver to react to an impending crash would allow the vehicle to potentially be slowed by an additional 6 mph (10 kph).

How does the traffic control device influence vehicle kinematics?

Driving context differs greatly by whether the driver is approaching a stop sign-controlled intersection or a signalized intersection. Accordingly, there are key differences in driver behavior that are important not only when reconstructing vehicle kinematics but also for the design and implementation of I-ADAS.

Drivers in the United States are required by law to come to a complete stop when approaching a stop sign. However, drivers frequently fail to come to a complete stop. In fact, using our 100-car dataset, I found that four-fifths (79.8%) of drivers failed to come to a complete stop (defined as minimum velocity < 1.2 m/s) at stop signs. A summary of this stopping behavior can be seen in Figure 7. The median stopping speed was found to be 6.2 mph, and 95% of stopping speeds were below 16.2 mph. As previously stated, drivers that enter the intersection at higher speeds are expected to benefit less from an I-ADAS system.

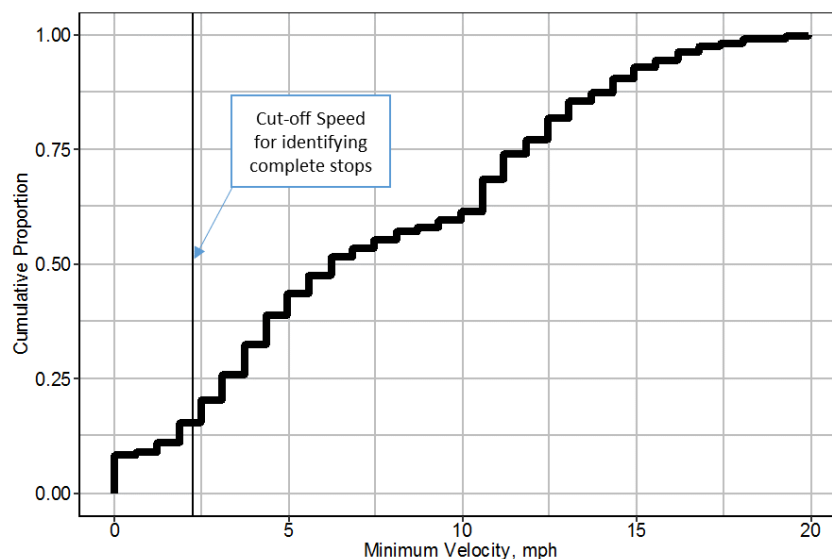


Figure 7. A cumulative distribution plot of minimum speeds for driver's that came to a complete stop at a stop sign-controlled intersection.

At signalized intersections, drivers are, of course, required to come to stop and wait during a red light. In the dataset examined in this study, 89.1% of drivers at signalized intersections came to a complete stop. Occasionally, drivers will experience a light phase change from red to green as they are slowing down for a traffic light. During these scenarios, rolling stops are observed. Rolling stops are also observed when drivers are slowing for stopped or slowed traffic. For these cases, drivers sometimes perform lane changes into a neighboring lane. In general, rolling stops are fairly rare in intersection crashes (2.0% of SCP crashes at signalized intersections in the simulation case set developed in Chapter 6). This study still seeks to model this behavior in order to ensure a comprehensive benefits model.

A key difference between stop sign-controlled and signalized intersections is the location where drivers begin their traversal (acceleration phase) into the intersection. Figure 8 depicts the variation in stopping location relative to the intersection entry location based on traffic control device. As previously stated, it is important to note that the intersection entry location was recorded differently for signalized and stop sign-controlled intersections. For signalized intersections, the location of intersection entry was indicated by the VTTI research team as the location where the traffic signal was last visible. For stop sign-controlled intersections, this location was indicated as the location where the stop bar was last visible. However, it can be easily deduced from the plot that there is substantially more variability in the traversal start location at signalized intersections. For drivers accelerating from a traffic light, the traversal start location for the middle 95% of drivers varied by 72.0 m. The median location for where drivers began accelerating was 41.0 m from the location where the traffic signal was last visible. The middle 95% of starting locations for drivers accelerating from a stop sign varied by 16.7 m. For stop sign-controlled traversal, the median location where drivers began accelerating was 0.2 m prior to where the stop bar was last visible.

Driving context can explain these differences. Drivers at stop signs do not begin accelerating until they have reached the intersection and had the chance to survey for oncoming vehicles. Conversely, a variety of factors influence the location where a driver at a signalized intersection may begin their acceleration traversal. For instance, drivers at signalized intersections frequently encounter queues. Additionally as previously stated, drivers may experience a light phase change that could lead to the driver transitioning from a deceleration phase to an acceleration phase prior to reaching the stop bar.

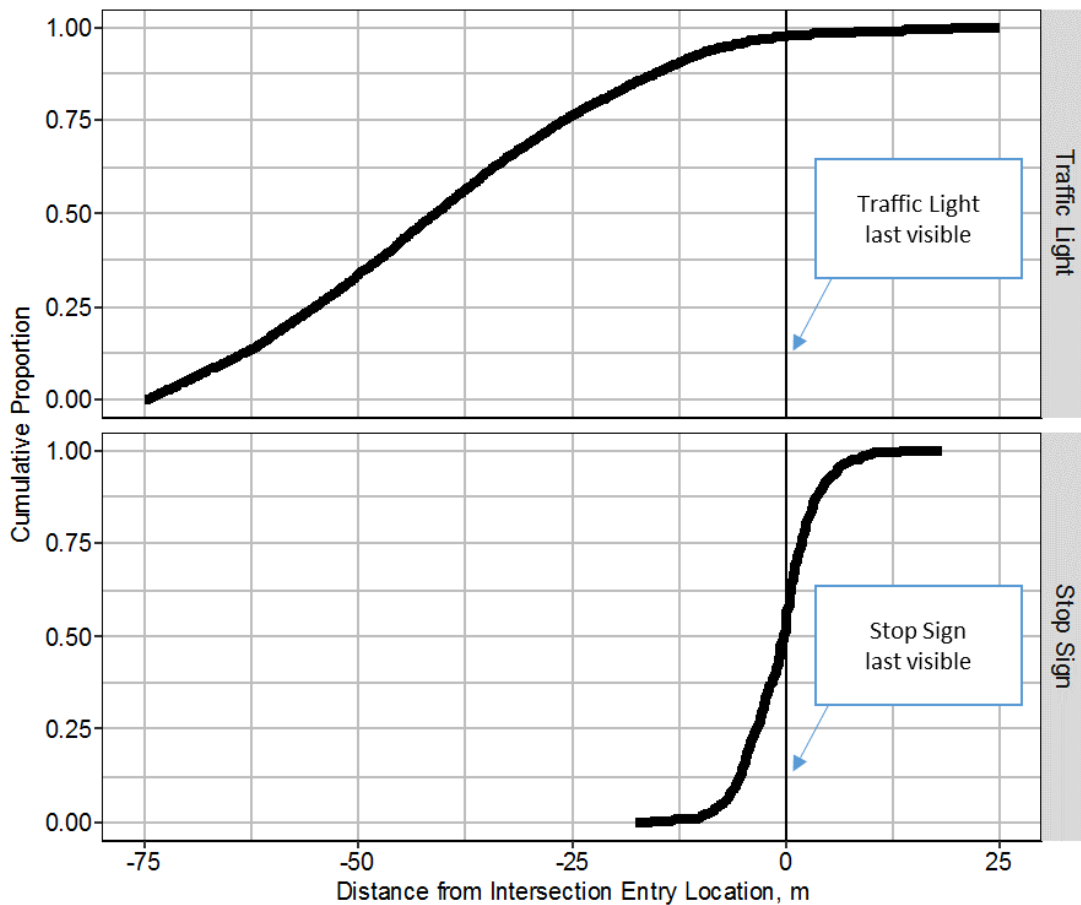


Figure 8. Cumulative distribution plots of the location where the driver began accelerating into the intersection relative to the point of intersection entry.

In addition to the aforementioned differences, the traffic control device type was found to be significantly correlated with maximum approach deceleration. Drivers approaching stop signs

(0.24 g) were found to have higher maximum deceleration magnitudes than drivers approaching traffic lights (0.21 g). No statistically significant differences were found for average traversal acceleration, maximum traversal acceleration, or average approach deceleration. The finding that maximum approach deceleration was influenced by traffic control device but not average approach deceleration is interesting, and suggests “shape” differences in the vehicle velocity time series between the two traffic control devices. For example, when drivers approach stop signs, there may be a period of higher vehicle decelerations as well as periods of lower deceleration, thereby offsetting one another.

This hypothesis was evaluated by examining approach and traversal kinematics by traffic control device and stopping movement, which can be seen in Figure 9. At traffic lights, the median vehicle speed 75 m from the intersection was 31.3 mph for rolling stopped drivers and 32.4 mph for completely stopped drivers. Likewise for stop signs, the median vehicle speed 75 m from the intersection was 31.8 mph for rolling stopped drivers and 30.5 mph for completely stopped drivers. Given that these drivers are at similar vehicle speeds at 75 m from the intersection, you would expect the average deceleration rates to be similar. However, the speeds at 30 m from the intersection differ more substantially. For traffic lights, the median speed for rolling stopped drivers was 21.3 mph and for completely stopped drivers was 21.2 mph. Conversely, for stop signs, the median speed for rolling stopped drivers was 24.3 mph and for completely stopped drivers was 23.6 mph. The higher speeds for stop signs at 30 m out during the intersection approach suggests that these drivers are decelerating at lower rates during the intersection approach phase followed by a period of higher deceleration toward the end of the approach phase.

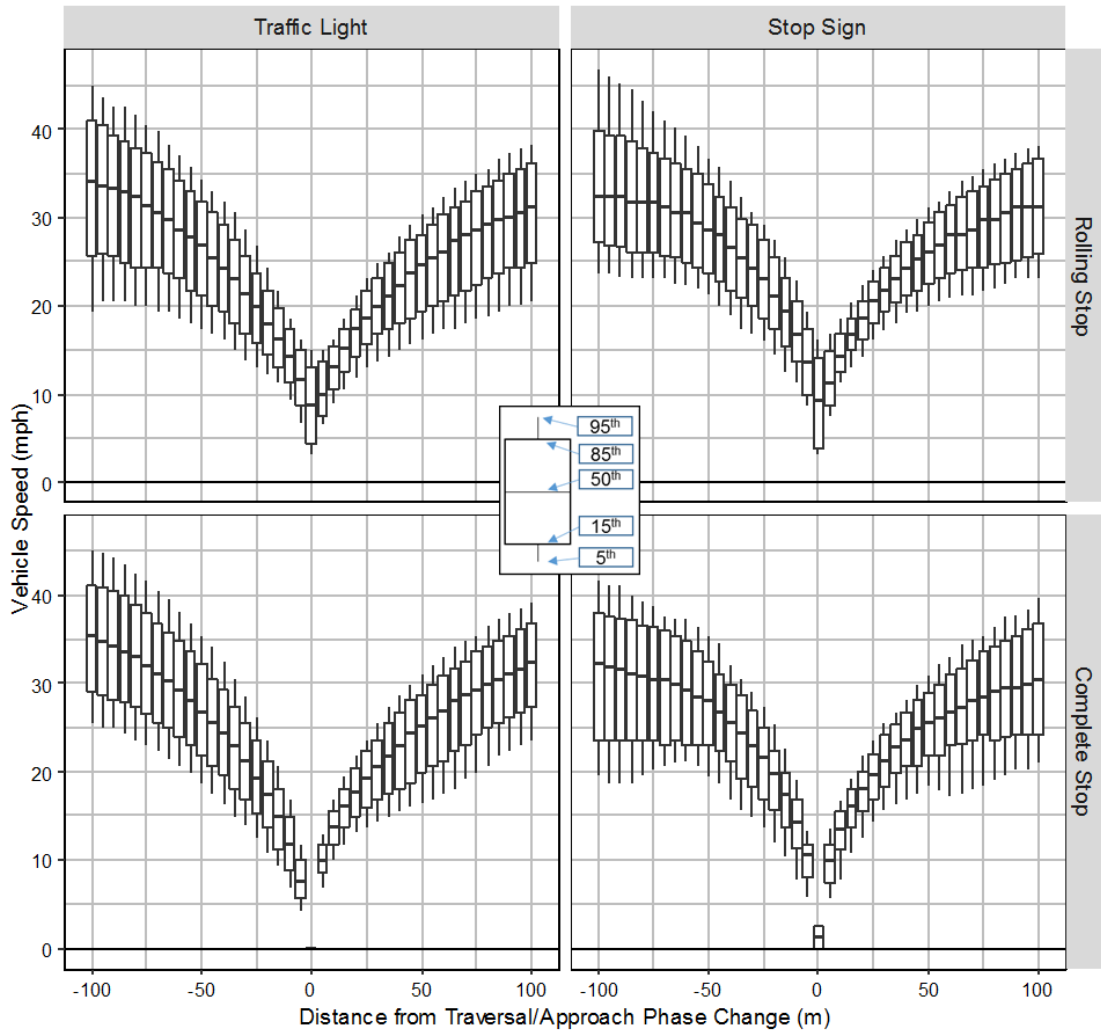


Figure 9. Approach and traversal kinematics by traffic control device and stopping behavior.

This finding can be explained by simply considering the driving context for drivers approaching each intersection type. At stop sign-controlled intersections, one motivation for having the approach velocity time series “shape” is that the driver will arrive at the intersection faster, and will therefore be able to proceed through the intersection in a shorter amount of time. However, at signalized intersections, there is little motivation for drivers to have a period of higher deceleration as the driver is required to stop and wait for the red light.

This is an important finding for the design and implementation of an active safety system that aims to stop drivers from inadvertently running through a stop sign. Although the vehicle speed change is less during the driver's early approach phase, it still typically begins at distances beyond 50 m from the intersection. Because of this, predictive models can be developed to differentiate between drivers that are aware and unaware of the stop sign. I explored this idea in Chapter 8.

In the following section, I further breakdown the analysis of traffic control device by also considering the turning behavior of the vehicle.

How does turning behavior affect approach and traversal kinematics?

This study examined both left turning and straight crossing behavior at intersections. Figure 10 shows vehicle kinematics for drivers as they approach and traverse intersections. Rolling stops were also compared with complete stops.

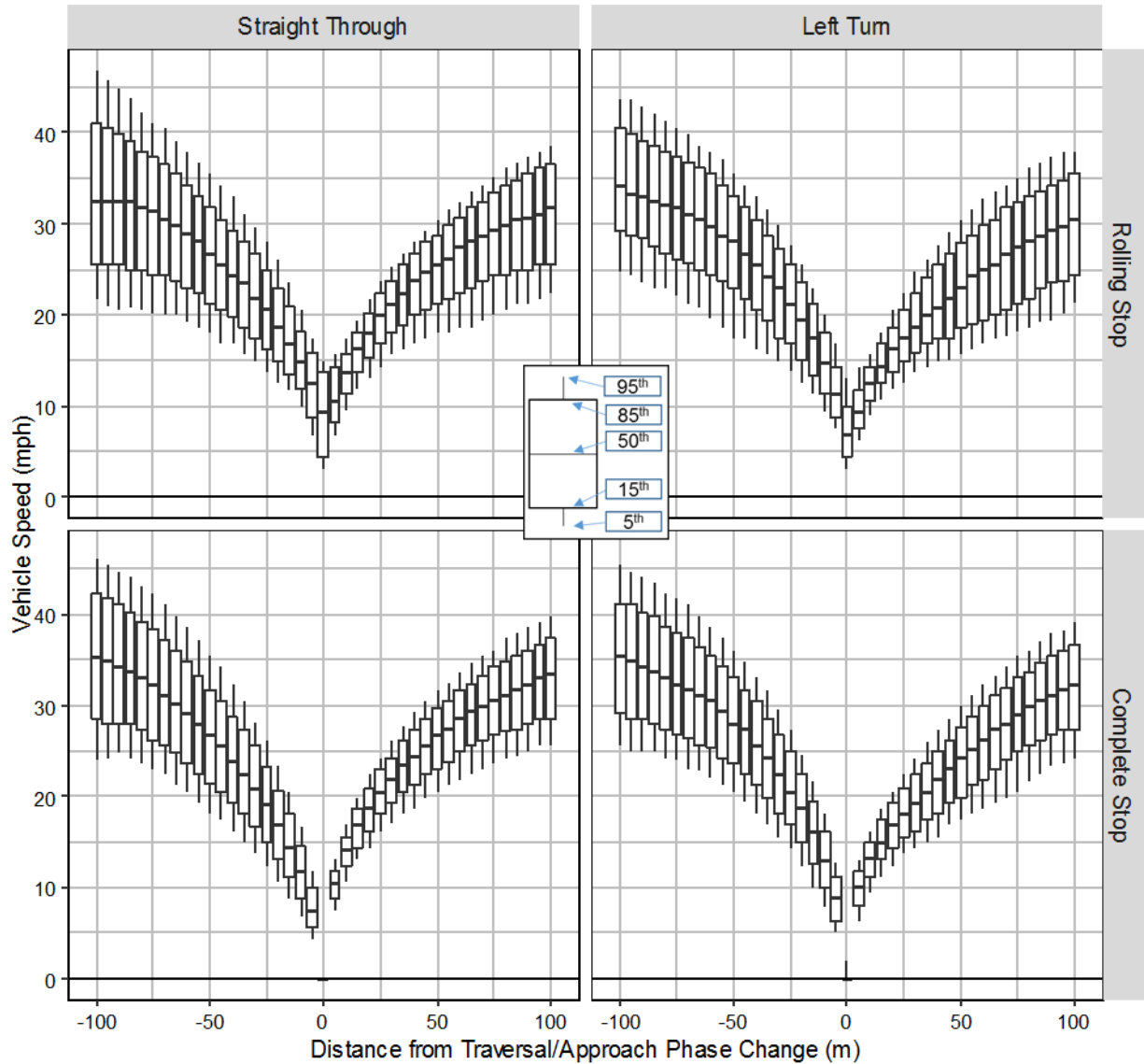


Figure 10. Approach and traversal vehicle kinematics by stopping behavior and turning behavior.

In general, left turning drivers were found to have a lower maximum traversal acceleration than straight crossing drivers. An interaction effect was also observed between turning behavior and

traffic control device for maximum traversal acceleration. A Tukey's Honest Significant difference (HSD) test was used to examine this interaction. Straight crossing drivers were only found to have a higher maximum traversal acceleration at signalized intersections. At stop signs, no difference in maximum traversal acceleration was observed between left turning and non-turning drivers. The generally higher maximum accelerations for straight crossing drivers has been observed in a prior study analyzing normal intersection traversal accelerations [131] and using the analysis presented in Chapter 4. Interestingly, Wang et al. [131] previously looked at intersection traversal accelerations after drivers came to complete stops at stop sign-controlled intersections. In their analysis using naturalistic data collected within the Atlanta urban area, they found that drivers tend on average to accelerate through the intersection at 0.13 g for straight crossing maneuvers and at 0.12 g for left turning maneuvers. These acceleration magnitudes are very similar to those observed in the current study for stop sign traversals (0.11 g for straight crossing and 0.12 g for left turns).

There were small differences in intersection approach kinematics between non-turning and left-turning vehicles. Average approach deceleration was found to be higher for straight crossing drivers (0.13 g) than for left turning drivers (0.12 g). For average approach deceleration, no interaction effect was found between turning behavior and the traffic control device. Turning behavior was found to have a nearly significant ($p=0.068$) effect on maximum vehicle deceleration. Drivers turning left (0.23 g) were found to have maximum decelerations that were very similar to straight crossing drivers (0.22 g). A significant interaction effect between turning behavior and traffic control device helped to better explain where the differences lie. The results from A Tukey's Honest Significant difference (HSD) test can be found in Table 5.

Table 5. Tabulations showing the results from the Tukey’s Post Hoc Analysis examining which levels of the traffic control device x turning intent interaction effect were statistically significant at predicting maximum vehicle deceleration. Factor levels that do not share a common letter were found to be different from one another.

		Traffic Control Device	
		Traffic Light	Stop Sign
Turning Intent	Straight Crossing	a	c
	Left Turning	b	c

For stop sign-controlled intersections, regardless of turning intent, drivers tend to come to rest or “roll” through the stop sign prior to accelerating into the intersection. There is no obvious reason to expect any differences in the approach kinematics for turning versus non-turning drivers. In fact, no statistical significant differences were observed in the stop sign approach kinematics between non-turning and left-turning drivers. The lack of statistical significance for stopping behavior at stop signs between turning groups indicates that, if any difference exists, they are likely very small. At signalized intersections, the maximum approach deceleration for non-turning drivers was found to be slightly less (by 0.02 g) than for left-turning drivers. This finding, although small, suggests differences in the signalized intersection approach kinematics between non-turning and left-turning drivers. In order to explain these differences, one must consider the different driving contexts for non-turning and left-turning drivers as they approach signalized intersections. Both non-turning drivers and left-turning drivers will perform rolling stops if they encounter a signal phase change or if they are required to slow for stopped or turning traffic. However, left-turning drivers can also perform left-turns if they are slowing to give the right away to a forward approach driver in a left turn across path opposite direction (LTAP/OD) scenario. Because this scenario is inherently different and only experienced by left turning drivers, it is unsurprising to

see small overall small differences between non-turning and left-turning vehicles approaching signalized intersections. This study was limited in the data available for determining an LTAP/OD scenario, but future work should look to explore this effect.

How does roadway speed limit affect intersection approach and traversal kinematics for stopped vehicles?

Speed limit was found to be significantly correlated with average approach deceleration, maximum approach deceleration, maximum traversal acceleration, average traversal acceleration, and the elapsed time for the first 30 m of the intersection traversal. No statistical significance was found for the effect on the elapsed time from 30 m into the approach until the traversal start time point. Signalized intersection approach and traversal speed profiles are shown in Figure 11. The graphic shows the dependence turning behavior, stopping behavior and speed limit on vehicle speeds for signalized intersections only.

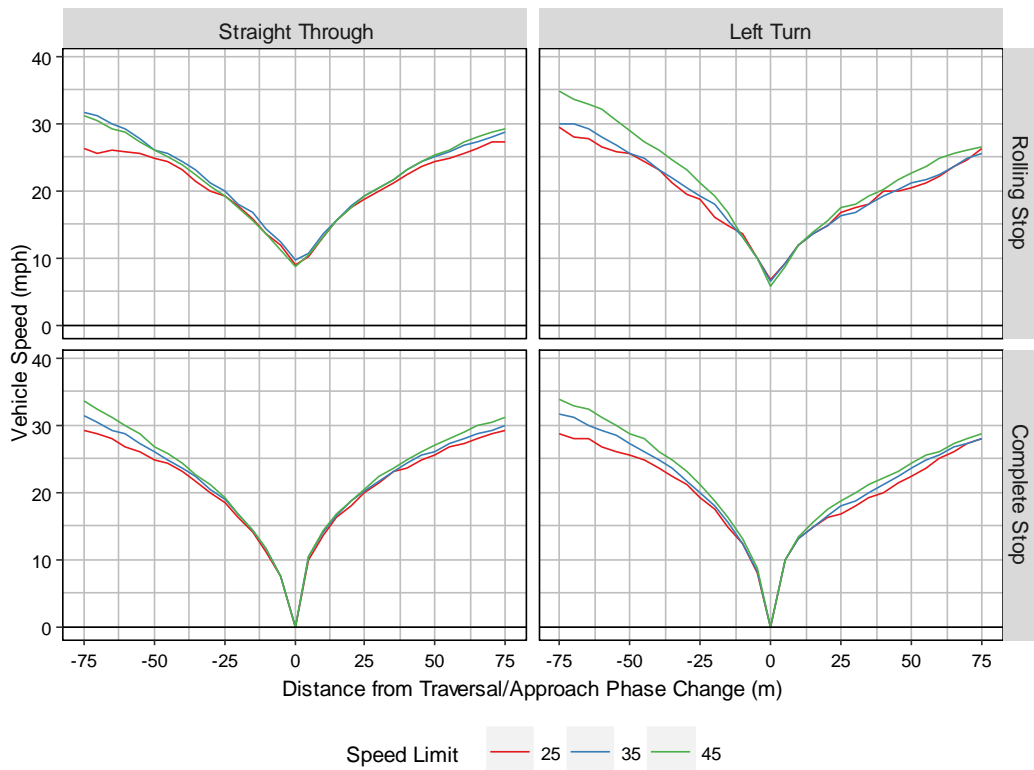


Figure 11. Median (50th percentile) intersection approach and traversal kinematics by turning behavior, stopping behavior, and speed limit. Only signalized intersection approaches are shown in this graphic.

The first important feature of the graphs to notice is that vehicle speeds during the approach begin to converge around 30 m prior to traversal start. The convergence would lead to little difference in the elapsed time during the final 30 m of the intersection approach, which explains the lack of significance in the statistical test.

Drivers on roads with higher speed limits tend to have higher approach and traversal speeds, which corresponded to higher maximum traversal acceleration values, higher maximum approach deceleration values, higher average approach decelerations, and higher average traversal acceleration values. Visually, the effect of speed limit appears to be most pronounced during the intersection approach phase. The mixed effects models predict that a 10 mph change in speed limit correlates approximately to a 0.007 g increase in maximum vehicle deceleration and a 0.008 g increase in average vehicle deceleration. The effect of starting approach speed on deceleration vehicle kinematics has been reported in a previous study analyzing intersection approaches at stop signs in the Atlanta metropolitan area [128]. Similar to the results of this study, they observed differences in vehicle kinematics during the early approach phase with the speed profiles converging during the later approach phase. However, their statistical analysis of average and maximum approach decelerations revealed an inconsistent dependency on speed limit. It should be noted that their study used only 428 deceleration events, whereas the current study uses nearly 45,000. It is possible that their dataset was too small to conclusively detect differences in approach kinematics.

Overall, the effect of speed limit on traversal acceleration kinematics appeared to be relatively small. The mixed effects models predict that a 10 mph change in speed limit corresponds to a 0.005 g increase in average traversal acceleration, a 0.005 g increase in maximum traversal acceleration, and 0.06 s less time to travel 30 m. Accordingly, the implications of higher speed

limits for I-ADAS appear to be small. Less than one-tenth of a second is relatively small when considering that a typical reaction time for a driver in an cross-traffic crash scenario is over one-second [129].

How do driver age and gender influence approach and traversal kinematics for stopped vehicles?

Driver age and gender were both investigated in this study. Driver gender, by itself, was not found to be significantly correlated with any kinematics feature. However, several interaction effects between driver gender and age were found to be significant. Driver age was found to significantly influence average traversal acceleration, and was found to be nearly significant in influencing the elapsed time during the late approach phase, maximum approach deceleration, and minimum rolling stop speed.

With regards to intersection approach kinematics, small, nearly-significant statistical differences were observed. The most pronounced effect was the effect of maximum approach deceleration, where an interaction effect between age and gender was also observed. For women, no effect of age was observed. For men, younger drivers were found to have a (0.05 g) higher maximum approach deceleration than senior drivers.

The effect of age was found to be significantly correlated with average traversal acceleration. This effect, however, was minimal. Senior drivers (0.09 g) were found to have an average traversal deceleration that was significantly lower than young (0.11 g) and adult (0.11 g) drivers. These results suggest that senior drivers tend to accelerate less aggressively than the younger population. This finding is consistent with several prior studies analyzing the relationship between driver age and driving aggressiveness [109, 132-134]. These prior studies have found a relationship between age and a number of aggressiveness-related factors, including crash history, risk-taking, and driver comfort levels.

MARS Models of Intersection Approach and Traversal Kinematics for stopped drivers

MARS models were generated for both the intersection approach and traversal phase. The independent variables used were distance from the beginning of the traversal acceleration into the intersection, stopping behavior, turning behavior, traffic control device, driver age, driver gender, and speed limit. Vehicle speed was used as a dependent variable. The approach and traversal phases were modeled separately due to the fact that speed limit before and after the intersection could be different from one another. In particular, this is expected to occur often for left turning drivers. Generating one full traversal model and including speed limit before and after the intersection was considered. However, this approach would have led to collinearity issues in the model.

The approach and traversal models for stopped vehicles can be found in the Appendix. MARS models are essentially the summation of a series of piecewise “Basis” functions, where each function is influenced by separate predictor variables. For the approach and traversal models respectively, Table 6 and Table 7 list the different combinations of predictor variables included in each model and the number of Basis functions using these combinations of predictor variables. As previously stated, the inclusion of a given combination of variables implies that the parameters improved the model fit.

Table 6. A list of the different predictor variable combinations used in this study for the approach phase model of drivers that came to a complete stop.

Combination #	List of variables	Basis Functions using this combination
0	Intercept	1
1	Distance from phase change	3
2	Turning Behavior	1
3	Age Group = Young	1
4	Distance from phase change Stopping Behavior	1
5	Distance from phase change Speed Limit	4
6	Distance from phase change Age Group = Senior	1
7	Turning Behavior Traffic Control Device	1
Final Count of Basis Functions		13

Table 7. A list of the different predictor variable combinations used in this study for the traversal phase model of drivers that came to a complete stop.

Combination #	List of variables	Basis Functions using this combination
0	Intercept	1
1	Distance from phase change	4
2	Turning Behavior	1
3	Driver Age = Young	1
4	Distance from phase change Stopping Behavior	1
5	Distance from phase change Speed limit	2
6	Distance from phase change Driver Age = Senior	1
7	Distance from phase change Stopping Behavior Speed Limit	1
8	Distance from phase change Traffic Control Device Speed Limit	1
Final Count of Basis Functions		13

Example approach and traversal trajectories can be found in Figure 12 and Figure 13, respectively. The approach model developed in this study will be used to develop the simulation case sets discussed in Chapter 6. This approach phase model will be “stitched” together with the acceleration profile model developed from EDR pre-crash data, which is described in Chapter 4. The location where distance is 0 (minimum speed location) will be used as the initial conditions for the acceleration profile model.

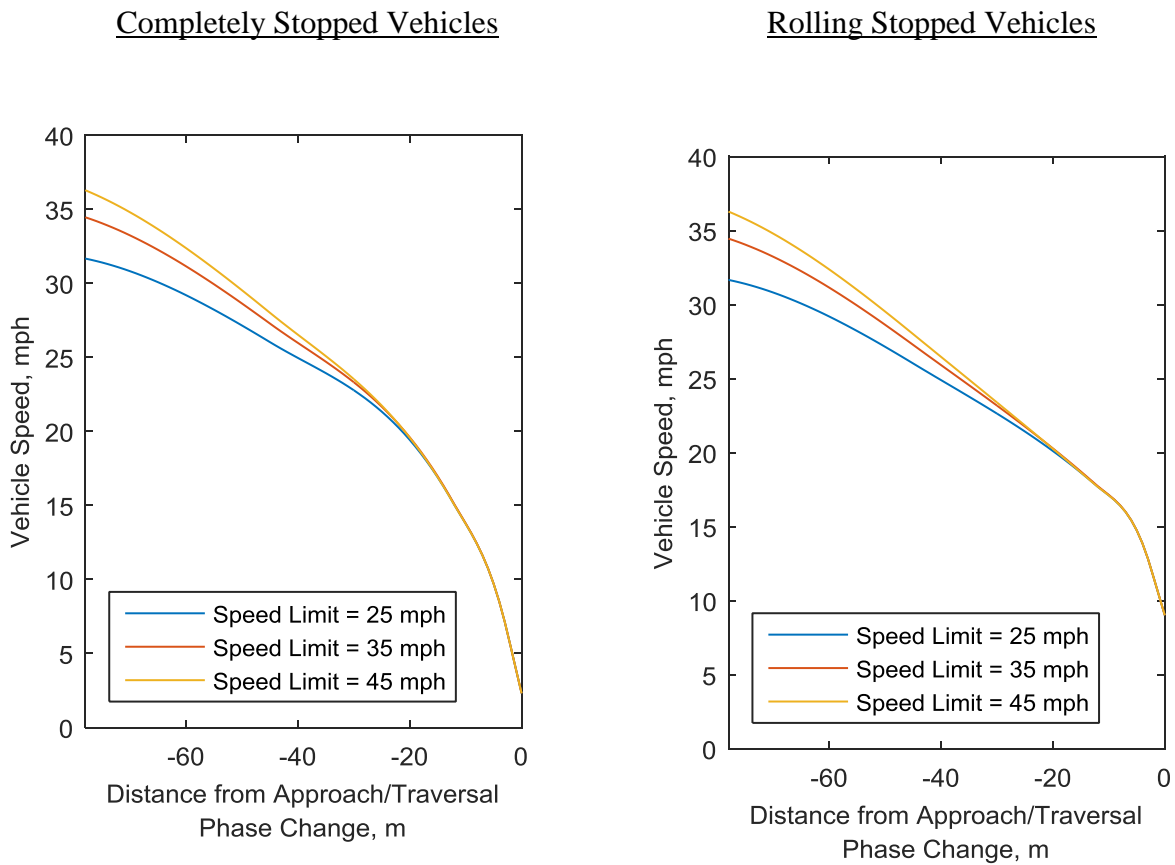
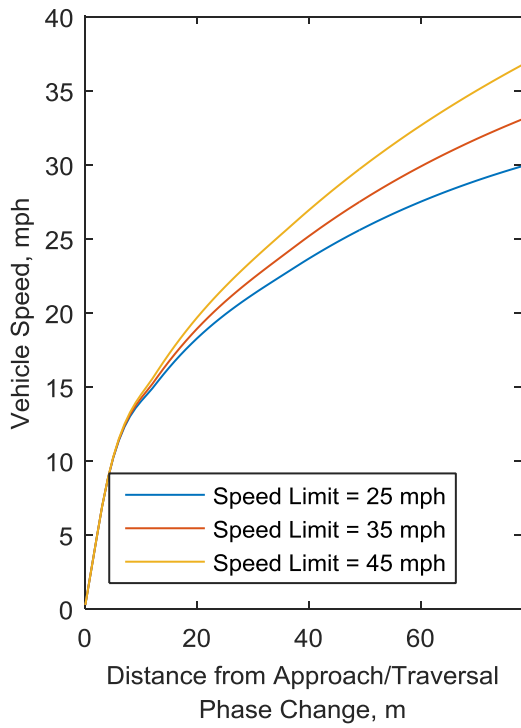


Figure 12. Example approach kinematics models generated for stopped vehicles. Several variations of this model are shown by speed limit and stopping behavior. The driver was assumed to be non-turning, not young or senior, a male, and approaching a stop sign controlled intersection.

Completely Stopped Vehicles



Rolling Stopped Vehicles

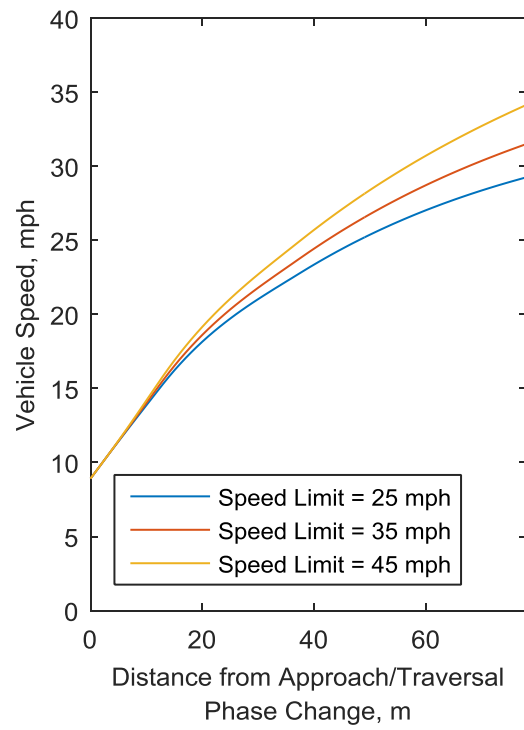


Figure 13. Example Traversal kinematics model outputs generated for stopped vehicles. Several variations of this model are shown by speed limit and stopping behavior. The driver was assumed to be non-turning, not young or senior, a male, and traversing through a stop sign controlled intersection.

Travelling Through Vehicles

As previously stated, our approach for the travelling through analysis was to only focus on signalized intersections. In general, it is very rare for a driver to travel through a stop sign-controlled intersection without yielding. In fact, less than 2% (8 total events) of the stop sign events analyzed in this study involved a travelling through vehicle.

How does turning behavior affect approach and traversal kinematics for travelling through drivers?

This study analyzed left turning and non-turning vehicles independently from one another. Driver behavior is inherently different between non-turning and left-turning for travelling through drivers. Figure 14 provides a clear illustration of these differences. For straight crossing drivers, drivers largely maintain a constant speed as the approach and traverse the intersection. Some drivers accelerate as they are approaching the intersection, which may be at least partially attributed to their trying to “beat the yellow” signal phase change [116]. On the contrary, left turning drivers have a tendency to slow as they approach the intersection in order to safely execute the left turn. This left turning behavior has been reported in several previous studies [116-118]. These left turning drivers additionally maintain a relatively constant speed as they are executing their left turn (assumed to occur around $d=0$, or the location where the traffic signal was last visible).

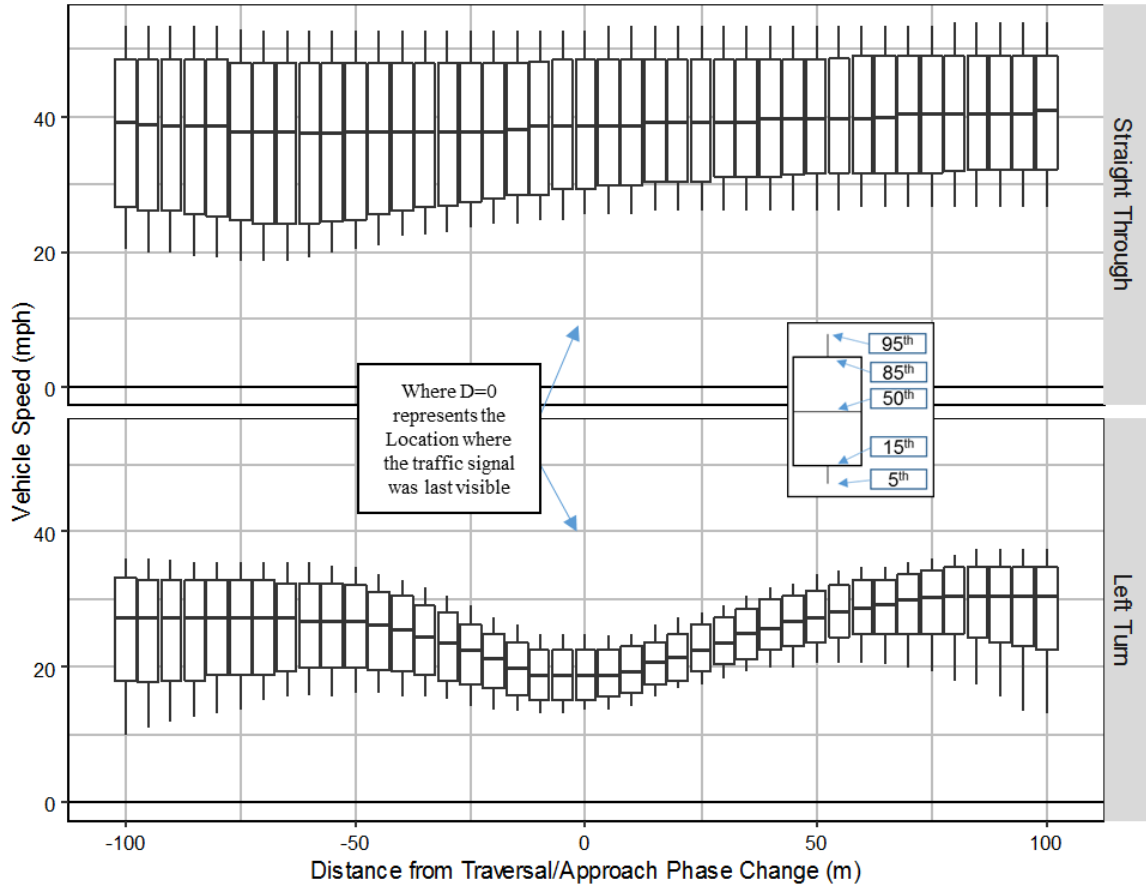


Figure 14. Intersection approach and traversal kinematics for travelling through drivers at signalized intersection. The graphs are separated by turning behavior. The location where distance = 0 represents the location where the traffic signal was last visible.

Statistical Analysis to Explore Factors Influencing Driver Behavior for Travelling Through Drivers

The influence of several predictor variables on vehicle kinematics metrics was explored using a mixed effects ANOVA. Non-turning and left-turning drivers were examined independently because of the inherent differences between the groups. A full summary of the results from this analysis can be found in Table 8. The vehicle kinematics metrics included the elapsed time during the final 30 m of the intersection approach phase, vehicle speed at traversal start, and the elapsed time during the first 30 m of the intersection traversal phase. The predictor variables were roadway speed limit, driver age group, and driver gender. An interaction effect for driver age and gender was also included in the model.

Each of the predictor variables with the exception of driver gender were found to be significantly correlated with some aspect of intersection approach and traversal kinematics for travelling through drivers. The influence of each predictor variable is discussed independently in each of the following sections.

Table 8. A summary of the results from the statistical analysis on the influence of several potentially important predictor variables on driver approach and traversal kinematics. A * was used to indicate statistical significance ($p < 0.05$). A + was used to indicate when a variable was nearly significant ($0.10 > p > 0.05$).

Turning Behavior	Dependent Variable	Parameter Group	p-value
Straight Crossing	Elapsed time during final 30 m of intersection approach	Speed Limit	<0.001*
		Driver Age	0.001*
		Driver Gender	0.934
		Age x Gender	0.756
	Speed at Traversal Start	Speed Limit	<0.001*
		Driver Age	<0.001*
		Driver Gender	0.924
		Age x Gender	0.963
	Elapsed time during first 30 m of intersection traversal	Speed Limit	<0.001*
		Driver Age	<0.001*
		Driver Gender	0.980
		Age x Gender	0.917
Left Turning	Elapsed time during final 30 m of intersection approach	Speed Limit	0.318
		Driver Age	0.234
		Driver Gender	0.968
		Age x Gender	0.538
	Speed at Traversal Start	Speed Limit	0.268
		Driver Age	0.136
		Driver Gender	0.588
		Age x Gender	0.751
	Elapsed time during first 30 m of intersection traversal	Speed Limit	<0.001*
		Driver Age	0.3221
		Driver Gender	0.135
		Age x Gender	0.190

How does roadway speed limit affect intersection approach and traversal kinematics for travelling through vehicles?

Speed limit was found to influence both intersection approach and traversal kinematics for travelling through vehicles. For straight crossing drivers, the model predicts that a 10 mph increase in speed limit correlates to drivers entering into the intersection at speeds 3.6 mph (5.8 kph) higher. Higher speed limits were also correlated with less time in the approach and traversal phase, which is simply due to the vehicles travelling faster. For left turning drivers, the effect of speed limit was only significant in influencing the elapsed time during the early traversal phase. Median traversal trajectories are shown Figure 15 for various speed limits.

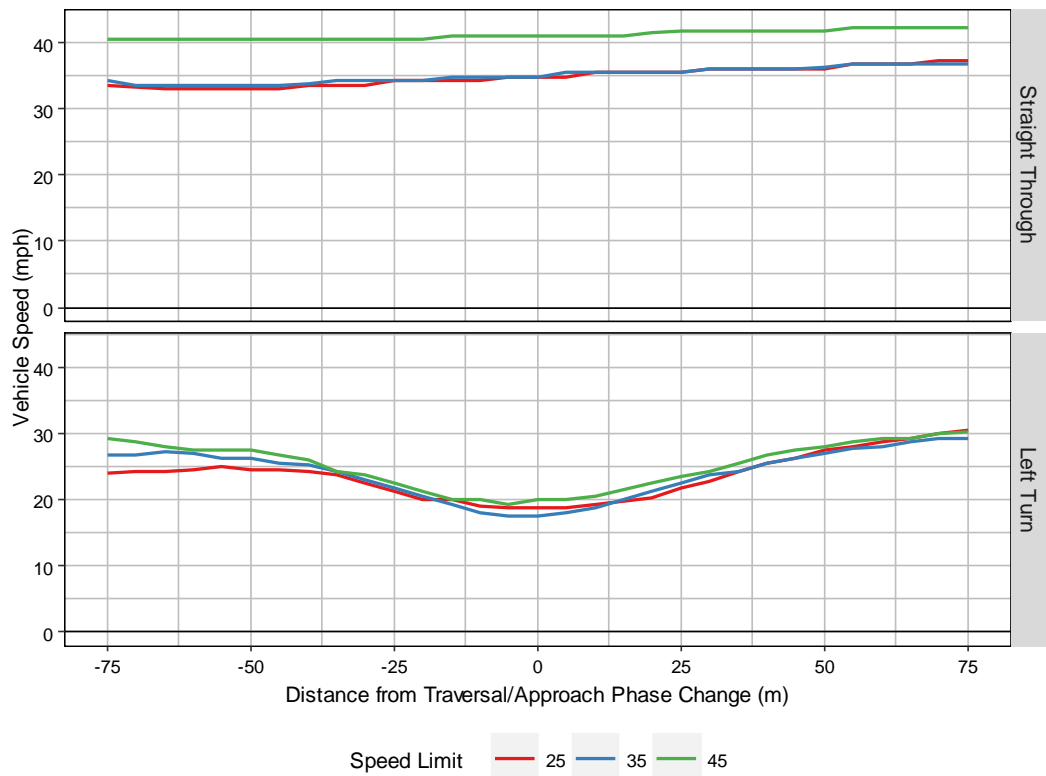


Figure 15. Median traversal kinematics by speed limit for non-turning and left-turning drivers approaching signalized intersections.

The effect of speed limit on traversal kinematics for left turning drivers was expected to be present but relatively small. The median trajectories shown in Figure 15 show a large jump in speeds from a 25-mph speed limit to a 35-mph speed limit, and a lesser difference from 35-mph to 45-mph. For left turns, drivers must restrict their speed in order to safely perform the turning without losing control of the vehicle. Higher speed limits are expected to be associated with larger intersections. Larger intersections imply larger turning radii, so drivers should be able to maintain higher speeds when traversing these intersection.

How do driver age and gender influence approach and traversal kinematics for travelling through vehicles?

Similar to the stopped vehicle kinematics, driver age was found to influence vehicle kinematics. However, differences were only observed between driver age groups during the intersection approach phase for straight crossing drivers. No effect of driver gender was observed.

A clear dependency of driver age on travelling through kinematics was seen for the straight crossing drivers. Senior drivers (1.97 s) were found to have significantly longer elapsed time during the final 30 m of the intersection approach than both adult (1.85 s) and young (1.79 s) drivers. Likewise for the elapsed time during the first 30 m of the traversal phase, senior drivers (1.91 s) had significantly longer early (first 30 m) traversal phase than adult (1.81 s) and young (1.74 s) drivers. Senior drivers (36.7 mph) also entered the intersection at slower speeds than adult (39.0 mph) and young (40.7 mph) drivers.

In general, senior drivers were found to be more conservative than the younger and adult driver groups. These results suggest that accounting for driver age is an important factor to consider when reconstructing intersection crashes for the simulation case set to be used for benefits estimates. Additionally, this finding suggests that driver age is an important factor to consider if I-ADAS designers are considering tailored systems for specific drivers.

MARS Models of Intersection Approach and Traversal Kinematics for stopped drivers

Two types of MARS models were generated for travelling through drivers in this study. The first looked to model the relationship between vehicle location and vehicle velocity. This was done for the approach and traversal phase for straight crossing and left turning drivers (i.e., four separate models). The second modeled vehicle acceleration versus vehicle location. This modeling strategy was only implemented for the approach phase of left turning drivers. This model will be used for modeling the approach phase of left turning drivers in the simulation case set discussed in Chapter 6. This is the only model that will be used in the benefits study, and the motivation for this technique is discussed in the later paragraphs.

The first model type aimed to generate a relationship between vehicle position relative to the intersection and vehicle velocity. The independent variables used were distance from phase transition, speed limit, driver gender, and driver age. Vehicle speed was used as a dependent variable. The approach and traversal phase were modeled separately due to the fact that speed limit could change from the approach phase to the traversal phase. In particular, this is expected to occur often for left turning drivers. Generating one full traversal model and including speed limit before and after the intersection was considered. However, this approach would have led to collinearity issues in the model.

All four models using the velocity versus position relation can be found in the appendix (Chapter 0) A summary of the basis functions used for each model can be found in Table 9, Table 10, Table 11, and Table 12 with model examples shown in Figure 16, Figure 17, Figure 18, and Figure 19.

Dependencies observed from the mixed effects ANOVA statistical model analysis are additionally present in our MARS model. Interestingly, although small, a driver gender effect was present in almost every model. The inclusion of driver gender in the model is likely due to the fact that the MARS model does not account for repeated measures.

Approach Phase – Non-Turning Drivers

Table 9. A list of the different predictor variable combinations used in this study for the approach phase model of non-turning drivers that travelled straight through the intersection.

Combination #	List of variables	Basis Functions using this combination
0	Intercept	1
1	Distance from phase change	2
2	Speed Limit	6
3	Driver Age = Young	1
4	Driver Age = Senior	1
5	Driver Age = Senior Driver Gender	1
7	Speed Limit Driver Age = Senior Driver Gender	1
Final Count of Basis Functions		13

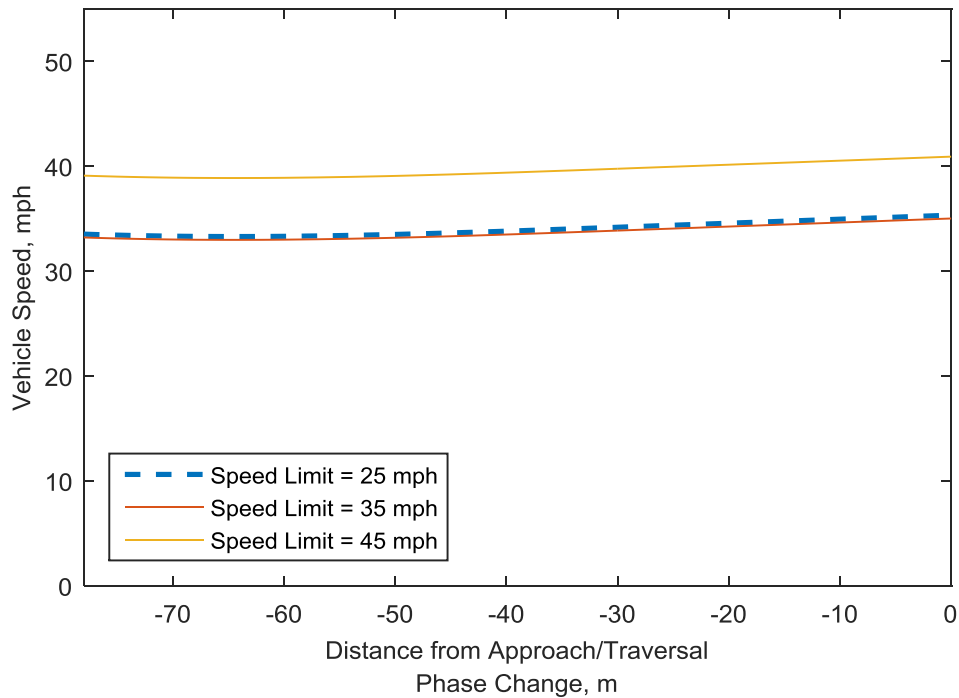


Figure 16. Example trajectories of the approach phase for non-turning drivers travelling through an intersection. Trajectories are for an adult male.

Traversal Phase – Non-Turning Drivers

Table 10. A list of the different predictor variable combinations used in this study for the approach phase model of non-turning drivers that travelled straight through the intersection.

Combination #	List of variables	Basis Functions using this combination
0	Intercept	1
1	Distance from phase change	2
2	Speed Limit	6
3	Driver Age = Young	1
4	Driver Age = Senior	1
5	Distance from phase change Speed Limit	2
6	Speed Limit Driver Age = Senior	2
Final Count of Basis Functions		15

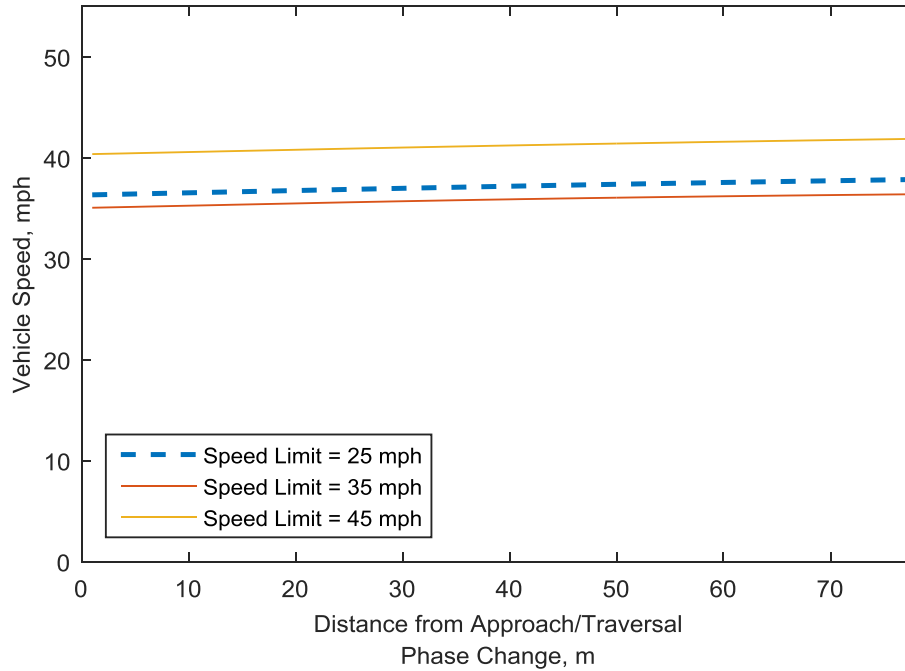


Figure 17. Example trajectories of the traversal phase for non-turning drivers travelling through an intersection. Trajectories are for an adult male.

Approach Phase – Left-Turning Drivers

Table 11. A list of the different predictor variable combinations used in this study for the approach phase model of left-turning drivers that travelled through the intersection.

Combination #	List of variables	Basis Functions using this combination
0	Intercept	1
1	Distance from phase change	3
2	Speed Limit	1
3	Driver Age = Senior	1
4	Distance from phase change Speed Limit	4
5	Speed Limit Diver Age = Young	2
6	Distance from phase change Speed Limit Driver Age = Young	1
Final Count of Basis Functions		13

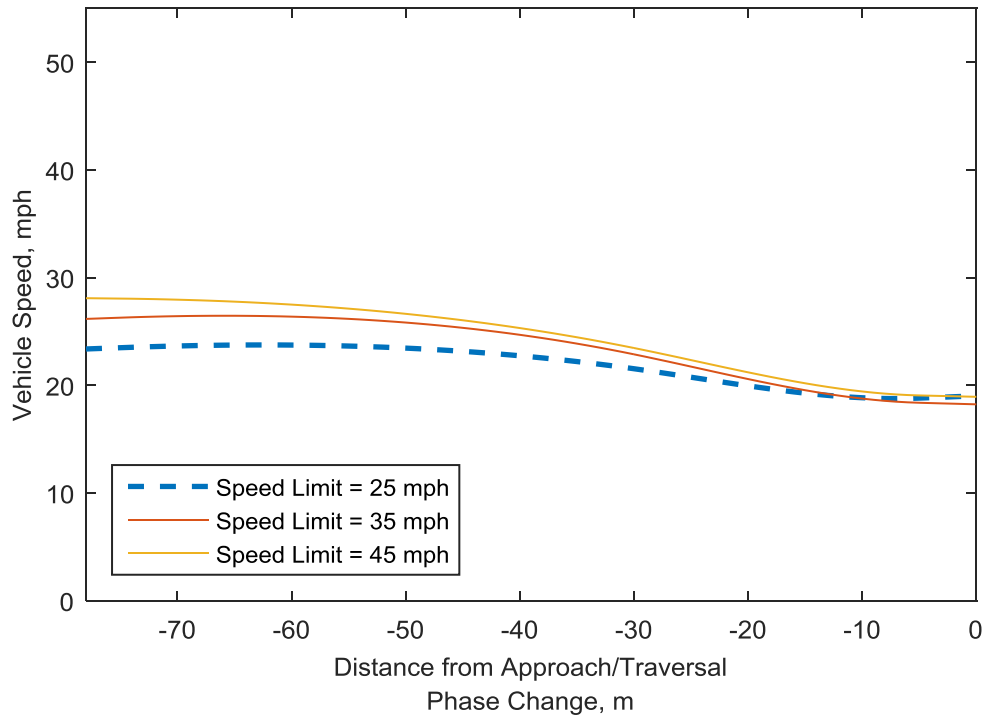


Figure 18. Example trajectories of the approach phase for left-turning drivers travelling through an intersection. Trajectories are for an adult male.

Traversal Phase – Left-Turning Drivers

Table 12. A list of the different predictor variable combinations used in this study for the approach phase model of non-turning drivers that travelled straight through the intersection.

Combination #	List of variables	Basis Functions using this combination
0	Intercept	1
1	Distance from phase change	2
2	Speed Limit	2
3	Driver Age = Young	1
4	Distance from phase change Speed Limit	4
5	Distance from phase change Driver Gender	1
6	Speed Limit Driver Age = Young	3
7	Driver Age = Young Driver Gender	1
8	Distance from phase change Driver Age = Young Driver Gender	2
Final Count of Basis Functions		17

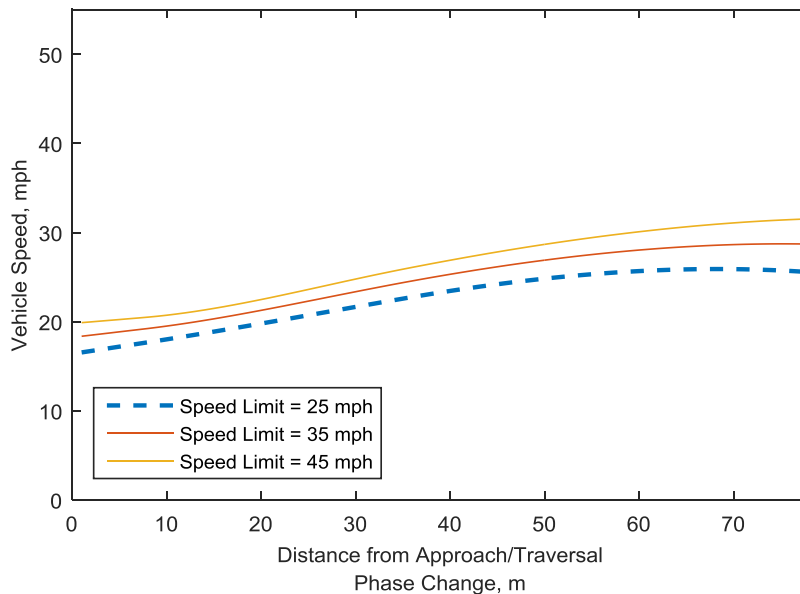


Figure 19. Example trajectories of the traversal phase for left-turning drivers travelling through an intersection. Trajectories are for an adult male.

The final model being developed was an acceleration versus distance relationship for the approach phase of the left turn model. This is the only model to be used for the benefits simulation case set. It should be noted that this travelling through, left-turn model at signalized intersections will also be used for reconstructing travelling-through, left-turn behavior at stop sign-controlled intersections (i.e. drivers that have a stop sign or no TCD on their intersection approach). This is proposed for two reasons. First, drivers taking left-turns with a stop sign very rarely fail to perform a complete or rolling stop during both normal driver and prior to real-world crashes. This was observed during a manual review of the crash investigator narratives for drivers in left turn across path lateral direction (LTAP/LD) and opposite direction (LTAP/OD) crashes, which is presented in the benefits study. This was also observed during the analysis of EDR records from left turning drivers in LTAP/LD and LTAP/OD crashes, which is also presented later in the manuscript. Second, the 100-car dataset of intersection traversals does not include left-turning behavior for drivers without a traffic control device on their intersection approach (e.g. for drivers at two-way stop sign controlled intersections).

Table 13. A list of the different predictor variable combinations used in this study for the approach phase model left-turning drivers that travelled through the intersection. This model uses an acceleration versus distance relationship.

Combination #	List of variables	Basis Functions using this combination
0	Intercept	1
1	Distance from phase change	2
2	Entry Speed	2
3	Speed Limit	2
4	Driver Age = Senior	1
5	Distance from phase change Entry Speed	4
6	Distance from phase change Speed Limit	1
7	Entry Speed Speed Limit	2
7	Distance from phase change Entry Speed Speed Limit	2
8	Distance from phase change Speed Limit Driver Age = Senior	1
Final Count of Basis Functions		18

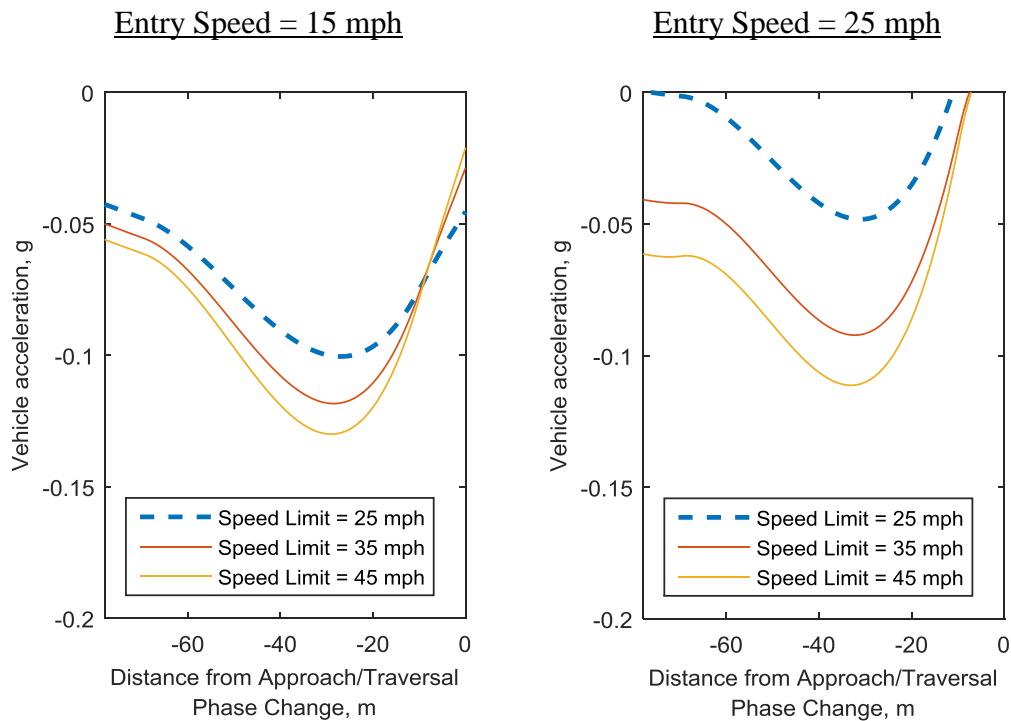


Figure 20. Example trajectories (acceleration versus distance) of the approach phase for left-turning drivers travelling through an intersection. Trajectories are for an adult male.

3.4 *Limitations*

There are several main limitations of this study that should be discussed. First, the dataset of intersection traversals used in this study were all performed in the northern Virginia / Washington, D.C. areas. The results from this study may not be representative of the entire U.S. population. Second, a limited number of predictor variables were considered in this study. Accounting for other variables, such as vehicle type, roadway conditions, and intersection characteristics, may help to limit driver variability. Third, the dataset used in this study is comprised of mainly traffic light intersection traversals. Even though traffic control device was used as a covariate, the model may still have some bias towards signalized intersections. Fourth, there can be considerable error in the recorded GPS position. This error, especially in areas concentrated with roadways, could have led to incorrect speed limits being assigned to a given traversal.

3.5 *Conclusions*

The main objectives of this study were to (a) determine factors influencing intersection traversal kinematics and (b) to develop driver models that can be used in future benefits studies. A number of potential predictor variables were considered in this study, including stopping behavior, turning behavior, traffic control device type, speed limit, driver age, and driver gender. Every one of these variables were found to have some influence on the kinematics features of intersection approach and traversal trajectories during normal driving. Using these dependencies, several approach and traversal models were developed using a MARS modeling technique. Several of these regression models will be directly used for benefits estimates. Lastly, this study identifies the implications of many normal driving features on the potential effectiveness of I-ADAS in the vehicle fleet.

4. Using Event Data Recorders to Model Driver Acceleration Behavior prior to Real-World Intersection Crashes¹

4.1 Introduction

Pre-crash vehicle kinematics are expected to highly influence the effectiveness of I-ADAS in real-world intersection crash scenarios. Pre-crash behavior can be divided into three primary phases [137]: the approach phase, the traversal phase, and any crash avoidance action that the driver may take (e.g., braking or steering [130]). During the intersection traversal phase, the ability of I-ADAS to detect an impending collision and deliver a timely warning will be greatly dependent on (a) the speeds that drivers enter the intersection and (b) acceleration magnitude.

The three most common intersection crash modes are straight crossing path (SCP) collisions, left turn across path lateral direction (LTAP/LD) collisions, and left turn across path opposite direction (LTAP/OD) collisions [2]. Approximately one-half of SCP intersection crashes in the U.S. involve a non-turning vehicle performing a rolling stop or complete stop prior to accelerating through the intersection [92, 137]. For LTAP/OD crashes, the left turning vehicle slows (71.6%) or stops (28.4%) prior to accelerating through the intersection [117]. Similarly in LTAP/LD crashes, the left turning vehicle typically slows or stops prior to entering the intersection [116]. To help drivers avoid intersection crashes, it is crucial that I-ADAS deliver a warning based on how drivers typically navigate across intersections in these crash modes. A timely warning is essential for ensuring that there is adequate time for an avoidance maneuver. However, warning drivers too

¹ The work shown in this study has been a part of several previously published peer-reviewed manuscripts, including:

135. Scanlon, J.M., K.D. Kusano, and H.C. Gabler. *A Preliminary Model of Driver Acceleration Behavior Prior to Real-World Straight Crossing Path Intersection Crashes Using EDRs*. in *Proceedings of the 2015 IEEE Intelligent Transportation Systems*. 2015. Canary Islands, Spain: IEEE.

136. Scanlon, J.M., R. Sherony, and H.C. Gabler, *Models of Driver Acceleration Behavior prior to Real-World Intersection Crashes (In Review)*. IEEE Transactions on intelligent transportation systems, 2016.

early could be perceived as a false-positive alert, which can affect driver response in a crash-imminent scenario [138-140] or lead to the driver turning off these systems altogether [141].

Several past studies have characterized and developed models of “typical” driver acceleration behavior. Two general methodologies were used to develop these models. One method is to mathematically model vehicle acceleration patterns as a function of relevant predictor variables, such as turning behavior, current speed, or distance from the intersection [125, 127, 131, 142, 143]. A second method is to construct a vehicle dynamics models that estimates vehicle acceleration based on vehicle body forces [144, 145]. The existing literature, however, focuses almost entirely on “normal” driving, i.e. non-crashes. The study of intersection traversal during crashes has been greatly hindered by a lack of detailed data on vehicle kinematics and driver behavior during these serious events.

There is reason to suspect pre-crash intersection traversals would vary from “normal” driving behavior. Driver aggressiveness and risk-taking behavior have been correlated with higher crash incidence [134, 146-148]. A large body of literature has examined characteristics of high-risk driving behaviors, which includes speeding [149, 150], maintaining a narrow following distance [109, 151], driving while impaired [152, 153], gap acceptance [154], and driving without a seat belt [151]. Additionally, an elevated number of high g-force events, e.g. hard braking, rapid acceleration, and faster turning, have been associated with elevated crash risk [155, 156]. Accelerometers measuring high g-force events have also been used as an in-vehicle evaluation tool of risky driving behavior [148, 157]. Some mechanisms that can explain this higher crash risk are (a) less time for crash avoidance action from threat detection to impact [158] and (b) loss of control [159].

The goal in this paper was to provide models of driver acceleration, which I-ADAS developers can use to project how quickly a driver will traverse a given intersection. Crash avoidance systems have to be “tuned” based on a number of factors, including how early on-board sensors could detect an oncoming vehicle, computational latency times for detecting conflicts, driver perception-reaction times, and any latency to activate actuators (e.g., applying brakes or steering). A vital part of this tuning is being able to predict a vehicle’s path through time. Determining acceleration traversal patterns can also be helpful for selecting appropriate sensor requirements for detecting oncoming vehicles [92, 158]. An ideal I-ADAS sensor should be capable of identifying potential collision partners at the first clear line-of-sight opportunity. Additionally, not only is this important for designers of these systems, but these models could also prove helpful for evaluators considering a future test that assesses intersection crash avoidance systems. These tests should be performed under crash conditions that replicate actual scenarios that occur in the crash population. Lastly, traversal models permit studies forecasting the population-wide feasibility of I-ADAS [137]. An important component of these studies is the simulation of vehicle behavior as it actually occurs during real-world crashes.

Event data recorders (EDR) can provide unique insights into pre-crash driver behavior. EDRs are the “black boxes” now installed in almost all new U.S. passenger vehicles, which directly measure and record pre-crash vehicle and driver behavior in the event of a collision [38]. EDRs have been used extensively for analyzing pre-crash and impact kinematics during both real-world crashes and staged crash tests [160-176]. EDRs record several pre-crash data elements which are key to understanding intersection traversal, including vehicle speed, accelerator application, brake application, yaw rate, and steering wheel angle [96]. For example, consider the EDR record of pre-crash speed from a real world crash shown in Figure 21. The red shaded vehicle performed a

complete stop, and then accelerated through the intersection. The driver that stopped attempted an evasive braking maneuver just prior to impacting the left side of a vehicle attempting to travel straight through the intersection.

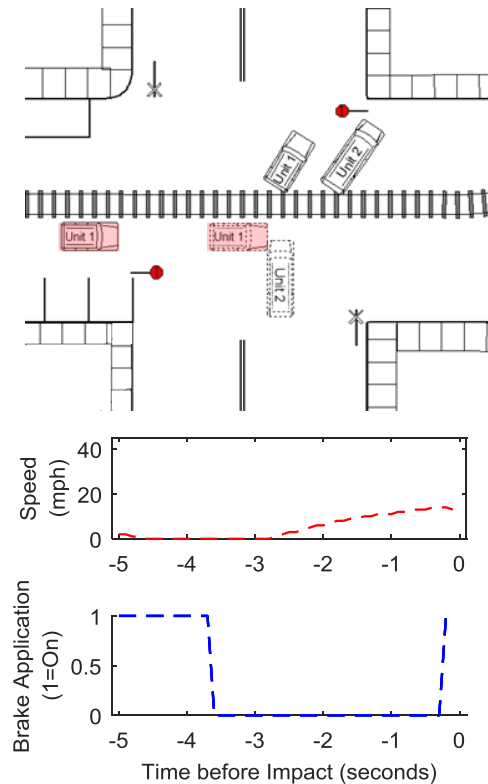


Figure 21. An EDR-recorded speed profile of a vehicle involved in a SCP intersection crash (NASS/CDS 2013-76-166) with the scene diagram prepared by the investigator of the crash.

This study analyzed the pre-crash kinematics of non-turning and left-turning vehicles accelerating into intersections using this EDR data. Our hypothesis was that drivers involved in crashes would accelerate more aggressively than the “typical” driving population. The objective of this study was to develop pre-crash acceleration models for non-turning drivers in SCP crashes and left-turning drivers in LTAP/LD and LTAP/OD crashes. Two research questions were proposed in this study. First, how representative are previously developed acceleration models of

pre-crash acceleration behavior? Second, can a more accurate acceleration profile model be developed to represent this pre-crash data?

4.2 *Methods*

Data Source

This study used EDR-recorded pre-crash speeds from vehicles involved in SCP, LTAP/LD, and LTAP/OD intersection collisions investigated as part of National Automotive Sampling System / Crashworthiness Data System (NASS/CDS) years 2000 to 2015. Chapter 2 details this data source, and the requirements for EDR module selection. EDR pre-crash speed and braking must have been recorded for a vehicle to be included in this study. Crashes with case weightings greater than 5,000 were excluded to limit skewing of the results [97].

To ensure similitude between the model dataset and all intersection crashes, the compositions of each dataset was compared with all similar crash events within the NASS/CDS database. Several potential confounding factors were compared. A Rao-Scott chi-squared test was used to identify differences in the composition of each dataset.

Extracting EDR-Recorded Intersection Traversal Accelerations

The goal of this study was to model the acceleration patterns of vehicles as they are attempting to safely pass through the intersection and prior to crash avoidance braking. Because these are EDR pre-crash records, evasive braking commonly occurs [130], which is accounted for using the methods in the following section.

Velocity time points from accelerating vehicles were extracted from the EDR records in two steps. The overall process is depicted in Figure 22. First, any time points in which evasive braking

occurred were removed from the time series. Evasive braking was determined by whether the brakes were applied at the last EDR-recorded time point. In the event of an evasive braking maneuver being indicated, all immediately prior time points where the service brake was engaged were removed.

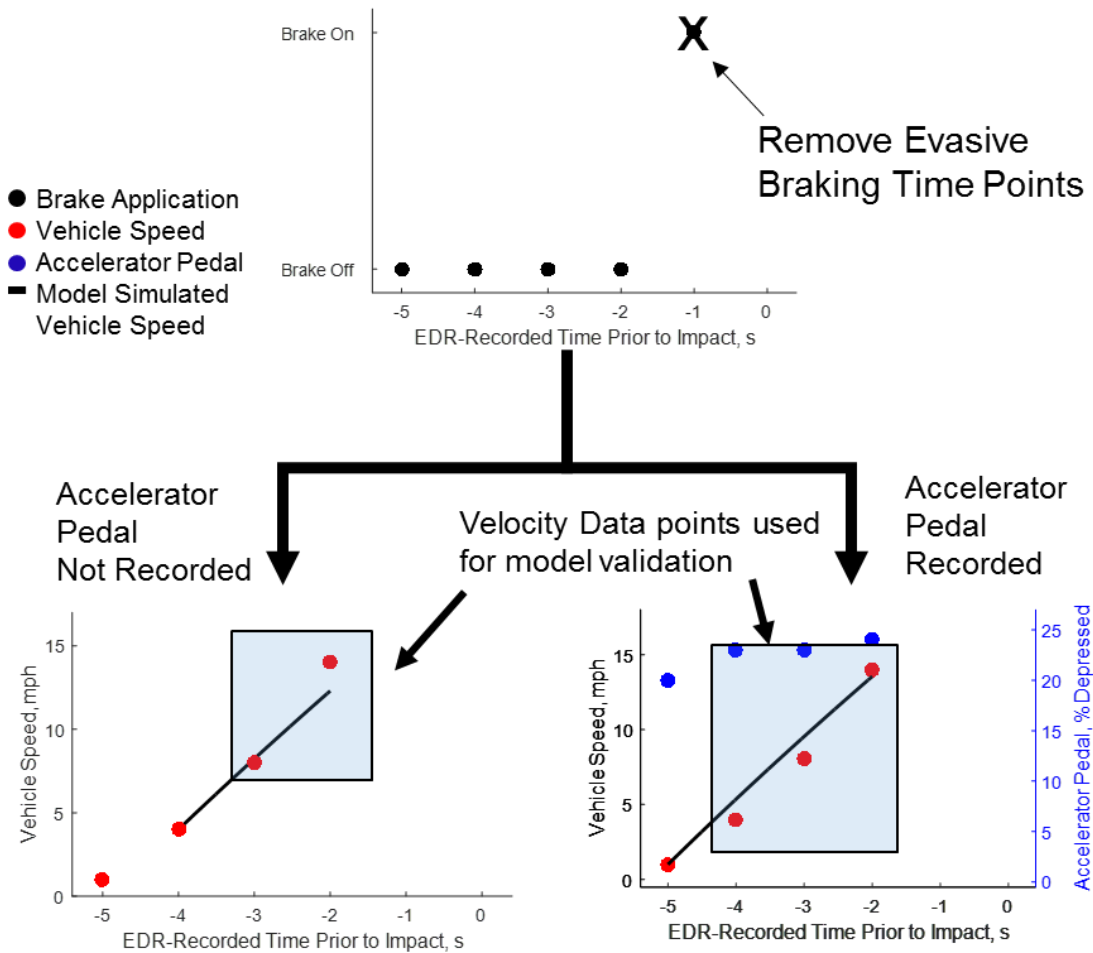


Figure 22. Extracting intersection traversal acceleration. The first step in this process required the removal of all EDR-recorded time points where evasive braking was indicated. The second step in the process required the extraction of the acceleration portion of the EDR record.

Second, the remaining data were used to determine if and at what EDR-recorded time points the driver was accelerating into the intersection. Some of the EDRs in our sample recorded

accelerator pedal position as a percentage of the fully-depressed position. When available, accelerator pedal application was used to determine when the driver was performing an acceleration maneuver. If the accelerator pedal was pressed at the last EDR-recorded time point prior to evasive braking, the driver was assumed to have been accelerating into the intersection. The time points with accelerator pedal application were then extracted as the acceleration time series. If accelerator pedal application was not recorded by the EDR, the speed profile was instead used to extract the acceleration time series. If an increase in velocity was observed between the two velocity time points prior to evasive braking application, the driver was assumed to have accelerated into the intersection, and all acceleration time points were extracted. However, without accelerator pedal application data, there is some uncertainty in whether the driver was accelerating at the earliest EDR-recorded acceleration time point. For example, the driver could have begun depressing the accelerator pedal just prior to the second acceleration time point but following the first acceleration time point. Accordingly, the first acceleration time point was removed from the acceleration time series for EDRs that did not record accelerator pedal application.

All model development and evaluation performed in this study used these extracted pre-crash traversal acceleration time series. The first data point in the extracted acceleration time series was used as an “initial condition”. All subsequent acceleration time points were used to evaluate the predictive power of the model.

Previously Developed Acceleration Profile Models

The studies discussed below have reported non-crash vehicle acceleration models developed for traffic engineers and intersection geometry design. The general form of each model can be seen in Figure 23.

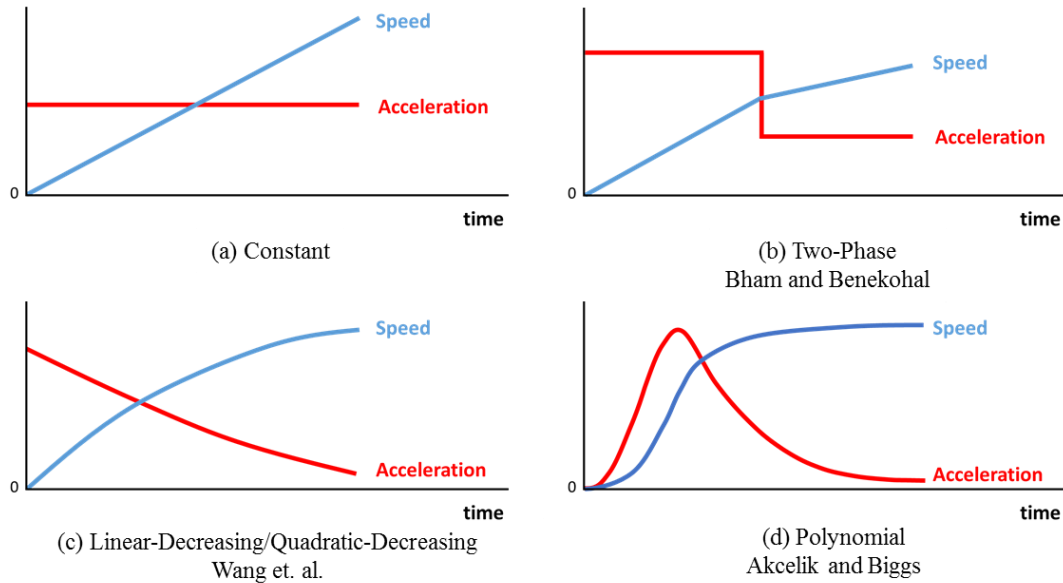


Figure 23. Example acceleration profiles of previously developed models.

The constant acceleration model is the simplest representation of driver acceleration into intersections. Using this model, the driver is assumed to maintain a constant acceleration until some target final speed is reached. This simplistic model has its drawbacks. First, this model assumes an instantaneous jerk at the initiation and conclusion of the acceleration event. Second, the model fails to account for changes in acceleration magnitude throughout the traversal that occur due to natural driving tendencies and changing gears [145]. Several studies have consistently found this model to be a poor approximation of real-world driver behavior [125, 127, 131], and as such, the constant acceleration model was not considered in this study's analyses.

Bham and Benekohal [127] developed a two-phase model that was evaluated in this study. Their model was based on acceleration data previously collected by Ohio State University using aerial photogrammetry [177]. The model assumed the driver would begin to accelerate at some higher constant value (1.10 m/s^2) until some vehicle speed had been reached (12.97 m/s), and then the vehicle would instantaneously begin to accelerate at some lower constant value (0.37 m/s^2). This relationship is shown in Equation 2. Integrating Equation 1 yields the velocity relation used in this study, as shown in Equation 3.

Equation 2 $a(t_i) = a_{1,2}$

Equation 3 $v(t_{i+1}) = a(t_i) \cdot \Delta t + v(t_i)$

Where,

- $a(t_i)$ = acceleration at the current time step, m/s
- a_1 = acceleration before $12.97 \text{ m/s} = 1.10 \text{ m/s}^2$
- a_2 = acceleration before $12.97 \text{ m/s} = 0.37 \text{ m/s}^2$
- $v(t_{i+1})$ = velocity at the next time step, m/s
- $v(t_i)$ = velocity at the current time step, m/s
- Δt = time step, s

Wang et al. [131] developed a linear-decreasing model and a quadratic-decreasing model which were assessed in this study. Like the two-phase model, both of these models assume drivers will initially accelerate at a higher rate followed by lower rates. The acceleration data for developing these models were taken from a naturalistic driving study that was performed in the Atlanta urban area. In this study, 100 vehicles were equipped with GPS systems and the coordinates of these vehicles were tracked. The researchers fit regression models to the acceleration vs. velocity relation of drivers as they were accelerating. Unique models were created for non-turning and left-turning vehicles. The fit models are shown in Table 14 for the linear (Equation 4 and Equation 5) and quadratic (Equation 6 and Equation 7) forms.

Table 14. Regression model equations developed by Wang et al. [131].

Equation Number	Turning Maneuver	Model Type	Equation
Equation 4	Straight	Linear Decreasing	$a(t) = 1.883 - 0.021 \cdot v(t)$
Equation 5	Turning	Linear Decreasing	$a(t) = 1.646 - 0.017 \cdot v(t)$
Equation 6	Straight	Quadratic decreasing	$a(t) = [1.381 - 0.011 \cdot v(t)]^2$
Equation 7	Turning	Quadratic decreasing	$a(t) = [1.289 - 0.009 \cdot v(t)]^2$

Where,

$a(t)$ = Acceleration at time point t in m/s^2 ,

t = time in s ,

$v(t)$ = Velocity in km/hr .

Akcelik and Biggs [125] developed a polynomial acceleration model which was also examined in this study. This model assumed that drivers begins to accelerate with zero jerk, ramps up vehicle acceleration to some maximum value, and then gradually decreases vehicle acceleration with zero jerk at acceleration offset. The data used to develop this model was collected in Sydney, Australia using the chase-car method. Data were collected in urban, suburban, and rural traffic. Using this technique, an instrumented vehicle randomly selects and follows vehicles in traffic. The equipped “chasing” car documents the movements of the lead vehicle. The general form of the polynomial model can be seen in Equation 7. The polynomial model provides a highly tunable option for representing a given acceleration profile. However, implementing this model requires several parameters that cannot be readily determined from pre-crash acceleration events, including vehicle speed at the end of the acceleration event, total acceleration time, and total acceleration distance. Each of these model inputs can only be determined if the driver completes the acceleration event, which very rarely occurs in intersection crash scenarios. As such, this model was not considered for this study’s analyses.

Equation 8
$$a(t) = r \cdot a_m \cdot \theta \cdot (1 - \theta^m)^2$$

Where,

- $a(t)$ = acceleration at time t in km/hr.s,
- a_m = maximum acceleration in m/s² dependent on initial velocity, final velocity, acceleration time, and acceleration distance,
- θ = time ratio, t / t_a ,
- t_a = acceleration time in s,
- r, m = model parameters dependent on initial velocity, final velocity, acceleration time, and acceleration distance.

Development of a New Pre-crash Acceleration Model

A linear-decreasing model and a quadratic-decreasing acceleration model were developed in this study to represent driver acceleration behavior prior to real-world intersection crashes. These models were selected for several reasons. First, these models can be developed from only partial acceleration profiles (i.e., the beginning and end of the traversal event is not required). Second, several prior studies have consistently found that driver’s accelerate at a higher degree early in the acceleration traversal [125, 127, 131]. Third, this model is computationally efficient, and can be readily applied for future applications. The general form of the linear-decreasing and quadratic-decreasing models are shown in Equation 9 and Equation 10, respectively.

Equation 9
$$a(t) = c_1 - c_2 \cdot v(t)^2$$

Equation 10
$$a(t) = [c_1 - c_2 \cdot v(t)]^2$$

Where,

- $a(t)$ = Acceleration at time point t in m/s²,
- t = time in s,
- $v(t)$ = Velocity in km/hr,
- c_1, c_2 = model parameters.

The model parameters, c_1 and c_2 , shown in Equation 9 and Equation 10 were computed using a simulated annealing global optimization algorithm [178]. An alternative, and perhaps preferable,

approach would be to compute parameters using regression methods. However, acceleration rates were not directly measured from EDR models and could not be determined from the low sampling rate and resolution that vehicle speed is typically collected. An overall error score shown Equation 10 was developed as an objective function to be minimized by the optimizer. The form of this equation was selected for several reasons. First, the squared residual allowed for an unsigned measure of observed versus predicted speed. Second, summing the squared residuals and normalizing by the total number of data points helped account for differences in sampling rates and acceleration durations. Third, each acceleration trace was weighted using the NASS case weighting factor. Accordingly, the resulting model parameters were selected based on real-world frequency.

Equation 11

$$\text{OverallError} = \frac{1}{\sum w_{\text{case}}} \sum_{i=1}^{N_{\text{Case}}} \sum_{j=1}^{N_{\text{traj}}} [(v_{\text{sim},i,j} - v_{\text{EDR},i,j})^2 \cdot \frac{w_{\text{case},i}}{N_{\text{traj},j}}]$$

Where,

Overall error	= Measure used to evaluate models in (m/s) ² ,
i	= index for case,
j	= index for time point in trajectory,
vEDR	= EDR recorded vehicle speed in m/s,
vsim	= Model predicted vehicle speed in m/s,
Ncase	= Total number of cases,
Ntraj	= Number of time points in acceleration trajectory,
wcase	= NASS case weight.

Model Evaluations

The accuracy of the developed models was compared with the previously developed non-crash acceleration profile models using a leave-one-out cross-validation procedure. Only cases up to year 2014 were included in the leave-one-out analysis. Using this technique, one observation is

withheld as a “testing dataset”, while the remaining n-1 observations (n = total number of observations) are used as a “training dataset” to develop the pre-crash acceleration models. The generated pre-crash models and previously developed models were then used to predict subsequent velocity time points in the testing dataset. This process was repeated n-times until velocity time point predictions had been generated for every acceleration profile. Using the overall error score shown in Equation 10, the overall ability of each model to accurately predict the observed EDR velocity time points was evaluated. Additionally, a regression line was fit through the observed versus predicted values. The slope of the line and R^2 were used to assess the predicted capacity of the models.

In addition, a trajectory error score, shown in Equation 12 was computed for each case in the dataset. Trajectory error is similar to the overall error score but is only calculated for a single trajectory and additionally retains whether each model tended to overestimate or underestimate acceleration behavior. The trajectory “error sign” was retained by taking the sign of the difference between the observed and predicted final velocity time points.

Equation 12
$$Trajectory\ Error = \sum_j^{N_{traj}} [(v_{sim,j} - v_{EDR,j})^2 \cdot \frac{1}{N_{traj}}] \cdot sgn(v_{sim,N_{traj}} - v_{EDR,N_{traj}})$$

Where,

- v_{EDR} = EDR recorded vehicle speed in m/s,
- v_{sim} = Model predicted vehicle speed in m/s ,
- N_{case} = Number of cases,
- N_{traj} = Number of time points in acceleration time series,
- w_{case} = NASS case weight.

Differences between the least squares means of trajectory error scores were examined to evaluate each model’s ability to predict pre-crash speeds. All statistical analyses were performed using the “SURVEYREG” procedure in the SAS 9.3 software package (SAS Institute, Cary, NC)

[179]. For a given crash mode, model type was used as the independent variable. Trajectory error, shown in Equation 11, was used as the dependent variable. An alpha level of 0.05 was used to determine significance.

As a second form of validation, a simple cross validation method was also used to compare the models generated in this study. Odd numbered case years were used to “train” the dataset. Even numbered case years were used to test the dataset. Overall error was used to evaluate the different models.

4.3 Results

Case Selection

A total of 348 EDR records were extracted for this study’s analyses from case years 2000 to 2015. Table I categorizes the dataset by intersection crash mode. The largest dataset of EDRs came from SCP crashes followed by LTAP/OD and LTAP/LD. A total of 1,308 data points from these cases were used in this study for development and validation of the model. Each of these data points are velocity measurements which occurred after the time point of first acceleration.

Table 15. Breakdown of included cases by crash mode.

Crash Mode (Turn)	Unweighted Case Count	Weighted Case Count
SCP (Straight)	138	53,708
LTAP/OD (Left)	125	58,530
LTAP/LD (Left)	85	26,493
Total	348	138,731

A summary of the EDR modules used in this study’s analyses can be found in Table II. A variety of module types were used in this study. Most of the records contained 5 s of pre-crash data, but a

few records (12 of 348) contained only 2.5 s. Most modules, in general, can record 5 s of pre-crash data, and modules with longer recordings also have a higher likelihood of containing an extractable acceleration profile. All of the records used collected vehicle speed at a resolution of at least 2.0 kph (1.2 mph). Additionally, most (245 of 348) of the EDRs used in this study collected vehicle speed at 1 Hz.

Table 16. Count of EDR modules by specifications.

Pre-crash Time Window	Sampling Rate	Velocity Sampling Resolution	EDR Count
5 s	1 Hz	0.16 kph [1.0 mph]	3
5 s	1 Hz	1.6 kph [1.0 mph]	216
5 s	1 Hz	2.0 kph [1.2 mph]	26
5 s	2 Hz	0.16 kph [0.1 mph]	7
5 s	2 Hz	1.0 kph [0.6 mph]	27
5 s	2 Hz	1.6 kph [1.0 mph]	29
5 s	5 Hz	1.6 kph [1.0 mph]	2
5 s	10 Hz	1.6 kph [1.0 mph]	26
2.5 s	2 Hz	1.6 kph [1.0 mph]	12
Total			348

Leave-one-out Cross-Validation Procedure

Table 17 shows least squares means of trajectory errors with comparisons between models for each crash mode. In general, the non-crash models tended to underestimate pre-crash vehicle speeds ($p < 0.001$). Using the leave-one-out method, the pre-crash models developed in this study were not found to not significantly underestimate or overestimate pre-crash acceleration patterns. When comparing the models, the new linear-decreasing and quadratic-decreasing models generated in this study were able to predict pre-crash acceleration behavior significantly ($p < 0.001$) better than each of the previously developed models for every crash mode. However, no differences were observed between the linear-decreasing and quadratic-decreasing models

generated in this study. It should also be noted that each of the previously developed models performed significantly different from one another ($p < 0.001$) for every crash mode variation.

Table 17. Least -squares means of trajectory error and mean differences between the various models.

Trajectory Error (m/s) ² (p-value)						
SCP						
Model		Bham 2-phase	Wang Linear	Wang Quad.	Scanlon Linear	Scanlon Quad.
		-3.17	-1.27	-1.54	0.00	-0.08
Bham 2-phase	-3.17	---	1.89 (<.001)	1.63 (<.001)	3.16 (<.001)	3.08 (<.001)
Wang Linear	-1.27	---	---	-0.26 (<.001)	1.27 (<.001)	1.19 (<.001)
Wang Quad.	-1.54	---	---	---	1.53 (<.001)	1.45 (<.001)
Scanlon Linear	0.00	---	---	---	---	-0.08 (0.290)
Scanlon Quad.	-0.08	---	---	---	---	---
LTAP/OD						
Model		Bham 2-phase	Wang Linear	Wang Quad.	Scanlon Linear	Scanlon Quad.
		-2.50	-1.26	-1.37	0.01	0.02
Bham 2-phase	-2.50	---	1.24 (<.001)	1.13 (<.001)	2.51 (<.001)	2.52 (<.001)
Wang Linear	-1.26	---	---	-0.11 (<.001)	1.27 (<.001)	1.28 (<.001)
Wang Quad.	-1.37	---	---	---	1.38 (<.001)	1.39 (<.001)
Scanlon Linear	0.01	---	---	---	---	0.01 (0.710)
Scanlon Quad.	0.02	---	---	---	---	---
LTAP/LD						
Model		Bham 2-phase	Wang Linear	Wang Quad.	Scanlon Linear	Scanlon Quad.
		-2.61	-1.36	-1.45	-0.11	-0.09
Bham 2-phase	-2.61	---	1.25 (<.001)	1.16 (<.001)	2.50 (<.001)	2.52 (<.001)
Wang Linear	-1.36	---	---	-0.09 (<.001)	1.24 (<.001)	1.27 (<.001)
Wang Quad.	-1.45	---	---	---	1.33 (<.001)	1.36 (<.001)
Scanlon Linear	-0.11	---	---	---	---	0.02 (0.470)
Scanlon Quad.	-0.09	---	---	---	---	---

Figure 24 presents a comparison of the simulated versus observed velocity time points for this study’s models and each of the previously developed models that were evaluated. Overall error scores for each model/crash mode variation can be found in Table 18. Each predicted velocity was generated using the Leave-one-out cross-validation procedure. All of the non-crash models being evaluated had greater overall error scores than the pre-crash models. The two-phase model underestimated the final velocity time point for 85%-97% of cases depending on the crash mode.

The Wang linear-decreasing underestimated 75%-84% of these final velocity time points, and the Wang quadratic-decreasing underestimated 76%-86% of final velocity time points. The new pre-crash linear-decreasing models developed in this study only underestimated 45-55% of final velocity time points, and the new quadratic-decreasing model underestimated 47-60% of final velocity time points.

Table 18. Overall Error scores for the various models and crash modes.

Overall Error (m/s)²			
Model	SCP	LTAP/OD	LTAP/LD
Bham 2-phase	3.19	2.62	2.63
Wang Linear	1.46	1.52	1.46
Wang Quad.	1.64	1.59	1.54
Scanlon Linear	0.91	0.89	1.02
Scanlon Quad.	0.92	0.89	1.05

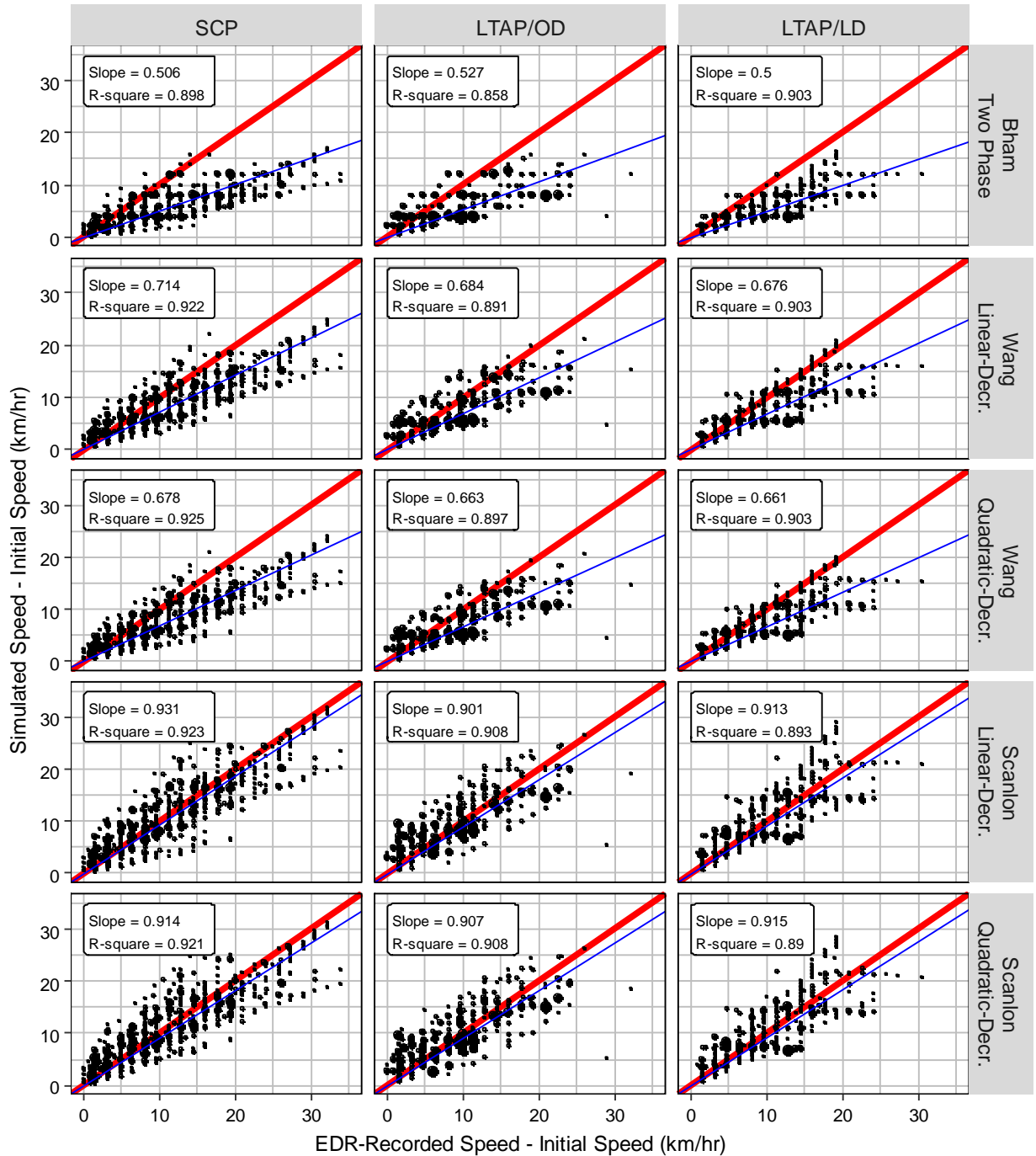


Figure 24. Simulated speeds versus EDR-recorded speed for every data point used in this study. Results were generated using the leave-one-out cross-validation method. Three previously generated models are shown in the figure, including the Bham two-phase, Wang linear-decreasing, and Wang quadratic-decreasing models. The Scanlon linear-decreasing and quadratic-decreasing models generated in this study are additionally presented in the figure. Data points are sized based on their NASS case weight.

Basic Cross-Validation Analysis

A supplemental cross-validation analysis was performed to further validate the findings of this study. A basic method was used, where odd NASS/CDS case years were used to “train” the model dataset, and even case years were used to “test” the model dataset. Overall error was used to test the predicted vehicle speeds with the recorded speed.

Figure 25 shows predicted speeds versus EDR-recorded speeds. Overlaid on the plots are the slope and R-square for a regression line fit through the data. Overall Error score is shown in Table 19. The pre-crash linear-decreasing and quadratic-decreasing models were found to predict pre-crash speeds more effectively the non-crash models as evidenced by the lower overall error values. Similar to the Leave-one-out analysis, the Wang linear-decreasing model was found to better predict the pre-crash data than the Wang quadratic-decreasing model. Also similar to the prior cross-validation analysis, the Bham model was found to greatly underestimate pre-crash speeds.

Table 19. Overall Error scores for the various models generated using the Basic Cross-Validation method.

Overall Error (m/s) ²			
Model	SCP	LTAP/OD	LTAP/LD
Bham 2-phase	3.19	2.62	2.63
Wang Linear	1.46	1.52	1.46
Wang Quad.	1.64	1.59	1.54
Scanlon Linear	0.91	0.89	1.02
Scanlon Quad.	0.92	0.89	1.05

*greyed cells represent pre-crash models developed in current study.

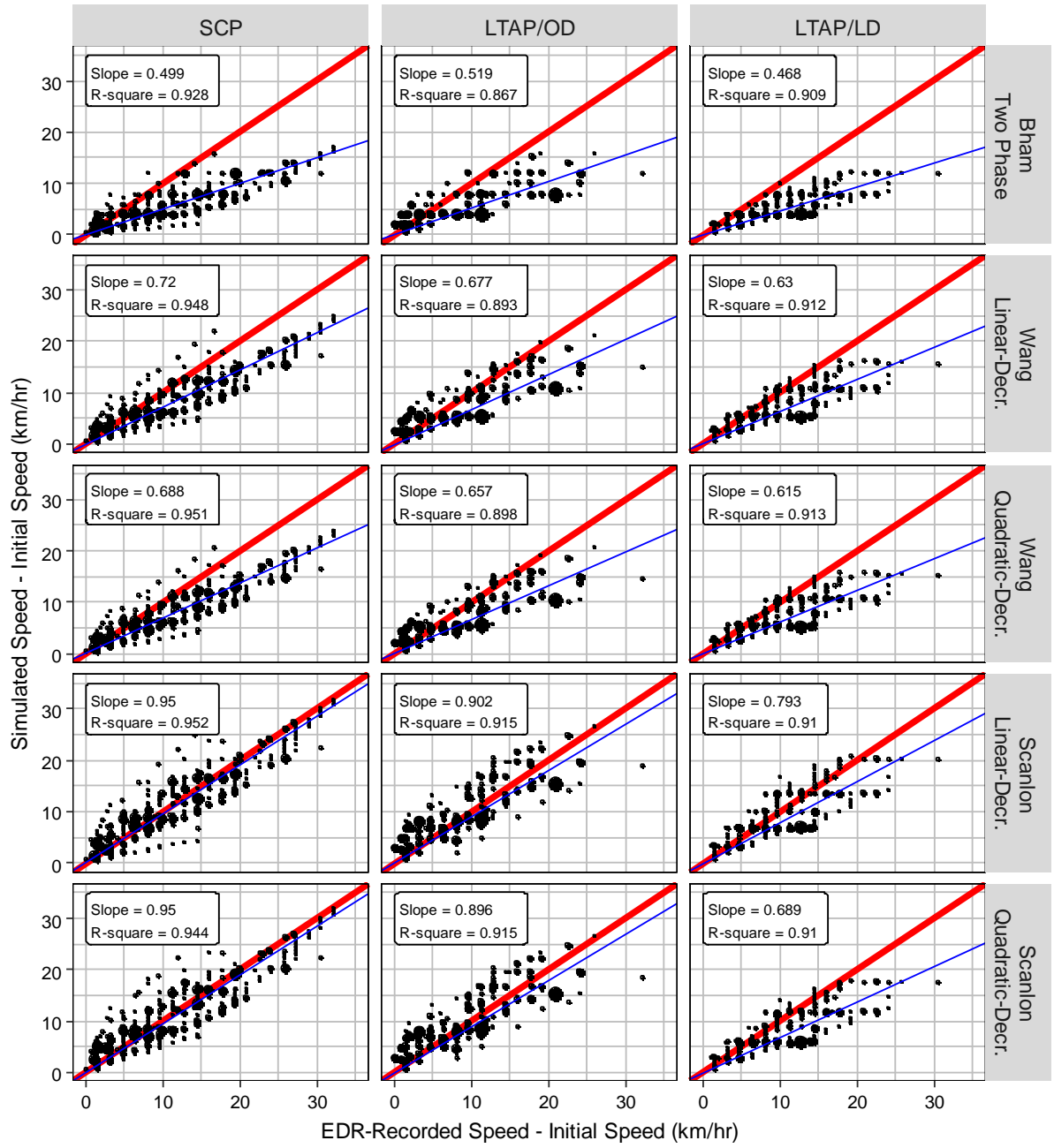


Figure 25. Comparing model predicted speed with recorded speed. These results were generated using the most basic cross-validation method.

Overall Model Fits

Optimum model parameters for the linear-decreasing and quadratic-decreasing models were then computed for each dataset of intersection crash modes. The resulting models can be presented in Equation 13-Equation 18 listed in Table 20. Figure 26 provides some example simulated trajectories for the three new linear-decreasing pre-crash models and each non-crash model. The quadratic-decreasing models produced similar trajectories to the linear-decreasing models and are not shown.

Table 20. Equations for overall pre-crash model fits.

Crash Mode (Turn)	Model	Equations
SCP (Straight)	Linear	$a(t) = 2.782 - 0.154 \cdot v(t)$ Equation 13
	Quad.	$a(t) = [1.745 - 0.090 \cdot v(t)]^2$ Equation 14
LTAP/OD (Left)	Linear	$a(t) = 2.924 - 0.247 \cdot v(t)$ Equation 15
	Quad.	$a(t) = [1.791 - 0.099 \cdot v(t)]^2$ Equation 16
LTAP/LD (Left)	Linear	$a(t) = 2.167 - 0.057 \cdot v(t)$ Equation 17
	Quad.	$a(t) = [1.489 - 0.025 \cdot v(t)]^2$ Equation 18

Where,

$a(t)$ = Acceleration at time point t in m/s^2 ,

$v(t)$ = Velocity at time point t in m/s ,

t = time in s .

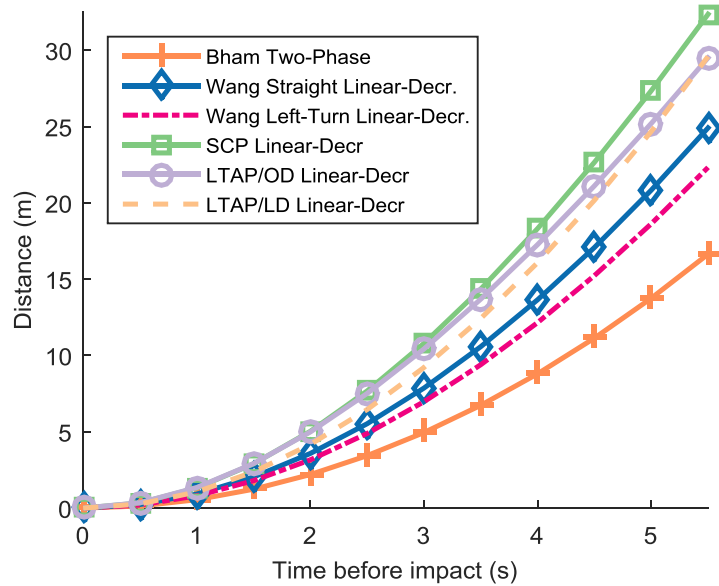


Figure 26. Simulated distance versus time trajectories for a vehicle accelerating from rest. Each acceleration trace corresponds to one of the models evaluated in this study.

The non-crash and crash models give dramatically different predictions of time to collision. Consider a crash that is going to occur 20-m after an I-ADAS vehicle begins to accelerate from rest into an intersection. The Bham and Benkohlal two-phase model predicts that the driver will reach the impact location in 6.03 s. The Wang et al. linear-decreasing and quadratic-decreasing models estimate that the crash will occur 4.89-4.97 s, respectively, following initial acceleration for non-turning vehicles. In contrast, the pre-crash models developed in this study predict that these crashes will occur much sooner. For SCP crashes, both models expect the crash to occur in 4.20-4.35 s – over 0.5 seconds earlier than the non-crash models predict.

For turning vehicles, the Wang et al. linear-decreasing and quadratic-decreasing models predict that the crash will occur 5.19-5.25 s, respectively. By contrast for LTAP/OD, the crash model anticipates the crash to occur in 4.31-4.36 s. For LTAP/LD, the crash model predicts the crash will occur in 4.47-4.48 s – substantially earlier than the non-crash models.

4.4 *Discussion*

The three non-crash models evaluated in this study underestimated pre-crash velocity. This finding provides support for our hypothesis that drivers involved in crashes may tend to accelerate differently than drivers in typical scenarios. The existing models were developed using non-crash data from “normal” driving. Additionally, some of the drivers, for example LTAP/OD crashes, may have seen the oncoming car, and attempted to rapidly accelerate to avoid an imminent collision. Gap selection errors due to misjudgment of available space and/or velocity of the oncoming driver is frequently cited as a contributing factor in real-world LTAP/OD crashes [117].

The findings of this paper have important implications for the design and evaluation of an I-ADAS. As previously stated, the acceleration patterns of vehicles as drivers enter and traverse intersections directly influences the amount of time available for crash avoidance action. The higher-than-normal acceleration behavior of driver’s prior to real-world crashes suggests that there is a need for I-ADAS design to account for this potentially more aggressive driving behavior. Using the Wang et. al. non-crash models and our new pre-crash model, we can compare drivers in crashes versus drivers in “normal” intersection traversal. For non-turning drivers, the new SCP pre-crash model predict that drivers typically involved in crashes will travel 20-m from a complete stop 0.54-0.77 s faster than a driver in a “normal” driving scenario. Likewise, for left-turning drivers, drivers in LTAP/OD and LTAP/LD crash scenarios will traverse 20-m from a stop 0.83-0.94 s and 0.71-0.78 s faster, respectively. Although only less than a second sooner, current active safety systems begin to warn drivers a mere 2-3 s prior to a collision occurring [23]. Given a typical crash avoidance braking magnitude of 0.6 g [130], a driver could slow their vehicle by 10 mph if

allotted an additional 0.8 s to react. This additional reduction in speed could not only be crucial for avoiding the crash but could also potentially reduce injuries in crashes which could not be avoided.

There do appear to be some differences in pre-crash acceleration behavior between the different crash modes. However, differences between the different crash modes was not tested in this study. In general, the acceleration of non-turning drivers in SCP crashes appears to be higher during the early traversal phase than left-turning drivers in LTAP/LD and LTAP/OD crashes. This finding is consistent with prior work comparing non-turning drivers with left-turning drivers [131]. The early acceleration of vehicles in LTAP/OD crashes also appears to be slightly greater than drivers in LTAP/LD crashes. As discussed previously, one reason for higher acceleration prior to real-world crashes may be that the driver saw the oncoming vehicle and then attempted to quickly accelerate through the gap in traffic. Gap selection, where the left-turning drivers sees the oncoming vehicle but still attempts to turn, commonly occurs in U.S. LTAP/OD crashes [117].

This study found insufficient statistical evidence to suggest that the linear-decreasing or the quadratic-decreasing model is a better representation of pre-crash traversal acceleration behavior. In fact, there appear to be only slight differences between the two models for predicting pre-crash data. Previous work by Wang et. al. [131] found that the linear-decreasing relationship of acceleration versus velocity tends to overestimate vehicle acceleration at higher speeds. In the current study, incomplete acceleration traces (limited EDR recording duration and final speed not reached due to being impacted) limited our ability to test this theory on the pre-crash data. In general, it is important to note that these models are only intended to simulate vehicle accelerations into the intersections.

A number of additional factors that were not considered in this study could influence vehicle acceleration rates. These include, but are not limited to, driver characteristics, vehicle characteristics, and roadway characteristics. It is important to recognize that I-ADAS systems do not currently consider factors such as intersection characteristics or driver characteristics. Future systems may be capable of adjusting based on specific factors. One factor not considered was roadway speed limit. Intuitively, we know that the acceleration of a driver speeding up to 45 mph will be different than that of a driver speeding up to 25 mph. What is not clear is if the differences lie in the acceleration magnitudes, acceleration duration, or both. Additional work on a larger dataset would help elucidate the effect of speed limit on intersection traversal kinematics. A second factor not considered was the size of the intersection. Drivers may be more likely to accelerate at higher rates if attempting to traverse a multilane high-speed road when compared to traveling through a smaller 4-way stop-controlled intersection. A third effect not considered was driver age and gender. Driver age and gender have both been correlated to more aggressive driving behavior and risk-taking [98, 109, 133, 146, 154, 155]. In particular, the young, male driving population has been consistently found to exhibit aggressive driving behavior. A fourth effect not considered was vehicle body type. There is obvious interplay between vehicle mass and engine power, among other factors, which dictate an individual vehicle's acceleration capacity. This study only considers cars, light trucks, and vans, and does not distinguish between the groups in the developed models. A fifth effect not considered was other drivers on the roadway. For example, if the driver was following some other vehicles on the roadway, their ability to accelerate may be restricted [127].

4.5 Validating the Composition of the EDR Dataset

The composition of the EDR model dataset used in this study was compared with all relevant intersection crashes in the NASS/CDS database. Given the moderate size of the dataset used in

this study, it is important to evaluate how the dataset used in this study compares with all similar events in NASS/CDS as a whole.

The first step was to develop a set of all intersection crashes in NASS/CDS. The dataset was developed by applying the same selection criteria that were used for the EDR model dataset. First, all intersection crashes were identified using the “RELINTER” variable. Second, using the “ACCTYPE” variable, straight crossing drivers in SCP crashes and left turning drivers in LTAP/OD and LTAP/LD crashes were extracted. Third, crashes with case weights greater than 5,000 were also excluded to avoid any potential skewing of the data.

The models developed in this study used a dataset of drivers that were accelerating into the intersection. It should be noted that the subset of NASS/CDS intersection events used for comparison do not exclusively contain drivers that accelerated into the intersection. Although this movement happens quite frequently in the intersection crash modes being analyzed, it is rarely coded in the NASS/CDS database (“PREMOVE” variable). EDRs provide a direct measurement of whether a driver was accelerating into the intersection. Therefore, acceleration behavior can be determined by examining pre-crash speed records.

Tabulations of factors for the model dataset can be found in Table 21. A number of factors discussed in the study could potentially influence driver acceleration behavior. These factors include, but are not limited to, driver age, driver gender, traffic control device, speed limit, and vehicle body type.

Table 21. Dataset composition used in the study to develop models of driver acceleration prior to real-world crashes.

Parameter	Value	Count (Weighted % of Total)		
		SCP	LTAP/OD	LTAP/LD
Driver Age	Unknown	11	8	7
	<= 25 y.o.	27	28	17
	26-54 y.o.	54	51	28
	>= 55 y.o.	46	38	33
Driver Gender	Female	77	61	55
	Male	51	56	23
	Unknown	10	8	7
Traffic Control Device	Traffic Signal	85	100	28
	Stop Sign	53	0	56
	Neither	0	25	1
Vehicle Body Type	Unknown	0	0	0
	Car	80	77	67
	LTV	58	48	18
Speed Limit	Unknown speed limit	1	0	1
	No Speed Limit	1	0	2
	<= 25 mph	25	5	20
	30-35 mph	54	50	27
	40-45 mph	44	55	23
	>= 50 mph	13	15	12
Total		138 (100%)	125 (100%)	85 (100%)

Additionally, a Rao-Scott chi-squared test was used to identify differences in the composition of each dataset. Statistical analyses were performed using the SURVEYFREQ procedure in the SAS 9.3 software package (SAS Institute, Cary, NC). Comparisons were done for each crash mode/parameter variation. Additionally, cases where an EDR was extracted were found to have a higher likelihood of containing a coded parameter. Because of this, for a given parameter, cases where the factor could not be determined (marked as “unknown” by the investigator) were not considered in the chi-squared analysis.

Driver age was first compared between the two datasets. The distribution of driver ages are shown in Figure 27. Significant differences in driver age were observed between the datasets ($p=0.009$). Senior drivers were found to be slightly overrepresented in the model dataset (35%) when compared to CDS events (22%). Young drivers were underrepresented in the model dataset (25%) in comparison to applicable NASS/CDS events (31%). One potential reason for differences in driver age demographics between the two datasets could have been the composition of automakers that make up the model dataset. EDR records were only available from four vehicle manufacturers, including General Motors (GM), Ford, Chrysler, and Toyota. GM comprised the majority of the dataset (68%), which is much a higher percentage than in the overall CDS dataset (32%). This large proportion is mainly because GM introduced EDRs into the vehicle fleet long before other OEMs. The entire NASS/CDS database was used to examine this possibility. The median age of drivers for these four vehicle manufacturers was found to be 4 years older than the median age of all other vehicle manufacturers. The senior driver age bracket was also found to be overrepresented (18%) for the four manufacturers when compared to all other automakers (12%).

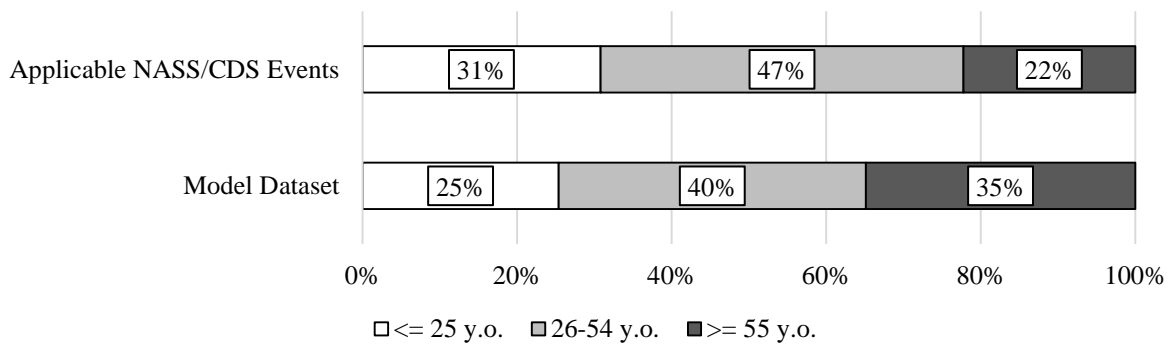


Figure 27. Comparing driver ages between the datasets.

The distribution of driver genders are shown in Figure 28. No statistical differences were observed for driver gender ($p=0.057$). Male drivers comprised 62% of the model dataset and 66% of similar NASS/CDS events.

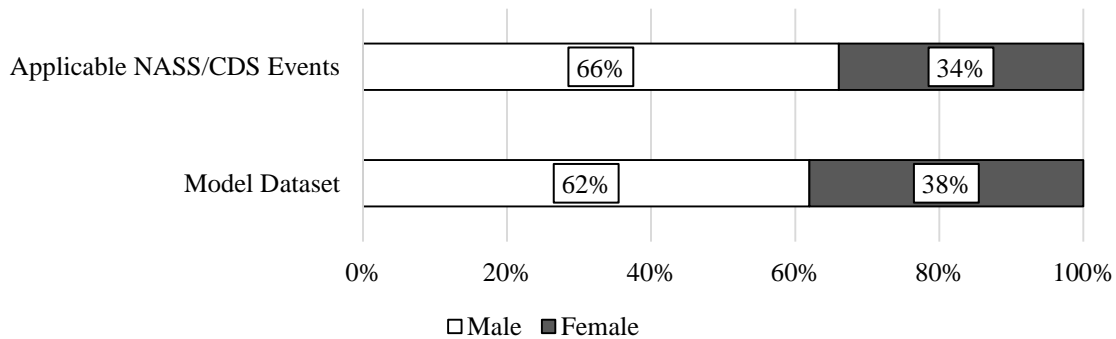


Figure 28. Comparing driver gender between the datasets.

Because NASS/CDS does not regularly code for acceleration behavior into intersections, a comparison was not made for traffic control device. Pre-crash actions are dependent on traffic control device, so performing this comparison would not be appropriate. As an example [137], for SCP crashes, about 30% of crashes at signalized intersections involve at least one of the vehicles having stopped then accelerated, whereas approximately 71% of crashes at two-way stop controlled intersections had a vehicle that stopped then accelerated.

The proportions of vehicle body type can be found in Figure 29. No statistical differences ($p=0.847$) were found in the proportions of vehicle body types between the two datasets. A total of 67% of the model dataset was comprised of cars. Cars comprised 66% of similar NASS/CDS events.

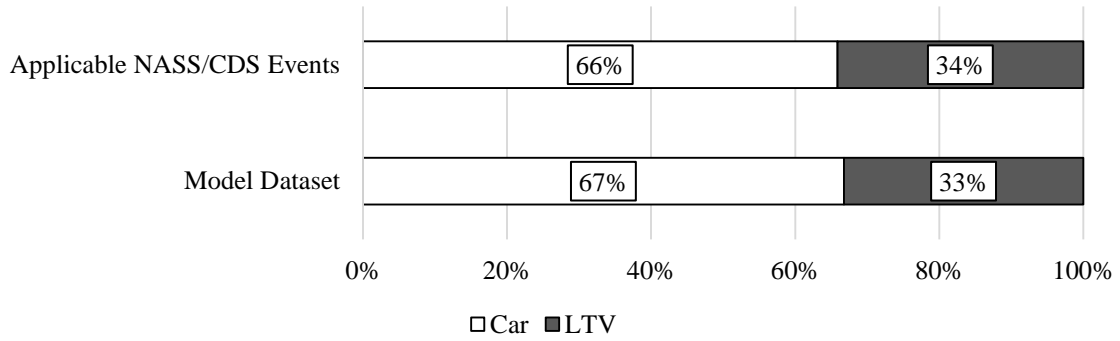


Figure 29. Comparing vehicle body types between the datasets.

No statistical differences ($p=0.658$) in roadway speed limits were observed between the two datasets. The proportions of these speed limits can be seen in Figure 30. For the model dataset, 41% of speed limits were 40 mph or greater. For similar NASS/CDS events, 38% of speed limits were 40 mph or greater.

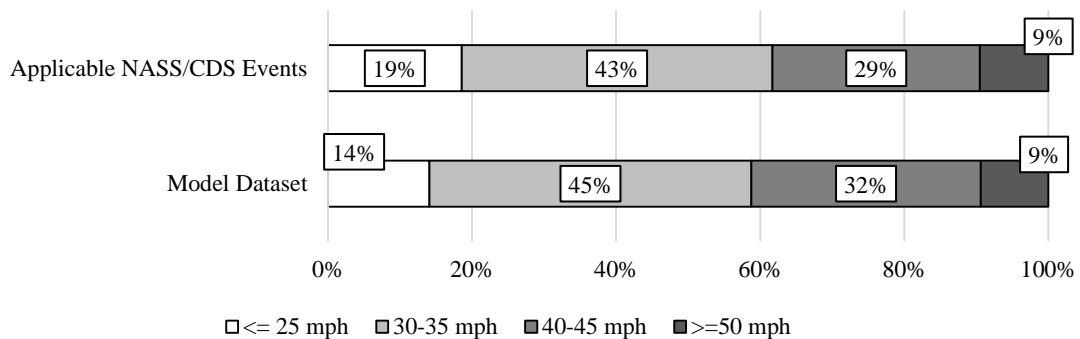


Figure 30. Comparing roadway speed limits between the datasets.

4.6 *Limitations*

There are several limitations that should be considered with regards to the dataset used in the current study. First, because NASS/CDS exclusively contains tow away crashes, the dataset may be biased toward more severe crashes. Additionally, for an EDR record to be considered in this study, the vehicle must have experienced either an airbag deployment and/or a delta-v greater than 5-mph. This may limit the generalizability of the results to less severe crashes. Second, it is important to recognize that the drivers included in this study did not complete their intersection traversal due to either (a) being impacted or (b) initiating crash avoidance braking. As such, caution should be used if attempting to use these models to simulate a full acceleration profile up to some desired speed.

4.7 *Conclusions*

This paper presents novel acceleration profile models that are representative of pre-crash acceleration behavior. These models were developed using EDR-recorded pre-crash data taken from vehicles involved in U.S. intersection crashes. A comparison of non-crash acceleration behavior in normal driving with pre-crash driver behavior suggests that drivers in intersection crashes may tend to accelerate more aggressively than drivers in non-crash traversals. These findings have important implications for designers of I-ADAS and for evaluators of active safety technology. Accounting for how drivers accelerate prior to real-world crashes is an important component for ensuring the effectiveness of I-ADAS in the U.S. vehicle fleet.

5. Analysis of Driver Evasive Maneuvering prior to Real-World Intersection Crashes²

5.1 Introduction

The analysis of evasive action during current intersection crashes may give important insight to designers of I-ADAS. First, analyzing the frequency of evasive action may indicate whether drivers were aware of an impending crash. The proportion of drivers that did not attempt to avoid the crash could serve as a metric for I-ADAS designers to improve upon. Second, if we can determine when drivers took evasive action to avoid a crash, this could provide I-ADAS designers with a target for when to provide warnings. Third, I-ADAS designers will need information about the direction that drivers currently perform evasive steering during intersection crashes. Any potential automated lateral evasive action taken by an I-ADAS system would likely depend on the direction that drivers currently undertake. Fourth, this study quantified the magnitude of these evasive actions. One strategy might be for future I-ADAS to amplify the braking or steering of drivers.

Several research questions were posed for the analysis of crash avoidance braking and steering behavior of drivers involved in intersection crashes. The first question was to simply determine whether current drivers were aware of an impending crash as measured by whether they took any evasive actions once they detected the impending crash. Conversely, a related question is how many drivers were unaware of the impending impact as measured by the lack of any evasive action. The next question was to determine when current drivers took evasive action. Finally, this study

² The work shown in this study has been a part of several previously published peer-reviewed manuscripts, including: 130. Scanlon, J.M., K.D. Kusano, and H.C. Gabler, *Analysis of Driver Evasive Maneuvering Prior to Intersection Crashes Using Event Data Recorders*. Traffic Injury Prevention, 2015. **16**(sup2): p. S182-S189.

looked to characterize any avoidance actions of current drivers, i.e. braking deceleration and steering input.

5.2 *Methods*

Data Source

This study used extracted EDR data from intersection collisions investigated as part of the NASS/CDS years 2001 to 2014. Chapter 2 describes this data source and the criteria used for EDR exclusion.

Three EDR pre-crash vehicle parameters were used in this study, i.e. vehicle indicated speed, brake application, and vehicle yaw rate. Vehicle indicated speed was measured based on wheel rotation. Brake application was recorded as whether the brake pedal had been pressed (0=Non-engaged, 1=Engaged). The vehicle's yaw rate was measured in degrees per second. EDR sampling rates depended on the pre-crash variable being analyzed and varied between 1, 2, 5, or 10 Hz. Pre-crash speed, braking, and steering data were always recorded at the same sampling rates, whereas the sampling rate of yaw rate was typically higher. EDR data was only included in this study if 5 seconds of pre-crash data were recorded.

Pre-crash Movement Classification

Each vehicle was assigned to one of three pre-crash movements: 1) “travelling through”, 2) “completely stopped”, or 3) “rolling stop”. Example cases of these pre-crash movements can be found in Figure 31, Figure 32, Figure 33, and Figure 34. Pre-crash movements were assigned based on recorded vehicle indicated speed data and turning behavior.

In general, a “completely stopped” driver was one who came to rest (zero-velocity) prior to accelerating through the intersection. A “rolling stopped” driver is one who slowed for a stop sign or red light and then accelerated into the intersection prior to coming to rest. Based on observations from the 100-Car NDS analysis and using EDR data, drivers that are performing rolling or complete stops generally stop before entering the intersection and then accelerate as they cross into the intersection. One exception to this is in LTAP/OD crashes, where it is not uncommon to see a driver stop within the intersection, wait for oncoming vehicles to pass, and accelerate through the intersection.

A “travelling through” driver is all remaining drivers who do not come to a complete or rolling stop. “Travelling Through” behavior would be observed, for example, if the driver had a green light on their approach or no traffic control device at all (i.e., two-way stop-controlled intersection). Occasionally, “travelling through” behavior is observed for drivers approaching a stop sign, which is typically the result of the driver failing to see the stop sign [180]. As discussed and observed in Chapter 3, travelling through driving behavior depends on the turning intention of the driver. Non-turning drivers (shown in Figure 32) tend to maintain a speed during the approach and traversal, and occasionally, accelerate if they attempt to “beat the yellow” signal phase change [116]. As shown in Figure 31, for left-turning drivers, drivers tend to slow as they approach and enter the intersection and accelerate as they leave the intersection [116-118].

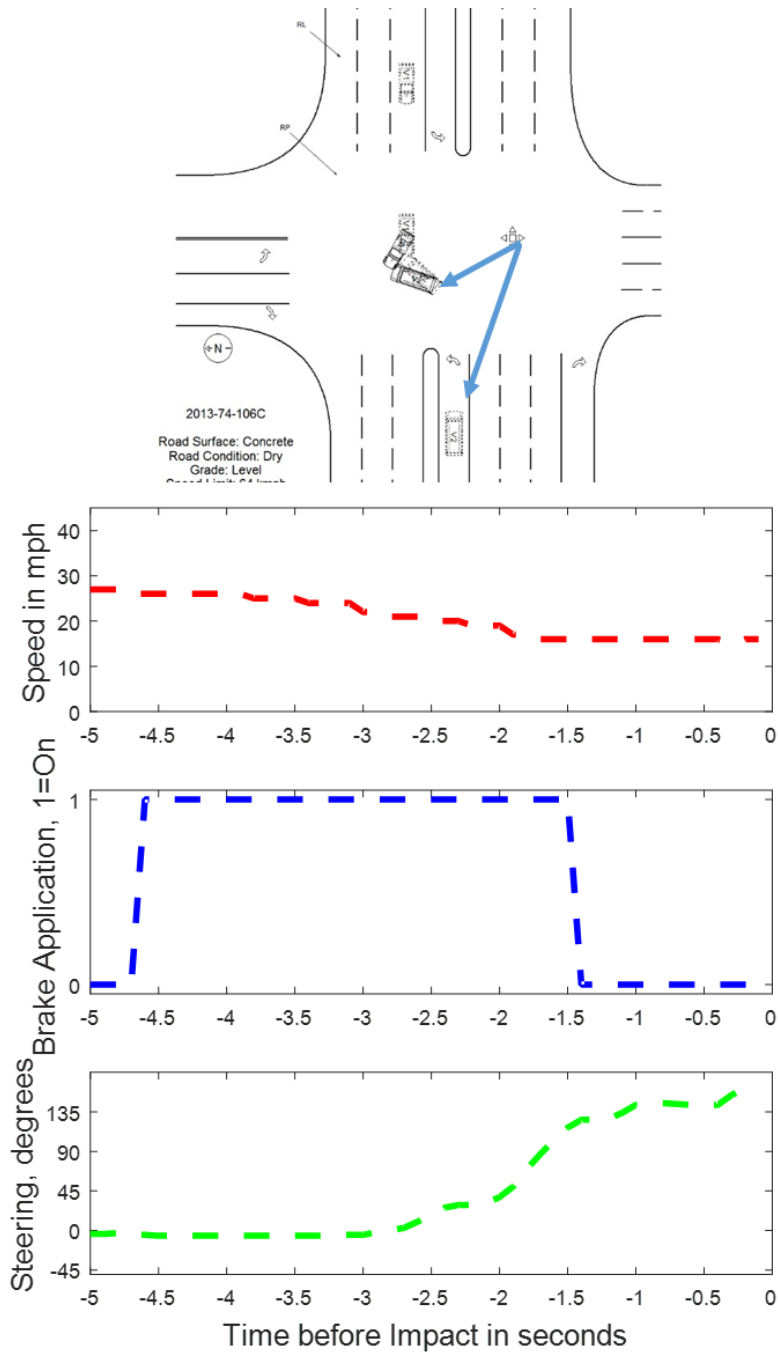


Figure 31. Example EDR (NASS/CDS 2013-74-106) recorded vehicle indicated speed profiles (sampled at 10 Hz). The subject vehicle (indicated by blue arrow) turned left while travelling through an intersection without yielding. The driver was then struck by a straight crossing vehicle travelling from the opposite direction. The subject vehicle did not take any evasive braking action. Based on a spike in yaw rate just before impact, which is not depicted, the driver likely attempted an evasive steering maneuver to the left just before impact. The image depicts a left turn across path/ opposite direction (LTAP/OD) intersection crash.

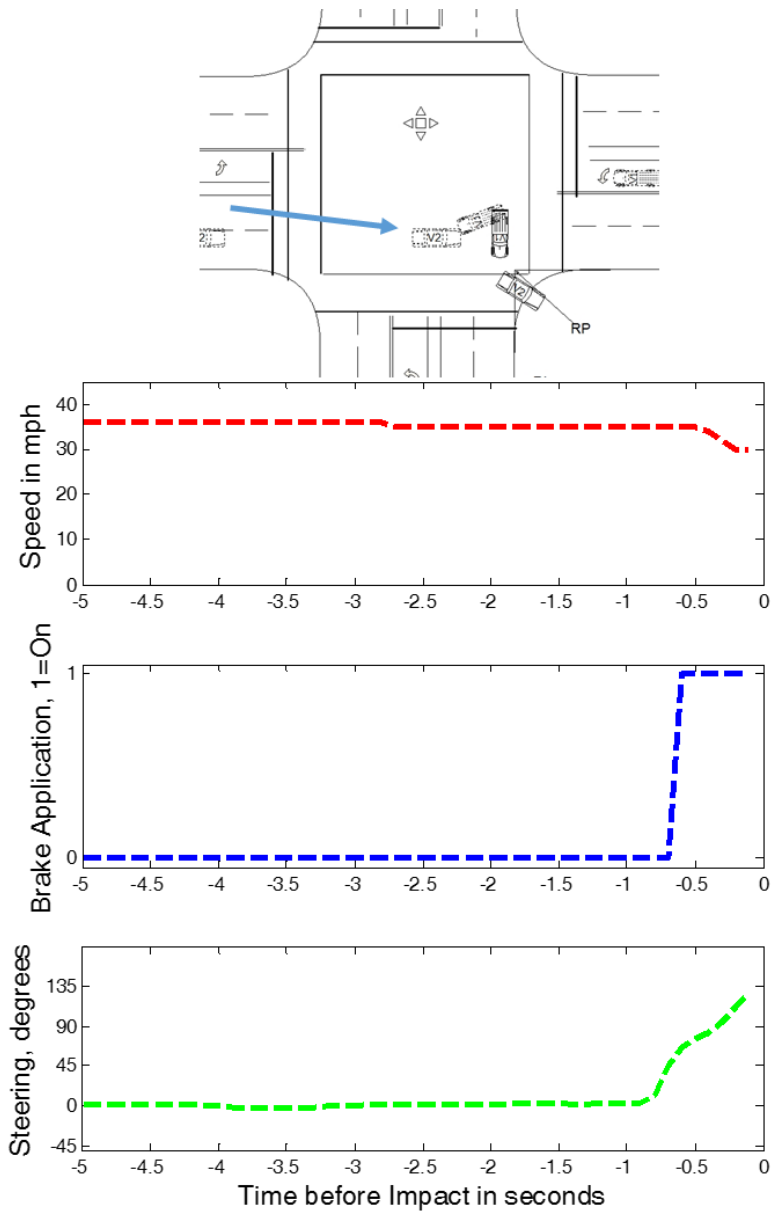


Figure 32. Example EDR (NASS/CDS 2013-78-145) recorded vehicle indicated speed profiles (sampled at 10 Hz). The subject vehicle (indicated by blue arrow) travelled straight through an intersection without yielding. The driver then struck a left turning vehicle. The subject vehicle performed an evasive braking and evasive steering maneuver in the last second (braking = 0.6 seconds, steering = 0.7 seconds) before impact. The image depicts a left turn across path/ opposite direction (LTAP/OD) intersection crash.

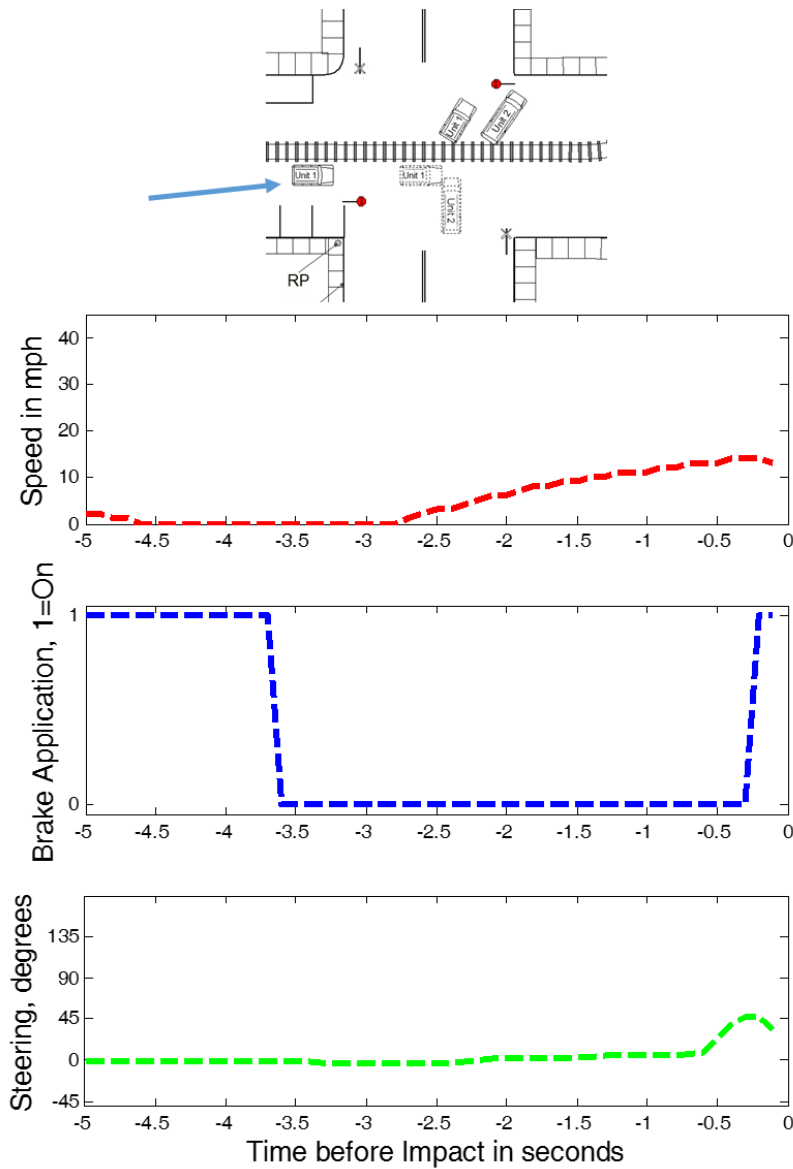


Figure 33. Example EDR (NASS/CDS 2013-76-166) recorded vehicle indicated speed profiles (sampled at 10 Hz). The subject vehicle (indicated by blue arrow) performed a complete stop, and then accelerated straight through an intersection. The driver then struck a vehicle that has the right-of-way. An evasive braking and steering maneuver were performed in the last second (braking = 0.2 seconds, steering = 0.5 seconds) before impact. The image depicts a straight cross path (SCP) intersection crash.

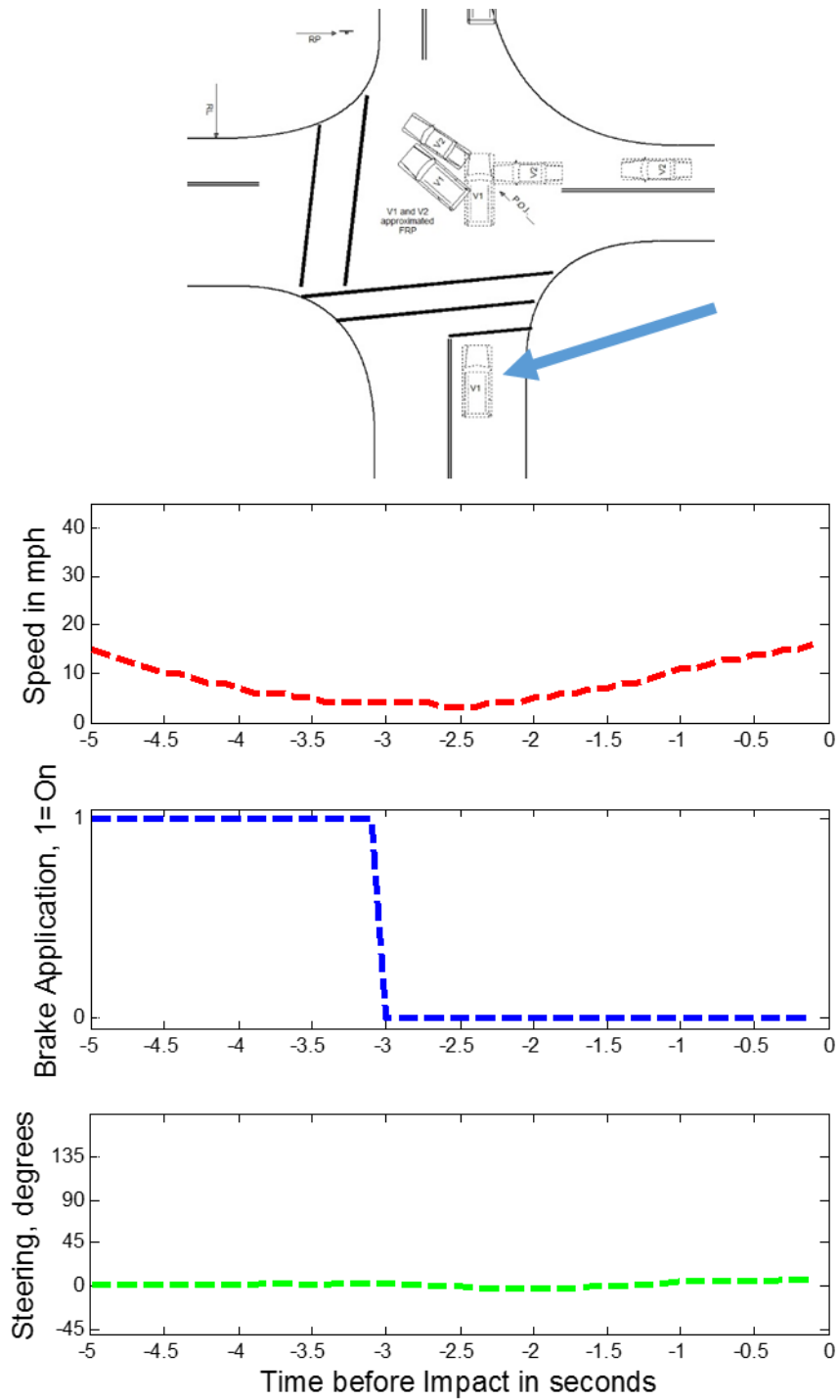


Figure 34. Example EDR (NASS/CDS 2011-43-163) recorded vehicle indicated speed profiles (sampled at 10 Hz). The subject vehicle (indicated by blue arrow) performed a rolling stop at 3 mph, and then accelerated straight across the intersection. The driver was then struck by a vehicle approaching from his left. The driver did not perform a steering or braking evasive maneuver. The image depicts a straight crossing path (SCP) intersection crash.

The criteria for labeling pre-crash movement can be found in Table 22. Vehicle indicated speed records were used to make pre-crash movement classifications.

Table 22. Pre-crash movement categories

Movement Group	Turning Behavior	Minimum Speed Threshold
Complete Stop	All	Minimum Speed == 0 mph
Rolling Stop	Straight	0 mph < Minimum Speed <= 20 mph
	left	0 mph < Minimum Speed <= 10 mph OR Minimum Speed > 10 mph AND Driver was accelerating when entering the intersection
Traveling Through	All	All remaining events

For a vehicle to be labeled as “completely stopped”, a zero-speed velocity followed by an acceleration into the intersection must have been observed in the pre-crash speed record.

Drivers must of course legally come to rest at stop signs. However, in the U.S. rolling stops are frequently observed at stop signs. At signalized intersections, drivers must stop at red lights. Occasionally, a traffic signal phase change occurs during the intersection approach, and the driver will then begin to accelerate into the intersection. In this study, the criteria for labeling a vehicle as “rolling stopped” depended on the turning behavior. For non-turning drivers to be “rolling stopped”, the vehicle velocity must have dipped below 20 mph (32 kph) followed by some acceleration through the intersection. In a prior analysis of stop sign violations [181], drivers that crossed into the intersections at speeds less than 20 mph tended to slow prior to entering the intersection. All remaining non-turning drivers were characterized as travelling through.

Left turning drivers were handled differently. As described previously, left turning drivers typically slow down as they approach intersections in order to complete the turn safely. Because

of this, a lower “rolling stopped” velocity dip threshold (10 mph, 24 kph) was used for drivers turning left at the intersection. This threshold was selected based on an analysis of 14,062 vehicle approaches to an instrumented intersection, and was collected by the Virginia Tech Transportation Institute (VTTI) using infrastructure based sensors as part of the Cooperative Intersection Avoidance System for Violation (CICAS-V) subtask 3.2 project [90]. Only drivers that had a green light while at least 40 m from entering the intersection were considered. Based on data observations, drivers that had a green light at 40 m from the intersection tended to be decelerating as they slowed down to complete the left turn (i.e., travelling through). In analyzing these 14,062 approaches, 99.9% of vehicles entered the intersection (crossed over the stop bar) at speeds in excess of 10 mph. There are some left turning drivers that may have performed a higher rolling stop speed and then accelerated as they entered intersection. In order to account for this behavior, if the driver was accelerating as they crossed into the intersection, the driver was also classified as rolling stopped. The location where the vehicle entered the intersection was determined by reconstructing the path of each vehicle prior to impact back to the location where the driver crossed the stop bar, crosswalk, or intersection boundary line. This technique is described at length in Chapter 7.

Determining whether Evasive Braking and Steering Occurred

Evasive braking and steering were analyzed in the current study. Many drivers began to first apply the brakes within 0.5 s prior to impact. This “last moment” braking behavior was classified as a crash avoidance maneuver. If at least 0.5 s of braking data was recorded, a 0.3 g deceleration threshold was used to determine whether the observed braking was, in fact, a crash avoidance maneuver. Many EDRs sample speed and braking data at 1 Hz, so for 1 Hz EDRs where drivers were decelerating for at least 1-s, deceleration was computed over the entire 1-s interval. This

deceleration threshold was established, because left turning drivers that are travelling through the intersection tend to apply the brakes during the intersection approach. Accordingly, brake application by itself is insufficient for identifying a braking maneuver. A 0.3 g threshold was selected based on an analysis of travelling through drivers extracted from the CICAS-V dataset (discussed in the preceding paragraph). The analysis of this compilation of 14,062 approaches revealed that 98.0% of drivers had a maximum deceleration less than 0.3 g (sample rate of 2 Hz) during the intersection approach.

Evasive steering was analyzed for non-turning drivers. The driver was assumed to have performed an evasive steering maneuver if a yaw rate greater than 4 degrees per second was recorded at the final time point prior to impact. This evasive steering trigger has been used previously during the 100-Car Naturalistic Driving Study to identify events such as crashes or near crashes [98]. The exclusion of left turning drivers is mainly due to difficulty in discerning normal turning behavior from evasive steering. Additionally, to further avoid any false-positive indications of evasive steering for non-turning drivers, vehicles that were on a curved road prior to impact or that were performing a lane change were excluded. These vehicles were identified using the coded “premove” variable in NASS/CDS.

Approach for Evasive Maneuver Frequency Analysis

The investigation first analyzed the frequency of evasive braking and steering for non-turning drivers. For inclusion in this investigation, the EDR module must have recorded both pre-crash braking and pre-crash yaw rate. As discussed, I restricted the analysis to straight crossing drivers that were not coded as having been travelling on a curved road or performing a lane change prior to impact.

In addition, the frequency of evasive braking was analyzed by itself, because of the large number of earlier generation EDRs available which recorded braking but not yaw rate data. This analysis was performed on straight crossing and left turning drivers. The purpose of this additional analysis was to examine factors that might influence likelihood that the driver takes some evasive action. A number of effects were explored, including driver gender, driver age, vehicle body type, pre-crash movement, traffic control device, turning behavior, and intersection crash mode.

To establish whether any of these effects significantly influenced likelihood of an evasive braking maneuver, logistic regression modeling was performed and a Wald test was used to determine significance (alpha level of 0.05). Whether or not the driver took evasive action was used as the dependent variable. logistic regression modeling for this study was performed using the “SURVEYLOGISTIC” procedure in the SAS 9.3 software package (SAS Institute, Cary, NC) [179]. In the event of statistical significance in one of the effects, the “LSMEANS” statement was used to perform a pairwise comparison between the different parameter levels.

Approach for Evasive Maneuver Timing Analysis

This study analyzed EDR pre-crash data to determine the timing of braking and steering with respect to time of impact. The timing of evasive braking for left turn, travelling through drivers was not performed. As discussed, these drivers commonly depress the brake pedal as they approach the intersection, and determining when evasive braking began cannot be done reliably for these drivers.

There are two sources of uncertainty in the time when either of these evasive actions was initiated. First, the EDR time coordinate system is not the same as the actual time coordinate system with respect to the time of impact. Because the time of impact is not, in general, recorded,

there is uncertainty in the offset between these two time axes. Second, pre-crash parameters are recorded at a relatively coarse frequency. There is some uncertainty in the timing of initial evasive maneuver time relative to the collected time point due to this discretization error. A further challenge when using EDR pre-crash data is that these sources of uncertainty vary by vehicle make, model, and year. The approach used in this study was to quantify the uncertainty in time for each case, and present a range of times for each data point of interest. In other words, I presented the earliest and latest time that drivers could have begun evasive maneuvering in each case.

A three-step approach was used to determine the beginning of evasive maneuvering relative to impact. The first step in this approach is to account for the offset between the EDR time coordinate system and the actual time coordinate system. Time offset represents the difference between the actual time zero and the EDR-recorded time zero as depicted in Figure 35.

Time Offset = Actual Time zero – EDR Time Zero

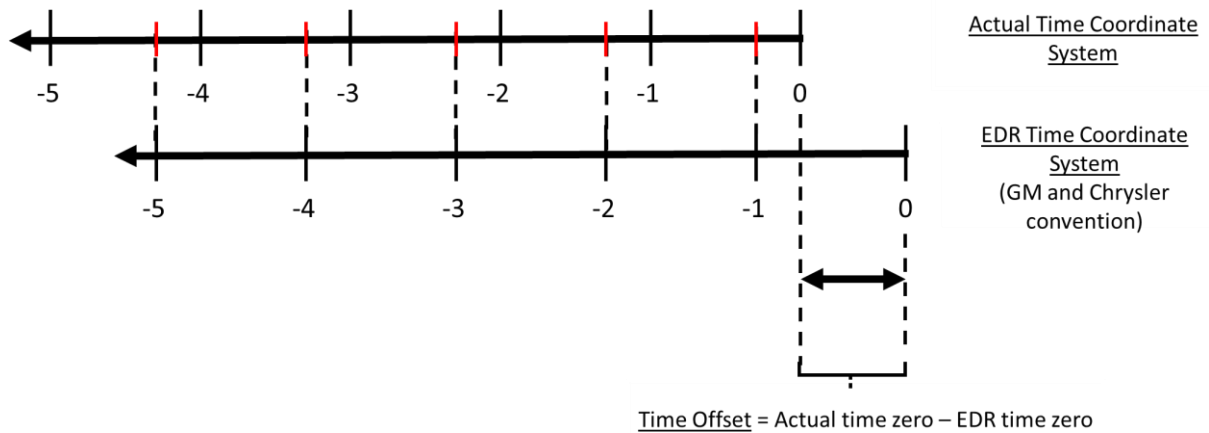


Figure 35. Comparison of the EDR time coordinate system and the actual time coordinate system.

EDR modules are continuously sampling data prior to any crash. In the event of a crash, pre-crash data recorded by the EDR for up to 5 seconds prior to impact is stored. However, in general,

it is unknown when these time points were collected relative to time of the impact. The convention of GM and Chrysler EDRs is to time stamp the last recorded EDR time point at $t = -1$ s, or as having been recorded at 1-second prior to impact [182, 183]. The convention of Ford EDRs is to time stamp the last recorded EDR time point at $t = 0$ s, or as having been recorded at impact [184]. Toyota EDR modules record an additional pre-crash value at impact, and record a “time from pre-crash to trigger” value, which can be used to determine the time offset [185]. “Time from pre-crash to trigger” was always rounded down to the nearest 100 ms, so each pre-impact time point could have been recorded up to 0.1s prior to the indicated time. The minimum and maximum time offset for pre-crash data collected at 1-Hz is shown for each vehicle manufacturer in Table 23.

Table 23. Minimum and maximum possible time offset uncertainty for EDRs of all four vehicle manufacturers included in this study. The table only shows the time offset uncertainty for a 1-Hz EDR.

Vehicle Manufacturer	Time Offset Uncertainty, s	Minimum Time offset, s	Maximum Time offset, s
GM	1.0	0.0	1.0
Chrysler	1.0	0.0	1.0
Ford	1.0	-1.0	0.0
Toyota	0.1	-0.1	0.0

The second step in this approach is to account for the uncertainty in the timing of initial evasive maneuver time relative to the collected time point. As an example, if brakes were off at $t = -4$ s, but on at $t = -3$ s, the driver could have begun braking anytime between $t = -4$ s and $t = -3$ s. We refer to the difference between the first recorded evasive maneuver time stamp and the actual start of the evasive maneuver as the discretization error. This discretization uncertainty refers to the difference between the maximum and minimum discretization error. Discretization uncertainty is directly dependent on the sampling rate of the data, which is shown in Table 24.

Discretization Error = Actual initial evasive maneuver time – First EDR-recorded evasive maneuver time

Discretization Uncertainty = Maximum Discretization Error – Minimum Discretization Error

Table 24. Minimum and maximum discretization error given EDR pre-crash sampling rate.

EDR recording rate (Hz)	Discretization Uncertainty, s	Minimum discretization error, s	Maximum discretization error, s
1	1.0	-1.0	0.0
2	0.5	-0.5	0.0
5	0.2	-0.2	0.0
10	0.1	-0.1	0.0

The final step in this approach is to determine the earliest and latest possible initial evasive maneuver time point. The total uncertainty for this initial evasive maneuver time point is equal to the sum of the time offset uncertainty and discretization uncertainty. In relation to the first EDR time-stamp of an evasive maneuver, the earliest and latest possible evasive maneuver time point can be determined using the equations below.

Total Uncertainty = Time Offset Uncertainty + Discretization Uncertainty

Latest Time = EDR Time Stamp + Max. Time Offset + Max. Discretization Error

Earliest Time = EDR Time Stamp - Min. Time Offset + Min. Discretization Error

An example of how each vehicle manufacturer records pre-crash data is shown in Figure 36. In this example case, the driver began to brake at 1.75 s prior to impact. We consider a scenario where

the EDR recorded pre-crash data at 1 Hz, and the last recorded data point was sampled 0.25 s prior to impact.

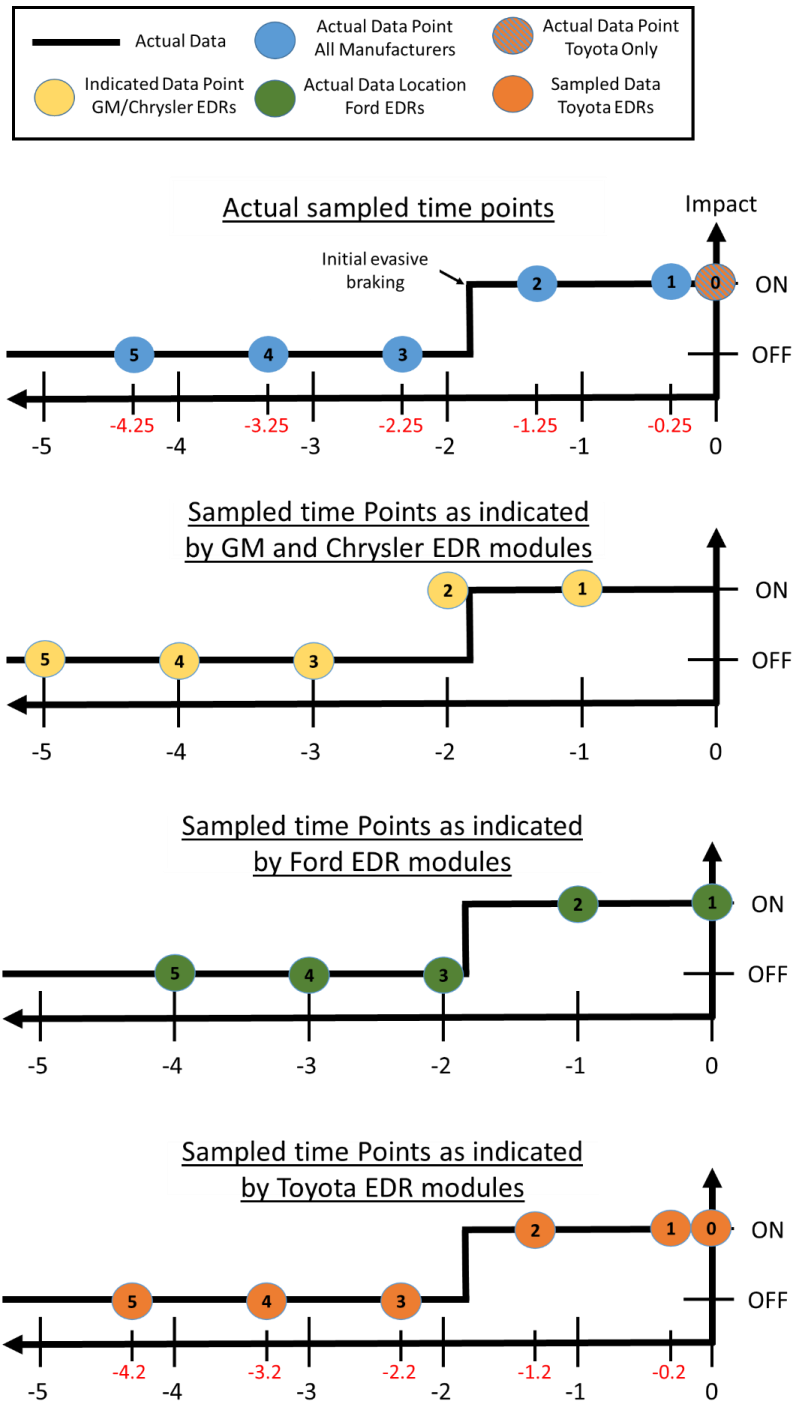


Figure 36. The figure depicts an example EDR braking time series. All of the data points are plotted on the actual time coordinate system. The actual points and timing of the EDR sampled time points are shown in

the first graph. The remaining three graphs show how each manufacturer EDR would timestamp the sampled data points.

The GM, Chrysler, and Ford EDRs would have recorded only 5 data points. The Toyota EDR would have recorded 1-extra data point at impact (a total of 6 time points). For the GM and Chrysler EDRs, the first braking time point would have been time-stamped at $t = -2$ s. For the Ford EDR, the first braking time point would have been time-stamped at $t = -1$ s. For the Toyota EDR, the first braking time point would have been time-stamped at $t = -1.2$ s. If given only the data recorded by each of these EDRs, there is uncertainty in when the braking began with respect to impact time. For the GM, Chrysler, and Ford modules, we only know that braking could have begun as early as $t = -3$ s and as late as $t = -1$ s, or 1 to 3 seconds prior to impact. For the Toyota modules, we know that braking could have begun as early as $t = -1.2$ s and as late as $t = -2.3$ s, or 1.2 to 2.3 seconds prior to impact. Given this uncertainty in the data, we present the earliest and latest possible times that evasive action could began. The computation for these times can be found in Table 25.

Table 25. Earliest and latest possible initial braking time point for an example case. The case assumes that an EDR that collects pre-crash data at 1-Hz was used. Vehicle braking began at 1.75 s prior to impact.

Vehicle Make	EDR time stamp, s	Min. Time offset, s	Max. Time offset, s	Min. discretization error, s	Max. discretization error, s	Earliest Possible Initial evasive time, s	Latest Possible Initial evasive time, s
GM	-2.0	0.0	1.0	-1.0	0.0	-3.0	-1.0
Chrysler	-2.0	0.0	1.0	-1.0	0.0	-3.0	-1.0
Ford	-1.0	-1.0	0.0	-1.0	0.0	-3.0	-1.0
Toyota	-1.2	-0.1	0.0	-1.0	0.0	-2.3	-1.2

Approach for Evasive Maneuver Kinematics Analysis

This study analyzed three sets of evasive maneuvering kinematics. First, evasive braking deceleration was analyzed. Second, maximum recorded yaw rate was analyzed. Third, the direction of any evasive steering maneuver was analyzed.

Average braking decelerations over the last 0.5 s prior to impact were extracted for drivers performing evasive braking. At least 0.5 seconds of braking must have been recorded by the EDR. Vehicle decelerations were not observed despite brake application for several cases with less than 0.5 seconds of braking, which is likely due to an inadequate amount of time to fully compress the brake pedal, and the low resolution and sampling rate at which some EDRs record vehicle indicated speed. If the vehicle was found to decelerate at over 1-g, wheel slip was assumed to have occurred, and the braking magnitude was not analyzed for that case. Vehicle indicated speed is inaccurate during wheel lockup due to slipping between the tire and ground, and can result in unrealistically high (> 1-g) deceleration values.

Evasive steering kinematics were analyzed for non-turning drivers that did not perform a lane change or that were not travelling on a curved road. Steering magnitude was analyzed using the maximum recorded yaw rate. The direction of the steering maneuver was analyzed by looking at the yaw rate sign at the maximum recorded value.

5.3 Results

Summary of Simulation Case Set

A total of 1,662 EDR modules that recorded pre-crash speed and were from 2000 to 2014 have been successfully extracted from U.S. intersection crashes investigated as a part of NAS/CDS. A total of 74 of these crashes were not an SCP, LTAP/LD, and LTAP/OD crash mode type. An

additional 10 cases were excluded for having case weights greater than 5,000. A total of 22 records were also excluded because of a low sampling rate (0.5 Hz) or because the vehicle was stopped for the entire pre-crash movement.

The remaining crashes were used to perform this study’s analyses. There were two unique EDR datasets that were used for this analysis. First, one dataset contains EDR modules with speed and braking data. This dataset consisted of 1,499 records, which were representative of 536,608 crashes nationally. A breakdown of this dataset can be found in Table 26. This dataset was used for performing the evasive braking analysis.

Table 26. Counts of EDRs containing vehicle speed and braking extracted are tabulated by crash mode. Tabulations with NASS/CDS case weights are additionally shown.

Intersection Crash Type	Turn Intent			
	Straight		Left	
	EDR Count (%)	Weighted Crashes (%)	EDR Count (%)	Weighted Crashes (%)
SCP	584 (54%)	191,724 (53%)	- (0.0%)	- (0.0%)
LTAP/OD	343 (32%)	119,002 (33%)	288 (69%)	133,435 (76%)
LTAP/LD	156 (14%)	49,413 (14%)	128 (31%)	43,036 (24%)
Total	1,083 (100%)	360,138 (100%)	416 (100%)	176,470 (100%)

Second, a smaller dataset containing EDR downloads with speed, braking, and vehicle yaw rate was extracted. A total of 164 records, which are representative of 63,409 crashes nationally were included. A summary of both datasets can be found in Table 27. This dataset was used for comparing evasive braking and evasive steering frequencies. As stated previously, left turning drivers and non-turning drivers that performed lane changes or that were travelling on a curved roads were excluded from this analysis.

Table 27. Counts of EDRs containing vehicle speed, braking, and yaw rate extracted are tabulated by crash mode. Tabulations with NASS/CDS case weights are additionally shown.

Intersection Crash Type	Turn Intent	
	Straight	
	EDR Count (%)	Weighted Crashes (%)
SCP	99 (60%)	37,769 (60%)
LTAP/LD	47 (29%)	19,224 (30%)
LTAP/OD	18 (11%)	6,416 (10%)
Total	164 (100%)	63,409 (100%)

How frequently do drivers take evasive action?

Braking vs. Steering Frequency

The frequency of evasive braking and steering was first examined using the dataset of 164 EDR modules with vehicle indicated speed, braking application, and vehicle yaw rate data. This smaller dataset where both elements were recorded in order to examine the frequency of braking and steering maneuvers together.

A summary of evasive maneuvering frequency by type can be found in Table 28. Evasive maneuvering was found to occur in 84% of analyzed crashes. Approximately one-third (33%) of the drivers performed both a braking and steering evasive maneuver. A total of 20% of drivers performed steering only, while 32% of drivers performed braking only. Around 16% of drivers did not perform any evasive maneuver.

Table 28. A summary of evasive maneuvering by maneuver type.

Evasive Maneuver	Unweighted		Weighted	
	Count	% of Total	Count	% of Total
Braking Only	42	26%	20,126	32%
Steering Only	26	16%	12,508	20%
Braking + Steering	61	37%	20,702	33%
No Evasive Maneuver	35	21%	10,073	16%
Total	164	100%	63,409	100%

Which factors potentially influence evasive braking frequency?

A detailed analysis of evasive braking used a second, larger dataset of 1,499 EDR modules that recorded vehicle indicated speed and braking application data. The purpose of this section was to observe effects on evasive braking frequency. A summary of some basic stats for evasive braking frequency by several parameters of interest can be found in Table 29. Overall, drivers performed an avoidance braking maneuver in 58% of all cases in this larger dataset with only braking data. This proportion is very similar to the previous dataset with braking and steering data (65%).

There are a few trends to observe from this data. First, the data suggests that young (49%) and senior drivers (39%) may take evasive braking action less often than adult drivers (65%). Second, drivers that performed complete and rolling stops (39%) evasively braked substantially less than drivers that were travelling through the intersection (68%). Third, evasive braking was less common when proceeding from a stop sign (37%) than compared to drivers at traffic lights (59%) and drivers without a traffic control device (66%). Fourth, the turning behavior of the driver and the traffic control device both appear to be correlated with evasive braking frequency. Drivers turning left that were involved in LTAP/OD (43%) and LTAP/LD (46%) crashes evasively braked less often than straight crossing drivers in SCP (56%), LTAP/OD (77%) and LTAP/LD (73%) crashes.

Table 29. Composition of Evasive Braking Dataset.

Factor	Factor Level	Unweighted				Weighted			
		Count		% of Total		Count		% of Total	
		No Brake	Brake	No Brake	Brake	No Brake	Brake	No Brake	Brake
All Cases	---	651	848	43%	57%	224,815	311,793	42%	58%
Driver Gender	Male	282	361	44%	56%	91,768	111,058	45%	55%
	Female	319	412	44%	56%	103,634	156,558	40%	60%
	Unknown	50	75	40%	60%	29,413	44,177	40%	60%
Vehicle Body Type	Car	413	509	45%	55%	141,224	197,883	42%	58%
	LTV	238	339	41%	59%	83,591	113,910	42%	58%
Driver Age Group	Young (age≤20)	71	84	46%	54%	29,980	28,685	51%	49%
	Adult (20<age<65)	405	583	41%	59%	113,824	207,149	35%	65%
	Senior (age≥65)	121	102	54%	46%	49,342	30,896	61%	39%
	Unknown	54	79	41%	59%	31,669	45,062	41%	59%
Driver Pre-crash maneuver	Stopped	319	163	66%	34%	114,217	71,653	61%	39%
	Travelling	332	685	33%	67%	110,598	240,140	32%	68%
Traffic Control Device	None	112	257	30%	70%	49,161	95,620	34%	66%
	Traffic Light	405	513	44%	56%	135,667	193,463	41%	59%
	Stop Sign	131	75	64%	36%	38,022	22,223	63%	37%
	Unknown / Other	3	3	50%	50%	1,965	488	80%	20%
Turning Behavior – Crash Mode	Straight SCP	277	307	47%	53%	84,953	106,770	44%	56%
	Straight LTAP/OD	81	262	24%	76%	27,337	91,664	23%	77%
	Left LTAP/OD	174	114	60%	40%	75,964	57,471	57%	43%
	Straight LTAP/LD	38	118	24%	76%	13,199	36,214	27%	73%
	Left Turn LTAP/LD	81	47	63%	37%	23,362	19,674	54%	46%

It is, of course, important to statistically analyze these effects in order to determine whether the observed differences in evasive frequency are, in fact, significant. Table 30 shows results from a Wald chi-square test for each of the aforementioned parameters of interest. Several significant differences (alpha level of 0.05) were observed for the various effects, including driver gender, driver age, and pre-crash maneuver. A near-significant difference was also observed for the turning maneuver / crash mode interaction effect.

Table 30. Results from the Wald test used to examine factors that significantly influence likelihood of taking evasive action. A * was used to identify parameters found to be statistically significant. A + was used to identify variables that were just above the established alpha level (0.05).

Variable	Parameter	Coefficient	χ^2	p-value
Intercept		-1.338	---	---
Driver Gender	Female	0.292	7.798	0.020*
	Unknown	1.872		
	male	0.000		
Vehicle Body Type	Car	0.165	0.635	0.426
	LTV	0.000		
Driver Age	Adult (20<age<65)	0.513	19.948	<0.001*
	Senior (age≥65)	-0.548		
	Unknown	-1.330		
	Young (age≤20)	0.000		
Driver Pre-crash maneuver	Stopped	-0.879	7.583	0.006*
	Travelling Through	0.000		
Traffic Control Device	None	1.521	5.625	0.131
	Traffic Light	1.310		
	Stop Sign	0.836		
	Unknown / Other	0.000		
Turning Behavior – Crash Mode	Left-LTAP/LD	0.374	9.137	0.058+
	Left-LTAP/OD	-0.277		
	Straight-LTAP/LD	0.386		
	Straight-LTAP/OD	0.768		
	Straight-SCP	0.000		

Pairwise comparisons were performed in order to evaluate which factor levels differed from one another. First, for driver gender, differences were observed between the male - unreported

gender comparison and female - unreported gender comparison. No differences were observed between male and female drivers, which was anticipated based on the prior proportional analysis. Second, for driver age, senior drivers were found to take evasive braking action less frequently than adult drivers. Specifically, adult drivers were found to be around 2.9 times more likely to take evasive braking action than their senior counterparts. Third, drivers that came to a complete or rolling stop were less likely to evasively brake than driver who travelled through the intersection. Drivers that travelled through the intersection were approximately 2.4 times more likely to take evasive braking action. Fourth, two differences were observed in the levels of the turning – intersection group interaction effect. However, because the variable effect was near-significant ($p=0.058$), the results should be interpreted with caution. The non-turning driver in LTAP/OD crashes was found to evasively braking about 2.8 times more frequently than the left turning driver in LTAP/OD crashes. In addition, non-turning drivers in LTAP/OD crashes were found to take evasive braking action 2.2 times more frequently than non-turning drivers in SCP crashes.

Initial Evasive Maneuver Time of Drivers prior to Intersection Crashes

The time when the brakes were first applied and steering first initiated was examined independently. A total of 788 subject vehicles that braked and 87 subject vehicles that steered were available to examine the timing of evasive maneuvering. As discussed in the methods, left turn, travelling through drivers were not included in the evasive braking time analysis. It should be noted that the timing of braking and steering were examined independently, and some drivers could have braked and steered. The results present the earliest and latest possible median initial evasive maneuver time given the inherent uncertainty in the timing of evasive maneuvering relative to impact.

First, an analysis was performed on the timing of evasive braking using the full set of 788 drivers that took evasive braking action. Cumulative distributions of the time of evasive braking can be found in Figure 37 . The median time of braking was found to be between 0.1 to 2.0 seconds prior to impact. Three-fourths of drivers began to brake sometime between 1.0 to 2.0 seconds prior to impact. Three-fourths of drivers began to brake sometime between 1.0 to 2.0 seconds prior to impact.

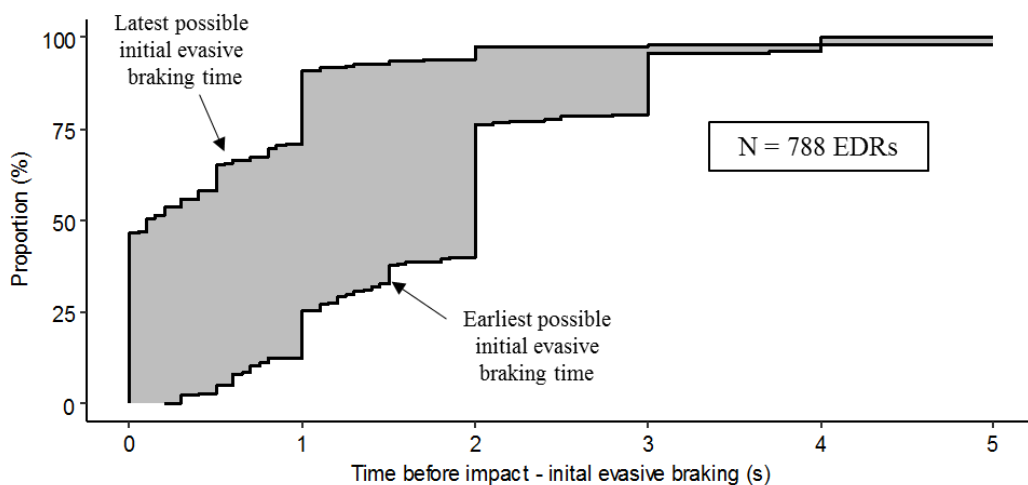


Figure 37. Weighted cumulative distributions of evasive braking time points. All EDR modules with evasive braking were considered. Due to uncertainty in the time at which the evasive maneuver began, minimum and maximum possible time points are provided.

As discussed, and as can be visualized by the grey area in Figure 37, there can be considerable uncertainty in the timing of evasive braking. In particular, this uncertainty is substantially higher for records with pre-crash braking recorded at 1 Hz (65% of extracted records). To better understand when evasive braking typically begins, a smaller dataset of 248 records, where braking was sampled at 2 Hz or higher was analyzed. The results from this analysis can be seen in Figure 38. The median range of times for when initial evasive braking started was found to be narrowed to between 0.4 s and 1.0 s prior to impact. A total of 75% of evasive braking events began 0.8 to 1.5 s prior to impact.

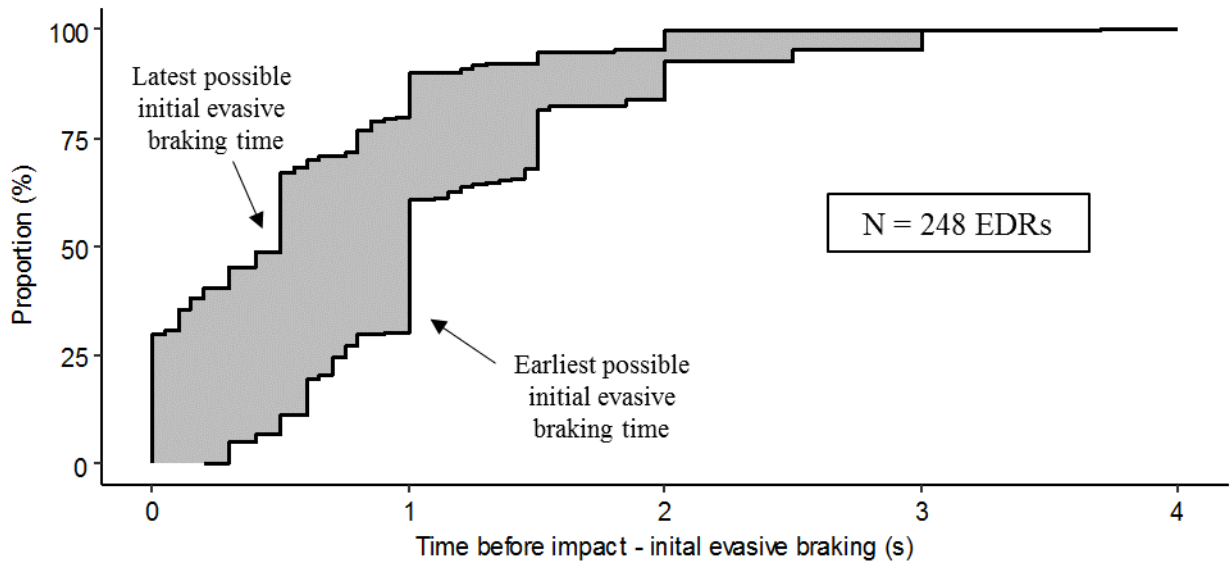


Figure 38. Weighted cumulative distributions of evasive braking time points. Only modules that recorded pre-crash braking at 2 Hz or higher were considered. Due to uncertainty in the time at which the evasive maneuver began, minimum and maximum possible time points are provided.

Next, an analysis was performed on the timing of evasive steering. Yaw rate is typically sampled at 5 or 10 Hz (85% of modules). This timing analysis focused solely on the 68 set of records where (a) the driver took evasive steering action and (b) yaw rate sampling was at least 5 Hz. The time when evasive steering began was found to be 0.2 to 0.4 s prior to impact. A total of 75% of evasive steering events were initiated 0.5 to 0.7 s prior to impact.

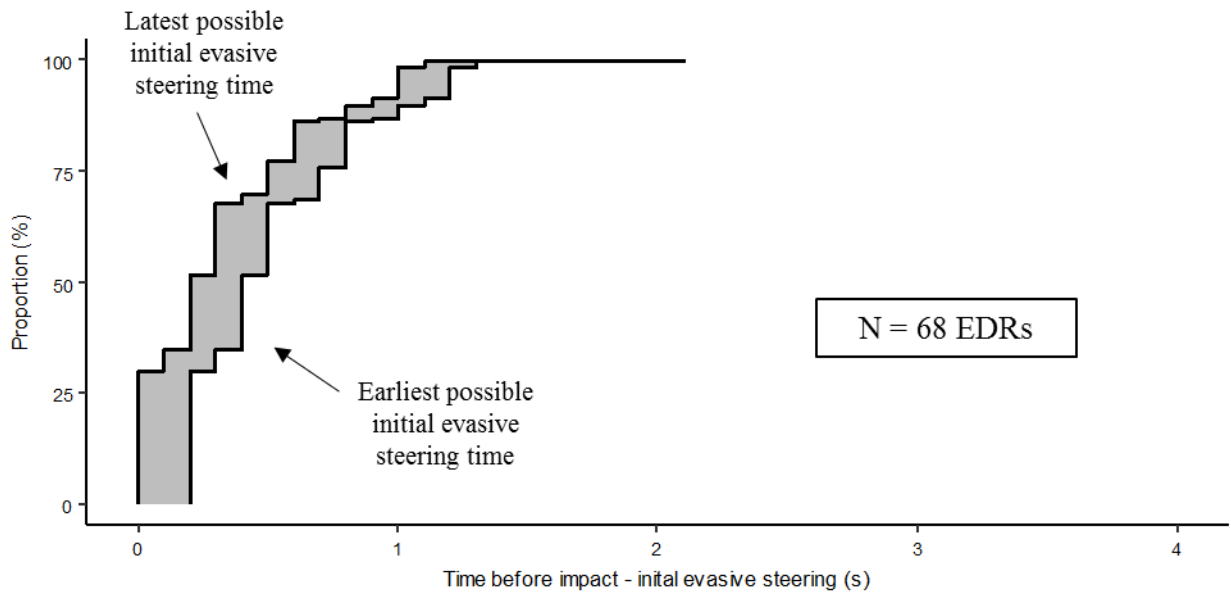


Figure 39. Weighted cumulative distributions of evasive steering time points. Due to uncertainty in the time at which the evasive maneuver began, minimum and maximum possible time points are provided.

Evasive Maneuver Kinematics

Evasive Braking Decelerations prior to Intersection Crashes

The next objective was to determine the magnitude of braking deceleration. As mentioned, only vehicles with at least 0.5 s of evasive braking and no wheel slip were considered for this analysis. Of the 843 records with evasive braking action, 332 records met the inclusion criteria.

Results from the evasive braking magnitude analysis can be found in Figure 40. The median average evasive braking deceleration recorded by the EDRs was found to be 0.55 g. A total of 75% and 95% of deceleration values fell below 0.72 g and 0.91 g, respectively.

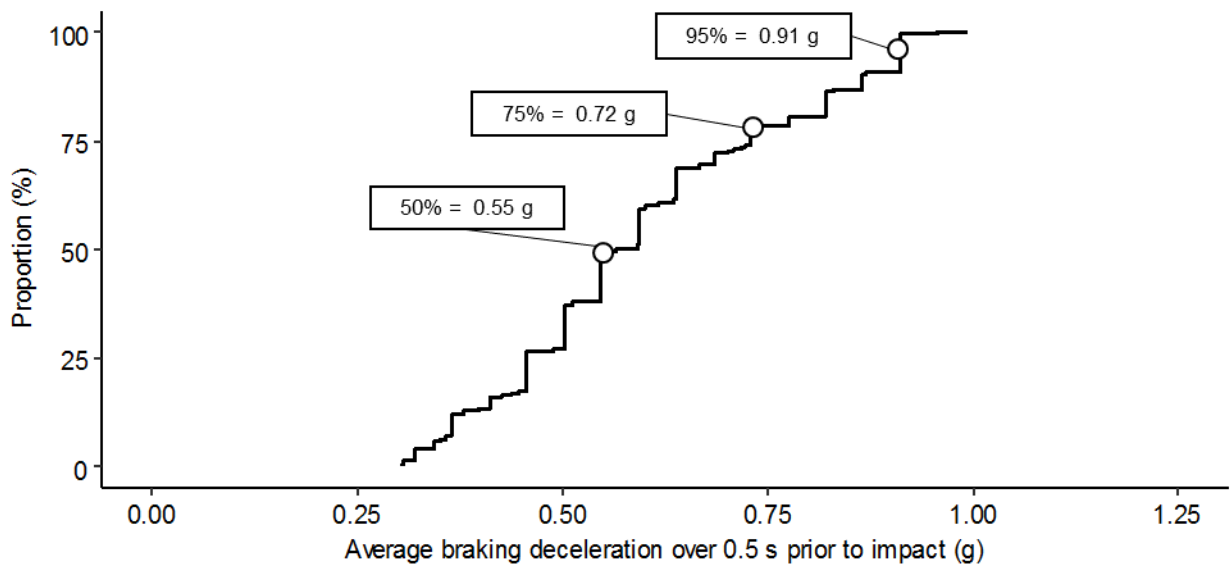
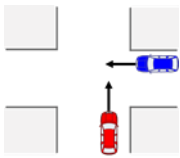
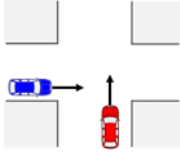
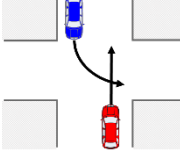
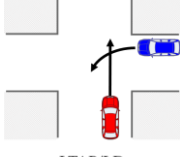


Figure 40. Weighted cumulative distribution of maximum evasive braking decelerations.

Evasive Steering Kinematics prior to Intersection Crashes

The 87 vehicles that performed an evasive steering maneuver were used to investigate evasive steering direction. A breakdown of evasive steering direction by crash configuration can be found in Table 31. In general, evasive steering tended to be to the right (61%), but this was not consistent across all crash modes. For SCP crashes with an oncoming vehicle approaching from the right, the driver steered to the right 69% of the time. In SCP crashes where the vehicle was approaching from the left, the driver steered to the right 42% of the time. In LTAP/OD crashes, the driver steered to the right 70% of the time. In LTAP/LD crashes, evasive steering was almost always to the right (86% of the time). Note that this analysis is based on a small sample, and should be revisited when additional EDR data becomes available.

Table 31. Frequency counts of evasive steering direction by crash configuration. The red car in the depicted scenes represent the EDR-equipped vehicle, while the blue car represents the other vehicle.

Crash Configuration	Steering Direction (red vehicle)	Unweighted		Weighted	
		Count	% of Total (within crash configuration)	Count	% of Total (within crash configuration)
 SCP (right)	Right	18	78%	7,232	69%
	Left	5	22%	3,223	31%
 SCP (left)	Right	13	52%	5,246	42%
	Left	12	48%	7,151	58%
 LTAP/OD	Right	17	59%	4,846	70%
	Left	12	41%	2,048	30%
 LTAP/LD	Right	7	70%	2,995	86%
	Left	3	30%	470	14%

Maximum evasive vehicle yaw rate was investigated using the 87 vehicles that performed an evasive steering maneuver. A cumulative distribution of maximum evasive yaw rates can be found in Figure 41. The median of the maximum evasive yaw rates was found to be 10 degrees/s. A total of 75% and 95% of maximum vehicle yaw rates were below 18 and 24 deg/s, respectively.

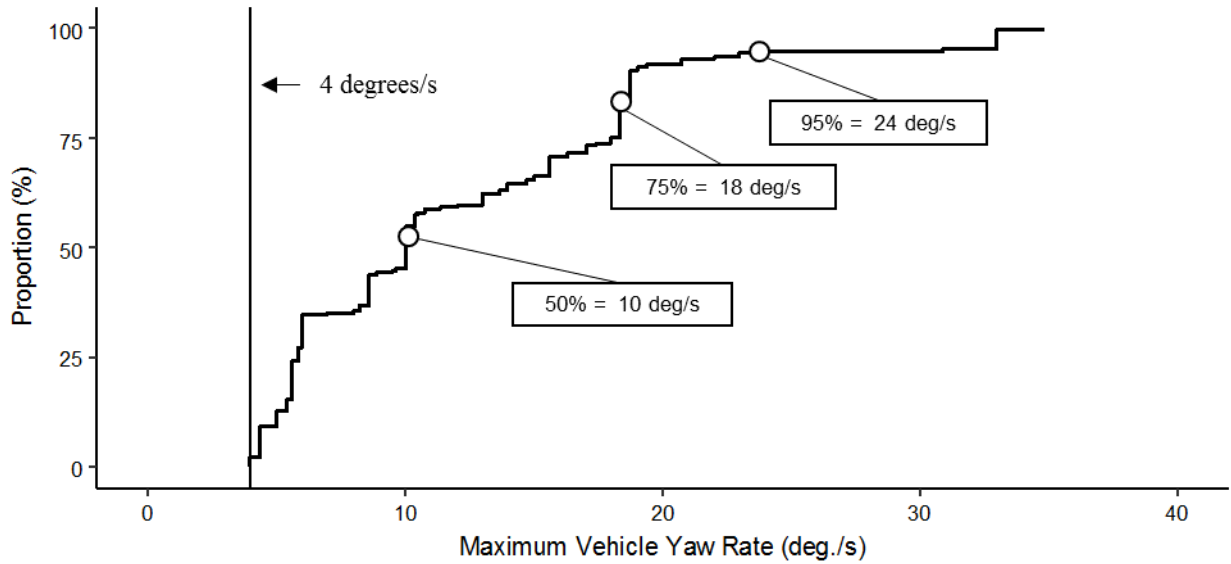


Figure 41. Weighted cumulative distribution of maximum evasive vehicle yaw rate.

5.4 Discussion

Implications for I-ADAS

Braking and Steering Frequency

The large proportion of drivers that performed some crash avoidance maneuver suggests that a majority of the drivers involved in intersection crashes were aware of an impending crash at some point prior to impact. Approximately one-third of drivers used a combination of both evasive steering and braking. Braking (32%) and steering (20%) by themselves occurred frequently as well. These findings are important for I-ADAS developers for two reasons. First, less than one-fifth of the drivers analyzed in this study failed to take any evasive action. One goal of an I-ADAS system may be to improve threat awareness for this group. Second, the large proportion of drivers that took evasive action offers promise that these drivers may have been sufficiently attentive to receive and react to an I-ADAS warning. However, it should be noted that this was not a hypothesis tested in this study, and additional information from the driver would be required to confirm this theory. Additionally, these findings should not be interpreted as a measure of the potential effectiveness of an I-ADAS alert. Many factors (e.g. timing of a warning, reaction time of the driver, appropriate reaction of the driver, and roadway/vehicle/crash characteristics) will all likely play a role in the driver response to an I-ADAS alert.

An analysis on a large sample of 1,499 modules that recorded evasive braking was performed to investigate the effects of various factors on likelihood of taking evasive action. There were two notable findings. First, the significantly smaller fraction of drivers that evasively braked following rolling and complete stops is an interesting finding of this study, and suggests that a majority of these drivers may not have been aware of an impending crash. As evidenced by findings later in

this dissertation, I-ADAS may be most effective at detecting and alerting drivers of an oncoming vehicle when the vehicle is proceeding into the intersection at a low speed (i.e., a greater amount of time to react to a potential threat). These results further suggest that I-ADAS, in general, may be most effective at alerting this subset of drivers that proceed into intersection from a rolling or complete stop by allowing them to take some evasive action either through providing a warning or utilizing AEB..

Second, senior drivers (over 65 years old) were found to be around 3 times less likely to evasive braking action less than adult drives (21-64 years old). A lower, insignificant proportion of younger drivers (20 years old or less) when compared to the adult bracket were found to have taken evasive braking action as well. One theory for these findings is that the lower proportion of evasive braking maneuvers is a result of less visual scanning for oncoming vehicles. Limited visual scanning during intersection entry has been well documented in past literature for both young and senior age groups [186, 187]. Additionally, senior drivers have shown diminished cognitive-motor abilities [188] and slower decision making [189-191]. These results provide evidence that I-ADAS may prove especially helpful for the senior demographic, which failed to detect and/or react soon enough to evade a potential collision partner.

Braking and Steering Timing

Three-fourths of drivers were found to begin braking at a maximum of 1.5 seconds prior to impact and steering at a maximum of 0.7 seconds prior to impact. The initial braking time of vehicles involved in intersection crashes was compared with the initial braking time of vehicles involved in rear-end crashes. Kusano and Gabler [42, 112] found that approximately 25% of drivers began evasively braking within the last second prior to impact. 75% of drivers began

evasive braking within the last two seconds prior to impact. Our study of intersection crash evasive braking found that most drivers brake at roughly the same time as drivers in rear-end crashes.

In a similar experimental study on evasive braking and steering in near-crash intersection scenarios, Mazzae et al. [192] examined the timing of evasive maneuvering in 192 research subjects while driving on dry pavement. They found that 52% of drivers steered before braking, and 46% of drivers braked before steering. The remaining 2% performed only one evasive maneuver. For drivers that braked before steering, they found subjects initiated braking 0.55 seconds earlier than steering.

Braking and Steering Kinematics

Three kinematics analyses were performed. The first examined the magnitude of evasive braking decelerations. The second examined the magnitude of evasive steering yaw rates. The third examined the direction of any evasive steering maneuver.

The median average deceleration observed in this study (0.55 g) was similar to that observed by Kusano and Gabler [42, 112] in a study analyzing EDR evasive braking during rear-end crashes. They found the average deceleration of vehicles to be 0.52 g. In general, quantifying magnitudes of both evasive braking and steering maneuvers may prove useful for calibrating I-ADAS technology. First, when developing these systems, it may help designers to have estimates of typical evasive action magnitudes during real-world crashes. One specific example is for projecting system effectiveness, such as in the benefits study presented in Chapter 11. Information on how drivers respond to a warning of a crash imminent scenarios can help in evaluating how effective this technology will be in the vehicle fleet. Second, automated emergency braking (AEB) is already present within the vehicle fleet [82, 83], and autonomous steering systems are likely to

emerge in the coming years [193, 194]. Knowledge of how drivers currently take evasive action could prove helpful in tuning systems toward how human drivers would respond.

It should be noted that this analysis focuses exclusively on driver action in scenarios where a crash was not avoided. It takes time to compress the brake pedal and turn the steering wheel. Accordingly, many of these evasive actions were likely incomplete, i.e. maximum steering and braking magnitudes not achieved. These results can, accordingly, be considered a lower bound for maximum evasive maneuvering action.

In all four crash configurations analyzed, evasive steering direction was found to be more frequently (61%) to the right. These results should be regarded with caution, because of the very low case counts available for this analysis. There are a number of crash-specific factors that could influence evasive steering. It is not clear if the evasive steering direction is dependent on the timing of when the driver initially became aware of an imminent crash, the direction of the oncoming vehicle, and/or some natural tendency for drivers to turn to the right (e.g., based on handedness [195]). For instance, it may not always be beneficial to evasively steer prior to intersection crashes. Other traffic on the roadway, unique road geometry, or adverse surface conditions in actual crashes may limit the driver's ability to perform an evasive steering maneuver in a particular direction. Additionally, on U.S. roadways, steering to the left could lead the driver to travel into the path of oncoming traffic.

5.5 *Limitations*

This study has a number of limitations. At least one vehicle had to be towed away from the scene to be included in this database. As such, our dataset may have been biased toward more severe crashes, where vehicles were travelling at faster speeds. These faster speeds would have

yielded less time for drivers to evasively react, and thus, this sample of crashes may underestimate the proportion of drivers that evasively maneuver in all crashes. Additionally, the dataset may be biased toward drivers that began evasively maneuvering closer to impact. Lastly, the amount of time available for the driver to react would influence the resulting evasive maneuver magnitude. There may be some limitations in generalizing these results to all crashes, such as, these crashes may occur closer to impact, which could limit the amount of time available to fully compress the brake pedal or steer the vehicle.

Caution should be used when interpreting the frequency of evasive steering and braking from the EDR results in this study. Our assumption was that any braking at the last EDR-recorded time point and/or a substantially high deceleration just prior to impact indicated an evasive braking maneuver. A yaw rate magnitude greater than 4 degrees per second immediately prior to impact was assumed to indicate an evasive maneuver attempt. There is no way to be certain that the braking and yaw rate observed in this study was in fact due to an evasive maneuver. Additionally, some drivers may have attempted an evasive maneuver after the last-EDR time point was recorded. As such, this study may underestimate the frequency of evasive maneuvering.

It should be noted that there is substantially more uncertainty in the timing of evasive braking than in the timing of evasive steering. As previously discussed, there is uncertainty in when the evasive maneuvers actually started due to discretization error and uncertainty in when the last recorded data point was collected relative to the impact. Because some EDRs sample yaw rate at a higher frequency than braking data, the timing of steering is known with greater certainty than the timing of evasive braking. Overall, the results suggest that braking and steering occur at approximately the same time.

Different triggers were used to determine evasive braking and evasive steering. Brake application is measured as a binary data element (on/off), whereas a yaw rate threshold was used as the evasive steering trigger. If both actions were started simultaneously, more time may have been required to produce a 4 degrees/s vehicle yaw rate than to compress the brake pedal to indicate braking application. However, the median evasive yaw acceleration was 33.7 degrees/s², which indicates that the evasive steering trigger would likely be indicated within around one-tenth of a second. This is a relatively short amount of time considering the 10 Hz sampling rate of yaw rate by most EDRs included in this study. This leads us to believe that there is little difference in the difference in the time required to trigger an evasive steering or braking event.

EDRs record pre-crash data elements in intervals independent of one another, as shown previously by Wilkinson et al. [196]. This could lead to some synchronicity error between pre-crash speed and braking. EDRs that sample data at slower rates will be most subject to this error.

5.6 .Conclusions

This study has examined the characteristics of driver evasive maneuvers in intersection crashes. Three research questions were posed in this study that aimed to characterize intersection crash avoidance frequency, timing, and vehicle kinematics. The majority of drivers involved in intersection crashes were alert enough to perform an evasive action. Evasive maneuvering was found to occur in over four out of every five crashes with braking and steering occurring at approximately the same frequency. Evasive braking was found to occur less frequently for senior drivers and when drivers accelerated into the intersection from a complete or rolling stop than when travelling through the intersection. After accounting for uncertainty in the timing of braking and steering data, the median initial braking time was found to be 0.4 to 1.0 seconds prior to impact. Median initial steering time was found to be 0.2 to 0.4 seconds prior to impact. Three-fourths of driver began braking at a maximum of 1.5 seconds prior to impact and steering at a maximum of 0.7 seconds prior to impact. For all four crash configurations analyzed (SCP approach from right, SCP approach from left, LTAP/OD, LTAP/LD), evasive steering direction was found to be most frequently to the right. The median average evasive braking deceleration for all cases was found to be 0.55 g after correcting for wheel slip. The median of the maximum evasive vehicle yaw rates was found to be 10 degrees per seconds.

Section 2:
Building Simulation Case Sets of
Real-World Cross Traffic
Intersection Crashes

6. Estimating Pre-crash Driver Actions for Travelling Through Drivers³

6.1 Introduction

An important part of this dissertation work is reconstructing the pre-crash actions of drivers in real-world intersection crashes. Although impact speed can be readily determined using well-established methods [198, 199], there is often uncertainty in the pre-impact behavior of the driver. Traditionally, to understand these crashes, investigators must rely on witnesses and evidence collected from the crash scene. However, this information is not always sufficient for determining both driver errors leading to the crash (e.g., speeding) and the actions taken to avoid the crash (e.g., braking).

These crash records play an important role in the analyses performed throughout this dissertation work, and in automotive safety research in general. Researchers, developers, and evaluators of vehicle technology around the world use large databases of crashes in an effort to understand the nature of crash modes and injury mechanisms and how these crashes and injuries could potentially be prevented. The motivation for conducting this study was for the development and evaluation of future crash avoidance technologies. Specifically, for the implementation of the simulation case set presented in Chapter 7 to be used for evaluating I-ADAS. Previous studies have utilized information from real-world crash investigations in order to predict the effectiveness of future crash avoidance systems [39, 137, 200-203] and to determine the needs of these technologies within the vehicle fleet [22, 130, 135, 158, 181, 204-206].

³ The work shown in this study has been a part of several previously published peer-reviewed manuscripts, including: 197. Scanlon, J.M., R. Sherony, and H.C. Gabler, *Estimating Pre-crash Driver Actions when You Don't Have an EDR (In Review)*. Accident Analysis & Prevention, 2016.

There is, however, often uncertainty in the pre-crash behavior of drivers in intersection crashes. One useful way for determining pre-crash kinematics is through the use of Event Data Recorders (EDR) [96]. In the event of a crash, an EDR has the ability to record pre-crash vehicle kinematics, such as vehicle speed and braking. However, this data is often not available for investigators following a crash. For example, EDRs do not always record the pre-crash event due to low impact severity. For an event to be recorded, the vehicle must have either (a) had an airbag deployment or (b) experienced a substantially high delta-v. Additionally, EDRs occasionally malfunction and fail to record the event.

In the absence of EDR pre-crash data, there is a need for quantitative methods that can be used to determine pre-crash driver behavior. This study seeks to develop statistical relationships to determine pre-crash vehicle kinematics using evidence that can be collected on-scene. Specifically, the current study generated statistical models for estimating likelihood that the driver took some evasive action and the speed at which the driver entered the intersection.

The three most common intersection crash modes in the United States are straight crossing path (SCP), left turn across path opposite direction (LTAP/OD), and left turn across path lateral direction (LTAP/LD) crashes. Together, these impact configurations account for 73% of all intersection crashes [33] and 93% of fatal intersection crashes [3]. The pre-crash behavior of drivers involved in these crashes can be divided into two main categories: (1) drivers that come to a complete or “rolling” stop prior to accelerating through the intersection and (2) drivers that travel through the intersection because for example they do not have a stop sign or red light. For each of the three most common intersection crash modes, nearly every intersection crash involves at least one vehicle travelling through the intersection [116, 117, 137]. For non-turning drivers, travelling through drivers (shown in Figure 32) tend to either (a) maintain a relatively constant velocity

throughout their intersection approach and traversal or (b) accelerate in order to “beat” the amber phase of a traffic signal [116]. For left-turning drivers, travelling through drivers (shown in Figure 31) typically decelerate as the approach and enter the intersection in order to safely complete the turn and accelerate as they are exiting the intersection [116-118].

The objective of this study was to develop predictive models that can be used to determine the most likely vehicle kinematics of travelling through drivers in intersection crashes. As a part of this effort, cross-validation was performed in order to evaluate the predictive power of each model. Two predictive models were developed. First, logistic regression modelling was used to predict likelihood of an evasive braking maneuver from evidence that can be obtained from a crash scene. This predictive power of this model was compared with what was recorded by the crash investigator. Second, linear regression modelling was used to estimate the drivers traversal speed based on whether an evasive braking maneuver was likely to have occurred. Model predicted traversal speeds were compared with what actually occurred using cross-validation.

6.2 *Methods*

Data Source

This study utilized EDR records downloaded from vehicles investigated as a part of the National Automotive Sampling System / Crashworthiness System (NASS/CDS). This data source, along with inclusion criteria, is discussed extensively in Chapter 2. In addition to the exclusion reasons discussed, cases were also excluded if driver age, impact location, speed limit, or traffic control device were unknown. Each of these predictor variables were used to develop this study's models. Also, as done in the previously described studies, if the vehicle experienced wheel slip (recorded acceleration over 1-g), the case was excluded.

Determining Traversal Speed and Impact Speed

The pre-crash path and pre-crash speed profile of each vehicle in the dataset was reconstructed in order to determine speed at intersection entry, which we define as traversal speed. The methods used in this study to reconstruct vehicle path is discussed extensively in Chapter 7. In general, measurements are taken using the investigator drawn scene diagram to trace the path of the vehicle backwards in time from the point of impact.

The location where the vehicles entered into the intersection were collected from scene diagram. The stop bar was used, if present, to indicate the intersection entry location. If only the crosswalk was present, it was used as the entry location. If neither were present, intersection boundary lines were drawn by extrapolating the road edges through the intersection, and this boundary was used for intersection entry.

The positional time series of each vehicle was reconstructed using the EDR pre-crash speed record. These methods are also discussed in Chapter 7. In general, pre-crash speed was integrated to determine the pre-crash position of the vehicle with respect to time.

Identifying Travelling Through Drivers

The same process for identifying travelling through drivers in Chapter 5 was used in the current study. The criteria for labeling pre-crash movement can be found in Table 22. Vehicle indicated speed records were used to make pre-crash movement classifications. In summary, prior to any evasive braking, non-turning drivers were assumed to be travelling through if they did not slow below 20 mph. Left turning, travelling through drivers either did not slow below 10 mph and were not accelerating as they entered the intersection. This 10 mph threshold was selected based on an analysis of 14,062 left turn intersection approaches at a protected green light, where 99.9% of the drivers entered the intersection at speeds in excess of 10 mph.

Table 32. Pre-crash movement categories

Movement Group	Turning Behavior	Minimum Speed Threshold
Complete Stop	All	Minimum Speed == 0 mph
Rolling Stop	Straight	0 mph < Minimum Speed <= 15 mph
	left	0 mph < Minimum Speed <= 10 mph OR Minimum Speed > 10 mph AND Driver was accelerating when entering the intersection
Traveling Through	All	All remaining events

Extracting Parameters of Interest from EDR Records

Three parameters were extracted from the pre-crash speed records, including vehicle speed at impact, vehicle speed at intersection entry, and whether evasive braking action was performed. Vehicle speed at impact and at intersection entry were taken directly from the reconstructed pre-crash kinematics. Toyota modules directly records pre-crash speed at the time the EDR is triggered to store an event (e.g., airbag deployment), which was assumed to be the impact speed [185]. GM, Ford, and Chrysler modules do not directly record impact speed [182, 185]. Impact speed was determined for these modules by extrapolating forward (and assuming the driver would maintain a constant acceleration) in time from the last recorded pre-crash speed. This method is presented in detail in Chapter 7.

A slightly different criteria was used in Chapter 5 than was implemented to characterize an evasive braking maneuver in the current study. In the prior analysis, “last moment” braking that began within 0.5 s of impact was classified as an evasive braking maneuver. In the current study, only the deceleration over last recorded 0.5 s prior to impact was considered when classifying evasive braking. If the EDR sampled speed at 1 Hz, the change in velocity over the last full second was considered to compute deceleration. The purpose of this work was to develop a model that could aid in reconstructing the pre-crash speeds of vehicles in real-world crashes. Drivers that were able to depress the brake pedal, but that did not result in a substantial change in vehicle speed, were not of interest in the current study.

A 0.3 g deceleration threshold was used to distinguish crash avoidance braking from non-emergency braking behavior. Non-emergency braking prior to impact is common for left turning drivers travelling through the intersection. As discussed in the evasive maneuvering analysis, a 0.3

g threshold was selected because it is an abnormally high magnitude deceleration for a left turning driver travelling through the intersection. Specifically, an analysis of 14,062 left turning, travelling through approaches revealed that 98.0% of drivers had a maximum deceleration less than 0.3 g (sample rate of 2 Hz).

Estimating Likelihood of an Evasive Braking Maneuver

Logistic regression modeling was used to predict whether an evasive braking maneuver occurred for vehicles that were travelling through the intersection. Two steps were used to develop and evaluate these models. First, the full dataset of pre-crash events were used to develop a model to predict whether evasive braking occurred. Second, leave-one-out cross-validation was used to examine the performance of the model form against NASS/CDS investigator indicated braking avoidance maneuvers.

Models were developed in this study using the “Survey” package [207] in the R programming language [121]. Within this package, this study used *svyglm* to fit the regression models and *regTermTest* to test which of the predictor variables were statistically significant. The *regTermTest* function uses a Wald test, which was used in this study to test whether each of the regression terms was zero (i.e., not significantly correlated to predict evasive braking). An alpha level of 0.05 was used to determine which of the predictor variables significantly contributed to the likelihood that evasive braking occurred.

Two separate regression models were generated, one for straight crossing and another for left turning drivers. Regression parameters were selected based on the dynamics of emergency braking and the prior analysis of evasive maneuvering presented in Chapter 5. For the straight crossing model, impact speed relative to the posted speed limit, the posted speed limit, driver age group,

and impact configuration were used. For left turning drivers, impact speed, driver age group, and impact configuration were used. The general forms of these regression equations for straight and left turning drivers can be seen in Equation 19 and Equation 20, respectively.

$$\text{Equation 19 } p(\text{evade, straight}) = \frac{1}{1 + e^{-(\beta_0 + \beta_1 \cdot (v_{\text{impact}} / \text{sl}) + \beta_2 \cdot \text{sl} + \beta_3 \cdot \text{Young} + \beta_4 \cdot \text{Senior} + \beta_5 \cdot \text{Near} + \beta_6 \cdot \text{Far})}}$$

$$\text{Equation 20 } p(\text{evade, left}) = \frac{1}{1 + e^{-(\beta_0 + \beta_1 \cdot v_{\text{impact}} + \beta_2 \cdot \text{Young} + \beta_3 \cdot \text{Senior} + \beta_4 \cdot \text{Near} + \beta_5 \cdot \text{Far})}}$$

Where,

- p_{evade} = probability evasive braking occurred,
- β_{0-6} = model coefficients,
- v_{impact} = impact speed in mph,
- sl = speed limit in mph,
- Young = 1 if driver age \leq 20 years and 0 if not,
- Senior = 1 if driver age \geq 65 years and 0 if not,
- Near = 1 if near-side impact and 0 if not,
- Far = 1 if far-side impact and 0 if not.

For straight crossing drivers, it was important to consider impact speed with respect to the posted speed limit. Lower impact speeds with respect to speed limit would imply a higher likelihood of evasive braking having had occurred. Conversely, for left turning drivers, impact speed by itself was only considered. Drivers slow when executing left turns, so the effect of speed limit was expected to be small.

The effect of speed limit by itself was included for non-turning drivers. Roadways with higher speed limits would have faster travelling vehicles which would allow less time for a driver to perceive and then react to an imminent crash.

Driver age was demonstrated in Chapter 5 to be significantly correlated with likelihood of evasive braking. This prior analysis demonstrated that senior drivers (65 years old or greater) were

substantially 3 times less likely to take evasive braking action than drivers 21 to 64 years old. This could be attributed to several physical causes, including limited visual scanning, cognitive-motor abilities, and slower decision making [186-191].

Impact configuration, i.e. whether the vehicle was front, left-side, or right-side impacted, was expected to be correlated with whether evasive braking took place. If a driver took evasive action, it was hypothesized that drivers would be more likely to then be involved in a frontal impact. Additionally, an evasive braking action might benefit a driver about to experience a frontal impact more than a driver about to experience a side impact.

Determining Travelling Speed from Evasive Braking

Linear regression modeling was used to predict the driver's most likely speed at intersection entry given that the driver took braking evasive action. Similar to the evasive braking likelihood model, the "Survey" package [207] in the R programming language [121] was used to generate and evaluate all regression models. A Wald test was also used to determine the statistical significance of each predictor variable. A regression model was generated for both straight crossing and left turning drivers, which can be seen in Equation 21 and Equation 22, respectively. For both regression models, two predictor terms were added from the evasive braking likelihood models. First, whether the driver took evasive braking was used as a predictor variable. For a given impact speed, a driver that took evasive braking action would, obviously, tend to have a higher traversal speed than a driver that did not take evasive braking action. Second, an interaction effect between impact speed and evasive braking was used. Any significant effect would imply that the relationship between impact speed and traversal speed depended on whether braking took place.

Equation 21

$$v_{traversal} = \beta_0 + \beta_1 \cdot (v_{impact} / sl) + \beta_2 \cdot sl + \beta_3 \cdot Young + \beta_4 \cdot Senior + \beta_5 \cdot Near + \beta_6 \cdot Far + \beta_7 \cdot Braked + \beta_8 \cdot Braked \cdot (v_{impact} / sl)$$

Equation 22

$$v_{traversal} = \beta_0 + \beta_1 \cdot v_{impact} + \beta_2 \cdot Young + \beta_3 \cdot Senior + \beta_4 \cdot Near + \beta_5 \cdot Far + \beta_5 \cdot Braked + \beta_6 \cdot Braked \cdot v_{impact}$$

Where,

$v_{traversal}$ = speed at intersection entry in mph,

β_{0-8} = model coefficients,

v_{impact} = impact speed in mph,

sl = speed limit in mph,

Signal = 1 if traffic signal and 0 if not,

Stop = 1 if stop sign and 0 if not,

Young = 1 if driver age \leq 20 years and 0 if not,

Senior = 1 if driver age \geq 65 years and 0 if not,

Near = 1 if near-side impact and 0 if not,

Far = 1 if far-side impact and 0 if not,

Braked = 1 if evasive braking occurred and 0 if not.

Evaluating the Regression Models

Leave-one-out cross-validation was used to assess how accurately both the evasive braking and traversal speed models were able to classify driver behavior. This method withholds one observation (single pre-crash event) as a testing dataset. The remaining observations are used to train the models. For the single case, some probability of an evasive braking maneuver and a most likely travel speed were assigned using the trained model. This process was then repeated for the remaining for all observations until each was assigned some prediction.

The evasive braking likelihood model was evaluated by examining the ratio of correctly identified evasive braking maneuvers (true-positive proportion), the ratio of incorrectly identified non-evasive braking maneuvers (false-positive proportion), and the accuracy of the model, in general. These proportions were then compared with what was identified by the NASS/CDS crash

investigator. The traversal speed model was assessed by comparing the model predicted traversal speed with the vehicle speed recorded by the EDR.

6.3 *Results and Discussion*

Dataset Composition

A total of 1,213 EDRs with pre-crash speed and braking and that were taken from SCP, LTAP/OD, and LTAP/LD intersection crashes were considered for this study's analysis. From this initial set, 145 EDRs were excluded due to potential wheel slip. An additional four cases were removed for having case weights above 5000. A total of 215 left turning and 146 straight crossing drivers were removed for having completely or rolling stopped prior to entering the intersection. Lastly, 92 cases were removed for missing case information, e.g. age, gender, or scene diagram. The final dataset consisted of 613 EDRs, where 93 were taken from left turning vehicles and 520 from straight crossing vehicles.

The Effect of Crash Avoidance Braking on Impact Speed

This study hinges on the hypothesis that impact speed can be used to determine whether a driver took evasive braking action. Additionally, this study tests the hypothesis that impact speed can be used as predictor of pre-crash traversal speed. As a first step, impact speeds with and without crash avoidance braking were examined for both straight crossing and left turning drivers. This relationship is shown in Figure 42.

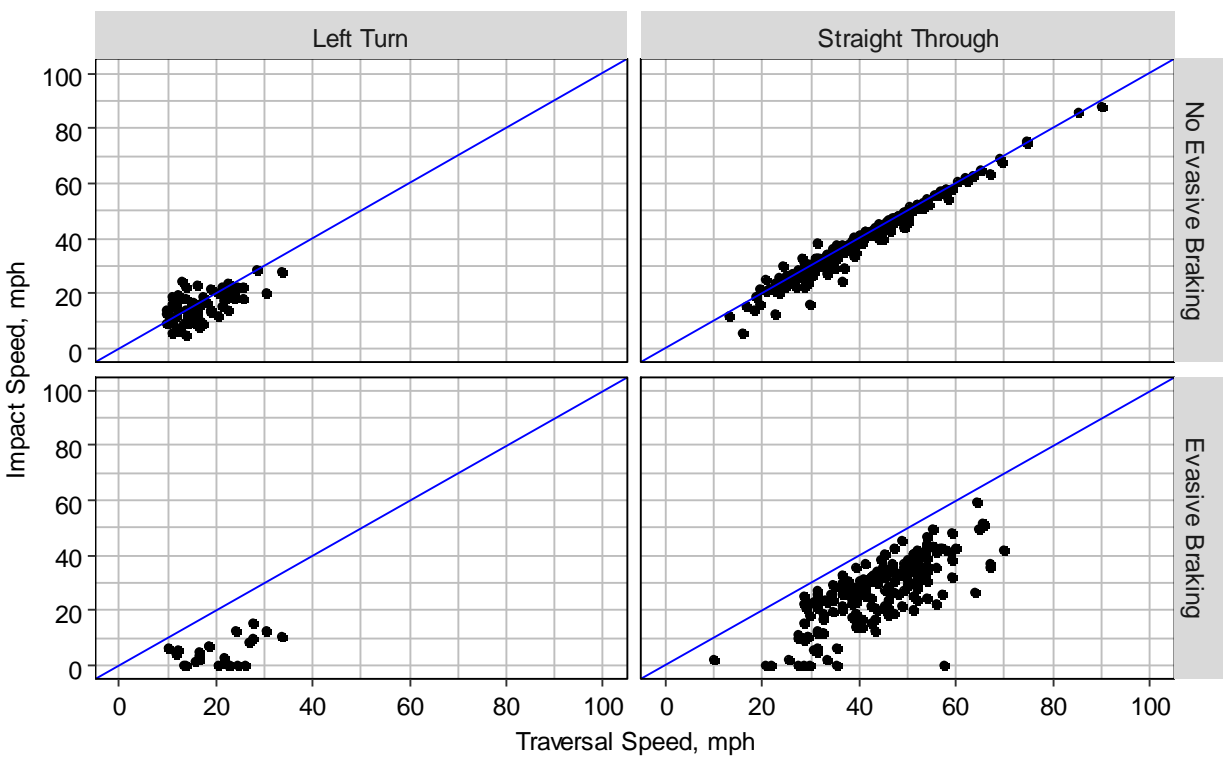


Figure 42. Impact speed as a function of traversal speed presented by turning behavior and evasive maneuvering.

It is important to note the relationship between crash avoidance braking and impact speed. First, as would be expected, drivers that evasively braked had, in general, lower impact speeds than initial traversal speeds. This was an encouraging sign that impact speed could be used, along with

other relevant covariates, as a means for estimating likelihood that evasive braking occurred and the driver's most likely traversal speed. Second, there appears to be an approximately linear relation between traversal speed and impact speed. Based on this observation, linear regression modeling seems appropriate. Third, for both left turning and straight crossing drivers that did not evasively brake, drivers appear to maintain a relatively constant speed from intersection entry until impact as evidenced by the data point falling approximately along on the blue line. There appears to be less difference between traversal speed and impact speed for straight crossing drivers, which was also anticipated because as discussed previously, left turning drivers tend to decelerate during intersection entry and accelerate while leaving the intersection. .

There are several additional important trends that should be observed. First, drivers taking left turns traverse intersections at substantially lower speeds than drivers travelling straight through the intersection. The median left turn traversal speed was 17 mph, while the median straight crossing speed was 39 mph. Second, the range of traversal speeds was higher for straight travelling drivers than left turning drivers. For drivers without crash avoidance braking, the middle 95% of traversal speeds for straight crossing drivers ranged from 21 to 62 mph, while the middle 95% of traversal speeds for left turning drivers fell between 11 and 27 mph. Several reasons can explain these generally lower vehicle speeds while turning, such as (a) frictional limitations between the road-tire interface and (b) drivers feeling uncomfortable during higher lateral accelerations [208].

Model Estimating Likelihood of an Evasive Braking Maneuver Having Occurred

Logistic regression was used to model likelihood of an evasive braking maneuver. Model parameters and statistical test results from the Wald-test can be found in Table 33 for straight crossing drivers and Table 34 for left turning drivers.

There were two significant findings that should be noted from the statistical analysis. First, as expected, impact speed was found to be significantly correlated with the probability of evasive braking for both straight crossing and left turning drivers. Second, an effect of impact location was observed for both straight crossing drivers and left turning drivers. Drivers involved in frontal impacts were more likely to have evasively braked than when involved in far side impacts. Intuitively, we would expect that drivers who brake would be more likely to be involved in a frontal crash, because they would have slowed down their vehicle allowing the oncoming vehicle to pass in front.

One interesting finding to note is that driver age was not found to be a significant predictor variable despite significance observations made in Chapter 5. In Chapter 5, driver age was used in a logistic regression to determine likelihood of taking evasive braking action. The results suggested that senior drivers were nearly three times less likely to have taken evasive action than adult drivers. The result in the current study is most likely due to the inclusion of impact speed in the current model. If adult drivers tend to brake (and possibly brake at a higher degree), they would have lower impact speeds than senior drivers. Therefore, the age effect may not be significant, because the effect is being accounted for in the impact speed effect. Accordingly, the lack of significance in the age effect observed in this study should not be interpreted to suggest no age-related differences in evasive braking action frequency.

Table 33. Parameters for the straight crossing evasive braking model. Reference parameters do not have coefficients are indicated by “---”.

Parameter	Parameter Value	Coefficient	Std. Error	F-Ratio	p-value
Intercept		5.375	1.361	---	---
Impact Speed / Speed Limit		-4.855	0.914	28.2	<0.001*
Speed Limit (mph)		-0.037	0.022	2.9	0.092
Age Group	Young (age < 20 yr.)	-0.299	0.748	0.5	0.591
	Adult (21 < age < 64 yr.)	---	---		
	Senior (age > 65 y.o.)	-0.512	0.508		
Impact Location	Front	---	---	5.4	0.005*
	Left-side	-0.849	0.507		
	Right-side	-2.109	0.748		

Table 34. Parameters for left turning evasive braking model. Reference parameters do not have coefficients are indicated by “---”.

Parameter	Parameter Value	Coefficient	Std. Error	F-Ratio	p-value
Intercept		3.905	1.065	---	---
Impact Speed (mph)		-0.554	0.163	11.5	0.001*
Age Group	Young (age < 20 y.o.)	-0.817	1.662	1.1	0.328
	Adult (21 < age < 65 y.o.)	---	---		
	Senior (age > 65 y.o.)	1.524	1.406		
Impact Location	Front	---	---	7.6	0.001*
	Left-side	2.789	1.424		
	Right-side	-4.827	1.423		

Comparing Evasive Braking Probability Model with Crash Investigator

Leave-one-out cross-validation was performed to compare the statistical models for predicting evasive braking with what was coded by the NASS/CDS investigator. Table 35 shows a direct comparison of the model performance versus what was indicated by the investigator. Table 36 shows a full summary of the coded braking maneuver with the actual braking maneuver indicated using the EDR in order to first examine the accuracy of the investigator. Table 37 shows a full summary the model predicted braking maneuver versus what actually occurred.

Table 35. Summary of model performance versus NASS/CDS investigator.

Evaluation Metric		Straight Crossing Drivers	Left Turning Drivers
% of Accurately Predicted Events	Model	75%	82%
	Investigator	49%	42%
False-Positive Percentage	Model	17%	18%
	Investigator	47%	46%
True-Positive Percentage	Model	64%	83%
	Investigator	43%	3%

The proposed statistical model was found to be, in general, more accurate than the NASS/CDS investigator. The model correctly predicted whether or not evasive braking occurred for 75% of straight crossing drivers and 82% of left turning drivers. The NASS/CDS investigator was only accurate for approximately one-half of the indicated braking avoidance maneuvers (49% of straight crossing drivers, and 42% of left turning drivers). The investigator had both high false-positive percentages of 47% and 46%, for straight crossing and left turning, and low true-positive percentages of 43% and 3% for left turning drivers. Comparatively, the model correctly predicted 64% and 83% of evasive braking maneuvers that occurred during straight crossings and left turns, respectively. The percentage of incorrectly identified non-evasive braking maneuvers was also

It should be noted that predictions were made using a 50% probability of braking threshold, which resulted in around 36% of straight crossing drivers that performed an evasive braking maneuver to be incorrectly identified as having not evasively braked. When applying this model, it is important to note that the evasive braking model simply provides some likelihood of evasive braking having occurred. There is inherent uncertainty when making any sort of prediction using

a probabilistic model. There are several potential ways to apply these models for crash reconstruction. One method is to simply classify a given vehicle as either had evasively braked or not. This can be done by selecting some probability threshold to classify whether crash avoidance braking occurred. If intending to use these models for this application, it is important to consider the false-positive and true-positive rates for various probability thresholds. Table 38 shows false-positive, true-positive, and accuracy rates using several probability thresholds. All rates were generated using leave-one-out cross-validation.

Table 36. Accuracy of NASS/CDS investigator coded avoidance maneuver determined using EDR-recorded avoidance maneuver.

Straight Crossing Drivers Count --- Weighted Count		Actual Braking Maneuver Determined Using EDR				Total	
		No Braking		Braking			
NASS/CDS Coded Avoidance Braking Maneuver	No Braking	182	46,650	67	29,820	249	76,470
	Braking	66	18,988	92	31,156	158	50,144
	Unknown	70	21,882	43	10,210	113	32,092
Total		318	87,521	202	71,186	520	158,707

Left Turning Drivers Count (Weighted Count)		Actual Braking Maneuver Determined Using EDR				Total	
		No Braking		Braking			
NASS/CDS Coded Avoidance Braking Maneuver	No Braking	45	16,614	11	4,389	56	21,003
	Braking	3	1,912	2	285	5	2,197
	Unknown	21	12,010	10	4,690	31	16,700
Total		69	30,536	23	9,364	92	39,900

Table 37. Accuracy of evasive braking likelihood model determined using leave-one-out cross-validation.

Straight Crossing Drivers Count --- Weighted Count		Actual Braking Maneuver Determined Using EDR				Total	
		No Braking		Braking			
Evasive Braking Model Prediction	No Braking	266	72,698	85	25,291	351	97,990
	Braking	52	14,822	117	45,894	169	60,717
Total		318	87,521	202	71,186	520	158,707

Left Turning Drivers Count (Weighted Count)		Actual Braking Maneuver Determined Using EDR				Total	
		No Braking		Braking			
Evasive Braking Model Prediction	No Braking	63	25,120	6	1,609	69	26,729
	Braking	6	5,416	17	7,755	23	13,171
Total		69	30,536	23	9,364	92	39,900

Table 38. Results from the leave-one-out cross-validation analysis of the evasive prediction model. Several probability thresholds are considered. Both the straight crossing and left turning models are shown.

Straight Crossing Drivers			
Probability Threshold	True-Positive Proportion, %	False-Positive Proportion, %	Accuracy, %
0.1	97%	81%	54%
0.2	93%	62%	63%
0.3	90%	45%	71%
0.4	72%	30%	71%
0.5	64%	17%	75%
0.6	55%	12%	73%
0.7	40%	7%	69%
0.8	22%	4%	63%
0.9	8%	0%	59%
Left Turning Drivers			
0.1	97%	26%	80%
0.2	86%	22%	80%
0.3	83%	18%	82%
0.4	83%	18%	82%
0.5	83%	18%	82%
0.6	81%	18%	82%
0.7	81%	14%	85%
0.8	54%	14%	79%
0.9	48%	0%	88%

Model Estimating Traversal Speed

Linear regression was used to determine traversal speed given impact speed and whether the driver took evasive action. Regression parameters and the results from the statistical analyses can be found in Table 39 and Table 40.

Table 39. Model parameters and statistical result for the straight crossing traversal speed linear regression model. Reference parameters do not have coefficients are indicated by “---”.

Parameter	Parameter Value	Coefficient	Std. Error	F-Ratio	p-value
Intercept (mph)		-31.462	2.599	---	---
Impact Speed / Speed Limit		36.613	1.613	515.5	<0.001*
Speed Limit (mph)		0.865	0.038	508.8	<0.001*
Age Group	Young (age < 20 years)	0.550	1.216	0.6	0.543
	Adult (21 < age < 65 years)	---	---		
	Senior (age < 65 years)	-0.453	0.524		
Impact Location	Front	---	---	0.7	0.476
	Left-side	0.798	0.658		
	Right-side	-0.446	1.097		
Evasive Braking	No Evasive Braking	---	---	224.7	<0.001*
	Evasive Braking	27.720	1.849		
(Impact Speed / Speed Limit) × (1 if braking, 0 if not)		-20.364	2.261	81.2	<0.001*

Table 40. Model parameters and statistical result for the left turning traversal speed linear regression model. Reference parameters do not have coefficients are indicated by “---”.

Parameter	Parameter Value	Coefficient	Std. Error	F-Ratio	p-value
Intercept (mph)		9.765	1.608	---	---
Impact Speed (mph)		0.619	0.085	53.2	<0.001*
Age Group	Young (age < 20 years)	-1.511	1.494	0.6	0.534
	Adult (21 < age < 65 years)	---	---		
	Senior (age < 65 years)	-2.155	2.060		
Impact Location	Front	---	---	8.5	0.001*
	Left-side	-4.293	1.247		
	Right-side	-1.476	1.082		
Evasive Braking	No Evasive Braking	---	---	14.0	0.001*
	Evasive Braking	9.902	2.642		
(Impact Speed) × (1 if evasive braking, 0 if not)		-0.172	0.359	0.2	0.634

As expected, impact speed and evasive braking were found to be important predictor variables for determining the vehicle’s most likely traversal speed. For straight crossing drivers, a significant interaction effect was observed between evasive braking and impact speed. This result suggests

that the relationship between impact speed and traversal speed depends on whether the driver took evasive braking actions.

The effect of speed limit was found to be a significant predictor variable for straight crossing drivers. The result suggests that, in general for this subset of drivers, drivers tend to “speed” less at higher speed limits. A 10 mph increase in speed limits corresponded to an 8.7 mph increase in traversal speed.

Left turning drivers that were involved in a frontal impact tended to have higher traversal speeds (3.6 mph) than drivers involved in a left side impact. One contributing factor may be glance direction, which could influence the amount (e.g., magnitude and duration) of evasive braking performed. Specifically, drivers involved in left side impacts were involved in a LTAP/LD type intersection crash, whereas the right side impacted drivers were involved in LTAP/OD crashes.

6.4 Evaluating the Traversal Speed Model

Figure 43 and Figure 44 show model predicted speed generated using the leave-one-out cross-validation method versus what was recorded by the EDR for straight crossing and left turning drivers, respectively. For the straight crossing model, 50% of traversal speeds predictions were within 2.0 mph of the EDR-recorded value, and 95% of predicted speeds were within 8.4% of actual recorded speed. For the left turning model, 50% of predicted speeds were within 3.0 mph, and 95% of values were within 8.6 mph.

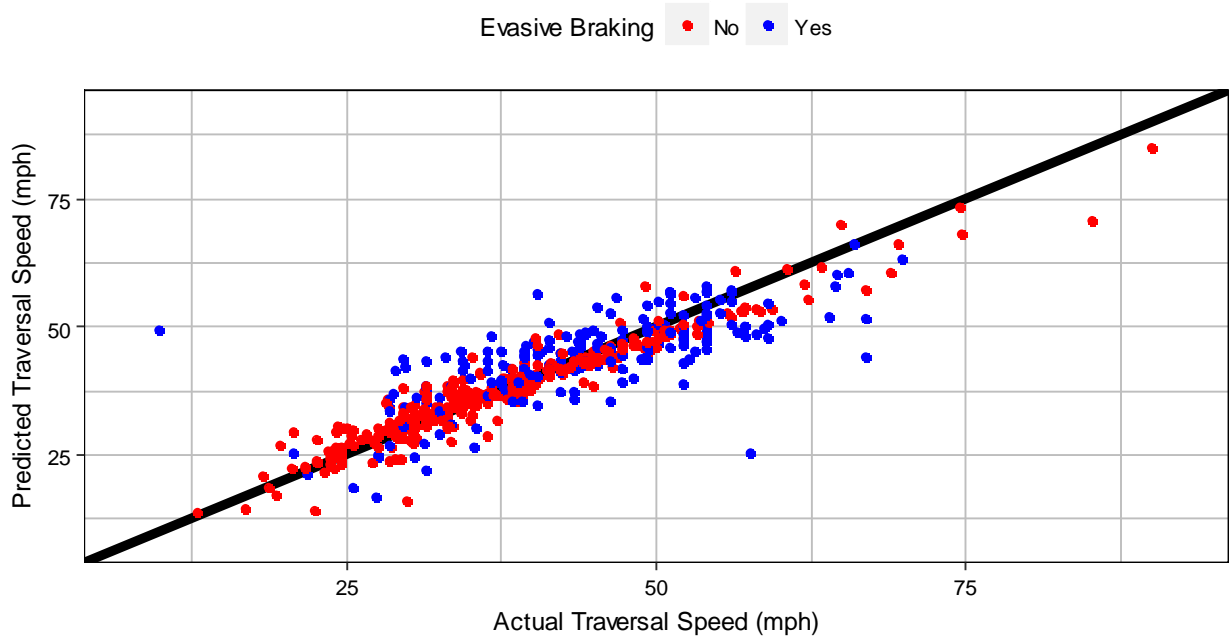


Figure 43. Model predicted speed versus vehicle speed recorded by the EDR for straight crossing drivers.

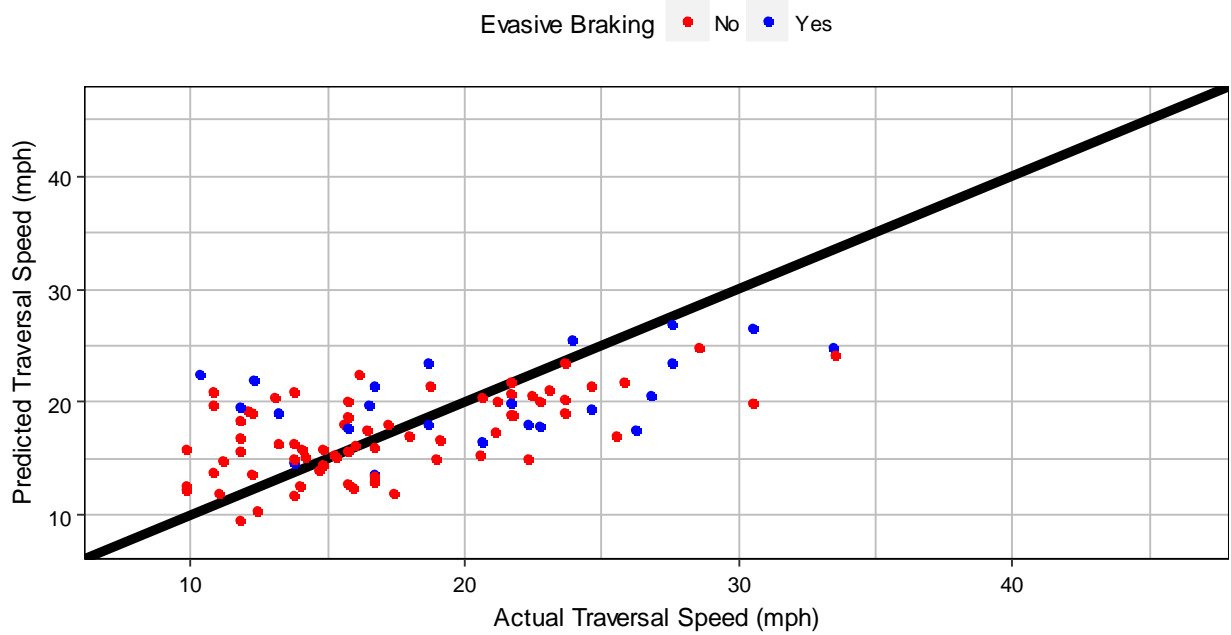


Figure 44. Model predicted speed versus vehicle recorded by the EDR for left turning drivers.

6.5 *Conclusions*

This study used event data recorders and information collected during crash investigations to develop models that could (a) determine the likelihood of an evasive braking maneuver having been performed and (b) determine the driver's most likely traversal speed prior to any braking. These models will be directly used to develop the simulation case set in Chapter 7. Models were evaluated using leave-one-out cross-validation method. The models generated in this study serve as a useful tool for individuals looking to reconstruct pre-crash vehicle kinematics from on-scene evidence. These models may prove particularly effective if attempting to reconstruct pre-crash behavior for cases in large crash databases where there is often uncertainty in what led to the crash.

7. Reconstructing the Pre-Crash Trajectories of Vehicles involved in Intersection Crashes

7.1 Reconstruction Strategy

A primary goal of this thesis work was to evaluate I-ADAS in real-world crash scenarios. Because I-ADAS is not yet in production cars, a retrospective analysis of accident statistics is not possible. My approach was to instead reconstruct real-world SCP, LTAP/LD, and LTAP/OD crashes between vehicles without I-ADAS. These crashes would then be simulated as if the vehicles were equipped with I-ADAS.

One limitation of reconstructing real-world intersection crashes is that there is often uncertainty in the pre-crash driver behavior (e.g. travel speed, evasive braking). Two simulation case sets were generated in this study using different methods for determining pre-crash behavior.

The first simulation case set was generated from NASS/CDS crashes where both vehicles were equipped with EDRs. This case set is referred to as the EDR dataset. SCP, LTAP/LD, and LTAP/OD crashes were used for this analysis. For this dataset, reconstructions were accomplished by coupling the pre-crash vehicle speed extracted from EDR downloads with the pre-crash path recorded by a scene investigator in a scene diagram. Example EDR downloads extracted from two vehicles involved in a SCP and LTAP/OD intersection crash are shown in Figure 45 and Figure 46, respectively.

The second simulation case set, referred to as the NMVCCS dataset, was generated from crashes investigated as a part of the NMVCCS study. Only SCP and LTAP/LD crashes were considered for this dataset. This dataset differed in several ways from the EDR dataset. First, the NMVCCS dataset is considerably larger. As presented in this study, over 650 SCP + LTAP/LD crashes were extracted. By comparison, the dataset of NASS/CDS crashes where both vehicles

were equipped with EDRs was composed of only 40 SCP + LTAP/LD crashes. One limitation of the NMVCCS dataset is the lack of EDR records. The NMVCCS dataset relies on driver models to estimate most likely vehicle kinematics.

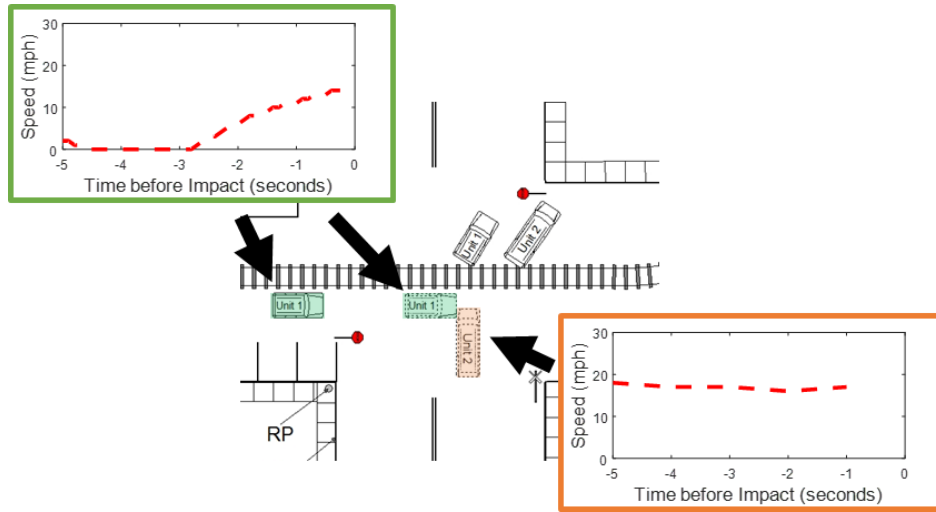


Figure 45. The downloaded EDRs for a SCP intersection crash (NASS/CDS 2013-76-166). The vehicle indicated in green stopped at a stop sign then accelerated into the intersection as indicated by the EDR download extracted from the vehicle. The vehicle indicated in orange did not have a traffic control device, and was travelling at approximately 20 mph for the 5-seconds prior to impact as indicated by the EDR download.

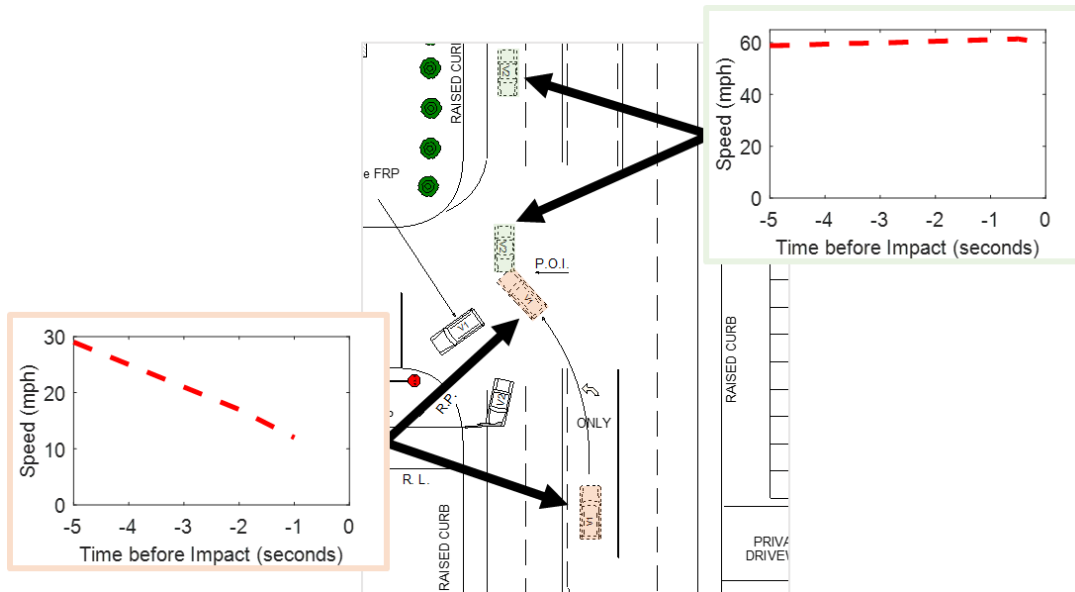


Figure 46. The scene diagram for NASS/CDS case 2014-4-55. The EDR speed profile records are additionally included for both vehicles. The left turning vehicle (red) slowed down throughout the intersection approach and left turn. The straight crossing vehicle (green) maintained a relatively constant speed approximately 15 mph higher than the posted speed limit (speed limit = 45 mph).

There were three main steps for generating the two simulation case sets. First, real-world intersection crashes were extracted from a U.S. national crash database. Second, path reconstructions were performed to quantitatively reconstruct the path of the vehicle prior to impact. Third, speed reconstructions were performed. For the EDR dataset, the pre-crash speed time series collected by the EDR were used to trace back the vehicles' positions through time. For the NMVCCS dataset, speed reconstructions were performed using driver models to determine each vehicle's most likely impact speed, crash avoidance maneuvers, intersection traversal kinematics, and intersection approach kinematics.

7.2 Data Sources

NMVCCS Dataset

This dataset reconstructed vehicle kinematics for SCP and LTAP/LD intersection crashes investigated as a part of NMVCCS (described in Chapter 2). A total of 1,129 crashes were extracted from NMVCCS using the “reljct” to isolate intersection-related crashes and “acctype” to select only SCP and LTAP/LD crashes. From these cases in NMVCCS, inclusion criteria were established based on (a) whether the case was correctly identified, (b) whether the case had missing information, or (c) the crash was not eligible for PC-Crash reconstruction. The following paragraphs detail the criterion used to select cases of interest. A detailed summary of the included cases can be found in Table 41. The final dataset used in this study consisted of a total of 661 crashes.

Table 41. Total number of crashes included in the final simulation case set.

Group		Count	Weighted Count
All CT Crashes in NMVCCS		1,129	420,781
Valid CT after Manual Inspection		1,042	390,984
Missing Case Information	Unknown pre-crash Movement	13	4,192
	No Posted Speed Limit on Roadway	8	1,331
	Missing Diagram/Photograph/Speed Limit	37	15,440
	Stop Location not provided in Diagram	56	17,464
PC-Crash Exclusion	Rollover	102	45,899
	3 or more Moving Vehicles Impacted	45	10,679
	Missing Vehicle in CVS database	68	23,014
	Scene Diagram Not Sufficient	39	15,310
Injury Benefits	Unknown driver age/gender	13	2,779
Final Dataset for CT Reconstruction		661	254,877

First, an SCP intersection crash was defined as having occurred when the collision involved two vehicles travelling straight at a crossing or connections of two roadways. An LTAP/LD

intersection crash was defined as one involving a left turning vehicle being involved in a collision with a vehicle approaching the left direction. Crashes involving driveways, alleys, or interchanges were excluded as well as crashes having one of the vehicles stopped in the intersection or involving a vehicle travelling in the wrong direction.

Second, cases were only included when all necessary information was provided within the database. Cases were excluded if vehicle approach photographs or scene diagrams were omitted from the database, if the speed limit of either of the intersecting roads was unknown, if either intersecting road did not have a speed limit, if pre-crash movements for either driver were unknown, and if the location of road markings (crosswalk, stop bar) could not be determined from the scene diagram.

Third, some inclusion criteria were used for selecting cases to reconstruct using PC-Crash. First, crashes were excluded if any of the vehicles in the crash could not be found within the Canadian Vehicle Specifications (CVS) [209] database that is used within PC-Crash v9.1 [199]. Occasionally, large work trucks and vans would be involved in these crashes, and would not be present within this vehicle database. Second, scene diagrams were sometimes scaled incorrectly. This was determined after large discrepancies were observed between the size of the vehicles loaded into the scene diagram and the size of the depicted vehicle body. Third, because these crashes were simulated in two-dimensions, rollover crashes were omitted from this study. Fourth, crashes occasionally involved collisions between more than two moving vehicles were excluded from further analysis. Because these crashes were simulated from the instance of initial impact, the initial location of any additional impacted moving vehicles were not provided in the scene diagram.

Fourth, there were some driver-specific criteria established for eventually computing injury benefits. Crashes were not considered in the reconstructed simulation case set if driver age and/or gender were not coded. Only 13 crashes involved drivers of unknown age or gender.

EDR Dataset

This study extracted crashes from a series of crashes investigated by the National Highway Traffic Safety Administration (NHTSA) as part of the National Automotive Sampling System / Crashworthiness Data System (NASS/CDS) for case years 2004 to 2014. Several additional criteria to those mentioned in Chapter 2 were required for a crash to be included in this study. First, only intersection crashes where both vehicles were equipped with an EDR were included in this study. Second, only SCP or LTAP/LD crashes that occurred in intersections were included. Third, the extracted EDR must have recorded pre-crash speed. Fourth, for SCP and LTAP/LD crashes, the pre-crash speed must have been sufficient for tracing the vehicle back to the intersection boundary line. For LTAP/OD crashes, the time point when the left turning vehicle first departed its initial travel lane was used. Most EDRs record up to 5-seconds of pre-crash data. Occasionally, this 5-seconds is not long enough to trace the vehicle position back to the earliest detection opportunity. Fifth, as has been previously done in the literature [97], cases with a national weighting factor greater than 5,000 crashes were excluded to eliminate skewing of the results. Sixth, crashes were excluded if the vehicle experienced a 1-g maximum deceleration. Unrealistically high vehicle decelerations are a sign that the vehicle experienced wheel slip.

A total of 91 SCP, LTAP/LD, and LTAP/OD crashes were extracted from NASS/CDS, where both vehicles were equipped with an EDR. Eight crashes excluded due to not having occur at the connection of two or more roadways. One crash was excluded due to a NASS case weighting

greater than 5,000 crashes. Fourteen additional crashes were excluded because at least one of the vehicles likely experienced wheel slip (maximum deceleration greater than 1-g). One LTAP/OD crashes were excluded because the pre-crash recording duration was not sufficient for tracing vehicle position back to the initial left turn lane departure. Three total SCP and LTAP/LD crashes were excluded because the recording duration did not capture the first intersection boundary line crossing.

The final dataset consisted of 35 LTAP/OD crashes, 21 SCP crashes, and 8 LTAP/LD crashes. As discussed in later sections, LTAP/OD crashes were examined independently of SCP and LTAP/LD crashes due to inherent differences between the crash modes.

7.3 Path Reconstructions

The paths of all vehicles involved in the simulation case set were reconstructed using measurements taken from the scene diagram. The full data collection protocol to be used by the researchers for collecting measurements to reconstruct vehicle paths can be found in the Appendix.

Scene diagrams contain the quantitative elements required for performing pre-crash path reconstructions. NASS/CDS stores these drawn-to-scale scene diagrams in Easy Street Draw (ESD) files (A-T Solutions Inc.). The ESD files include intersection geometry, road markings, and the vehicle locations of the crash impact location within the intersection. For this study, reviewers downloaded the scene diagrams and make supplemental measurements as detailed in this section. These measurements were then used to reconstruct the full pre-crash path taken by each vehicle.

Measurements for Reconstructing Vehicle Paths

Impact locations were determined by measuring the relative positions of both vehicles. These positions and orientations were determined using what is depicted in the scene diagram.

Vehicle dimensions were obtained for both vehicles. For the EDR dataset, the vehicle dimensions recorded by the crash investigator were used. For the NMVCCS dataset, vehicle dimensions were determined using the Canadian Vehicle Specifications (CVS) database [209]. This database is compiled annually by the Collision Investigation and Research Division of Transport Canada.

The path reconstruction measurements were used to determine the path taken by the vehicle prior to impact. The lateral movement categories depicted in Figure 47 were used to determine the required path reconstruction measurements. Example measurements for each of these scenarios can be found in the data collection protocol in the Appendix. The following paragraphs detail the various measurements recorded.

Seven categories were used to describe the movements of the vehicle prior to impact. These categories are depicted in Figure 47. The potential lateral movements included (a) a road curvature prior to the intersection, (b) a road curvature prior to and within the intersection, (c) a lane misdirection that requires the vehicle to change heading angles, (d) a lane offset within the intersection that requires the entering vehicle to move laterally to continue on the same road, (e) a lane change prior to or within the intersection, (f) an evasive steering maneuver, and (g) a left turn that was performed at the intersection.

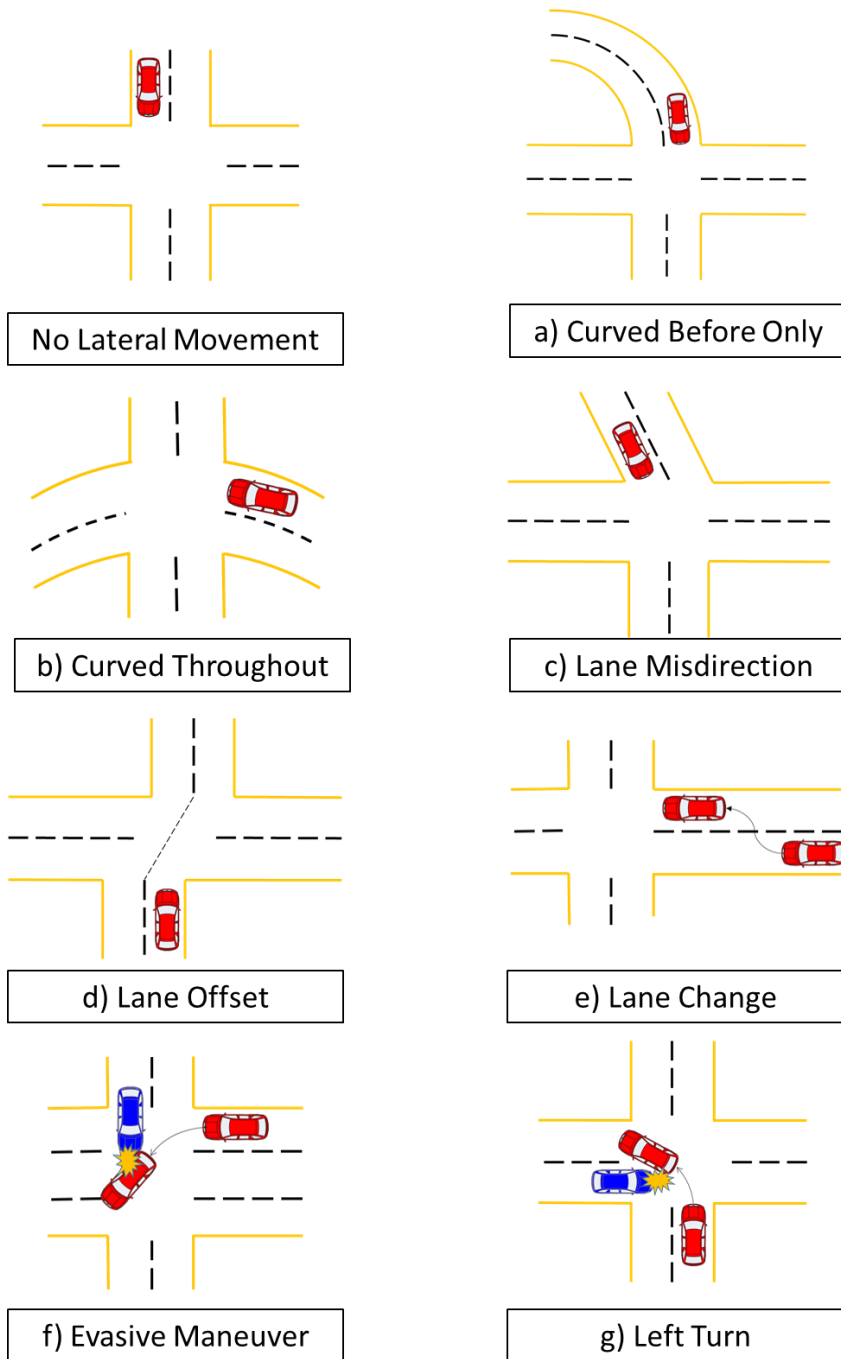


Figure 47. Seven pre-crash movement categories that were used to reconstruct vehicle paths.

If no lateral movement was performed prior to the crash, the only metric required to reconstruct the vehicle path was the vehicle heading prior to entering the intersection. The driver was then assumed to have maintained this heading throughout the entire pre-crash approach.

The measurements required for curved roads depended on whether the road curvature was prior to the intersection or extended through the intersection. If the road was only curved prior to the intersection, two measurements were required, i.e. the vehicle path radius of curvature and the distance from the end of the curved road to the intersection boundary line. For roads with curvature that extended through the intersection, only the vehicle path radius of curvature was measured. In addition to these measurements, the direction of the curvature (i.e. to the left or right) was also indicated.

Vehicle paths with a lane offset or lane misdirection were modeled as taking a straight path from the intersection boundary to the impact location. For an evasive steering maneuver, the vehicle was assumed to have taken a straight path from the start of the evasive maneuver (as indicated on the scene diagram) to the impact location. The distance that each vehicle travelled laterally (with respect to vehicle heading prior to entering the intersection or beginning the evasive maneuver) was measured. For drivers that performed an evasive maneuver, the longitudinal travelling distance (with respect to vehicle heading prior to evasive maneuver) from the evasive starting point to the impact location was measured. In addition, the direction of the lateral movement (i.e. to the left or right) was indicated.

Lane changes were modeled as being an instantaneous change in lateral position. The location of where the lane change was indicated as having started was measured relative to the intersection boundary. The lateral direction of the lane change was also indicated.

Left turns were modeled using an arc of constant radius. This method allowed for the retention of the depicted heading at impact and the heading prior to the initiation of the left turn.

Intersection Entry Location

The location where each driver entered the intersection was determined for every crash. If a stop bar was present, it was used as the intersection entry location. If a stop bar was not present but a crosswalk was present, the location where the vehicle first crossed the crosswalk was taken as the intersection entry location. If neither a stop bar nor crosswalk was present, the intersection boundary line was used as the intersection entry location. Intersection boundary lines were drawn for every scene diagram. These lines were drawn by extrapolating the road edge throughout the intersection. Examples of drawing these intersection boundary lines can be found for two cases in Figure 48.

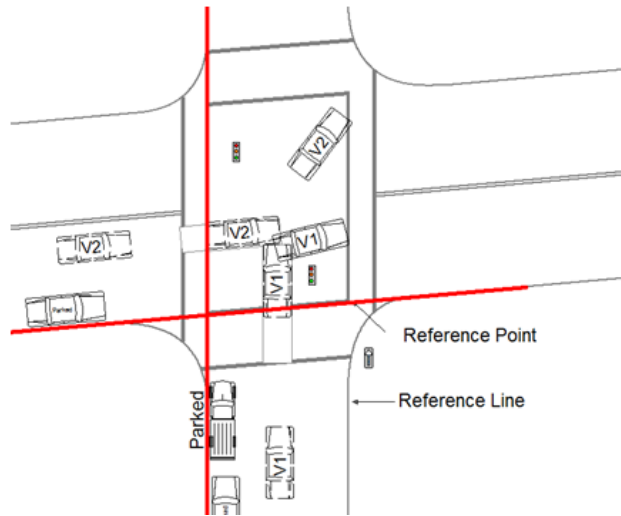
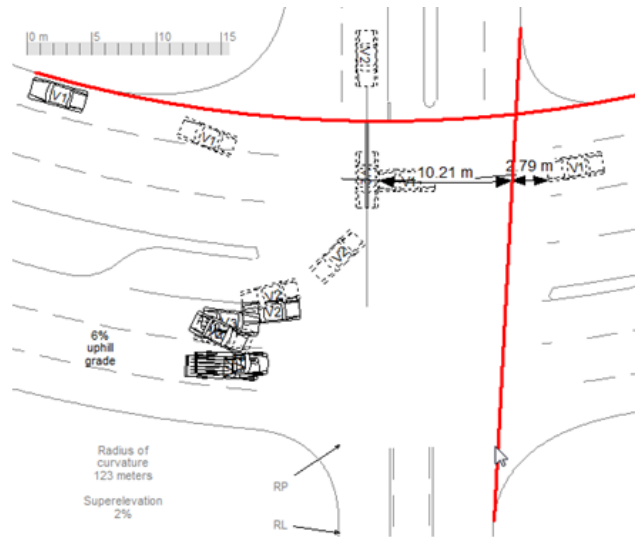


Figure 48. Examples for how intersection boundary lines were drawn. The scene diagram on the top was taken from NMVCCS case 2007-74-62. The scene diagram on the bottom comes from NMVCCS case 2006-03-043.

7.4 *Speed Reconstructions*

EDR Dataset

The EDR pre-crash vehicle speed was used to reconstruct the location of the vehicle through time. This was accomplished in three steps.

First, in general, there is some uncertainty in the time stamp associated with a given EDR pre-crash record. EDRs continuously collect pre-crash data, while the vehicle is being driven. In the event of some triggering event, such as an airbag deployment or high delta-v, the EDR stores the pre-crash data to memory. However, the EDR time axis is not the same as the actual time axis with respect to the time of impact. With the exception of Toyota EDRs, most vehicle manufacturers do not record vehicle speed at the point of impact, i.e. the last EDR-recorded vehicle speed was obtained at some point within the sample time prior to impact. For example, GM EDRs always indicate the last pre-crash speed data point as having been collected at one sample time prior to impact (1 Hz EDR would indicate last data point as occurring 1-second prior to impact). This source of uncertainty is accentuated by the relatively coarse frequency (1 Hz) most EDRs collect data, and is further complicated by the fact that the sampling strategy varies by make, model, and year of the vehicle.

To account for this uncertainty, the last EDR-recorded speed was assumed to have been obtained at one-half the sample time prior to the crash. In reality, the final time point could have been collected as early as one-full sample time prior to impact. However, the exact time when the final time point was collected cannot be determined from the EDR. Impact speed was then determined using linear extrapolation. A depiction of this method can be found in Figure 49 for a typical GM EDR.

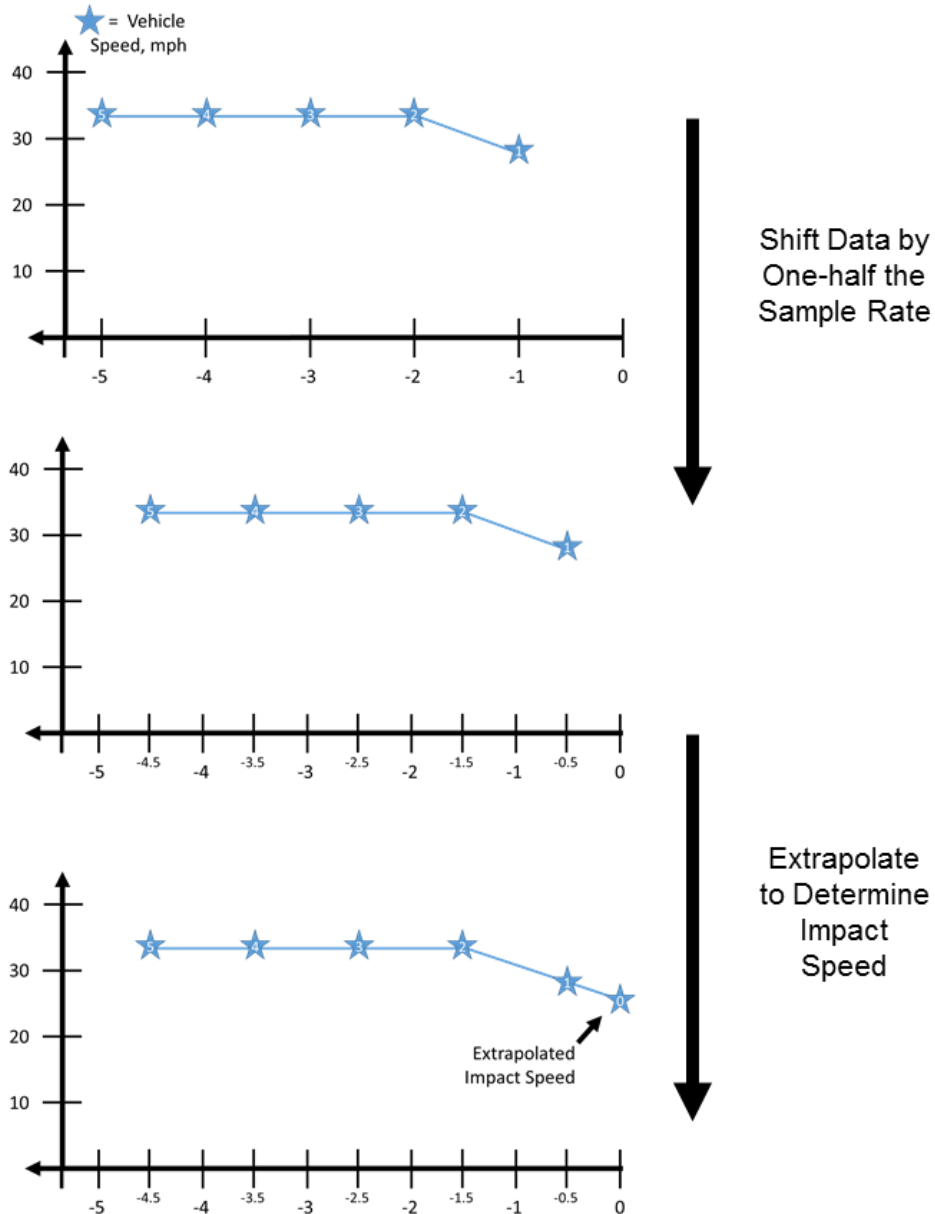


Figure 49. An example case for accounting for uncertainty in sample time step using a 1-Hz EDR. The top-figure shows a typical GM EDR recording of vehicle speed. Time zero represents impact. The last EDR-recorded vehicle speed (labeled as 1) was recorded at some point within 1-second prior to impact. In the middle figure, due to uncertainty in when the last EDR-recorded vehicle speed was recorded, the time series was shifted by one-half the sample time (0.5 s). In the bottom figure, impact speed was determined through linear extrapolation.

Second, the modified velocity profile was numerically integrated using trapezoidal integration in order to determine the position of the vehicle throughout the pre-crash time series. Third, travel

distances were compared to the distance measured from intersection entry to impact. In cases where the recorded travel distance was less than the measured distance, the case was excluded due to insufficient EDR data.

Overview

The kinematics of vehicles involved in SCP and LTAP/LD intersection crashes can be divided into four main phases, which are shown in Figure 50. Vehicle kinematics include the impact speed and crash kinematics, any evasive maneuvering prior to impact, within the intersection kinematics prior to any evasive maneuvering, and the intersection approach kinematics.

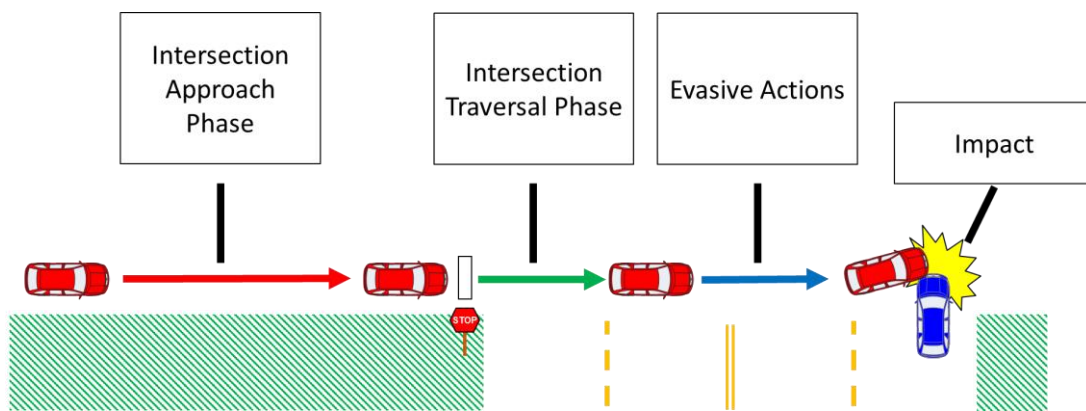


Figure 50. The four main components of pre-intersection crash vehicle kinematics.

Pre-crash Movement Categories

Vehicle behavior prior to the collision is a critical component of reconstructing intersection crashes. The pre-crash movement of each driver was placed into one of three categories. These categories were established based on observations made during our normal and pre-crash driving analysis in Section 1. Drivers that proceeded into the intersection from a full-stop were labeled as “Completely Stopped”. Drivers that accelerated into the intersection after slowing, but not coming to rest, were labeled as “Rolling Stopped”. For non-turning drivers, drivers that did not slow prior to entering the intersection were labeled as “Travelling Through”. For left turning drivers, drivers that slowed as they entered the intersection in order to complete the left turn were classified as “Travelling Through”.

The pre-crash movement of each driver was determined by examining the coded “PREMOVE” variable and the crash narrative prepared by the investigator. The “PREMOVE” variable was occasionally found to be inconsistent with the crash narrative in coding for drivers that stopped. Additionally, the variable lacks details regarding if the driver performed a complete or rolling stop. The scene narrative was used in conjunction with the “PREMOVE” variable in order to determine each vehicle’s most likely movements.

Impact Speed Reconstruction

Overview

Impact speed reconstructions were performed using PC-Crash reconstruction software [199, 210]. PC-Crash uses a collection of trajectory and collision models to simulate the kinematics and kinetics of vehicles before, during, and after the crash. This study utilized the software’s impulse-restitution model to simulate crashes in 2D from the point of impact to the vehicles’ final resting positions. Using the impulse-restitution model, vehicle impacts were modeled in two phases (compression and restitution) as equal and opposite forces about a single point of impact. Simulations were iteratively performed using the PC-Crash optimizer tool in order to determine the most likely impact speeds. Both the impact model [211] and collision optimizer [212] features of PC-Crash have been previously validated using staged crash tests.

PC-Crash includes a “collision optimizer” program, which takes the initial, intermediate, and final vehicle locations and iteratively simulates crashes to find the most likely impact speeds. The PC-Crash collision optimization tool works by minimizing the error between the simulated and the observed intermediate and final vehicle positions. This study used the genetic optimization approach within the PC-Crash software in order to optimize impact velocities, points of impact,

and contact planes within the crash. A schematic of the point of impact and contact plane are shown in Figure 51. Impact velocities correspond to the initial velocity applied to each vehicle at the first simulation point (the initial impact location). The point of impact corresponds to the point where forces were applied to each vehicle during an impact. The impulse-restitution model used in this study models forces about an infinitely small point. The contact plane is used to define the direction of normal and friction forces between the vehicles during an impact.

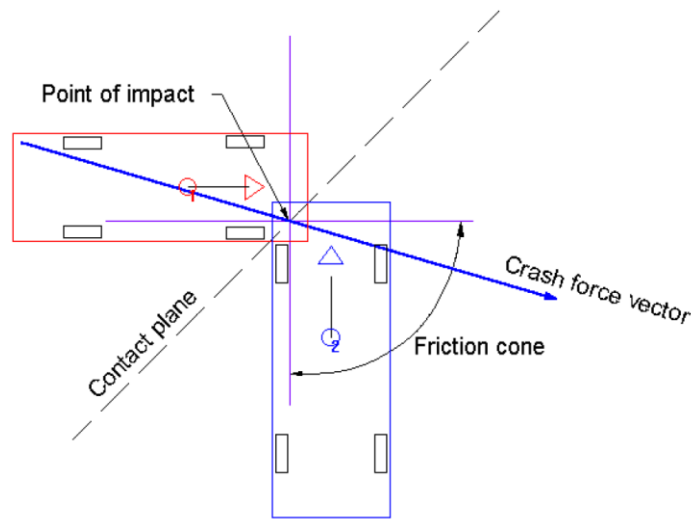


Figure 51. A depiction of point of impact and contact plane using PC-Crash (Figure taken from PC-Crash user manual [213]).

Reconstructions were manually performed by a team of researchers. A summary of the reconstructions methods used in this study can be found in Figure 52. The first step was to prepare the crash scene in PC-Crash followed by determining the impact speeds using the PC-Crash collision optimizer tool. A number of measures were taken to expedite the reconstruction process and ensure its repeatability, including the usage of a customized case viewer and the generation of a detailed reconstruction protocol provided in the Appendix. The customized case viewer contains a link to an internally stored scene diagram, a written scene narrative prepared by the NMVCCS

investigator, and photographs from the crash scene and of each vehicle. The reconstruction protocol contains a detailed description of the reconstruction methods that were followed closely by each reviewer. The following sections detail the reconstruction protocol.

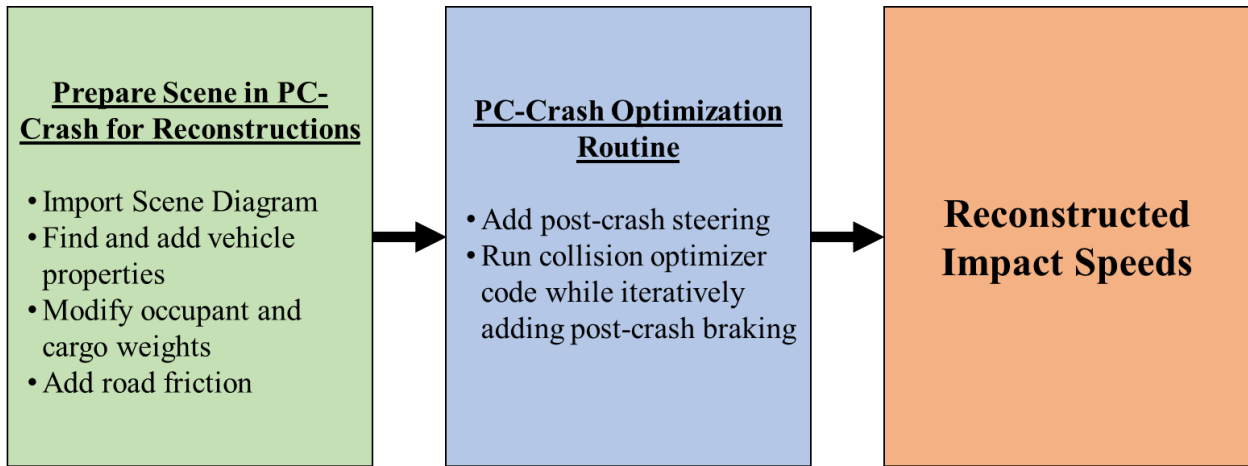


Figure 52. A depiction of the PC-Crash reconstruction protocol.

PC-Crash Scene Preparation

PC-Crash provides a comprehensive platform for inputting unique characteristics from a given crash. This includes the ability to input scene diagrams with impact and post-crash vehicle positions, a large library of vehicles with relevant properties e.g. size, weight, suspension characteristics, and crash stiffness, and customizable road conditions.

Scene diagrams contain a scaled depiction of the crash scene. NMVCCS stores these drawn-to-scale scene diagrams in Easy Street Draw (ESD) files (A-T Solutions Inc.). The ESD files include intersection geometry, road markings, and vehicle locations prior to and following the crash. For each crash, these scaled scene diagrams were exported as an image from ESD then imported into PC-Crash. This scene diagram was then used in PC-Crash to position all vehicles and objects.

PC-Crash uses the Canadian Vehicle Specifications (CVS) database of vehicle properties dating back to model year 1972 [209] . The make, model, and model year of each vehicle involved in the crashes were determined first using the scene narrative. In the event that any of the vehicles were not included in the scene narrative, they were determined using the coded information within the NMVCCS database. The model of the car provided in the scene narrative and coded database are occasionally not specific enough in describing the vehicle involved in the crash, so that it could be associated with a vehicle listed in the PC-Crash vehicle database. For instance, engine sizes (e.g. v4, v6, v8), the number of doors (e.g. 2-door, 4-door), the size of the cargo space (e.g. extended cab packages), and transmission arrangement (e.g. 4-wheel driver vs. 2-wheel drive) may be specified in PC-Crash but not in the NMVCCS records. Accordingly, vehicle photos were used to determine the appropriate vehicle model. For example, markings on the rear or side of the vehicle can provide more detail on optional equipment compared to the make and model alone.

If a specific make and model was not available in the PC-Crash database, a mechanical clone was found either from the same generation or a related manufacturer. For example, if a 1999 Chevrolet Silverado was involved in a crash but not present within the PC-Crash library, a mechanical clone would need to be found. This Silverado was produced from 1999 to 2006 using a similar design, or generation. An alternative Chevrolet Silverado would then be searched for throughout these years. In addition, the 1999 GMC Sierra is a mechanical clone, and has similar vehicle properties.

After appropriate vehicle models were selected, they were placed into their respective impact locations as indicated by the scene diagram. The impact location serves as the initial time point for the impact speed reconstruction. Rest positions, intermediate vehicle locations, and tire marking locations are then added to the simulation using the scene diagram. These initial, intermediate, and

final positions are all considered by the PC-Crash optimizer tool for determining most likely impact speeds.

Occupant and cargo weight are then added for each of the involved vehicles. Cargo weight is documented by the NMVCCS investigator and is available as the “CARGOWGT” variable in the NMVCCS database. Cargo weight was assumed to be in the trunk of the vehicle. The weight of each vehicle occupant was determined using coded variables (“WEIGHT”) within the NMVCCS database. However, the weight of the occupant is not always provided. If the weight is not provided but the occupant gender is, the occupant weight was assumed to be the national average for that gender of individuals aged 20 and over (88.7 kg for male, 75.4 kg for female) determined from the National Health and Nutrition Examination Survey (NHANES) [214].

Each vehicle wheel was inspected for wheel lockup due to damage. This was determined by the researcher using the scene photographs. Wheel lockup almost exclusively occurs after direct contact. For a given wheel, lockup was indicated if the wheel was visibly knocked out of alignment. If wheel lockup is determined for any wheel, 100% braking was applied to the effected wheel, which is recommended by the PC-Crash user manual for these scenarios [213].

Roadside objects were added to the scene diagram at their respective position. These objects were only be included if they are impacted during the crash. Some examples of observed roadside objects are light poles, mailboxes, or trees.

Road friction were modified within the crash space using the road friction tool. The “surcond” variable within the NMVCCS coded database were used to determine the road surface conditions. There are 5 possible surface conditions that can be input into PC-Crash, including dry, wet, very

wet, snow, and ice. The methods for correlating the coded NMVCCS road conditions with the input PC-Crash surface conditions can be found in Table 42.

Table 42. Table for matching coded NMVCCS road conditions within inputted PC-Crash surface conditions.

PC-Crash Surface Conditions	NMVCCS road conditions	Simulated Coefficient of Friction (μ)
Dry	“Dry” “Sand, Dirt”	0.8
Wet	“Wet”	0.5
Very Wet	“Standing water (1/4 inch or deeper)”	0.4
Snow	“Snow covered” “Slush”	0.3
Ice	“Ice”	0.1

PC-Crash Impact Speed Optimization

PC-Crash includes a “collision optimizer” program, which takes the initial, intermediate, and final vehicle locations and iteratively simulates crashes to find the most likely impact speeds. The PC-Crash collision optimization tool works by minimizing the error between simulated and observed the intermediate and final vehicle positions. This study used the programs genetic optimization approach in order to optimize impact velocities, points of impact, and contact planes within the crash. Point of impact and contact plane can be visualized in Figure 53. Impact velocities correspond to the initial velocity applied to each vehicle at the first simulation point (the initial impact location). The point of impact corresponds to the point where forces were applied to each vehicle during an impact. The impulse-restitution model that were used in this study models forces

about an infinitely small point. The contact plane is used to define the direction of normal and friction forces between the vehicles during an impact.

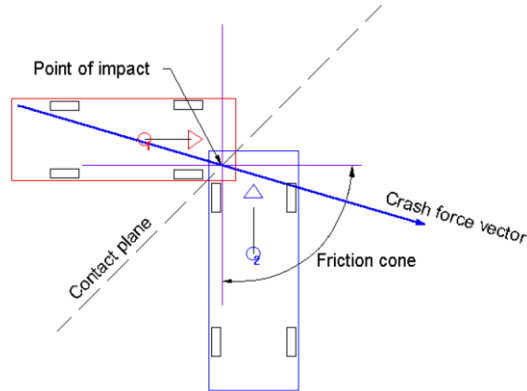


Figure 53. A depiction of point of impact and contact plane using PC-Crash (Figure taken from PC-Crash user manual [213]).

Vehicle braking and steering cannot be optimized using the collision optimizer tool, but are generally needed in order to properly replicate the final crash positions. Braking was iteratively adjusted in 10% of maximum increments for both vehicles to determine the braking combination that minimized error between the simulated and observed vehicle positions. Steering was applied if the post-collision trajectory could not be achieved using braking alone. For example, braking would not be sufficient in a crash where a vehicle pulled over to the road side immediately following impact. Steering was added for vehicles using the follow path tool. This tool is used by laying out the path that the vehicle took post collision. The vehicle would then attempt to follow the path post impact, but is restricted by what is physically possible by the vehicle given its current state. This tool is ideal because it allows for multiple steering sequences.

Accounting for Evasive Braking

Evasive braking occurs frequently in intersection crashes. The NMVCCS database contains coded variables for whether evasive braking and steering occurred. An analysis of this database

indicated that only 15% of drivers in these crashes were indicated as performed an evasive braking maneuver. In contrast, in the chapter 5 avoidance maneuver analysis using EDRs from NASS/CDS, nearly three out of five drivers in SCP, LTAP/OD, and LTAP/LD crashes took evasive braking action.

This observation led to an investigation into the reliability of the coded avoidance maneuver variable as input by the NHTSA investigator. Because only a small sample of NMVCCS EDRs were available, I performed an analysis on the 1,499 NASS/CDS EDR records extracted in Chapter 5. These EDRs were taken from vehicles in SCP, LTAP/OD, and LTAP/LD crashes. The investigator was accurate in indicating whether or not evasive braking occurred for 44% of crashed vehicles. The percentage of false-positive and true-positive indications were 36% and 30%, respectively. This result led to a search for an alternative method to indicate whether evasive braking occurred.

Rather than rely on the NMVCCS recorded avoidance maneuver variable, two methods were used to determine whether an evasive maneuver was performed. First, if the driver completely stopped or performed a rolling stop prior to entering the intersection, the pre-crash acceleration pattern and PC-Crash reconstructed impact speed were used to determine whether evasive braking occurred. Second, if the driver was travelling through the intersection without stopping, logistic regression models formulated using the EDR dataset were used to predict whether evasive braking occurred. The development and validation of this model is shown in Chapter 6.

Evasive braking was modeled by assuming an initial jerk of -11.0 m/s^3 down to some maximum deceleration value. This jerk magnitude is within the range of values typically observed by drivers during conflict situations [215]. In general, maximum vehicle deceleration capacity depends on a

number of factors, including vehicle characteristics, surface conditions, vehicle speed, and surface type [216-218]. This study used maximum deceleration values of 0.3 g, 0.4 g, or 0.8 g based on whether the road conditions were icy, wet, or dry, respectively.

Completely and Rolling Stopped Vehicles

Overview of Methods for Reconstructing Rolling or Completely Stopped Vehicles

The speed profiles of completely and rolling stopped drivers were reconstructed using similar methods. First, the deceleration and acceleration phases of the vehicles were estimated and “stitched” together. Second, the impact speed was used to determine if the driver was likely to have taken evasive braking action. The overall approach can be seen in Figure 54.

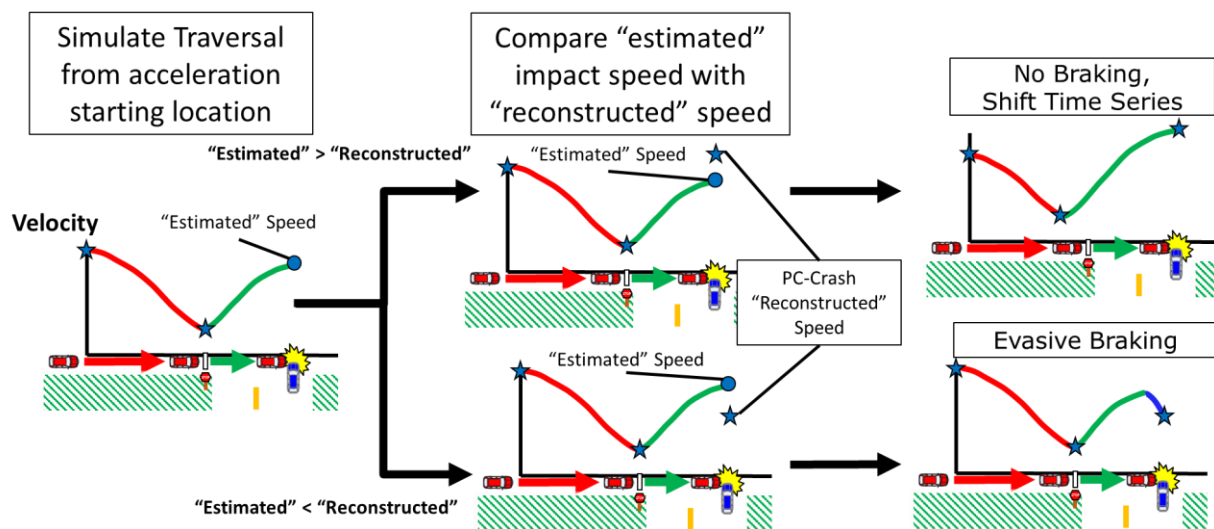


Figure 54. Overview of approach for determining “most-likely” kinematics of drivers that completely or rolling stopped prior to entering the intersection.

Drivers that performed a complete or rolling stop prior to entering the intersection were initially assumed to begin their acceleration into the intersection at the location that the driver entered the intersection. (i.e., stop bar, crosswalk, intersection boundary). An acceleration profile model, described in the following sections, was used to simulate vehicle acceleration from the intersection entry location to the impact location as if no evasive braking had taken place. If the speed at the impact location is higher than the previously reconstructed impact speed, an evasive braking

maneuver was assumed to have occurred. For this scenario, the driver would be modeled as starting their acceleration into the intersection from the starting location followed by evasive braking down to the reconstructed impact speed. If the speed at the impact location fell below the previously reconstructed impacted speed, the driver was assumed to have not performed an evasive braking maneuver. In this scenario, the acceleration starting location was moved away from the intersection until the simulated speed at the impact location and reconstructed impact speed were identical.

Intersection Approach Model

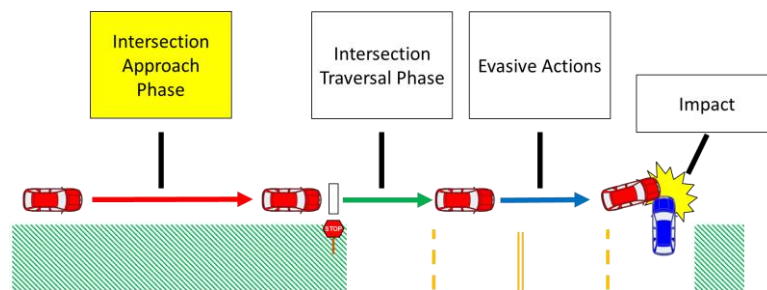


Figure 55. The intersection approach phase is highlighted among the four main components of pre-intersection crash vehicle kinematics.

The intersection approach model developed and described in Chapter 3 was used to determine the deceleration kinematics of the vehicle on the intersection approach. This model was developed using the 100-Car Naturalistic Driving Study (NDS) data collected by the Virginia Tech Transportation Institute (VTTI) [98]. To develop this model, approximately 12,000 previously identified [99] speed traces of intersection approaches for complete and rolling stopped drivers were extracted from the NDS dataset. These developed models account for differences in approach kinematics due to a variety of factors, including stopping behavior (rolling vs. complete stop), turning behavior, and traffic control device. Model development was performed in Matlab using the ARESLab toolbox [123].

Intersection Traversal Model

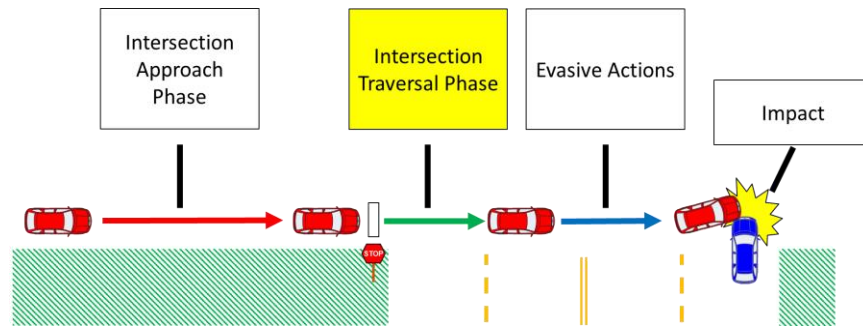


Figure 56. The intersection traversal phase is highlighted among the four main components of pre-intersection crash vehicle kinematics.

The intersection traversal acceleration models developed and evaluated in Chapter 4 were used to model acceleration kinematics into the intersection. These models were developed using pre-crash EDR data. A major finding of this analysis was that drivers in crashes tend to accelerate at higher magnitudes than during normal driving. Accurately reconstructing real-world acceleration patterns is important for accurate assessment of I-ADAS technology.

Travelling Through Vehicles

Overview of Methods for Reconstructing Travelling Through the Intersection Vehicles

Vehicles travelling through the intersection were modeled based on their turning behavior. Non-turning vehicles were assumed to not slow or speed up prior to entering the intersection. Left turning vehicles were assumed to decelerate during the intersection approach down to some safe left turn traversal speed. These behaviors are depicted in Figure 57 and Figure 58. For both sets of behaviors, the traversal speed and evasive braking action must be estimated. The following sections detail the methods used to reconstruct pre-crash kinematics for travelling through vehicles.

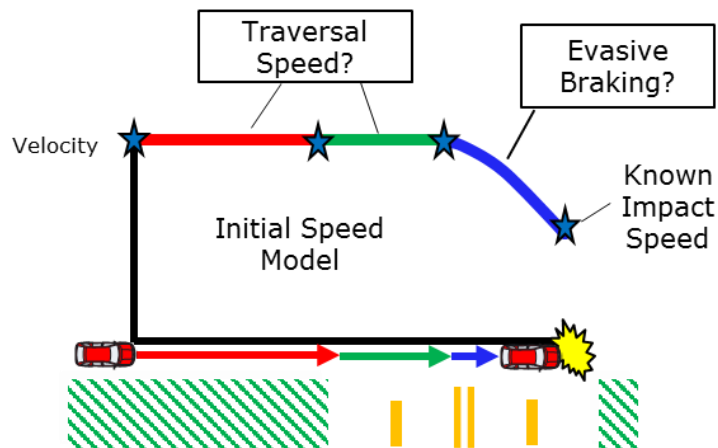


Figure 57. Example travelling through profile for non-turning vehicle.

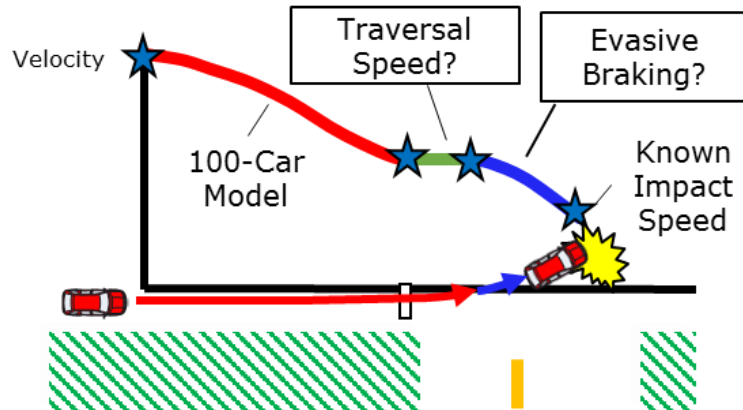


Figure 58. Example travelling through profile for vehicle turning left.

Travelling through vehicle speeds were reconstructed in two phases. First, a developed logistic regression model was used to estimate the likelihood that crash avoidance braking occurred given the reconstructed impact speed. Second, each speed profile was then reconstructed with and without evasive braking. The probability of an evasive braking action having occurred was used to weight each scenario. The most likely traversal speed for the trajectory with evasive braking was estimated using a developed linear regression model. Figure 59 gives a general outline of these methods.

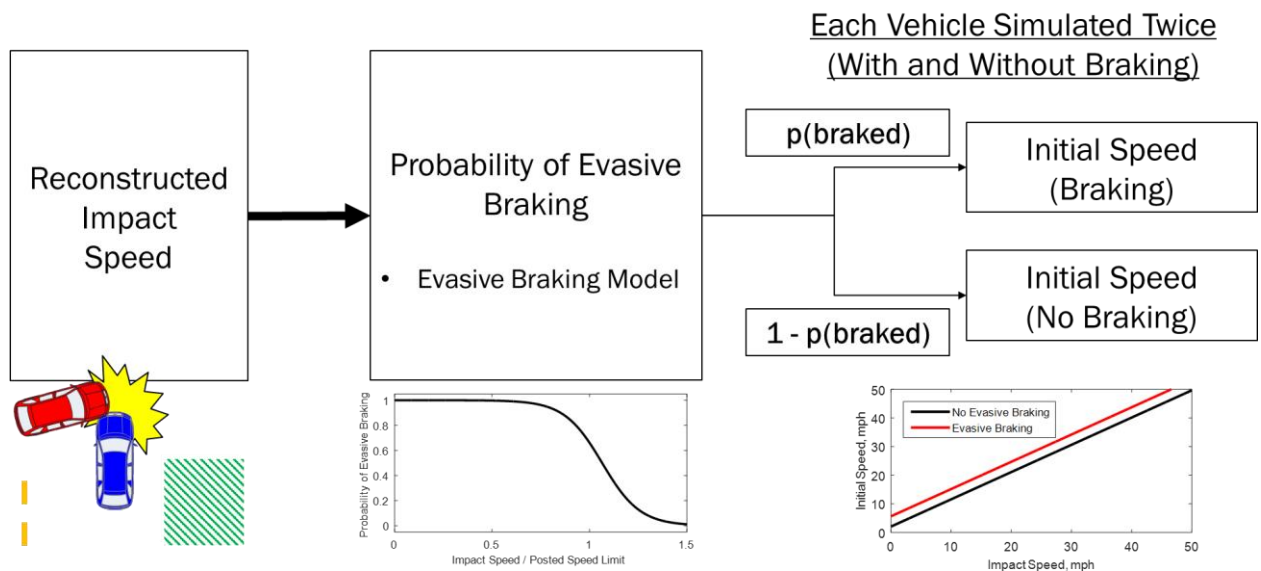


Figure 59. Steps that will be used to reconstruct the kinematics of travelling through vehicles.

Evasive Braking for Travelling Through Vehicles

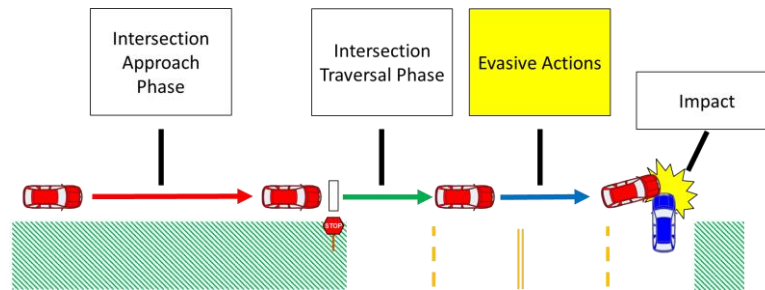


Figure 60. The evasive actions phase is highlighted among the four main components of pre-intersection crash vehicle kinematics.

Logistic regression models were developed in Chapter 6 for predicting whether a travelling through driver was likely to have taken evasive action. These model used the reconstructed impact speed in order to estimate the likelihood that an evasive braking maneuver attempt occurred. Two scenarios were then modeled: one without evasive braking and one with evasive braking. Both scenarios were weighted based on their likelihood of having occurred as indicated by the regression model.

The one exception to performing the simulation twice was if the impact speed was excessively high or low. These cases would suggest either a very high or very low likelihood of evasive braking having occurred. Specifically, if the probability of an evasive braking maneuver having or having not occurred was above 99%, only the more likely scenario was simulated. Additionally, if the impact speed was below 15 mph for straight crossing drivers or 7 mph for left turning drivers, only a scenario where the driver evasive braked was simulated. Using the dataset from Chapter 6, non-evasive braking drivers rarely (2% for left turning and 3% for straight crossing) have impact speeds below these speeds.

Traversal Speeds for Travelling through Drivers

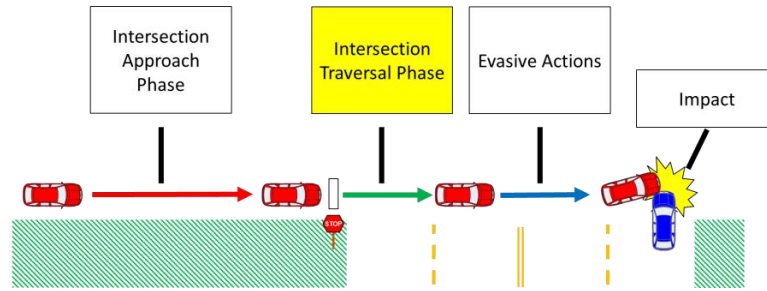


Figure 61. The traversal phase is highlighted among the four main components of pre-intersection crash vehicle kinematics.

The travel speed prior to any evasive action was determined using the linear regression models developed in Chapter 6. The driver was assumed to have maintained this traversal speed from intersection entry until the beginning of any evasive braking. This regression model used the drivers known impact speed to make an estimate of the driver's most likely traversal speed. In the event of no evasive braking, the driver was assumed to have maintained their impact speed throughout the traversal.

Approach Speeds for Travelling through Drivers

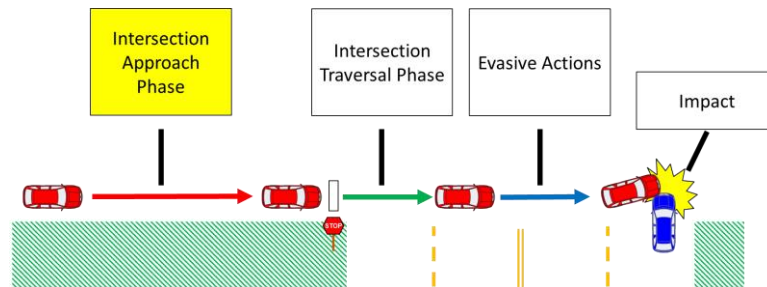


Figure 62. The approach phase of the pre-crash action is highlighted.

The approach phase was handled differently for the different turning behaviors. If the vehicle was non-turning, they were assumed to have maintained their traversal speed throughout the

intersection approach. If the vehicle was left-turning, the driver was assumed to have been decelerating up until the point of intersection entry (i.e., stop bar, crosswalk, or boundary line).

The approach model for left turn, travelling through drivers was generated in Chapter 3. The model was developed from a set of 1,132 left turn, travelling through approaches extracted from the 100-Car study. The model represents approach kinematics as an acceleration versus distance relationship, which allows continuity in the speed profile between the approach and traversal phase. The independent variables used were distance from phase transition, speed at intersection entry, speed limit, driver gender, and driver age. Example trajectories from this model can be seen in Figure 63.

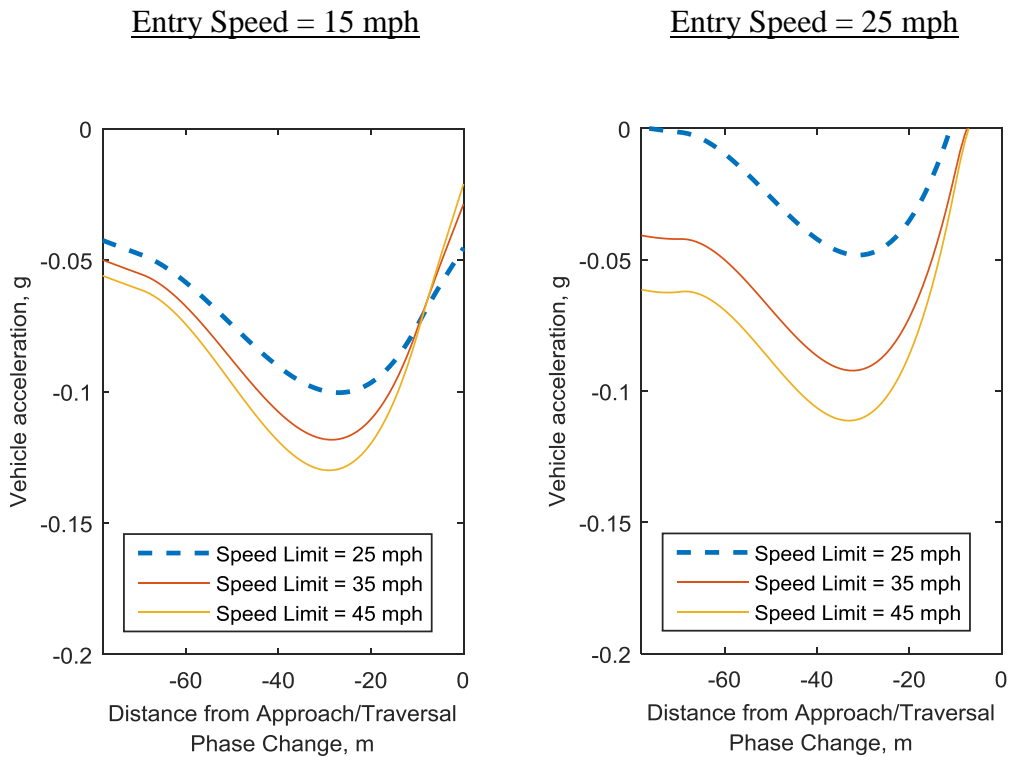


Figure 63. Example trajectories (acceleration versus distance) of the approach phase for left-turning drivers travelling through an intersection. Trajectories are for an adult male.

7.5 Overview of NMVCCS Dataset

A total of 1,531 (1,139 SCP and 392 LTAP/LD) crash reconstructions were performed in this study. These simulations were based generated using 448 SCP crashes and 213 LTAP/LD from the NMVCCS database. These crashes were representative of 254,877 U.S. crashes.

The following sections detail the composition of the included cases in the simulation case set. Several parameters were considered, including speed limit, traffic control device, and pre-crash stopping behavior. It should be noted that this dataset was generated exclusively from U.S. crash data, so generalizing this dataset to other countries should be done with caution. Additionally, because inclusion criteria were used to subset all available crashes in NMVCCS, a comparison of all cases “Valid after manual inspection” were compared with the simulation case set in order to ensure similitude.

Traffic Control Devices

There are, in general, four traffic control device variations that are represented in U.S. SCP and LTAP/LD crashes. The relative proportion of each variation for the simulation case set is shown in Figure 64. Signalized (SCP = 55%, LTAP/LD 36%) and two-way stop-controlled (SCP = 41%, LTAP/LD 58%) intersections comprised nearly the entire dataset. Very few of the crashes occurred at four-way stop-controlled (SCP = 4%, LTAP/LD 1%) or at unsignalized (SCP = 0.3%, LTAP/LD 3%) intersections.

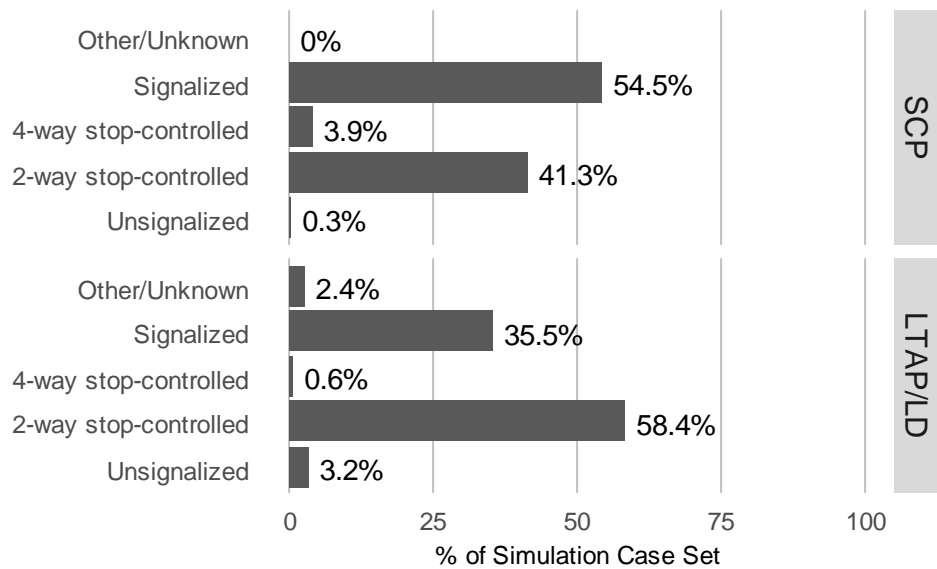


Figure 64. Crashes within this study’s simulation case set by traffic control devices.

These proportions were compared with the full simulation case set prior to case exclusion. The composition of the case set prior to exclusion can be seen in Figure 65. In general, the composition of traffic control devices in the simulation case set was very similar to that of the original set of crashes extracted.

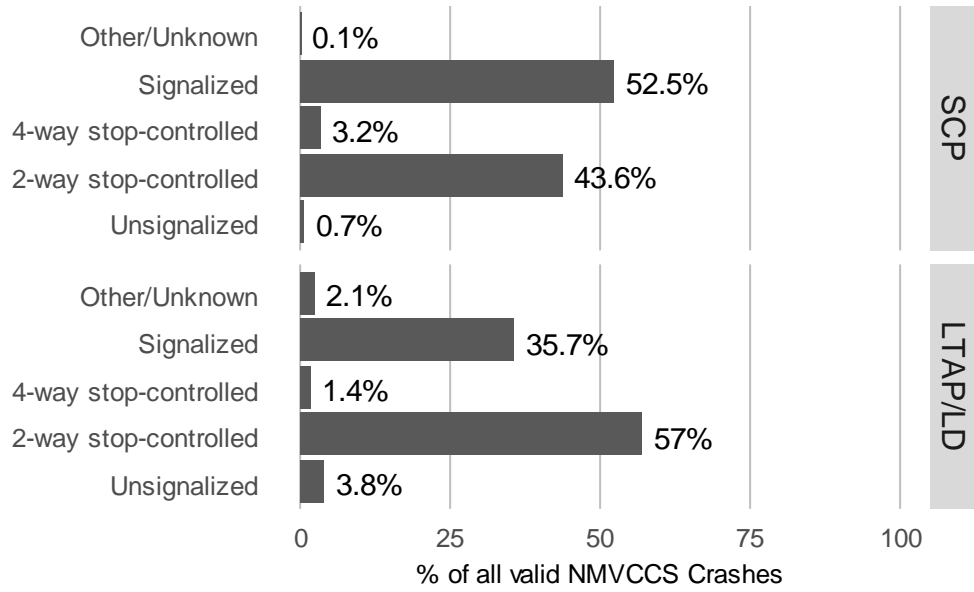


Figure 65. Original set of cases extracted crashes broken down by traffic control devices.

Speed Limits

Speed limits are provided in Figure 66 for the simulation case set by whether the vehicle had the right of way. In general, the majority (64%) of SCP crashed vehicles in the simulation case set were travelling on roads with a speed limit less than or equal to 35 mph. A lower proportion (44%) of LTAP/LD crashed vehicles were travelling on roads with speed limits of 35 mph or lower.

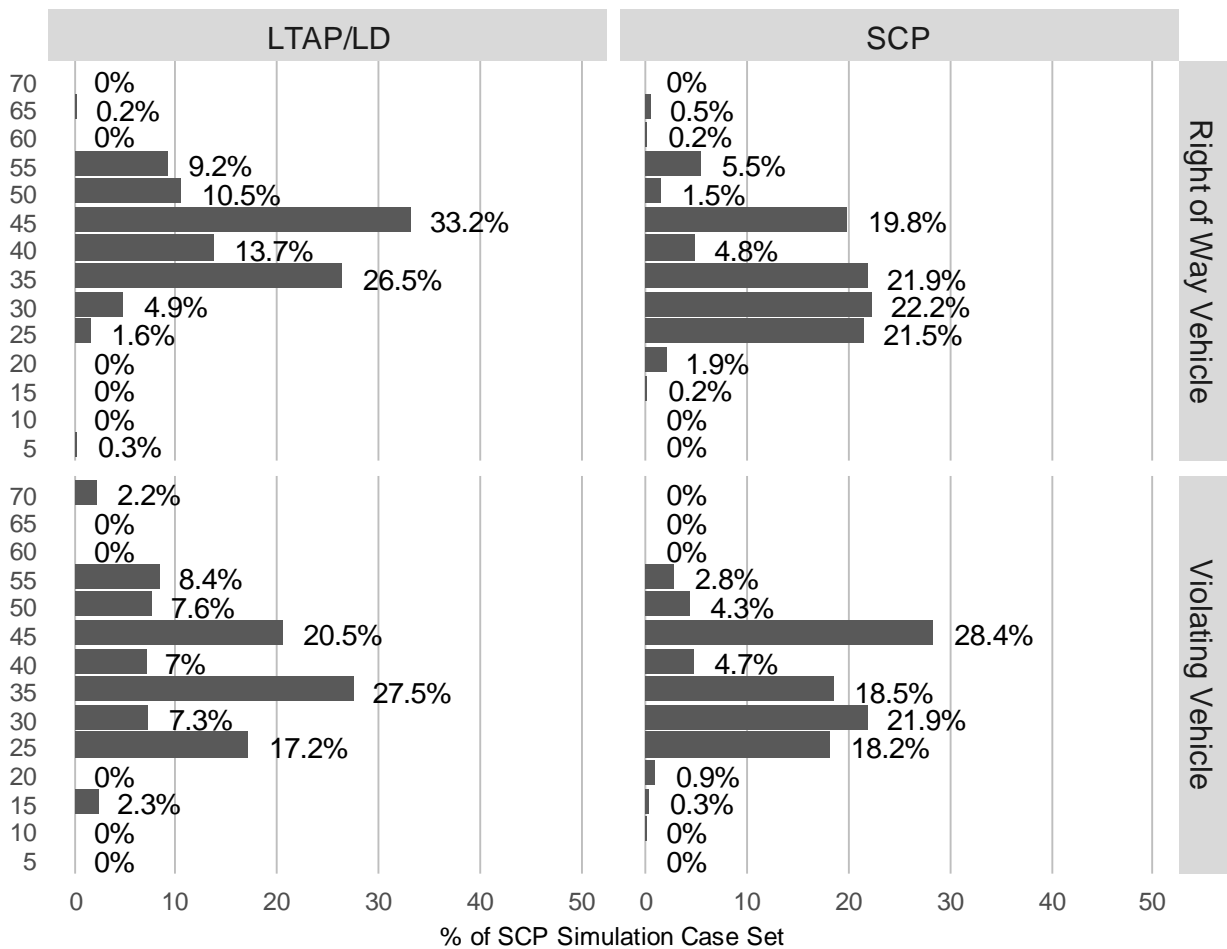


Figure 66. The distribution of speed limits for the simulation case set used in this study.

Speed limit distributions in the simulation case set were then compared with the original full set of NMVCCS SCP and LTAP/LD crashes. The full dataset composition can be seen in Figure 67. In general, the distribution of speed limits in the simulation case set were very similar to the

all valid crashes available in NMVCCS. For example, when considering all valid SCP crashes in the NMVCCS dataset, 63% of vehicles had a speed limit less than or equal to 35 mph, which is comparable to the 64% of cases in the simulation case set. Likewise for LTAP/LD crashes, the set of all valid LTAP/LD crashed vehicles were travelling on roads with speed limits of 35 mph or less in 46% of crashes, which compared well to the 44% in the simulation case set.

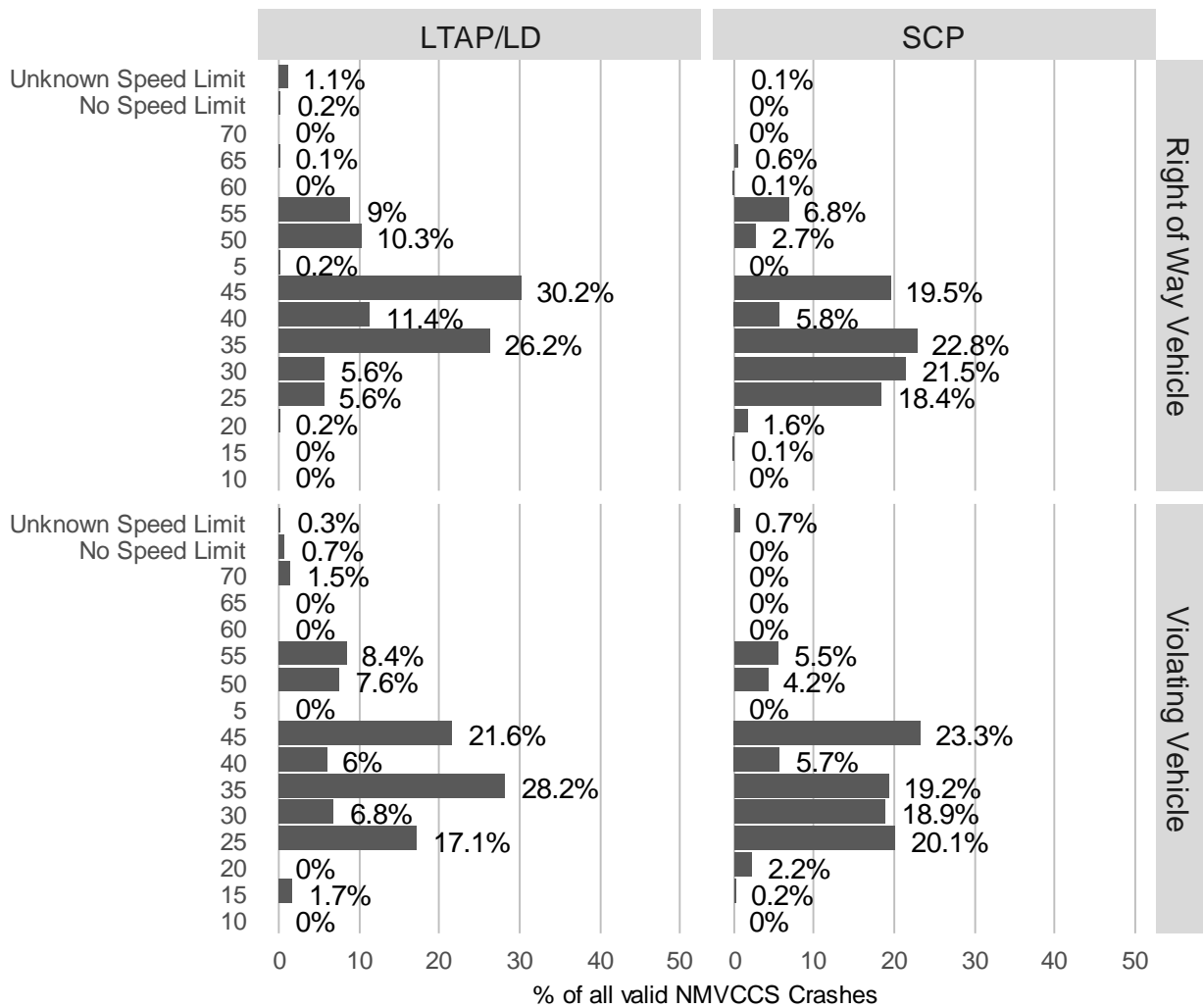


Figure 67. The distribution of speed limits for the original set of extracted crashes prior to exclusion.

Pre-Crash Behavior

Accounting for different pre-crash movements was an important aspect of this study’s reconstruction methods. Whether the vehicle stops (completely or rolling) or travels through the intersection influences (a) the available time for I-ADAS response and (b) the requirements for sensor detection. Consequentially, pre-crash movements are expected to influence expected benefits. Based on this, it can be hypothesized that, in general, I-ADAS will be more effective in LTAP/LD crashes than in SCP crash. A summary of the pre-crash movements observed in this dataset can be found in Table 43. It is important to note the relatively high proportion of SCP crashes that occur between two vehicles that did not perform a rolling or complete stop (53.8%). When compared to LTAP/LD, these pre-crash movement scenario is much less common, only comprising around 11.3% of all LTAP/LD crashes.

Table 43. Summary of pre-crash movements observed in this study.

Crash Mode	Pre-Crash Movement		Count	% of Crash Mode	Weighted Count	Weighted % of Crash Mode
	No Right-of-way	Right-of-way				
SCP	Stopped	Stopped	6	1.3	2,093	1.4
	Stopped	Moving	118	26.3	48,020	32.0
	Moving	Stopped	83	18.5	83	22.2
	Moving	Moving	241	53.8	66,781	44.5
LTAP/LD	Stopped	Stopped	0	0.0	0	0.0
	Stopped	Moving	151	70.9	67,162	64.1
	Moving	Stopped	38	17.8	29,719	28.4
	Moving	Moving	24	11.3	7,837	7.5
Total			661	100.0	254,877	100.0

There are several reasons why a higher proportion of LTAP/LD crashes had at least one of the vehicles coming to a complete or rolling stop. First, for LTAP/LD crashes at signalized intersections, the straight crossing vehicle is more likely (about 74% of the time) to have been the

violating vehicle and run the red light. This finding suggests that, at signalized intersections, left turning vehicles are less likely to run a red light than straight crossing vehicles. Because of this, 81% of LTAP/LD signalized crashes involved at least one vehicle stopping prior to entering the intersection. Conversely for SCP crashes, 44% of these crashes involved at least one of the vehicles stopping before entering the intersection.

Second, left turning vehicles were less likely to run a stop sign. The left turning vehicle is almost always (96%) the violating vehicle at stop sign controlled intersections. Our analysis revealed that 83% of these left turning violating vehicles came to a complete stop, 16% performed a rolling stop, and the remaining 1% was classified as travelling through. One of the travelling through, left turning vehicles inadvertently ran the stop sign, while the other two vehicles were describes as having failed to either “pause or stop” or having “continued through the intersection without stopping”. In general, only 0.6% of LTAP/LD crashes at stop sign-controlled involved both vehicles travelling through. Conversely, for SCP scenarios, 30% of the stop sign-controlled crashes occurred with both vehicles having travelled through. These crashes typically occurred when one of the drivers inadvertently runs the stop sign [180].

Driver pre-crash movements were compared with all valid cases extracted from NMVCCS. Figure 68 shows pre-crash movements for all valid SCP and LTAP/LD crashes extracted from NMVCCS. In general, the proportions of travelling through vehicles in the simulation case set were comparable to the all valid extracted crashes. In the full set of valid SCP crashes, 72% of crashed vehicles were travelling through. Similarly for the simulation case set, 71% of crashes vehicles were travelling through. Likewise for LTAP/LD crashes, 54% of crashed vehicles were traveling through in the simulation case set, which compared well to the 53% of crashed vehicles for all valid NMVCCS crashes.

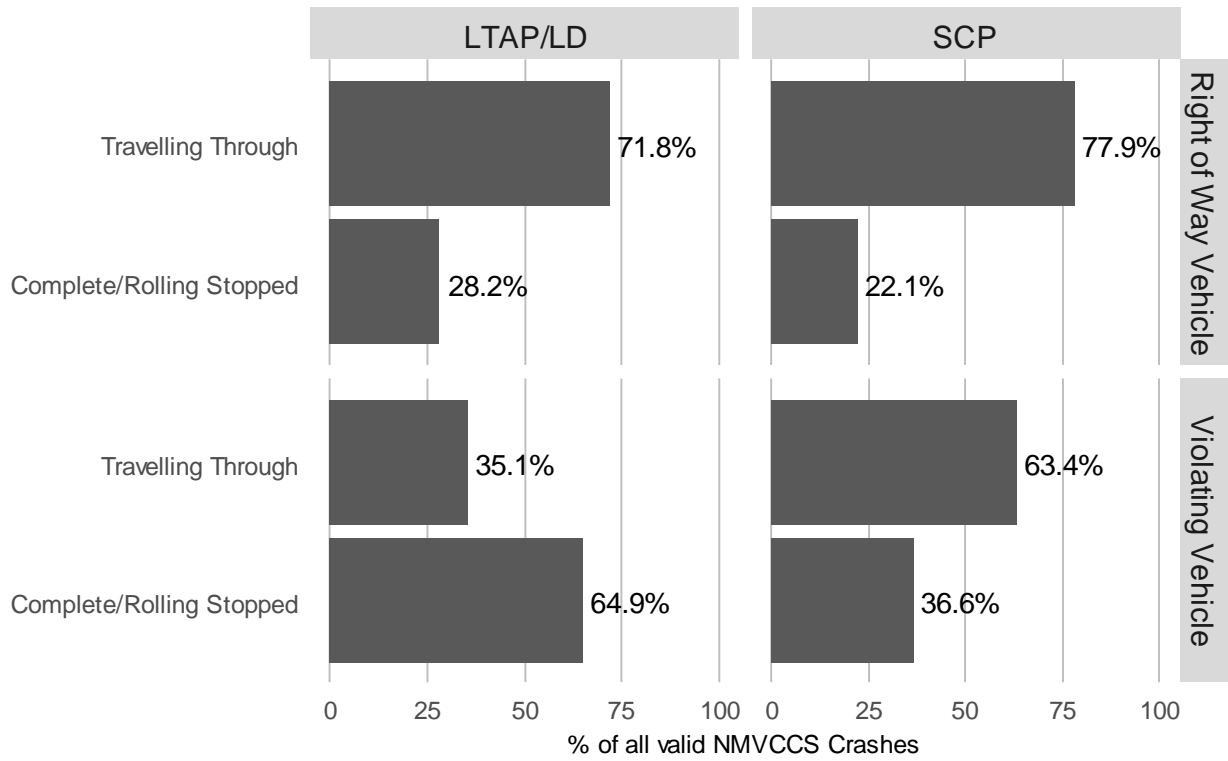


Figure 68. The pre-crash movements for all vehicles extracted from valid NMVCCS SCP crashes.

Section 3:
Evaluating I-ADAS Capabilities

8. Predicting Crash-Relevant Violations at Stop Sign-Controlled Intersections for the Development of an Intersection Driver Assistance System⁴

8.1 Introduction

One I-ADAS function will be to detect approaching vehicles using onboard sensors, such as radar or lidar. Current technology in the vehicle fleet uses forward-facing radar for cross-traffic object detection [82, 83], and future systems may use side-facing sensors to detect oncoming vehicles from greater distances [92, 158]. However, this strategy of detecting oncoming vehicles will be less effective if vehicles fail to yield prior to entering the intersection because less time will be available to detect and avoid an imminent crash. Failure to yield at an intersection is a substantial priority. For straight crossing path (SCP) intersection crashes in the U.S., approximately one-third [91, 92] of stop sign-controlled crashes and nearly all (95%) [92] of signalized intersection crashes involved a vehicle failing to yield for the traffic control device.

An alternative strategy may be to alert the driver of an impending traffic signal violation earlier in the intersection approach, while the driver still has time to yield for the traffic control device. Previous work estimates that 90% of drivers that run stop signs failed to detect the traffic control device during the approach [180]. The first challenge is to detect an upcoming stop sign or signalized intersection. Vehicle-to-infrastructure (V2I) communication of vehicle position is possible [219], but may be prohibitively expensive in the case of stop-sign controlled intersections. Current vehicle-based technologies could however make this approach feasible. For example, advances in automated traffic sign detection utilize vision-based technology to detect traffic

⁴ The work shown in this study has been a part of several previously published peer-reviewed manuscripts, including:
181. Scanlon, J.M., R. Sherony, and H.C. Gabler, *Predicting Crash-Relevant Violations at Stop Sign-Controlled Intersections for the Development of an Intersection Driver Assistance System*. Traffic Injury Prevention, 2016. **17**(sup1): p. 59-65.

control signs, such as stop signs [220-224]. Another approach is to couple GPS traces with map data for detecting an upcoming intersection [225-227].

There are two competing priorities when designing an I-ADAS that accurately notifies a driver of an impending violation. First, the system should aim to maximize the number of correctly predicted violations, or the true-positive proportion. The true-positive proportion is the ratio of correctly identified violations to the total number of violations. However, when maximizing correctly identified violations, there is a tradeoff in the number of false alarms that might be delivered to the driver, or the false-positive proportion. The false-positive proportion is the ratio of non-violations incorrectly identified as violations to the total number of non-violations. Accordingly, the second priority when designing these systems should be to limit false-positive warnings. Maintaining this balance of identifying violations while not delivering false alarms is important for the implementation of a driver warning system. Drivers that receive too many false-positive alerts could become annoyed and as a result become less reactive when a true alert is given [139, 140] or turn off these alarms altogether [141]. Additionally, for drivers to trust in the warning system, the driver expects to be warned early enough to be able to stop the vehicle [138].

The objective of this study was to develop a stop sign violation detection algorithm, and evaluate its ability to provide an accurate and timely detection. Three research questions were posed in this study. First, how often would drivers be alerted? Second, when would drivers be alerted? Third, could the vehicle be stopped at this earliest violation detection opportunity?

8.2 *Methods*

Defining a Stop Sign Violation

By law, drivers must come to a complete stop at stop signs in the United States. Although any non-complete stop is considered a violation from a legal standpoint, drivers frequently “roll” through stop sign-controlled intersections in real-world scenarios [85]. Because this stopping behavior is so typical, warning drivers every time they perform a rolling stop could lead to driver annoyance and/or poor acceptance of the technology. In an ideal scenario, drivers would receive warnings only when they are unaware of an approaching stop sign. However, there is no perfect speed threshold that can distinguish between drivers that are aware or unaware of an imminent stop sign. An alternative approach is to select a speed threshold that is atypical during “normal” driving but commonly observed during pre-crash scenarios. This study defined a stop sign violation as a vehicle which travelled at a speed in excess of 20 mph (32 kph) throughout the entire intersection approach. Previous work indicates that drivers rarely cross stop bars at speeds in excess of 20 mph (0.2%) [85]. Using the 100-Car naturalistic driving dataset extracted in this study, drivers were similarly found to have travelled in excess of 20 mph throughout the entire intersection approach in only 1.1% of samples. Conversely, in pre-crash scenarios, drivers frequently travel at speeds in excess of 20 mph. In fact, of the 90 event data recorder (EDR) records considered for this study’s analysis that were taken from SCP intersection crashes, 27% of the drivers were travelling at speeds in excess of 20 mph throughout the intersection approach.

Data Sources

This study used two data sources for generating a single dataset of typical driver behavior (100-Car Naturalistic Driving Study) and violations (EDR downloads from real-world crashes). These data sources are detailed in Chapter 2.

The 100-Car NDS study instrumented vehicles with measurement devices that recorded a number of data elements, including speed and braking. The intersection events to be used in this study were previously identified as part of the CICAS-V study [99]. This dataset of stop sign-controlled intersection traversals were found using GPS coordinates from (1) a list of intersections provided by the Virginia Department of Transportation (VDOT) as having elevated crash frequencies and (2) intersections frequently traversed by study participants. The inclusion criteria established in Chapter 2 were used to extract a set of stop sign approaches from this dataset.

EDR records downloaded from stop sign violating vehicles were also used in the current study. In addition to the inclusion criteria established in Chapter 2 for extracting EDR records, only stop sign violations were of interest in this study.

Overview of Methods for Developing and Evaluating Stop Sign Violation Detection Model

This study's overall strategy is depicted in Figure 69. A dataset of stop sign violations and non-violations were first extracted. Vehicle positions through time during the intersection approach were reconstructed for each case. A leave-one-out cross-validation technique was performed to assess the potential violation detection capacity of the hypothetical stop sign warning algorithm. Using this method, one approach is withheld as a testing dataset, while the remaining approaches were used as a training batch. The training dataset was used to develop a stop sign warning algorithm. The developed model was then validated using the approach in the testing dataset. The

process was then repeated for the remaining approaches until a violation prediction was obtained for every traversal.

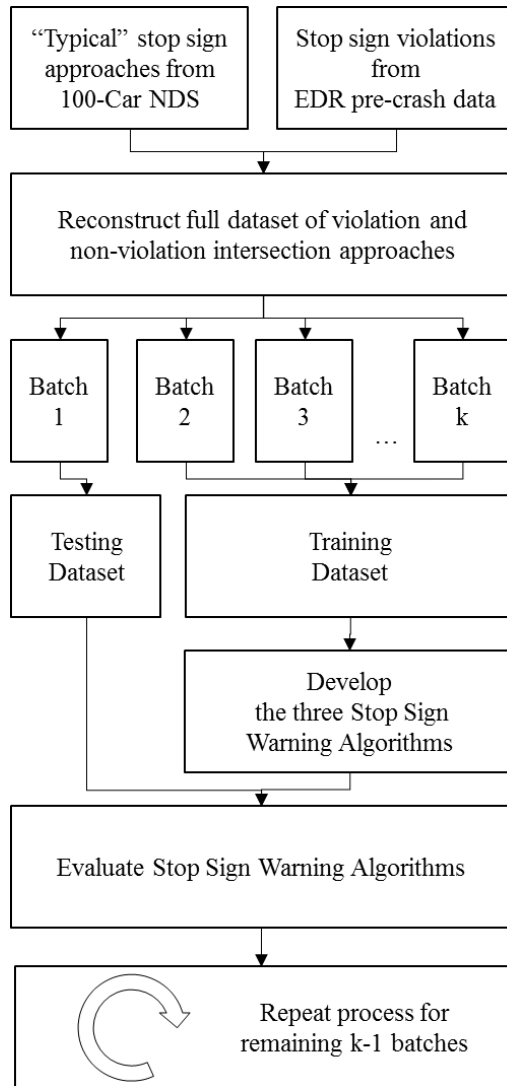


Figure 69. The flowchart depicts this study's overall strategy.

Intersection Approach Reconstructions

For the 100-Car dataset, vehicle speed collected from the vehicle CAN bus was used to reconstruct vehicle position throughout the intersection approach. The time step where the stop bar was last visible was assumed to be the end of the intersection approach.

For the EDR dataset, the protocol established in Chapter 7 was used to trace back the position of the vehicle during the intersection approach. EDR-recorded pre-crash speed was used to reconstruct the vehicle's position through time. In current EDRs, there is some uncertainty in the timing of pre-crash speed and braking records with respect to the time of impact, which was accounted for using the methods detailed in Chapter 7 for tracing back vehicle positions through time. The scene diagram prepared by the NASS/CDS investigator was used to determine the end of the intersection approach. The stop bar was used as the end of the intersection approach if present. If no stop bar was present, the intersection boundary was used as the end of the intersection approach. Intersection boundary lines were drawn by extrapolating the road edge through the intersection.

Numerical integration was used to estimate the location of the vehicle throughout the reconstructed intersection approach up to 50 m prior to the vehicle entering the intersection. As discussed later in this paper, our stop sign detection algorithm was assumed to begin monitoring for potential stop sign running at 50 m from the intersection.

Hypothetical Stop Sign Warning Algorithm

This paper evaluates the potential of a hypothetical stop sign warning algorithm for an I-ADAS. A unique algorithm was developed for each training batch. The proposed system evaluates the likelihood of a stop sign violation at discrete locations along the intersection approach using a

series of logistic regression models. The algorithm begins to monitor the likelihood of a violation beginning 50 m prior to intersection entry, and continues to reevaluate the likelihood of a stop sign violation at intervals of 2.5 m. The hypothetical system was assumed to be deactivated if (a) the vehicle's velocity fell below 20 mph (32 kph) (i.e. the vehicle was no longer "violating") or (b) the vehicle was within 10 m from entering the intersection. An earliest violation detection distance of 50 m was selected because an earlier analysis of the dataset showed that most non-violating drivers (60%) begin to decelerate before this distance before the intersection. The 10 m threshold helps limit false alarm warnings for drivers that have already yielded (slowed or stopped) and began accelerating into the intersection. Early analysis of the non-violation dataset showed that 98.6% of drivers began accelerating within 10 m prior to entering the intersection.

It should be noted that, in a production car, the proposed system would evaluate the likelihood of a stop sign violation continuously through time, i.e. at discrete time points. If the system was modeled as assessing violation likelihood at some sampling rate, the algorithm would still need to use a relevant logistic regression model. For example, if the system reevaluated the likelihood of a violation at 18.8 m before the intersection, the system might use the logistic regression model for 17.5 m or 20 m, neither of which would be perfectly appropriate. As an alternative, the algorithm developed in this study evaluates likelihood of a violation at discrete 2.5 m increments as a uniform means of assessment. For a vehicle travelling at 30 mph, the system would reevaluate likelihood of a violation once every 0.2 s (5 Hz), and at 60 mph, the system would reevaluate likelihood of a violation once every 0.1 s (10 Hz). The detection refresh rate was considered to be realistic given the refresh rate of current collision avoidance systems [228-230].

Three violation detection algorithms were explored in this study, including an "early detection", "intermediate detection", and "delayed detection" model. The early detection algorithm detects

violations at the earliest time point during the intersection approach. However, this algorithm is the most susceptible to false alarms. Vice versa, the delayed detection algorithm is the least prone to false alarms, but will tend to deliver later alarms. These three algorithms were developed by setting different cut-off violation prediction probabilities. If the probability of a violation exceeds this cut-off value at a given location, an alert would be delivered to the driver, and this location would be labeled the “earliest violation detection location”. For each model and training batch, unique violation prediction probability thresholds were selected for each location along the intersection approach. At a given location along the intersection approach, the thresholds selected for the early, intermediate, and delayed detection models were set so that 5%, 1%, and 0.5% of non-violations were incorrectly identified as violations.

Logistic Regression Model Development

Logistic regression models were developed in this study using the *glm* function in the R programming language [121]. Weighting factors were applied to weight the non-violations and violations according to how often they might occur in the real-world. Violations were assumed to represent 0.2% of intersection traversals, which was taken from the results of the previously discussed naturalistic driving study dataset [85, 86, 90]. Each violation in this study was given a weight of 1, and the weight for the non-violation approaches was calculated using Equation 23.

Equation 23.
$$\text{weight}_{\text{non-violations}} = \frac{99.8\%}{0.2\%} \cdot \frac{N_{\text{violation}}}{N_{\text{non-violations}}}$$

Where,

- Weight_{non-violation} = weighting factor assigned to non-violations,
- N_{violation} = Number of violations in dataset,
- N_{non-violations} = Number of non-violations in dataset.

Two measures were used to model likelihood of a stop sign violation. The first measure was RDP, shown in Equation 24. RDP is defined as the average deceleration magnitude required to stop the vehicle given some velocity and stopping distance. RDP is a useful measure for determining a vehicle's capacity to yield for a stop sign. The second measure was current brake application status, which was used to assess whether the driver was actively attempting to slow the vehicle (i.e. drivers that were braking more likely to stop). Braking data is stored as a binary variable, i.e. 1 = brake pedal depressed and 0 = driver not braking.

Equation 24
$$RDP = \frac{v^2}{2 \times D_{SL}}$$

Where

- RDP = Required deceleration parameter
- v = Current vehicle speed
- D_{SL} = Distance from the stop location

The logistic equation was used to generate a single composite metric that can be used to calculate the probability of a stop sign violation at a given distance from the intersection. This relationship is shown in Equation 25.

Equation 25
$$P_{\text{violation}} = \frac{1}{1 + e^{-(\beta_0 + \beta_1 \cdot RDP + \beta_2 \cdot Brake)}}$$

Where

- P_{violation} = probability of a violation (0-1)
- β₀₋₃ = Model Parameters
- RDP = Required deceleration parameter
- Brake = 1 is on / 0 is off

Evaluation of Stop Sign Warning Algorithm

The timing of the warning was evaluated using RDP after some driver reaction time, which can be calculated using Equation 26. RDP after reaction time represents the required deceleration to stop the vehicle after some elapsed perception-reaction time (PRT). This study used a PRT of 1.0 s, which is within the bounds of typical reaction times observed during an experimental study looking at how drivers respond to an in-vehicle alert of a potential intersection violation [231] .

Equation 26
$$\text{RDP (after PRT)} = \frac{v^2}{2 \times (D_{SL} - v \times \text{PRT}) \times g}$$

Where

RDP (after PRT)	=	Required deceleration parameter after perception-reaction time
v	=	Current vehicle speed
D_{SL}	=	Distance from the stop location
PRT	=	Perception-reaction time
g	=	gravitational constant

The study evaluated the braking capacity of vehicles with respect to RDP. Maximum vehicle deceleration capacity will play an important role in the effectiveness of stop sign violation warning systems, and depend on a number of factors, including vehicle characteristics, surface conditions, vehicle speed, and surface type [216-218]. Nominal maximum braking decelerations on wet and dry pavement/asphalt/concrete are 0.7 g to 0.8 g, respectively [39]. In snow, this maximum braking deceleration decreases to 0.4 g. When evaluating RDP in this study, three possible surface conditions were considered, i.e. poor (max. braking = 0.4 g), moderate (max. braking = 0.6 g), and good (max. braking = 0.8 g) braking conditions.

8.3 *Results*

Dataset Summary

This study's dataset consisted of 696 total intersection approaches. A total of 665 of those approaches came from the 100-car dataset, while 31 approaches came from the EDR dataset of violations. Of the 665 100-Car approaches, 7 of the drivers were classified as violators. In total, the final dataset consisted of 38 stop sign violations. Violations were weighted using a factor of 1, whereas non-violations were assigned a factor of 28.8 using Equation 23. These weighting factors were applied in order to weight violations and non-violations based on how often they occur in real-world scenarios.

A total of 967 previously identified stop sign intersection approaches from the 100-Car study were considered for this study. A total of 41 cases were excluded due to the traversal occurring too near the beginning or end of the vehicle trip. An additional 124 cases and 137 cases were excluded due to invalid brake and speed data, respectively.

A total of 126 EDR records were considered for this study. Two of the cases were excluded after a manual review revealed that the cases had been incorrectly identified as SCP intersection crashes. A total of 90 of the remaining 124 vehicles (73%) were non-violations and were excluded from the dataset. Two additional crashes were excluded due to the stop bar not being included in the scene diagram despite being present in on-scene photographs. One additional crash was excluded due to likely wheel slip (braking $> 1G$).

Statistical Models Using Entire Dataset

Logistic regression models were fit to the entire dataset for various distances prior to intersection entry. Model regression parameters for 2.5 m steps can be found in Table 44. The

results from the Wald χ^2 tests to examine the significance of each predictor are shown. For every distance analyzed, brake application and RDP were found to be statistically significant ($p < 0.05$) predictors of stop sign violations. It should be noted that these model coefficients represent a fit to the entire dataset. For the leave-one-out cross-validation procedure used in this study to evaluate the model, 20 different models (fit from 20 unique training batches) were generated for each detection distance. AUC with confidence intervals are also shown. AUC values were very high (> 0.90) for every distance analyzed, which indicates that each model has good predictive power.

Table 44. Model coefficients, the area under the ROC curve (AUC) with 95% confidence intervals, and Wald χ^2 test results for overall dataset regressions. Regression models are generated for distances from intersection entry ranging from 10 m to 50 m prior to intersection entry in 2.5 m increments. Several distances along the intersection approach are considered. The violation detection probability thresholds for three false positive proportions (FPP) are presented. In this study, the early, intermediate, and delayed detection algorithms were developed by selecting violation detection probability thresholds that resulted in FPP values of 5%, 1%, and 0.5%, respectively.

Distance from Intersection Entry (m)	AUC (2.5%, 97.5%)	Violation Detection Probability Threshold			Intercept, l=Violation	RDP, g		Brake Application, l=ON	
		FPP = 5%	FPP = 1%	FPP = 0.5%		Coefficient	z-statistic (p-value)	Coefficient	z-statistic (p-value)
50	0.930 (0.883,0.976)	0.0053	0.0236	0.0354	-10.74	30.41	10.38 (<0.001)	-4.38	-7.45 (<0.001)
47.5	0.936 (0.893,0.978)	0.0049	0.0169	0.0276	-10.71	29.87	10.42 (<0.001)	-4.56	-7.51 (<0.001)
45	0.948 (0.909,0.986)	0.0047	0.0198	0.0250	-11.27	33.45	9.59 (<0.001)	-5.69	-7.53 (<0.001)
42.5	0.955 (0.922,0.989)	0.0047	0.0191	0.0260	-11.22	32.78	9.51 (<0.001)	-5.66	-7.47 (<0.001)
40	0.960 (0.929,0.992)	0.0041	0.0165	0.0273	-11.07	32.05	9.01 (<0.001)	-5.69	-7.43 (<0.001)
37.5	0.969 (0.943,0.995)	0.0031	0.0148	0.0262	-10.79	31.42	8.67 (<0.001)	-5.90	-7.47 (<0.001)
35	0.977 (0.956,0.997)	0.0024	0.0206	0.0253	-10.58	31.21	7.98 (<0.001)	-6.12	-7.16 (<0.001)
32.5	0.982 (0.967,0.998)	0.0022	0.0219	0.0300	-10.07	28.67	7.94 (<0.001)	-5.83	-7.34 (<0.001)
30	0.969 (0.943,0.994)	0.0023	0.0170	0.0231	-9.03	23.31	8.92 (<0.001)	-4.99	-7.90 (0.001)
27.5	0.973 (0.950,0.996)	0.0018	0.0163	0.0275	-8.76	24.19	8.83 (<0.001)	-5.88	-7.48 (<0.001)
25	0.978 (0.959,0.997)	0.0015	0.0100	0.0391	-9.03	24.00	8.84 (<0.001)	-5.46	-7.49 (<0.001)
22.5	0.983 (0.967,0.999)	0.0013	0.0102	0.0225	-8.91	26.07	8.54 (<0.001)	-6.61	-6.62 (<0.001)
20	0.987 (0.970,1.000)	0.0010	0.0068	0.0229	-9.89	28.20	8.10 (<0.001)	-7.13	-6.62 (<0.001)
17.5	0.990 (0.975,1.000)	0.0009	0.0084	0.0156	-10.62	27.35	8.01 (<0.001)	-7.02	-6.61 (<0.001)
15	0.999 (0.998,1.000)	0.0002	0.0050	0.0114	-14.82	38.80	4.78 (<0.001)	-9.23	-4.92 (<0.001)
12.5	1.000 (0.999,1.000)	0.00003	0.0016	0.0045	-18.41	46.05	3.51 (<0.001)	-11.29	-3.28 (0.001)
10	0.999 (0.998,1.000)	0.0001	0.0051	0.0117	-16.82	29.56	4.02 (<0.001)	-5.71	-3.07 (0.002)

Cross-Validation Evaluation of Hypothetical Stop Sign Warning Algorithm

The proportion of correctly identified violations and non-violations at various locations along the intersection approach can be found in Table 45. The results indicate that all three detection algorithms would be able to detect each of the violations at some point during the intersection approach. However, the number of incorrectly identified non-violations greatly differed. For the early detection algorithm, false alarms would be delivered to 22.3% of non-violating drivers. For the intermediate detection algorithm, false alarms would be delivered to 5.6% of non-violating drivers. For the delayed detection algorithm, false alarms would be delivered to 3.3% of non-violating drivers.

Table 45. Results from the cross-validation evaluation of the models at several distances along the intersection approach prior to intersection entry are shown.

	Distance from Intersection Entry (m)	Correctly Identified Violations (%)	Correctly Identified Non-Violations (%)
Early Detection Algorithm	50	68.4%	95.3%
	45	76.3%	95.4%
	40	84.2%	95.0%
	35	86.8%	95.4%
	30	86.8%	94.8%
	25	89.5%	95.0%
	20	94.7%	94.8%
	15	100.0%	94.8%
	10	100.0%	95.1%
Intermediate Detection Algorithm	50	63.2%	98.8%
	45	68.4%	98.8%
	40	68.4%	98.8%
	35	76.3%	98.6%
	30	76.3%	98.8%
	25	81.6%	98.6%
	20	86.8%	98.9%
	15	97.4%	98.8%
	10	94.7%	98.9%
Delayed Detection Algorithm	50	63.2%	99.4%
	45	68.4%	99.4%
	40	68.4%	99.2%
	35	73.7%	99.2%
	30	73.7%	99.2%
	25	73.7%	99.2%
	20	81.6%	99.4%
	15	94.7%	99.4%
	10	92.1%	99.4%

Figure 70 provides a graphical depiction of the required braking deceleration magnitude to stop the vehicle at the earliest violation detection time points. Speed versus distance at these time points are shown for each stop sign warning algorithm, and lines are provided to show how these data points correspond to RDP before and after a 1.0 s PRT. Tabulations of the percent of cases where braking demand (RDP) did not exceed maximum braking capabilities are shown in Table 46. Given good surface conditions (dry asphalt), maximum braking capabilities of vehicles are around 0.8 g. For all three algorithms, 97.4% of violations could have been successfully detected while RDP before PRT was less than 0.8 g. However, RDP after PRT was less than 0.8 g for only 55.3% - 71.1% of cases. Given poor conditions (snow), maximum braking capabilities fall to 0.4 g. A total of 55.3% - 65.8% could have been detected while RDP before PRT was less than 0.4 g. Alternatively, RDP after PRT was less than 0.4 g for 10.5% - 26.3% of drivers.

Table 46. A tabulation of violations where braking capacity exceeded braking demand is shown. Results from all three detection algorithms are presented. Three maximum braking capacity values were considered that are dependent on road surface conditions. RDP before and after an elapsed reaction time were considered.

Detection Algorithm	Surface Conditions (maximum braking capability)	% of Violations RDP before reaction time < max. braking capability	% of Violations RDP after reaction time < max. braking capability
Early	Poor (0.4 g)	65.8%	26.3%
	Moderate (0.6 g)	89.5%	52.6%
	Good (0.8 g)	97.4%	71.1%
Intermediate	Poor (0.4 g)	55.3%	26.3%
	Moderate (0.6 g)	89.5%	50.0%
	Good (0.8 g)	97.4%	60.5%
Delayed	Poor (0.4 g)	55.3%	13.2%
	Moderate (0.6 g)	89.5%	44.7%
	Good (0.8 g)	97.4%	55.3%

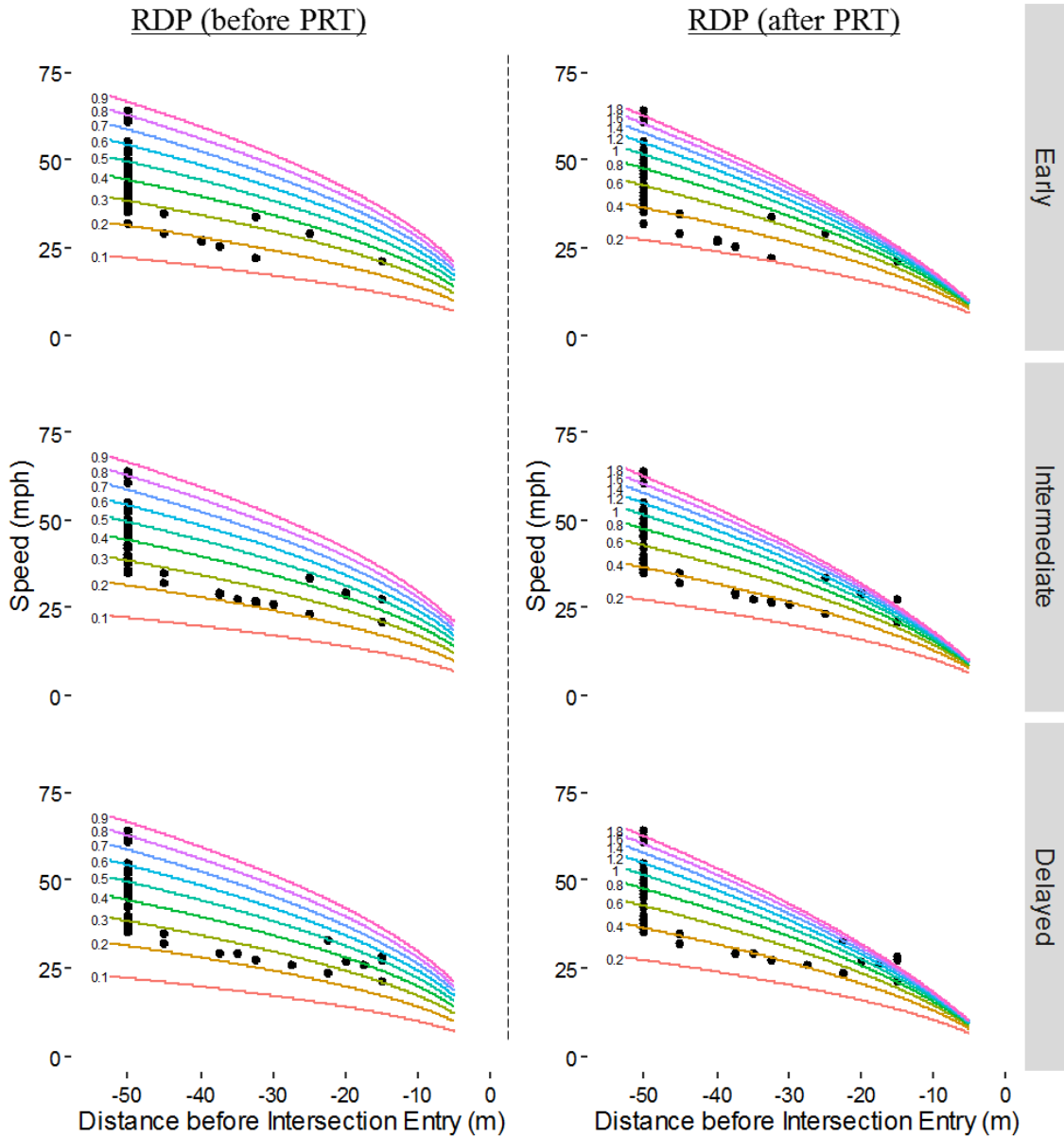


Figure 70. The figure provides graphical depictions of the braking deceleration magnitude that is required to stop the vehicle given vehicle kinematics at the earliest violation detection time point. Each data point on the graph depicts a unique speed and distance from intersection entry at the earliest violation detection time point. Lines are additionally shown to indicate corresponding RDP values. The graph on the left shows lines representing RDP at the time that the violation was detected, i.e. before a PRT. The graph on the right shows lines representing RDP after a 1.0 s PRT. Each row of graphs corresponds to the results of each unique violation detection algorithm.

8.4 *Discussion*

The overall objective of this study was to evaluate how an I-ADAS warning algorithm might perform in a real-world scenario. All three detection algorithms were able to predict an intersection violation at some point prior to the vehicle reaching 10 m from the stopping location, but violation detection did improve with increasing proximity to intersection entry. The early detection algorithm, as designed, was able to detect imminent violations earlier in the intersection approach. However, although the false-positive proportion at each distance was designed to be around 5% for this early detection algorithm, false alarms accumulated throughout the intersection approach, and approximately 1 out of every 4 non-violations (22.9%) were incorrectly identified. Conversely, the delayed detection algorithm sacrificed some time for alerting the driver, but would deliver false alarms in only 1 out of every 30 (3.3%) non-violations.

The ability of the vehicle to be stopped was assessed by comparing RDP before and after a PRT with the maximum braking capacity of vehicles given various surface conditions. For an I-ADAS that alerts the driver of an impending violation, RDP after a PRT is a useful measure of what would be required by the driver to completely stop the vehicle. Given good surface conditions (max. braking capabilities = 0.8g) and maximum effort, about three-fourths of drivers would be able to stop the vehicle by the stop bar regardless of the detection algorithm. In addition to warning drivers, another strategy may be to implement automatic emergency braking (AEB) into I-ADAS technology, which is already present in production vehicles for frontal crash prevention [23] and I-ADAS [82]. If vehicles were equipped with AEB, the results suggest that, given good surface conditions and maximum brake effort, nearly every vehicle could potentially stop. These results highlight the importance of an earlier reaction, which allow lower required braking decelerations, on the potential effectiveness of this technology.

8.5 *Limitations*

There are several limitations with regards to this study's findings. First, it should be noted that two unrelated datasets were used to develop this study's violation detection algorithms. The weighting factors used in this study were based on a small sample of stop sign-controlled intersections, and caution should be used if trying to extrapolate the results and models to a larger population. Additionally, each of violations were weighted equally to one another. In reality, some violations are more likely to occur than others.

The second major limitation of the study relates to the datasets used. The 100-Car study was conducted within a small region and included a limited number of drivers and intersection. This dataset may not be representative of the entire U.S. population. A larger scale analysis is required to translate these results to additional regions and demographics. The EDR dataset comprises only vehicles that were involved in an "airbag deployment-level" collision. Because of this, the dataset may be biased toward more severe crashes, and may not translate well for (1) lower severity crashes, (2) near-crashes, and (3) violations that did result in a crash or near-crash. It should also be noted that speed and braking data were not sampled at a uniform rate across all cases. Depending on vehicle make, model, and year, EDR data were sampled at 1 Hz to 10 Hz, and 100-Car data were sampled at 3 Hz to 10 Hz. Additionally, EDR pre-crash data has a limited duration and there is uncertainty associated with the timing of the collected data. Pre-crash data elements are recorded in intervals independent of one another, and thus synchronicity error between the signals can be present [196]. Also, wheel slip during heavy braking could cause an underestimation of vehicle speed and lead to error in the reconstructed position vs. speed profile [232].

8.6 *Conclusions*

This study used a dataset of typical driver behavior (100-car naturalistic driving study) and violations (Event Data Recorders downloaded from real-world crashes) to develop and evaluate a predictive model for detecting whether a stop sign violation was imminent. Two methodologies for preventing violations were considered: (a) a warning-based I-ADAS and (b) an AEB-based I-ADAS. The findings demonstrated and quantified the inherent trade-off between timely detection of imminent stop sign violations and false-positive activation. Additionally, a predictive algorithm is proposed and demonstrated against real-world data. The findings should be regarded by designers and evaluators considering a stop sign violation detection algorithm. Additionally, repeating the analysis on a larger, more extensive dataset will allow for the development of a more comprehensive algorithm to further validate the findings.

9. Evaluating the Sensor Detection Capabilities of I-ADAS for Preventing Left Turn Across Path Opposite Direction Crashes⁵

9.1 Introduction

The left turn across path with a vehicle travelling from the opposite direction (LTAP/OD) crash mode accounts for approximately one-third (32%) of all fatal intersection crashes and one-fourth (26%) of all intersection crashes. LTAP/OD crashes are second only to straight crossing path (SCP) collisions in terms of frequency and fatal outcomes in intersection crashes [3, 33]. A schematic of an LTAP/OD crash is shown in Figure 71. These crashes almost always (99% [93]) occur when either (a) both vehicles had a signal or (b) neither vehicle had a signal or stop sign on their approach. These crashes tend to occur when the turning driver either (a) failed to detect the oncoming vehicle or (b) misjudged the gap required to successfully perform the left turn. In fact, distraction (48%) and judgment errors (34%) are overwhelmingly the most commonly cited critical reasons for the crash having occurred [93].

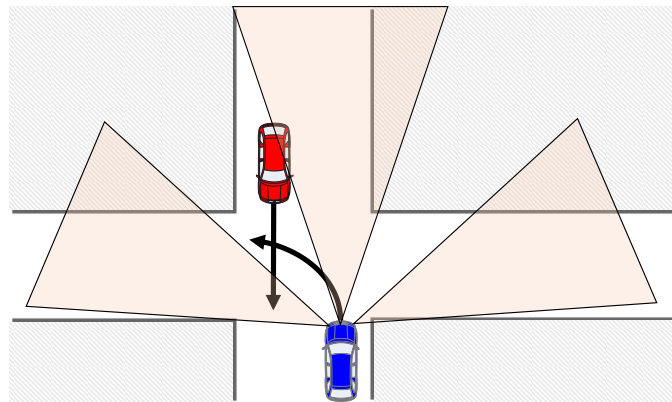


Figure 71. A depiction of an LTAP/OD crash scenario. The blue (left turning) vehicle is equipped with hypothetical forward and side facing sensors.

⁵ The work shown in this study has been a part of several previously published peer-reviewed manuscripts, including:
233. Scanlon, J.M., et al., *Earliest Sensor Detection Opportunity for Left Turn Across Path Opposite Direction Crashes (In Review)*. IEEE Transactions on Intelligent Vehicles, 2017.

Turning left at intersections with oncoming vehicles is an inherently complex maneuver. Drivers must scan for vehicles, yield the right of way when appropriate, and make a decision on when the intersection can be safely traversed. Older drivers have been found to be particularly vulnerable when performing left turns at intersections [234-236]. Frequently cited mechanisms for this susceptibility are that senior drivers tend to misjudge whether they have adequate time to make a left turn across another vehicles path in an intersection [187, 237, 238] or they failed to see the oncoming vehicle altogether [237]. A number of age-related deficiencies can explain this, including diminished cognitive-motor abilities [188], inadequate visual scanning [186, 187], and slower decision making [189-191]. The objective of I-ADAS is to continuously scan and detect oncoming vehicles and enhance the capacity for the crash to be avoided by either providing a warning or autonomously evading the crash. Accordingly, this technology may prove useful for these senior drivers, which fail to detect or misjudge the location of a potential collision partner.

One challenge when designing I-ADAS is selecting sensor specifications that ensure that oncoming vehicles can be consistently detected in a timely manner. Most crash avoidance technologies rely on cameras or radar for vehicle detection [23, 82, 83, 239-242], and some future vehicles will use a 360-degree lidar [243, 244]. The sensor specifications, such as detection range, field of view, and orientation, will directly influence performance of I-ADAS. These three parameters are depicted in Figure 72. In an LTAP/OD crash, selecting appropriate sensor specifications are complicated by (a) detection requirements depending on which vehicle is equipped (i.e., the left turning or straight crossing) and (b) potential sight obstructions [117]. Both of these elements are explored in the current study.

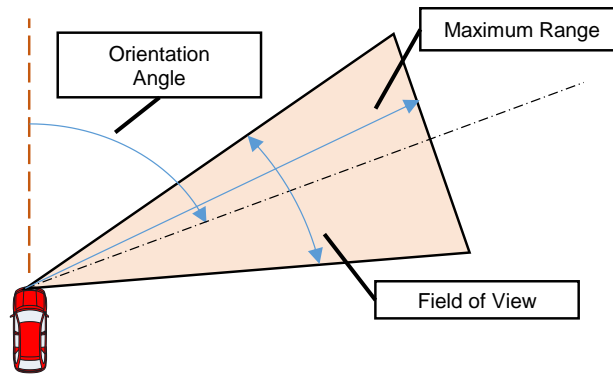


Figure 72. A depiction of sensor orientation, maximum range, and field of view for detecting oncoming vehicles.

One method for determining appropriate design specifications is through the reconstruction of real-world crashes [137, 158, 181]. By tracing back the position of the vehicle throughout time, crashes can then be simulated forward as if either vehicle had been equipped with I-ADAS. In doing so, design specifications can be determined in the context of the real-world scenarios that these technologies aim to prevent. Given the uncertainty associated with impact speed, crash avoidance action [130], and approach/traversal vehicle kinematics [135, 142], the most reliable method for tracing back the pre-crash positions of vehicles is with the use of Event Data Recorders (EDRs) which are present in 96% of new U.S. passenger vehicles [38]. As an example, consider the case depicted in Figure 73, which was included in this study's case set. In the event of a crash, the EDR has the potential to record a number of pre-crash parameters, such as vehicle speed, brake application, yaw rate, and steering wheel angle [96].

The objective of this study was to determine the required sensing specifications to ensure that an I-ADAS could detect an oncoming vehicle at the earliest possible opportunity. Three research questions were posed. First, how much time is available for crash avoidance from detection of an oncoming vehicle until impact? Second, what detection range and azimuth is required for sensors

to detect an oncoming vehicle at the earliest opportunity? Third, how will sensor specifications influence vehicle detection capacity?

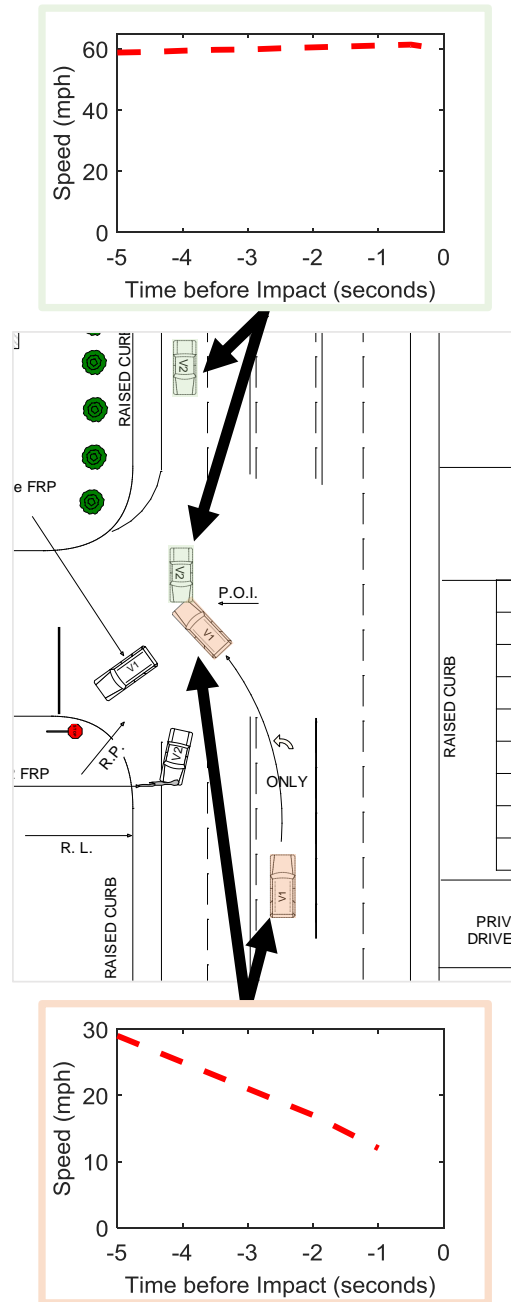


Figure 73. The scene diagram for NASS/CDS case 2014-4-55. The EDR speed profile records are additionally included for both vehicles. The left turning vehicle (red) slowed down throughout the intersection approach and left turn. The straight crossing vehicle (green) maintained a relatively constant speed approximately 15 mph higher than the posted speed limit (speed limit = 45 mph).

9.2 *Methods*

Data Source

This study used 35 reconstructed LTAP/OD crashes from the EDR dataset discussed in Chapter 7. A total of 44 crashes were considered for this study's analysis. One of the cases was excluded for missing a scene diagram in the case documentation. An additional 6 cases were excluded because at least one of the vehicles likely experienced wheel slip (maximum deceleration greater than 1-g). Two cases were removed because the EDR pre-crash records were not sufficient for tracing the vehicle path back to the best-case detection opportunity.

The simulation case set developed in Chapter 7 and used in the current study traced the pre-crash positions of each vehicle from the beginning of the EDR pre-crash records up until the point of impact. Positions were reconstructed using the scene diagram prepared by the crash investigator. Methods employed in a prior study were used to take measurements of the vehicle's path leading up to the crash [92, 137, 158, 181]. These measurements, among others, included any evasive steering the driver may have performed, any turning on curved roads, any lane changes, and the turning path while traversing the intersection. The pre-crash time series of each vehicle was then reconstructed using the EDR pre-crash vehicle speed records.

Sensor Reconstructions

A primary objective of this study was to determine the range, field-of-view, and orientation required for on-board sensors to detect oncoming vehicles. This study modeled I-ADAS as monitoring for a potential collision partner only after the left turning vehicle first left its initial travel lane. At this time point, it was assumed the collision avoidance system would have recognized that a left turn was being attempted.

Other vehicles on the roadway in adjacent lanes could obstruct the sightline to any oncoming vehicles for some proportion of these crashes [117]. Two scenarios were considered for I-ADAS. First, we considered a best-case scenario, where a clear line-of-sight would have been available throughout the entire pre-crash. In this scenario, the earliest detection opportunity would have been the location where the left turning vehicle first departed its initial travel lane (i.e., where I-ADAS would begin monitoring for a collision partner). Second, we considered a worst-case scenario. In this scenario, as shown in Figure 74, vehicles in adjacent lanes could obstruct the view from the left turning vehicle to the straight crossing vehicle. A queue of stopped vehicles were modeled as being present in the adjacent lane of the straight crossing vehicle. For this scenario, the earliest detection opportunity was modeled as occurring only after the left turning vehicle left its initial travel lane *and* a clear line-of-sight was available. It should be noted that not all LTAP/OD involve a straight crossing driver with adjacent lanes that could obstruct line-of-sight. Accordingly, for crashes such as those occurring on a two-lane roadway, the best-case and worst-case earliest detection opportunities were assumed to occur at the same location (initial travel lane departure by left turning vehicle). Additionally, in the event that the left turning vehicle stopped beyond the earliest detection opportunity (as determined using the EDR records), the instance when the turning vehicle began accelerating was taken as the earliest detection opportunity.

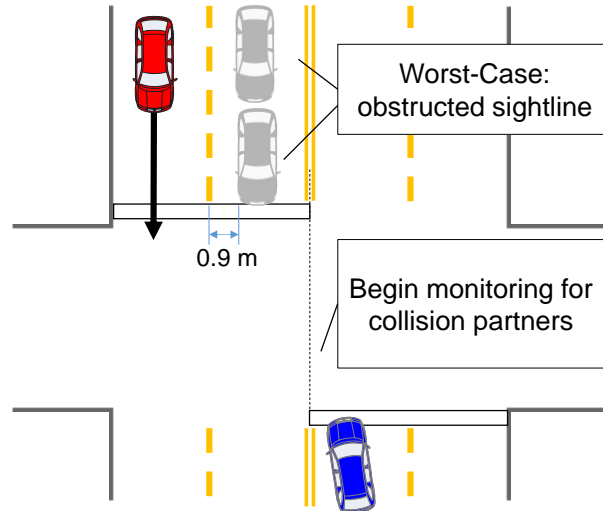


Figure 74. The opportunities for earliest vehicle detection given sight obstructions. The worst-case earliest detection opportunity represents a scenario where (a) the left turning vehicle has begun initiating a left turn and (b) line-of-sight was obstructed by a queue of vehicles.

At both of these locations, the required detection distance and angle with respect to vehicle heading were of interest. Examples of these two measures can be found in Figure 75. For example, a vehicle that was directly straight ahead and 20-m away would have a required detection distance of 20-m and a required detection angle of 0° . All distance and angle measurements were taken from the front-center of the “equipped” vehicle. The perspective of either vehicle having been equipped was considered.

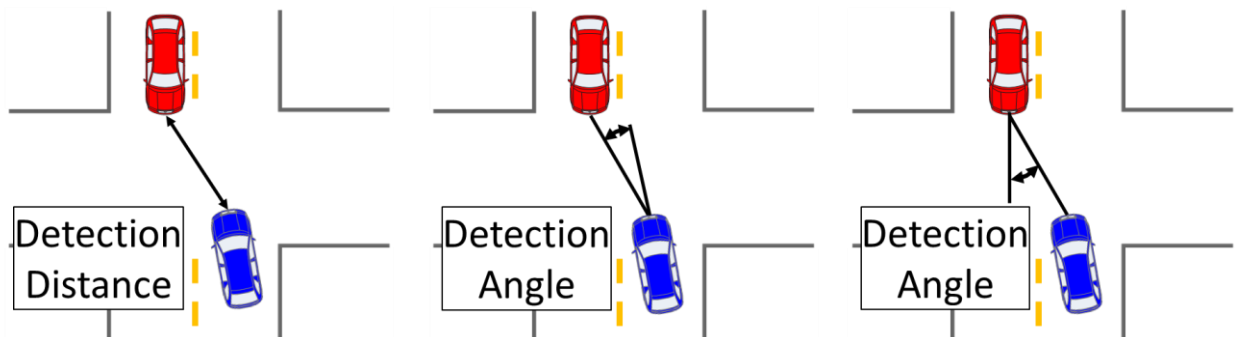


Figure 75. Detection distance and angle measurements used to describe the relative positions of the two vehicles.

Additionally, several hypothetical sensors were considered, including a short-wide beam, a long-narrow beam, and an intermediate beam. Sensor characteristics that were used in this study are shown in Table 47. The specifications used are within the capacity of several commercially available vehicle-based radars, including Delphi Corporation’s Electronically Scanning Radar, Smartmicro’s UMRR Automotive Radar Sensors, and Eaton’s VORAD® VS-400. All simulations were performed with the assumption that the sensor would be oriented in the direction of the vehicle heading.

Table 47. Sensor specifications that were examined in the current study.

	Wide Beam	Intermediate Beam	Narrow Beam
Range	30 m	90 m	150
Azimuth	+/- 45°	+/- 30°	+/- 15°

9.3 Results and Discussions

How much time is available for crash avoidance from detection of an oncoming vehicle until impact?

This study's first analysis examined the time available to avoid a crash after an oncoming vehicle could have been potentially detected. Two time points were considered. First, the best-case scenario was taken, i.e., a clear sightline was available at the instant the left turning vehicle initially departed in its initial travel lane. Second, the worst-case scenario was considered, where a queue of cars would have obscured the view to any oncoming vehicles. The time from crossing these time points until impact can be seen in Figure 76. For the best-case scenario, 50% of the intervals from detection to impact fell below 1.8 s and 95% of the intervals fell below 3.6 s. For the worst-case scenario, the median time to impact was 1.2 s and 95% of times fell below 2.7 s.

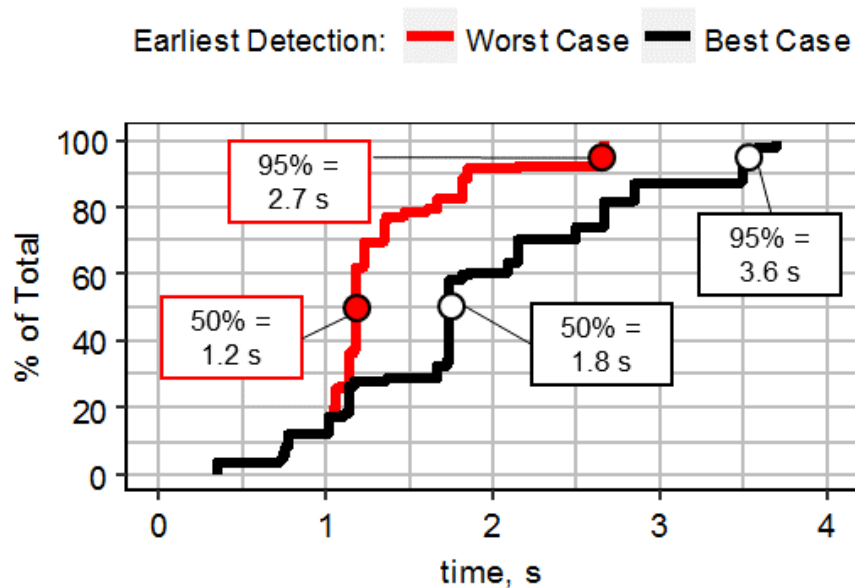


Figure 76. Interval between detection and impact under best-case and worst-case scenarios.

One concern of these active safety systems is whether there would be sufficient time for a driver to respond to a warning. One major limitation of using a warning is perception-reaction time. In a previous simulator study at Monash University Research Center (MUARC) in Australia [129], researchers had participants drive down a stretch of road that consisted of several signalized intersections. While driving, right turning drivers (Australia has left-hand traffic) occasionally turned across the path of the subject vehicle at which point the driver would receive an audible or visual warning and respond by either braking or steering. The median reaction time (interval between warning and evasive action start) for these straight crossing drivers was 1.5 s. In a second simulator study performed by BMW Group Research and technology [245], forty males participated in a driving simulator study that replicated the participant being an occupant in a vehicle being driven by another person. Similar to that of a driving instructor, the participant was instructed to press a brake pedal if they judged a situation to be potentially dangerous. These drivers then experienced several scenarios where the subject vehicle instead took a left turn across the path of a straight crossing driver and a visual warning was delivered. The median perception-reaction time (interval between warning and brake pedal press) for these drivers was also 1.5 s. In the current study, because 72% of best-case scenario times exceed 1.5 s, if every driver was to respond after 1.5 s we would expect these drivers to have the potential to *begin* reacting following a warning. This does not imply, however, that these drivers would have been able to successfully avoid the crash. Additionally, a mere 22% of drivers would have had 1.5 s to react if they received a warning at the worst-case earliest detection opportunity.

A second method for I-ADAS crash avoidance would be for the system to autonomously evade the crash. The previous few years have seen the emergence of AEB and autonomous steering systems are also being developed and considered by designers [193]. The major advantage of

automated crash evasion is a faster reaction than that of a driver. Although this technology is most commonly installed in frontal crash avoidance systems [23], Volvo released an updated version of “City Safety” in 2014 [82, 246], which is a combination of crash avoidance functions that aim to prevent a number of crash modes commonly occurring in cities, including LTAP/OD intersection crashes. The system specifically employs AEB if the equipped vehicle begins to turn left across the path of an

What detection range and azimuth is required for sensors to detect an oncoming vehicle at the earliest opportunity?

This study's second analysis examined the required detection range and azimuth for detecting the opposing vehicle. As in the prior analysis, both the best-case and worst-case scenarios were considered. Figure 77 shows the range between the vehicles given the best and worst cases. The median detection range for the worst-case detection scenario was 20.5 m and 95% of distances fell below 61.0 m. In the best-case scenario, the median range was 33.5 m and 95% of distances fell below 86.5 m. This result suggests that in the absence of potential sight occlusions I-ADAS sensors with a maximum range capacity of 90 m would have the capacity to detect all oncoming vehicles in the dataset. Although sight occlusions are expected to be a limiting factor for I-ADAS, it is important that these systems have adequate sensing capacity for the ideal scenario (i.e., no sight occlusions). Failing to design for these more extreme scenarios could lead to failed crash avoidance in an otherwise avoidable scenario.

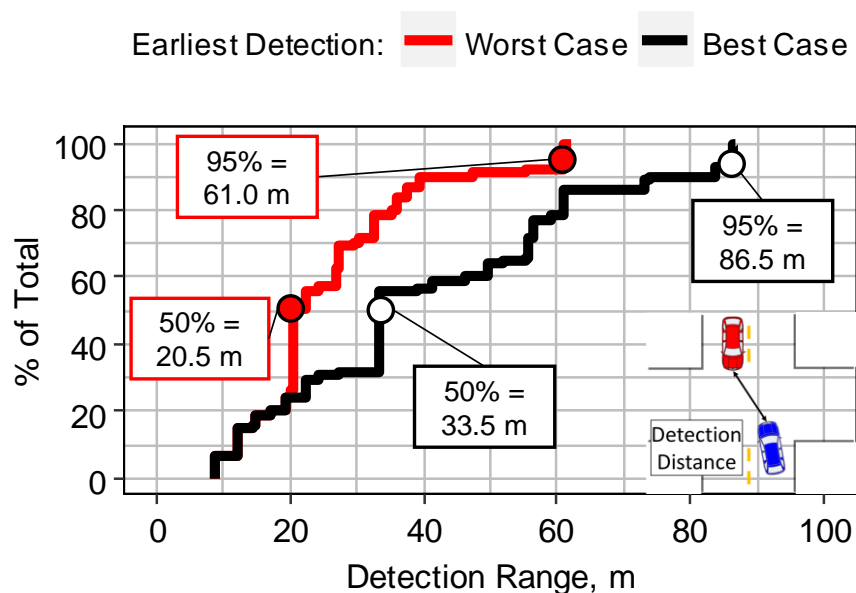


Figure 77. Detection distance between the front-center of the vehicles at the best-case and worst-case earliest detection opportunities.

Figure 78 shows detection angle values for the left turning vehicles at the best- and worst-case possible detection opportunities. At the best-case earliest time point, the left turning vehicle had a median required detection angle of 10.8° and 95% of angle values fell below 26.7°. As the vehicle continues its left turn, we would expect the detection angle values to grow. Accordingly, at the worst-case time point, the median required detection angle was 17.0° and 95% of azimuth values fell below 30.4°.

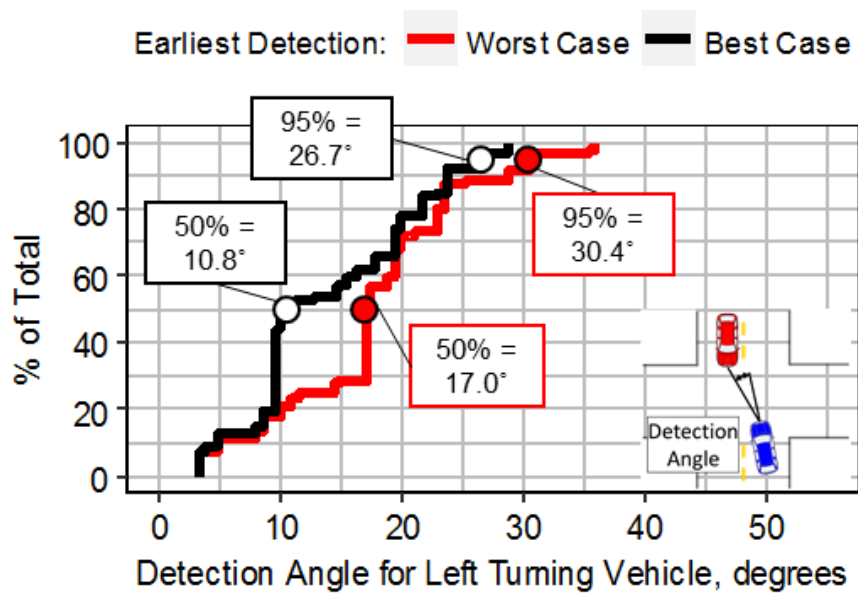


Figure 78. Detection angle between the front-center of the vehicles for the left turning vehicle at the best-case and worst-case earliest detection opportunities.

Figure 79 shows required detection azimuth values for the straight crossing driver. At the best-case earliest detection time point, the median azimuth was 7.9° and 95% of values fell below 19.5°. Similarly at the worst-case earliest detection time point, the median azimuth was 9.2° and 95% of values fell below 21.8°. Two competing factors that dictate azimuth for the straight crossing driver are (1) the proximity of the left turning vehicle and (2) the lateral position of the left turning

vehicle. If the left turning vehicle never turned across the path of the straight crossing driver, the azimuth value would inherently become larger due to a narrowing of the longitudinal distance between the vehicles. Because these are all LTAP/OD crashes, the left turning driver is moving laterally into the path of the straight crossing driver, which is working to decrease the detection azimuth of the non-turning vehicle. These two competing mechanisms led to only slightly higher azimuth values at the worst-case earliest detection time point.

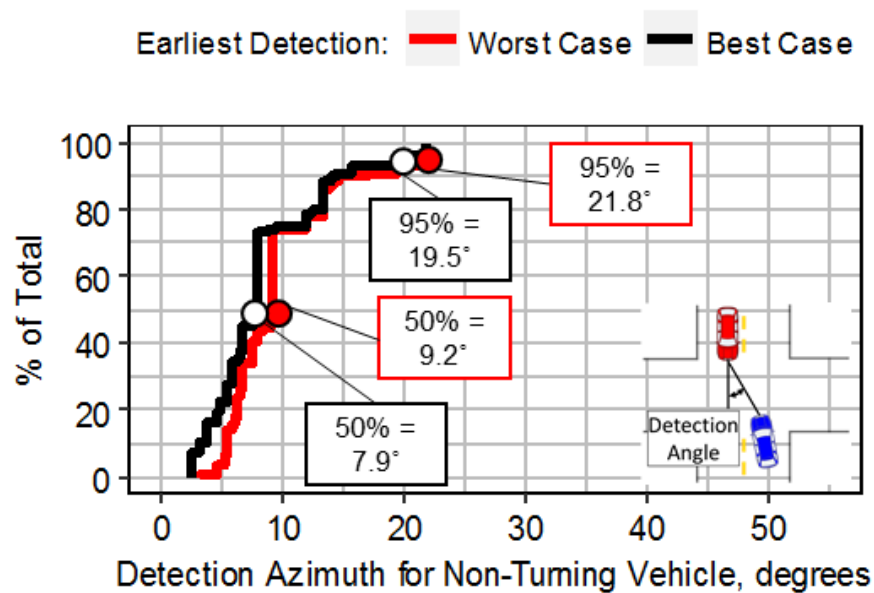


Figure 79. Detection azimuth between the front-center of the vehicles for the straight crossing vehicle at best-case and worst-case earliest detection opportunities.

How will sensor specifications influence vehicle detection capacity?

The next objective was to determine the capacity for an onboard sensor to detect an oncoming vehicle. It is important, of course, to consider the perspective of both vehicles, because either vehicle could in theory take avoidance action. The convention shown in Figure 80 was used to trace the position of the oncoming vehicle from the perspective of the equipped vehicle. The straight ahead position was taken to be the longitudinal direction. The origin was taken as the front-center of the equipped vehicle. The position of the oncoming vehicle with respect to the wide, intermediate, and narrow sensors orientated in the longitudinal direction was considered.

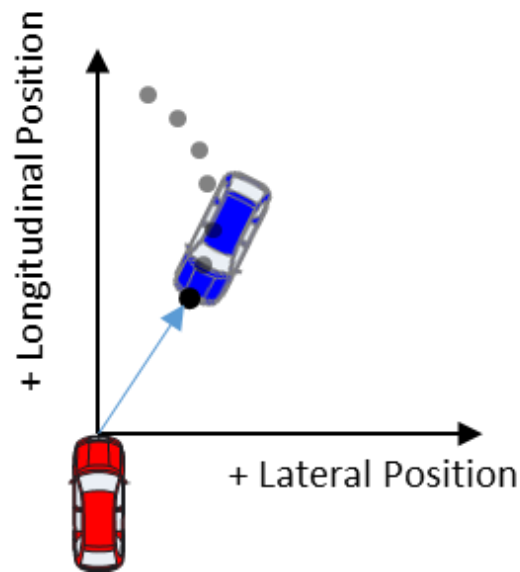


Figure 80. Convention used to describe relative location of oncoming vehicle (blue vehicle) with respect to the equipped vehicle (red vehicle).

The perspective of the left turning driver was first considered. The position of the oncoming straight crossing vehicle from the best-case detection opportunity until impact is shown in Figure 81. The specifications of three sensor beams orientated in the direction of the vehicle heading are also shown. A total of 92% of trajectories stayed within the intermediate beam from the best-case detection opportunity until the worst-case detection opportunity. All of the trajectories were in the

sensor beam at the best-case detection time point. Conversely, only 31% and 28% of the trajectories stayed within the wide and narrow beams, respectively.

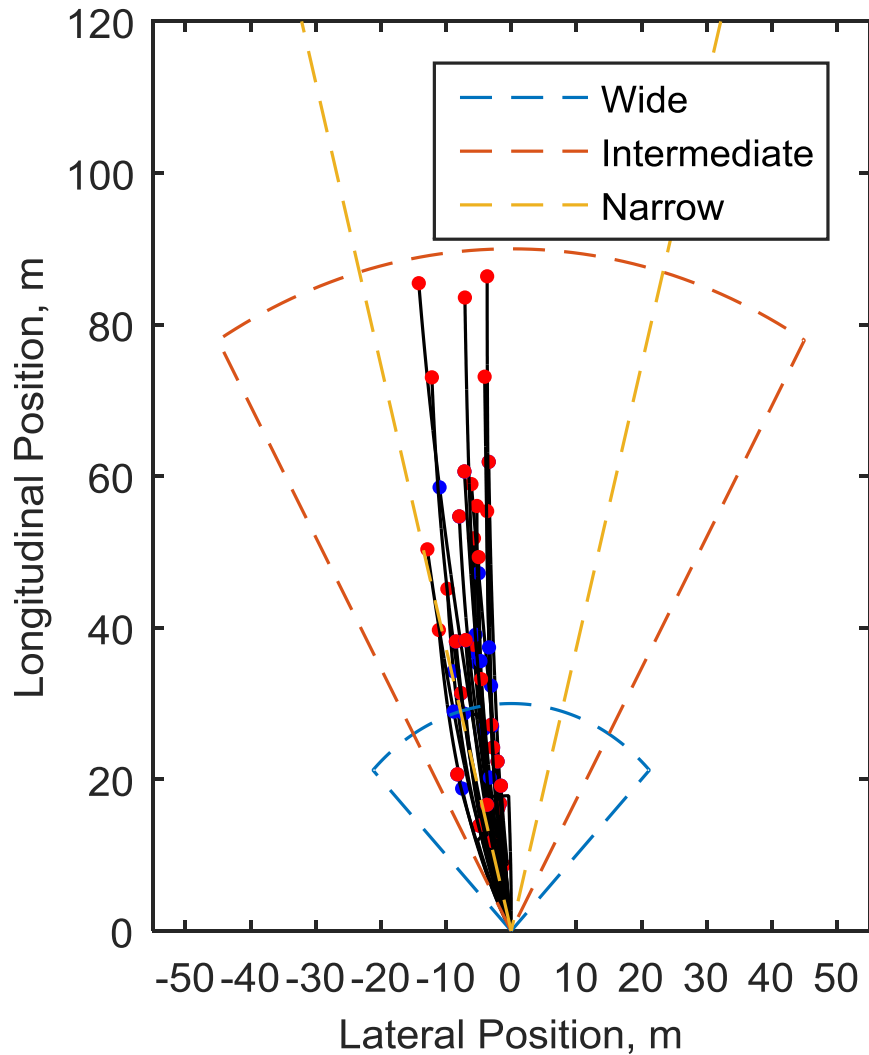


Figure 81. The position of the straight crossing vehicle (oncoming) from the perspective of the left turning vehicle (equipped). The red dot indicates the best-case detection opportunity, while the blue dot represents the worst-case detection opportunity. The trace terminates at the point of impact. Three sensor beams are considered with the assumption that the sensor was oriented in the direction of the vehicle heading.

The perspective of the straight crossing vehicle was then considered in Figure 82. The oncoming vehicle was within the intermediate and narrow beams from the best-case to worst-case time points for 79% and 69% of cases, respectively. All of the trajectories were in the intermediate sensor beam at the best-case detection time point. The wide beam was less effective as only 20% of vehicles were within the sensor beam throughout this time period.

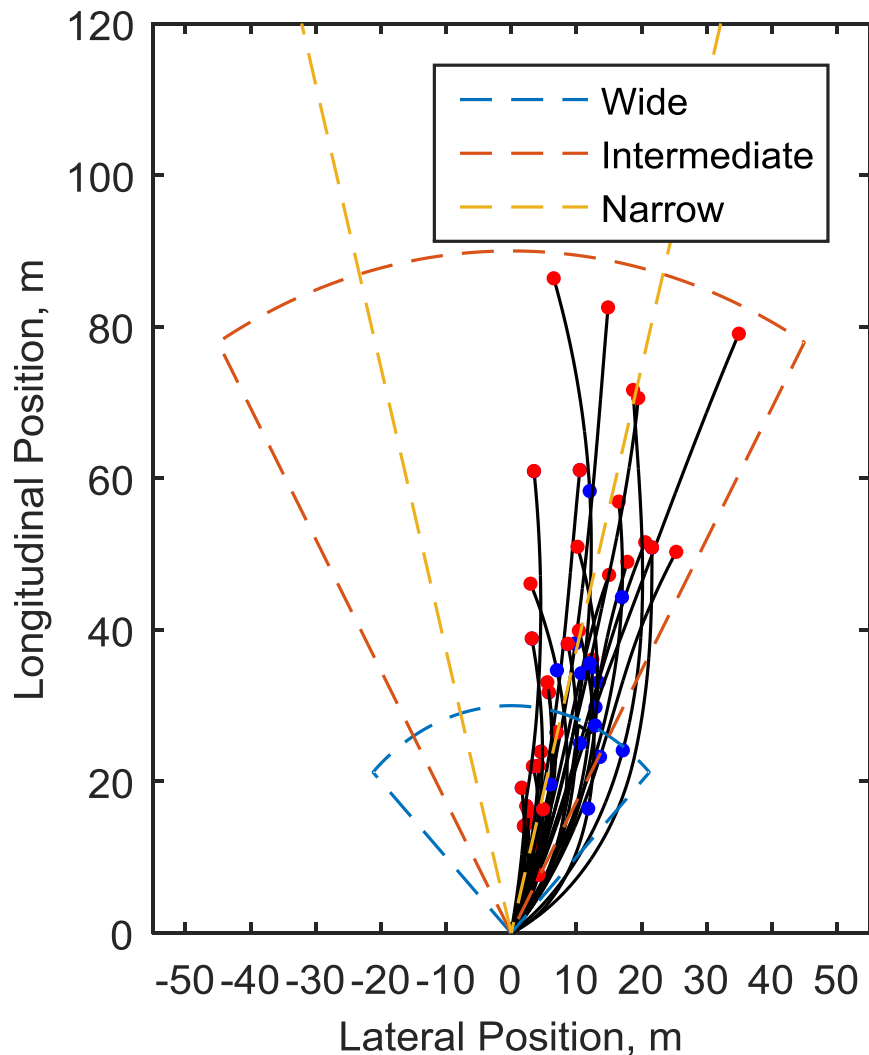


Figure 82. The position of the left turning vehicle (oncoming) from the perspective of the straight crossing vehicle (equipped). The red dot indicates the best-case detection opportunity, while the blue dot represents the worst-case detection opportunity. The trace terminates at the point of impact. Three sensor beams are considered with the assumption that the sensor was oriented in the direction of the vehicle heading.

There are several important findings from this analysis. First, if a forward facing sensor was used, the intermediate beam specifications seem most appropriate for detecting oncoming vehicle. These sensors should, of course, be tuned to accommodate vehicle sensing throughout the encroachment. Second, only a forward facing sensor is considered in this analysis. Current I-ADAS technology used by vehicles on the market [82, 83] utilize a forward facing radar. I-ADAS designers should consider incorporating side-facing sensors to ensure continuous vehicle detection.

9.4 *Limitations*

There are a number of limitations to note in the current study. First, path reconstructions were made based on the depiction of pre-crash vehicle locations in the scene diagram prepared by the crash investigator. Some geometrical assumptions were made in order to interpolate vehicle position between these depicted positions. Second, EDR data is limited in recording duration, resolution, and sampling rate. Third, other roadway traffic which could limit sensor capacity was considered for only two discrete locations (best-case and worst-case). In a real-world scenario, we would expect earliest sensor detection to occur at some point between these two locations. Third, for an EDR record to be included in this study, the vehicle must have experienced an airbag deployment or a delta-v greater than 5-mph. Additionally, one of the vehicles had to have been towed from the scene to have been included in NASS/CDS. This dataset has some bias toward more severe intersection crashes, which should be considered when interpreting results or trying to translate these results to lower-speed collisions.

9.5 *Conclusions*

This study reconstructed 35 real-world LTAP/OD crashes that occurred in the U.S. vehicle fleet. The results suggest that sight occlusions due to other vehicles on the roadway will substantially limit the available time from detection to avoidance action. The time interval from detection to impact is, in general, well below typical perception-reaction times observed for drivers in previous simulator studies. Accordingly, this finding indicates that I-ADAS has the potential to be greatly limited if utilizing a warning for the driver rather than taking automated evasive action, such as with AEB. Required detection specifications, specifically the required detection distance and azimuth, are highlighted in the results. For left turning vehicles, maximum required detection azimuth tends to occur near the midpoint of the left turn. An intermediate sensor beam (90 m, +/- 30°) was found to perform superior to both a wide or narrow beam sensor. The results highlight the need for careful tuning of sensor capabilities and the need to consider side-facing sensors for ensuring vehicle tracking prior to any conflict.

10. Evaluating the Sensor Detection Capabilities of I-ADAS for Preventing Cross Traffic Intersection Crashes⁶

10.1 Introduction

Onboard vehicle detection sensors are becoming increasingly more common within the U.S. vehicle fleet. Forward collision warning (FCW) systems are emerging systems that use a forward facing radar to detect an imminent forward collision [23]. In addition, some early intersection assistance systems utilize this forward radar for cross traffic object detection (pedestrian, vehicle, animal) [82, 83]. Side-facing sensors are currently being implemented for blind spot detection [239, 241] and rear cross traffic alert systems [239], and may be useful for a future automated lane change system [240, 242]. However, no commercially available vehicles currently utilize a side-facing sensor on the front of the vehicle for vehicle detection.

Two of the most frequent intersection crash modes observed in the U.S. are Straight Crossing Path (SCP) and Left Turn Across Path Lateral Direction (LTAP/LD) crashes, which are depicted in Figure 83. Together these scenarios account for one-half (50.4%) of all U.S. intersection crashes [2]. Unlike LTAP/OD crashes presented in Chapter 9, vehicles approach one another from lateral directions in SCP and TLAP/LD crashes. Accordingly, vehicles may benefit from this side-facing sensor sensors during these scenarios.

⁶ The work shown in this study has been a part of several previously published peer-reviewed manuscripts, including:

158. Scanlon, J.M., et al., *Using Event Data Recorders from Real-World Crashes to Investigate the Earliest Detection Opportunity for an Intersection Advanced Driver Assistance System (No. 2016-01-1457)*. SAE Technical Paper, 2016.

92. Scanlon, J.M., et al. *Potential of Intersection Driver Assistance Systems to Mitigate Straight Crossing Path Crashes Using U.S. Nationally Representative Crash Data*. in *Proceedings of the 2015 IEEE Intelligent Vehicles Symposium*. 2015. Seoul, Korea.

247. Page, K.I., et al. *The Potential for Intersection Advanced Driver Assistance System to Reduce Straight Crossing Path Crashes*. in *Proceedings of the 2015 AAAM Student Research Symposium*. 2015. Philadelphia, Pennsylvania.

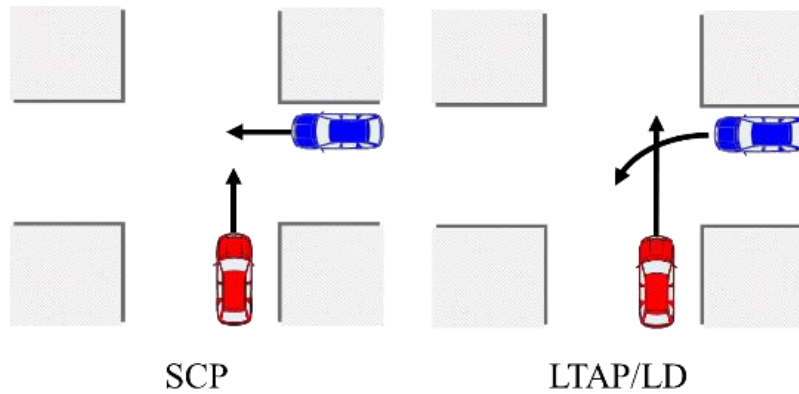


Figure 83. A depiction of SCP and LTAP/LD intersection crash modes.

The performance of an I-ADAS will depend on the ability of the onboard sensors to detect an imminent collision early enough for an I-ADAS to respond in a timely manner. There are several vehicle sensing technologies potentially useful for I-ADAS implementation, including radar, lidar, and cameras. Many commercially available vehicles currently rely on cameras or radar for vehicle detection [82, 83, 239]. More futuristic cars, such as the Google’s self-driving car [243] and OEM research vehicles [244], utilize a 360 degrees lidar located on top of the vehicle or lidar sensors located in the bumpers for vehicle detection. However, there are limitations to consider when designing these systems. First, these sensors are limited in the distance, or range, that they can detect an oncoming vehicle. Second, with the exception of the 360 degrees lidar, these sensors have a limited field of view, or azimuth. Additionally, there is an inherent trade-off between the range and azimuth for which these sensors can detect oncoming vehicles (i.e. longer range sensors have a narrower azimuth). Figure 84 depicts three important sensor specifications, which are expected to play an important role in the detection capabilities of these systems.

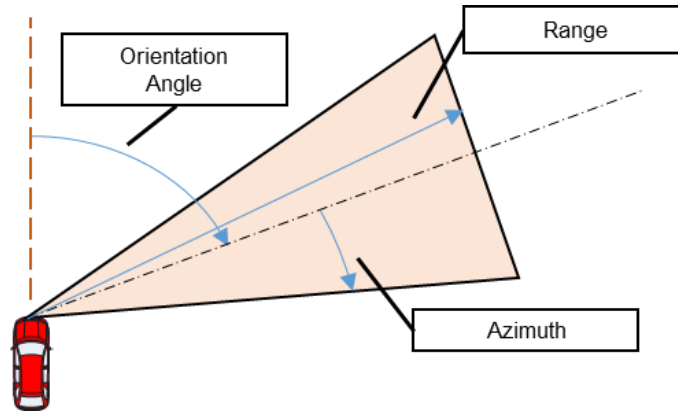


Figure 84. A depiction of sensor orientation, range, and azimuth for detecting an oncoming vehicle.

Typical driver action and vehicle kinematics will also likely play a part in the performance of I-ADAS, because these factors directly influence the available time for the system to respond. Specifically, these systems must accommodate how drivers currently navigate through intersections prior to real-world crashes. For example, crashes involving at least one vehicle stopped prior to entering the intersection (approximately one-half of all SCP crashes and nine- of every ten LTAP/LD crashes [based on NMVCCS cases analyzed in Chapter 7]) would yield greater time for an I-ADAS to respond. The previous work in Chapter 4 showed that drivers in intersection crashes typically accelerate faster into intersections than in normal driving [135]. Lastly, the work in Chapter 5 indicated four-fifths of drivers already take some form of evasive action (i.e. steering and/or braking) during real-world intersection crashes [130]. Proposed I-ADAS systems should seek to improve upon the timing of current driver evasive actions.

Sightline restrictions from an I-ADAS equipped vehicle to the oncoming vehicle will limit the ability of an I-ADAS sensor to detect the approaching vehicle. This study assumes that no sightline obstructions were present after the first vehicle enters the intersection. The time point when the first vehicle enters the intersection is referred to as the earliest detection opportunity. This is of

course a best case scenario as sightline obstructions can impede the performance of I-ADAS. This study investigates the requirements of a side-facing sensor given the need to detect the oncoming vehicle at the earliest detection opportunity.

A useful technique for evaluating the potential sensor detection needs of I-ADAS is through reconstructing real-world intersection crashes and then simulating the crashes as if the vehicles had been equipped with an I-ADAS. There are only a few vehicles [82, 83] commercially available that are equipped with these systems, and at the time of this study, none of these vehicles used side-facing sensors. This study simulates real-world crashes as they actually occurred, but includes hypothetical I-ADAS sensors in order to investigate their potential vehicle detection capability in a real-world crash scenario.

This study seeks to answer three research questions. First, we were interested in determining “What were the detection distances and angles at the earliest detection opportunity?”. Given range and azimuth limitations in I-ADAS sensor technology, this information provides basic requirements for the design of these systems. Second, what were the time-to-collision (TTC) values at the earliest detection opportunity? TTC is the elapsed time from the earliest detection opportunity until impact. TTC at this earliest detection opportunity is important to consider when designing I-ADAS, because sufficient time is required both for an I-ADAS to alert the driver and for the driver to react to the warning. Third, how does varying sensor position, orientation, and range/azimuth specifications influence the sensor detection capability of I-ADAS?

10.2 *Methods*

Data Source

This study's analysis was based on the NMVCCS simulation case set of 661 reconstructed SCP and LTAP/LD intersection.

Detection Distance and Angle Calculations

Detection distance and angle values were generated for each vehicle at the earliest detection opportunity for each simulation. Sightline restrictions from an I-ADAS equipped vehicle to the oncoming vehicle will limit the ability of an I-ADAS sensor to detect the approaching vehicle. This study assumes that no sightline obstructions were present after the first vehicle enters the intersection. The time point when the first vehicle enters the intersection is referred to as the earliest detection opportunity. This is of course a best case scenario as sightline obstructions can impede the performance of I-ADAS. This study investigates the requirements of a side-facing sensor given the need to detect the oncoming vehicle at the earliest detection opportunity.

. If a stop bar was present, it was used as the earliest detection opportunity. If a stop bar was not present but a crosswalk was present, the location where the vehicle first crossed the crosswalk was taken as the earliest detection opportunity. If neither a stop bar nor crosswalk was present, the intersection boundary line was used as the earliest detection opportunity. Intersection boundary lines were drawn for every scene diagram. These lines were drawn by extrapolating the road edge throughout the intersection. Examples of drawing these intersection boundary lines can be found for two cases in Figure 85.

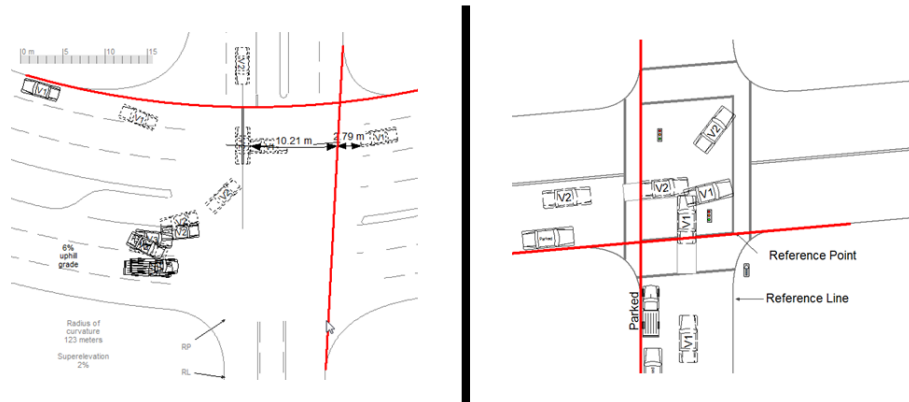


Figure 85. Examples for how intersection boundary lines were drawn. The scene diagram on the left was taken from NMVCCS case 2007-74-62. The scene diagram on the right comes from NMVCCS case 2006-03-043.

Detection distance was computed as the distance between the vehicles at the earliest detection opportunity. The detection angle was computed for both the entering vehicle and the oncoming vehicle. The entering vehicle refers to the first vehicle to enter the intersection. The oncoming vehicle has not entered the intersection, and is approaching the intersection. Both measurements can be visualized in Figure 86.

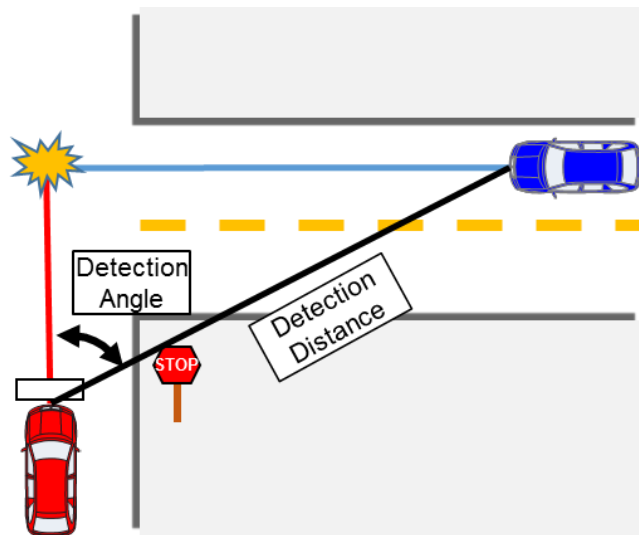


Figure 86. A graphical representation of range and azimuth. The Red vehicle represents the vehicle from which range and azimuth are computed.

Sensor Modeling

The ability of three radar sensors in nine configurations to detect an oncoming vehicle were analyzed. The three sensors modeled were intended to represent wide, intermediate, and narrow beam radars, where there is an inherent trade-off between sensor range and azimuth capabilities. A depiction of the three specifications analyzed in this study can be seen in Figure 87.

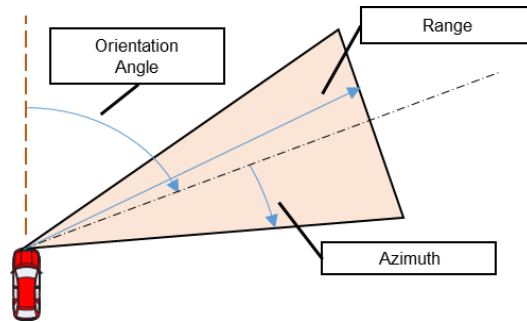


Figure 87. A depiction of sensor orientation, range, and azimuth for detecting an oncoming vehicle.

Radar sensor specifications were based on several commercially available, vehicle-based radars, including Delphi Corporation’s Electronically Scanning Radar, Smartmicro’s UMRR Automotive Radar Sensors, and Eaton’s VORAD® VS-400. The sensors were modeled as being pointed in one of six unique orientations, including 0, 15, 30, 45, 60, and 75 degrees. The eighteen total combinations of sensor specifications and configurations are shown in Table 48.

Table 48. Sensor combinations modeled in this study.

Orientation (degrees)	Range (m)	Azimuth (+/- degrees)	Sensor Orientation (degrees relative to forward direction)					
			0°	15°	30°	45°	60°	75°
Sensor Type	Wide Beam		0°	15°	30°	45°	60°	75°
			40 m	40 m	40 m	40 m	40 m	40 m
		+/- 90°	+/- 90°	+/- 90°	+/- 90°	+/- 90°	+/- 90°	
	Intermediate Beam		0°	15°	30°	45°	60°	75°
			80 m	80 m	80 m	80 m	80 m	80 m
		+/- 75°	+/- 75°	+/- 75°	+/- 75°	+/- 75°	+/- 75°	
Narrow Beam		0°	15°	30°	45°	60°	75°	
		120 m	120 m	120 m	120 m	120 m	120 m	
	+/- 60°	+/- 60°	+/- 60°	+/- 60°	+/- 60°	+/- 60°		

The sensor was always modeled as being located on the front center of the vehicle. A sensor was assumed to detect an approaching vehicle if the C.G. of the vehicle fell within the radar beam. A depiction of a scenario with and without vehicle detection are shown in Figure 88.

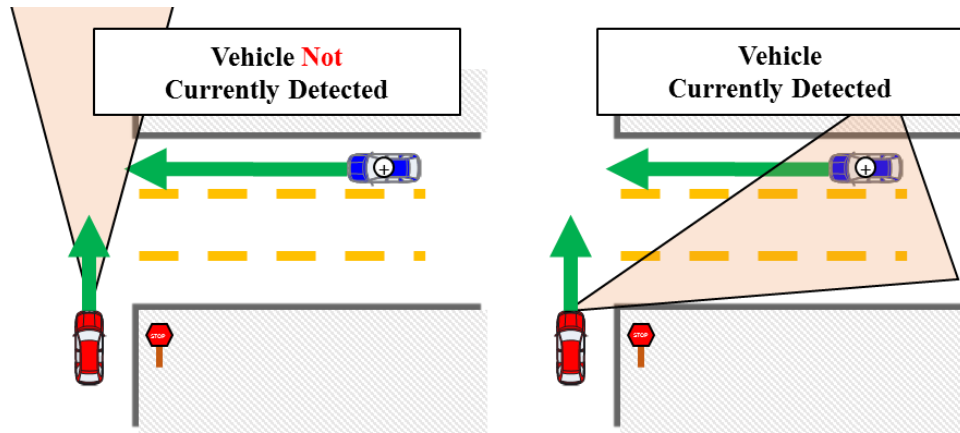


Figure 88. The figure on the left shows a sensor-equipped red vehicle whose front-facing radar beam does not detect an approaching blue vehicle. The figure on the right depicts a side-facing radar beam that does detect an oncoming blue vehicle.

10.3 *Results and Discussions*

A total of 1,531 (1,139 SCP and 392 LTAP/LD) crash reconstruction simulations were run in this study. These simulations were based generated using 448 SCP crashes and 213 LTAP/LD from the NMVCCS database. These crashes were representative of 254,877 U.S. crashes.

What was Detection Distance and Angles when Vehicles Enter the Intersection?

The primary objective of the study was to determine the required detection distance and angles between vehicles at the earliest detection opportunity. Detection distance and angle were analyzed from the perspective of both the entering vehicle and the oncoming vehicle. The effects of stopping behavior and intersection crash mode were also investigated.

Analysis of all CT Crashes

The first analysis examined detection distance and angle distributions for all CT crashes (SCP + LTAP/LD). These values generated provide a general sense for the range and azimuth requirements of sensors to detect oncoming vehicles in CT crash modes. In general, either vehicle could have been equipped with an I-ADAS. This analysis examines the perspective of either vehicle.

Figure 89 shows the distribution of detection distance at the earliest detection opportunity. One-half of cases had range values less than 33 m. A total of 95% of cases had range values below 86 m.

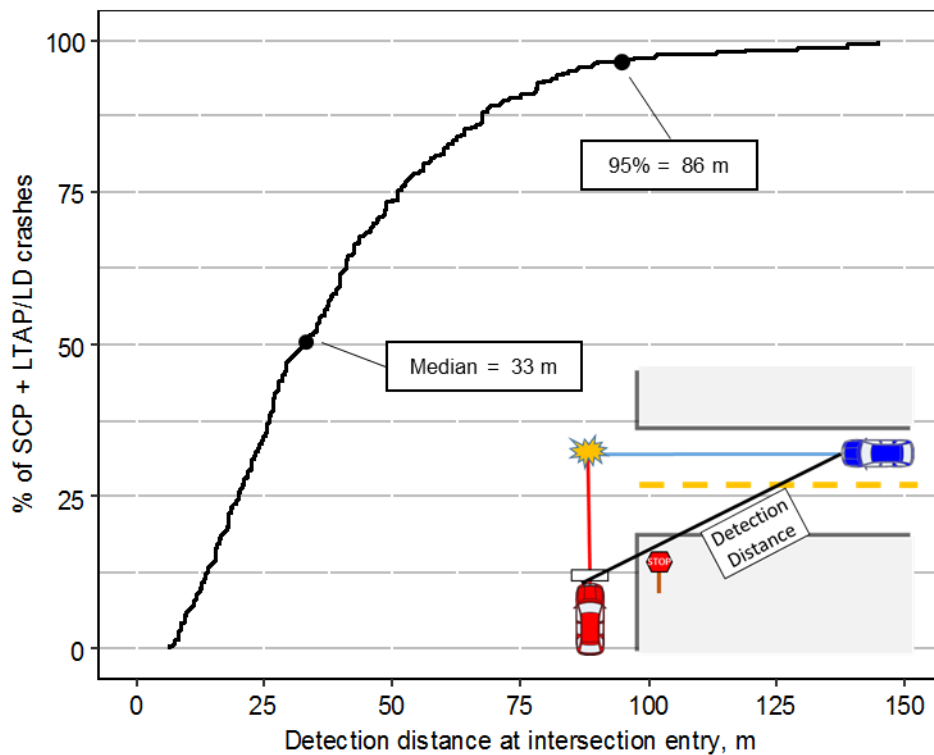


Figure 89. A cumulative distribution plot of range for the first vehicle to enter the intersection

Figure 90 shows a distribution of detection angle values at the earliest detection opportunity for the first vehicle to enter the intersection. The median detection angle was found to be 66 degrees. The middle 95% of the data fell between 28 degrees and 87 degrees.

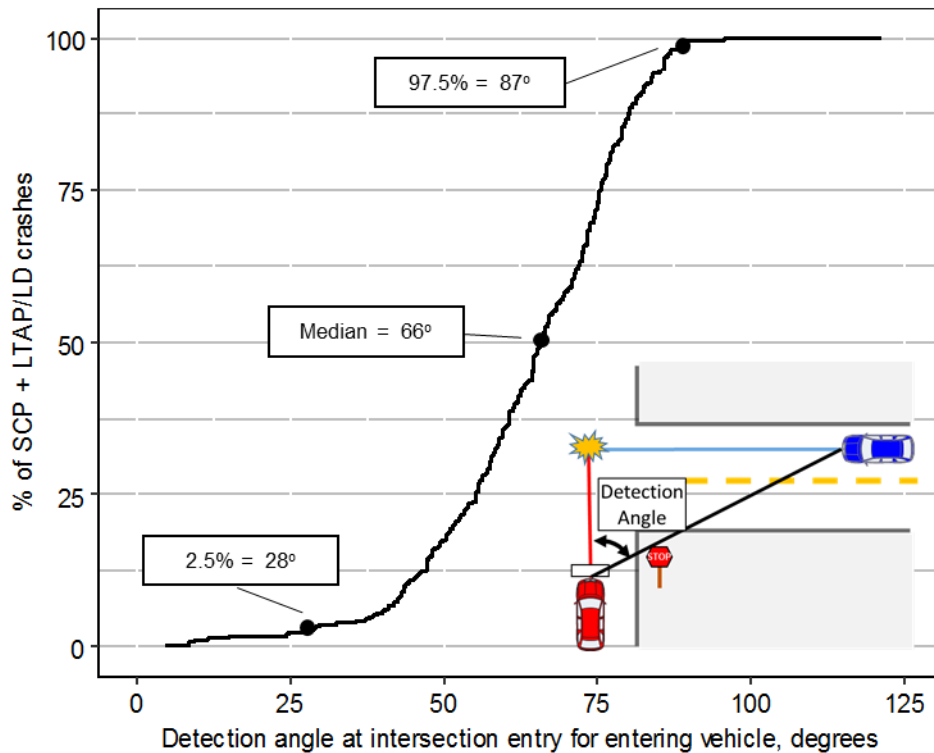


Figure 90. A cumulative distribution plot of azimuth at the earliest detection opportunity from the perspective of the entering vehicle.

The perspective of the oncoming vehicle was also considered, which is shown in Figure 91. At the earliest sensor detection opportunity, the azimuth values were much less for the oncoming vehicle than the first entering vehicle. The median detection angle was 27 degrees. The middle 95% of detection angles fell between 5 degrees and 64 degrees.

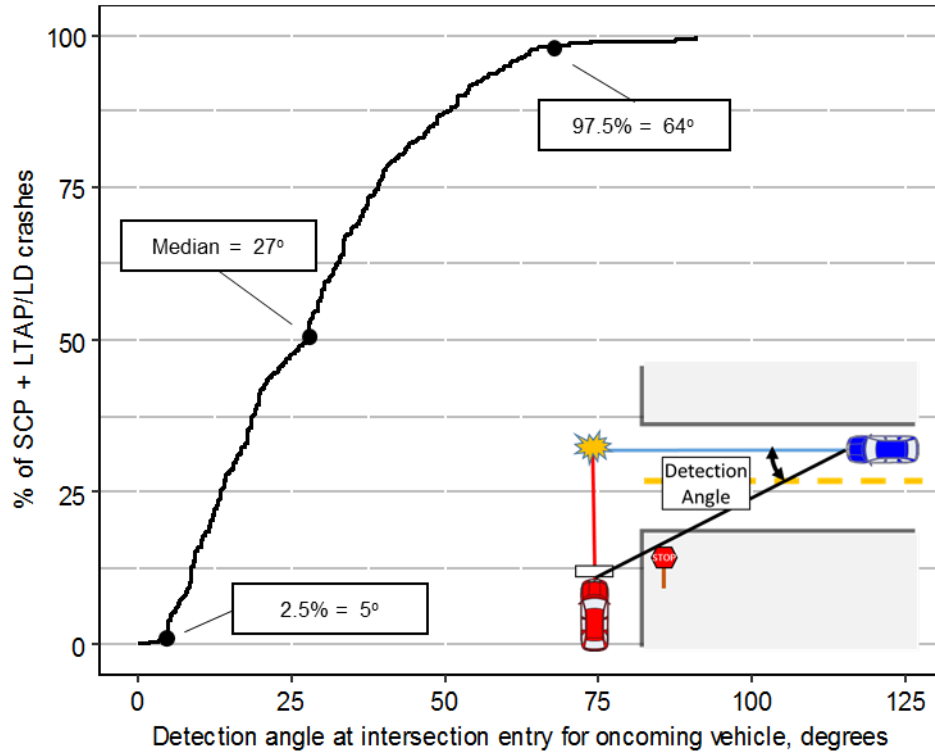


Figure 91. A cumulative distribution plot of azimuth at the earliest detection opportunity from the perspective of the oncoming vehicle.

There are several important findings from this set of results. First, at the earliest detection opportunity, nearly all (97%) of the vehicles were less than 100 m away from each other. Sensors with range capacity of 100 m will have the capacity to detect oncoming vehicles at or near the time of the earliest detection opportunity. Second, the sensor detection angle requirements appear to be different for the first entering vehicle and the oncoming vehicle. This indicates that required azimuth specification and sensor orientation should be considered for each vehicle perspective.

Analysis by Crash Mode

The second analysis examined the influence of crash mode on detection distance and angle requirements. During SCP and LTAP/LD crashes, vehicles are approaching one another from lateral directions. Accordingly, the sensor detection requirements were expected to be somewhat similar. However, differences in vehicle kinematics would lead to differences between the crash modes. Specifically, in LTAP/LD crashes, a substantially higher proportion (92.5%) of crashes occur between vehicles where at least one stopped prior to entering the intersection. For SCP crashes, only 55.5% of crashes involve at least one vehicle that stopped. Additionally, for drivers that stopped and are accelerating into the intersection, left turning drivers tend to accelerate at lower rate than straight crossing drivers, which was demonstrated in Chapters 3 and 4.

Figure 92 shows the distribution of detection distance values by crash mode at the earliest detection opportunity. Clear differences were observed between the SCP and LTAP/LD crash modes. The median detection distance for SCP crashes was 29 m. For LTAP/LD crashes, the median detection distance was 37 m. Similarly, 95% of detection distances fell below 75 m for SCP crashes. Conversely for LTAP/LD crashes, 95% of detection distances fell below 97 m.

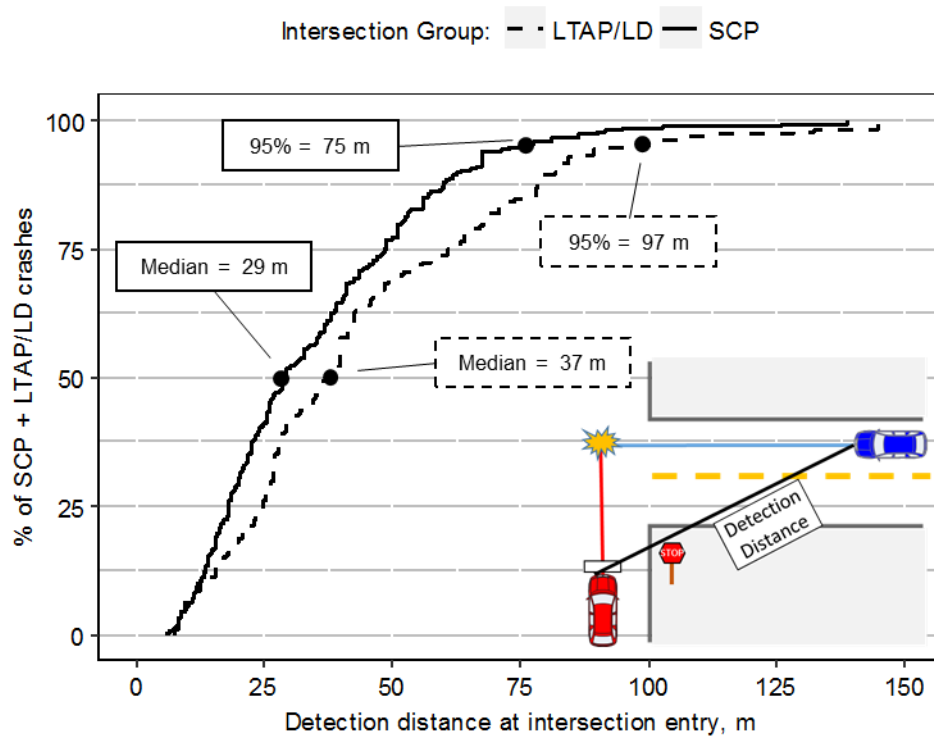


Figure 92. A cumulative distribution of detection distance requirements by intersection group.

Figure 93 shows the distribution of detection angles for the entering vehicle at the earliest detection opportunity. The results are shown by crash mode. The median detection angle for entering vehicles in the SCP crash mode was 72 degrees. In the LTAP/LD crash mode, the median detection angle was lower at 62 degrees. The middle 95% of detection angles for the SCP crash mode was narrower than for the LTAP/LD crash mode. For SCP, 95% of detection angles fell

between 38 degrees and 88 degrees (~50 degrees difference). For LTAP/LD, these 95% of detection angles ranged from 10 degrees to 84 degrees (~75 degrees difference).

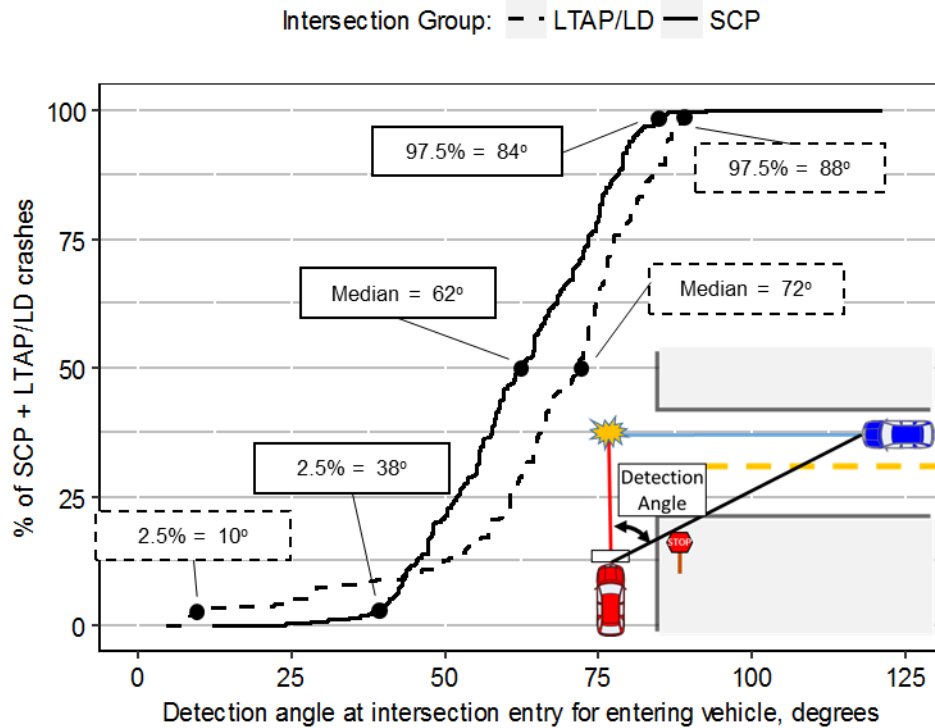


Figure 93. A cumulative distribution plot of detection angle for the entering vehicle at the earliest detection opportunity. Results are shown by crash mode.

The greater variability in detection angle for LTAP/LD crashes can be attributed, at least partially, to the fact that the entering vehicle is often turning left (86% of the time). For some of these crashes, the left turning vehicle was initiating the left turn at the earliest detection opportunity, which would decrease the detection angle.

Figure 94 shows the distribution of detection angles for the oncoming vehicle at the earliest detection opportunity. The median detection angle for SCP crashes was 32 degrees, while for LTAP/LD, the median detection angle was 16 degrees. A total of 95% of detection angles ranged from 6-64 degrees for SCP crashes and 4-76 degrees for LTAP/LD crashes.

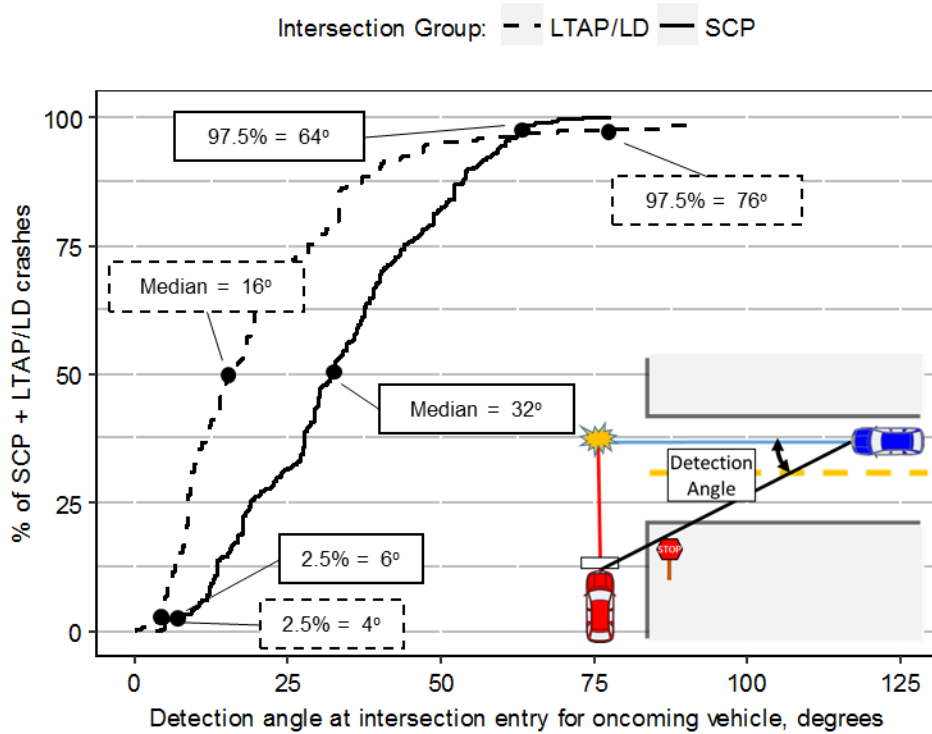


Figure 94. A cumulative distribution plot of detection angle for the oncoming vehicle at the earliest detection opportunity. Results are shown by crash mode.

The lower detection angles for the oncoming vehicle in LTAP/LD crashes can be primarily attributed to these vehicles being, in general, at farther distances away from the intersection at the earliest detection opportunity. The earliest detection opportunity for SCP crashes occurs while these vehicles are closer to one another, which implies a larger detection angle for the oncoming vehicle.

Analysis by Stopping Behavior

As demonstrated in the next section analyzing elapsed time following intersection entry, stopping behavior has a substantial influence on the available time for I-ADAS response. This stopping behavior effect translates itself into stark differences in detection distance and angle requirements. There are two general trends that can be observed. First, the sensor range requirements for crashes where at least one of the vehicles stopped is approximately 50% higher than for crashes where neither vehicle stopped. Second, stopping behavior in crashes, in general, leads to an increase in the detection angle of the entering vehicle and a decrease in the detection angle for the oncoming vehicle.

Figure 95 shows detection distance values by whether one of the vehicles stopped prior to entering the intersection. If at least one of the vehicles stopped (rolling or completely) prior to entering the intersection, one-half of detection distances fell below 38 m, and 95% of detection distances were below 91 m. Conversely, for crashes where neither vehicle stopped, the median detection distance was 25 m, and 95% of values fell below 59 m.

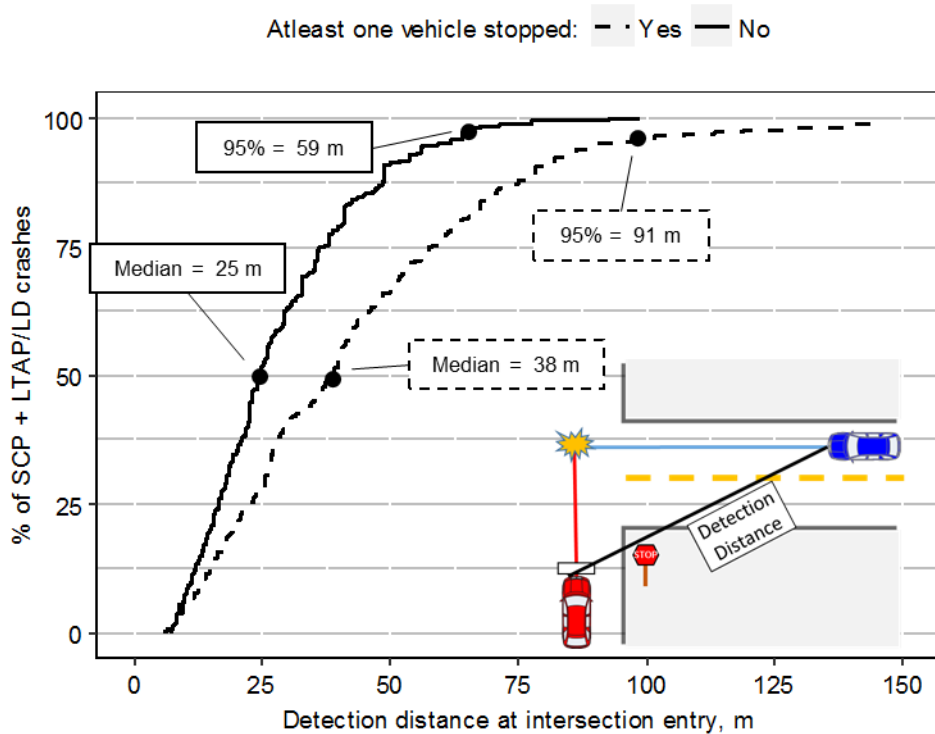


Figure 95. Cumulative distribution plots of detection distance at the earliest detection opportunity by whether at least one of the vehicles stopped.

Figure 96 shows detection angle for the entering vehicle at the earliest detection opportunity. The results are shown by whether either of the vehicles stopped. When at least one of the vehicles stopped, the median detection angle was 72 degrees with the middle 95% of angles ranging from 24 to 88 degrees. When neither vehicle stopped, the median detection angle was 59 degrees, and the middle 95% of detection angles ranged from 24 to 77 degrees.

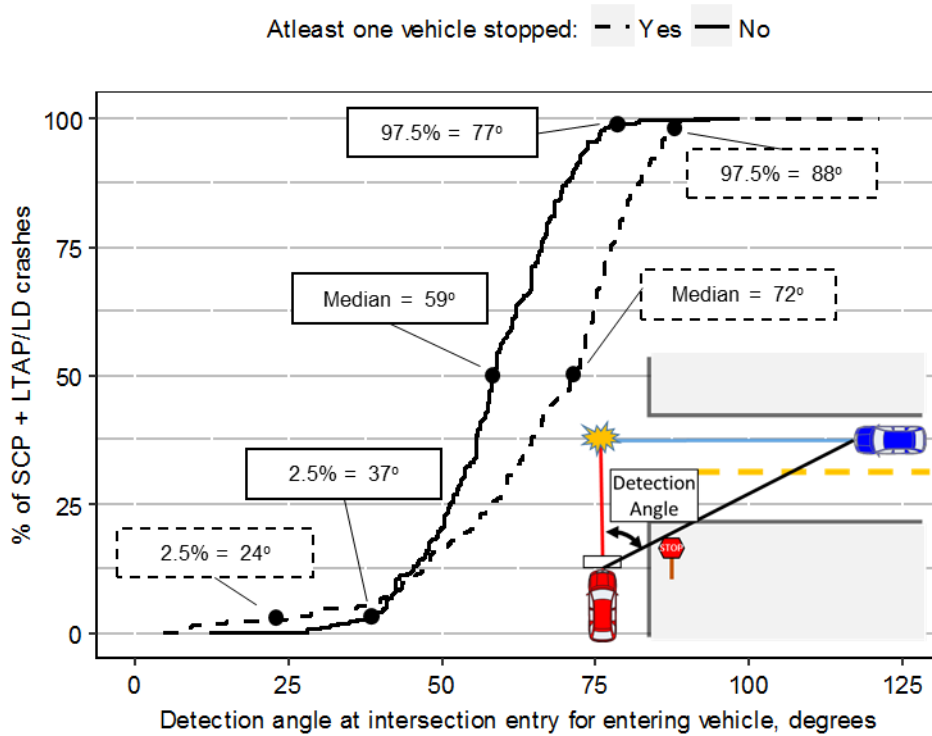


Figure 96. Cumulative distribution plots of detection angle at the earliest detection opportunity for the first vehicle to enter the intersection. The results are shown by whether at least one of the vehicles stopped.

Figure 97 shows detection angles at the earliest detection opportunity for the oncoming vehicle. Results are shown by stopping behavior. For crashes where at least one vehicle stopped, the median detection angle was 19 degrees, and the middle 95% of detection angles ranged from 5 to 64 degrees. When neither vehicle stopped, the median detection angle was 37 degrees, and the middle 95% of detection angle values ranged from 16 to 66 degrees.

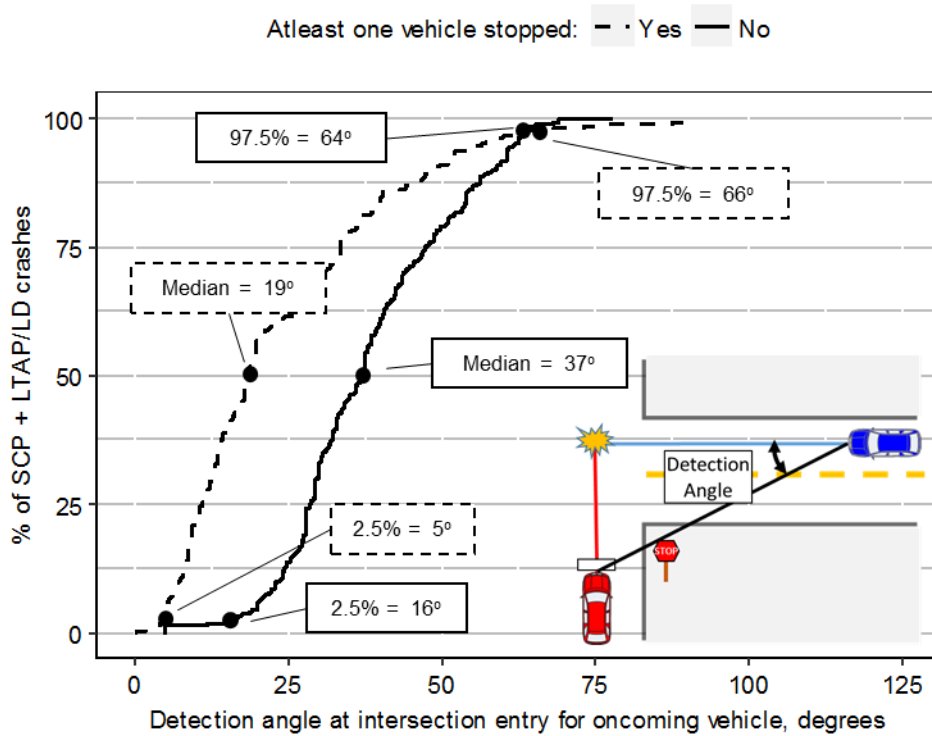


Figure 97. Cumulative distribution plots of detection angle at the earliest detection opportunity for the oncoming vehicle. The results are shown by whether at least one of the vehicles stopped.

How much time elapsed from the earliest detection opportunity to impact?

The first analysis examined the time-to-collision (TTC) at the earliest detection opportunity. As previously stated, the earliest detection opportunity is defined as the instance the driver crosses the stop bar (if provided), crosswalk (if stop bar is not provided), or intersection boundary line (if neither are present).

Figure 98 shows a cumulative distribution plot of elapsed time from the earliest detection opportunity until impact. The median elapsed time was 1.7 s, and 95% of times fell below 4.1 s.

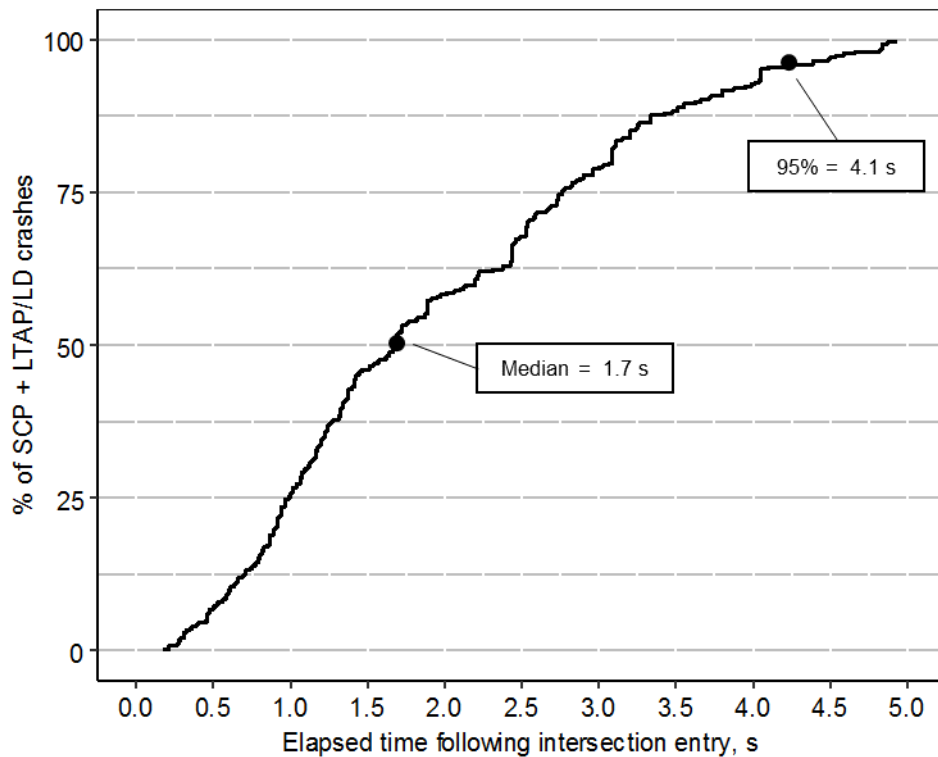


Figure 98. A cumulative distribution plot of elapsed time to collision following the earliest detection opportunity.

These results were further broken down by crash mode in Figure 99. There was considerably less time for SCP crashes. The median elapsed time was 1.4 s, and 95% of elapsed time values were below 3.8 s. Conversely, for LTAP/LD crashes, the median elapsed time was 2.1 s, and 95% of times fell below 4.5 s. As stated in the preceding section, LTAP/LD crashes more often occur in scenarios where at least one of the vehicles stopped prior to entering the intersection.

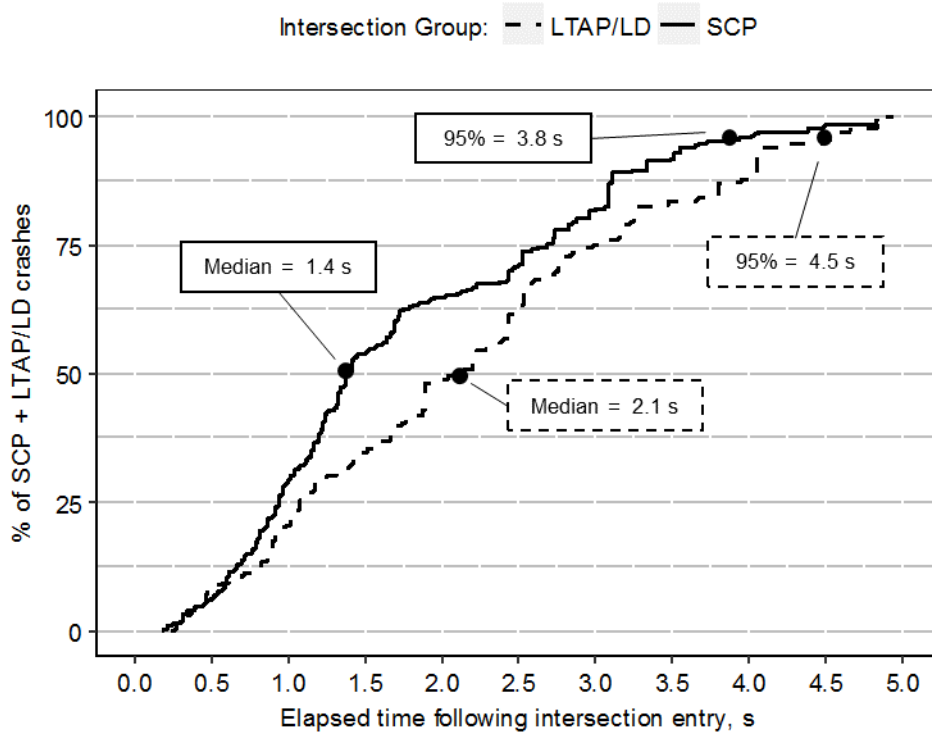


Figure 99. A cumulative distribution plot of time to collision following the earliest detection opportunity. Results are shown by the intersection crash mode.

The elapsed time following the earliest detection opportunity until impact was also examined with respect to stopping behavior in Figure 100. In crashes where at least one vehicle stopped, the median elapsed time after the earliest detection opportunity was 2.2 s, and 95% of times fell below 4.5 s. Conversely, if neither vehicle stopped, the median time was 1.2 s, and 95% of values fell below 2.8 s.

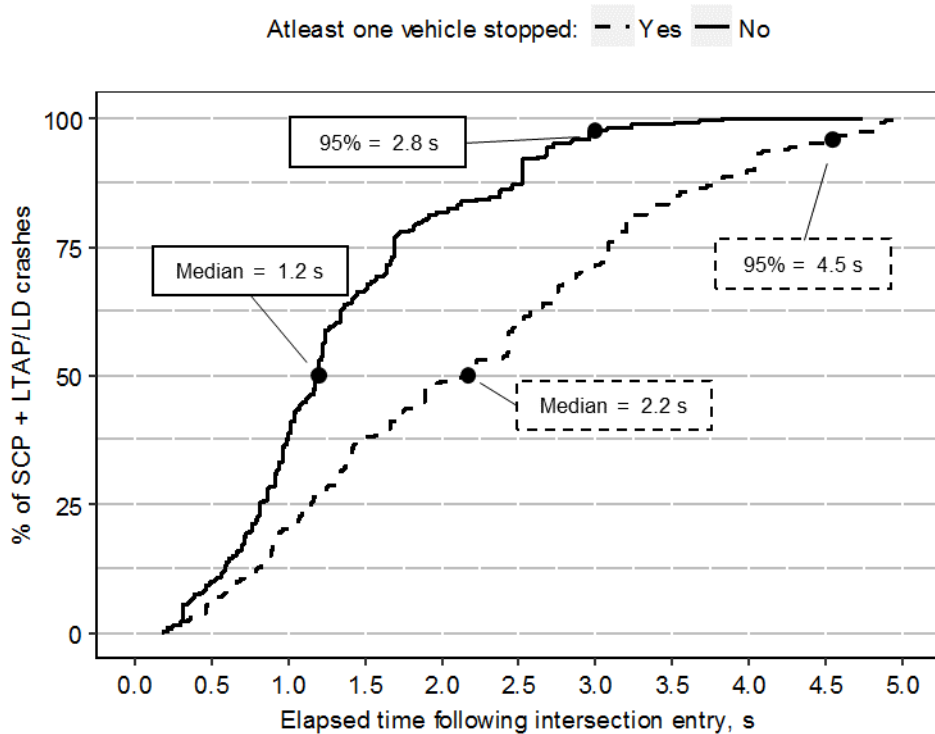


Figure 100. A cumulative distribution plot of time to collision following the earliest detection opportunity. Results are shown by the stopping behavior of the vehicles.

These time intervals are very low when considering an I-ADAS that alerts the driver of an approaching vehicle at the instant the vehicle enters the intersection. In one experimental study performed by Mazzae et al. [192] investigated typical braking reaction time in response to an intersection incursion. This NHTSA sponsored study placed 245 subjects in vehicles and had them drive on a test track with wet or dry pavement. A two-way stop-controlled intersection was setup on the track with the experimental vehicle having no stop sign on their intersection approach. After

some time a foam car was towed into the intersection in order to simulate an incursion. The results indicated the average driver response time to an intersection incursion begin within the range of 1.37 s to 1.51 s.

In a second simulator-based study at the Monash University Research Center (MUARC), 32 participants performed three test drives along a given stretch of road [129]. Each stretch of road consisted of 7 to 8 signalized intersections. During 3 of the intersection traversals for each of the drives (i.e. 9 events per participant), the driver experienced one of three imminent intersection crash scenarios (two of which were SCP related). When the crash scenario occurred, the participant either received (1) no warning, (2) a visual warning, or (3) an auditory warning. Similar to the results of the prior study, the average reaction time was found to be approximately 1.28 s. The median reaction time was found to be 0.99 s, and the 17th and 83rd percentiles of reaction times were 0.70 s and 1.89 s, respectively.

Given that it takes 1 s to respond to an imminent crash, our findings suggest that a moderate proportion of CT crashes (29% of SCP and 20% of LTAP/LD) are occurring too quickly for a warning-based I-ADAS to be effective. This result suggests that alternative techniques, such as utilizing automatic emergency braking (AEB), may be necessary in crashes occurring in too short of time following the earliest detection opportunity. This theory is further tested in the work presented in the Chapter 11 benefits analysis.

Which Sensor Specifications and Orientations Would Be Appropriate for Cross-Traffic Crashes?

The orientation and specifications of an I-ADAS sensor will determine its ability to detect an approaching vehicle. Two perspectives were considered: (a) the perspective of the first entering vehicle and (b) the perspective of the oncoming vehicle. As demonstrated in the preceding section, the detection angle requirements are dependent on the vehicle perspective. The ability of an I-ADAS sensor to detect an approaching vehicle at the earliest detection opportunity was investigated for three sets of sensor specifications (wide, intermediate, and narrow beam) and six orientations (0° , 15° , 30° , 45° , 60° , and 75° from the forward direction).

Figure 101 shows how sensor detection will vary with sensor orientation and specifications for the entering vehicle. Our results indicate that the narrow beam detected the highest proportion (98%) of oncoming vehicles at the earliest detection opportunity. Over 98% of oncoming vehicles detected was achieved for sensor orientations ranging from 44 to 68 degrees. The highest proportion of vehicles detected for the wide and intermediate beams were 62% and 93%, respectively.

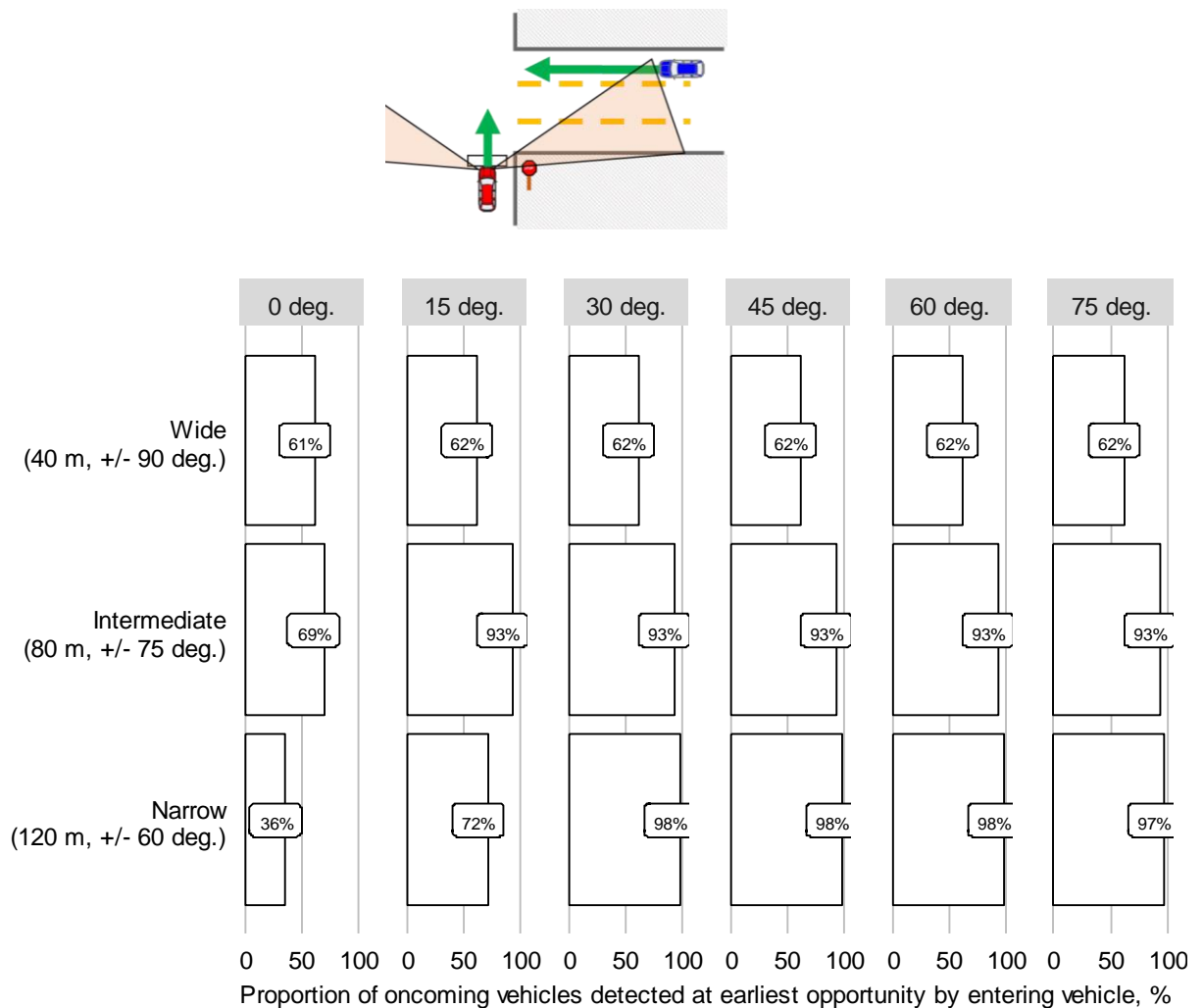


Figure 101. The proportion of oncoming vehicles detected at the earliest detection opportunity are shown. The perspective of the entering vehicle is depicted.

Figure 102 shows the proportion of entering vehicles potentially detectable by on-board sensors equipped on the oncoming vehicle. The performance of the three sensor beam types were very similar for the entering and oncoming vehicle. The best performing sensor was found to be the narrow beam, which detected 98% of entering vehicles. Maximum performance for the narrow beam was achieved when the sensor was oriented at 31 to 61 degrees. The highest proportion of entering vehicles detected by the wide and intermediate beams were 62% and 93%, respectively.

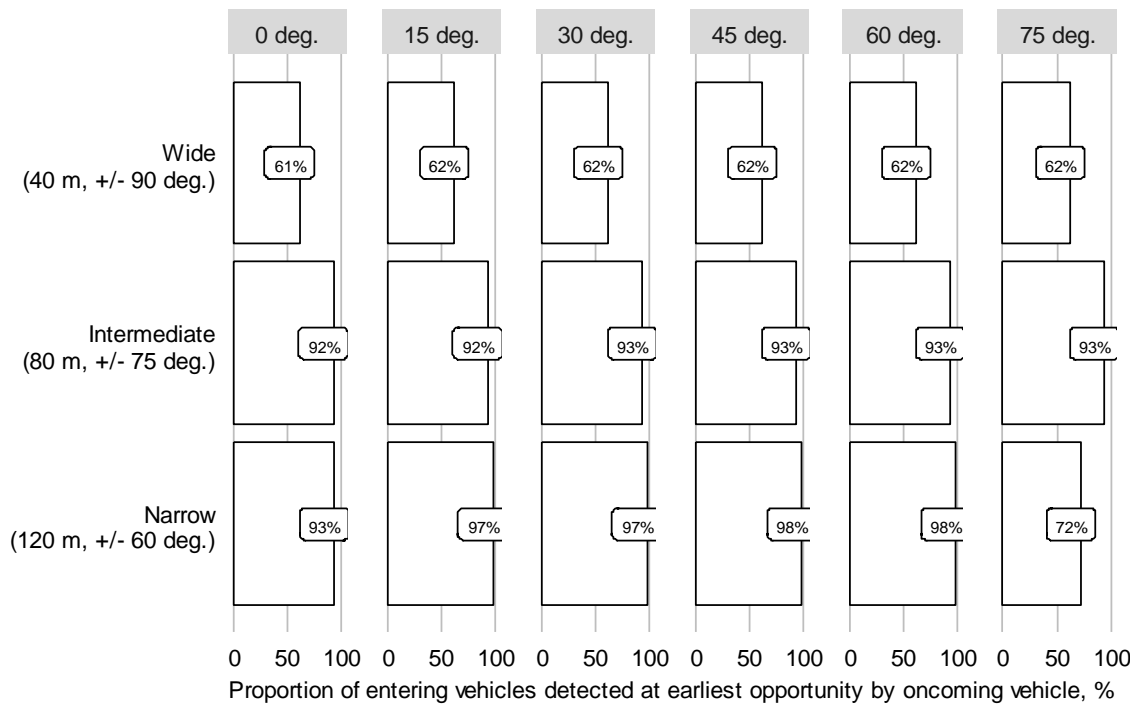
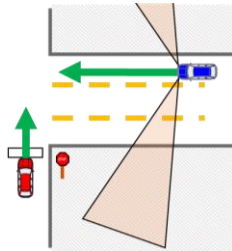


Figure 102. The proportion of entering vehicles detected at the earliest detection opportunity are shown. The perspective of the oncoming vehicle is depicted.

Compare Results with EDR Dataset

One limitation of reconstructing real-world crashes is that there is often uncertainty in pre-crash driver behavior (e.g. travel speed, evasive braking). The EDR dataset developed in Chapter 7 has the advantage of including each vehicle's actual pre-crash speed profile. However, the NMVCCS dataset has the advantage of containing a substantially larger dataset of crashes. As a form of validation for the findings from the NMVCCS dataset, detection distances, detection angles, and timings were compared with the 29 SCP and LTAP/LD crashes in the EDR dataset.

All measurements for this comparative analysis were taken from the time point when the first vehicle crossed the intersection boundary line. Figure 85 shows this location, which was drawn by extrapolating out the road edge through the intersection. The other analyses in this study used the stop bar or crosswalk, if present, as the earliest detection opportunity. Due to the limited duration that most EDRs record the pre-crash (most record up to 5-s of data), the EDR recording duration was insufficient for tracing back vehicle positions back to the stop bar for nearly one-half of the available records. Most (~90%) of the records considered for this study had a sufficiently long recording for capturing the time point when the first vehicle crossed the intersection boundary line.

One important observation to point out from these analyses is the shape of the cumulative distribution curves for the two datasets. The EDR dataset contains only 29 cases. Fewer cases (using weighted data) makes the "steps" in the distribution more pronounced. Consequentially, it becomes difficult to analyze the true distribution of the population. This observation, in itself, provides motivation for expanding the analysis to the much larger NMVCCS dataset (661 Cases), where the distribution has a much "smoother" shape.

Detection distances at initial intersection boundary line crossing were first compared between the two datasets. These results can be seen in Figure 103. Overall the detection distances compared well despite the case counts in the EDR dataset. The median detection distance of the EDR dataset was 16 m, and 95% of the values fell below 45 m. For the NMVCCS dataset, the median detection distance was 22 m, and 95% of distances were below 58 m. It should be noted that the EDR dataset does not capture the long upper “tail” of distances in the NMVCCS dataset. Potential explanations for this finding are presented at the end of the section.

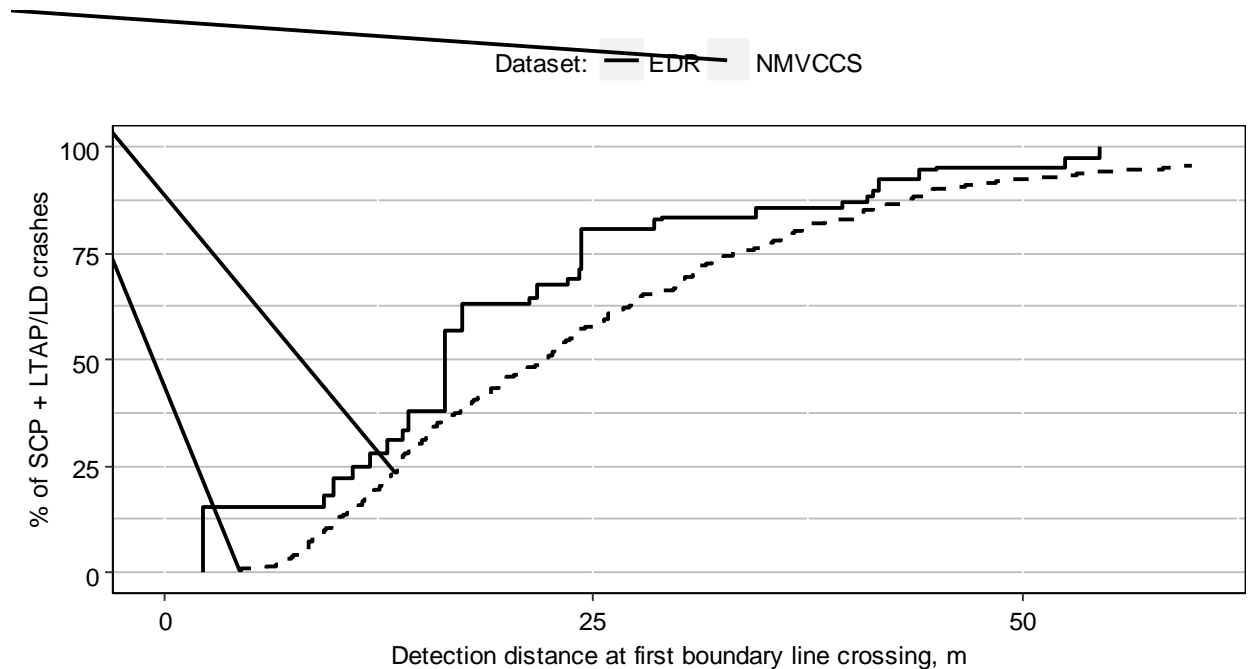


Figure 103. Detection distance requirements at the time point when the first vehicle crosses over the intersection boundary line. Estimates were generated for the EDR dataset and the NMVCCS dataset.

Detection angles for the entering vehicles were compared next between the two datasets. The EDR dataset was tended to have smaller detection angles, which suggest that the oncoming vehicle was more toward the forward position of the oncoming vehicle. This is typically observed if the oncoming vehicles are a farther distance apart. The median azimuth for the EDR dataset (51 degrees), and the middle 95% of values fell between 30 to 90 degrees. The median azimuth for the NMVCCS dataset was 65 degrees, and the middle 95% of values were between 29 to 89 degrees. While the median angles did not align, the range of the middle 95% of values were nearly identical.

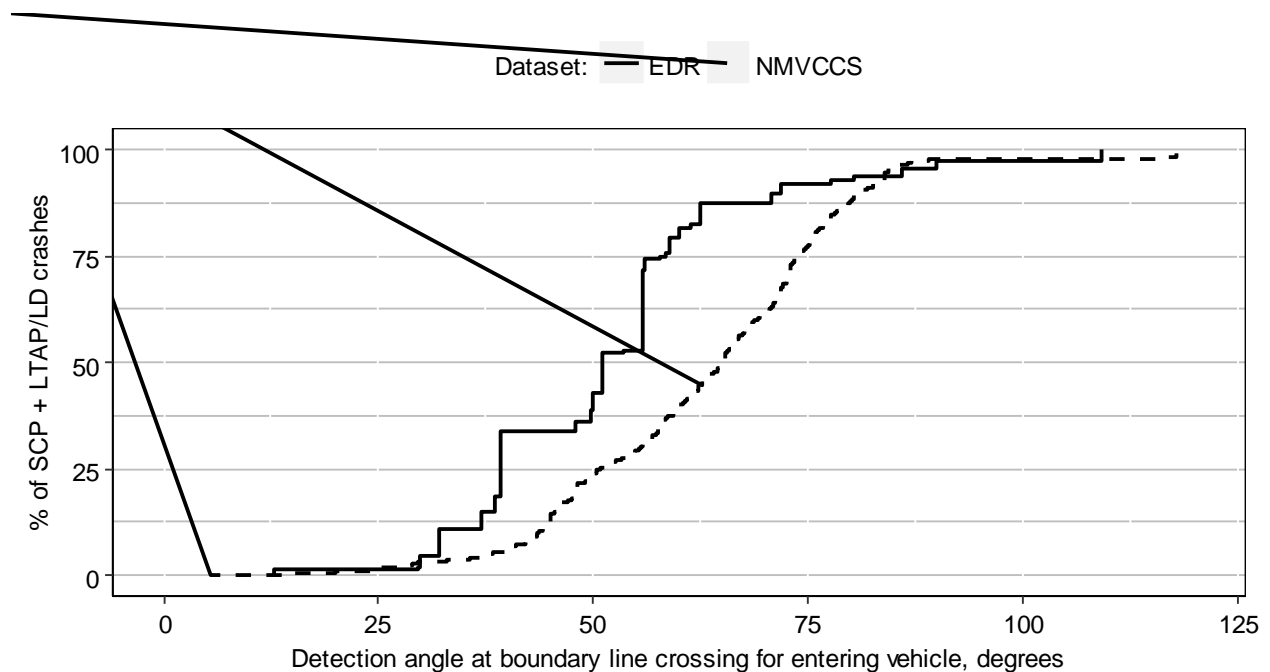


Figure 104. Detection angle requirements at the time point when the first vehicle crosses over the intersection boundary line. The perspective of the first vehicle to enter the intersection (entering vehicle) is considered. Estimates were generated for the EDR dataset and the NMVCCS dataset.

Detection angles for the oncoming vehicle were then compared. Consistent with the previous findings, closer proximity of vehicles at the boundary line for the EDR dataset translated to slightly larger detection angles for the oncoming vehicle at first boundary line crossing. The median oncoming vehicle detection angle in the EDR dataset was 34 degrees, and 95% of values fell between 6 and 58 degrees. For the NMVCCS dataset, the median value was 28 degrees, and 95% of values fell between 5 and 66 degrees.

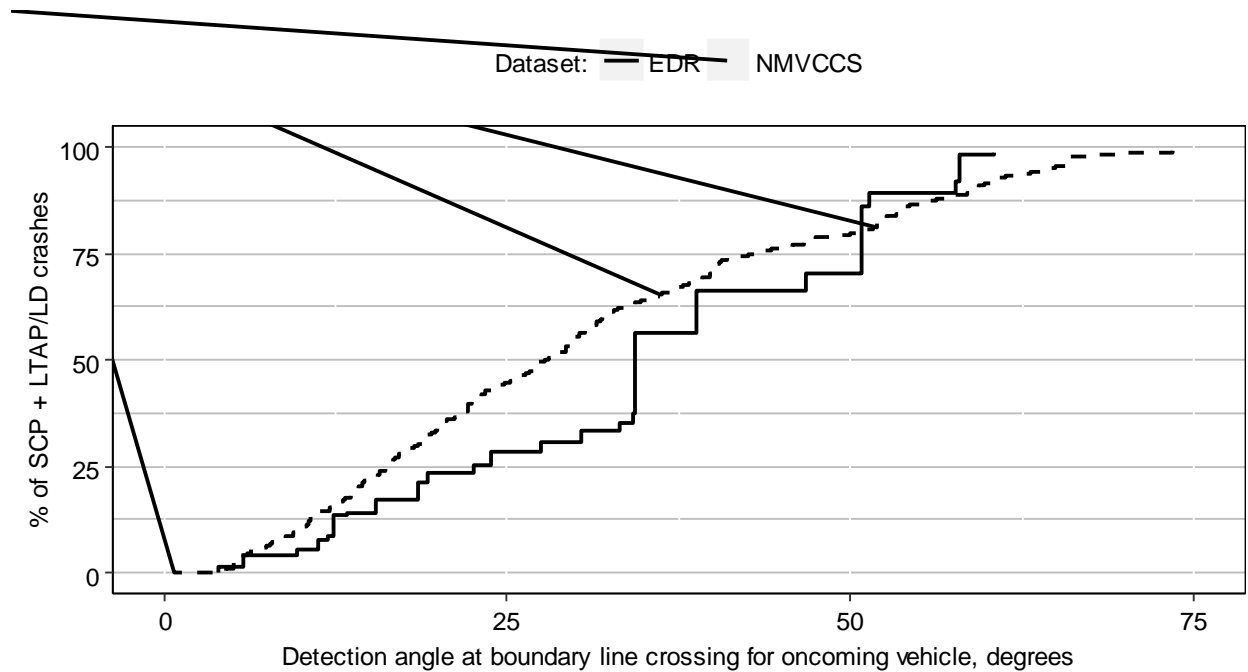


Figure 105. Detection angle requirements at the time point when the first vehicle crosses over the intersection boundary line. The perspective of the vehicle approaching the intersection when the entering vehicle crosses the boundary line. Estimates were generated for the EDR dataset and the NMVCCS dataset.

The last comparison made was the elapsed time following the first crossing of the intersection boundary line. The EDR dataset was found to have similar elapsed time values, but fails to capture the upper “tail” of elapsed time values. For the EDR dataset, the median elapsed time following boundary crossing was 1.4 s, and 95% of values fell below 1.8 s. For the NMVCCS dataset, the median time was 1.1 s, and 95% of times fell below 2.9 s.

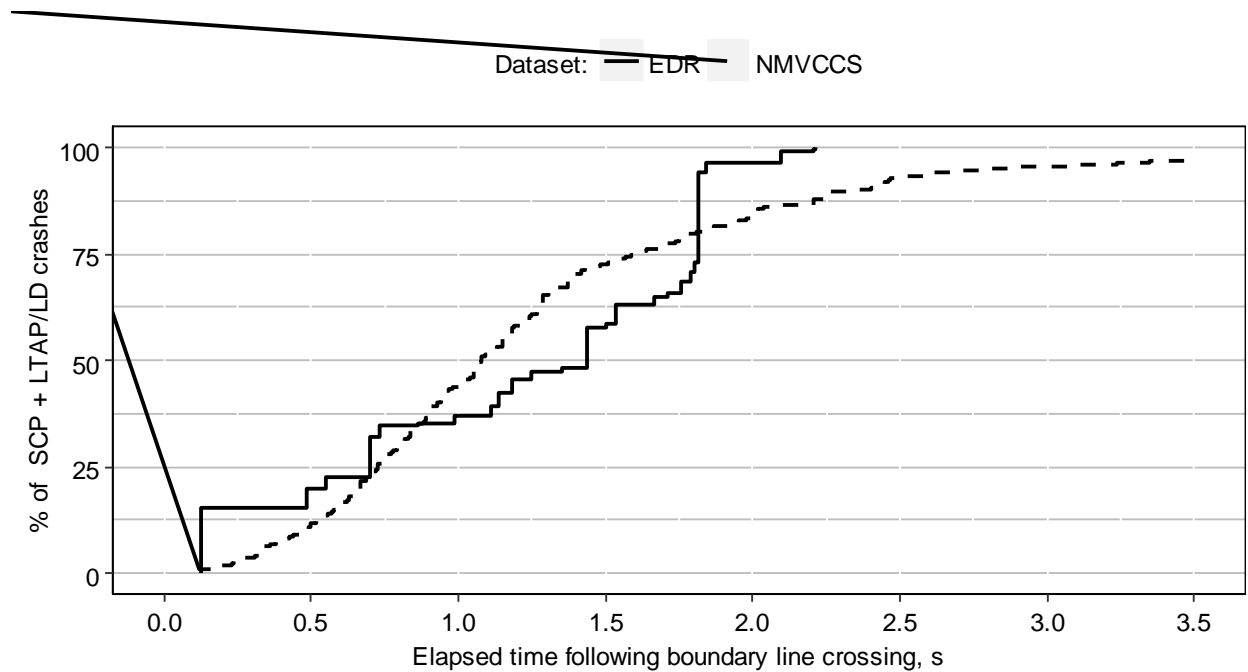


Figure 106. A cumulative distribution plot of the time-to-collision at the time point when the first vehicle first crosses the intersection boundary line. Estimates were generated for the EDR dataset and the NMVCCS dataset.

In general, the results from the EDR dataset compare well with the NMVCCS dataset. This result suggests that the speed reconstructions performed in the NMVCCS dataset, in general, reflect realistic real-world speed profiles.

There were some key differences between the results of the two datasets. First, in general, the elapsed time following boundary crossing were, in general, shorter for the EDR dataset. Second, detection distance values for the EDR dataset were, in general, smaller in the EDR dataset. Both of these results can be at least partially explained by the inclusion criteria used for selecting the EDR dataset. The EDR dataset is comprised of crashes where each vehicle experienced “deployment-level” impact severities. This criterion was established to ensure that the record being analyzed corresponded to the crash being investigated. However, this criteria likely produces some bias in the severity of the crashes being included. Specifically, I would expect that these crashes typically involve higher speed vehicles. Higher speeds imply shorter traversal times and smaller detection distances, which is consistent with the results from this study.

It should also be noted that the EDR recording duration was not always sufficient for tracing the vehicle positions back to the point of initial intersection boundary crossing. Specifically, three crashes from the EDR dataset (~10%) were removed for this reason. Two of these crashes had vehicles with 5-s worth of pre-crash data. The other crash had an EDR record with only 2.5 s of pre-crash. This inclusion criteria leads to including crashes with shorter traversal times and smaller detection distances. It should also be noted that there tends to be a long “tail” for higher times and detection distance values that was not as pronounced in the EDR dataset. This inclusion criteria likely contributed to this finding.

10.4 *Limitations*

This study has a number of limitations that should be addressed. First, the NMVCCS case set uses a collection of driver models to estimate pre-crash vehicle positions. The approach for estimating pre-crash deceleration and acceleration rates was to model the 50th percentile of drivers. Some general assumptions were also made with regards for modeling evasive braking action. As a form of validation for this approach, the results taken from the NMVCCS dataset were compared with NASS/CDS EDR dataset, where each vehicle had to have an EDR that recorded pre-crash speeds. Overall, this study found good agreement between the results from the two datasets.

Second, only EDRs with ample pre-crash data were included in the EDR dataset used in this study, i.e. cases were excluded if the EDR did not record vehicle's crossing over the intersection boundary line. This biases this study's results toward crashes with shorter elapsed time from intersection entry to impact and lower detection distance values. Approximately one out of every thirteen cases were excluded due to this criteria. Also, crashes in the EDR dataset were only considered if one of the vehicle's experienced an airbag deployment or a delta-v greater than 5-mph. As such, the dataset is likely biased toward more severe crashes, where the vehicles may have been travelling faster prior to impact.

Third, this study makes some assumptions regarding sightline obstructions. In general, sightline restrictions at intersections can be divided into two main categories: fixed and moving. This study's assumptions handle the bulk of fixed obstructions. Our study assumes that sightlines are completely obstructed until the first vehicle enters the intersection. Vehicles in our model cannot see around corners. This assumption corresponds to vehicles operating in an "urban canyon". But, this assumption would also subsume cases in which approaches to intersections were obstructed

by trees, shrubs, and signs. There were a few cases where objects/trees in the median could lead to a later earliest detection opportunity. Likewise, in many crashes in more open environments, vehicles could have a clear sightline earlier than was modeled, which could lead to an earlier earliest detection opportunity. Moving obstructions, such as roadway traffic or parked vehicles, were not accounted for in this study. By not accounting for these moving obstructions, the earliest detection opportunities would likely have occurred later than modeled for some crashes.

10.5 *Conclusions*

This study estimated range and azimuth at intersection entry for a set of 448 SCP crashes and 213 LTAP/LD intersection crashes. The pre-crash positions of every vehicle involved in these crashes were reconstructed using a combination of previously developed driver models. Overall, this study found that a narrow beam radar beam (120 m range, +/- 60° field of view) directed at 44 to 61 degrees from the vehicle heading would allow for maximum vehicle detection capacity at the earliest detection opportunity for either vehicle in a CT intersection crash. The influence of stopping behavior and intersection crash mode was also investigated. I-ADAS will have more time from the earliest detection opportunity to impact in LTAP/LD crashes when compared to SCP crashes. This can be largely attributed to (a) a higher proportion of LTAP/LD crashes involving at least one of the vehicles performing a rolling or complete stop prior to accelerating into the intersection and (b) lower acceleration rates by left turning drivers than straight crossing drivers. These results have important implications for designers of an I-ADAS considering the necessary range, azimuth, and orientation for detecting an approaching vehicle.

11. Crash and Safety Benefits of I-ADAS for SCP and LTAP/LD crashes in the U.S. Vehicle Fleet ⁷

11.1 *Introduction*

Preventing and/or mitigating crashes and injuries that occur in intersection crashes are among the highest priority for designers, evaluators, and regulatory agencies [31, 83, 84, 246]. Crash avoidance systems aimed at preventing intersection crashes are currently being developed and deployed throughout the vehicle fleet. One promising method is to I-ADAS. Using I-ADAS, the onboard system must evaluate (a) whether there is a potential collision partner and (b) if it is necessary to take crash avoidance action. If the system does detect an imminent threat, I-ADAS can respond by either (a) warning the driver and/or (b) autonomously preventing the crash (e.g., using automated emergency braking, or AEB). This system is likely to be influenced by the available time from earliest vehicle detection until impact. Accordingly, the effectiveness of this technology is expected to be a strong function of computational latency time [249], sightline restrictions [158], driver perception reaction time [129], sensor specifications [158], and triggering algorithms [23].

There are several additional methods being explored for preventing intersection crashes. These other technologies can be divided into two basic groups: (1) vehicle-to-infrastructure (V2I) and (2) vehicle-to-vehicle (V2V). V2I uses infrastructure-based communication systems to relay information, such as upcoming traffic control devices, the location of other roadway users, and

⁷ The work shown in this study has been a part of several previously published peer-reviewed manuscripts, including:
137. Scanlon, J.M., R. Sherony, and H.C. Gabler. *Preliminary potential crash prevention estimates for an Intersection Advanced Driver Assistance System in straight crossing path crashes*. in *Intelligent Vehicles Symposium (IV), 2016 IEEE*. 2016. Gothenburg, Sweden: IEEE.
248. Scanlon, J.M., R. Sherony, and H.C. Gabler. *Injury Mitigation Estimates for an Intersection Driver Assistance System in Straight Crossing Path Crashes in the US*. Traffic Injury Prevention, 2017. **ESV Special Issue**.

changes in speed limit, to surrounding vehicles [219, 250, 251]. V2V is similar to V2I but relies on information relayed between vehicles [250]. Both technologies have the potential to use data collected by either (a) vehicle-based sensors [252, 253] or (b) roadside sensors [219, 254]. Like I-ADAS, these technologies will require vehicle path prediction and crash threat detection algorithms, and will need to make an appropriate intervention decision. One major advantage of V2V and V2I for intersection crashes is that by communicating the position of other neighboring vehicles, sight obstruction limitations can be overcome. This limitation, as demonstrated in the current study, is expected to play a major restrictive role in I-ADAS effectiveness. Although V2I and V2V are promising crash avoidance solutions, fleet wide implementation will be gradual. Specifically, these technologies (a) are still being developed and tested, (b) may be prohibitively expensive to implement in some locations (e.g., rural, less frequently traversed roads) [254], and (c) will take time to be deployed throughout the vehicle fleet. In fact, in December 2015, NHTSA set forth a proposed framework of testing procedures for a future intersection collision avoidance system that uses vehicle-to-vehicle (V2V) communications [31]. Accordingly, I-ADAS serves as a promising, near-term alternative that is already present within the vehicle fleet [83, 84, 246].

Two of the most common intersection crash modes in the U.S. are the straight crossing path (SCP) and the left turn across path lateral direction (LTAP/LD) scenarios. These crashes are depicted in Figure 107. Altogether, these scenarios account for one-half of all intersection crashes and three-fifths of all fatal intersection crashes [2]. The SCP and LTAP/LD crash modes have similarities, which make potential preventive measures similar. First, both scenarios involve vehicles approaching one another from lateral directions. Accordingly, as demonstrated in Task 3.2, side-facing or 360-degree vehicle detection sensors are required in order to detect oncoming vehicles in a timely manner [92, 158]. Second, at signalized intersections, both of these crash

modes involve one of the vehicles having violated the traffic signal, i.e., running a red light [116, 255]. Traffic light violators can largely be divided into (a) those attempting to “beat the yellow”, or cross through the intersection during the amber phase, or (b) those inadvertently crossing into an intersection on a red light. Third, at stop signs, these crashes mainly occur at two-way stop-controlled intersections [116]. Examining crashes in the NHTSA database reveals that 43% of SCP and 59% of LTAP/LD crashes occur at two-way stop-sign controlled intersection. For SCP crashes, driver at the stop sign typically (two-thirds of the time) stops prior to entering the intersection, but occasionally will travel through the intersection without stopping. A majority of these “travelling through” drivers ran failed to see the stop sign during the intersection approach. For LTAP/LD crashes, 95% of crashes involve a driver accelerating into the intersection after a complete or rolling stop. This driver accelerating from the stop sign is almost always (96% of the time) the left turning driver.

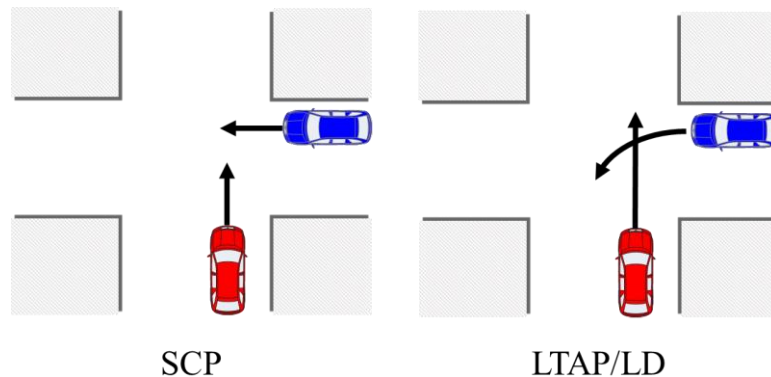


Figure 107. Scenarios being considered in the current benefits study.

There is a need to forecast the ability of I-ADAS technology to prevent and mitigate real-world intersection crashes. Using a benefits study, designers, evaluators, and regulators of this technology can quantify how effective the technology may be and identify design requirements

and limitations. The current study retrospectively simulated SCP and LTAP/LD intersection crashes as if one of the vehicles had been equipped with an I-ADAS. Additionally, a scenario where both vehicles was equipped was also considered. The objective of this study was to estimate the proportion of crashes and vehicles with seriously injured drivers that could be reduced if, for every CT intersection crash in the U.S., one of, or both of, the vehicles had been equipped with I-ADAS. Additionally, we analyzed the influence of I-ADAS design on system effectiveness. This included (1) examining both a system that either delivers a warning or autonomously brakes, (2) investigating the influence of computational latency time, and (3) investigating the influence of activation timing thresholds.

11.2 Methods

Overall Strategy

There were four main steps in this study. These four steps are depicted in Figure 108. First, a set of crashes were extracted from a U.S., nationally-representative database. Second, each crash was reconstructed from the intersection approach through impact using information collected by the crash investigator. These first two steps were completed in prior task reports, and are thoroughly summarized in Task 3.2. Third, each scenario was simulated as if one, or both, of the involved vehicles had been equipped with an I-ADAS. Fourth, the crash outcomes with and without I-ADAS were used to estimate the proportion of crashes and seriously injured drivers that could have potentially been prevented.

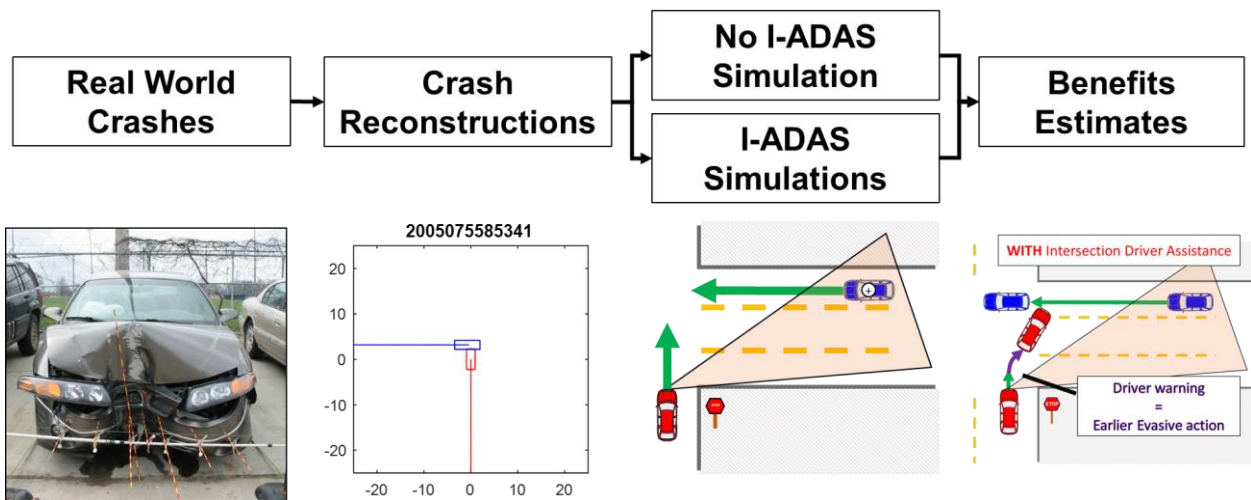


Figure 108. Outline of study methods.

Simulation Case Sets

The NMVCCS dataset developed in Chapter 7 was used in the current study. This simulation case set contains detailed crash reconstructions that accounts for the approach, traversal, evasive maneuvering, and impact speeds of vehicles involved in the crashes.

I-ADAS Simulations

An overview of the approach of the hypothetical I-ADAS modeled is shown in Figure 109. Onboard sensors were assumed to be continuously scanning for oncoming vehicles. At the instant the first vehicle entered the intersection, a clear line-of-sight was modeled between the vehicles. After the oncoming vehicle was first within sensor range, some computational time would be required for the sensor to detect the approaching vehicle. I-ADAS would then either autonomously brake or deliver a warning to the driver if the crash was deemed imminent (i.e., if the crash was estimated to occur within a pre-defined time window). For a system that delivers a warning, driver reaction would have occurred only after some perception-reaction time.

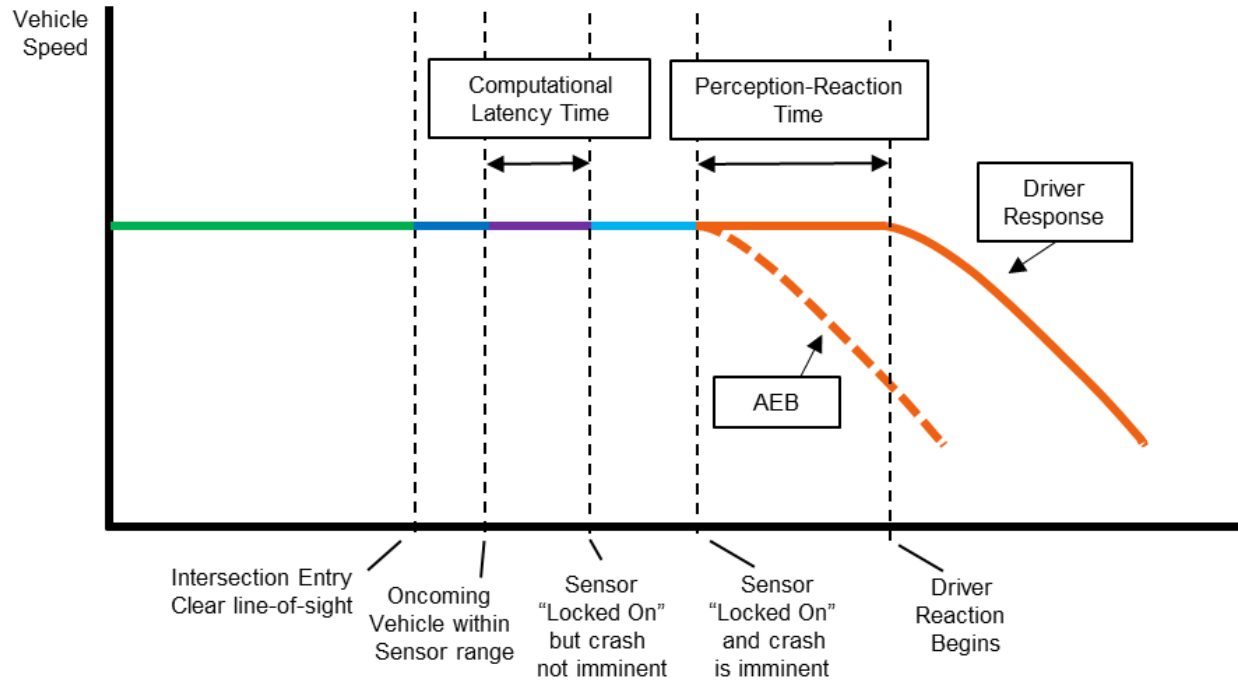


Figure 109. Overview of the approach for modeling I-ADAS in the current study.

A total of 30 variations of I-ADAS were considered in this study, which consisted of five separate time-to-collision (TTC) thresholds, three separate computational latencies, and two different I-ADAS response modalities (i.e., a warning or AEB). Every crash was simulated as if one, or both, of the vehicles had been equipped with an I-ADAS. To model I-ADAS, this study assumed the equipped vehicle had two frontal-side vehicle detection sensors. Each sensor was modeled as being oriented at 45-degrees away from the vehicle heading, having a maximum detection range of 120 m, and having a field of view +/- 60 degrees. These specifications correspond to the narrow beam, which was investigated in Chapter 10. These specifications are within the capacity of several commercially-available, vehicle-based radars, such as Delphi Corporation's Electronically Scanning Radar, Smartmicro's UMRR Automotive Radar Sensors,

and Eaton's VORAD® VS-400. Additionally, the analysis of these specifications indicated that 98% of oncoming vehicles could have been detected at the earliest detection opportunity.

At a given time point, a warning to the driver or autonomous braking was only assumed to occur (a) if the oncoming vehicle could have been detected by the onboard sensors, (b) if the TTC fell below a pre-defined threshold, and (c) after some computational latency time. The earliest vehicle detection opportunity was assumed to be at the time point when the first vehicle entered the intersection (e.g., crossed over the stop bar). Because sightline restrictions are expected to limit sensor detection capacity during the intersection approach, this assumption implies that a clear line-of-sight is only possible after one of the vehicles had crossed into the intersection.

There is some inherent computational latency time while I-ADAS is processing incoming sensor data. Latency time can depend on a variety of factors, such as the number of vehicles being detected by the sensor [249]. Three separate latency times were considered in this study: 0, 0.25, and 0.5 s delays.

A crash was deemed imminent if the TTC fell below a pre-defined threshold. TTC was calculated by assuming the I-ADAS equipped vehicle would maintain its current acceleration until the point of impact. The distance until the two vehicles would impact was calculated by extrapolating forward each vehicle's positions until they intersected. This calculation can be found in Equation 27. A depiction of the metrics required for calculating TTC can be seen in Figure 110. Like other active safety systems [23], the timing thresholds used for these system are automaker and model specific. Accordingly, five separate TTC values were evaluated in this study, including 1.0, 1.5, 2.0, 2.5, and 3.0 s thresholds.

Equation 27.
$$TTC = \frac{-v + \sqrt{v^2 - 2 \cdot d \cdot a}}{a}$$

Where,

TTC = time-to-collision,

a = acceleration of I-ADAS equipped vehicle traversing the intersection,

v = velocity of I-ADAS equipped vehicle traversing the intersection,

d = distance until the I-ADAS vehicle crosses the path of the oncoming vehicle.

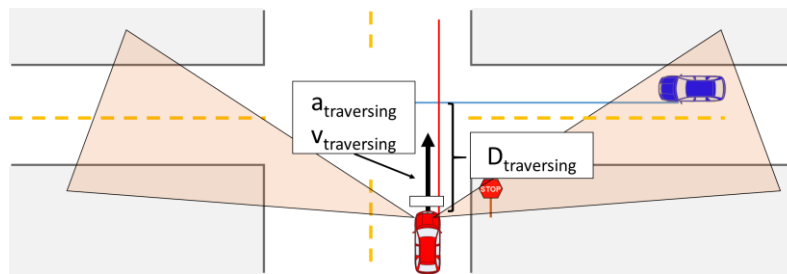


Figure 110. Depiction of how TTC can be estimated from the kinematics of the I-ADAS equipped vehicle.

Two types of I-ADAS were evaluated in this study: one that delivers a warning and a second that autonomously brakes. For the system that delivers a warning, the driver was assumed to take crash avoidance braking action after some perception-reaction time. A previous simulator study analyzing driver reaction times in response to a warning in cross-traffic intersection crash scenarios was used to determine an appropriate reaction time between warning delivery and driver response [129]. The raw data from this study, which were graciously provided by the Monash research group, can be visualized in Figure 111. As can be visualized, there is a relatively broad distribution of times for how long it would take a driver to respond to an I-ADAS warning. Accordingly, every reconstructed crash was simulated with three equally-probable reaction time values, 0.70, 0.99,

and 1.89 s, which represent the 17th, 50th, and 83rd percentiles of reaction times, accordingly. Autonomous braking was assumed to begin without the delay of reaction time.

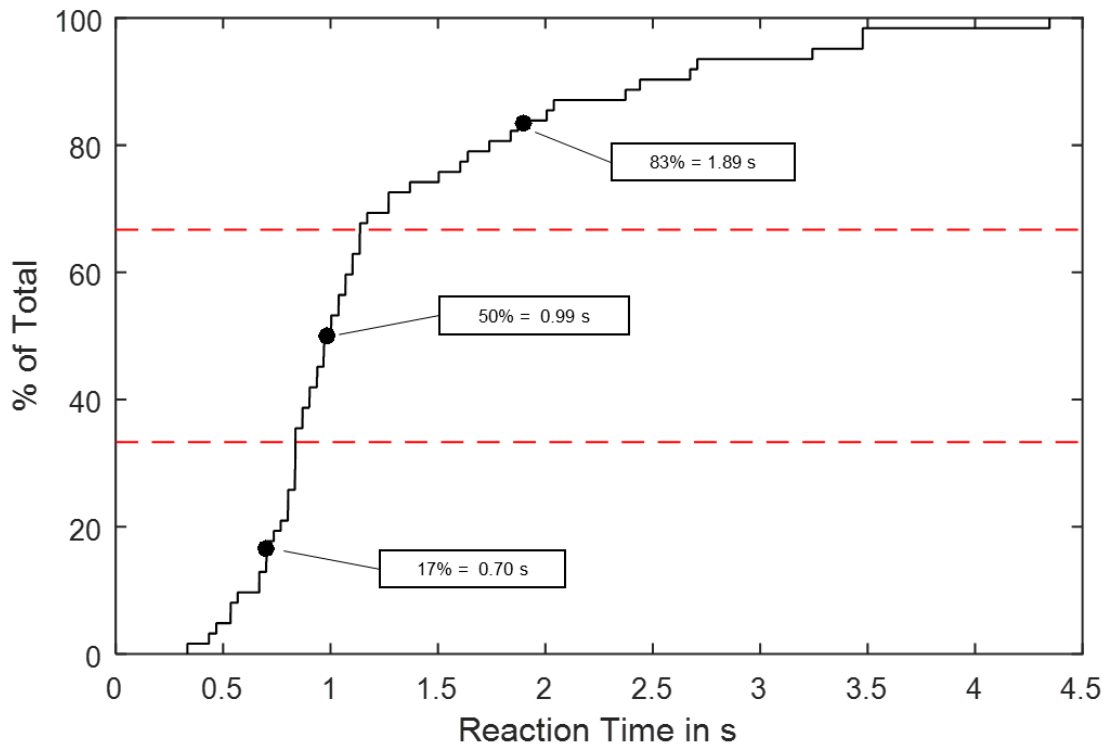


Figure 111. Reaction time values provided from the Monash group for cross-traffic crashes.

Drivers were assumed to brake with a jerk value of -11m/s^3 [215], whereas autonomous braking was modeled using a substantially higher value of -35m/s^3 [256]. Following the approach of the crash reconstructions, maximum evasive braking deceleration magnitudes were assumed to be dependent on the road surface conditions. In general, maximum vehicle deceleration capacity depends on a number of factors, including vehicle characteristics, surface conditions, vehicle speed, and surface type [216-218]. This study used maximum deceleration values of 0.3 g, 0.4 g, or 0.8 g based on whether the road conditions were icy, wet, or dry, respectively.

Injury Risk Modeling

A key objective of this study was to project the potential reduction of injuries with and without I-ADAS in a future fleet. Because NMVCCS was compiled from 2005-2007, the proportion of crashed vehicles equipped with side airbags was expected to be substantially lower in the current fleet. Likewise, not all NMVCCS vehicles were equipped with frontal airbags. Because the intent of this study was to project I-ADAS effectiveness in a future fleet, all vehicles were modeled in the study as though they were equipped with both frontal and side airbags.

Injury risk was modeled as a function of total delta-v and other covariates. In order to determine delta-v, impacts with and without I-ADAS were simulated using PC Crash simulation software [199, 210]. Simulations were performed by placing each vehicle in their respective impact position and orientation. Each vehicle was then assigned their respective impact speeds and the impact simulation was run. Total delta-v was computed for each impact from the total change in vehicle velocity over the first 300 ms of impact.

There are several methods for estimating injury risk through simulation. These strategies can be broken down into two broad categories: (1) detailed and (2) statistical. Finite element modeling is a common detailed modeling strategy for analyzing occupant injury risk [257-261]. Although this modeling strategy is useful for in-depth injury risk analyses, it is limited by (a) being time consuming and (b) requiring input information that is simply not available using NMVCCS. This study used statistical methods, specifically logistic regression modeling, to estimate injury risk from impact conditions, which is one of the most common methods for estimating injury likelihood [22, 39, 97, 262-273].

A total of 13,744 crashed (9,149 frontal, 2,366 near-side, and 2,229 far-side impacts) passenger vehicles were used to develop injury risk models. Case years 1998 to 2014 from the NASS/CDS database were used. This database is ideal because it not only includes detailed injury records, but it also includes relevant information about the occupants, vehicles, and crash severity [274]. Several criteria were required for a vehicle to be included in this analysis. First, the first crash must have involved two passenger vehicles. For example, crashes involving heavy trucks, motorcycles, or buses were excluded. Second, the first impact that the vehicle was involved in must have also been the most severe impact (highest delta-v) experienced by the vehicle, as indicated by the crash investigator (“accseq1” variable in NASS/CDS). This helps give assurance that the injuries sustained correspond to the first described impact. Third, the first impact must have been a frontal, left-side, or right-side impact. Third, vehicles were excluded if any of the following information was not coded: (a) injury severity, (b) driver age, (c) driver gender, (d) total delta-v, and (e) vehicle body type. Occasionally, this information is not available. Fourth, as has been previously done in the literature [97], cases with a national weighting factor greater than 5,000 crashes were excluded to limit skewing of the results. Fifth, the vehicle model year must have been 1998 or after. Airbags play an important role in reducing and preventing occupant injuries [71, 275]. The Federal Motor Vehicle Safety Standard 208 (FMVSS 208) was amended in 1998 to mandate that all newly manufactured vehicles be equipped with depowered airbags to prevent injuries to out-of-position occupants [276]. Sixth, the CDS database must have coded whether or not the vehicle was equipped with a side airbag (“restype” variable in NASS/CDS).

All logistic regression modeling for this study was performed using the “SURVEYLOGISTIC” procedure in the SAS 9.3 software package (SAS Institute, Cary, NC) [179]. Three injury risk models were created based on where the vehicle was impacted, including (1) a frontal, (2) a near-

side, and (3) a far-side model. Impact location plays an important role in injury risk [277-287]. The 1998 update of the Abbreviated Injury Scale (AIS) was used to determine injury severity [288]. A maximum AIS score of 3 or greater (MAIS3+) was assumed to represent a seriously injured driver.

Several predictor variables were used as independent variables for the model. First, total delta-v is a commonly used metric of impact severity [39, 97], and was used in this study. Total delta-v describes the total change in velocity experienced over the impact. Delta-v serves as a measure of impact severity, and inherently accounts for a variety of factors, such as vehicle mass, stiffness, and crash compatibility [289-293]. The total delta-v values presented in NASS/CDS are computed using the WinSMASH program which uses the vehicle's crush stiffness and crush damage in order to estimate the vehicles change in velocity. Second, belt use was also be used. Belt use is an important countermeasure for preventing occupant injuries [294-297]. Third, driver characteristics, including age [298, 299] and gender [300-302], are both important indicators of driver injury risk, and this study used both variables to predict injury risk. Two driver age groups were defined in this study, including (1) senior (age \geq 65 years old) and (2) non-senior (age < 65 year old). Fourth, for the near-side and far-side impact predictive models, whether the vehicle was equipped with some type of side airbag was included in the model.

The final form of the injury risk models can be found in Equation 28, Equation 29, Equation 30, and Equation 31 show the logits for the frontal, near-side, and far-side impact models, respectively.

Equation 28
$$p[MAIS3+] = \frac{1}{1 + e^{-\text{logit}}}$$

Equation 29
$$\text{logit}_{\text{frontal}} = \beta_0 + \beta_1 \cdot \Delta v + \beta_2 \cdot \text{belted} + \beta_3 \cdot \text{unknownbelt} + \beta_4 \cdot \text{senior} + \beta_5 \cdot \text{male}$$

Equation 30
$$\text{logit}_{\text{near}} = \beta_0 + \beta_1 \cdot \Delta v + \beta_2 \cdot \text{belted} + \beta_3 \cdot \text{unknownbelt} + \beta_4 \cdot \text{senior} + \beta_5 \cdot \text{male} + \beta_6 \cdot \text{sidebag}$$

Equation 31
$$\text{logit}_{\text{far}} = \beta_0 + \beta_1 \cdot \Delta v + \beta_2 \cdot \text{belted} + \beta_3 \cdot \text{unknownbelt} + \beta_4 \cdot \text{senior} + \beta_5 \cdot \text{male} + \beta_6 \cdot \text{sidebag}$$

Where,

- p[MAIS3+] = probability of a seriously injured driver (0-1)
- β_{0-5} = Model Parameters
- Δv = total change in velocity (kph),
- Belted = 1 if driver was known to be belted / 0 if not,
- Unknown belt = 1 if unknown whether driver was belted or unbelted / 0 if not,
- Senior = 1 if driver age \geq 65 y.o., 0 if driver age $<$ 65 y.o.,
- Male = 1 if driver gender is male, 0 if driver gender is female,
- Sidebag = 1 if equipped, 0 if not.

Table 49 shows the regression coefficients for the injury risk models shown in Equation 29, Equation 30, and Equation 31. In addition, a Wald-test was performed to test the hypothesis that all coefficients of a particular parameter are zero. Serious injury risk versus delta-v for frontal and side impacts can be found in Figure 112.

Table 49. Parameters for logistic regression function used to predict driver MAIS3+ injuries. A Wald-test was also performed for each of the predictor variables in order to show significant predictors. * was used to show statistical significance (p-value < 0.05). + was used to indicate a near-significant correlation (0.05 < p-value < 0.10)

Frontal Impact				
Variable	Parameter	Coefficient	χ^2	p-value
---	β_0 , Intercept	-5.916	---	---
Delta-v	β_1 , delta-v (kph)	0.116	200.27	<0.001*
Belt Use	β_2 , Belted	-1.044	22.77	<0.001*
	β_3 , Unknown Belt Use	0.479	1.20	0.273
Driver Age	β_4 , Age \geq 65 y.o.	0.810	13.49	<0.001*
Driver Gender	B_5 , Gender = male	-0.374	10.40	0.001*
Near-Side Impact				
Coefficient	Parameter	Coefficient	χ^2	p-value
---	β_0 , Intercept	-5.146	---	---
Delta-v	β_1 , delta-v (kph)	0.127	69.58	<0.001*
Belt Use	β_2 , Belted	-0.113	0.12	0.730
	β_3 , Unknown Belt Use	-0.898	3.55	0.060+
Driver Age	β_4 , Age \geq 65 y.o.	1.089	25.86	<0.001*
Driver Gender	B_5 , Gender = male	-0.318	3.50	0.061+
Side Bag	B_6 , Side bag equipped	-1.138	17.28	<0.001
Far-Side Impact				
---	β_0 , Intercept	-5.762	---	---
Delta-v	β_1 , delta-v (kph)	0.123	85.89	<0.001*
Belt Use	β_2 , Belted	-1.234	14.21	<0.001*
	β_3 , Unknown Belt Use	-0.203	0.17	0.685
Driver Age	β_4 , Age \geq 65 y.o.	0.859	5.25	0.022*
Driver Gender	B_5 , Gender = male	0.142	0.70	0.402
Side Bag	B_6 , Side bag equipped	-0.431	0.63	0.429

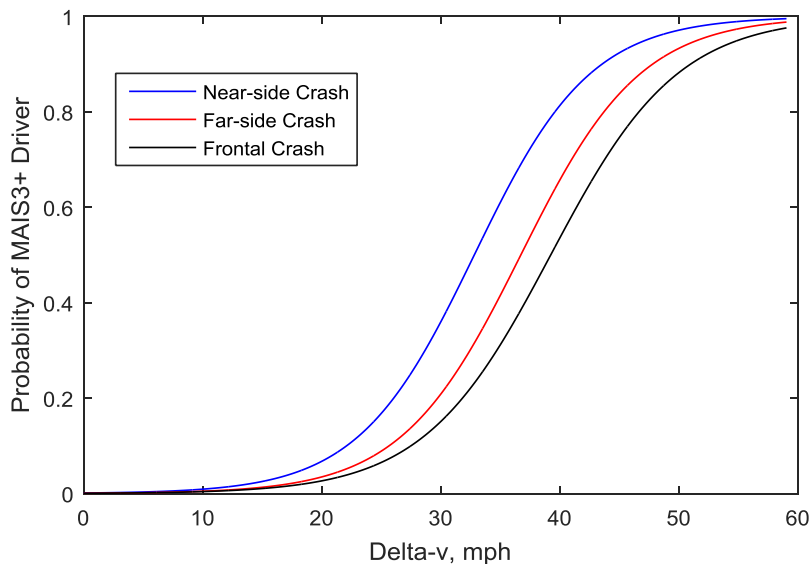


Figure 112. Example injury risk curves generated during the current study.

Benefits Estimates Calculation

As a first step for generating benefits estimates for a single I-ADAS variation, the number of crashes with I-ADAS was calculated. Equation 32 and Equation 33 shows how the number of crashes with and without I-ADAS were calculated. Cases were simulated multiple times and weighted based on likelihood of occurring in order to (a) account for uncertainty in evasive braking action, (b) account for uncertainty in driver perception-reaction time, and (c) consider a scenario where either of the vehicles was equipped with I-ADAS.

Equation 32.
$$N_{crashes\ w/\ IADAS} = \sum_{i=1}^{\#Cases} \sum_{j=1}^{\#Sim} crashed_{i,j} \cdot \frac{w_i}{\#Sim}$$

Equation 33.
$$N_{crashes\ w/o\ IADAS} = \sum_{i=1}^{\#Cases} \sum_{j=1}^{\#Sim} \frac{w_i}{\#Sim}$$

Where,

- $N_{crashes\ w/o\ I-ADAS}$ = Number of weighted crashes in simulation case set,
- $N_{crashes\ w/\ I-ADAS}$ = Number of crashes estimated to have occurred with I-ADAS,
- $Crashed_{i,j}$ = binary value denoting outcome of I-ADAS simulation (1 = crash, 0 = no crash)
- $\# Cases$ = Total number of cases in simulation case set,
- $\# Sim$ = Total number of simulations performed for case i,
- w_i = Case weight for case i.

As a second step, the total number of seriously injured drivers with and without I-ADAS were calculated. Equation 34 and Equation 35 show the computation required to estimate the number of seriously injured drivers with and without I-ADAS, respectively. It is important to note that either vehicle could have had a seriously injured driver. In theory, the total number of seriously injured drivers is two times that of the total number of crashes.

Equation 34.
$$N_{MAIS3+\ w/\ IADAS} = \sum_{i=1}^{\#Cases} \sum_{j=1}^{\#Sim} (p[MAIS3+,ROW]_{i,j,w/IADAS} + p[MAIS3+,Violate]_{i,j,w/IADAS}) \cdot \frac{w_i}{\#Sim}$$

Equation 35

$$N_{MAIS3+ w/o IADAS} = \sum_{i=1}^{\#Cases} \sum_{j=1}^{\#Sim} (p[MAIS3+,ROW]_{i,j,w/o IADAS} + p[MAIS3+,Violate]_{i,j,w/o IADAS}) \cdot \frac{w_i}{\#Sim}$$

Where,

- $N_{MAIS3+ w/ I-ADAS}$ = Number of seriously injured drivers with I-ADAS,
- $N_{MAIS3+ w/o I-ADAS}$ = Number of seriously injured drivers without I-ADAS,
- $p[MAIS3+]_{i,j}$ = probability of a seriously injured driver for case i and simulation j (0-1),
- # Cases = Total number of cases in simulation case set,
- # Sim = Total number of simulations performed for Case i,
- ROW = Right of way vehicle,
- Violate = violating vehicle,
- w_i = Case weight for case i.

As a final step, the effectiveness of the system can be calculated. The computation is the same for the crash and safety benefits, and is shown in Equation 36.

Equation 36.

$$\varepsilon = 1 - \frac{N_{w/IADAS}}{N_{w/o IADAS}}$$

Where,

- ε = Proportion of crashes/MAIS3+ that could be prevented by I-ADAS,
- $N_{w/I-ADAS}$ = Number of crashes/MAIS3+ drivers with I-ADAS,
- $N_{w/o I-ADAS}$ = Number of crashes/MAIS3+ drivers without I-ADAS.

11.3 *Results and Discussion*

A total of 1,531 (1,139 SCP and 392 LTAP/LD) crash reconstruction simulations were run in this study. These simulations were based generated using 448 SCP crashes and 213 LTAP/LD from the NMVCCS database. These crashes were representative of 254,877 U.S. crashes.

Summary of Benefits Estimates if One Vehicle Was Equipped

Potential crash prevention estimates for all 30 variants of I-ADAS that were evaluated in this study can be found in Figure 113. The model predicted that 30-64% of CT crashes are potentially preventable by an I-ADAS that autonomously brakes via an AEB system. Conversely, for an I-ADAS that delivers an alert to the driver, the potential crash prevention effectiveness drops to merely 0-27% of CT crashes. For crashes that were found to be unavoidable but where the driver/AEB was able to begin evasive braking earlier, modified impact conditions were observed. The proportion of modified impacts depended on the design of the I-ADAS and was as high as 44% of all CT crashes.

Even if a crash cannot be successfully avoided, by reducing impact speeds there is the potential for injury mitigation/prevention. Figure 114 shows the proportion of vehicles with seriously injured drivers that could be potentially prevented if one of the involved vehicles had been equipped with an I-ADAS. The model predicts that up to 79% of vehicles with a seriously injured driver are potentially preventable with an I-ADAS that uses AEB. For an I-ADAS that uses a warning to the driver, up to only 33% of seriously injured drivers were estimated to be potentially preventable.

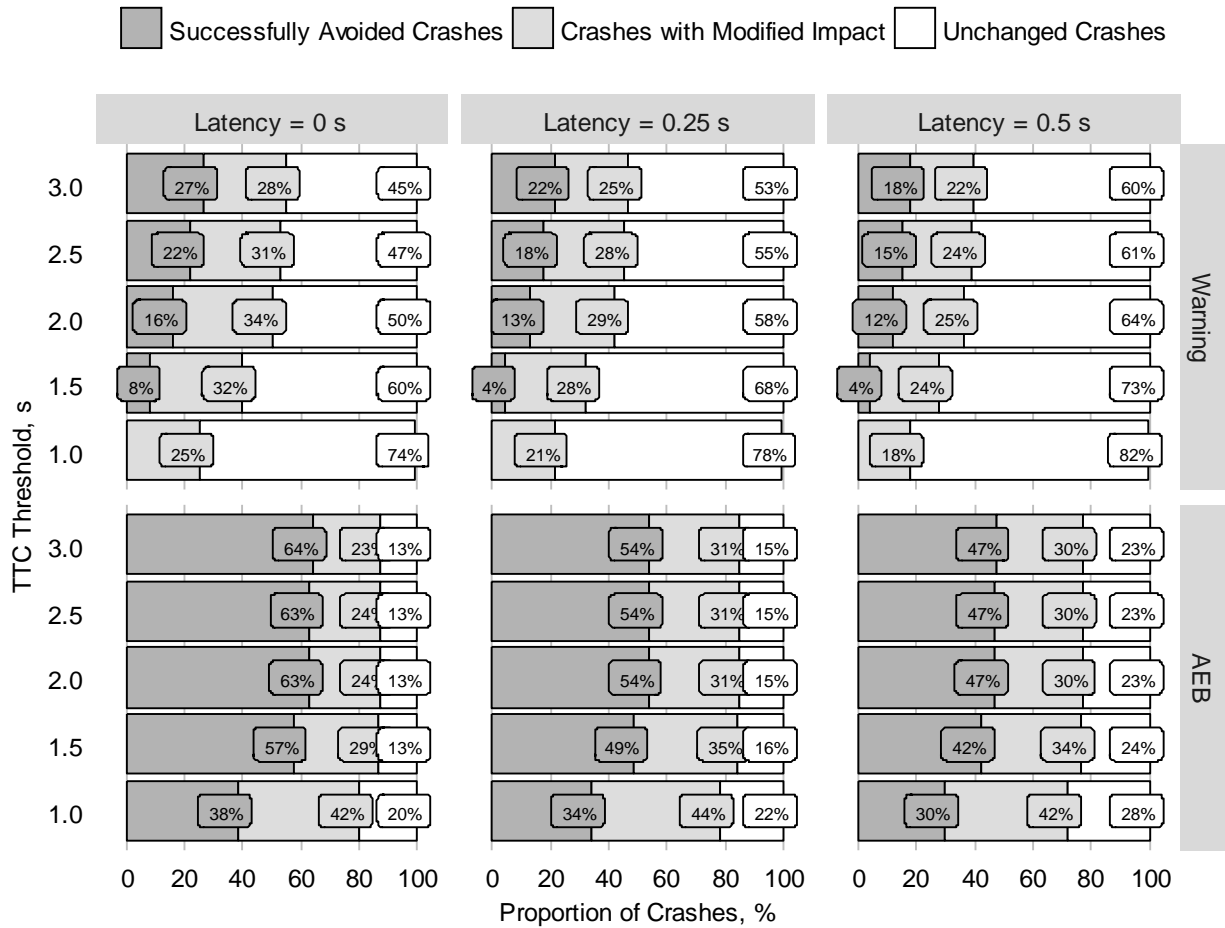


Figure 113. Proportion of CT crashes within the simulation case set that (a) were avoided, (b) had modified impact conditions, or (c) had unchanged impact conditions. All 30 variations of I-ADAS considered in this study are shown.

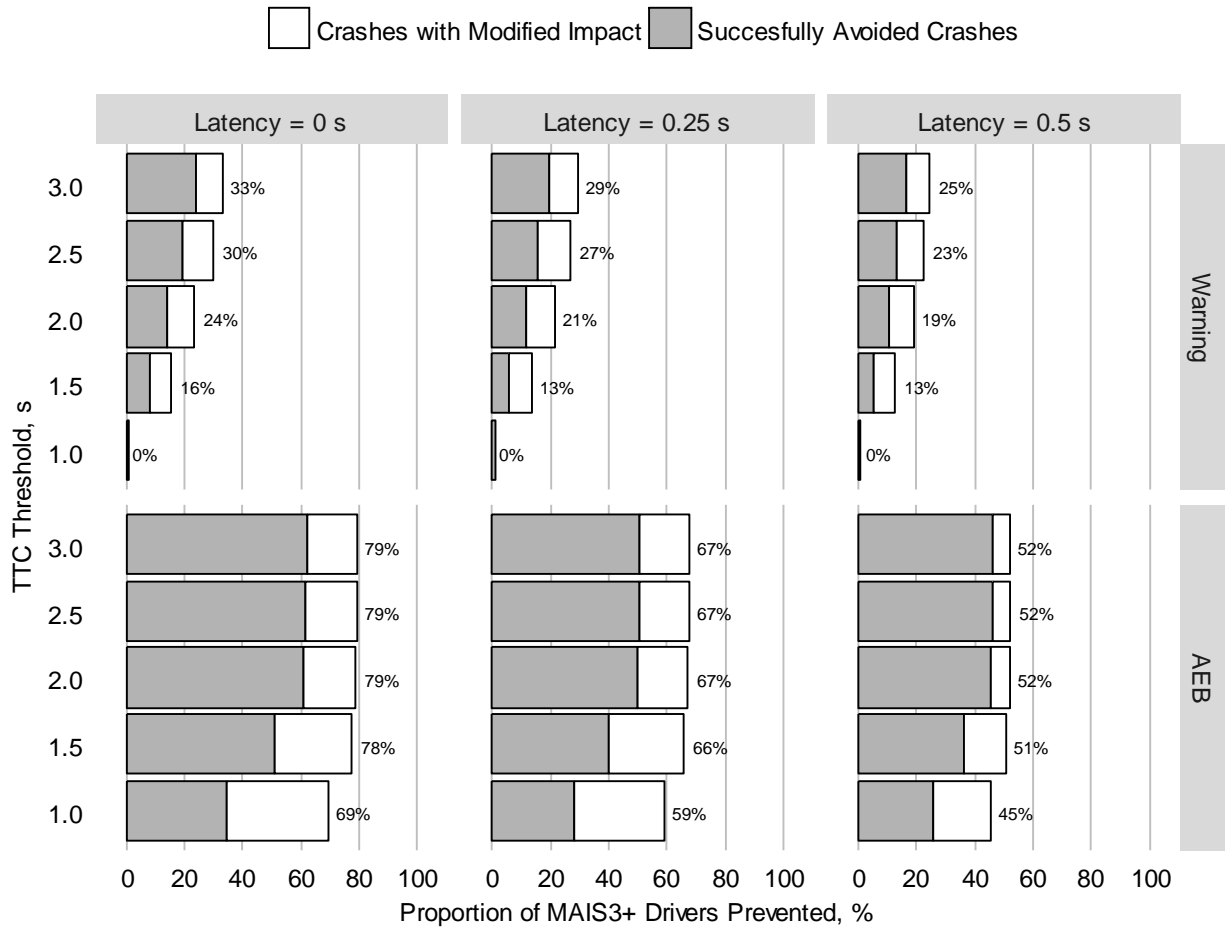


Figure 114. The proportion of seriously injured drivers potentially preventable if an I-ADAS had been equipped on one of the vehicles. All CT crashes are shown. The contribution of completely avoided crashes and crashes with modified impact conditions are shown.

There are several important findings that can be observed from this analysis. First, any computational latency time from initial sensor detection to I-ADAS warning/AEB will limit system effectiveness [249]. The results suggest that increasing computational latency time from 0 to 0.5 s would result in the system being substantially less effective. Without any latency, up to 27% of crashes were potentially preventable by an I-ADAS that uses a warning, and 64% of crashes were potentially preventable if AEB was used. If latency time was 0.5 s, the maximum

proportion of crashes potentially preventable dropped to 18% with a warning-based system and 47% with a system that used AEB.

Second, the TTC-threshold for determining when to deliver a warning or begin automated evasive action may influence the potential effectiveness of I-ADAS. For an I-ADAS that delivers an alert, crash/injury prevention effectiveness steadily increased from a TTC-threshold of 1.0 s (no crashes or injuries prevented) to 3.0 s (18-27% of crashes, 25-33% of MAIS3+ drivers). For an I-ADAS that autonomously brakes, a substantial increase in the proportion of crashes/injuries that could be prevented was observed from 1.0 s (30-38% of crashes, 45-69% of MAIS3+ drivers) to 1.5 s (42-57% of crashes, 51-78% of MAIS3+ drivers). Beyond 1.5 s, the predicted effectiveness estimates largely plateaued. This leveling-off time point for AEB is notable, and can be interpreted as the amount of time required to ensure that a potentially avoidable crash is, in fact, avoided. The remaining crashes beyond this time point represent those with too short of an available time window for crash avoidance (i.e., elapsed time from earliest detection until impact).

The effect of TTC-threshold is important to consider given the need for I-ADAS to give both a “timely” response and ensure driver acceptance of the technology. A sufficiently early I-ADAS response is essential for ensuring that crash prevention/injury mitigation is possible. Responses too late run the risk of limiting system effectiveness, while responses too early could lead to a higher proportion of false-alarms, driver annoyance, less reactive drivers, and/or drivers turning off the systems altogether [138-141, 181, 303].

It is also important to consider these TTC values in the context of currently available ADAS technologies. Frontal crash avoidance systems (primarily intended for rear-end impacts), in general, deliver warnings at TTC-values of around 2-3 s [23]. For vehicles equipped with AEB,

automated braking begins shortly after in the event that sufficient crash avoidance action has not been taken [82-84, 239, 304]. It is likely unrealistic for implemented I-ADAS technology to initiate AEB at such high deceleration rates earlier than 2-s prior to a potential impact, especially given anticipated false-positive activations. The results from this study suggest that it may be appropriate for I-ADAS to first deliver a warning, and if necessary, apply emergency braking to help avoid a potential collision. Specifically, the model results suggest that, if the driver fails to adequately respond by 1.5 s prior to the crash, AEB activation would ensure near-maximum potential benefits.

Third, we were interested in comparing effectiveness estimates for an I-ADAS that utilizes an alert to the driver with an I-ADAS that autonomously brakes via AEB. The advantages of an AEB system are that it has the capacity to (a) respond sooner than a driver and (b) ramp up vehicle acceleration at a higher rate (i.e., higher jerk) [215, 256]. In general, the results of this study suggest that I-ADAS will be 2-3 times more effective if an autonomous braking system is utilized over a warning-based system.

Effect of Crash Mode

SCP and LTAP/LD crash modes are examined in this study. As demonstrated in Chapter 10, differences in pre-crash kinematics behaviors between the two crash modes influence the available time for I-ADAS sensor detection and activation. Specifically, LTAP/LD crashes tend to have greater elapsed time from the earliest detection opportunity to impact. The LTAP/LD crash mode most often (~93% of the time) involves at least one of the vehicles having accelerated into the intersection from a stop. Whereas, in SCP crashes, at least one vehicle stops in only ~56% of crashes. Additionally, as demonstrated in Task 2.2 and Task 2.4.2, drivers turning left at intersections tend to travel at slower speeds and accelerate at lower rates.

These differences in pre-crash kinematics translated to higher predicted benefits for vehicles involved in LTAP/LD crashes. To illustrate these differences, Figure 115 shows the proportion of crashes potentially prevented by intersection crash modes. Results are only shown for an I-ADAS without any latency time, but the trends were similar across all latency times. For SCP crashes, up to 23% of crashes were potentially preventable if an I-ADAS that warns the driver was used, and up to 59% of crashes were potentially preventable for an AEB-based I-ADAS. Conversely, in LTAP/LD crashes, the maximum potential crash benefits were 32% and 71% for the warning-based and AEB-based I-ADAS, respectively.

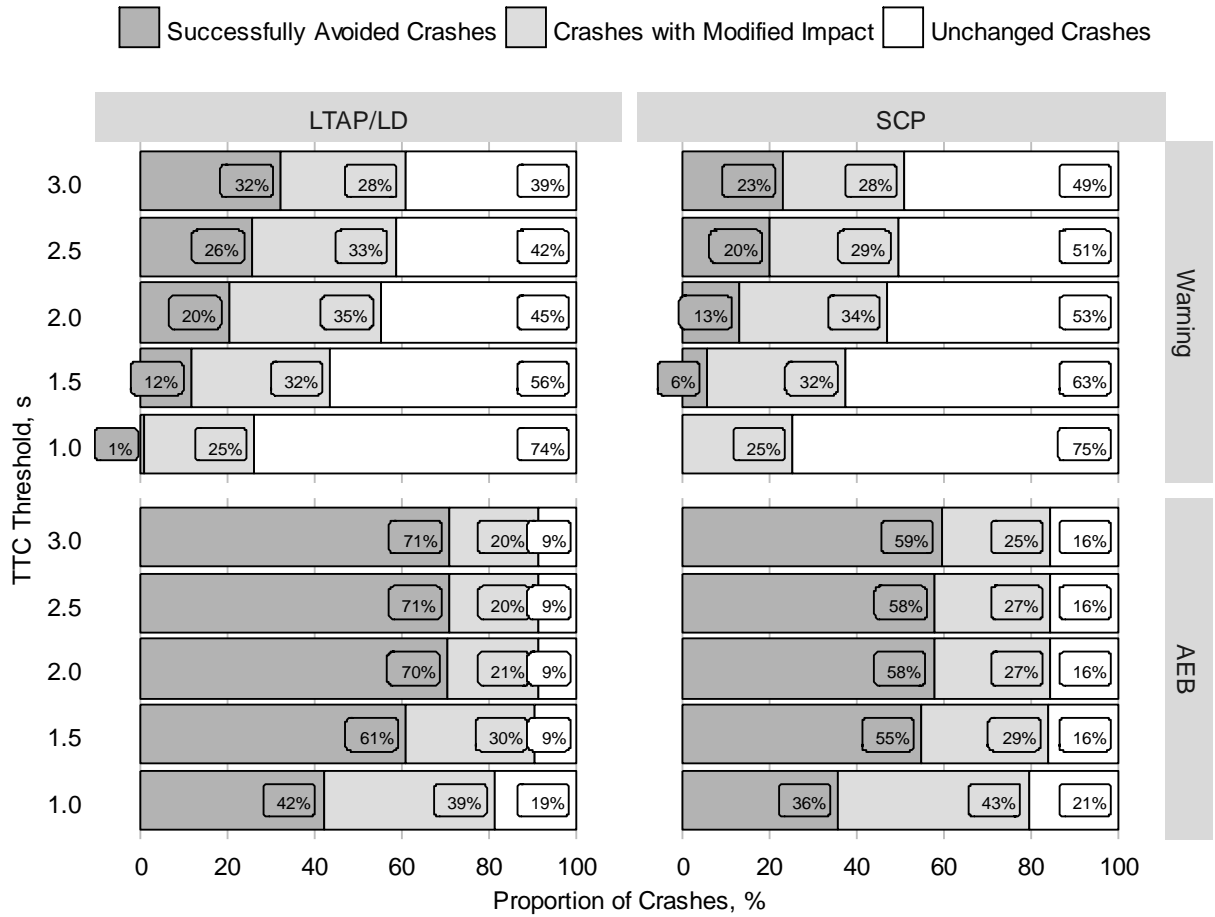


Figure 115. The proportion of crashes potentially preventable for an I-ADAS with no latency time. Results are shown by intersection crash mode.

Effect of Stopping Behavior

Pre-crash stopping behavior was found to be an important governing factor influencing the effectiveness of I-ADAS. For drivers that slow or stop prior to accelerating into the intersection, I-ADAS is afforded additional time to detect and respond to an imminent crash. Figure 116 shows the proportion of crashes potentially preventable by whether at least one of the involved drivers slowed or stopped prior to entering the intersection. For crashes where at least one vehicle stopped, the maximum computed potential benefits was 34% for a warning-based I-ADAS and 73% for an I-ADAS that utilized AEB. For crashes where neither vehicle stopped, the maximum potential benefits dropped dramatically to 9% of crashes if a warning-based I-ADAS was used and 43% for an I-ADAS with AEB.

For a warning-based I-ADAS, the model predicted that the system has the potential to be over three times more effective in scenarios where one of the involved vehicles stopped. Given no computational latency and the most conservative TTC-threshold (i.e., earliest TTC time of 3.0 s), only one out of every ten crashes was estimated to be potentially preventable for crashes where neither vehicle stopped. Conversely, as many as 43% of crashes in which one vehicle stopped were potentially preventable if AEB was utilized. These results suggest that, if I-ADAS for CT crashes is introduced with a warning-based technology, these systems would have substantially greater success in crashes where at least one of the vehicles stopped are targeted.

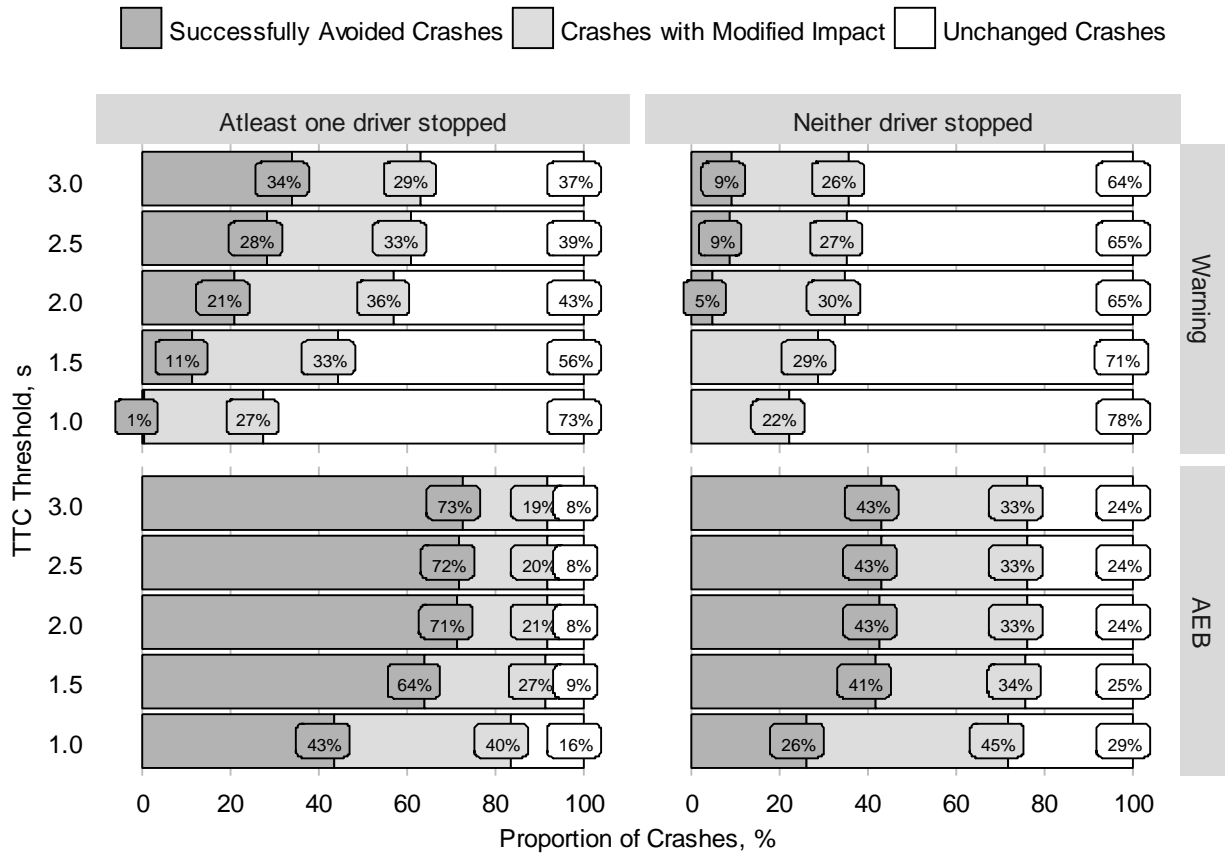


Figure 116. The proportion of crashes potentially preventable by whether one of the vehicles stopped or slowed prior to entering the intersection. Results are presented only for a system without computational latency time.

Effect of Reaction Time

This study took the approach of modeling three equally probably reaction times. Each simulation was then weighted as equally probable. This approach was used for each of the previous sections.

We were also interested in investigating how reaction time would influence the effectiveness of I-ADAS. We considered the three reaction times investigated in this study, which represent the 17th, 50th, 83rd percentiles. Figure 117 shows the proportion of crashes potentially preventable by driver reaction time. Only the system without any computational latency time was considered. For comparison, the AEB-based system is shown for comparison.

The slowest reacting 1/3 of driver (reaction time of 1.89 s) were found to have the potential to successfully avoid 12% of all CT crashes. For the fastest reacting drivers (0.70 s), I-ADAS was estimated to be approximately three times more effective (38% of CT crashes). However, even the fastest reacting drivers were still only around one-half as effective as an I-ADAS that utilized AEB.

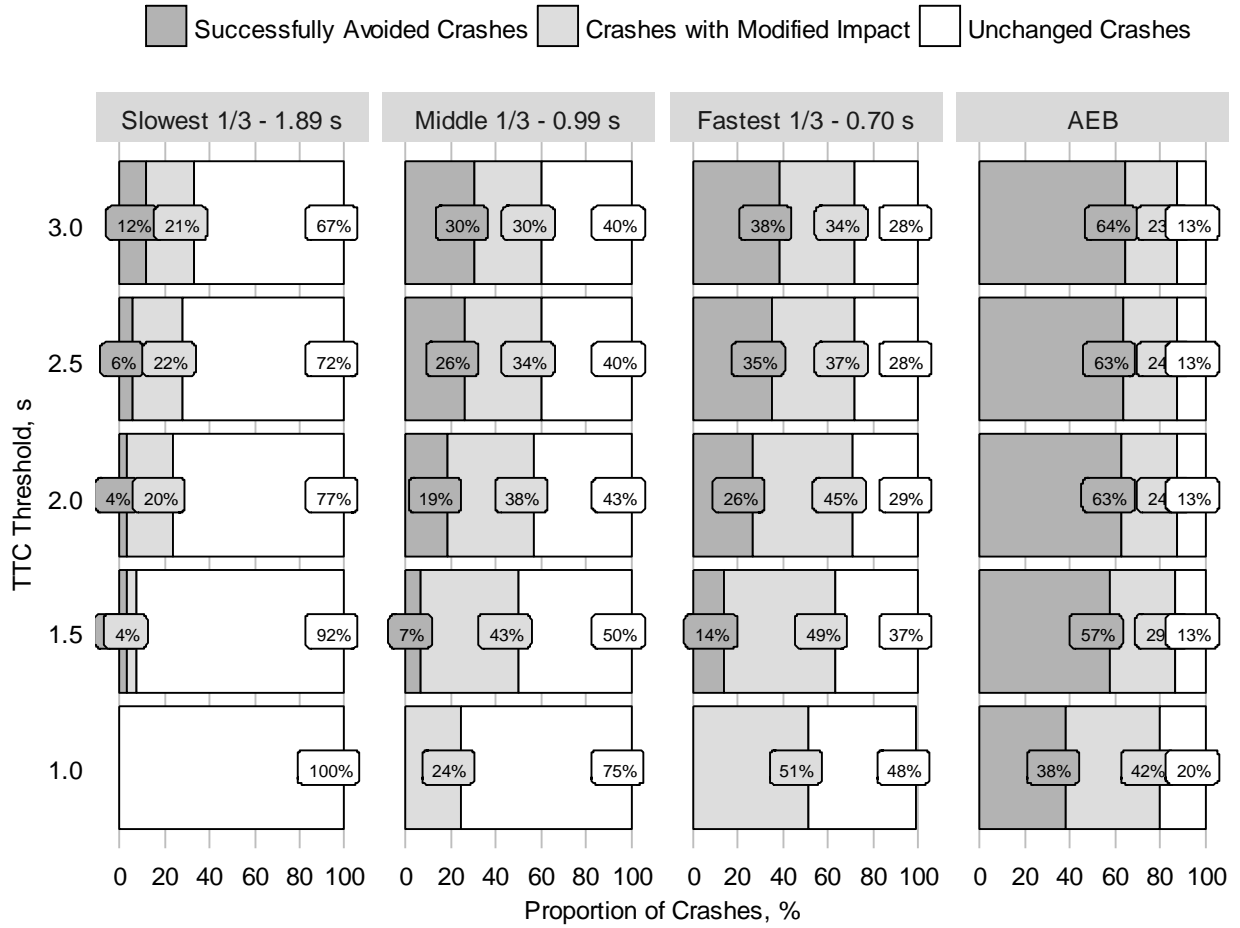


Figure 117. The proportion of crashes potentially preventable by driver reaction time or being AEB-equipped. Results are presented only for a system without computational latency time.

Potential Disbenefits of I-ADAS

For crashes with modified impact conditions, it is important to consider whether activation of I-ADAS may result in disbenefits in some crashes. The model indicates that the driver was able to respond to the I-ADAS alert, but was unsuccessful in avoiding the crash, for 18-44% of crashes. An analysis of potential disbenefits was performed on this dataset of crashes with modified impact conditions. Disbenefits were assumed to have occurred if there was an increase in the combined risk (sum of probability) of MAIS3+ injury for the drivers involved in the crash.

To illustrate a scenario where I-ADAS could have a disbenefit for the **I-ADAS-equipped** driver consider the crash depicted in Figure 118. The red vehicle was originally struck in the far-side rear quarter panel. After having been equipped with I-ADAS, the system autonomously brakes at the earliest detection opportunity. Although the red vehicle had a lower impact speed, the principle direction of force (PDOF) of the impact is now directed more toward the red vehicle's C.G., which causes the red vehicle to experience a higher delta-v. Using the models developed in this study, an increase in delta-v translates to an increased risk of serious injury.

To illustrate a scenario where I-ADAS could have a disbenefit for the **non-I-ADAS-equipped** driver consider the crash depicted in Figure 119. This time the red vehicle was originally struck in the far-side front quarter panel. After having been equipped with I-ADAS, the system autonomously brakes at the earliest detection opportunity. The red vehicle is able to slow down the vehicle, which leads to the non-equipped vehicle passing in front of the red vehicle. The non-equipped vehicle is then side impacted in the near-side, front quarter panel. Despite the 5-kph decrease in impact speed, the models developed in this study estimate a slightly higher injury risk, because the vehicle was now involved impacted in the near-side.

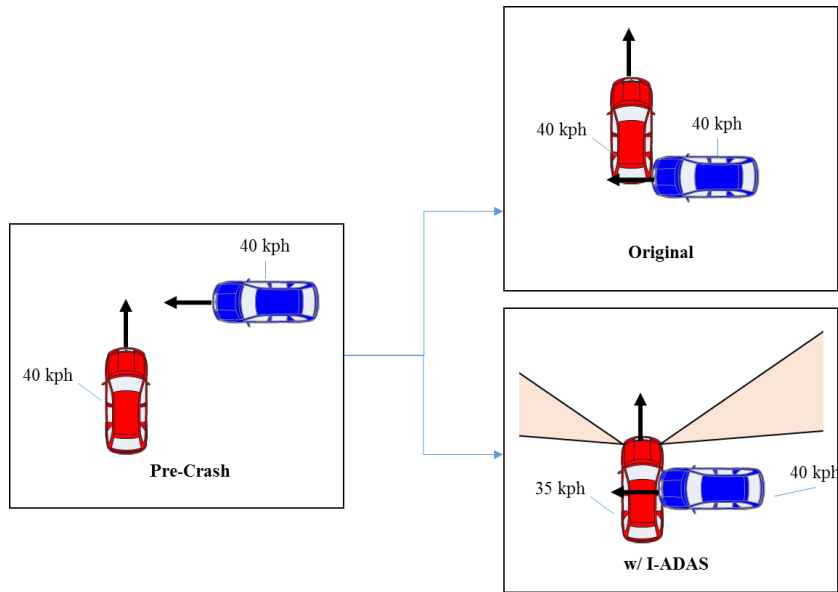


Figure 118. Example of a case where disbenefits could potentially result for the I-ADAS-equipped driver. Here, the I-ADAS-equipped vehicle applies brakes and slows from 40 to 35 kph.

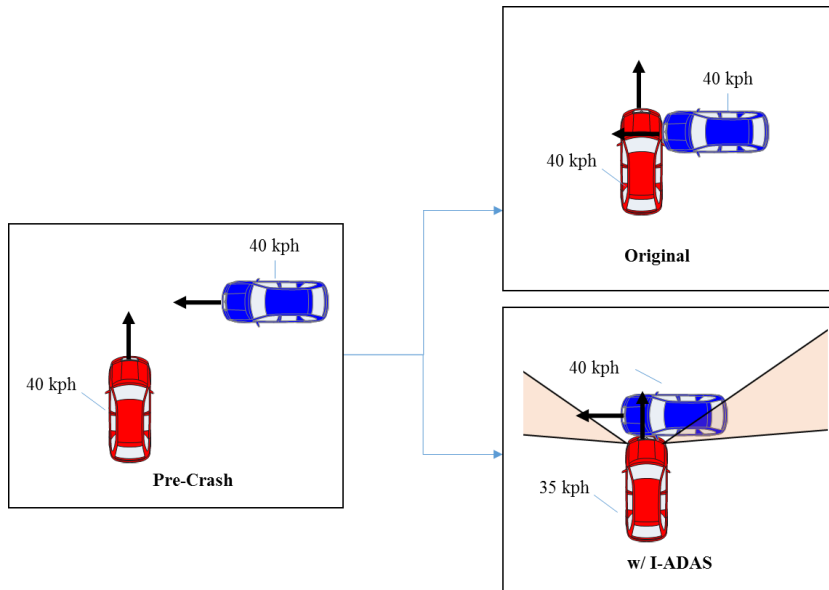


Figure 119. Example of a case where disbenefits could potentially result for the non-equipped driver. Here, the I-ADAS-equipped vehicle applies brakes and slows from 40 to 35 kph.

Figure 120 shows the proportion of crashes with potentially higher injury risk. Around 5 to 10% of CT crashes had potential disbenefits. This result can be interpreted as the proportion of CT crashes where I-ADAS could lead to a higher proportion of seriously injured drivers than in the original crash mode.

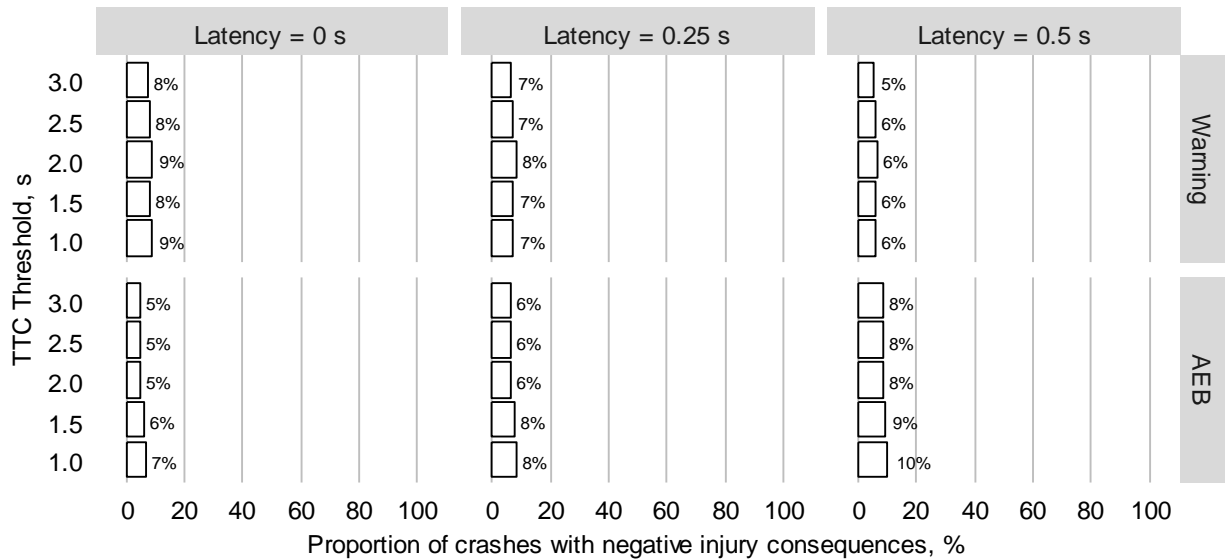


Figure 120. Proportion of all CT crashes with disbenefits in I-ADAS activation.

Figure 121 shows the proportion of crashes with modified impact conditions that had potential disbenefits. The results suggest that negative injury consequences could occur between 16 to 36% of the time for crashes where I-ADAS enables an earlier evasive reaction, but the crash cannot be successfully avoided.

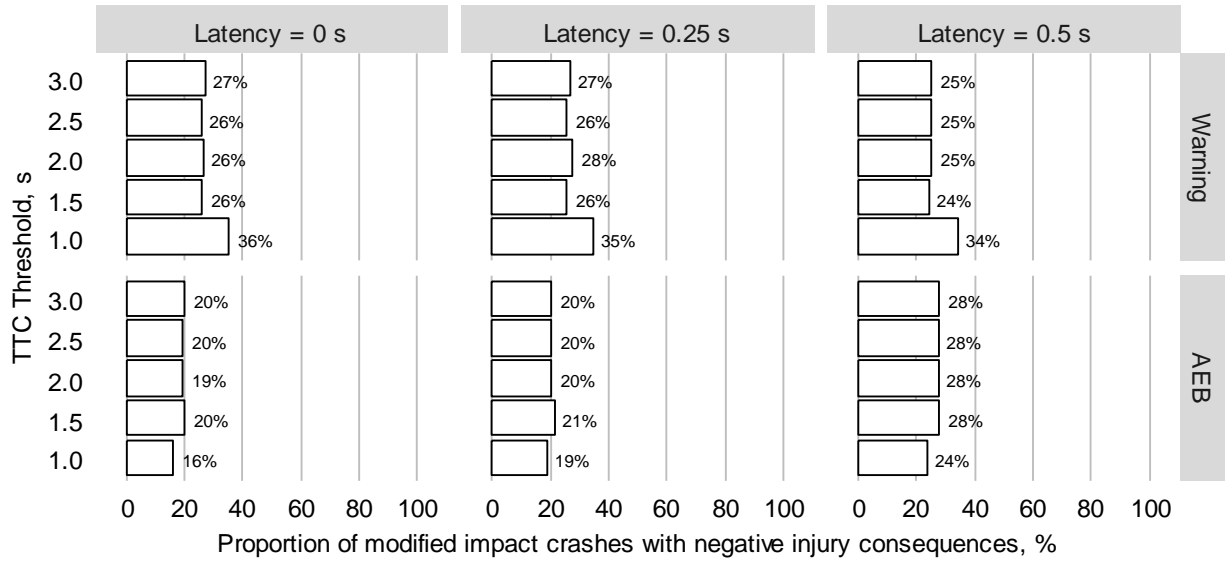


Figure 121. Proportion of CT crashes with modified impact conditions that resulted in MAIS3+ injury risk.

These proportions do not consider the severity of the increase in injury risk, only that there was some increase in MAIS3+ probability. The next question posed was: How does the number of added MAIS3+ injuries compare with the original number of MAIS3+ injuries? To address this, I compared the number of added MAIS3+ injuries to the total number of MAIS3+ injuries in the simulation case set, which can be seen in Figure 122. The results suggest that 2 to 10% of the total number of MAIS3+ drivers could potentially be added due to disbenefit.

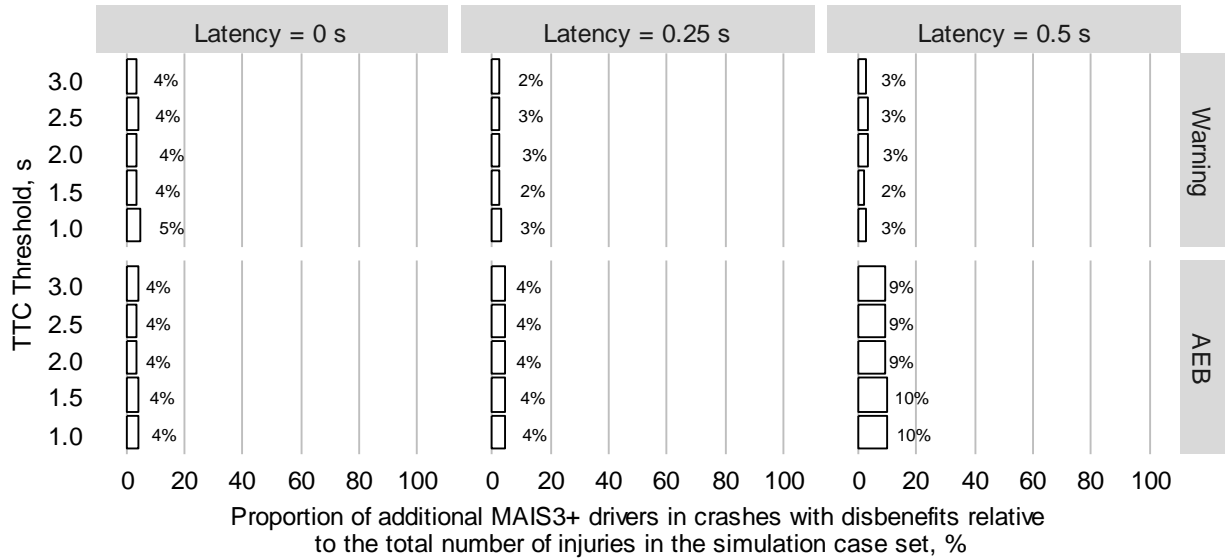


Figure 122. The proportion of added MAIS3+ injuries compared to original number of MAIS3+ injuries.

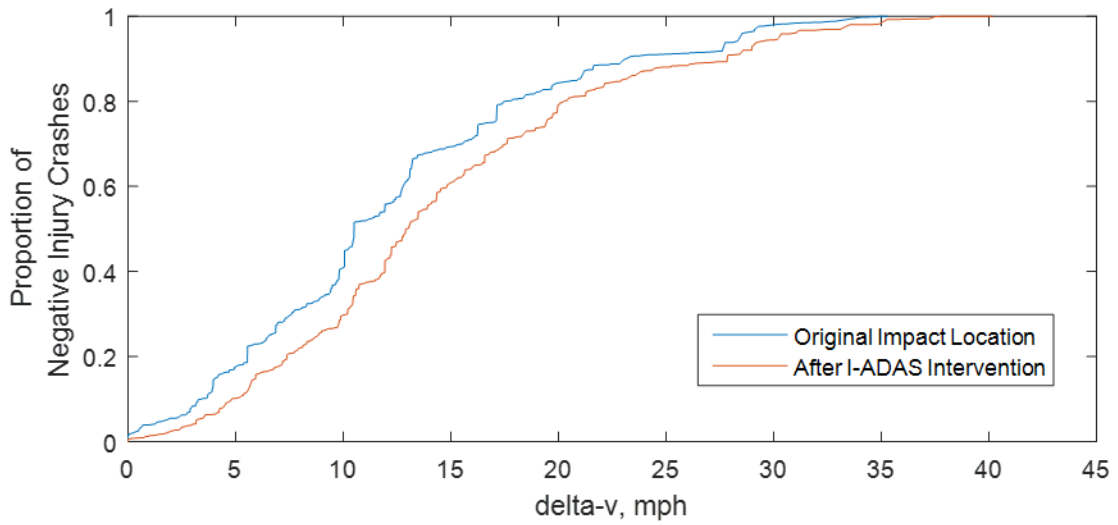
There are two mechanisms that can cause an increase in injury risk using the models developed for this study. One mechanism is changing the impact location (e.g., frontal to near-side). The second mechanism is causing a higher delta-v. To examine both of these effects, the results from two I-ADAS systems were considered:

- (1) latency = 0.25 s, warning-based, TTC-threshold = 2.5 s
- (2) latency = 0.25 s, AEB-based, TTC-threshold = 1.5 s

Figure 123 shows how impact location changed before and after an I-ADAS intervention only for cases where negative injury consequences were predicted to have occurred. One theory is that negative injury consequences will be a result of the impact location shifting from a frontal impact to a side impact. However, the results suggest that this mechanism is not particularly prevalent in crashes with negative injury consequences. For the warning-based I-ADAS, 2% of the crashed vehicles with negative injury consequence had impact locations that shifted from a frontal to a side

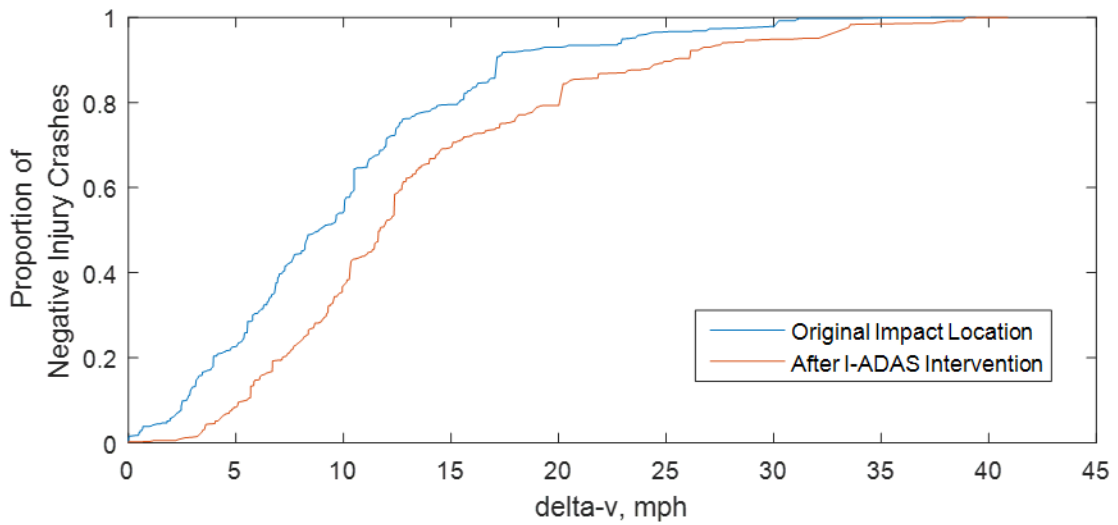
impacts. For the AEB-based I-ADAS, 6% of the crashed vehicles experienced this shift. The results suggest that vehicles which experienced negative injury consequences only had a slight increase in the number of side impact over frontal impacts. Although a side impact is known to have higher injury risk than a frontal crash, for a frontal impact to be changed to a side impact in an intersection crash scenario with I-ADAS, the driver has to apply substantial braking or steering to cause this shift in impact location. In the model used in this study, only emergency braking is applied in response to the I-ADAS activation. So for crashes which experienced a shift from a frontal impact to a side impact, the striking vehicle would have had a lower impact speed, and thus, a lower impact severity.

higher injury risk? To investigate this possibility, Figure 124 was created to examine delta-v before and after I-ADAS intervention for these crashes with negative injury consequences. In general, the distributions verify this theory. For the warning-based I-ADAS, the 50th percentile delta-v after I-ADAS intervention was 2.5 mph higher. For the AEB-based I-ADAS, the 50th percentile delta-v after I-ADAS intervention was 2.8 mph higher.



latency = 0.25 s, warning-based, TTC-threshold = 2.5 s

Crashes with negative injury consequences (8% of crash population)



latency = 0.25 s, AEB-based, TTC-threshold = 1.5 s

Crashes with negative injury consequences (6% of crash population)

Figure 124. Changes in delta-v before and after an I-ADAS intervention. Only crashes that were shown to have negative injury consequences were considered. Two hypothetical I-ADAS warning algorithms are depicted.

Limitations in Disbenefits Analysis

The disbenefits analysis in the current study is based on an I-ADAS algorithm that does not use any sort of path planning algorithm. More advanced algorithms may have the potential to suppress I-ADAS activation if the system detects a crash configuration with a potential disbenefit. Additionally, the modeled I-ADAS only assumes that the driver and autonomous evasive system will brake to avoid the crash. This may, of course, not always be the optimal course of action. For example, in the crash configuration depicted in Figure 118, activating I-ADAS led to the equipped-vehicle being side impacted in the occupant compartment. In this case, an algorithm that suppressed I-ADAS activation or enabled automated acceleration may have allowed the original crash to be avoided. Lastly, the injury risk models strictly use delta-v to compute risk. There is, of course, energy transferred to rotational motion, which could lead to an increase in injury risk.

Full Implementation: Equipping the Entire Vehicle Fleet

The benefits results thus far have focused on a scenario where only one of the involved vehicles had been equipped with I-ADAS. As this technology becomes more commonplace within the vehicle fleet, potential CT intersection crash scenarios involving two I-ADAS-equipped vehicles will become more common. Eventually, when this technology has been near-fully implemented in the vehicle fleet, virtually all CT intersection crash scenarios will occur between I-ADAS-equipped vehicles. This section focuses on this future fleet.

Figure 125 shows the model-predicted proportion of CT intersection crashes potentially preventable if I-ADAS were equipped on all vehicles throughout the vehicle fleet. Figure 126 shows the proportion of seriously injured drivers within these crashed vehicles that could have been potentially prevented. In this future fleet, up to 34% of crashes and 39% of vehicles with seriously injured drivers are potentially preventable if a warning-based I-ADAS is used. If an AEB-based I-ADAS is used, the results suggest that up to 70% of crashes could have been avoided, and 89% of vehicles with seriously injured drivers were potentially preventable.

These results were compared with the results from the analysis of equipping only one of the vehicles. In this analysis, the anticipated benefits were up to 27% of crashes and 33% of MAIS3+ drivers prevented if a warning was used. For an AEB-based benefits, the potential benefits were up to 64% of crashes and 79% of MAIS3+ drivers.

The potential effectiveness of I-ADAS was, of course, anticipated to be lower for crashes where only one of the vehicles was equipped. However, this increase in potential benefits when equipping both vehicles was relatively moderate. Additionally, a large proportion of crashes (30%) were still considered “unpreventable” even with the best performing I-ADAS (no latency, TTC =

3.0 s, AEB) being modeled on both vehicles. There were some notable attributes for the unavoidable crashes where both vehicles were equipped with this I-ADAS. First, only 50% of crashes were avoidable if neither of the vehicles performed a complete or rolling stop. Conversely, 79% of crashes were avoidable if one of the vehicles came to a stop. Second, a larger proportion SCP crashes at signalized intersections (74%) were avoided than crashes at stop sign-controlled intersections (56%). Similarly in LTAP/LD crashes, 89% of signalized crashes were avoidable, while only 71% of stop sign controlled intersection crashes were avoided.

From these findings, two primary factors can be deduced as limiting the effectiveness of I-ADAS technology in this full implementation fleet. Both of these factors lead to these crashes being unavoidable unless the violation can be stopped altogether. First, drivers that do not slow or stop prior to entering the intersection will end up traversing the intersection much more quickly. This limits the available time for I-ADAS to take crash avoidance action. Second, in the U.S., stop sign-controlled intersections tend to be smaller than signalized intersections. In fact, for 43% of the signalized crashes in the dataset, the first vehicle travelled into at least the third lane prior to being impacted. Conversely, at stop sign-controlled intersections, only 21% of these crashes involved the first vehicle to enter the intersection having travelled across more than two lanes. Shorter distances travelled into the intersection also translates to less available time following the earliest detection opportunity.

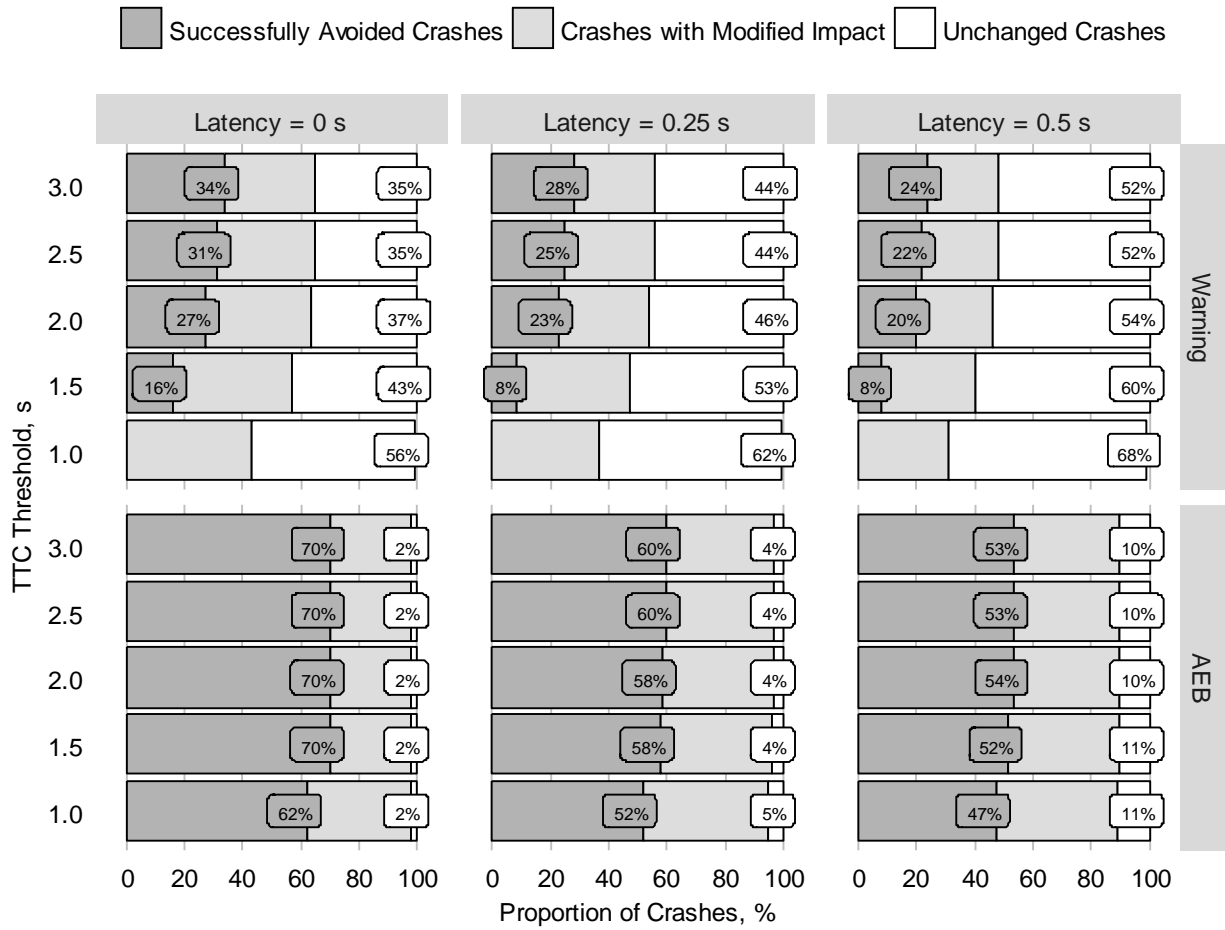


Figure 125. Potential proportion of CT intersection crashes potentially preventable if I-ADAS was equipped on all vehicles throughout the entire vehicle fleet.

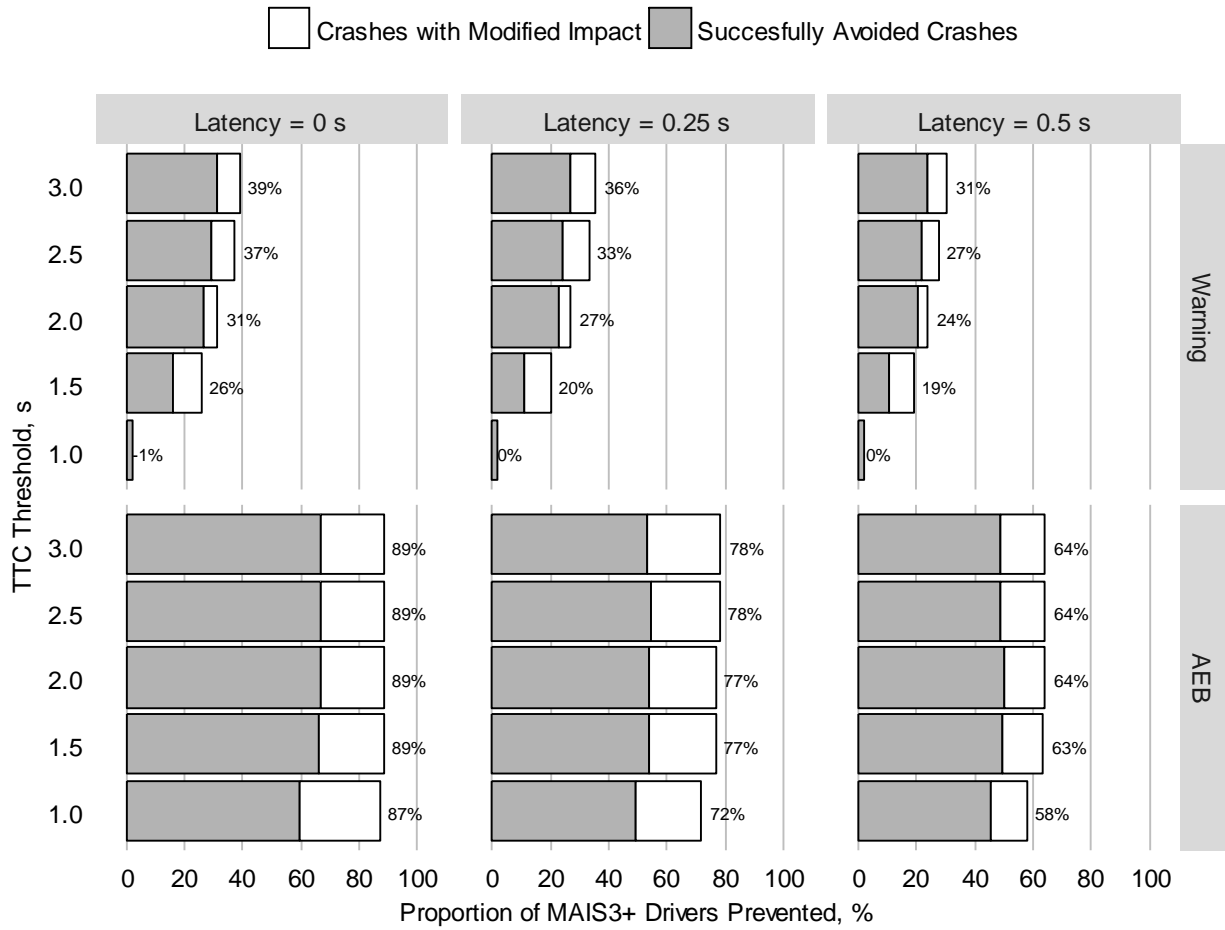


Figure 126. Proportion of potentially prevented vehicles with MAIS3+ drivers if I-ADAS was equipped on all vehicles throughout the entire vehicle fleet.

11.4 *Limitations*

This study has a number of limitations. First, variability in certain aspects of how drivers approach and traverse intersections was not considered in this study. Factors, such as acceleration rates, deceleration rates, and rolling stop speeds, will influence the available time for an I-ADAS to deliver a warning or begin autonomous braking. This study took the approach of using models taken from the 50th percentile of driver behavior. Other factors, such as evasive braking action and reaction time, were simulated under several possible scenarios, and weighted based on their likelihood of having occurred. Drivers were also assumed to apply maximum braking deceleration given enough time to fully press the brake pedal (i.e., dependent on assumed braking jerk value and initial reaction time). Not accounting for variability in driver behavior could limit the generalizability of the results to various driving “styles” (e.g., accounting for aggressive driving styles). Expansions to the current study should focus on examining and accounting for the variability that exists in how drivers navigate intersections and react to imminent collisions.

Second, our study makes several assumptions about obstructions. In general, sightline restrictions at intersections can be divided into two main categories: fixed and moving. This study’s assumptions handle the bulk of fixed obstructions. Our study assumes that sightlines are completely obstructed until the first vehicle enters the intersection. Vehicles in our model cannot see around corners. This assumption corresponds to vehicles operating in an “urban canyon”. But, this assumption would also subsume cases in which approaches to intersections were obstructed by trees, shrubs, and signs. There were a few cases where objects/trees in the median could lead to the effectiveness being overestimated in some cases. Likewise, in many crashes in more open environments, vehicles could have a clear sightline earlier than was modeled, which could lead to an underestimation of effectiveness. Moving obstructions, such as roadway traffic or parked

vehicles, were not accounted for in this study. By not accounting for these moving obstructions, effectiveness estimates are likely to be overestimated for some crashes.

Third, our study used a hypothetical I-ADAS algorithm. The exact specifications and algorithms developed by automakers are highly proprietary. In an effort to examine sensitivity to TTC-threshold and computational latency time, our study considered several potential algorithms. Although this approach allows for a general analysis of I-ADAS, examining algorithms actually utilized by designers would allow for a general comparison of design. Fourth, drivers and autonomous crash avoidance systems could use steering to avoid a crash, but this countermeasure was not considered in this study's simulations. Higher benefits estimates would be expected if this extra degree of freedom was considered in the model. It should be noted, however, that automated steering technology is still being developed, and is not currently implemented in existing I-ADAS technology. Fifth, in some cases, although the simulated first collision may have been avoided, there is always the potential for a separate vehicle to have been impacted. This assumption could lead to overestimates of system effectiveness in some crashes.

11.5 *Conclusions*

This study estimated crash and safety benefits for a set of 661 CT intersection crashes. These crashes were extracted from the NHTSA national crash database. This study reconstructed each of these crashes, and simulated them as if one of the involved vehicles had been equipped with I-ADAS. A scenario was also considered where both vehicles had been equipped (i.e., after full implementation in a future vehicle fleet) Thirty variations of I-ADAS were considered, including (a) 5 activation timing thresholds, (b) 3 computational latency times, and (c) either a warning-based or AEB-based system. Each of these components of I-ADAS were quantitatively assessed. The influence of crash mode (SCP vs. LTAP/LD) and stopping behavior were also investigated. Lastly, the effect of reaction time on potential effectiveness was discussed.

12. Conclusions

Intersection crashes are among the most frequent and lethal crash models in the United States. Intersection Advanced Driver Assistance Systems (I-ADAS) are emerging active safety systems which aim to help drivers safely navigate intersections. The primary function of I-ADAS will be to detect oncoming vehicles, and in the event of an imminent collision, either (a) alert the driver and/or (b) autonomously evade the crash. A potential secondary function of I-ADAS may be to detect and prevent imminent traffic signal violations (i.e. running a red light or stop sign) earlier in the intersection approach, while the driver still has time to yield for the traffic control device.

As shown in Figure 127, the three most common intersection crash modes in the U.S. were straight crossing path (SCP), left turn across path / opposite direction (LTAP/OD), and left turn across path / lateral direction (LTAP/LD), which together accounted for 73% of all intersection crashes and 93% of fatal intersection crashes [2]. I-ADAS is expected to have the greatest impact on reducing crashes, injuries, and fatalities if focused on these most common modes.

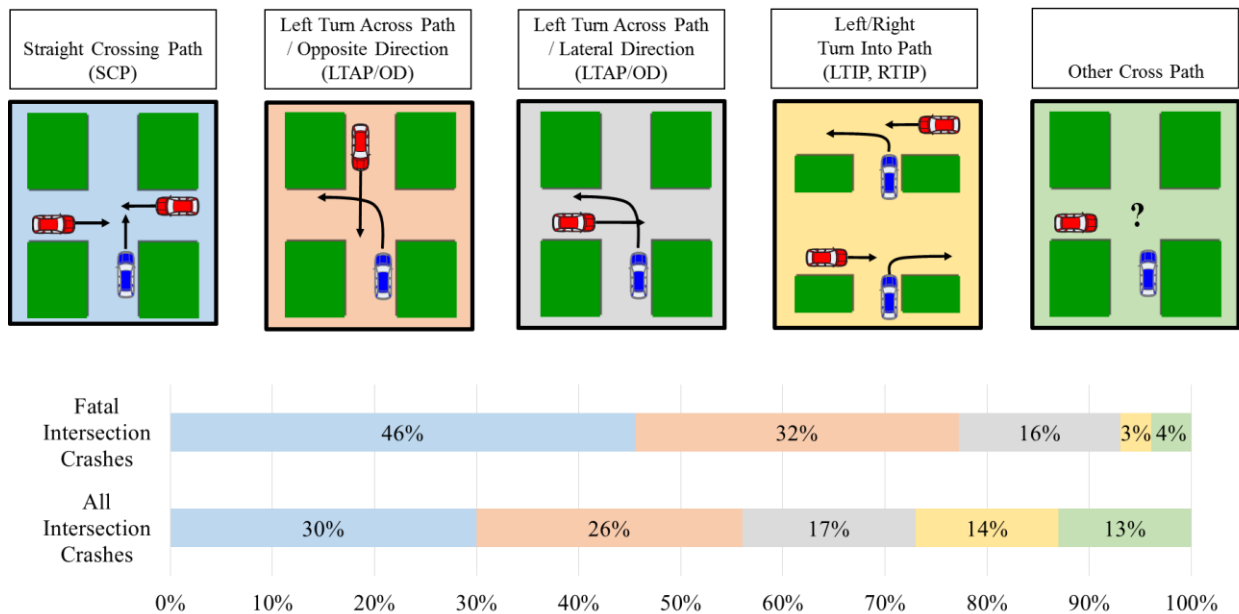


Figure 127. Tabulations of the most common intersection crash modes in the U.S. crash population. Tabulations are shown for all police-reported intersection crashes and all fatal intersection crashes.

Driver Behavior Models for Intersections

Developing models of driver behavior was a critical component of this work evaluating the effectiveness of I-ADAS. These models were particularly useful in the reconstruction of real-world crashes. As a part of this effort several data sources were examined, including data from the 100-Car Naturalistic Driving Study and pre-crash data from EDR downloads extracted from NASS/CDS crashed vehicles.

As shown in Figure 128, the kinematics of vehicles involved in SCP, LTAP/LD, and LTAP/OD intersection crashes can be divided into four main phases. Vehicle kinematics include the impact speed and crash kinematics, any evasive maneuvering prior to impact, within the intersection kinematics prior to any evasive maneuvering, and the intersection approach kinematics.

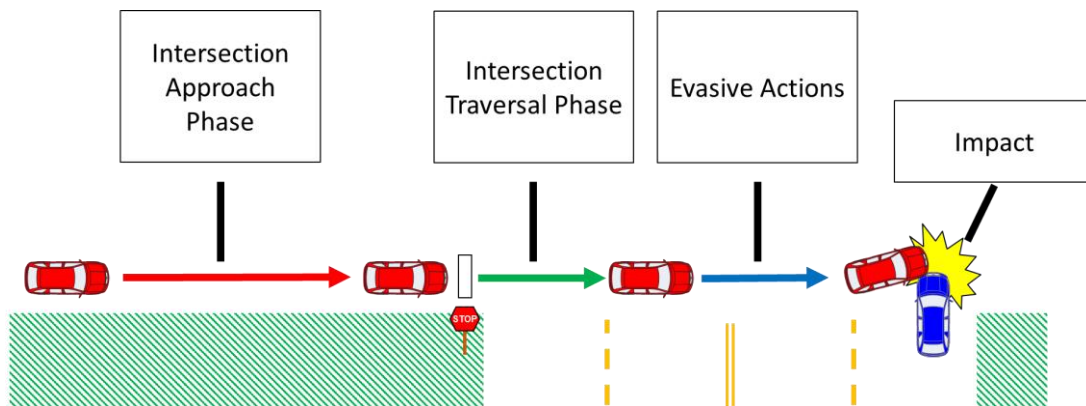


Figure 128. The four main components of pre-intersection crash vehicle kinematics.

Approach and Traversal Observations

An important part of this work was first visualizing the different ways that drivers approach and traverse intersections. Approximately 45,000 intersection approach and traversal trajectories were used to examine typical driver behavior at intersections. These observations helped to establish the four main pre-crash movement groups utilized in the crash reconstruction methods. As shown in Figure 129, the first two categories established were rolling stopped drivers and completely stopped drivers. As shown in Figure 130, the other two categories were straight crossing-travelling through and left turning-travelling through.

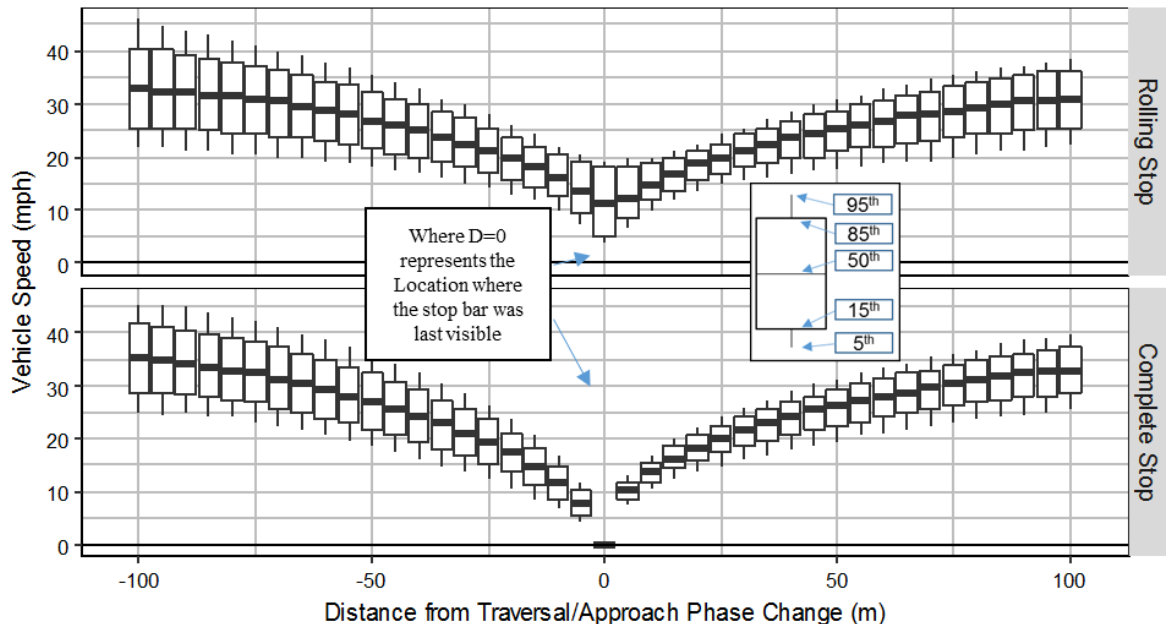


Figure 129. Box plots of vehicle speed versus distance from the beginning of the intersection traversal phase. Two pre-crash movements are shown, including rolling stopped and completely stopped. Every deceleration and acceleration phase were shifted in order to have the driver reach their minimum velocity at $d=0$.

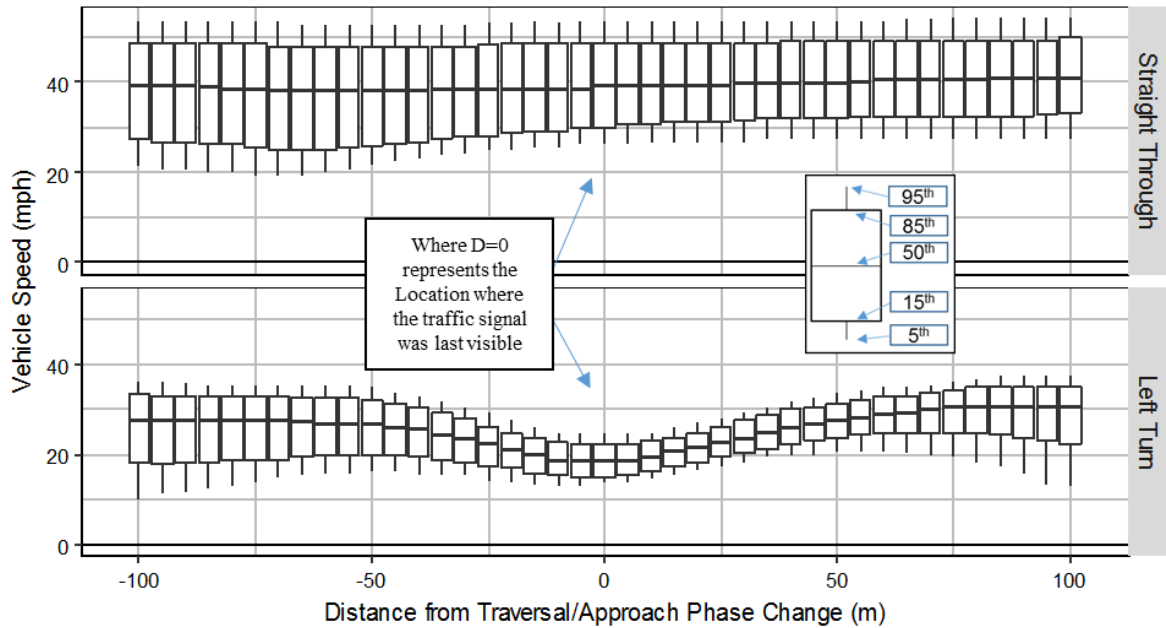


Figure 130. Intersection approach and traversal kinematics for travelling through drivers at signalized intersection. The graphs are separated by turning behavior. The location where distance = 0 represents the location where the traffic signal was last visible

Approach Models for Complete and Rolling Stopped Drivers

An intersection approach model was developed and used to determine the deceleration kinematics of completely and rolling stopped vehicles on the intersection approach for this work’s I-ADAS evaluation analysis. This model was developed using the 100-Car Naturalistic Driving Study (NDS) data collected by the Virginia Tech Transportation Institute (VTTI) [98]. To develop this model, approximately 12,000 previously identified [99] speed traces of intersection approaches for complete and rolling stopped drivers were extracted from the NDS dataset. These developed models account for differences in approach kinematics due to a variety of factors, including stopping behavior (rolling vs. complete stop), turning behavior, and traffic control device. Model development was performed in Matlab using the ARESLab toolbox [123]. Example trajectories from this model can be seen in Figure 131. This approach phase model was “stitched”

together with the acceleration profile model developed from EDR pre-crash data as part of developing a simulation case set.

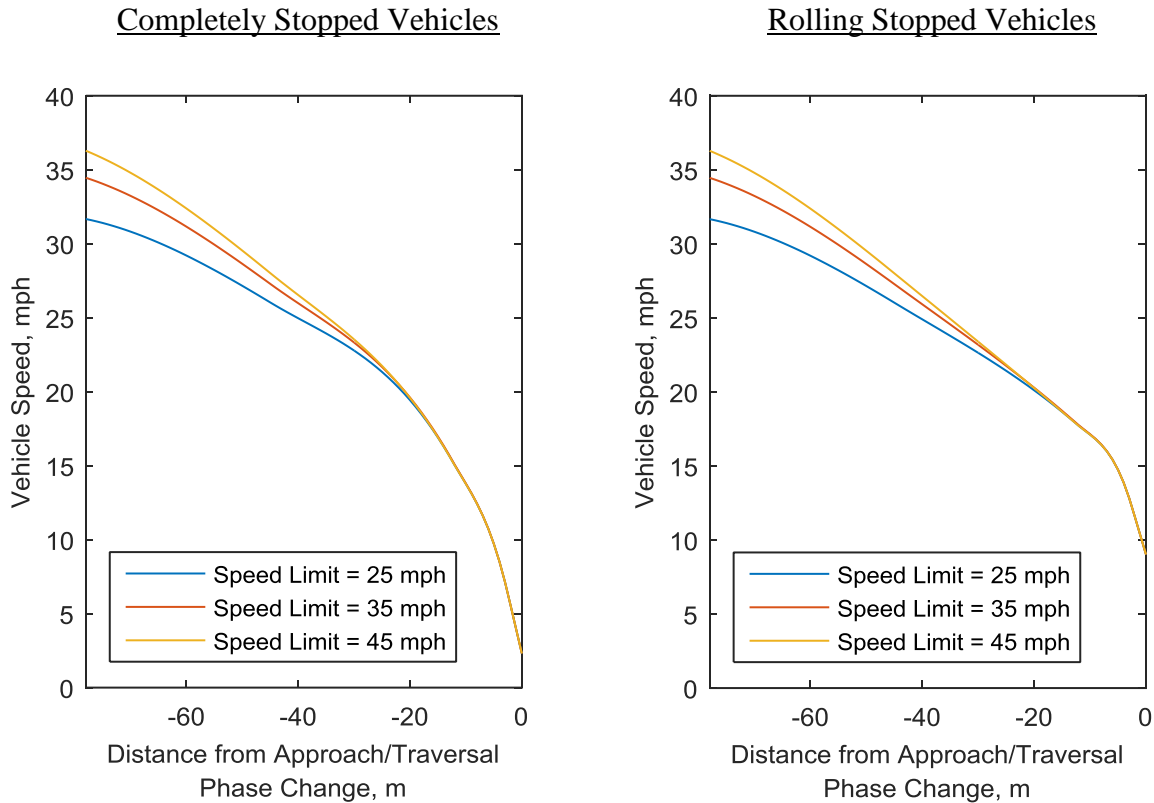


Figure 131. Example approach kinematics models generated for stopped vehicles. Several variations of this model are shown by speed limit and stopping behavior. The driver was assumed to be non-turning, not young or senior, a male, and approaching a stop sign controlled intersection.

Traversal Models for Complete and Rolling Stopped Drivers

The study next developed models of intersection traversals for drivers accelerating into an intersection from a complete or rolling stop. The approach was to utilize 348 Event Data Recorder (EDR) pre-crash records taken from SCP, LTAP/OD, and LTAP/LD crashes investigated as part of National Automotive Sampling System / Crashworthiness Data System (NASS/CDS). Acceleration models were generated from this pre-crash data, and were evaluated using a leave-

one-out cross-validation procedure. Additionally, the predictive power of several non-crash driver models were evaluated using this pre-crash data. The resulting models from our analysis can be found in Table 50. Additionally, a comparison of the overall model fits against pre-existing non-violation models can be found in Figure 132.

Previously developed non-crash models from the literature were compared with the pre-crash models. Our hypothesis was that drivers involved in crashes would accelerate more aggressively than the “typical” driving population. This result suggests that drivers in pre-crash scenarios tend to accelerate more aggressively than drivers in normal scenarios ($p < 0.001$). This has important implications for the design of I-ADAS. Specifically, higher acceleration results in less available time for I-ADAS to detect and respond to an imminent collision..

Table 50. Equations for overall pre-crash model fits.

Crash Mode (Turn)	Model	Equations	
SCP (Straight)	Linear	$a(t) = 2.782 - 0.154 \cdot v(t)$	Equation 37
	Quad.	$a(t) = [1.745 - 0.090 \cdot v(t)]^2$	Equation 38
LTAP/OD (Left)	Linear	$a(t) = 2.924 - 0.247 \cdot v(t)$	Equation 39
	Quad.	$a(t) = [1.791 - 0.099 \cdot v(t)]^2$	Equation 40
LTAP/LD (Left)	Linear	$a(t) = 2.167 - 0.057 \cdot v(t)$	Equation 41
	Quad.	$a(t) = [1.489 - 0.025 \cdot v(t)]^2$	Equation 42

Where,
 $a(t)$ = Acceleration at time point t in m/s^2 ,
 $v(t)$ = Velocity at time point t in m/s ,
 t = time in s .

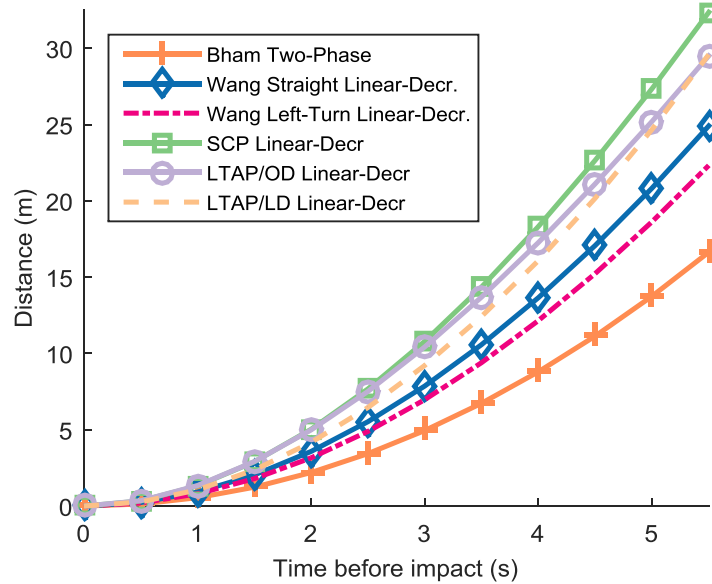


Figure 132. Simulated distance versus time trajectories for a vehicle accelerating from rest. Each acceleration trace corresponds to one of the models evaluated in this study.

Overview of Travelling Through Vehicles at Intersections

Vehicles travelling through the intersection can be modeled based on their turning behavior. Non-turning vehicles typically do not slow or speed up prior to entering the intersection. Left turning vehicles tend to decelerate during the intersection approach down to some safe left turn traversal speed. These behaviors are depicted in Figure 133 and Figure 134. For both sets of behaviors, the traversal speed and evasive braking action must be estimated. The following sections detail the driver models that were used to reconstruct pre-crash kinematics for travelling through vehicles.

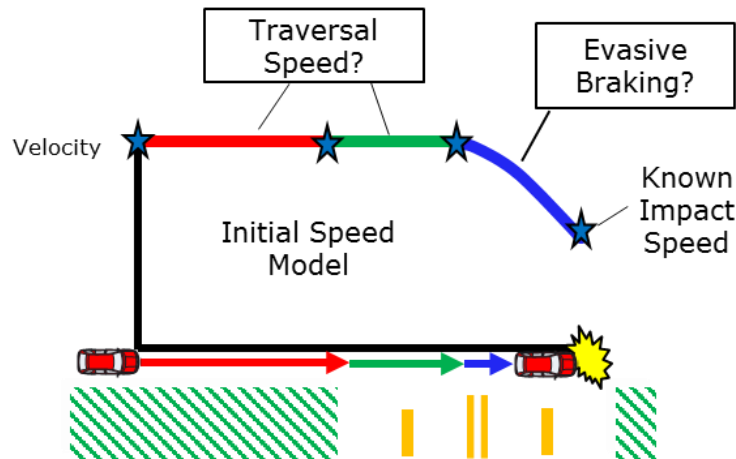


Figure 133. Example travelling through profile for non-turning vehicle.

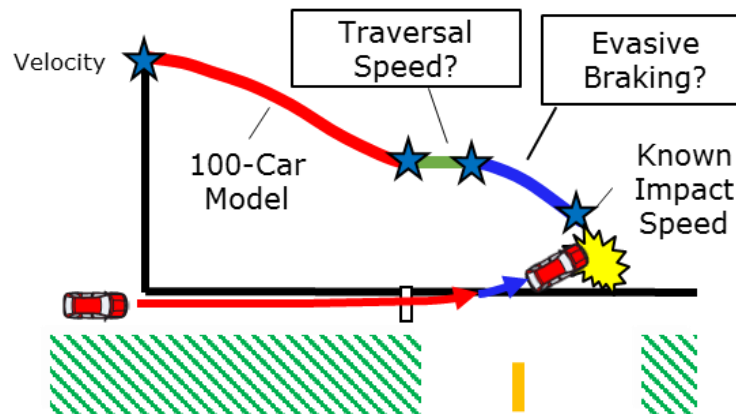


Figure 134. Example travelling through profile for vehicle turning left.

Evasive Braking Models for Travelling Through Drivers

Regression models were developed to predict whether a travelling through driver was likely to have taken evasive action. These models use reconstructed impact speed in order to estimate the likelihood that an evasive braking maneuver attempt occurred. The models were based off of 623 EDR recorded extracted from vehicles involved in crashes investigated as part of the National Automotive Sampling System – Crashworthiness Data System (NASS/CDS).

Logistic regression modeling was used to predict whether an evasive braking maneuver occurred for vehicles that were travelling through the intersection. Models were developed in this study using the “Survey” package [207] in the R programming language [121]. Within this package, this study used the *svyglm* to fit the regression models and *regTermTest* to test which of the predictor variables were statistically significant. The *regTermTest* function uses a Wald test, which was used in this study to test whether each of the regression terms was zero (i.e., not significantly correlated to predict evasive braking). An alpha level of 0.05 was used to determine which of the predictor variables significantly contributed to the likelihood that evasive braking occurred. Two separate regression models were generated, one for straight crossing and another for left turning drivers. For the straight crossing model, impact speed relative to the posted speed limit, the posted speed limit, driver age group, and impact configuration were used. For left turning drivers, impact speed, driver age group, and impact configuration were used. The general forms of these regression equations can be found in Figure 135 and Figure 136.

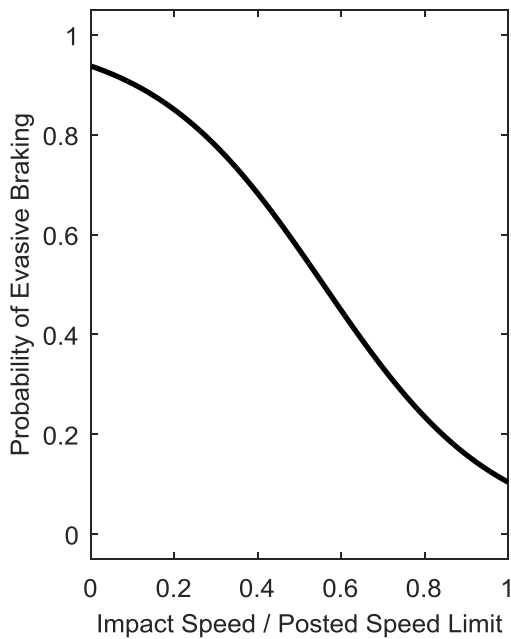


Figure 135. Evasive braking probability based on impact speed relative to the posted speed limit for a straight crossing driver.

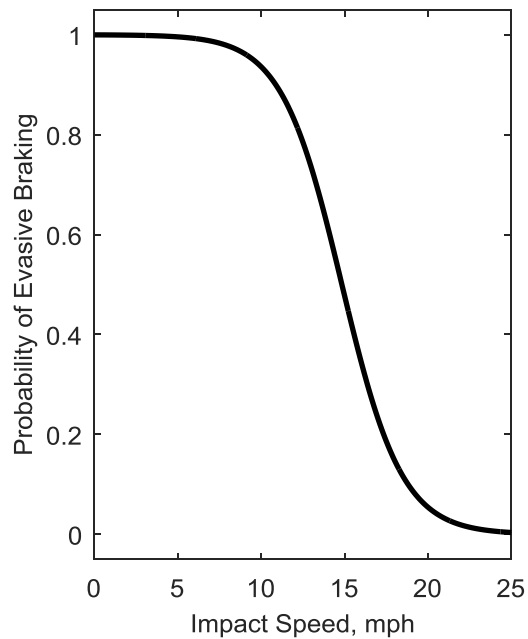


Figure 136. Evasive braking likelihood based on impact speed for a left turning travelling through vehicle.

Traversal Speed Models for Travelling Through Drivers

Regression models were developed to predict the traversal speed of drivers traveling through the intersection. The same dataset as used in the evasive braking model described above was used for the traversal speed model. Linear regression modeling was used to predict the driver’s most likely speed at intersection entry given that the driver took braking evasive action. Similar to the evasive braking likelihood model, the “Survey” package [207] in the R programming language [121] was used to generate and evaluate all regression models. A Wald test was also used to determine the statistical significance of each predictor variable. A regression model was generated for both straight crossing and left turning drivers, which can be seen in Figure 137 and Figure 138, respectively. For both regression models, two predictor terms were added from the evasive braking

likelihood models. First, whether the driver took evasive braking was used as a predictor variable. For a given impact speed, a driver that took evasive braking action would, obviously, tend to have a higher traversal speed than a driver that did not take evasive braking action. Second, an interaction effect between impact speed and evasive braking was used. Any significant effect would imply that the relationship between impact speed and traversal speed depended on whether braking took place.

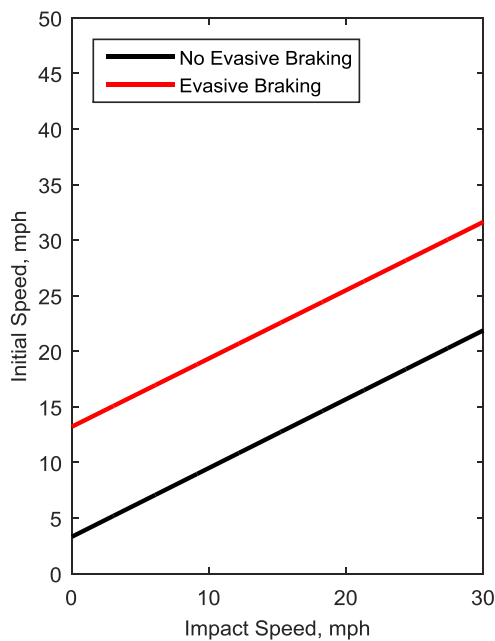


Figure 137. Most likely traversal speed based on impact speed relative to the posted speed limit and whether evasive braking was performed for a straight crossing driver. This equation form was generated for a senior driver travelling on a 35 mph road that was impacted in the near-side.

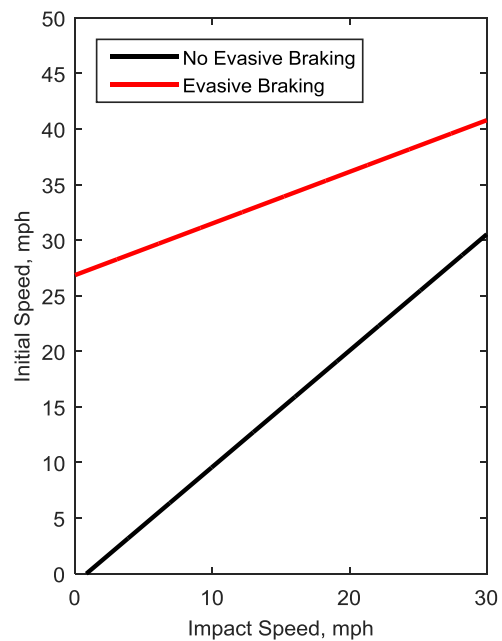


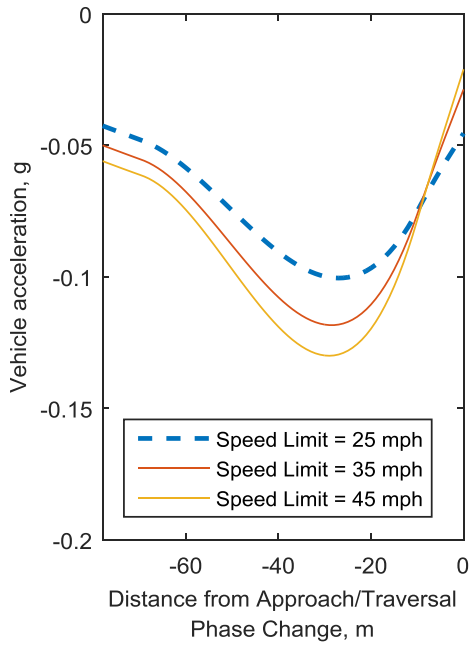
Figure 138. Most likely traversal speed based on impact speed limit and whether evasive braking was performed for a straight crossing driver. This equation form was generated for a senior driver that was impacted on the near-side.

Approach Models for Travelling Through Drivers

In general, the project modeled the approach phase based on whether the driver was straight crossing or turning left at the intersection. If the vehicle was non-turning, they were assumed to have maintained their traversal speed throughout the intersection approach. If the vehicle was left-turning, the driver was assumed to have decelerated up until the point of intersection entry (i.e., stop bar, crosswalk, or boundary line).

The study next developed an approach model for left turning travelling through drivers. The approach model was generated using a dataset of 1,132 left turn, travelling through approaches extracted from the 100-Car study. The model presents an acceleration versus distance relationship for the approach phase of the left turn model. An acceleration versus distance model allows continuity in the speed profile between the approach and traversal phase. Other independent variables used were distance from phase transition, speed at intersection entry, speed limit, driver gender, and driver age. Model development was performed in Matlab using the ARESLab toolbox [123]. Example trajectories from this model can be seen in Figure 139

Entry Speed = 15 mph



Entry Speed = 25 mph

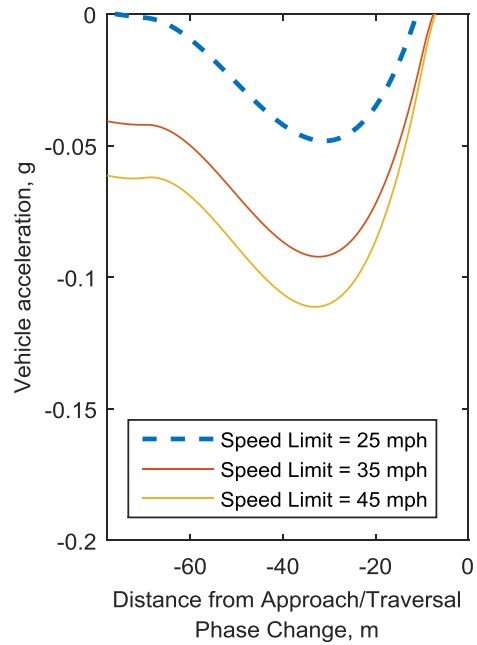


Figure 139. Example trajectories (acceleration versus distance) of the approach phase for left-turning drivers travelling through an intersection. Trajectories are for an adult male.

I-ADAS Reaction Model

An important part of this work was modeling how a driver would respond to an I-ADAS warning. The first important component was modeling an appropriate perception reaction time. The reaction times from the Monash study were used to model an appropriate reaction time between warning delivery and driver response [129]. This simulator study examined driver reaction to an in-vehicle warning when presented with a cross-traffic crash scenarios. There is a distribution of times for how long it would take a driver to respond to an I-ADAS warning. The Monash research group provided us with the raw reaction time data from their study. A distribution of reaction time values from this study can be seen in Figure 140. The approach used was to simulate three equally-probable reaction time values, 0.70 s, 0.99 s, and 1.89 s, which represent the 17th, 50th, and 83rd percentiles of reaction times, accordingly. Autonomous braking was assumed to begin without the delay of reaction time.

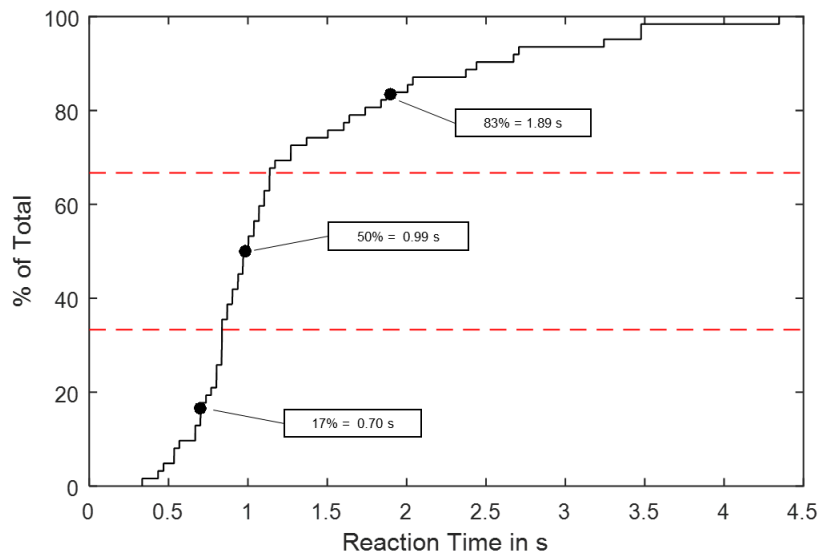


Figure 140. Reaction time values provided from the Monash group for cross-traffic crashes.

An analysis of different studies suggest average crash avoidance decelerations in response to an I-ADAS would likely range from 0.4 g to 0.6 g [129, 130, 231]. There is, of course, some ramp up of deceleration rate as a driver depresses the brake. Drivers were assumed to brake with a jerk value of -11 m/s^3 [215]. Braking deceleration magnitudes was assumed to be dependent on the road surface conditions. In general, maximum vehicle deceleration capacity depends on a number of factors, including vehicle characteristics, surface conditions, vehicle speed, and surface type [216-218]. Our study used maximum deceleration values of 0.3 g, 0.4 g, or 0.8 g based on whether the road conditions were icy, wet, or dry, respectively.

Building a Simulation Case Set

The research project established and implemented a detailed methodology for performing crash reconstructions and building a simulation case set. These simulation case sets were utilized in the studies examining the capacity of I-ADAS to successfully prevent and mitigate U.S. intersection crashes.

Data Source

The safety benefits work was based on two set of real-world intersection crashes investigated by the National Highway Traffic Safety Administration (NHTSA) as part of National Automotive Sampling System / Crashworthiness Data System (NASS/CDS) and the National Motor Vehicle Crash Causation Survey (NMVCCS). Crashes in the NASS/CDS simulation case set must have had involved two vehicles with extractable EDR records, and was referred to as the EDR dataset. The final EDR dataset consisted of 35 LTAP/OD crashes, 21 SCP crashes, and 8 LTAP/LD crashes. A total of 448 SCP crashes and 213 LTAP/LD from the NMVCCS database were extracted.

Path Reconstructions

The paths of all vehicles involved in the simulation case set were reconstructed using measurements taken from the scene diagram. The path reconstruction process included finding the location where the driver entered the intersection.

Speed Reconstructions

After the pre-crash vehicle path was determined, speed reconstructions were performed. The EDR dataset had the advantage of containing actual pre-crash speed data from the vehicles involved in the crash. This speed data was used to trace back vehicle position.

This NMVCCS dataset utilized the work performed in both the driver modeling studies and the impact speed reconstruction work to generate pre-crash kinematics. PC-Crash reconstructed impact speeds were used as the starting point for predicting the most likely vehicle pre-crash kinematics. For drivers travelling through the intersection, statistical driver models for predicting evasive braking and pre-evasive travelling speeds were generated in this study from pre-crash data acquired from Event Data Recorders. For drivers that stopped prior to entering the intersection, intersection approach kinematics were reconstructed using models developed from 100-Car naturalistic data, intersection traversal kinematics were reconstructed produced using a pre-crash acceleration model developed from real-world intersection crashes, and any avoidance action was determined using their reconstructed impact speed.

Evaluating I-ADAS Capabilities

Predicting Crash-Relevant Violations at Stop Sign-Controlled Intersections

Objectives

The objective of this study was to develop a stop sign violation detection algorithm, and evaluate its ability to provide an accurate and timely detection. Three research questions were posed in this study. First, how often would drivers be alerted? Second, when would drivers be alerted? Third, could the vehicle be stopped at this earliest violation detection opportunity?

Data Source

Passenger vehicle intersection approaches were extracted from a dataset of typical driver behavior (100-car naturalistic driving study) and violations (Event Data Recorders downloaded from real-world crashes), and were assigned weighting factors based on real-world frequency. A total of 38 violating and 658 non-violating approaches were used in the analysis.

Methods

Leave-one-out cross-validation was used to develop and evaluate three hypothetical stop sign warning algorithms (i.e. early, intermediate, and delayed) for detecting an impending violation during the intersection approach. Violation detection models were developed using logistic regression models that evaluate likelihood of a violation at various locations along the intersection approach. Two potential indicators of driver intent to stop, i.e., required deceleration parameter (RDP) and brake application, were used to develop the predictive models. The earliest violation detection opportunity was then evaluated for each detection algorithm in order (1) to evaluate the

violation detection accuracy and (2) to compare braking demand versus maximum braking capabilities.

Results

All three algorithms were able to detect a violation at some point during the intersection approach. The early detection algorithm, as designed, was able to detect violations earlier than all other algorithms during the intersection approach, but gave false alarms for 22.3% of approaches. In contrast, the delayed detection algorithm sacrificed some time for detecting violations, but was able to substantially reduce false alarms to only 3.3% of all non-violating approaches. Given good surface conditions (max. braking capabilities = 0.8g) and maximum effort, most drivers (55.3% - 71.1%) would be able to stop the vehicle regardless of the detection algorithm. However, given poor surface conditions (max. braking capabilities = 0.4g), few drivers (10.5% - 26.3%) would be able to stop the vehicle. Automatic emergency braking (AEB) would allow for early braking prior to driver reaction. If equipped with an AEB system, the results suggest that, even for the poor surface conditions scenario, over one-half (55.3% - 65.8%) of the vehicles could have been stopped. This study demonstrates the potential of I-ADAS to incorporate a stop-sign violation detection algorithm. Repeating the analysis on a larger, more extensive dataset will allow for the development of a more comprehensive algorithm to further validate the findings.

Sensor Detection Needs of I-ADAS in LTAP/OD Crashes

Objectives

The objective of this study was to examine the earliest detection opportunity for I-ADAS in LTAP/OD intersection crashes. Three research questions were posed. First, how much time is available for crash avoidance from detection of an oncoming vehicle until impact? Second, what detection range and azimuth is required for sensors to detect an oncoming vehicle at the earliest opportunity? Third, how will sensor specifications influence vehicle detection capacity?

Data Source

The simulation case set of 35 LTAP/OD crashes investigated as a part of NASS/CDS were considered for the current study. The pre-crash positions of each vehicle prior to impact were reconstructed using each vehicle's actual pre-crash records.

Methods

This study looks at the sensor detection needs of I-ADAS in LTAP/OD crashes for two distinct scenarios: one with and one without potential sight occlusions. Without sight obstructions, the “best-case” scenario earliest detection opportunity was taken to be the time point the left turning vehicle first departed their initial lane. The “worst-case” scenario, shown in Figure 141, assumes an obstructed sightline due to a queue of vehicles in the roadway.

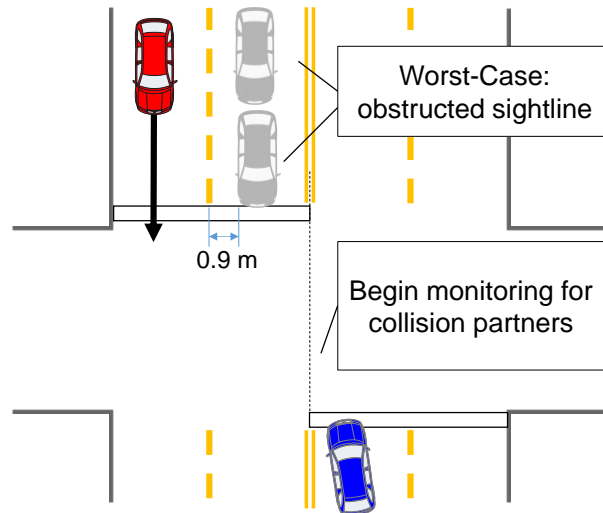


Figure 141. The opportunities for earliest vehicle detection given sight obstructions. The worst-case earliest detection opportunity represents a scenario where (a) the left turning vehicle has begun initiating a left turn and (b) line-of-sight was obstructed by a queue of vehicles.

Results

What was Detection Distance and Angles when Vehicles Enter the Intersection? The median detection range for the worst-case detection scenario was 20.5 m and 95% of distances fell below 61.0 m. In the best-case scenario, the median range was 33.5 m and 95% of distances fell below 86.5 m. This result suggests that in the absence of potential sight occlusions I-ADAS sensors with a maximum range capacity of 90 m would have the capacity to detect all oncoming vehicles in the dataset. Although sight occlusions are expected to be a limiting factor for I-ADAS, it is important that these systems have adequate sensing capacity for the ideal scenario (i.e., no sight occlusions). Failing to design for these more extreme scenarios could lead to failed crash avoidance in an otherwise avoidable scenario.

How much time elapsed from the earliest detection opportunity to impact? The time from crossing the worst and best case time points until impact can be seen in Figure 142. For the best-

case scenario, 50% of the intervals from detection to impact fell below 1.8 s and 95% of the intervals fell below 3.6 s. For the worst-case scenario, the median time to impact was 1.2 s and 95% of times fell below 2.7 s.

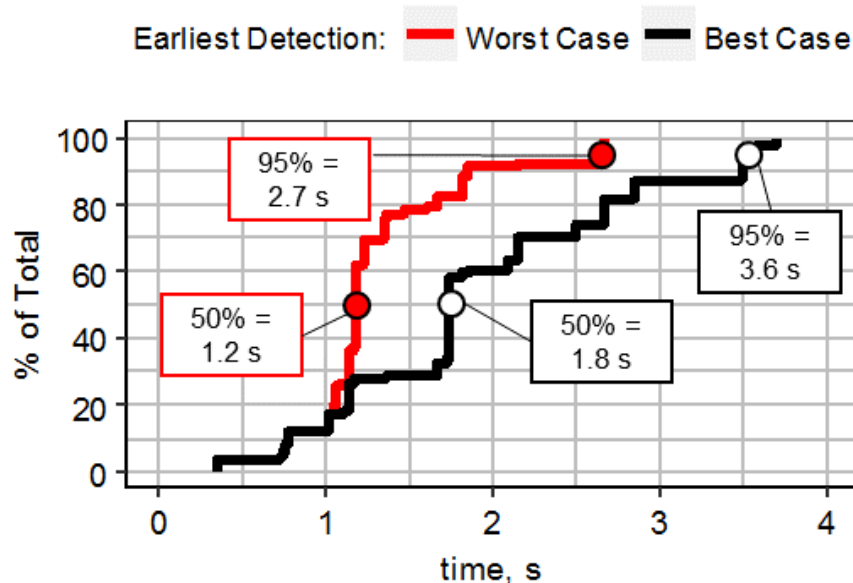


Figure 142. Interval between detection and impact under best-case and worst-case scenarios.

Which sensor specifications and orientations best detected an oncoming vehicle at intersection entry? There are several important findings from this analysis. First, if a forward facing sensor was used, the intermediate beam specifications (90 m, +/- 30 degrees) was found to be most appropriate for detecting oncoming vehicle. In fact, for both vehicle perspectives, all of the trajectories were in the intermediate sensor beam at the best-case detection time point. These sensors should, of course, be tuned to accommodate vehicle sensing throughout the encroachment. Second, only a forward facing sensor is considered in this analysis. Current I-ADAS technology used by vehicles on the market [82, 83] utilize a forward facing radar. I-ADAS designers should consider

incorporating side-facing sensors to ensure continuous vehicle detection if the oncoming vehicle happens to pass outside of the sensor field of view during the approach.

Sensor Detection Needs of I-ADAS in SCP and LTAP/LD Crashes

Objective

Three research questions were posed for this analysis. First, we were interested in determining “What were the detection distances and angles at the earliest detection opportunity?”. This study assumed that the first opportunity for a clear sightline would have occurred when the first vehicle entered the intersection. Second, we investigated “How much time elapsed from the earliest detection opportunity impact?”. Third, we analyzed “Which sensor specifications and orientations best detected an oncoming vehicle at the earliest detection opportunity?”.

Data Source

This study used the simulation case set of SCP and LTAP/LD crashes developed in Chapter 7.

Detection Distance and Angle Calculations

Detection distance and angle values were generated for each vehicle at the earliest detection opportunity for each simulation. The range was computed as the distance between the vehicles. The detection angle was computed for both the entering vehicle and the oncoming vehicle. The entering vehicle refers to the first vehicle to enter the intersection. The oncoming vehicle has not entered the intersection, and is approaching the intersection. Both measurements can be visualized in Figure 143.

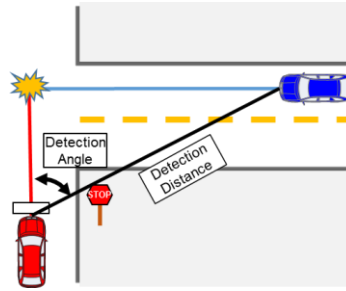


Figure 143. A graphical representation of range and azimuth. The Red vehicle represents the vehicle from which range and azimuth are computed.

Sensor Modeling

The ability of three radar sensors in nine orientations to detect an oncoming vehicle were analyzed. The three sensors modeled were intended to represent wide, intermediate, and narrow beam radars, where there is an inherent trade-off between sensor range and azimuth capabilities. The eighteen total combinations of sensor specifications and configurations are shown in Table 51.

Table 51. Sensor combinations modeled in this study.

Orientation (degrees) Range (m) Azimuth (+/- degrees)		Sensor Orientation (degrees relative to forward direction)					
		0°	15°	30°	45°	60°	75°
Sensor Type	Wide Beam	0°	15°	30°	45°	60°	75°
		40 m	40 m	40 m	40 m	40 m	40 m
	Intermediate Beam	+/- 90°	+/- 90°	+/- 90°	+/- 90°	+/- 90°	+/- 90°
		0°	15°	30°	45°	60°	75°
		80 m	80 m	80 m	80 m	80 m	80 m
		+/- 75°	+/- 75°	+/- 75°	+/- 75°	+/- 75°	+/- 75°
Narrow Beam	0°	15°	30°	45°	60°	75°	
	120 m	120 m	120 m	120 m	120 m	120 m	
		+/- 60°	+/- 60°	+/- 60°	+/- 60°	+/- 60°	

Results

What was Detection Distance and Angles when Vehicles Enter the Intersection? There are several important findings from this set of results. First, at the earliest detection opportunity, nearly all (97%) of the vehicles were less than 100 m away from each other. Sensors with range capacity of 100 m will have the capacity to detect oncoming vehicles at or near the time of the earliest detection opportunity. Second, the sensor detection angle requirements appear to be different for the first entering vehicle and the oncoming vehicle. This indicates that required azimuth specification and sensor orientation should be considered for each vehicle perspective.

How much time elapsed from the earliest detection opportunity to impact? Figure 144 shows a cumulative distribution plot of elapsed time from the earliest detection opportunity until impact. The median elapsed time was 1.7 s, and 95% of times fell below 4.1 s. When considering the average driver reaction time to an intersection incursion is between 1.37 s to 1.51 s [192], these elapsed times are very low if a system is to deliver a warning to the driver at intersection entry.

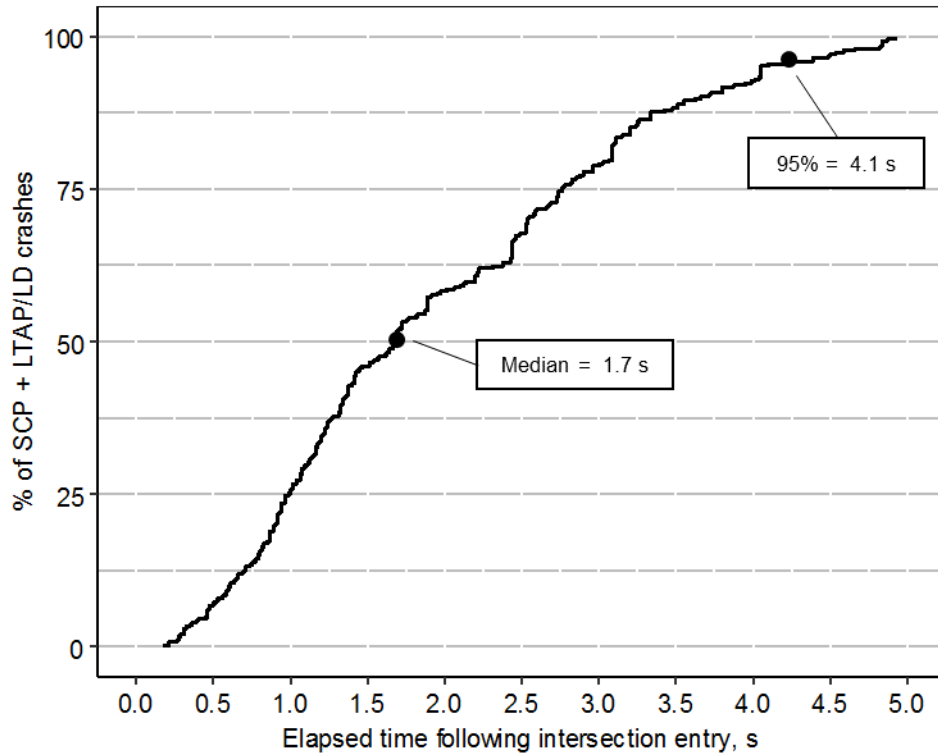


Figure 144. A cumulative distribution plot of elapsed time to collision following the earliest detection opportunity.

Which sensor specifications and orientations best detected an oncoming vehicle at intersection entry? The results indicate that the narrow beam (120 m, +/- 60 degrees) detected the highest proportion (98%) of oncoming vehicles at the earliest detection opportunity. Over 98% of oncoming vehicles detected was achieved for sensor orientations ranging from 44 to 68 degrees. The highest proportion of vehicles detected for the wide (40 m, +/- 90 degrees) and intermediate (80 m, +/- 75 degrees) beams were 62% and 93%, respectively.

Safety Benefits of I-ADAS: Crash and Injury Prevention in SCP and LTAP/LD Crashes

Overview

The approach of the benefits analysis was to use the developed simulation case sets for examining the potential effectiveness of I-ADAS at preventing and mitigating crashes. The benefits estimates approach involved the four steps depicted in Figure 145. The first step involved extracting real-world CT cases from a U.S. national crash database. The second step was to reconstruct each crash case. The third step was to perform pre-crash and impact simulations with and without I-ADAS. The fourth step of the study was to determine the potential number of crashes and seriously injured drivers that could be prevented.

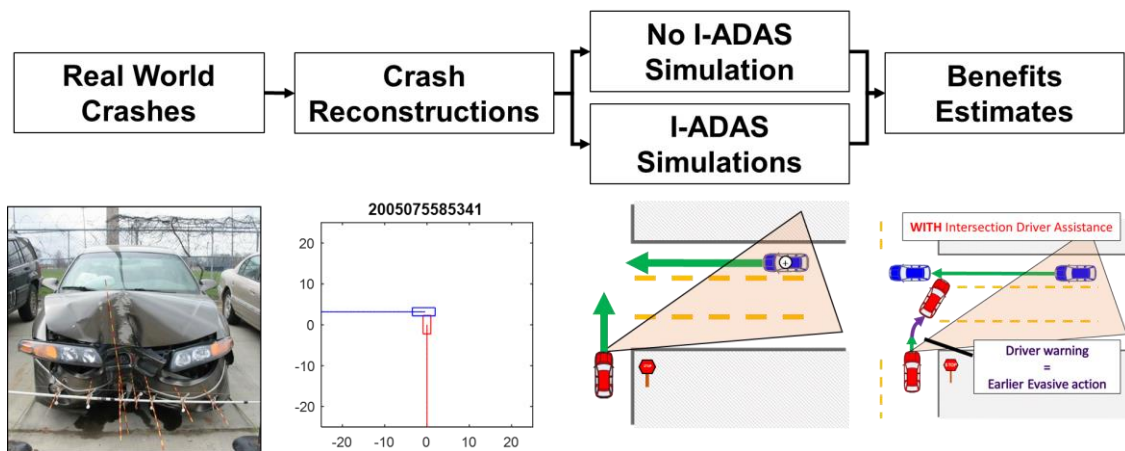


Figure 145. Outline of Benefits Study Approach.

Objective

The current study estimated the benefits of I-ADAS in SCP and LTAP/LD intersection crashes in the case where only one of the vehicles had been equipped with an I-ADAS. This scenario corresponds to the benefits of I-ADAS from a single driver operating in a non-equipped fleet (i.e.,

during the initial introduction of I-ADAS in the U.S. fleet). In addition, benefits estimates were produced for a scenario where both vehicles had been equipped. Eventually, this technology will have been fully implemented in the vehicle fleet (i.e., many years after the initial introduction of I-ADAS in the fleet). In this second scenario, all CT intersection crash scenarios will occur between I-ADAS-equipped vehicles.

The objective of this study was to estimate the proportion of crashes and vehicles with seriously injured drivers that could be reduced if, for every CT intersection crash in the U.S., one of the vehicles, or both, had been equipped with I-ADAS. Additionally, we analyzed the influence of I-ADAS design on system effectiveness. This included (1) examining both a system that either delivers a warning or autonomously brakes, (2) investigating the influence of computational latency time, and (3) investigating the influence of activation timing thresholds. The effects of intersection crash mode, stopping behavior, and reaction time were also investigated.

I-ADAS Modeling and Driver Response

The approach for modeling I-ADAS response can be found in Figure 146. Onboard sensors were assumed to be continuously scanning for oncoming vehicles. At the instant the first vehicle entered the intersection, a clear line-of-sight was modeled between the vehicles. After the oncoming vehicle was first within sensor range, some computational time would be required for the sensor to detect the approaching vehicle. I-ADAS would then either autonomously brake or deliver a warning to the driver if the crash was deemed imminent (i.e., if the crash was estimated to occur within a pre-defined time window). For a system that delivers a warning, driver reaction would have occurred only after some perception-reaction time.

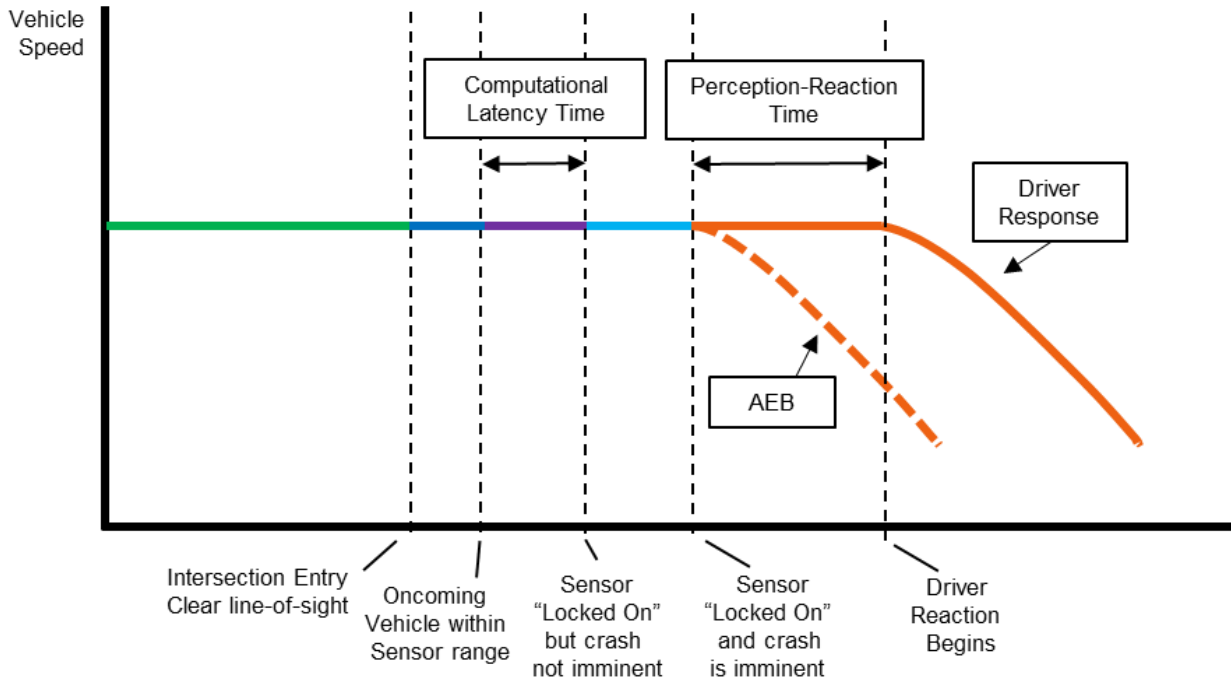


Figure 146. Approach for modeling I-ADAS reaction.

Impact and Injury Modeling

The probability of a seriously injured driver was estimated from impact conditions using logistic regression modeling. Two injury risk models for frontal and side impacts were generated. Independent variables used to model injury risk include delta-v, belt use, driver age, driver gender, occupant compartment intrusion, and the side of the vehicle that was impacted. The .0Abbreviated Injury Scale (AIS) was used to describe injury severity [288]. A maximum AIS score of 3 or greater (MAIS3+) was used to represent a seriously injured driver.

Results

How many CT intersection crashes and seriously injured drivers could be prevented if one of the vehicles was equipped with an I-ADAS? Figure 147 shows the proportion of CT crashes potentially preventable with I-ADAS. The model predicted that 30-64% of CT crashes are potentially preventable by an I-ADAS that autonomously brakes via an AEB system. Conversely, for an I-ADAS that only delivers an alert to the driver, the potential crash prevention effectiveness drops to 0-27% of CT crashes. For crashes that were found to be unavoidable but where the driver/AEB was able to begin evasive braking earlier, modified impact conditions were observed. The proportion of modified impacts depended on the design of the I-ADAS and was as high as 44% of all CT crashes.

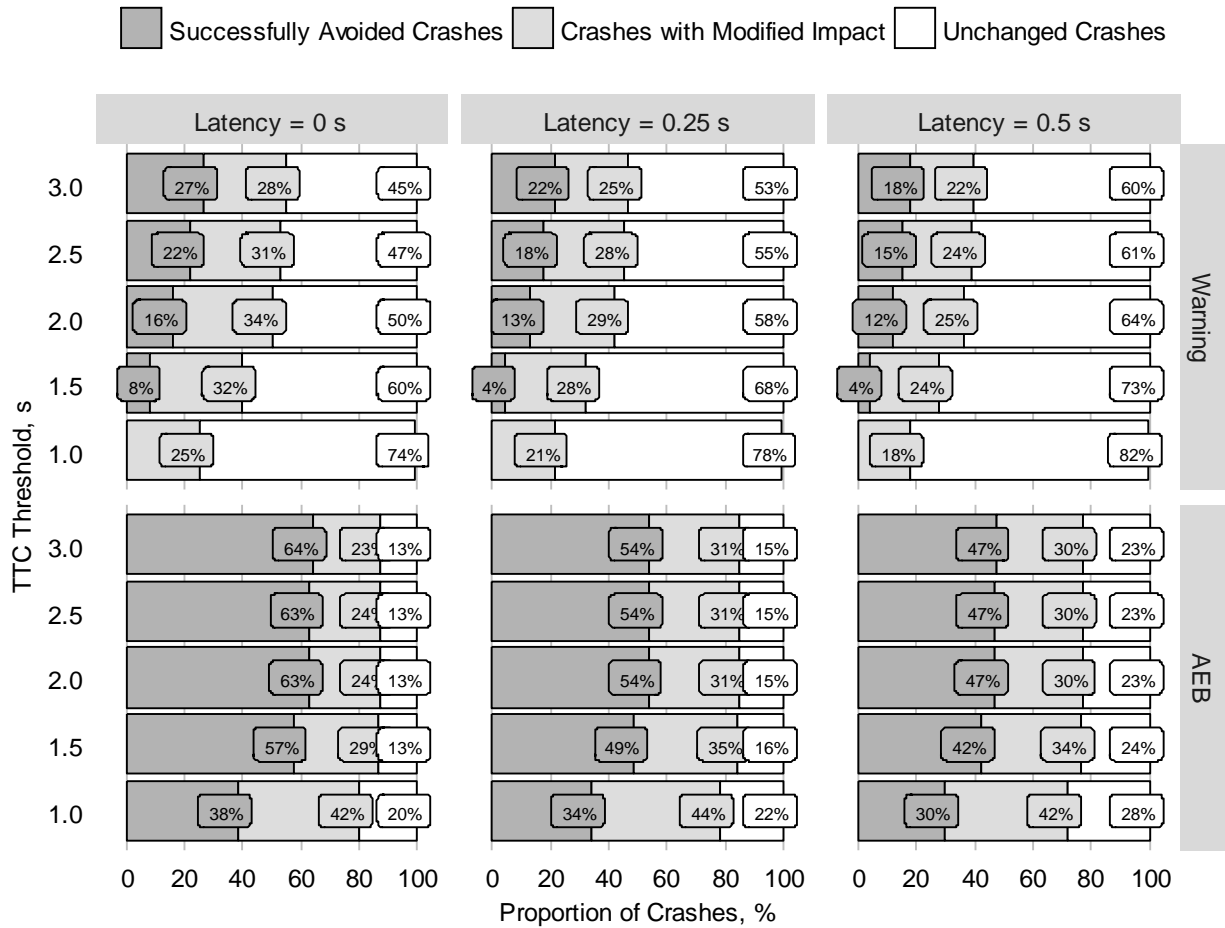


Figure 147. Proportion of CT crashes within the simulation case set that (a) were avoided, (b) had modified impact conditions, or (c) had unchanged impact conditions. All 30 variations of I-ADAS considered in this study are shown.

Even if a crash cannot be successfully avoided, by reducing impact speeds there is the potential for injury mitigation/prevention. Figure 148 shows the proportion of vehicles with seriously injured drivers that could be potentially prevented if one of the involved vehicles had been equipped with an I-ADAS. The model predicts that up to 79% of vehicles with a seriously injured driver are potentially preventable with an I-ADAS that uses AEB. For an I-ADAS that uses a warning to the driver, up to only 33% of seriously injured drivers were estimated to be potentially preventable.

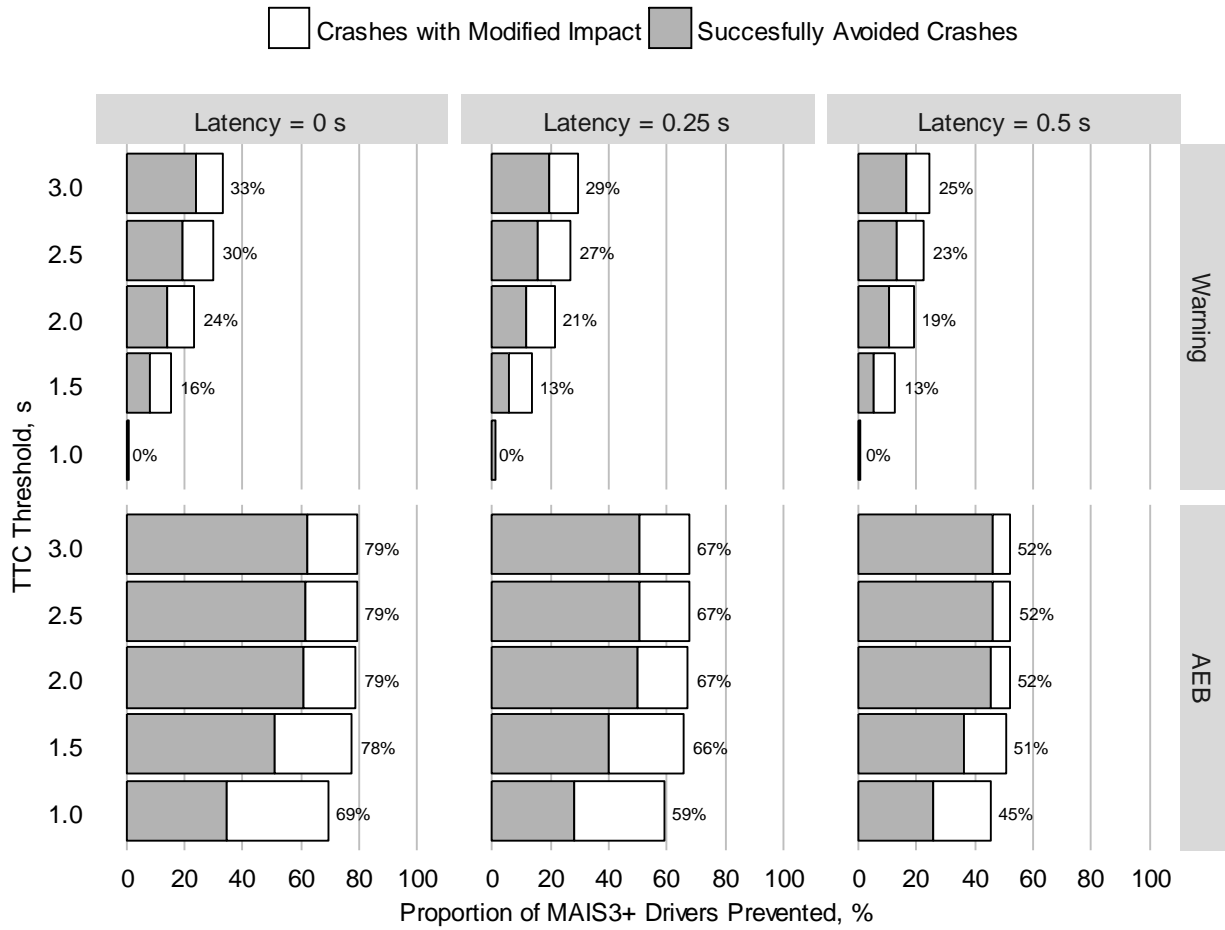


Figure 148. The proportion of seriously injured drivers potentially preventable if an I-ADAS had been equipped on one of the vehicles. All CT crashes are shown. The contribution of completely avoided crashes and crashes with modified impact conditions are shown.

How many CT intersection crashes and seriously injured drivers could be prevented if all vehicles in the U.S. vehicle fleet were equipped with an I-ADAS? Figure 149 shows the model-predicted proportion of CT intersection crashes potentially preventable if I-ADAS were equipped on all vehicles throughout the vehicle fleet. Figure 150 shows the proportion of seriously injured drivers within these crashed vehicles that could have been potentially prevented. In this future fleet, up to 34% of crashes and 39% of vehicles with seriously injured drivers are potentially preventable if a warning-based I-ADAS is used. If an AEB-based I-ADAS is used, the results suggest that up to 70% of crashes could have been avoided and 89% of vehicles with seriously injured drivers were potentially preventable.

The potential effectiveness of I-ADAS was, of course, anticipated to be lower for crashes where only one of the vehicles was equipped. However, this increase in potential benefits when equipping both vehicles was relatively moderate. Additionally, a large proportion of crashes (30%) were still considered “unpreventable” even with the best performing I-ADAS (no latency, TTC = 3.0 s, AEB) being modeled on both vehicles. There were some notable attributes for the unavoidable crashes where both vehicles were equipped with this I-ADAS. First, only 50% of crashes were avoidable if neither of the vehicles performed a complete or rolling stop. Conversely, 79% of crashes were avoidable if one of the vehicles came to a stop. Second, a larger proportion SCP crashes at signalized intersections (74%) were avoided than crashes at stop sign-controlled intersections (56%). Similarly in LTAP/LD crashes, 89% of signalized crashes were avoidable, while only 71% of stop sign controlled intersection crashes were avoided.

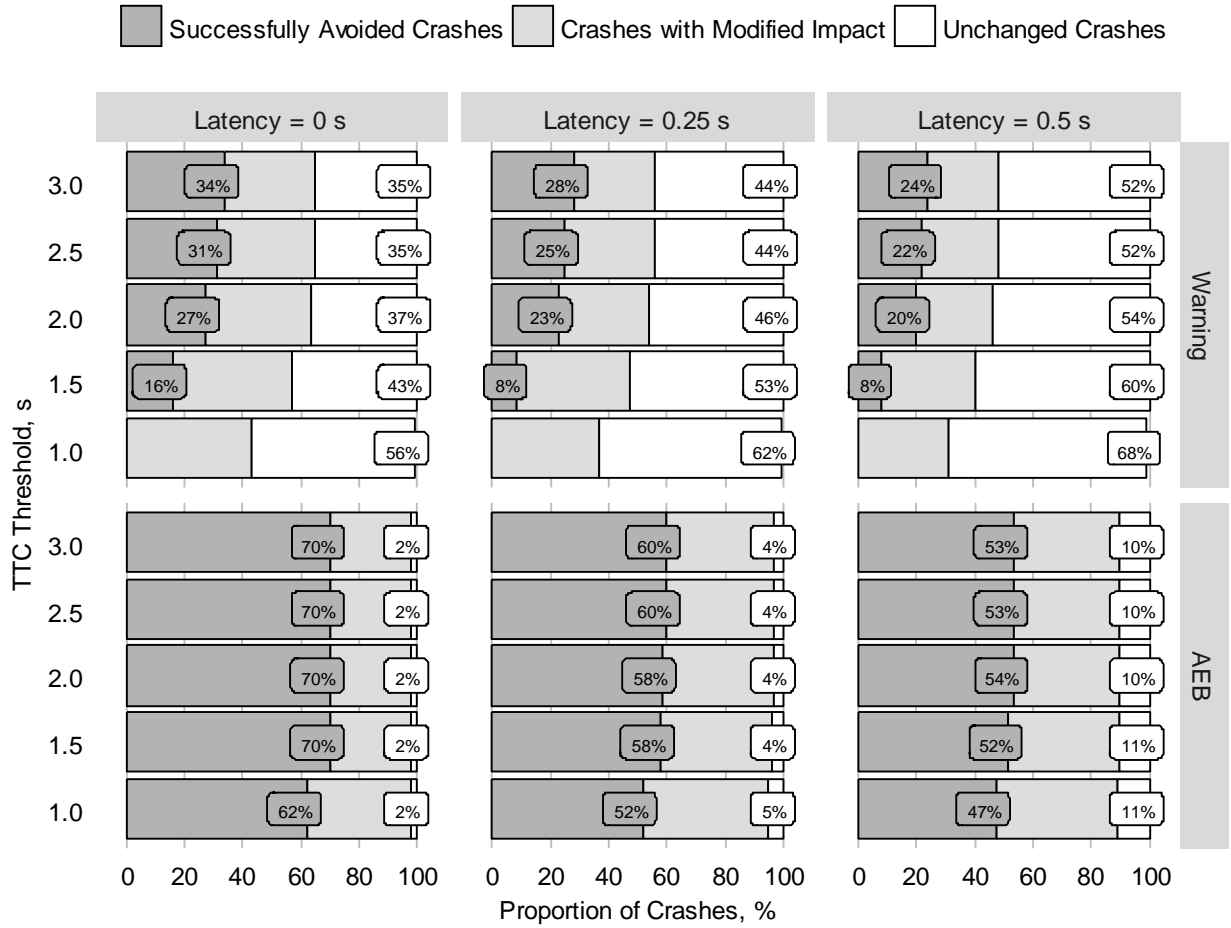


Figure 149. Potential proportion of CT intersection crashes potentially preventable if I-ADAS was equipped on all vehicles throughout the entire vehicle fleet.

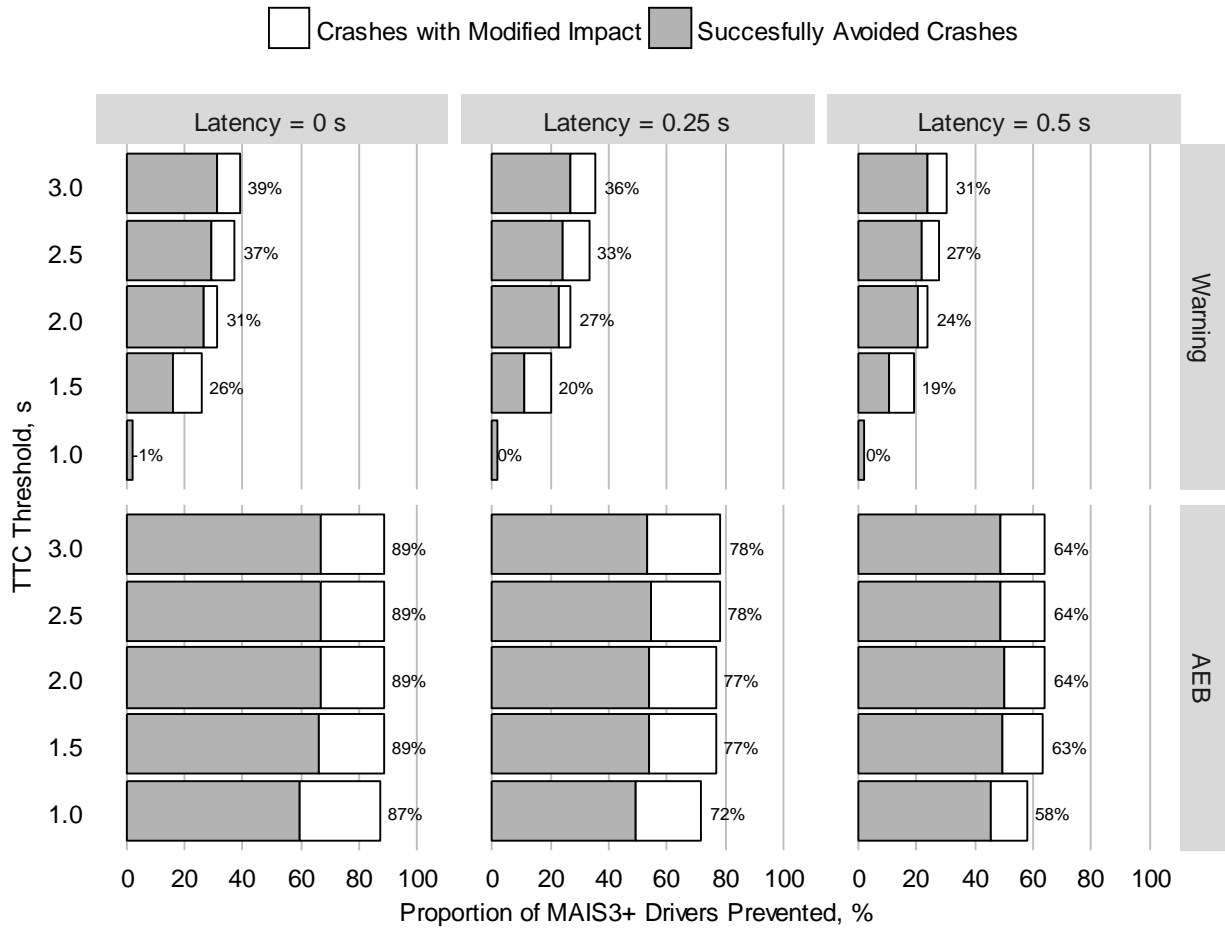


Figure 150. Proportion of potentially prevented vehicles with MAIS3+ drivers if I-ADAS was equipped on all vehicles throughout the entire vehicle fleet.

What are the potential disbenefits of I-ADAS?

For crashes with modified impact conditions, it is important to consider whether activation of I-ADAS may result in disbenefits in some crashes. The model indicates that the driver was able to respond to the I-ADAS alert, but was unsuccessful in avoiding the crash, in 18-44% of crashes. An analysis of potential disbenefits was performed on this dataset of crashes with modified impact conditions. Disbenefits were assumed to have occurred if there was an increase in the combined risk (sum of probability) of MAIS3+ injury for the drivers involved in the crash.

Figure 151 shows the proportion of crashes with potentially higher injury risk. Around 5 to 10% of CT crashes had potential disbenefits. This result can be interpreted as the proportion of CT crashes where I-ADAS could lead to a higher proportion of seriously injured drivers than in the original crash mode.

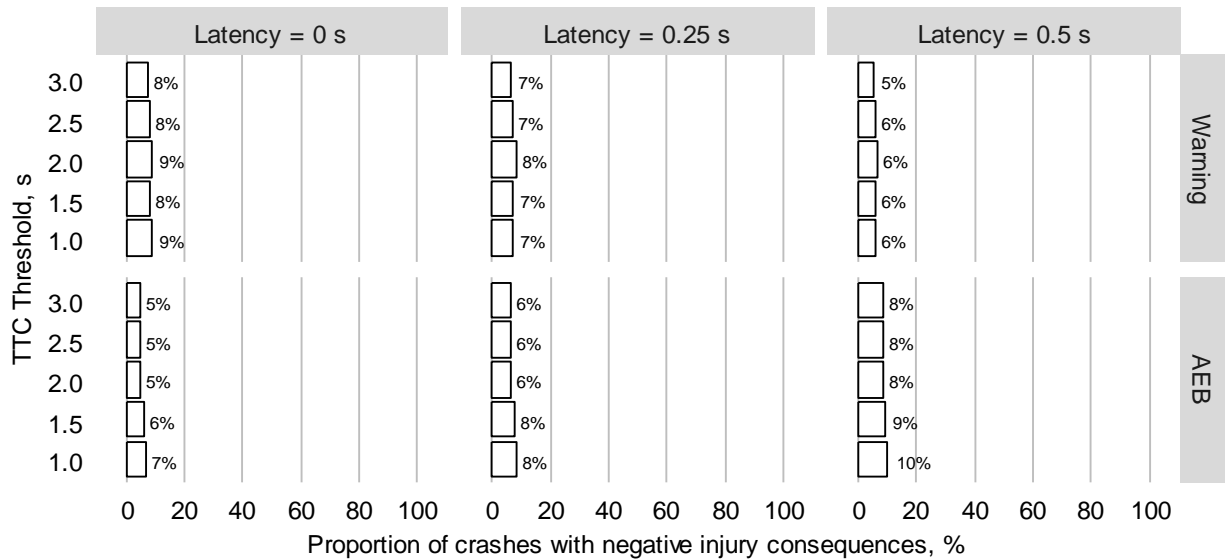


Figure 151. Proportion of all CT crashes with disbenefits in I-ADAS activation.

The disbenefits analysis in the current study is based on an I-ADAS algorithm that does not use any sort of path planning algorithm. More advanced algorithms may have the potential to suppress

I-ADAS activation if the system detects a crash configuration with a potential disbenefit. Additionally, the modeled I-ADAS only assumes that the driver and autonomous evasive system will brake to avoid the crash. This may, of course, not always be the optimal course of action, or the maneuver that would have been performed by the driver. For example, in the crash configuration depicted in Figure 152, activating I-ADAS led to the equipped-vehicle being side impacted in the occupant compartment. In this case, an algorithm that suppressed I-ADAS activation or enabled automated acceleration may have allowed the original crash to be avoided.

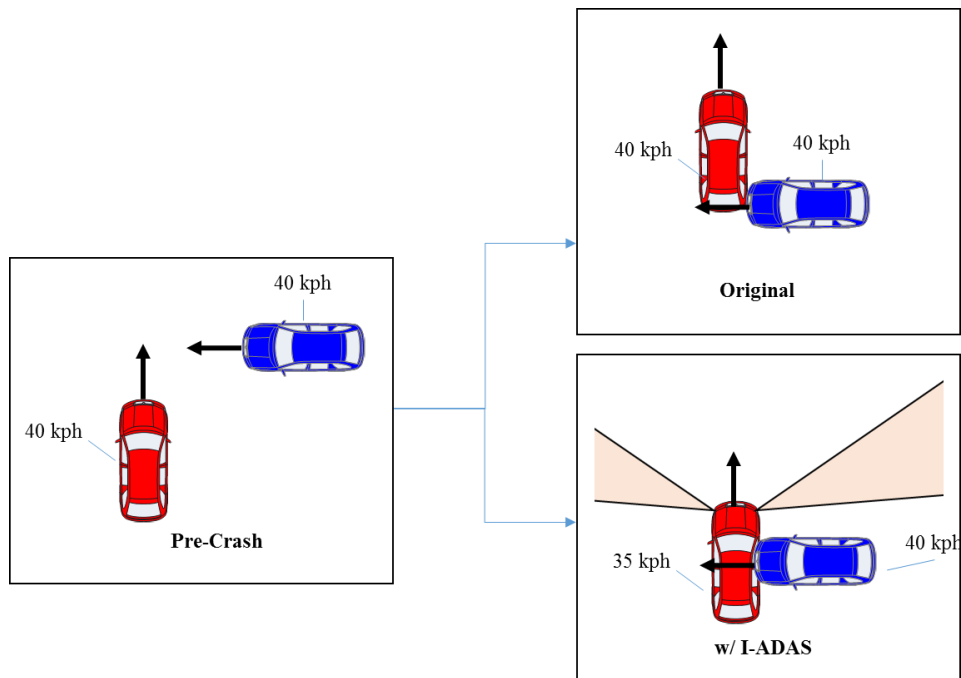


Figure 152. Example of a case where disbenefits could potentially result for the I-ADAS-equipped driver. Here, the I-ADAS-equipped vehicle applies brakes and slows from 40 to 35 kph.

13.Current and Anticipated Contributions to Literature

To date, the research presented in this dissertation, and completed by Scanlon and Gabler, have been the subject of several peer-reviewed publications. Additionally, a number of papers from this work are currently under review or are anticipated in the near-future. The following lists the manuscripts that are published, in print, under review, or anticipated:

Manuscripts currently published, in print or under review

- 1) Scanlon, J. M., Kusano, K. D., & Gabler, H. C. (2015). Analysis of Driver Evasive Maneuvering Prior to Intersection Crashes Using Event Data Recorders. *Traffic injury prevention*, 16, S182-S189.
- 2) Page, Kerry I, Scanlon, John M, Kusano, Kristofer D, & Gabler, Hampton C. (2015). The Potential for Intersection Advanced Driver Assistance System to Reduce Straight Crossing Path Crashes. Paper presented at the Proceedings of the 2015 AAAM Student Research Symposium, Philadelphia, Pennsylvania.
- 3) Scanlon, John M, Kusano, Kristofer D, & Gabler, Hampton C. (2015). A Preliminary Model of Driver Acceleration Behavior prior to Real-World Straight Crossing Path Crashes Using EDRs. Paper presented at the Proceedings of the 2015 IEEE Intelligent Transportation Systems, Canary Islands, Spain.
- 4) Scanlon, John M, Kusano, Kristofer D, Sherony, Rini, & Gabler, Hampton C. (2015). Potential of Intersection Driver Assistance Systems to Mitigate Straight Crossing Path Crashes Using U.S. Nationally Representative Crash Data. Paper presented at the Proceedings of the 2015 IEEE Intelligent Vehicles Symposium, Seoul, Korea.
- 5) Noble, A. M., Kusano, K. D., Scanlon, J. M., Doerzaph, Z., & Gabler, H. C. (2016). Driver Approach and Traversal Trajectories for Signalized Intersections Using Naturalistic Data. Paper presented at the 95th Annual Meeting of the Transportation Research Board, Washington, DC.
- 6) Scanlon, J. M., Page, K., Sherony, R., & Gabler, H. C. (2016). Using Event Data Recorders from Real-World Crashes to Evaluate the Vehicle Detection Capability of an Intersection Advanced Driver Assistance System (No. 2016-01-1457). SAE Technical Paper.
- 7) Scanlon, J. M., Kusano, K. D., & Gabler, H. C. (2016). Preliminary Potential Crash Prevention Estimates for an Intersection Advanced Driver Assistance System in Straight Crossing Path Crashes. Paper presented at the Proceedings of the 2016 IEEE Intelligent Vehicles Symposium, Gothenburg, Sweden.
- 8) Scanlon, J. M., Sherony, R., & Gabler, H. C. (2016). Predicting Crash-Relevant Violations at Stop Sign-Controlled Intersections for the Development of an Intersection Driver Assistance System. *Traffic injury prevention*, 17, 59-65
- 9) Scanlon, J. M., Sherony, R., & Gabler, H. C. (2017). Injury Mitigation Estimates for an Intersection Driver Assistance System in Straight Crossing Path Crashes in the US. *Traffic injury prevention* (Accepted – DOI: 10.1080/15389588.2017.1300257).

- 10) Scanlon, J. M., Sherony, R., & Gabler, C. (2017). Preliminary Effectiveness Estimates for Intersection Driver Assistance Systems in LTAP/OD Crashes. Proceedings of the 2017 FAST-zero Symposium, Nara, Japan.
- 11) Scanlon, J. M., Kusano, K. D., & Gabler, H. C. (2016). Lane Departure Warning and Prevention Systems in the US Vehicle Fleet: Influence of Roadway Characteristics on Potential Safety Benefits. Transportation Research Record: Journal of the Transportation Research Board(2559), 17-23.
- 12) Scanlon, J. M., Kusano, K. D., Sherony, R., & Gabler, H. C. (2015). Potential Safety Benefits of Lane Departure Warning and Prevention Systems in the U.S. Vehicle Fleet. Paper presented at the Proceedings of the 24th International Enhanced Safety of Vehicles Conference, Gothenburg, Sweden, Paper Number 15-0080.

Potential Titles of Anticipated Manuscripts in the Near-Future

- 13) Scanlon, J. M., Sherony, R., & Gabler, H. C. (2016). Models of Driver Acceleration Behavior prior to Real-World Intersection Crashes (In Review). *IEEE Transactions on Intelligent Transportation Systems*.
- 14) Scanlon, J. M., Sherony, R., & Gabler, H. C. (2016). Estimating Pre-crash Driver Actions when You Don't Have an EDR (In Review). Accident Analysis & Prevention.
- 15) Scanlon, J. M., Sherony, R., Ota, K., & Gabler, C. (2017). Earliest Sensor Detection Opportunity for Left Turn Across Path Opposite Direction Crashes (In Review). *IEEE Transactions on Intelligent Vehicles*.
- 16) Factors Influencing Intersection Approach and Traversal Driver Behavior
- 17) The Sensor Detection Needs of I-ADAS Technology in SCP and LTAP/LD Crashes
- 18) The Potential of I-ADAS to Prevent and Mitigate U.S. LTAP/LD Crashes
- 19) The Potential of I-ADAS to Prevent and Mitigate U.S. LTAP/OD Crashes

References

1. Kusano, K.D. and H.C. Gabler, *Comprehensive target populations for current active safety systems using national crash databases*. Traffic injury prevention, 2013. **15**(7): p. 753-761.
2. Kusano, K.D. and H.C. Gabler, *Target Population for Intersection Advanced Driver Assistance Systems in the US*. SAE International Journal of Transportation Safety, 2015. **3**(2015-01-1408): p. 1-16.
3. NHTSA, *Fatality Analysis Reporting System (FARS): Analytical User's Manual 1975-2015*. 2016, U.S. Department of Transportation.
4. Chang, J., et al., *CICAS-V research on comprehensive costs of intersection crashes*. National Highway Traffic Safety Administration, Washington DC, Report, 2007(07-0016).
5. NHTSA, U.S. DOT, *National Safety Council Launch 'Road to Zero' Coalition to End Roadway Fatalities*. 2016.
6. Tingvall, C. and N. Haworth. *Vision Zero: an ethical approach to safety and mobility*. in *6th ITE International Conference Road Safety & Traffic Enforcement: Beyond*. 2000.
7. Elliott, M.R., et al., *Effectiveness of child safety seats vs seat belts in reducing risk for death in children in passenger vehicle crashes*. Archives of pediatrics & adolescent medicine, 2006. **160**(6): p. 617-621.
8. Brasel, K.J., et al., *Seat belts are more effective than airbags in reducing thoracic aortic injury in frontal motor vehicle crashes*. Journal of Trauma and Acute Care Surgery, 2002. **53**(2): p. 309-313.
9. Evans, L., *Restraint effectiveness, occupant ejection from cars, and fatality reductions*. Accident Analysis & Prevention, 1990. **22**(2): p. 167-175.
10. Evans, L., *The effectiveness of safety belts in preventing fatalities*. Accident Analysis & Prevention, 1986. **18**(3): p. 229-241.
11. Yi, Q., et al., *Development of Bicycle Surrogate for Bicyclist Pre-Collision System Evaluation*. 2016, SAE Technical Paper.
12. Belgiovane, D.J., et al., *Surrogate Bicycle Design for Millimeter-Wave Automotive Radar Pre-Collision Testing*. IEEE Transactions on Intelligent Transportation Systems, 2017.
13. Chien, S.Y.-P., et al., *Bicycle apparatuses for use in automotive testing*. 2016, Google Patents.
14. Sherony, R. and C. Zhang. *Pedestrian and Bicyclist Crash Scenarios in the US*. in *Intelligent Transportation Systems (ITSC), 2015 IEEE 18th International Conference on*. 2015. IEEE.
15. Lefler, D.E. and H.C. Gabler, *The fatality and injury risk of light truck impacts with pedestrians in the United States*. Accident Analysis & Prevention, 2004. **36**(2): p. 295-304.

16. Gabler, H.C. *The risk of fatality in motorcycle crashes with roadside barriers*. in *Proceedings of the 20th international conference on enhanced safety of vehicles, Lyons, France*. 2007.
17. Daniello, A. and H.C. Gabler, *Fatality risk in motorcycle collisions with roadside objects in the United States*. *Accident Analysis & Prevention*, 2011. **43**(3): p. 1167-1170.
18. Daniello, A. and H. Gabler, *Effect of barrier type on injury severity in motorcycle-to-barrier collisions in North Carolina, Texas, and New Jersey*. *Transportation Research Record: Journal of the Transportation Research Board*, 2011(2262): p. 144-151.
19. Gabler, H.C. *The Emerging Risk of Fatal Motorcycle Crashes with Guardrails*. in *86th Annual Meeting of the Transportation Research Record, Washington, DC*. 2007.
20. Daniello, A., H. Gabler, and Y. Mehta, *Effectiveness of motorcycle training and licensing*. *Transportation Research Record: Journal of the Transportation Research Board*, 2009(2140): p. 206-213.
21. Daniello, A., D. Cristino, and H. Gabler, *Relationship between rider trajectory and injury outcome in motorcycle-to-barrier crashes*. *Transportation Research Record: Journal of the Transportation Research Board*, 2013(2388): p. 47-53.
22. Scanlon, J.M., K.D. Kusano, and H.C. Gabler, *Lane Departure Warning and Prevention Systems in the US Vehicle Fleet: Influence of Roadway Characteristics on Potential Safety Benefits*. *Transportation Research Record: Journal of the Transportation Research Board*, 2016(2559): p. 17-23.
23. Kusano, K.D. and H.C. Gabler, *Comparison of expected crash and injury reduction from production forward collision and lane departure warning systems*. *Traffic injury prevention*, 2015. **16**(sup2): p. S109-S114.
24. Kusano, K.D., et al. *Comparison of Event Data Recorder and Naturalistic Driving Data for the Study of Lane Departure Events*. in *24th International Technical Conference on the Enhanced Safety of Vehicles (ESV)*. 2015.
25. Kusano, K.D., H. Gabler, and T.I. Gorman, *Fleetwide safety benefits of production forward collision and lane departure warning systems*. *SAE International Journal of Passenger Cars-Mechanical Systems*, 2014. **7**(2014-01-0166): p. 514-527.
26. NHTSA, *Federal Motor Vehicle Safety Standards; Electronic Stability Control Systems; Controls and Displays, 49 CFR Parts 571 and 585*. 2007.
27. NHTSA, *U.S. DOT and IIHS announce historic commitment of 20 automakers to make automatic emergency braking standard on new vehicles* 2016.
28. NHTSA, *Lane Departure Warning System Confirmation Test and Lane Keeping Support Performance Documentation*. 2013, U.S. Department of Transportation.
29. NHTSA, *Forward Collision Warning System Confirmation Test*. 2013, U.S. Department of Transportation.

30. Institute, I.H.L.D. *About our tests: Front Crash Prevention Tests*. 03/29/2016]; Available from: <http://www.ihs.org/ihs/ratings/ratings-info/front-crash-prevention-tests>.
31. NHTSA, *Characterization Test Procedures for Intersection Collision Avoidance Systems Based on Vehicle-to-Vehicle Communications*. 2015, U.S. Department of Transportation.
32. Euro, N., *2020 Roadmap, Revision 1*. 2015, March.
33. NHTSA, *National Automotive Sampling System (NASS) General Estimates System (GES): Analytical User's Manual 1988-2015*. 2016, U.S. Department of Transportation.
34. Wilson, F.A. and J.P. Stimpson, *Trends in fatalities from distracted driving in the United States, 1999 to 2008*. American journal of public health, 2010. **100**(11): p. 2213-2219.
35. Rakauskas, M.E., L.J. Gugerty, and N.J. Ward, *Effects of naturalistic cell phone conversations on driving performance*. Journal of safety research, 2004. **35**(4): p. 453-464.
36. Beede, K.E. and S.J. Kass, *Engrossed in conversation: The impact of cell phones on simulated driving performance*. Accident Analysis & Prevention, 2006. **38**(2): p. 415-421.
37. Strayer, D.L., F.A. Drews, and W.A. Johnston, *Cell phone-induced failures of visual attention during simulated driving*. Journal of experimental psychology: Applied, 2003. **9**(1): p. 23.
38. NHTSA, *U.S. DOT Proposes Broader Use of Event Data Recorders to Help Improve Vehicle Safety*. 2012.
39. Kusano, K.D. and H.C. Gabler, *Safety benefits of forward collision warning, brake assist, and autonomous braking systems in rear-end collisions*. Intelligent Transportation Systems, IEEE Transactions on, 2012. **13**(4): p. 1546-1555.
40. Rakha, H., et al., *Evaluation of safety benefits from a heavy-vehicle forward collision warning system*. Transportation Research Record: Journal of the Transportation Research Board, 2010(2194): p. 44-54.
41. Jermakian, J.S., *Crash avoidance potential of four passenger vehicle technologies*. Accid Anal Prev, 2011. **43**: p. 732-740.
42. Kusano, K.D. and H.C. Gabler, *Method for Estimating Time to Collision at Braking in Real-World, Lead Vehicle Stopped Rear-End Crashes for Use in Pre-Crash System Design*, W. SAE International Technical Paper Series, P.A., Paper Number 2011-01-0576, Editor. 2011.
43. Kusano, K.D., et al., *Potential Occupant Injury Reduction in the US Vehicle Fleet for Lane Departure Warning-Equipped Vehicles in Single-Vehicle Crashes*. Traffic injury prevention, 2014. **15**(sup1): p. S157-S164.
44. Gordon, T., et al. *Advanced Crash Avoidance Technologies (ACAT) Program - Final Report of the Volvo-Ford-UMTRI Project: Safety Impact Methodology for Lane Departure Warning - Method Development and Estimation of Benefits*. 2010. Department of Transportation.

45. Houser, A., et al., *Analysis of benefits and costs of lane departure warning systems for the trucking industry*. 2009.
46. Krueger, S., et al., *Exploratory study on the potential socio-economic impact of the introduction of intelligent safety systems in road vehicles*. VDI/VDE Innovation+ Technik GmbH, Institute for Transport Economics at the University of Cologne, Tech. Rep, 2005.
47. Najm, W. and A. Burgett. *Benefits estimation for selected collision avoidance systems*. in *MOBILITY FOR EVERYONE. 4TH WORLD CONGRESS ON INTELLIGENT TRANSPORT SYSTEMS, 21-24 OCTOBER 1997, BERLIN.(PAPER NO. 1022)*. 1997.
48. Scanlon, J.M., et al. *Potential Safety Benefits of Lane Departure Warning and Prevention Systems in the U.S. Vehicle Fleet*. in *Proceedings of the 24th International Enhanced Safety of Vehicles Conference*. 2015. Gothenburg, Sweden, Paper Number 15-0080.
49. Tanaka, S., et al., *Benefit Estimation of a Lane Departure Warning System using ASSTREET*. SAE International Journal of Passenger Cars-Electronic and Electrical Systems, 2012. **5**(2012-01-0289): p. 133-145.
50. Teraoka, E.Y.M., S. Tanaka, and T. Mochida, *Benefit Estimation Method for Lane Departure Warning Systems in the American Traffic Environment*. 2014, SAE Technical Paper.
51. Pomerleau, D., et al., *Run-off-road collision avoidance using IVHS countermeasures*. DOT HS, 1999. **809**(170): p. 88.
52. Scanlon, J.M., K.D. Kusano, and H.C. Gabler. *Influence of Roadway Characteristics on Potential Safety Benefits of Lane Departure Warning and Prevention Systems in the US Vehicle Fleet*. in *Transportation Research Board 95th Annual Meeting*. 2016.
53. Scanlon, J.M., K.D. Kusano, and H.C. Gabler. *The influence of roadway characteristics on potential safety benefits of lane departure warning and prevention systems in the U.S. vehicle fleet*. in *FAST-zero'15: 3rd International Symposium on Future Active Safety Technology Toward zero traffic accidents*. 2015. Chalmers University of Technology. SAFER Vehicle and Traffic Safety Centre.
54. Kusano, K.D. and H.C. Gabler, *Characterization of lane departure crashes using event data recorders extracted from real-world collisions*. SAE International journal of passenger cars-mechanical systems, 2013. **6**(2013-01-0730): p. 705-713.
55. Kusano, K. and H. Gabler, *Characterization of opposite-direction road departure crashes in the united states*. Transportation Research Record: Journal of the Transportation Research Board, 2013(2377): p. 14-20.
56. Kusano, K.D. and H.C. Gabler, *Field relevance of the new car assessment program lane departure warning confirmation test*. SAE International Journal of Passenger Cars-Mechanical Systems, 2012. **5**(2012-01-0284): p. 253-264.
57. Gorman, T.I., Kusano, K. D., Gabler, H. C. *Model of Fleet-Wide Safety Benefits of Lane Departure Warning Systems*. in *16th International IEEE Conference on Intelligent Transportation Systems (ITSC)*. 2013. The Hague, The Netherlands.

58. Kusano, K.D., Daniello, A.L. , and Gabler, H. C. *Evaluation of a Driver Model for Lane Departure Warning Benefits Estimates*. in *Future Active Safety Technology Toward Zero Traffic Accidents (FAST-Zero) Conference*. 2013. Nagayo, Japan.
59. Gabler, H.C., Kusano, K. D., and Gorman, T. I. *Mathematical Model of Road Departure Events and Estimates of Lane Departure Warning Benefits*. in *2nd International Symposium on Future Active Safety Technology Towards Zero Traffic Accidents (FAST-zoer'13)*. 2013. Nagoya, Japan.
60. Daniello, A.L., Kusano, K. D., and Gabler, H. C. , *Validation of a Driver Recovery Model Using Real-World Departure Cases*, in *SAE International Technical Paper Series, Warrendale, P.A., Paper Number 2013-01-0723*. 2013.
61. Kusano, K.D. and H.C. Gabler. *Model of collision avoidance with lane departure warning in real-world departure collisions with fixed roadside objects*. in *Intelligent Transportation Systems (ITSC), 2012 15th International IEEE Conference on*. 2012. IEEE.
62. Johnson, N.S. and H.C. Gabler, *Reduction in fatal longitudinal barrier crash rate due to electronic stability control*. Transportation Research Record: Journal of the Transportation Research Board, 2015(2521): p. 79-85.
63. Johnson, N.S. and H.C. Gabler, *Injury outcome in crashes with guardrail end terminals*. Traffic injury prevention, 2015. **16**(sup2): p. S103-S108.
64. Johnson, N.S., R. Thomson, and H.C. Gabler, *Improved method for roadside barrier length of need modeling using real-world trajectories*. Accident Analysis & Prevention, 2015. **80**: p. 162-171.
65. Johnson, N.S. and H.C. Gabler, *Injury Risk in Frontal Crashes with Guardrail and Guardrail End Terminals*. 2013.
66. Johnson, N.S., *Serious and Fatal Injury Risk in Road Departure Crashes with Guardrail*. 2015.
67. Hampton, C.E. and H.C. Gabler, *Development of a missing post repair guideline for longitudinal barrier crash safety*. Journal of Transportation Engineering, 2012. **139**(6): p. 549-555.
68. Hampton, C.E. and H.C. Gabler, *Crash performance of strong-post W-beam guardrail with missing blockouts*. International Journal of Crashworthiness, 2012. **17**(1): p. 93-103.
69. Hampton, C., D. Gabauer, and H. Gabler, *Limits of acceptable rail-and-post deflection in crash-damaged strong-post W-beam guardrail*. Transportation Research Record: Journal of the Transportation Research Board, 2010(2195): p. 95-105.
70. Gabauer, D.J. and H.C. Gabler. *Differential rollover risk in vehicle-to-traffic barrier collisions*. in *Annals of advances in automotive medicine. Association for the Advancement of Automotive Medicine. Scientific Conference*. 2009. Association for the Advancement of Automotive Medicine.
71. Gabauer, D.J. and H.C. Gabler, *The effects of airbags and seatbelts on occupant injury in longitudinal barrier crashes*. Journal of safety research, 2010. **41**(1): p. 9-15.

72. Gabauer, D.J. and H.C. Gabler, *Evaluation of current repair criteria for longitudinal barrier with crash damage*. Journal of Transportation Engineering, 2009. **135**(4): p. 225-234.
73. Gabler, H.C. and D.J. Gabauer. *Opportunities for reduction of fatalities in vehicle-guardrail collisions*. in *Annu Proc Assoc Adv Automot Med*. 2007.
74. Gabauer, D.J., et al., *Pendulum testing as a means of assessing the crash performance of longitudinal barrier with minor damage*. International Journal of Impact Engineering, 2010. **37**(11): p. 1121-1137.
75. Gabauer, D.J. and H.C. Gabler. *Review of Current Damage-Level Criteria for Longitudinal Barrier Repair*. in *Proceedings of the 87 th Annual Meeting of the Transportation Research Record*. 2008.
76. Kusano, K.D. and H.C. Gabler. *Rural Road Departure Crashes: Why Is Injury Severity Correlated with Lane Markings?* in *TRB 91st Annual Meeting Compendium of Papers DVD*. 2012.
77. Stanley, L.M. *Haptic and auditory cues for lane departure warnings*. in *Proceedings of the Human Factors and Ergonomics Society Annual Meeting*. 2006. Sage Publications.
78. Suzuki, K. and H. Jansson, *An analysis of driver's steering behaviour during auditory or haptic warnings for the designing of lane departure warning system*. JSAE Review, 2003. **24**: p. 65-70.
79. Chen, M., T. Jochem, and D. Pomerleau. *AURORA: A vision-based roadway departure warning system*. in *Intelligent Robots and Systems 95.'Human Robot Interaction and Cooperative Robots', Proceedings. 1995 IEEE/RSJ International Conference on*. 1995. IEEE.
80. Kim, S.-Y. and S.-Y. Oh. *A driver adaptive lane departure warning system based on image processing and a fuzzy evolutionary technique*. in *Intelligent Vehicles Symposium, 2003. Proceedings. IEEE*. 2003. IEEE.
81. Rudin-Brown, C. and Y. Ian Noy, *Investigation of behavioral adaptation to lane departure warnings*. Transportation Research Record: Journal of the Transportation Research Board, 2002(1803): p. 30-37.
82. Volvo Car Corporation, *2016 Volvo XC90 Owner's Manual*. 2015.
83. Mercedes-Benz USA, *2016 S-Class Operator's Manual*. 2015, Daimler AG: Stuttgart, Germany.
84. Audi, *2016 Audi Q7 Owner's Manual*. 2015, Audi AG: Germany.
85. Doerzaph, Z., *Development of a threat assessment algorithm for intersection collision avoidance systems*. 2007, Virginia Polytechnic Institute and State University: Blacksburg, VA.

86. Doerzaph, Z., V. Neale, and R. Kiefer. *Cooperative intersection collision avoidance for violations: threat assessment algorithm development and evaluation method*. in *Transportation Research Board 89th Annual Meeting*. 2010.
87. Elhenawy, M., et al., *Modeling driver stop/run behavior at the onset of a yellow indication considering driver run tendency and roadway surface conditions*. *Accident Analysis & Prevention*, 2015. **83**: p. 90-100.
88. Jahangiri, A., H. Rakha, and T.A. Dingus. *Predicting red-light running violations at signalized intersections using machine learning techniques*. in *Transportation Research Board 94th Annual Meeting*. 2015.
89. Jahangiri, A., H.A. Rakha, and T.A. Dingus. *Adopting Machine Learning Methods to Predict Red-light Running Violations*. in *Intelligent Transportation Systems (ITSC), 2015 IEEE 18th International Conference on*. 2015. IEEE.
90. Doerzaph, Z., et al., *Cooperative Intersection Collision Avoidance System Limited to Stop Sign and Traffic Signal Violations (CICAS-V) Subtask 3.2 Interim Report: Naturalistic Infrastructure-Based Driving Data Collection and Intersection Collision Avoidance Algorithm Development*. National Highway Traffic Safety Administration, Tech. Rep, 2008.
91. Retting, R.A., H.B. Weinstein, and M.G. Solomon, *Analysis of motor-vehicle crashes at stop signs in four US cities*. *Journal of Safety Research*, 2003. **34**(5): p. 485-489.
92. Scanlon, J.M., et al. *Potential of Intersection Driver Assistance Systems to Mitigate Straight Crossing Path Crashes Using U.S. Nationally Representative Crash Data*. in *Proceedings of the 2015 IEEE Intelligent Vehicles Symposium*. 2015. Seoul, Korea.
93. Bellis, E. and J. Page, *National Motor Vehicle Crash Causation Survey SAS Analytical Users Manual*. 2008, National Highway Traffic Safety Administration: Washington, DC.
94. NHTSA, *National Automotive Sampling System — Crashworthiness Data System: 2015 Analytical User's Manual*. 2016, U.S. Department of Transportation.
95. NHTSA, *National Motor Vehicle Crash Causation Survey: Report to Congress*. 2008, U.S. Department of Transportation.
96. Gabler, H.C., J.A. Hinch, and J. Steiner, *Event Data Recorders. A Decade of Innovation*. 2008, Warrendale, PA: Society of Automotive Engineers.
97. Kononen, D.W., C.A. Flannagan, and S.C. Wang, *Identification and validation of a logistic regression model for predicting serious injuries associated with motor vehicle crashes*. *Accident Analysis & Prevention*, 2011. **43**(1): p. 112-122.
98. Dingus, T.A., et al., *The 100-car naturalistic driving study, Phase II-results of the 100-car field experiment*, NHTSA, Editor. 2006: Washington, DC.
99. Sudweeks, J., et al., *Cooperative Intersection Collision Avoidance Systems Limited to Stop Sign and Traffic Signal Violations (CICAS-V) Subtask 3.1 Report: Mining of the 100-Car Naturalistic Database to Determine Factors Related to Intersection Violations and Near Violations*. 2007, Washington, DC: National Highway Traffic Safety Administration.

100. ESRI, *ArcMap 10.3*. 2014, ESRI Redlands, CA.
101. Johnson, T., et al., *Investigation of driver lane keeping behavior in normal driving based on naturalistic driving study data*. SAE International Journal of Transportation Safety, 2016. **4**(2016-01-1449): p. 236-244.
102. Johnson, T., R. Sherony, and H.C. Gabler. *Driver lane keeping behavior in normal driving using 100-car naturalistic driving study data*. in *Intelligent Vehicles Symposium (IV), 2016 IEEE*. 2016. IEEE.
103. Chen, R., R. Sherony, and H.C. Gabler, *Comparison of Time to Collision and Enhanced Time to Collision at Brake Application during Normal Driving*. 2016, SAE Technical Paper.
104. Chen, R., K.D. Kusano, and H.C. Gabler. *Age and gender difference in braking behavior from the 100-Car Naturalistic Driving Study: the implication for autonomous braking system design*. in *FAST-zero'15: 3rd International Symposium on Future Active Safety Technology Toward zero traffic accidents, 2015*. 2015.
105. Kusano, K.D., R. Chen, and H.C. Gabler. *Effect of driving context on time to collision at brake application during car following*. in *FAST-zero'15: 3rd International Symposium on Future Active Safety Technology Toward zero traffic accidents, 2015*. 2015.
106. Chen, R., K.D. Kusano, and H.C. Gabler, *Driver behavior during overtaking maneuvers from the 100-Car Naturalistic Driving Study*. Traffic injury prevention, 2015. **16**(sup2): p. S176-S181.
107. Thor, C.P. and H.C. Gabler. *Assessing the residual teen crash risk factors after graduated drivers license implementation*. in *Annals of Advances in Automotive Medicine/Annual Scientific Conference*. 2010. Association for the Advancement of Automotive Medicine.
108. Kusano, K.D., et al., *Population distributions of time to collision at brake application during car following from naturalistic driving data*. Journal of safety research, 2015. **54**: p. 95. e29-104.
109. Montgomery, J., K.D. Kusano, and H.C. Gabler, *Age and gender differences in time to collision at braking from the 100-car naturalistic driving study*. Traffic injury prevention, 2014. **15**(sup1): p. S15-S20.
110. Kusano, K.D., et al. *Comparison of Event Data Recorder and Naturalistic Driving Data for the Study of Lane Departure Events*. in *Proc. 24th Enhanc. Saf. Veh. Conf.* 2015.
111. Kusano, K.D., J. Montgomery, and H.C. Gabler. *Methodology for identifying car following events from naturalistic data*. in *Intelligent Vehicles Symposium Proceedings, 2014 IEEE*. 2014. IEEE.
112. Kusano, K.D. and H.C. Gabler. *Real-world Driver Crash Avoidance Maneuvers in Rear-end Collisions using Event Data Recorders*. in *Road Safety and Simulation International Conference*. 2013. Rome, Italy.

113. Gabler, H.C. and J. Hinch. *Feasibility of using event data recorders to characterize the pre-crash behavior of drivers in rear-end collisions*. in *Twenty-first International Conference on Enhanced Safety of Vehicles*. 2009.
114. Kusano, K.D., R. Sherony, and H.C. Gabler, *Methodology for using advanced event data recorders to reconstruct vehicle trajectories for use in Safety impact methodologies (SIM)*. *Traffic injury prevention*, 2013. **14**(sup1): p. S77-S86.
115. Kusano, K. and H. Gabler. *Driver response to road departures in the 100-car naturalistic study*. in *Proceedings of the 4th Road Safety and Simulation International Conference. Rome, Italy*. 2013.
116. Ragland, D.R. and A.A. Zabyshny, *Intersection decision support project: Taxonomy of crossing-path crashes at intersections using GES 2000 data*. Safe Transportation Research & Education Center, 2003.
117. Chovan, J.D., et al., *Examination of intersection, left turn across path crashes and potential IVHS countermeasures (Rep. no. DOT HS 808 154)*. 1994, National Highway Traffic Safety Administration: Cambridge, MA.
118. Wolfermann, A., W.K. Alhajyaseen, and H. Nakamura. *Modeling speed profiles of turning vehicles at signalized intersections*. in *3rd International Conference on Road Safety and Simulation RSS2011, Transportation Research Board TRB, Indianapolis*. 2011.
119. Federal Highway Administration, *Manual on Uniform Traffic Control Devices*, U.S. Department of Transportation, Editor. 2009: Washington, D.C.
120. Bates, D., et al., *Fitting linear mixed-effects models using lme4*. arXiv preprint arXiv:1406.5823, 2014.
121. R Core Team, *R: A Language and Environment for Statistical Computing*. 2015, R Foundation for Statistical Computing: Vienna, Austria.
122. Lenth, R.V. and M. Hervé, *lsmeans: Least-Squares Means. R package version 2.11*. URL <http://CRAN.R-project.org/package=lsmeans>, 2014.
123. Jekabsons, G., *ARESLab: Adaptive regression splines toolbox for Matlab/Octave*. 2015: <http://www.cs.rtu.lv/jekabsons/>.
124. Akçelik, R. and M. Besley. *Acceleration and deceleration models*. in *23rd Conference of Australian Institutes of Transport Research (CAITR 2001), Monash University, Melbourne, Australia*. 2001.
125. Akçelik, R. and D. Biggs, *Acceleration profile models for vehicles in road traffic*. *Transportation Science*, 1987. **21**(1): p. 36-54.
126. Bham, G.H. and R.F. Benekohal. *Development, Evaluation, and Comparison of Acceleration Models*. in *81st Annual Meeting of the Transportation Research Board*. 2002. Washington, D.C.

127. Bham, G.H. and R.F. Benekohal, *A high fidelity traffic simulation model based on cellular automata and car-following concepts*. Transportation Research Part C: Emerging Technologies, 2004. **12**(1): p. 1-32.
128. Wang, J., et al., *Normal deceleration behavior of passenger vehicles at stop sign-controlled intersections evaluated with in-vehicle global positioning system data*. Transportation Research Record: Journal of the Transportation Research Board, 2005. **1937**(1): p. 120-127.
129. Chen, H., L. Cao, and D.B. Logan, *Investigation into the effect of an intersection crash warning system on driving performance in a simulator*. Traffic injury prevention, 2011. **12**(5): p. 529-537.
130. Scanlon, J.M., K.D. Kusano, and H.C. Gabler, *Analysis of Driver Evasive Maneuvering Prior to Intersection Crashes Using Event Data Recorders*. Traffic Injury Prevention, 2015. **16**(sup2): p. S182-S189.
131. Wang, J., et al., *Normal acceleration behavior of passenger vehicles starting from rest at all-way stop-controlled intersections*. Transportation Research Record: Journal of the Transportation Research Board, 2004. **1883**(1): p. 158-166.
132. Deery, H.A. and B.N. Fildes, *Young novice driver subtypes: Relationship to high-risk behavior, traffic accident record, and simulator driving performance*. Human Factors: The Journal of the Human Factors and Ergonomics Society, 1999. **41**(4): p. 628-643.
133. Özkan, T. and T. Lajunen, *Why are there sex differences in risky driving? The relationship between sex and gender - role on aggressive driving, traffic offences, and accident involvement among young Turkish drivers*. Aggressive behavior, 2005. **31**(6): p. 547-558.
134. Jonah, B.A., *Accident risk and risk-taking behaviour among young drivers*. Accident Analysis & Prevention, 1986. **18**(4): p. 255-271.
135. Scanlon, J.M., K.D. Kusano, and H.C. Gabler. *A Preliminary Model of Driver Acceleration Behavior Prior to Real-World Straight Crossing Path Intersection Crashes Using EDRs*. in *Proceedings of the 2015 IEEE Intelligent Transportation Systems*. 2015. Canary Islands, Spain: IEEE.
136. Scanlon, J.M., R. Sherony, and H.C. Gabler, *Models of Driver Acceleration Behavior prior to Real-World Intersection Crashes (In Review)*. IEEE Transactions on intelligent transportation systems, 2016.
137. Scanlon, J.M., R. Sherony, and H.C. Gabler. *Preliminary potential crash prevention estimates for an Intersection Advanced Driver Assistance System in straight crossing path crashes*. in *Intelligent Vehicles Symposium (IV), 2016 IEEE*. 2016. Gothenburg, Sweden: IEEE.
138. Abe, G. and J. Richardson, *Alarm timing, trust and driver expectation for forward collision warning systems*. Applied Ergonomics, 2006. **37**(5): p. 577-586.

139. Dingus, T.A., et al., *Human factors design issues for crash avoidance systems*. Human factors in intelligent transportation systems. 1998, New York, NY: Psychology Press. 55-93.
140. Neale, V. and T. Dingus, *Motor vehicle warnings*, in *Handbook of warnings*, E. M. S. Wogalter, Editor. 2006, Lawrence Erlbaum Associates: Mahwah, NJ. p. 687-700.
141. Bliss, J.P. and S.A. Acton, *Alarm mistrust in automobiles: how collision alarm reliability affects driving*. Applied ergonomics, 2003. **34**(6): p. 499-509.
142. Noble, A.M., et al. *Driver Approach and Traversal Trajectories for Signalized Intersections Using Naturalistic Data*. in *95th Annual Meeting of the Transportation Research Board*. 2016. Washington, DC.
143. Long, G., *Acceleration characteristics of starting vehicles*. Transportation Research Record: Journal of the Transportation Research Board, 2000. **1737**(1): p. 58-70.
144. Rakha, H., et al., *Vehicle dynamics model for predicting maximum truck acceleration levels*. Journal of transportation engineering, 2001. **127**(5): p. 418-425.
145. Searle, J., *Equations for Speed, Time and Distance for Vehicles Under Maximum Acceleration*. 1999, SAE Technical Paper.
146. Turner, C. and R. McClure, *Age and gender differences in risk-taking behaviour as an explanation for high incidence of motor vehicle crashes as a driver in young males*. Injury control and safety promotion, 2003. **10**(3): p. 123-130.
147. Elander, J., R. West, and D. French, *Behavioral correlates of individual differences in road-traffic crash risk: An examination of methods and findings*. Psychological bulletin, 1993. **113**(2): p. 279.
148. Simons-Morton, B.G., et al., *The effect of passengers and risk-taking friends on risky driving and crashes/near crashes among novice teenagers*. Journal of Adolescent Health, 2011. **49**(6): p. 587-593.
149. Wasielewski, P., *Speed as a measure of driver risk: Observed speeds versus driver and vehicle characteristics*. Accident Analysis & Prevention, 1984. **16**(2): p. 89-103.
150. Konecni, V., E.B. Ebbeson, and D.K. Konecni, *Decision processes and risk taking in traffic: Driver response to the onset of yellow light*. Journal of Applied Psychology, 1976. **61**(3): p. 359.
151. Evansm, L., P. Wasielewski, and C.R. Von Buseck, *Compulsory seat belt usage and driver risk-taking behavior*. Human Factors: The Journal of the Human Factors and Ergonomics Society, 1982. **24**(1): p. 41-48.
152. Borkenstein, R.F., R. Crowther, and R. Shumate, *The role of the drinking driver in traffic accidents (The Grand Rapids Study)*. Blutalkohol, 1974. **11**(Suppl.): p. 1-131.
153. McLean, A.J., O.T. Holubowycz, and B.L. Sandow, *ALCOHOL AND CRASHES. IDENTIFICATION OF RELEVANT FACTORS IN THIS ASSOCIATION*. 1980.

154. Yan, X., E. Radwan, and D. Guo, *Effects of major-road vehicle speed and driver age and gender on left-turn gap acceptance*. *Accident Analysis & Prevention*, 2007. **39**(4): p. 843-852.
155. Toledo, T., O. Musicant, and T. Lotan, *In-vehicle data recorders for monitoring and feedback on drivers' behavior*. *Transportation Research Part C: Emerging Technologies*, 2008. **16**(3): p. 320-331.
156. af Wåhlberg, A.E., *Aggregation of driver celeration behavior data: Effects on stability and accident prediction*. *Safety science*, 2007. **45**(4): p. 487-500.
157. Knipling, R.R., *Safety for the long haul: Large truck crash risk, causation, & prevention*. 2009: American Trucking Association Arlington, VA.
158. Scanlon, J.M., et al., *Using Event Data Recorders from Real-World Crashes to Investigate the Earliest Detection Opportunity for an Intersection Advanced Driver Assistance System (No. 2016-01-1457)*. SAE Technical Paper, 2016.
159. Tavris, D.R., E.M. Kuhn, and P.M. Layde, *Age and gender patterns in motor vehicle crash injuries: importance of type of crash and occupant role*. *Accident Analysis & Prevention*, 2001. **33**(2): p. 167-172.
160. Tsoi, A., et al., *Validation of Event Data Recorders in High Severity Full-Frontal Crash Tests*. *SAE International Journal of Transportation Safety*, 2013. **1**(2013-01-1265): p. 76-99.
161. Tsoi, A., N. Johnson, and H. Gabler, *Validation of event data recorders in side-impact crash tests*. *SAE International journal of transportation safety*, 2014. **2**(2014-01-0503): p. 130-164.
162. Ruth, R.R. and A. Tsoi, *Accuracy of Translations Obtained by 2013 GIT Tool on 2010-2012 Kia and Hyundai EDR Speed and Delta V Data in NCAP Tests*. 2014, SAE Technical Paper.
163. Tsoi, A.H., J. Hinch, and H. Gabler, *Analysis of Event Data Recorder Survivability in Crashes with Fire, Immersion, and High Delta-V*. 2015, SAE Technical Paper.
164. Tsoi, A.H., et al., *Survivability of Event Data Recorder Data in Exposure to High Temperature, Submersion, and Static Crush*. 2015, SAE Technical Paper.
165. Johnson, N.S. and H.C. Gabler, *Evaluation of NASS-CDS side crash Delta-V estimates using event data recorders*. *Traffic injury prevention*, 2014. **15**(8): p. 827-834.
166. Johnson, N.S., H.C. Gabler, and D. Sharma. *Preliminary Evaluation of NASS-CDS Side Crash Delta-V Estimates Using Event Data Recorders*. in *23rd International Technical Conference on the Enhanced Safety of Vehicles (ESV)*. 2013.
167. Bowman, D., A. Marinik, and H. Gabler, *Assessment of Heavy Vehicle EDR Technologies*. 2013, SAE Technical Paper.
168. Johnson, N.S. and H.C. Gabler, *Accuracy of a damage-based reconstruction method in NHTSA side crash tests*. *Traffic injury prevention*, 2012. **13**(1): p. 72-80.

169. Hampton, C.E. and H.C. Gabler, *Evaluation of the accuracy of NASS/CDS Delta-V estimates from the enhanced WinSmash algorithm*. Ann Adv Automot Med, 2010. **54**: p. 241-52.
170. Hampton, C.E. and H.C. Gabler, *NASS/CDS delta-V estimates: the influence of enhancements to the WinSmash crash reconstruction code*. Annals of advances in automotive medicine, 2009. **53**: p. 91-102.
171. Gabler, H.C. and J. Hinch. *Evaluation of advanced air bag deployment algorithm performance using event data recorders*. in *Annals of Advances in Automotive Medicine/Annual Scientific Conference*. 2008. Association for the Advancement of Automotive Medicine.
172. Funk, J.R., J.M. Cormier, and H.C. Gabler, *Effect of delta-V errors in NASS on frontal crash risk calculations*. Ann Adv Automot Med, 2008. **52**: p. 155-164.
173. Gabler, H.C. and J. Hinch. *Characterization of Advanced Air Bag Field Performance using Event Data Recorders*. in *Proceedings of the 20th International Conference on Enhanced Safety of Vehicles*. 2007.
174. Niehoff, P. and H.C. Gabler. *The accuracy of WinSmash delta-V estimates: the influence of vehicle type, stiffness, and impact mode*. in *Annual Proceedings of the Association for the Advancement of Automotive Medicine*. 2006.
175. Gabler, H.C., C.E. Hampton, and J. Hinch, *Crash severity: a comparison of event data recorder measurements with accident reconstruction estimates*. 2004, SAE Technical Paper.
176. Gabler, H.C., C. Hampton, and T. Roston. *Estimating crash severity: can event data recorders replace crash reconstruction?* in *Proceedings: International Technical Conference on the Enhanced Safety of Vehicles*. 2003. National Highway Traffic Safety Administration.
177. Treiterer, J., *Investigation of traffic dynamics by aerial photogrammetry techniques*. 1975.
178. Goffe, W.L., G.D. Ferrier, and J. Rogers, *Global optimization of statistical functions with simulated annealing*. Journal of Econometrics, 1994. **60**(1): p. 65-99.
179. SAS Institute Inc., *SAS/STAT 9.3 User's Guide*. 2011: Cary, NC.
180. Tijerina, L., et al., *Examination of Signalized Intersection, Straight Crossing Path Crashes and Potential IVHS Countermeasures. Final Report*. 1994.
181. Scanlon, J.M., R. Sherony, and H.C. Gabler, *Predicting Crash-Relevant Violations at Stop Sign-Controlled Intersections for the Development of an Intersection Driver Assistance System*. Traffic Injury Prevention, 2016. **17**(sup1): p. 59-65.
182. Bare, C., et al., *Analysis of Pre-Crash Data Transferred over the Serial Data Bus and Utilized by the SDM-DS Module*. 2011, SAE Technical Paper.
183. Bortolin, R., et al., *Chrysler Airbag Control Module (ACM) Data Reliability*. SAE International Journal of Passenger Cars-Mechanical Systems, 2010. **3**(1): p. 653-674.

184. Ruth, R. and J. Daily, *Accuracy and Timing of 2013 Ford Flex Event Data Recorders*. 2014, SAE Technical Paper.
185. Brown, R., et al., *Confirmation of Toyota EDR Pre-crash Data*. 2012, SAE Technical Paper.
186. Bao, S. and L.N. Boyle, *Age-related differences in visual scanning at median-divided highway intersections in rural areas*. *Accident Analysis & Prevention*, 2009. **41**(1): p. 146-152.
187. Oxley, J., et al., *Intersection design for older drivers*. *Transportation Research Part F: Traffic Psychology and Behaviour*, 2006. **9**(5): p. 335-346.
188. Stelmach, G.E. and A. Nahom, *Cognitive-motor abilities of the elderly driver*. *Human Factors: The Journal of the Human Factors and Ergonomics Society*, 1992. **34**(1): p. 53-65.
189. Janke, M.K., *Age related disabilities that may impair driving and their assessment*. 1994.
190. Chown, S.M., *Age and the rigidities*. *Journal of Gerontology*, 1961.
191. Birren, J.E., *Age changes in speed of behavior: Its central nature and physiological correlates*. *Behavior, aging and the nervous system*, 1965: p. 191-216.
192. Mazzae, E.N., et al., *Driver crash avoidance behavior with ABS in an intersection incursion scenario on dry versus wet pavement*, W. SAE International Technical Paper Series, P.A., Paper Number 1999-01-1290, Editor. 1999.
193. Nissan Motor Corporation, *Nissan Announces "Autonomous Emergency Steering System"*. 2012.
194. Toyota Motor Corporation, *Toyota Develops New Pedestrian Safety Technology*. 2013.
195. Scharine, A.A. and M.K. McBeath, *Right-handers and Americans favor turning to the right*. *Human Factors: The Journal of the Human Factors and Ergonomics Society*, 2002. **44**(2): p. 248-256.
196. Wilkinson, C.C., et al., *The Timing of Pre-Crash Data Recorded in General Motors Sensing and Diagnostic Modules*. 2006, SAE Technical Paper.
197. Scanlon, J.M., R. Sherony, and H.C. Gabler, *Estimating Pre-crash Driver Actions when You Don't Have an EDR (In Review)*. *Accident Analysis & Prevention*, 2016.
198. Brach, R.M., *Mechanical impact dynamics: rigid body collisions*. 1991.
199. Dr. Steffan Datentechnik GmbH, *PC-Crash 9.1*, D.H. Steffan, Editor. 2011: Linz, Austria.
200. Anderson, R., et al., *Potential benefits of forward collision avoidance technology*. *Injury*, 2012. **44**(15): p. 24.
201. Gordon, T., et al., *Advanced crash avoidance technologies (ACAT) program—Final report of the Volvo-Ford-UMTRI project: safety impact methodology for lane departure warning—Method development and estimation of benefits*. 2010.

202. Van Auken, R., et al., *Advanced crash avoidance technologies (ACAT) program—final report of the Honda-DRI team, volume I: Executive summary and technical report*. DOT HS, 2011. **811**.
203. Luo, X., W. Du, and J. Zhang. *Safety benefits of motorized seat belt as a component in ADAS in front-end collisions*. in *Intelligent Transportation Systems (ITSC), 2014 IEEE 17th International Conference on*. 2014. IEEE.
204. Thorat, S. and J.U.A.S.D. SanketThorve, *Design and Implementation of Automatic Emergency Braking System*. 2016.
205. Wiacek, C., J. Bean, and D. Sharma. *Real-World Analysis of Fatal Rear-End Crashes*. in *24th International Technical Conference on the Enhanced Safety of Vehicles (ESV)*. 2015.
206. Kusano, K.D. and H.C. Gabler, *Target Population for Intersection Advanced Driver Assistance Systems in the U.S.* 2015, SAE Technical Paper (2015-01-1408).
207. Lumley, T., *Analysis of complex survey samples*. Journal of Statistical Software, 2004. **9**(1): p. 1-19.
208. Prokop, G., *Modeling human vehicle driving by model predictive online optimization*. Vehicle System Dynamics, 2001. **35**(1): p. 19-53.
209. *Canadian Vehicle Specifications*, C.I.a.R.D.o.T. Canada, Editor. 2015: Canadian Association of Road Safety Professionals.
210. Datentechnik, D.S., *PC-Crash: A Simulation Program for Vehicle Accidents - Technical Manual*. 2011: Linz, Austria.
211. Cliff, W.E. and D.T. Montgomery, *Validation of PC-Crash - A momentum-based accident reconstruction program*. 1996, SAE Technical Paper.
212. Cliff, W.E. and A. Moser, *Reconstruction of twenty staged collisions with PC-Crash's optimizer*. 2001, SAE Technical Paper.
213. Datentechnik, D.S., *PC-Crash Operating Manual*. May 2009: Linz, Austria.
214. Fryar, C.D., Q. Gu, and C.L. Ogden, *Anthropometric reference data for children and adults: United States, 2007-2010*. Vital and health statistics. Series 11, Data from the national health survey, 2012(252): p. 1-48.
215. Nygård, M., *A method for analysing traffic safety with help of speed profiles*. 1999.
216. Baker, J.S., *Traffic accident investigation manual, 1st ed.*, in *Northwestern University Traffic Institute*. 1975: Evanston, IL.
217. Blau, P.J., *Friction science and technology: from concepts to applications*. 2008, Boca Raton, FL: CRC press.
218. Franck, H. and D. Franck, *Mathematical methods for accident reconstruction: a forensic engineering perspective*. 2009: CRC Press.

219. Papadimitratos, P., et al., *Vehicular communication systems: Enabling technologies, applications, and future outlook on intelligent transportation*. Communications Magazine, IEEE, 2009. **47**(11): p. 84-95.
220. Bahlmann, C., et al. *A system for traffic sign detection, tracking, and recognition using color, shape, and motion information*. in *Intelligent Vehicles Symposium, 2005. Proceedings. IEEE*. 2005. IEEE.
221. De La Escalera, A., et al., *Road traffic sign detection and classification*. Industrial Electronics, IEEE Transactions on, 1997. **44**(6): p. 848-859.
222. Garcia-Garrido, M.A., M.A. Sotelo, and E. Martm-Gorostiza. *Fast traffic sign detection and recognition under changing lighting conditions*. in *Intelligent Transportation Systems Conference, 2006. ITSC'06. IEEE*. 2006. IEEE.
223. Akatsuka, H. and S. Imai, *Road signposts recognition system*. 1987, SAE Technical Paper.
224. Franke, U., et al. *Steps towards an intelligent vision system for driver assistance in urban traffic*. in *Intelligent Transportation System, 1997. ITSC'97., IEEE Conference on*. 1997. IEEE.
225. Mardirossian, A., *For monitoring and detecting traffic violations*. 1999: United States.
226. Yamaki, T. and T. Nishizaka, *Traffic violation warning and traffic violation storage apparatus*. 2004, Google Patents.
227. Pierowicz, J.A., et al., *Intersection collision avoidance using ITS countermeasures*. 2000: US Department of Transportation, National Highway Traffic Safety Administration.
228. Jansson, J., J. Johansson, and F. Gustafsson, *Decision making for collision avoidance systems*. Society of Automotive Engineering SAE, 2002. **1**: p. 0403.
229. Kallhammer, J., *Imaging: The road ahead for car night-vision*. Nature Photon, 2006. **5**: p. 12-13.
230. Lindgren, A., et al., *Driver behaviour when using an integrated advisory warning display for advanced driver assistance systems*. Intelligent Transport Systems, IET, 2009. **3**(4): p. 390-399.
231. Neale, V., et al., *Cooperative Intersection Collision Avoidance System Limited to Stop Sign and Traffic Signal Violations (CICAS-V) Subtask 3.3 Interim Report: Test of Alternative Driver-Vehicle Interfaces on the Smart Road*. National Highway Traffic Safety Administration, Tech. Rep, 2008.
232. Ruth, R. and T. Brown, *2009 Crown Victoria PCM EDR Accuracy in Steady State and ABS Braking Conditions*. 2010, SAE Technical Paper.
233. Scanlon, J.M., et al., *Earliest Sensor Detection Opportunity for Left Turn Across Path Opposite Direction Crashes (In Review)*. IEEE Transactions on Intelligent Vehicles, 2017.
234. Aizenberg, R. and D.M. McKenzie, *Teen and senior drivers*. 1997, California Department of Motor Vehicles, Research and Development Section: Sacramento, CA.

235. Sifrit, K.J., et al. *Intersection Crashes among Drivers in their 60s, 70s and 80s*. in *proceedings of the human factors and ergonomics society annual meeting*. 2010. SAGE Publications.
236. Reinfurt, D.W., et al., *Investigations of crashes and casualties associated with older drivers*. Project G. 8. Chapel Hill, NC: University of North Carolina Highway Safety Research Center, 2000.
237. Braitman, K.A., et al., *Factors leading to older drivers' intersection crashes*. *Traffic Injury Prevention*, 2007. **8**(3): p. 267-274.
238. Chandraratna, S. and N. Stamatiadis, *Problem driving maneuvers of elderly drivers*. *Transportation Research Record: Journal of the Transportation Research Board*, 2003(1843): p. 89-95.
239. Toyota Motor Corporation, *Lexus 2016 NX300H Owners Manual*. 2016.
240. Schubert, R., K. Schulze, and G. Wanielik, *Situation assessment for automatic lane-change maneuvers*. *Intelligent Transportation Systems, IEEE Transactions on*, 2010. **11**(3): p. 607-616.
241. Pakett, A.G., *Smart blind spot sensor*. 1994, Google Patents.
242. Hatipoglu, C., Ü. Özgüner, and K. Redmill, *Automated lane change controller design*. *Intelligent Transportation Systems, IEEE Transactions on*, 2003. **4**(1): p. 13-22.
243. Guizzo, E., *How google's self-driving car works*. *IEEE Spectrum Online*, October, 2011. **18**.
244. Toyota Motor Corporation, *Toyota Brings Advanced Automated Vehicle Technology to U.S. Roads*. 2014: Ann Arbor, Mich. .
245. Thoma, S., T. Lindberg, and G. Klinker, *Evaluation of a generic warning for multiple intersection assistance systems*. *Human factors, security and safety*, 2009: p. 173-188.
246. Volvo Car USA, *City Safety by Volvo Cars – outstanding crash prevention that is standard in the all-new XC90*. 2014.
247. Page, K.I., et al. *The Potential for Intersection Advanced Driver Assistance System to Reduce Straight Crossing Path Crashes*. in *Proceedings of the 2015 AAAM Student Research Symposium*. 2015. Philadelphia, Pennsylvania.
248. Scanlon, J.M., R. Sherony, and H.C. Gabler, *Injury Mitigation Estimates for an Intersection Driver Assistance System in Straight Crossing Path Crashes in the US*. *Traffic Injury Prevention*, 2017. **ESV Special Issue**.
249. Kaempchen, N. and K. Dietmayer. *Data synchronization strategies for multi-sensor fusion*. in *Proceedings of the IEEE Conference on Intelligent Transportation Systems*. 2003. Citeseer.
250. Glielmo, L., *Vehicle-to-vehicle/vehicle-to-infrastructure control*. *The Impact of Control Technology*, 2011.

251. IEEE Connected Vehicles, *First Toyota cars to include V2V and V2I communication by the end of 2015*, in *IEEE Connected Vehicles Initiative*. 2015.
252. Li, X., et al., *Performance evaluation of vehicle-based mobile sensor networks for traffic monitoring*. IEEE transactions on vehicular technology, 2009. **58**(4): p. 1647-1653.
253. Fuerstenberg, K.C., K.C. Dietmayer, and V. Willhoeft. *Pedestrian recognition in urban traffic using a vehicle based multilayer laserscanner*. in *Intelligent Vehicle Symposium, 2002. IEEE*. 2002. IEEE.
254. Cho, Y. and J. Rice, *Estimating velocity fields on a freeway from low-resolution videos*. IEEE Transactions on intelligent transportation systems, 2006. **7**(4): p. 463-469.
255. Retting, R., A. Williams, and M. Greene, *Red-light running and sensible countermeasures: Summary of research findings*. Transportation Research Record: Journal of the Transportation Research Board, 1998(1640): p. 23-26.
256. Grover, C., et al., *Automated emergency brake systems: Technical requirements, costs and benefits*. Automated emergency brake systems: technical requirements, costs and benefits, 2013. **1**(1): p. 1-109.
257. Sherwood, C.P., et al., *Prediction of cervical spine injury risk for the 6-year-old child in frontal crashes*. Traffic injury prevention, 2003. **4**(3): p. 206-213.
258. Van Rooij, L., et al., *The effects of vehicle seat belt parameters on the injury risk for children in booster seats*. SAE transactions, 2003. **112**(6): p. 470-482.
259. Snedeker, J.G., M.H. Muser, and F.H. Walz. *Assessment of pelvis and upper leg injury risk in car-pedestrian collisions: comparison of accident statistics, impactor tests and a human body finite element model*. in *SAE CONFERENCE PROCEEDINGS P*. 2003. SAE; 1999.
260. Moorcroft, D.M., et al., *Computational model of the pregnant occupant: predicting the risk of injury in automobile crashes*. American journal of obstetrics and gynecology, 2003. **189**(2): p. 540-544.
261. Weaver, A.A., et al., *Biomechanical modeling of eye trauma for different orbit anthropometries*. Journal of biomechanics, 2011. **44**(7): p. 1296-1303.
262. Chen, R. and H.C. Gabler, *Risk of thoracic injury from direct steering wheel impact in frontal crashes*. Journal of trauma and acute care surgery, 2014. **76**(6): p. 1441-1446.
263. Peng, Y., et al., *A study of adult pedestrian head impact conditions and injury risks in passenger car collisions based on real-world accident data*. Traffic injury prevention, 2013. **14**(6): p. 639-646.
264. Zhang, P., et al., *Prediction of thoracic injury severity in frontal impacts by selected anatomical morphomic variables through model-averaged logistic regression approach*. Accident Analysis & Prevention, 2013. **60**: p. 172-180.
265. Tsoi, A.H. and H.C. Gabler, *Evaluation of vehicle-based crash severity metrics*. Traffic injury prevention, 2015. **16**(sup2): p. S132-S139.

266. Kusano, K. and H.C. Gabler, *Comparison and validation of injury risk classifiers for advanced automated crash notification systems*. Traffic injury prevention, 2014. **15**(sup1): p. S126-S133.
267. Kusano, K.D. and H.C. Gabler, *Automated crash notification: Evaluation of in-vehicle principal direction of force estimations*. Transportation research part C: emerging technologies, 2013. **32**: p. 116-128.
268. Gabauer, D.J. and H.C. Gabler. *Can delta-V be adjusted with structural and occupant restraint performance to improve prediction of chest acceleration?* in *Annals of Advances in Automotive Medicine/Annual Scientific Conference*. 2008. Association for the Advancement of Automotive Medicine.
269. Gabauer, D.J. and H.C. Gabler, *Comparison of roadside and vehicle crash test injury criteria in frontal crash tests*. International Journal of Vehicle Safety, 2008. **3**(1): p. 1-13.
270. Gabauer, D.J. and H.C. Gabler, *Comparison of roadside crash injury metrics using event data recorders*. Accident Analysis & Prevention, 2008. **40**(2): p. 548-558.
271. Gabauer, D. and H.C. Gabler. *Evaluation of the acceleration severity index threshold values utilizing event data recorder technology*. in *Proceedings of the 84th Annual Meeting of the Transportation Research Board, Washington, DC*. 2005.
272. Gabauer, D. and H. Gabler, *Methodology to evaluate the flail space model by using event data recorder technology*. Transportation Research Record: Journal of the Transportation Research Board, 2004(1890): p. 49-57.
273. Stitzel, J.D., et al. *A population-based comparison of CIREN and NASS cases using similarity scoring*. in *Annu Proc Assoc Adv Automot Med*. 2007.
274. Gabler, H.C., A.A. Weaver, and J.D. Stitzel, *Automotive Field Data in Injury Biomechanics*, in *Accidental Injury*. 2015, Springer. p. 33-49.
275. Braver, E.R., et al., *Reductions in deaths in frontal crashes among right front passengers in vehicles equipped with passenger air bags*. Jama, 1997. **278**(17): p. 1437-1439.
276. Hollowell, W.T., et al., *Updated review of potential test procedures for FMVSS No. 208*. NHTSA Docket, 1999: p. 6407-6.
277. Digges, K., et al. *Characteristics of the injury environment in far-side crashes*. in *Annu Proc Assoc Adv Automot Med*. 2005.
278. Fildes, B., et al. *Chest and abdominal injuries to occupants in far side crashes*. in *The 20th International Technical Conference on Enhanced Saefy of Vehicles Proceedings*. Lyon, France. 2007.
279. Fildes, B.N., et al. *Determining side impact priorities using real-world crash data and harm*. in *Proceedings of the 2000 International IRCOBI Conference on the Biomechanics of Impact, Mont Pellaire, France*. 2000.

280. Gabler, H.C., et al. *Far side impact injury risk for belted occupants in Australia and the United States*. in *Proceedings of the nineteenth international conference on enhanced safety of vehicles, paper*. 2005.
281. Gabler, H.C., B.N. Fildes, and M. Fitzharris, *Improved side impact protection: a search for systems modelling priorities*. Proceedings of DETR, 2000: p. 109.
282. Bostrom, O., et al. *Injury reduction opportunities of far side impact countermeasures*. in *52nd Annals of Advances in Automotive Medicine Annual Conference*. Sandiego, Association for the Advancement of Automotive Medicine. 2008.
283. Fildes, B., et al. *Occupant protection in far side crashes*. in *Proceedings of the Nineteenth International Conference on Enhanced Safety of Vehicles, Washington, DC, USA*. 2005.
284. Newland, C., et al., *Occupant-to-occupant interaction and impact injury risk in side impact crashes*. Stapp car crash journal, 2008. **52**: p. 327.
285. Digges, K.H. and H.C. Gabler, *Opportunities for reducing casualties in far-side crashes*. 2006, SAE Technical Paper.
286. Fildes, B., et al. *Side Impact Crashes and Countermeasures*. in *Proceedings of the Fourth International Forum of Automotive Traffic Safety*. 2005.
287. Gabler, H.C., et al., *Side impact injury risk for belted far side passenger vehicle occupants*. 2005, SAE Technical Paper.
288. AAAM, *The Abbreviated Injury Scale-1990, Update 1998*. 1998: Des Plaines, IL.
289. Gabler, H.C. and W.T. Hollowell, *The aggressivity of light trucks and vans in traffic crashes*. 1998, SAE Technical Paper.
290. Gabler, H.C. and W.T. Hollowell, *The crash compatibility of cars and light trucks*. Journal of Crush Prevention and Injury Control, 2000. **2**(1): p. 19-31.
291. Gabler, H.C., *The evolution of side crash compatibility between cars, light trucks and vans*. 2003, SAE Technical Paper.
292. Donoughe, K., J. Whitestone, and H.C. Gabler. *Analysis of firetruck crashes and associated firefighter injuries in the United States*. in *Annals of Advances in Automotive Medicine/Annual Scientific Conference*. 2012. Association for the Advancement of Automotive Medicine.
293. Chen, R., et al. *An Analysis of Hybrid and Electric Vehicle Crashes in the US*. in *24th International Technical Conference on the Enhanced Safety of Vehicles (ESV)*. 2015.
294. Durbin, D.R., M.R. Elliott, and F.K. Winston, *Belt-positioning booster seats and reduction in risk of injury among children in vehicle crashes*. Jama, 2003. **289**(21): p. 2835-2840.
295. Durbin, D.R., et al., *Effects of seating position and appropriate restraint use on the risk of injury to children in motor vehicle crashes*. Pediatrics, 2005. **115**(3): p. e305-e309.
296. Kemper, A.R., et al., *Biomechanical response of the human clavicle: the effects of loading direction on bending properties*. Journal of applied biomechanics, 2009. **25**(2): p. 165-174.

297. Gayzik, F.S., et al., *Characterization of crash-induced thoracic loading resulting in pulmonary contusion*. *Journal of Trauma and Acute Care Surgery*, 2009. **66**(3): p. 840-849.
298. McCoy, G., R. Johnstone, and R. Duthie, *Injury to the elderly in road traffic accidents*. *Journal of Trauma and Acute Care Surgery*, 1989. **29**(4): p. 494-497.
299. Langford, J. and S. Koppel, *Epidemiology of older driver crashes—identifying older driver risk factors and exposure patterns*. *Transportation Research Part F: Traffic Psychology and Behaviour*, 2006. **9**(5): p. 309-321.
300. Beck, L.F., A.M. Dellinger, and M.E. O'neil, *Motor vehicle crash injury rates by mode of travel, United States: using exposure-based methods to quantify differences*. *American Journal of Epidemiology*, 2007. **166**(2): p. 212-218.
301. Yau, K.K., *Risk factors affecting the severity of single vehicle traffic accidents in Hong Kong*. *Accident Analysis & Prevention*, 2004. **36**(3): p. 333-340.
302. Mock, C.N., et al., *The relationship between body weight and risk of death and serious injury in motor vehicle crashes*. *Accident Analysis & Prevention*, 2002. **34**(2): p. 221-228.
303. Abe, G. and J. Richardson, *The influence of alarm timing on driver response to collision warning systems following system failure*. *Behaviour & Information Technology*, 2006. **25**(5): p. 443-452.
304. Lopez, A., et al. *Analysis of the Braking Behaviour in Pedestrian Automatic Emergency Braking*. in *Intelligent Transportation Systems (ITSC), 2015 IEEE 18th International Conference on*. 2015. IEEE.

Appendix

A.1 Extracting Speed Limit Data from Shape Files

Methods were written for ArcMap 10.3.1. As later versions are released, the following instructions may need to be updated.

Performing a Join

Instructions for using the Join function in ArcMap 10.3.1 to join a shapefile with an excel file with GPS coordinates. The accuracy of these instructions depends on updates and versions of the ArcMap program being used.

1. Open ArcMAP
2. Click Add Data 
3. Find your data file and shapefile
 - a. if you cannot get to your folder click the “Connect to Folder” button  at the top right side and find your folder
4. After adding in data right click on the table name in the Table of Contents window and look at the properties
5. If the properties say yes next to the “Has Object-ID” field in the “Source” tab then move on to step 6, otherwise continue with following steps
 - a. Right-click the layer in the table of contents, point to “Data”, then click “Export...”
 - b. Click the Export drop-down arrow and click All records
 - c. Click the Browse button  and navigate to a location to save the exported data
 - d. Type the name for the output data source
 - e. Click OK
 - f. Right-click on the new data file you just exported
 - g. Select the “Display XY Data...” option
 - h. Choose which fields correspond to the latitudinal and longitudinal columns in your data
 - i. Click OK. This should cause your points to appear on the map
6. Right click the title of dataset of GPS coordinates, select Joins and Relates → “Join...”
7. Make sure that the first drop down menu says “Join data from another layer based on spatial location”
8. Choose your shapefile for the second drop down menu choice
9. Choose the second option for the second question
10. Make sure the path is saving your join file where you want it

11. Click okay
12. Now when you go to the join file you just created and click “Open Attribute Table” it will show you your joined data set along with all of the information for the road closest to your data point.
13. Click select all in the file button and then copy it over to a blank excel sheet.

Finding Road Intersections

1. Open ArcMAP
2. Click Add Data 
3. Find your road shapefile
 - a. if you cannot get to your folder click the “Connect to Folder” button  at the top right side and find your folder
4. Click Geoprocessing -> Intersect
5. In the ‘Input Features’ drop down select your road shapefile
6. In the ‘Output Feature Class’ section either go with the default save area and name or browse and find a new place to save your data
7. Scroll all the way down to the bottom of the window and find the ‘Output Type’ section. Change this to read ‘POINT’ instead of ‘INPUT’
8. Click ‘OK’

Exporting Attributes Table to a .csv

ArcMap was not originally designed to be able to export directly to Excel, so when you try to export your attributes table you won't see an option for either .xls or .csv. However, you can use this method to export your attributes table as a .csv without having to export as a .txt and then convert the .txt file to a .csv file.

1. Open the Attributes Table
2. Click the ‘Table Options’ drop down menu  and select ‘Export’
3. In the ‘Output table’ section browse to where you want the csv file saved
4. Name the file and select .txt for the file type
 - a. This will probably automatically add a .txt suffix to the end of your file name, saving the file like this will save it as a .txt file. However, if you delete the .txt from the end of the file name then saving the file will save it as a .csv file
5. Click ‘OK’

A.2 MARS Model Outputs for Intersection approach and traversal models

The following tables show the MARS models for each category of crossing data. The independent variables used in the regression models are denoted using the following parameters:

- d=Distance from intersection traversal start point (m, negative value for before traversal start)
- isroll = Driver performed rolling stop
- tcd = traffic control device (1=signalized, 2=stop sign-controlled)
- turn = turning behavior (0=non-turning, 1=left-turning)
- sl = speed limit in mph
- isyoung = driver age \leq 20 y.o.
- issenior = driver age \geq 50 y.o
- ismale = gender (0 = female, 1 = male)

Table A1. Printout for model for the approach phase of drivers that came to a rolling or complete stop.

<pre> if (d <= -45) then f1_1 = 0 if (-45 < d < -12.5) then begin p1_1 = (2*(-12.5) + (-45) - 3*(-20)) / ((-12.5) - (-45))^2 r1_1 = (2*(-20) - (-12.5) - (-45)) / ((-12.5) - (-45))^3 f1_1 = p1_1*(d-(-45))^2 + r1_1*(d-(-45))^3 end if (d >= (-12.5)) then f1_1 = d - (-20) BF1 = f1_1 if (isroll <= 0.5) then f2_2 = -(isroll - (1)) if (0.5 < isroll < 1) then begin p2_2 = (3*(1) - 2*(0.5) - (1)) / ((0.5) - (1))^2 r2_2 = ((0.5) + (1) - 2*(1)) / ((0.5) - (1))^3 f2_2 = p2_2*(isroll-(1))^2 + r2_2*(isroll-(1))^3 end if (isroll >= (1)) then f2_2 = 0 BF2 = BF1 * f2_2 if (d <= -45) then f3_1 = -(d - (-20)) if (-45 < d < -12.5) then begin p3_1 = (3*(-20) - 2*(-45) - (-12.5)) / ((-45) - (-12.5))^2 r3_1 = ((-45) + (-12.5) - 2*(-20)) / ((-45) - (-12.5))^3 f3_1 = p3_1*(d-(-12.5))^2 + r3_1*(d-(-12.5))^3 end if (d >= (-12.5)) then f3_1 = 0 if (sl <= 10) then f3_2 = 0 if (10 < sl < 17.5) then begin p3_2 = (2*(17.5) + (10) - 3*(15)) / ((17.5) - (10))^2 r3_2 = (2*(15) - (17.5) - (10)) / ((17.5) - (10))^3 f3_2 = p3_2*(sl-(10))^2 + r3_2*(sl-(10))^3 end if (sl >= (17.5)) then f3_2 = sl - (15) BF3 = f3_1 * f3_2 if (d <= -45) then f4_1 = -(d - (-20)) if (-45 < d < -12.5) then begin p4_1 = (3*(-20) - 2*(-45) - (-12.5)) / ((-45) - (-12.5))^2 r4_1 = ((-45) + (-12.5) - 2*(-20)) / ((-45) - (-12.5))^3 f4_1 = p4_1*(d-(-12.5))^2 + r4_1*(d-(-12.5))^3 end if (d >= (-12.5)) then f4_1 = 0 if (sl <= 10) then f4_2 = -(sl - (15)) if (10 < sl < 17.5) then begin p4_2 = (3*(15) - 2*(10) - (17.5)) / ((10) - (17.5))^2 r4_2 = ((10) + (17.5) - 2*(15)) / ((10) - (17.5))^3 f4_2 = p4_2*(sl-(17.5))^2 + r4_2*(sl-(17.5))^3 end if (sl >= (17.5)) then f4_2 = 0 BF4 = f4_1 * f4_2 if (isyoung <= 0) then f5_1 = 0 if (0 < isyoung < 0.5) then begin p5_1 = (2*(0.5) + (0) - 3*(0)) / ((0.5) - (0))^2 r5_1 = (2*(0) - (0.5) - (0)) / ((0.5) - (0))^3 f5_1 = p5_1*(isyoung-(0))^2 + r5_1*(isyoung-(0))^3 end if (isyoung >= (0.5)) then f5_1 = isyoung - (0) BF5 = f5_1 if (d <= -85) then f6_1 = 0 if (-85 < d < -45) then begin p6_1 = (2*(-45) + (-85) - 3*(-70)) / ((-45) - (-85))^2 r6_1 = (2*(-70) - (-45) - (-85)) / ((-45) - (-85))^3 f6_1 = p6_1*(d-(-85))^2 + r6_1*(d-(-85))^3 end if (d >= (-45)) then f6_1 = d - (-70) BF6 = f6_1 if (d <= -12.5) then f7_1 = 0 if (-12.5 < d < -2.5) then begin p7_1 = (2*(-2.5) + (-12.5) - 3*(-5)) / ((-2.5) - (-12.5))^2 r7_1 = (2*(-5) - (-2.5) - (-12.5)) / ((-2.5) - (-12.5))^3 f7_1 = p7_1*(d-(-12.5))^2 + r7_1*(d-(-12.5))^3 end if (d >= (-2.5)) then f7_1 = d - (-5) BF7 = f7_1 if (turn <= 0.5) then f8_1 = -(turn - (1)) </pre>	<pre> if (0.5 < turn < 1) then begin p8_1 = (3*(1) - 2*(0.5) - (1)) / ((0.5) - (1))^2 r8_1 = ((0.5) + (1) - 2*(1)) / ((0.5) - (1))^3 f8_1 = p8_1*(turn-(1))^2 + r8_1*(turn-(1))^3 end if (turn >= (1)) then f8_1 = 0 BF8 = f8_1 if (tcd <= 1) then f9_2 = 0 if (1 < tcd < 1.5) then begin p9_2 = (2*(1.5) + (1) - 3*(1)) / ((1.5) - (1))^2 r9_2 = (2*(1) - (1.5) - (1)) / ((1.5) - (1))^3 f9_2 = p9_2*(tcd-(1))^2 + r9_2*(tcd-(1))^3 end if (tcd >= (1.5)) then f9_2 = tcd - (1) BF9 = BF8 * f9_2 if (d <= -12.5) then f10_1 = -(d - (-5)) if (-12.5 < d < -2.5) then begin p10_1 = (3*(-5) - 2*(-12.5) - (-2.5)) / ((-12.5) - (-2.5))^2 r10_1 = ((-12.5) + (-2.5) - 2*(-5)) / ((-12.5) - (-2.5))^3 f10_1 = p10_1*(d-(-2.5))^2 + r10_1*(d-(-2.5))^3 end if (d >= (-2.5)) then f10_1 = 0 if (issenior <= 0) then f10_2 = 0 if (0 < issenior < 0.5) then begin p10_2 = (2*(0.5) + (0) - 3*(0)) / ((0.5) - (0))^2 r10_2 = (2*(0) - (0.5) - (0)) / ((0.5) - (0))^3 f10_2 = p10_2*(issenior-(0))^2 + r10_2*(issenior-(0))^3 end if (issenior >= (0.5)) then f10_2 = issenior - (0) BF10 = f10_1 * f10_2 if (d <= -12.5) then f11_1 = -(d - (-5)) if (-12.5 < d < -2.5) then begin p11_1 = (3*(-5) - 2*(-12.5) - (-2.5)) / ((-12.5) - (-2.5))^2 r11_1 = ((-12.5) + (-2.5) - 2*(-5)) / ((-12.5) - (-2.5))^3 f11_1 = p11_1*(d-(-2.5))^2 + r11_1*(d-(-2.5))^3 end if (d >= (-2.5)) then f11_1 = 0 if (sl <= 17.5) then f11_2 = 0 if (17.5 < sl < 37.5) then begin p11_2 = (2*(37.5) + (17.5) - 3*(20)) / ((37.5) - (17.5))^2 r11_2 = (2*(20) - (37.5) - (17.5)) / ((37.5) - (17.5))^3 f11_2 = p11_2*(sl-(17.5))^2 + r11_2*(sl-(17.5))^3 end if (sl >= (37.5)) then f11_2 = sl - (20) BF11 = f11_1 * f11_2 if (d <= -12.5) then f12_1 = -(d - (-5)) if (-12.5 < d < -2.5) then begin p12_1 = (3*(-5) - 2*(-12.5) - (-2.5)) / ((-12.5) - (-2.5))^2 r12_1 = ((-12.5) + (-2.5) - 2*(-5)) / ((-12.5) - (-2.5))^3 f12_1 = p12_1*(d-(-2.5))^2 + r12_1*(d-(-2.5))^3 end if (d >= (-2.5)) then f12_1 = 0 if (sl <= 17.5) then f12_2 = -(sl - (20)) if (17.5 < sl < 37.5) then begin p12_2 = (3*(20) - 2*(17.5) - (37.5)) / ((17.5) - (37.5))^2 r12_2 = ((17.5) + (37.5) - 2*(20)) / ((17.5) - (37.5))^3 f12_2 = p12_2*(sl-(37.5))^2 + r12_2*(sl-(37.5))^3 end if (sl >= (37.5)) then f12_2 = 0 BF12 = f12_1 * f12_2 y = 13.306 - 0.061935*BF1 - 0.14981*BF2 + 0.0018017*BF3 - 0.01205*BF4 + 0.64148*BF5 - 0.094225*BF6 - 0.41426*BF7 - 0.46506*BF8 + 1.0921*BF9 - 0.009344*BF10 - 0.00042349*BF11 + 0.0070384*BF12 </pre>
---	--

Table A2. Printout of model for the traversal phase of drivers that came to a rolling or complete stop.

<pre> if (d <= 12.5) then f1_1 = 0 if (12.5 < d < 37.5) then begin p1_1 = (2*(37.5) + (12.5) - 3*(20)) / ((37.5) - (12.5))^2 r1_1 = (2*(20) - (37.5) - (12.5)) / ((37.5) - (12.5))^3 f1_1 = p1_1*(d-(12.5))^2 + r1_1*(d-(12.5))^3 end if (d >= (37.5)) then f1_1 = d - (20) BF1 = f1_1 if (d <= 12.5) then f2_1 = -(d - (20)) if (12.5 < d < 37.5) then begin p2_1 = (3*(20) - 2*(12.5) - (37.5)) / ((12.5) - (37.5))^2 r2_1 = ((12.5) + (37.5) - 2*(20)) / ((12.5) - (37.5))^3 f2_1 = p2_1*(d-(37.5))^2 + r2_1*(d-(37.5))^3 end if (d >= (37.5)) then f2_1 = 0 BF2 = f2_1 if (d <= 2.5) then f3_1 = -(d - (5)) if (2.5 < d < 12.5) then begin p3_1 = (3*(5) - 2*(2.5) - (12.5)) / ((2.5) - (12.5))^2 r3_1 = ((2.5) + (12.5) - 2*(5)) / ((2.5) - (12.5))^3 f3_1 = p3_1*(d-(12.5))^2 + r3_1*(d-(12.5))^3 end if (d >= (12.5)) then f3_1 = 0 BF3 = f3_1 if (d <= 2.5) then f4_1 = 0 if (2.5 < d < 12.5) then begin p4_1 = (2*(12.5) + (2.5) - 3*(5)) / ((12.5) - (2.5))^2 r4_1 = (2*(5) - (12.5) - (2.5)) / ((12.5) - (2.5))^3 f4_1 = p4_1*(d-(2.5))^2 + r4_1*(d-(2.5))^3 end if (d >= (12.5)) then f4_1 = d - (5) if (sl <= 10.5) then f4_2 = 0 if (10.5 < sl < 37.5) then begin p4_2 = (2*(37.5) + (10.5) - 3*(20)) / ((37.5) - (10.5))^2 r4_2 = (2*(20) - (37.5) - (10.5)) / ((37.5) - (10.5))^3 f4_2 = p4_2*(sl-(10.5))^2 + r4_2*(sl-(10.5))^3 end if (sl >= (37.5)) then f4_2 = sl - (20) BF4 = f4_1 * f4_2 if (d <= 2.5) then f5_1 = 0 if (2.5 < d < 12.5) then begin p5_1 = (2*(12.5) + (2.5) - 3*(5)) / ((12.5) - (2.5))^2 r5_1 = (2*(5) - (12.5) - (2.5)) / ((12.5) - (2.5))^3 f5_1 = p5_1*(d-(2.5))^2 + r5_1*(d-(2.5))^3 end if (d >= (12.5)) then f5_1 = d - (5) if (sl <= 10.5) then f5_2 = -(sl - (20)) if (10.5 < sl < 37.5) then begin p5_2 = (3*(20) - 2*(10.5) - (37.5)) / ((10.5) - (37.5))^2 r5_2 = ((10.5) + (37.5) - 2*(20)) / ((10.5) - (37.5))^3 f5_2 = p5_2*(sl-(37.5))^2 + r5_2*(sl-(37.5))^3 end if (sl >= (37.5)) then f5_2 = 0 BF5 = f5_1 * f5_2 if (isroll <= 0) then f6_2 = 0 if (0 < isroll < 0.5) then begin p6_2 = (2*(0.5) + (0) - 3*(0)) / ((0.5) - (0))^2 r6_2 = (2*(0) - (0.5) - (0)) / ((0.5) - (0))^3 f6_2 = p6_2*(isroll-(0))^2 + r6_2*(isroll-(0))^3 end if (isroll >= (0.5)) then f6_2 = isroll - (0) BF6 = BF3 * f6_2 if (d <= 37.5) then f7_1 = -(d - (55)) if (37.5 < d < 77.5) then begin p7_1 = (3*(55) - 2*(37.5) - (77.5)) / ((37.5) - (77.5))^2 r7_1 = ((37.5) + (77.5) - 2*(55)) / ((37.5) - (77.5))^3 f7_1 = p7_1*(d-(77.5))^2 + r7_1*(d-(77.5))^3 end if (d >= (77.5)) then f7_1 = 0 BF7 = f7_1 if (turn <= 0) then f8_1 = 0 </pre>	<pre> if (0 < turn < 0.5) then begin p8_1 = (2*(0.5) + (0) - 3*(0)) / ((0.5) - (0))^2 r8_1 = (2*(0) - (0.5) - (0)) / ((0.5) - (0))^3 f8_1 = p8_1*(turn-(0))^2 + r8_1*(turn-(0))^3 end if (turn >= (0.5)) then f8_1 = turn - (0) BF8 = f8_1 if (d <= 2.5) then f9_1 = 0 if (2.5 < d < 12.5) then begin p9_1 = (2*(12.5) + (2.5) - 3*(5)) / ((12.5) - (2.5))^2 r9_1 = (2*(5) - (12.5) - (2.5)) / ((12.5) - (2.5))^3 f9_1 = p9_1*(d-(2.5))^2 + r9_1*(d-(2.5))^3 end if (d >= (12.5)) then f9_1 = d - (5) if (issenior <= 0.5) then f9_2 = -(issenior - (1)) if (0.5 < issenior < 1) then begin p9_2 = (3*(1) - 2*(0.5) - (1)) / ((0.5) - (1))^2 r9_2 = ((0.5) + (1) - 2*(1)) / ((0.5) - (1))^3 f9_2 = p9_2*(issenior-(1))^2 + r9_2*(issenior-(1))^3 end if (issenior >= (1)) then f9_2 = 0 BF9 = f9_1 * f9_2 if (isroll <= 0.5) then f10_3 = -(isroll - (1)) if (0.5 < isroll < 1) then begin p10_3 = (3*(1) - 2*(0.5) - (1)) / ((0.5) - (1))^2 r10_3 = ((0.5) + (1) - 2*(1)) / ((0.5) - (1))^3 f10_3 = p10_3*(isroll-(1))^2 + r10_3*(isroll-(1))^3 end if (isroll >= (1)) then f10_3 = 0 BF10 = BF4 * f10_3 if (tcd <= 1.5) then f11_3 = -(tcd - (2)) if (1.5 < tcd < 2) then begin p11_3 = (3*(2) - 2*(1.5) - (2)) / ((1.5) - (2))^2 r11_3 = ((1.5) + (2) - 2*(2)) / ((1.5) - (2))^3 f11_3 = p11_3*(tcd-(2))^2 + r11_3*(tcd-(2))^3 end if (tcd >= (2)) then f11_3 = 0 BF11 = BF4 * f11_3 if (isyounge <= 0) then f12_1 = 0 if (0 < isyounge < 0.5) then begin p12_1 = (2*(0.5) + (0) - 3*(0)) / ((0.5) - (0))^2 r12_1 = (2*(0) - (0.5) - (0)) / ((0.5) - (0))^3 f12_1 = p12_1*(isyounge-(0))^2 + r12_1*(isyounge-(0))^3 end if (isyounge >= (0.5)) then f12_1 = isyounge - (0) BF12 = f12_1 y = 10.117 +0.02794*BF1 -0.1401*BF2 -0.79903*BF3 +0.0016223*BF4 +0.00063186*BF5 +0.77133*BF6 -0.058128*BF7 -0.71169*BF8 +0.0075698*BF9 +0.0006273*BF10 -0.0012163*BF11 +0.31755*BF12 </pre>
---	---

Table A3. Printout of velocity versus distance model for approach phase of drivers that took a left turn while travelling through a signalized intersection.

<pre> if (d <= -75) then f1_1 = 0 if (-75 < d < -30) then begin p1_1 = (2*(-30) + (-75) - 3*(-50)) / ((-30) - (-75))^2 r1_1 = (2*(-50) - (-30) - (-75)) / ((-30) - (-75))^3 f1_1 = p1_1*(d-(-75))^2 + r1_1*(d-(-75))^3 end if (d >= (-30)) then f1_1 = d - (-50) BF1 = f1_1 if (d <= -75) then f2_1 = -(d - (-50)) if (-75 < d < -30) then begin p2_1 = (3*(-50) - 2*(-75) - (-30)) / ((-75) - (-30))^2 r2_1 = ((-75) + (-30) - 2*(-50)) / ((-75) - (-30))^3 f2_1 = p2_1*(d-(-30))^2 + r2_1*(d-(-30))^3 end if (d >= (-30)) then f2_1 = 0 if (sl <= 45) then f2_2 = 0 if (45 < sl < 52.5) then begin p2_2 = (2*(52.5) + (45) - 3*(50)) / ((52.5) - (45))^2 r2_2 = (2*(50) - (52.5) - (45)) / ((52.5) - (45))^3 f2_2 = p2_2*(sl-(45))^2 + r2_2*(sl-(45))^3 end if (sl >= (52.5)) then f2_2 = sl - (50) BF2 = f2_1 * f2_2 if (isyoun <= 0.5) then f3_1 = -(isyoun - (1)) if (0.5 < isyoun < 1) then begin p3_1 = (3*(1) - 2*(0.5) - (1)) / ((0.5) - (1))^2 r3_1 = ((0.5) + (1) - 2*(1)) / ((0.5) - (1))^3 f3_1 = p3_1*(isyoun-(1))^2 + r3_1*(isyoun-(1))^3 end if (isyoun >= (1)) then f3_1 = 0 if (sl <= 12.5) then f3_2 = 0 if (12.5 < sl < 27.5) then begin p3_2 = (2*(27.5) + (12.5) - 3*(15)) / ((27.5) - (12.5))^2 r3_2 = (2*(15) - (27.5) - (12.5)) / ((27.5) - (12.5))^3 f3_2 = p3_2*(sl-(12.5))^2 + r3_2*(sl-(12.5))^3 end if (sl >= (27.5)) then f3_2 = sl - (15) BF3 = f3_1 * f3_2 if (isyoun <= 0.5) then f4_1 = -(isyoun - (1)) if (0.5 < isyoun < 1) then begin p4_1 = (3*(1) - 2*(0.5) - (1)) / ((0.5) - (1))^2 r4_1 = ((0.5) + (1) - 2*(1)) / ((0.5) - (1))^3 f4_1 = p4_1*(isyoun-(1))^2 + r4_1*(isyoun-(1))^3 end if (isyoun >= (1)) then f4_1 = 0 if (sl <= 12.5) then f4_2 = -(sl - (15)) if (12.5 < sl < 27.5) then begin p4_2 = (3*(15) - 2*(12.5) - (27.5)) / ((12.5) - (27.5))^2 r4_2 = ((12.5) + (27.5) - 2*(15)) / ((12.5) - (27.5))^3 f4_2 = p4_2*(sl-(27.5))^2 + r4_2*(sl-(27.5))^3 end if (sl >= (27.5)) then f4_2 = 0 BF4 = f4_1 * f4_2 if (sl <= 27.5) then f5_1 = -(sl - (40)) if (27.5 < sl < 45) then begin p5_1 = (3*(40) - 2*(27.5) - (45)) / ((27.5) - (45))^2 r5_1 = ((27.5) + (45) - 2*(40)) / ((27.5) - (45))^3 f5_1 = p5_1*(sl-(45))^2 + r5_1*(sl-(45))^3 end if (sl >= (45)) then f5_1 = 0 BF5 = f5_1 if (d <= -30) then f6_1 = 0 if (-30 < d < -5) then begin p6_1 = (2*(-5) + (-30) - 3*(-10)) / ((-5) - (-30))^2 r6_1 = (2*(-10) - (-5) - (-30)) / ((-5) - (-30))^3 f6_1 = p6_1*(d-(-30))^2 + r6_1*(d-(-30))^3 end if (d >= (-5)) then f6_1 = d - (-10) BF6 = f6_1 if (d <= -30) then f7_1 = -(d - (-10)) if (-30 < d < -5) then begin p7_1 = (3*(-10) - 2*(-30) - (-5)) / ((-30) - (-5))^2 r7_1 = ((-30) + (-5) - 2*(-10)) / ((-30) - (-5))^3 f7_1 = p7_1*(d-(-5))^2 + r7_1*(d-(-5))^3 </pre>	<pre> end if (d >= (-5)) then f7_1 = 0 BF7 = f7_1 if (isold <= 0) then f8_1 = 0 if (0 < isold < 0.5) then begin p8_1 = (2*(0.5) + (0) - 3*(0)) / ((0.5) - (0))^2 r8_1 = (2*(0) - (0.5) - (0)) / ((0.5) - (0))^3 f8_1 = p8_1*(isold-(0))^2 + r8_1*(isold-(0))^3 end if (isold >= (0.5)) then f8_1 = isold - (0) BF8 = f8_1 if (sl <= 12.5) then f9_2 = 0 if (12.5 < sl < 27.5) then begin p9_2 = (2*(27.5) + (12.5) - 3*(15)) / ((27.5) - (12.5))^2 r9_2 = (2*(15) - (27.5) - (12.5)) / ((27.5) - (12.5))^3 f9_2 = p9_2*(sl-(12.5))^2 + r9_2*(sl-(12.5))^3 end if (sl >= (27.5)) then f9_2 = sl - (15) BF9 = BF1 * f9_2 if (d <= -75) then f10_1 = 0 if (-75 < d < -30) then begin p10_1 = (2*(-30) + (-75) - 3*(-50)) / ((-30) - (-75))^2 r10_1 = (2*(-50) - (-30) - (-75)) / ((-30) - (-75))^3 f10_1 = p10_1*(d-(-75))^2 + r10_1*(d-(-75))^3 end if (d >= (-30)) then f10_1 = d - (-50) if (sl <= 12.5) then f10_2 = -(sl - (15)) if (12.5 < sl < 27.5) then begin p10_2 = (3*(15) - 2*(12.5) - (27.5)) / ((12.5) - (27.5))^2 r10_2 = ((12.5) + (27.5) - 2*(15)) / ((12.5) - (27.5))^3 f10_2 = p10_2*(sl-(27.5))^2 + r10_2*(sl-(27.5))^3 end if (sl >= (27.5)) then f10_2 = 0 if (isyoun <= 0.5) then f10_3 = -(isyoun - (1)) if (0.5 < isyoun < 1) then begin p10_3 = (3*(1) - 2*(0.5) - (1)) / ((0.5) - (1))^2 r10_3 = ((0.5) + (1) - 2*(1)) / ((0.5) - (1))^3 f10_3 = p10_3*(isyoun-(1))^2 + r10_3*(isyoun-(1))^3 end if (isyoun >= (1)) then f10_3 = 0 BF10 = f10_1 * f10_2 * f10_3 if (sl <= 27.5) then f11_1 = 0 if (27.5 < sl < 45) then begin p11_1 = (2*(45) + (27.5) - 3*(40)) / ((45) - (27.5))^2 r11_1 = (2*(40) - (45) - (27.5)) / ((45) - (27.5))^3 f11_1 = p11_1*(sl-(27.5))^2 + r11_1*(sl-(27.5))^3 end if (sl >= (45)) then f11_1 = sl - (40) if (d <= -75) then f11_2 = 0 if (-75 < d < -30) then begin p11_2 = (2*(-30) + (-75) - 3*(-50)) / ((-30) - (-75))^2 r11_2 = (2*(-50) - (-30) - (-75)) / ((-30) - (-75))^3 f11_2 = p11_2*(d-(-75))^2 + r11_2*(d-(-75))^3 end if (d >= (-30)) then f11_2 = d - (-50) BF11 = f11_1 * f11_2 if (sl <= 27.5) then f12_1 = 0 if (27.5 < sl < 45) then begin p12_1 = (2*(45) + (27.5) - 3*(40)) / ((45) - (27.5))^2 r12_1 = (2*(40) - (45) - (27.5)) / ((45) - (27.5))^3 f12_1 = p12_1*(sl-(27.5))^2 + r12_1*(sl-(27.5))^3 end if (sl >= (45)) then f12_1 = sl - (40) if (d <= -75) then f12_2 = -(d - (-50)) if (-75 < d < -30) then begin p12_2 = (3*(-50) - 2*(-75) - (-30)) / ((-75) - (-30))^2 r12_2 = ((-75) + (-30) - 2*(-50)) / ((-75) - (-30))^3 f12_2 = p12_2*(d-(-30))^2 + r12_2*(d-(-30))^3 end if (d >= (-30)) then f12_2 = 0 BF12 = f12_1 * f12_2 y = 13.698 - 0.082337*BF1 - 0.022494*BF2 - 0.020313*BF3 + 3.7329*BF4 - 0.084238*BF5 + 0.10175*BF6 - 0.01759*BF7 - 0.32978*BF8 - 0.0016456*BF9 - 0.094934*BF10 + 0.0037205*BF11 + 0.0046223*BF12 </pre>
---	---

Table A4. Printout of velocity versus distance model for traversal phase of drivers that took a left turn while travelling through a signalized intersection.

<pre> if (d <= 35) then f1_1 = 0 if (35 < d < 80) then begin p1_1 = (2*(80) + (35) - 3*(60)) / ((80) - (35))^2 r1_1 = (2*(60) - (80) - (35)) / ((80) - (35))^3 f1_1 = p1_1*(d-(35))^2 + r1_1*(d-(35))^3 end if (d >= (80)) then f1_1 = d - (60) BF1 = f1_1 if (d <= 35) then f2_1 = -(d - (60)) if (35 < d < 80) then begin p2_1 = (3*(60) - 2*(35) - (80)) / ((35) - (80))^2 r2_1 = ((35) + (80) - 2*(60)) / ((35) - (80))^3 f2_1 = p2_1*(d-(80))^2 + r2_1*(d-(80))^3 end if (d >= (80)) then f2_1 = 0 BF2 = f2_1 if (sl <= 17.5) then f3_1 = 0 if (17.5 < sl < 32.5) then begin p3_1 = (2*(32.5) + (17.5) - 3*(20)) / ((32.5) - (17.5))^2 r3_1 = (2*(20) - (32.5) - (17.5)) / ((32.5) - (17.5))^3 f3_1 = p3_1*(sl-(17.5))^2 + r3_1*(sl-(17.5))^3 end if (sl >= (32.5)) then f3_1 = sl - (20) BF3 = f3_1 if (sl <= 17.5) then f4_1 = -(sl - (20)) if (17.5 < sl < 32.5) then begin p4_1 = (3*(20) - 2*(17.5) - (32.5)) / ((17.5) - (32.5))^2 r4_1 = ((17.5) + (32.5) - 2*(20)) / ((17.5) - (32.5))^3 f4_1 = p4_1*(sl-(32.5))^2 + r4_1*(sl-(32.5))^3 end if (sl >= (32.5)) then f4_1 = 0 BF4 = f4_1 if (d <= 7.5) then f5_2 = 0 if (7.5 < d < 35) then begin p5_2 = (2*(35) + (7.5) - 3*(10)) / ((35) - (7.5))^2 r5_2 = (2*(10) - (35) - (7.5)) / ((35) - (7.5))^3 f5_2 = p5_2*(d-(7.5))^2 + r5_2*(d-(7.5))^3 end if (d >= (35)) then f5_2 = d - (10) BF5 = BF3 * f5_2 if (d <= 7.5) then f6_2 = -(d - (10)) if (7.5 < d < 35) then begin p6_2 = (3*(10) - 2*(7.5) - (35)) / ((7.5) - (35))^2 r6_2 = ((7.5) + (35) - 2*(10)) / ((7.5) - (35))^3 f6_2 = p6_2*(d-(35))^2 + r6_2*(d-(35))^3 end if (d >= (35)) then f6_2 = 0 BF6 = BF3 * f6_2 if (isyoung <= 0) then f7_1 = 0 if (0 < isyoung < 0.5) then begin p7_1 = (2*(0.5) + (0) - 3*(0)) / ((0.5) - (0))^2 r7_1 = (2*(0) - (0.5) - (0)) / ((0.5) - (0))^3 f7_1 = p7_1*(isyoung-(0))^2 + r7_1*(isyoung-(0))^3 end if (isyoung >= (0.5)) then f7_1 = isyoung - (0) BF7 = f7_1 if (ismale <= 0) then f8_2 = 0 if (0 < ismale < 0.5) then begin p8_2 = (2*(0.5) + (0) - 3*(0)) / ((0.5) - (0))^2 r8_2 = (2*(0) - (0.5) - (0)) / ((0.5) - (0))^3 f8_2 = p8_2*(ismale-(0))^2 + r8_2*(ismale-(0))^3 end if (ismale >= (0.5)) then f8_2 = ismale - (0) BF8 = BF1 * f8_2 if (ismale <= 0.5) then f9_2 = -(ismale - (1)) if (0.5 < ismale < 1) then begin p9_2 = (3*(1) - 2*(0.5) - (1)) / ((0.5) - (1))^2 r9_2 = ((0.5) + (1) - 2*(1)) / ((0.5) - (1))^3 f9_2 = p9_2*(ismale-(1))^2 + r9_2*(ismale-(1))^3 end </pre>	<pre> if (ismale >= (1)) then f9_2 = 0 BF9 = BF7 * f9_2 if (sl <= 47.5) then f10_2 = 0 if (47.5 < sl < 52.5) then begin p10_2 = (2*(52.5) + (47.5) - 3*(50)) / ((52.5) - (47.5))^2 r10_2 = (2*(50) - (52.5) - (47.5)) / ((52.5) - (47.5))^3 f10_2 = p10_2*(sl-(47.5))^2 + r10_2*(sl-(47.5))^3 end if (sl >= (52.5)) then f10_2 = sl - (50) BF10 = BF7 * f10_2 if (sl <= 47.5) then f11_2 = -(sl - (50)) if (47.5 < sl < 52.5) then begin p11_2 = (3*(50) - 2*(47.5) - (52.5)) / ((47.5) - (52.5))^2 r11_2 = ((47.5) + (52.5) - 2*(50)) / ((47.5) - (52.5))^3 f11_2 = p11_2*(sl-(52.5))^2 + r11_2*(sl-(52.5))^3 end if (sl >= (52.5)) then f11_2 = 0 BF11 = BF7 * f11_2 if (sl <= 12.5) then f12_2 = 0 if (12.5 < sl < 17.5) then begin p12_2 = (2*(17.5) + (12.5) - 3*(15)) / ((17.5) - (12.5))^2 r12_2 = (2*(15) - (17.5) - (12.5)) / ((17.5) - (12.5))^3 f12_2 = p12_2*(sl-(12.5))^2 + r12_2*(sl-(12.5))^3 end if (sl >= (17.5)) then f12_2 = sl - (15) BF12 = BF1 * f12_2 if (sl <= 12.5) then f13_2 = -(sl - (15)) if (12.5 < sl < 17.5) then begin p13_2 = (3*(15) - 2*(12.5) - (17.5)) / ((12.5) - (17.5))^2 r13_2 = ((12.5) + (17.5) - 2*(15)) / ((12.5) - (17.5))^3 f13_2 = p13_2*(sl-(17.5))^2 + r13_2*(sl-(17.5))^3 end if (sl >= (17.5)) then f13_2 = 0 BF13 = BF1 * f13_2 if (sl <= 32.5) then f14_2 = -(sl - (45)) if (32.5 < sl < 47.5) then begin p14_2 = (3*(45) - 2*(32.5) - (47.5)) / ((32.5) - (47.5))^2 r14_2 = ((32.5) + (47.5) - 2*(45)) / ((32.5) - (47.5))^3 f14_2 = p14_2*(sl-(47.5))^2 + r14_2*(sl-(47.5))^3 end if (sl >= (47.5)) then f14_2 = 0 BF14 = BF7 * f14_2 if (d <= 2.5) then f15_3 = 0 if (2.5 < d < 7.5) then begin p15_3 = (2*(7.5) + (2.5) - 3*(5)) / ((7.5) - (2.5))^2 r15_3 = (2*(5) - (7.5) - (2.5)) / ((7.5) - (2.5))^3 f15_3 = p15_3*(d-(2.5))^2 + r15_3*(d-(2.5))^3 end if (d >= (7.5)) then f15_3 = d - (5) BF15 = BF9 * f15_3 if (d <= 2.5) then f16_3 = -(d - (5)) if (2.5 < d < 7.5) then begin p16_3 = (3*(5) - 2*(2.5) - (7.5)) / ((2.5) - (7.5))^2 r16_3 = ((2.5) + (7.5) - 2*(5)) / ((2.5) - (7.5))^3 f16_3 = p16_3*(d-(7.5))^2 + r16_3*(d-(7.5))^3 end if (d >= (7.5)) then f16_3 = 0 BF16 = BF9 * f16_3 y = 11.857 - 0.041537*BF1 - 0.079309*BF2 + 0.053571*BF3 + 0.13866*BF4 + 0.00054741*BF5 + 0.001609*BF6 - 0.96916*BF7 - 0.019657*BF8 - 1.0474*BF9 + 0.64901*BF10 + 0.32793*BF11 + 0.0019523*BF12 + 0.01531*BF13 - 0.3136*BF14 + 0.0082424*BF15 + 0.082534*BF16 </pre>
---	--

Table A5. Printout of velocity versus distance model for approach phase of non-turning drivers travelling through a signalized intersection.

<pre> if (sl <= 15) then f1_1 = 0 if (15 < sl < 27.5) then begin p1_1 = (2*(27.5) + (15) - 3*(25)) / ((27.5) - (15))^2 r1_1 = (2*(25) - (27.5) - (15)) / ((27.5) - (15))^3 f1_1 = p1_1*(sl-(15))^2 + r1_1*(sl-(15))^3 end if (sl >= (27.5)) then f1_1 = sl - (25) BF1 = f1_1 if (isold <= 0) then f2_1 = 0 if (0 < isold < 0.5) then begin p2_1 = (2*(0.5) + (0) - 3*(0)) / ((0.5) - (0))^2 r2_1 = (2*(0) - (0.5) - (0)) / ((0.5) - (0))^3 f2_1 = p2_1*(isold-(0))^2 + r2_1*(isold-(0))^3 end if (isold >= (0.5)) then f2_1 = isold - (0) BF2 = f2_1 if (d <= -82.5) then f3_1 = 0 if (-82.5 < d < -32.5) then begin p3_1 = (2*(-32.5) + (-82.5) - 3*(-65)) / ((-32.5) - (-82.5))^2 r3_1 = (2*(-65) - (-32.5) - (-82.5)) / ((-32.5) - (-82.5))^3 f3_1 = p3_1*(d-(-82.5))^2 + r3_1*(d-(-82.5))^3 end if (d >= (-32.5)) then f3_1 = d - (-65) BF3 = f3_1 if (d <= -82.5) then f4_1 = -(d - (-65)) if (-82.5 < d < -32.5) then begin p4_1 = (3*(-65) - 2*(-82.5) - (-32.5)) / ((-82.5) - (-32.5))^2 r4_1 = ((-82.5) + (-32.5) - 2*(-65)) / ((-82.5) - (-32.5))^3 f4_1 = p4_1*(d-(-32.5))^2 + r4_1*(d-(-32.5))^3 end if (d >= (-32.5)) then f4_1 = 0 BF4 = f4_1 if (isyoung <= 0.5) then f5_1 = -(isyoung - (1)) if (0.5 < isyoung < 1) then begin p5_1 = (3*(1) - 2*(0.5) - (1)) / ((0.5) - (1))^2 r5_1 = ((0.5) + (1) - 2*(1)) / ((0.5) - (1))^3 f5_1 = p5_1*(isyoung-(1))^2 + r5_1*(isyoung-(1))^3 end if (isyoung >= (1)) then f5_1 = 0 BF5 = f5_1 if (sl <= 27.5) then f6_1 = 0 if (27.5 < sl < 31.5) then begin p6_1 = (2*(31.5) + (27.5) - 3*(30)) / ((31.5) - (27.5))^2 r6_1 = (2*(30) - (31.5) - (27.5)) / ((31.5) - (27.5))^3 f6_1 = p6_1*(sl-(27.5))^2 + r6_1*(sl-(27.5))^3 end if (sl >= (31.5)) then f6_1 = sl - (30) BF6 = f6_1 if (sl <= 36.5) then f7_1 = -(sl - (40)) if (36.5 < sl < 42.5) then begin p7_1 = (3*(40) - 2*(36.5) - (42.5)) / ((36.5) - (42.5))^2 r7_1 = ((36.5) + (42.5) - 2*(40)) / ((36.5) - (42.5))^3 f7_1 = p7_1*(sl-(42.5))^2 + r7_1*(sl-(42.5))^3 end if (sl >= (42.5)) then f7_1 = 0 BF7 = f7_1 if (ismale <= 0) then f8_2 = 0 if (0 < ismale < 0.5) then begin p8_2 = (2*(0.5) + (0) - 3*(0)) / ((0.5) - (0))^2 r8_2 = (2*(0) - (0.5) - (0)) / ((0.5) - (0))^3 f8_2 = p8_2*(ismale-(0))^2 + r8_2*(ismale-(0))^3 end if (ismale >= (0.5)) then f8_2 = ismale - (0) BF8 = BF2 * f8_2 if (sl <= 50) then f9_3 = 0 if (50 < sl < 60) then begin p9_3 = (2*(60) + (50) - 3*(55)) / ((60) - (50))^2 r9_3 = (2*(55) - (60) - (50)) / ((60) - (50))^3 f9_3 = p9_3*(sl-(50))^2 + r9_3*(sl-(50))^3 end </pre>	<pre> if (sl >= (60)) then f9_3 = sl - (55) BF9 = BF8 * f9_3 if (sl <= 42.5) then f10_1 = 0 if (42.5 < sl < 50) then begin p10_1 = (2*(50) + (42.5) - 3*(45)) / ((50) - (42.5))^2 r10_1 = (2*(45) - (50) - (42.5)) / ((50) - (42.5))^3 f10_1 = p10_1*(sl-(42.5))^2 + r10_1*(sl-(42.5))^3 end if (sl >= (50)) then f10_1 = sl - (45) BF10 = f10_1 if (sl <= 42.5) then f11_1 = -(sl - (45)) if (42.5 < sl < 50) then begin p11_1 = (3*(45) - 2*(42.5) - (50)) / ((42.5) - (50))^2 r11_1 = ((42.5) + (50) - 2*(45)) / ((42.5) - (50))^3 f11_1 = p11_1*(sl-(50))^2 + r11_1*(sl-(50))^3 end if (sl >= (50)) then f11_1 = 0 BF11 = f11_1 if (sl <= 31.5) then f12_1 = 0 if (31.5 < sl < 36.5) then begin p12_1 = (2*(36.5) + (31.5) - 3*(33)) / ((36.5) - (31.5))^2 r12_1 = (2*(33) - (36.5) - (31.5)) / ((36.5) - (31.5))^3 f12_1 = p12_1*(sl-(31.5))^2 + r12_1*(sl-(31.5))^3 end if (sl >= (36.5)) then f12_1 = sl - (33) BF12 = f12_1 y = 14.532 - 0.33156*BF1 - 1.0053*BF2 + 0.017158*BF3 + 0.022491*BF4 - 0.83376*BF5 + 0.93488*BF6 + 0.19719*BF7 + 0.34721*BF8 + 1.1231*BF9 + 0.10861*BF10 - 0.089475*BF11 - 0.31659*BF12 </pre>
---	--

Table A6. Printout of velocity versus distance model for the traversal phase of non-turning drivers travelling through a signalized intersection.

<pre> if (sl <= 31.5) then f1_1 = 0 if (31.5 < sl < 34) then begin p1_1 = (2*(34) + (31.5) - 3*(33)) / ((34) - (31.5))^2 r1_1 = (2*(33) - (34) - (31.5)) / ((34) - (31.5))^3 f1_1 = p1_1*(sl-(31.5))^2 + r1_1*(sl-(31.5))^3 end if (sl >= (34)) then f1_1 = sl - (33) BF1 = f1_1 if (isyoung <= 0) then f2_1 = 0 if (0 < isyoung < 0.5) then begin p2_1 = (2*(0.5) + (0) - 3*(0)) / ((0.5) - (0))^2 r2_1 = (2*(0) - (0.5) - (0)) / ((0.5) - (0))^3 f2_1 = p2_1*(isyoung-(0))^2 + r2_1*(isyoung-(0))^3 end if (isyoung >= (0.5)) then f2_1 = isyoung - (0) BF2 = f2_1 if (d <= 22.5) then f3_1 = 0 if (22.5 < d < 72.5) then begin p3_1 = (2*(72.5) + (22.5) - 3*(45)) / ((72.5) - (22.5))^2 r3_1 = (2*(45) - (72.5) - (22.5)) / ((72.5) - (22.5))^3 f3_1 = p3_1*(d-(22.5))^2 + r3_1*(d-(22.5))^3 end if (d >= (72.5)) then f3_1 = d - (45) BF3 = f3_1 if (d <= 22.5) then f4_1 = -(d - (45)) if (22.5 < d < 72.5) then begin p4_1 = (3*(45) - 2*(22.5) - (72.5)) / ((22.5) - (72.5))^2 r4_1 = ((22.5) + (72.5) - 2*(45)) / ((22.5) - (72.5))^3 f4_1 = p4_1*(d-(72.5))^2 + r4_1*(d-(72.5))^3 end if (d >= (72.5)) then f4_1 = 0 BF4 = f4_1 if (sl <= 15) then f5_1 = 0 if (15 < sl < 22.5) then begin p5_1 = (2*(22.5) + (15) - 3*(20)) / ((22.5) - (15))^2 r5_1 = (2*(20) - (22.5) - (15)) / ((22.5) - (15))^3 f5_1 = p5_1*(sl-(15))^2 + r5_1*(sl-(15))^3 end if (sl >= (22.5)) then f5_1 = sl - (20) BF5 = f5_1 if (sl <= 15) then f6_1 = -(sl - (20)) if (15 < sl < 22.5) then begin p6_1 = (3*(20) - 2*(15) - (22.5)) / ((15) - (22.5))^2 r6_1 = ((15) + (22.5) - 2*(20)) / ((15) - (22.5))^3 f6_1 = p6_1*(sl-(22.5))^2 + r6_1*(sl-(22.5))^3 end if (sl >= (22.5)) then f6_1 = 0 BF6 = f6_1 if (isold <= 0.5) then f7_1 = -(isold - (1)) if (0.5 < isold < 1) then begin p7_1 = (3*(1) - 2*(0.5) - (1)) / ((0.5) - (1))^2 r7_1 = ((0.5) + (1) - 2*(1)) / ((0.5) - (1))^3 f7_1 = p7_1*(isold-(1))^2 + r7_1*(isold-(1))^3 end if (isold >= (1)) then f7_1 = 0 BF7 = f7_1 if (sl <= 27.5) then f8_1 = 0 if (27.5 < sl < 31.5) then begin p8_1 = (2*(31.5) + (27.5) - 3*(30)) / ((31.5) - (27.5))^2 r8_1 = (2*(30) - (31.5) - (27.5)) / ((31.5) - (27.5))^3 f8_1 = p8_1*(sl-(27.5))^2 + r8_1*(sl-(27.5))^3 end if (sl >= (31.5)) then f8_1 = sl - (30) BF8 = f8_1 if (sl <= 34) then f9_1 = 0 if (34 < sl < 37.5) then begin p9_1 = (2*(37.5) + (34) - 3*(35)) / ((37.5) - (34))^2 r9_1 = (2*(35) - (37.5) - (34)) / ((37.5) - (34))^3 f9_1 = p9_1*(sl-(34))^2 + r9_1*(sl-(34))^3 end </pre>	<pre> if (sl >= (37.5)) then f9_1 = sl - (35) BF9 = f9_1 if (sl <= 37.5) then f10_2 = 0 if (37.5 < sl < 52.5) then begin p10_2 = (2*(52.5) + (37.5) - 3*(40)) / ((52.5) - (37.5))^2 r10_2 = (2*(40) - (52.5) - (37.5)) / ((52.5) - (37.5))^3 f10_2 = p10_2*(sl-(37.5))^2 + r10_2*(sl-(37.5))^3 end if (sl >= (52.5)) then f10_2 = sl - (40) BF10 = BF3 * f10_2 if (sl <= 37.5) then f11_2 = -(sl - (40)) if (37.5 < sl < 52.5) then begin p11_2 = (3*(40) - 2*(37.5) - (52.5)) / ((37.5) - (52.5))^2 r11_2 = ((37.5) + (52.5) - 2*(40)) / ((37.5) - (52.5))^3 f11_2 = p11_2*(sl-(52.5))^2 + r11_2*(sl-(52.5))^3 end if (sl >= (52.5)) then f11_2 = 0 BF11 = BF3 * f11_2 if (sl <= 22.5) then f12_1 = -(sl - (25)) if (22.5 < sl < 27.5) then begin p12_1 = (3*(25) - 2*(22.5) - (27.5)) / ((22.5) - (27.5))^2 r12_1 = ((22.5) + (27.5) - 2*(25)) / ((22.5) - (27.5))^3 f12_1 = p12_1*(sl-(27.5))^2 + r12_1*(sl-(27.5))^3 end if (sl >= (27.5)) then f12_1 = 0 BF12 = f12_1 if (sl <= 5.5) then f13_2 = 0 if (5.5 < sl < 15) then begin p13_2 = (2*(15) + (5.5) - 3*(10)) / ((15) - (5.5))^2 r13_2 = (2*(10) - (15) - (5.5)) / ((15) - (5.5))^3 f13_2 = p13_2*(sl-(5.5))^2 + r13_2*(sl-(5.5))^3 end if (sl >= (15)) then f13_2 = sl - (10) BF13 = BF7 * f13_2 if (sl <= 5.5) then f14_2 = -(sl - (10)) if (5.5 < sl < 15) then begin p14_2 = (3*(10) - 2*(5.5) - (15)) / ((5.5) - (15))^2 r14_2 = ((5.5) + (15) - 2*(10)) / ((5.5) - (15))^3 f14_2 = p14_2*(sl-(15))^2 + r14_2*(sl-(15))^3 end if (sl >= (15)) then f14_2 = 0 BF14 = BF7 * f14_2 y = 20.285 - 2.9861*BF1 + 0.94698*BF2 + 0.0034605*BF3 - 0.010054*BF4 - 0.74082*BF5 + 1.4095*BF6 + 0.91477*BF7 + 2.3378*BF8 + 1.6836*BF9 + 0.00086277*BF10 + 0.00025168*BF11 - 1.1394*BF12 - 0.0081437*BF13 - 0.69938*BF14 </pre>
--	---

Table A7. Printout of acceleration versus distance model for approach phase of left-turning drivers travelling through a signalized intersection.

<pre> if (d <= -69.517) then f1_1 = 0 if (-69.517 < d < -9.8368) then begin p1_1 = (2*(-9.8368) + (-69.517) - 3*(-13.007)) / ((-9.8368) - (-69.517))^2 r1_1 = (2*(-13.007) - (-9.8368) - (-69.517)) / ((-9.8368) - (-69.517))^3 f1_1 = p1_1*(d-(-69.517))^2 + r1_1*(d-(-69.517))^3 end if (d >= (-9.8368)) then f1_1 = d - (-13.007) BF1 = f1_1 if (d <= -69.517) then f2_1 = -(d - (-13.007)) if (-69.517 < d < -9.8368) then begin p2_1 = (3*(-13.007) - 2*(-69.517) - (-9.8368)) / ((-69.517) - (-9.8368))^2 r2_1 = ((-69.517) + (-9.8368) - 2*(-13.007)) / ((-69.517) - (-9.8368))^3 f2_1 = p2_1*(d-(-9.8368))^2 + r2_1*(d-(-9.8368))^3 end if (d >= (-9.8368)) then f2_1 = 0 BF2 = f2_1 if (sl <= 12.5) then f3_1 = 0 if (12.5 < sl < 17.5) then begin p3_1 = (2*(17.5) + (12.5) - 3*(15)) / ((17.5) - (12.5))^2 r3_1 = (2*(15) - (17.5) - (12.5)) / ((17.5) - (12.5))^3 f3_1 = p3_1*(sl-(12.5))^2 + r3_1*(sl-(12.5))^3 end if (sl >= (17.5)) then f3_1 = sl - (15) BF3 = f3_1 if (sl <= 12.5) then f4_1 = -(sl - (15)) if (12.5 < sl < 17.5) then begin p4_1 = (3*(15) - 2*(12.5) - (17.5)) / ((12.5) - (17.5))^2 r4_1 = ((12.5) + (17.5) - 2*(15)) / ((12.5) - (17.5))^3 f4_1 = p4_1*(sl-(17.5))^2 + r4_1*(sl-(17.5))^3 end if (sl >= (17.5)) then f4_1 = 0 BF4 = f4_1 if (entry_speed <= 5.4167) then f5_1 = 0 if (5.4167 < entry_speed < 13.472) then begin p5_1 = (2*(13.472) + (5.4167) - 3*(6.1111)) / ((13.472) - (5.4167))^2 r5_1 = (2*(6.1111) - (13.472) - (5.4167)) / ((13.472) - (5.4167))^3 f5_1 = p5_1*(entry_speed-(5.4167))^2 + r5_1*(entry_speed-(5.4167))^3 end if (entry_speed >= (13.472)) then f5_1 = entry_speed - (6.1111) BF5 = f5_1 if (entry_speed <= 5.4167) then f6_1 = -(entry_speed - (6.1111)) if (5.4167 < entry_speed < 13.472) then begin p6_1 = (3*(6.1111) - 2*(5.4167) - (13.472)) / ((5.4167) - (13.472))^2 r6_1 = ((5.4167) + (13.472) - 2*(6.1111)) / ((5.4167) - (13.472))^3 f6_1 = p6_1*(entry_speed-(13.472))^2 + r6_1*(entry_speed-(13.472))^3 end if (entry_speed >= (13.472)) then f6_1 = 0 BF6 = f6_1 if (d <= -9.8368) then f7_2 = 0 if (-9.8368 < d < -3.3333) then begin p7_2 = (2*(-3.3333) + (-9.8368) - 3*(-6.6667)) / ((-3.3333) - (-9.8368))^2 r7_2 = (2*(-6.6667) - (-3.3333) - (-9.8368)) / ((-3.3333) - (-9.8368))^3 f7_2 = p7_2*(d-(-9.8368))^2 + r7_2*(d-(-9.8368))^3 end if (d >= (-3.3333)) then f7_2 = d - (-6.6667) BF7 = BF5 * f7_2 if (d <= -9.8368) then f8_2 = -(d - (-6.6667)) if (-9.8368 < d < -3.3333) then begin p8_2 = (3*(-6.6667) - 2*(-9.8368) - (-3.3333)) / ((-9.8368) - (-3.3333))^2 r8_2 = ((-9.8368) + (-3.3333) - 2*(-6.6667)) / ((-9.8368) - (-3.3333))^3 f8_2 = p8_2*(d-(-3.3333))^2 + r8_2*(d-(-3.3333))^3 end if (d >= (-3.3333)) then f8_2 = 0 BF8 = BF5 * f8_2 if (sl <= 17.5) then f9_2 = 0 if (17.5 < sl < 37.5) then begin p9_2 = (2*(37.5) + (17.5) - 3*(20)) / ((37.5) - (17.5))^2 r9_2 = (2*(20) - (37.5) - (17.5)) / ((37.5) - (17.5))^3 f9_2 = p9_2*(sl-(17.5))^2 + r9_2*(sl-(17.5))^3 </pre>	<pre> if (sl >= (37.5)) then f10_2 = 0 BF10 = BF5 * f10_2 if (entry_speed <= 2.3611) then f11_2 = 0 if (2.3611 < entry_speed < 5.4167) then begin p11_2 = (2*(5.4167) + (2.3611) - 3*(4.7222)) / ((5.4167) - (2.3611))^2 r11_2 = (2*(4.7222) - (5.4167) - (2.3611)) / ((5.4167) - (2.3611))^3 f11_2 = p11_2*(entry_speed-(2.3611))^2 + r11_2*(entry_speed-(2.3611))^3 end if (entry_speed >= (5.4167)) then f11_2 = entry_speed - (4.7222) BF11 = BF1 * f11_2 if (entry_speed <= 2.3611) then f12_2 = -(entry_speed - (4.7222)) if (2.3611 < entry_speed < 5.4167) then begin p12_2 = (3*(4.7222) - 2*(2.3611) - (5.4167)) / ((2.3611) - (5.4167))^2 r12_2 = ((2.3611) + (5.4167) - 2*(4.7222)) / ((2.3611) - (5.4167))^3 f12_2 = p12_2*(entry_speed-(5.4167))^2 + r12_2*(entry_speed-(5.4167))^3 end if (entry_speed >= (5.4167)) then f12_2 = 0 BF12 = BF1 * f12_2 if (sl <= 17.5) then f13_2 = -(sl - (20)) if (17.5 < sl < 37.5) then begin p13_2 = (3*(20) - 2*(17.5) - (37.5)) / ((17.5) - (37.5))^2 r13_2 = ((17.5) + (37.5) - 2*(20)) / ((17.5) - (37.5))^3 f13_2 = p13_2*(sl-(37.5))^2 + r13_2*(sl-(37.5))^3 end if (sl >= (37.5)) then f13_2 = 0 BF13 = BF1 * f13_2 if (isseniior <= 0.5) then f14_1 = -(isseniior - (1)) if (0.5 < isseniior < 1) then begin p14_1 = (3*(1) - 2*(0.5) - (1)) / ((0.5) - (1))^2 r14_1 = ((0.5) + (1) - 2*(1)) / ((0.5) - (1))^3 f14_1 = p14_1*(isseniior-(1))^2 + r14_1*(isseniior-(1))^3 end if (isseniior >= (1)) then f14_1 = 0 BF14 = f14_1 if (d <= -69.517) then f15_1 = 0 if (-69.517 < d < -9.8368) then begin p15_1 = (2*(-9.8368) + (-69.517) - 3*(-13.007)) / ((-9.8368) - (-69.517))^2 r15_1 = (2*(-13.007) - (-9.8368) - (-69.517)) / ((-9.8368) - (-69.517))^3 f15_1 = p15_1*(d-(-69.517))^2 + r15_1*(d-(-69.517))^3 end if (d >= (-9.8368)) then f15_1 = d - (-13.007) if (sl <= 17.5) then f15_2 = 0 if (17.5 < sl < 37.5) then begin p15_2 = (2*(37.5) + (17.5) - 3*(20)) / ((37.5) - (17.5))^2 r15_2 = (2*(20) - (37.5) - (17.5)) / ((37.5) - (17.5))^3 f15_2 = p15_2*(sl-(17.5))^2 + r15_2*(sl-(17.5))^3 end if (sl >= (37.5)) then f15_2 = sl - (20) if (isseniior <= 0.5) then f15_3 = -(isseniior - (1)) if (0.5 < isseniior < 1) then begin p15_3 = (3*(1) - 2*(0.5) - (1)) / ((0.5) - (1))^2 r15_3 = ((0.5) + (1) - 2*(1)) / ((0.5) - (1))^3 f15_3 = p15_3*(isseniior-(1))^2 + r15_3*(isseniior-(1))^3 end if (isseniior >= (1)) then f15_3 = 0 BF15 = f15_1 * f15_2 * f15_3 if (d <= -126.24) then f16_3 = 0 if (-126.24 < d < -69.517) then begin p16_3 = (2*(-69.517) + (-126.24) - 3*(-126.03)) / ((-69.517) - (-126.24))^2 r16_3 = (2*(-126.03) - (-69.517) - (-126.24)) / ((-69.517) - (-126.24))^3 f16_3 = p16_3*(d-(-126.24))^2 + r16_3*(d-(-126.24))^3 end if (d >= (-69.517)) then f16_3 = d - (-126.03) BF16 = BF9 * f16_3 if (d <= -126.24) then f17_3 = -(d - (-126.03)) if (-126.24 < d < -69.517) then begin p17_3 = (3*(-126.03) - 2*(-126.24) - (-69.517)) / ((-126.24) - (-69.517))^2 r17_3 = ((-126.24) + (-69.517) - 2*(-126.03)) / ((-126.24) - (-69.517))^3 f17_3 = p17_3*(d-(-69.517))^2 + r17_3*(d-(-69.517))^3 end if (d >= (-69.517)) then f17_3 = 0 </pre>
---	--

<pre> end if (sl >= (37.5)) then f9_2 = sl - (20) BF9 = BF5 * f9_2 if (sl <= 17.5) then f10_2 = -(sl - (20)) if (17.5 < sl < 37.5) then begin p10_2 = (3*(20) - 2*(17.5) - (37.5)) / ((17.5) - (37.5))^2 r10_2 = ((17.5) + (37.5) - 2*(20)) / ((17.5) - (37.5))^3 f10_2 = p10_2*(sl-(37.5))^2 + r10_2*(sl-(37.5))^3 end </pre>	<pre> BF17 = BF9 * f17_3 y = -0.68883 +0.029864*BF1 +0.0067515*BF2 -0.004821*BF3 +0.24995*BF4 +0.11631*BF5 +0.10855*BF6 -0.015595*BF7 - 0.00090795*BF8 -0.0046825*BF9 -0.045731*BF10 +0.0046381*BF11 - 0.079854*BF12 +0.0080147*BF13 -0.12327*BF14 +0.00080716*BF15 +4.1176e-05*BF16 -0.00026563*BF17 </pre>
--	--

Protocol for Manual Review of Scene Evidence from SCP and LTAP/LD Intersection Crashes

Protocol Written By John Scanlon

**For use in completion of the “Safety Benefits of Intersection Assistance Systems”
sponsored by the Toyota Collaborative Safety Research Center**

Intersection Case Review

The protocol has two general steps. First, a series of questions must be answered within the case viewer. These questions are intended to (1) verify the crash as a SCP or LTAP/LD crash at an intersection, (2) describe intersection characteristics, and (3) examine the scene for potential sight obstructions. Second, measurements should be taken from the scene diagram. These measurements will allow for reconstruction of the vehicle path prior to impact. Spreadsheets will be used for all measurement inputs. The sheets will contain the key for identifying the vehicle, and columns to enter variables of interest.

Enter into Case Viewer

1) Is the crash a valid intersection crash?

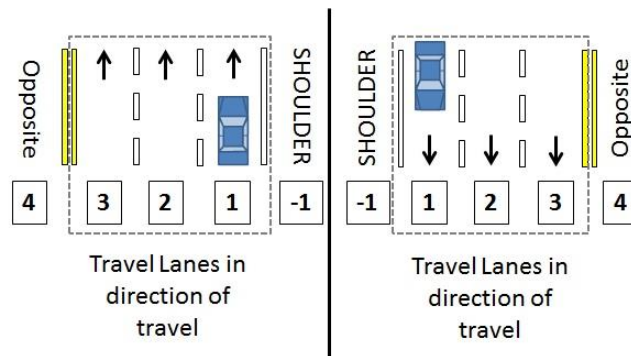
The reviewer will select either yes or no in the drop down. If a series of crashes occurs, the order of collisions is generally clearly marked. If it is still not clear, the reviewer will select unknown. Cases should be marked as invalid if any of the following are true:

- a. The case depicted was incorrectly marked as a SCP or LTAP/LD intersection crash (put **“Not Valid”** into the Leave Message for Case).
- b. The Case is missing important information
 - i. If photos are missing, put **“Photo”** into the Leave Message for Case.
 - ii. If the scene diagram is missing, put **“Diagram”** into the Leave Message for Case.

If the case is marked as not being valid... Click the first option for all remaining questions, save the answers, and move onto the next case.

2) Intersection Characteristics.

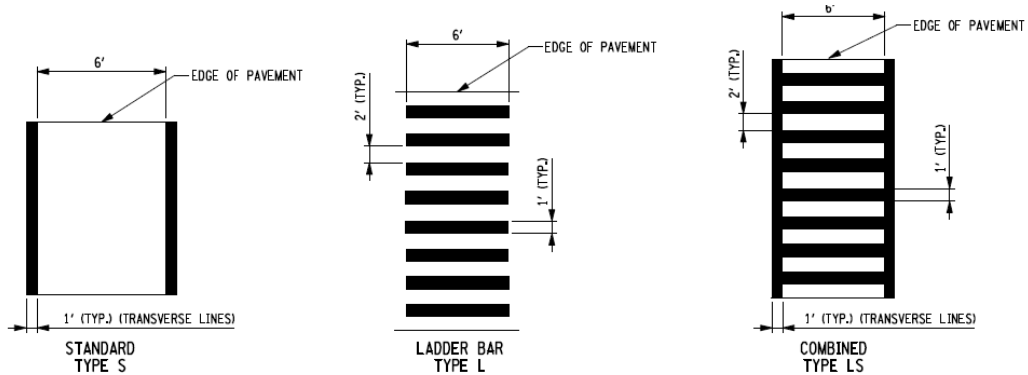
There will be six total inputs of the intersection characteristics. For each vehicle there will be three variables. First, the total number of lanes on the road being traveled on by both vehicles should be recorded. As an example, there are four total number of lanes for both instances shown below. Second, the number of lanes in the travel direction should be recorded. As an example, there are three total number of lanes in the travel direction for both instances shown below. Third, the travel lane should be recorded. For the examples below, the vehicles travel lane is 1. The parking lane should NOT be included when counting lanes.



3) From scene photos, was a stop bar present?

4) From scene photos, was a crosswalk present, and what type was it?

The type of crosswalks (e.g. S, L, LS type, or other) are provided below.



5) From vehicle approach photos, does terrain obstruct vision of vehicles entering the intersection?

This should be analyzed for both vehicles at the farthest back photo of the vehicle approaching the intersection. Potential terrain sight obstructions include a crest in the road or a median with trees in it.

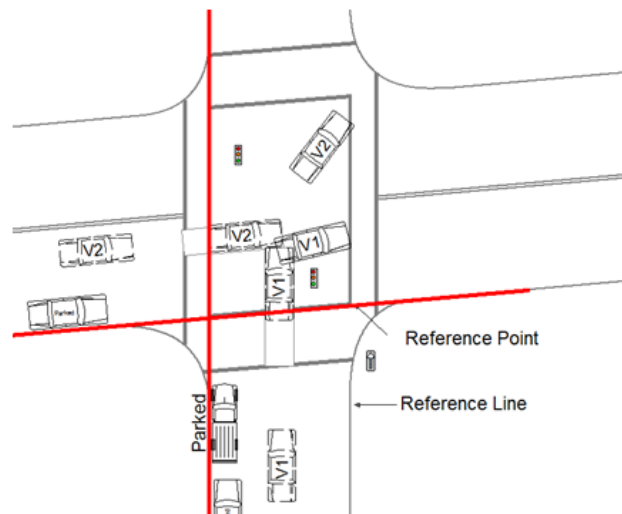
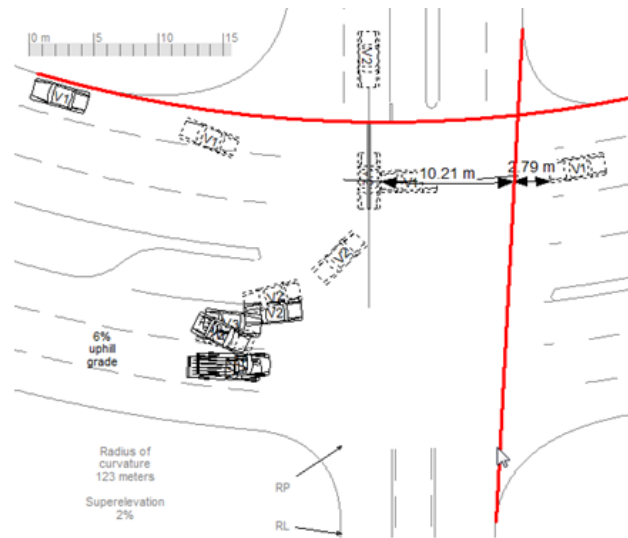
6) From vehicle approach photos, are there any objects on the side of the road that could obstruct vision?

This should be analyzed for both vehicles at the farthest back photo of the vehicle approaching the intersection. From this farthest back photo, if the view of the stop bar/ crosswalk of an entering vehicle is obstructed, the type of object should be entered into the program. Potential object sight obstructions include things like trees or parked vehicles.

Enter into the Measurement Spreadsheet

1) Draw the intersection boundary line.

This can be done by extrapolating the road edge through the intersection. This ONLY needs to be done for the corner between the two vehicle trajectories (as shown below).

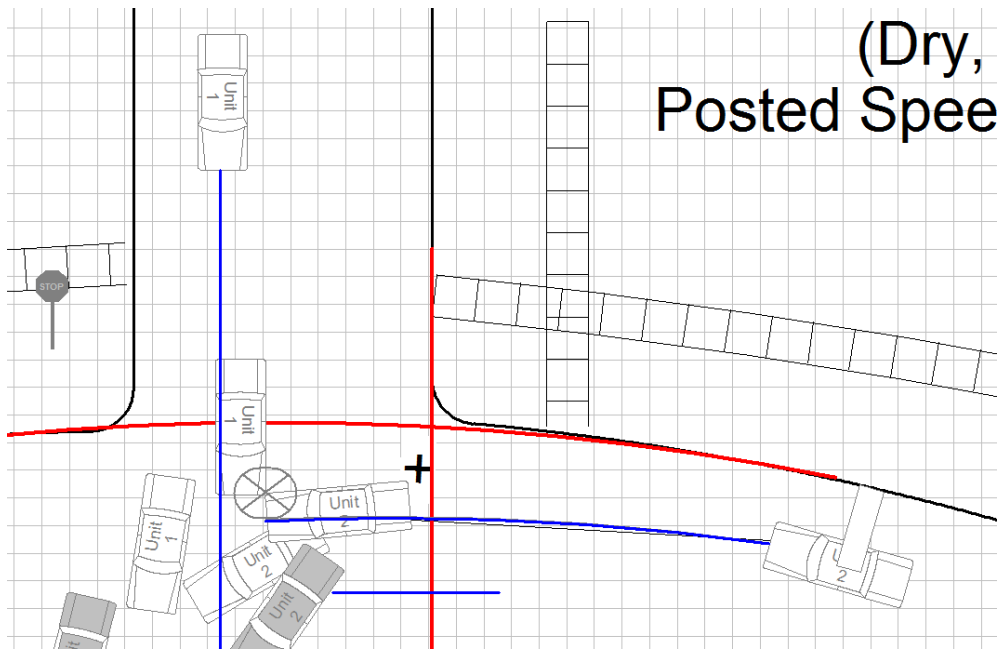


2) Draw the vehicle trajectory lines.

This line should be extrapolated from the front center of the vehicle in the direction of:

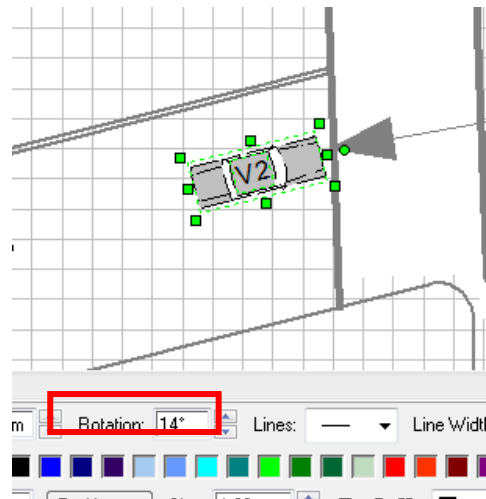
- a. The vehicle heading if the vehicle is travelling straight.
- b. Along the turning radius if the road has a radius of curvature.

In the case depicted, Vehicle 1 is travelling straight, and Vehicle 2 is travelling on a curved road. Vehicle 1's trajectory line can be drawn using a line or 0cm width rectangle. The rectangle should be used when the vehicle heading is not an increment of 90 degrees. The Vehicle 2 trajectory line should be drawn at the radius of curvature of Vehicle 2. In this case, you would find the outside road edge radius of curvature, and subtract the perpendicular distance to the center line of vehicle 2. The arc tool can then be used to draw the vehicle's trajectory throughout the turn.

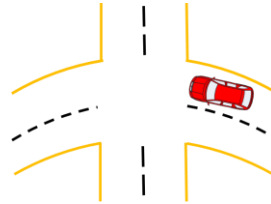


3) What are the vehicle headings?

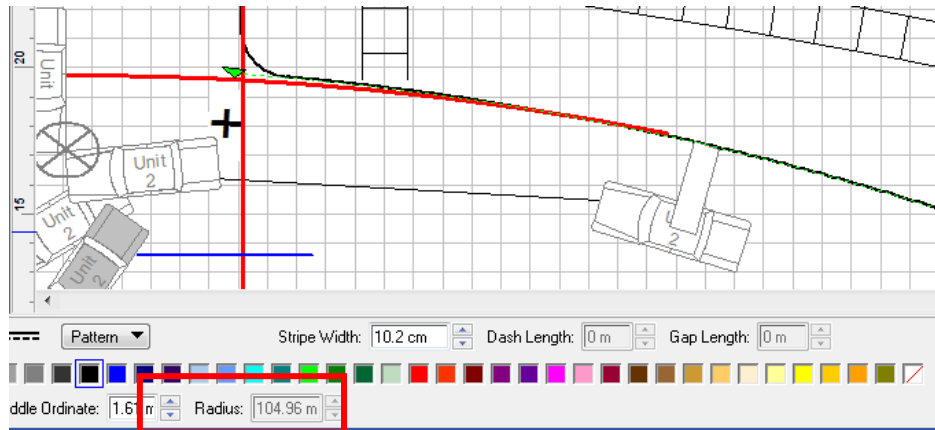
The reviewer will input angles in degrees as shown below. Vehicle angles can be extracted from the scene photograph by selecting the vehicles, while in the symbols layer, and looking at the rotation variable in the bottom left panel of the screen. This measurement should be taken at the last position before any evasive maneuvering. For turning vehicles, vehicle heading should additionally be recorded at the point of impact



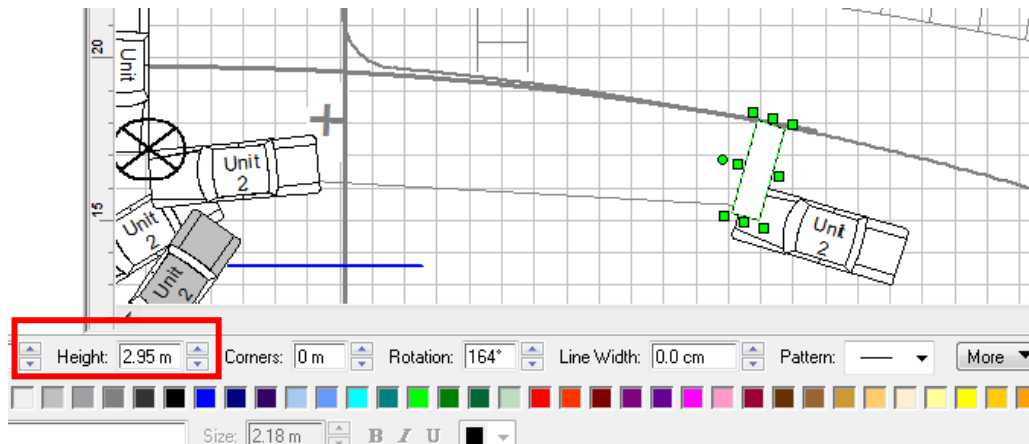
- 5) Finding the vehicle turning radius? This measurement should only be found for cases where the road was curved through the intersection (depicted below).



The vehicle turning radius of curvature can be found in two steps. **First**, double click the outside road edge. This will reveal this road edges radius or curvature, which is placed in a red box in the figure below. The road edge radius of curvature is 104.96 meters.



Second, use a rectangle perpendicular to the vehicle heading at any depicted location prior to evasive maneuvering to find the difference between the road edge radius of curvature and the vehicle turning radius of curvature. In the depicted figure below, the difference in radius is 2.95 meters.

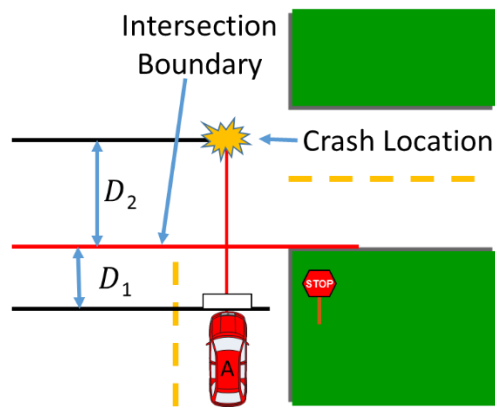


Using these two measurements, we find the vehicle turning radius of curvature to be $104.96 \text{ m} - 2.95 \text{ m}$ or approximately 102 m.

- 6) Determine the longitudinal travelling distance from the encroachment location for vehicles

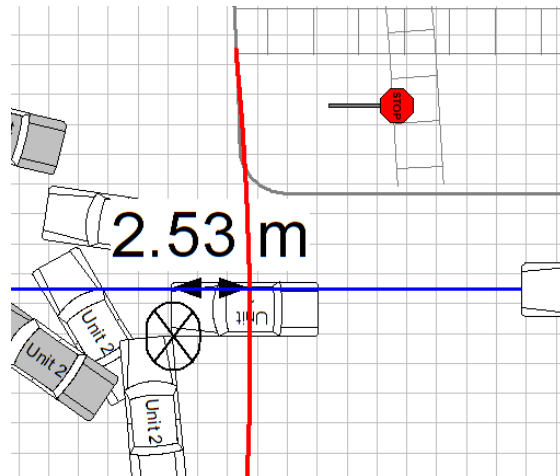
All measurements should be made to and from the FRONT CENTER of the vehicles. The measurements will be broken down into two components, D_1 and D_2 . For left turning vehicles, D_2 is further divided into $D_{2\text{-longitudinal}}$ and $D_{2\text{-lateral}}$. The longitudinal direction represents the initial heading direction. The lateral direction is perpendicular to this direction. D_1 represents the longitudinal travelling distance from the encroachment location (stop bar/crosswalk) to the intersection boundary line. D_2 , or $D_{2\text{-longitudinal}}$ for left turning drivers, represents the longitudinal travelling distance in the direction of the initial vehicle heading from the intersection boundary line to impact. $D_{2\text{-lateral}}$ should be collected for left turning to represent the lateral distance travelled from the intersection boundary until the impact location.

The figure below depicts these measurements.

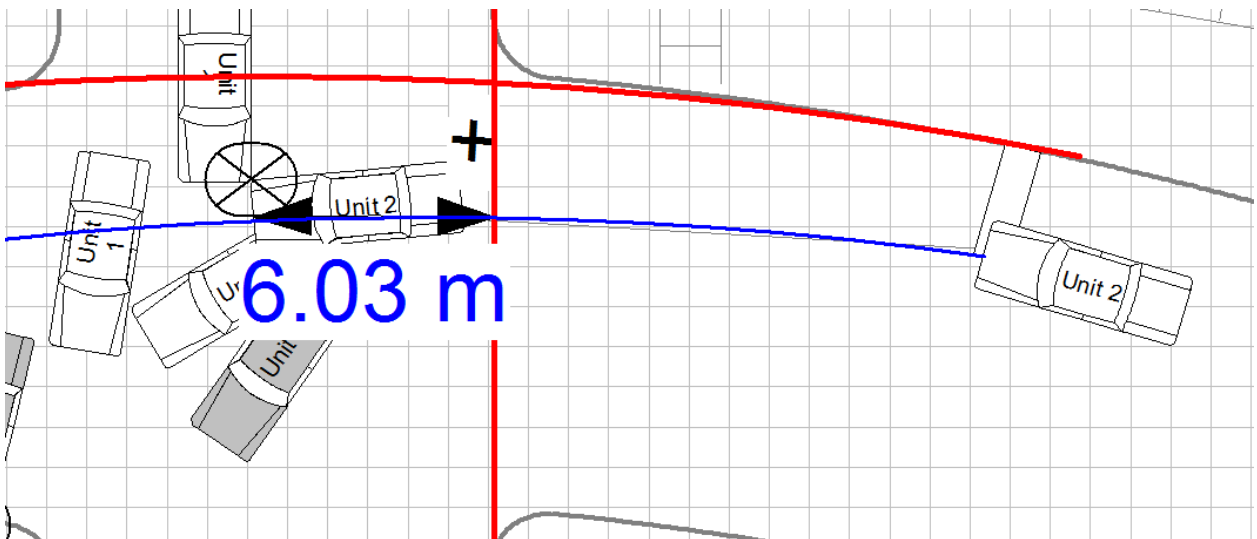


These measurements are dependent on whether the entry location is present and if the road is straight or curved. The entry location represents the position where the driver began their intersection traversal. If the scene photographs show that a stop bar is present, calculate D_1 using the stop bar as encroachment location. If the scene photographs show that only a crosswalk is present, the crosswalk will be used as the encroachment location. If neither the stop bar nor crosswalk are present in the scene photographs, do not measure D_1 .

The figure below depicts the D_2 measurement for a straight travelling vehicle. The vehicle proceeded from a stop sign. No road markings (stop bar/crosswalk) were present, so D_1 was not required. Very little evasive maneuvering was performed in this case, so the measurement was taken using the measurement tool only. D_2 was found to be 2.53 meters.

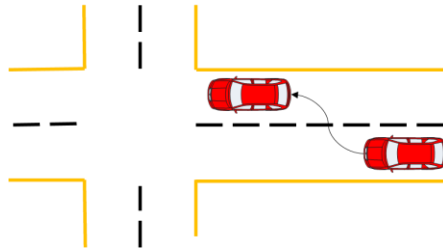


The figure below depicts the D_2 measurement for a vehicle travelling on a curved road. No road markings were present for this vehicle, so D_1 was not required. The dimension line tool was given a radius of curvature equal to the vehicle turning radius. The dimension line was then overlaid on the vehicle trajectory line. D_2 was found to be 6.03 meters.



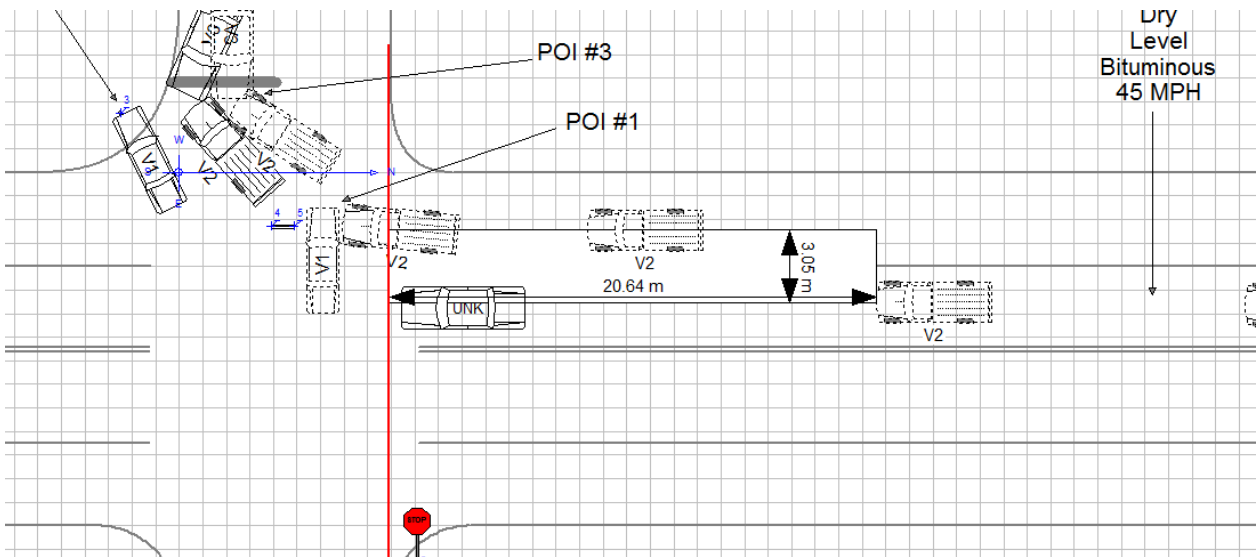
7) The following measurements only apply to cases with the described criteria.

LANE CHANGE

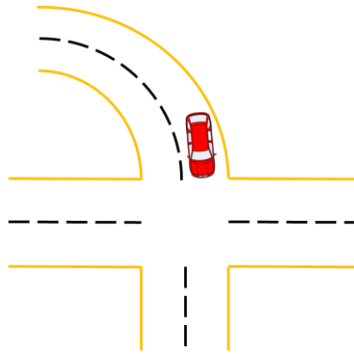


Three measurements are required. First, the direction of the lane change. Second, the starting location of the lane change relative to the intersection boundary line. If the lane change starting location is not provided, put “999” into the provided space. Third, the amount of lateral movement that took place.

In the scene below, the vehicle made a lane change to the right. The lane change started 20.64 m prior to the intersection boundary. The vehicle moved 3.05 meters laterally during the lane change.



CURVED ROAD BEFORE INTERSECTION



Three measurements are required for curved roads prior to the intersection: 1) the turning direction is needed, 2) the distance from the end of the radius to the intersection boundary line, and 3) the radius of curvature of the curve.

In the scene depicted, the vehicle is turning to the left. The radius of curvature begins at the intersection boundary, so this distance is equal to 0 meters. The radius of curvature was found using the inside radius (20.84 m) and the distance to the front center of the vehicle (3.53 m), and was found to be $20.84 \text{ m} + 3.53 \text{ m} = 24.37 \text{ m}$.

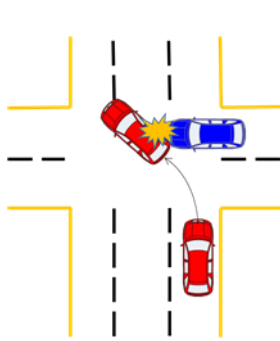


In the second scene depicted, the vehicle is turning to the left. The curve begins 36.24 m prior to the intersection boundary. The radius of curvature for the inside portion of the lane is 112.5 m. A rectangle oriented at the vehicle heading of Vehicle 1 can be used to measure the additional distance from the inside radius to the center of the vehicle (2.03 m). The radius is then the inside radius + the distance to the center of the vehicle (ROCB = $112.5 \text{ m} + 2.03 \text{ m} = 114.53 \text{ m}$).

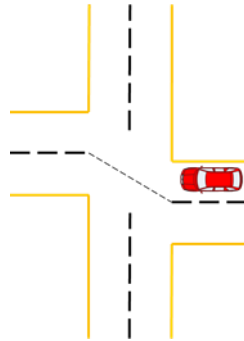


EVASIVE MANEUVER, LANE OFFSET, OR LANE MISDIRECTION (NON-TURNING VEHICLES ONLY)

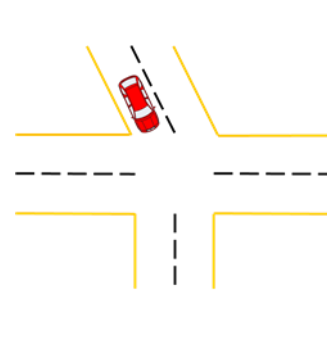
If the vehicle travels outside of the vehicle trajectory line prior to impact, the vehicle is assumed to have performed one of the following maneuvers.



Evasive Maneuver



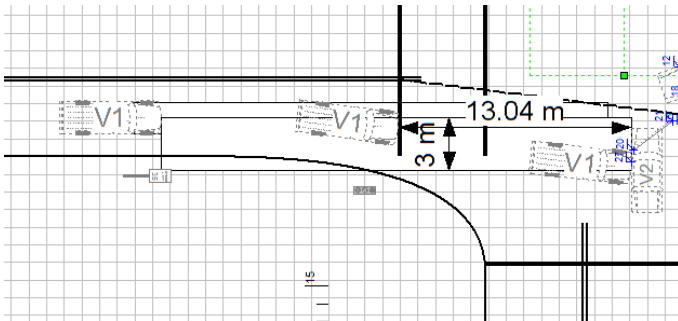
Lane Offset



Lane Misdirection

Three things should be calculated for these cases, including 1) the direction of the maneuver, 2) the starting point of the evasive maneuver relative to impact (evasive maneuver only), and 3) the lateral offset from original vehicle trajectory line.

In the scene depicted, the vehicle performs an evasive maneuver to the right. The distance travelled from the depicted initial evasive maneuver location to the impact location is 13.04 m. The lateral offset was depicted as 3.00 m.



Protocol for Reconstructing Impact Speeds of SCP, LTAP/OD. and LTAP/LD Crashes

PC-Crash Reconstruction

Overview

Objective: To determine the impact velocities of vehicles involved in SCP intersection crashes within the NMVCCS

Required Tools:

- 1) Data Input Spreadsheet (Results.xlsx): Reconstruction results will be put into this spreadsheet.
- 2) Vehicle Information Spreadsheet (Vehicle_Info.xls): Two sheets are contained in this spreadsheet.
 - a. *Generation Table* contains vehicle make, model, year, generation years, and alternative models. This table will be useful for determining if the vehicle chosen from the vehicle database is appropriate.
- 3) Case Viewer Program (NASS_PIC.exe): Will contain two important components for completing reconstructions. An annotated image of the case viewer program interface can be seen in the following sections.
 - a. *Scene narrative* is included on the right side of the case viewer. This summary contains a detailed account of the crash and crash conditions. The involved vehicle makes and models, road conditions, and road gradient can all be found in this account.
 - b. *Easy Street Draw File Link* is shown by the button “Open Scene Diagram in Easy Street Draw”. This scene diagram will be used for reconstructions.
- 4) Easy Street Draw software: An annotated screen shot of the program interface can be seen in the following sections.
- 5) PC-Crash Reconstruction Software: This software will be the platform for performing all crash reconstructions.

Step 1: Setup

Prior to beginning the reconstruction protocol, five files/applications/folders should be open.

- 1) The case viewer program should be opened.
- 2) The “Results.xlsx” spreadsheet should be opened for data input
- 3) The “Vehicle_Info.xlsx” spreadsheet should be opened for finding vehicle parameters.
- 4) PC-Crash should be opened.
- 5) The “Case Folders” directory should be opened on the share-drive. A folder has been generated for each case and should be used to store the completed case reconstructions.

Step 2: Importing a Scaled Scene Diagram into PC-Crash

The scene diagram acts a tool for overlaying the crash scene for accurate reconstructions. Step

2 describes the process for importing a scaled diagram into the PC-Crash program.

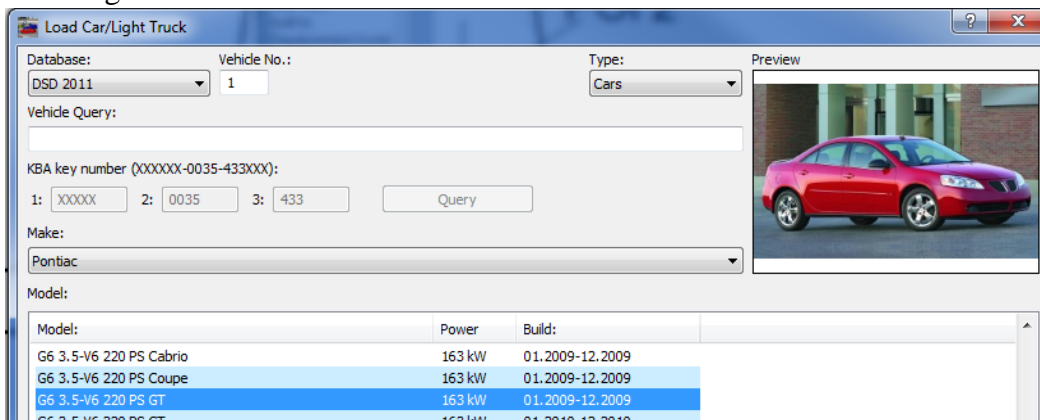
- 1) Within the search tool in the case viewer program, use the case “key” to select the crash of interest.
- 2) Click “Open Scene Diagram in Easy Street Draw” to open the scene diagram in easy street draw.
- 3) Use the measuring tape tool to draw a 10-meter long scale.
- 4) Left click the measuring tape and check the “include Measuring Tape in Printed Drawing” check box in the bottom panel of the window.
- 5) Select the “Save as Image” option on the top left corner of the interface.
 - a. Save the image as a .tif and place it into its appropriate folder.
- 6) Load the scene diagram into PC-Crash by selecting file→ Import→Bitmap and browsing for the case file
- 7) Scale the scene diagram using the  tool. This tool works by selecting the 0 and 10 m location on the sale, then imputing the “actual distance” as 10 m.

Step 3: Adding Vehicles to PC-Crash

Every intersection crash that will be reconstructed will involve at least two vehicles. Occasionally, additional vehicle(s) may be involved. It is important to add all involved vehicles for accurate reconstructions.

The following protocol should be repeated for all involved vehicles.

- 1) Load the vehicle by selecting the  icon.
- 2) Use the case viewer scene narrative to correspond the vehicle number in the scene diagram to a make, model, and year
- 3) Search for the make and model within the DSD 2011 database
 - a. If the vehicle cannot be found, use the generation sheet in the Vehicle Info spreadsheet to search for a suitable alternative model.
 - b. Compare the track width and vehicle length in the vehicle info table to verify the selected vehicle in the DSD database is appropriate
 - c. Input the selected vehicle into the results spreadsheet.
- 4) Modify vehicle specifications by right clicking in the window and selecting “vehicle settings”
 - a. Select “occupants and cargo” tab
 - b. Add the weights in the results spreadsheet into the appropriate front occupants, rear occupants, and trunk cargo columns
- 5) Use the  tool to move the vehicle to its respective impact location
 - a. The impact location represents the location where that that vehicle was first contacted.
 - b. Cars should be overlapping at this position.
 - c. Note: The car can be moved and rotated by clicking and dragging the center and edge of the vehicle, respectively.
 - d. Note: all positions prior to impact are irrelevant for this analysis and should be ignored.



Step 4: Adding Roadside Objects to the Scene

Roadside objects should only be added if they are impacted. If you are unsure whether an object was impacted, refer to the scene narrative and scene pictures in the case viewer. As a rule of thumb, when in doubt, include the object.

Roadside objects can be added using the following protocol:

1. On the right side of the page in the explorer tool bar, select custom vehicles → objects to find a list of roadside objects.
2. Three potential objects that can be added are trees (assign poles as trees), walls, and road side barriers.
3. Modify the object geometry by right clicking in blank space → selecting vehicle settings → selecting the object of interest in the drop down → modifying the height and width of the object.
 - a. Note: Height and width of the object can be determined by taking measurements using the  on the scene diagram.

Step 5: Adding Intermediate/rest Vehicle Positions and tire marks

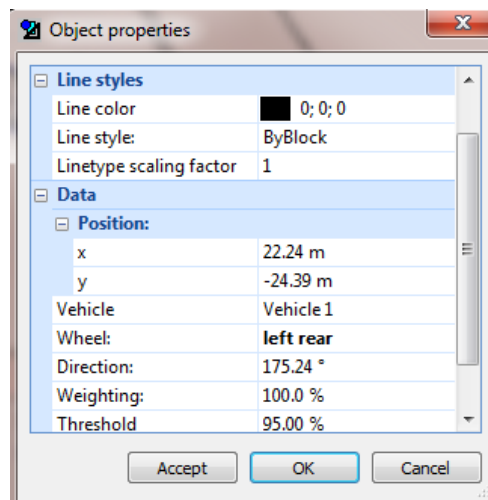
Adding vehicle positions and tire marks post impact give the collision optimizer a means an objective trajectory.

Intermediate and rest vehicle positions can be input using the following protocol:

1. Select Impact → Intermediate → Intermediate Position # OR
Select Impact → Rest
 - a. Note: Intermediate Position 1 corresponds to the first depicted position post impact.
2. A tow truck will appear and can be used to drag the impact vehicle to the intermediate vehicle positions.
 - a. Note: this will not move the impact vehicle, but will create a new vehicle that can be moved.

If present, tiremarks should be added at their appropriate locations. These tiremarks are important for the collision optimizer. The tiremark can be moved and rotated, and do not have a length component. The tiremark should be added to the beginning of the tiremark at the angle depicted.

1. Select  to add a tiremark.
2. Use  to select, move, and rotate the tiremark.
 - a. Note: a tiremark can be removed by selecting a tiremark, then deleting it using the  tool.
 - b. Note: The tiremark cross should be moved to the beginning tiremark, then rotated to follow the depicted markings.
3. After placing the tiremark in its location and direction double click on the tiremark cross using the .
4. The tiremark now must be assigned to the vehicle and tire of interest.
 - a. Under Data, Position change the vehicle and wheel to their appropriate setting.

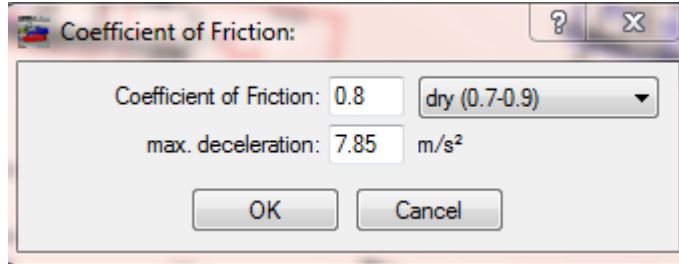


Step 6: Modify Road Friction

Road friction should be modified within for the entire depicted trajectories of both vehicles. Surface conditions can be determined. There are five possible selections for road friction: (1) dry, (2) wet, (3) very wet, (4) snow, and (5) ice. These are already given for you in the Results.xlsx spreadsheet.

Road friction should be modified using the following protocol:

- 1) Locate the following toolbar: .
- 2) Select the  button in the tool bar.
- 3) Left click to draw a polygon around the entire depicted trajectories.
- 4) After the polygon is completed, right click to finish drawing.
- 5) A coefficient of friction window will automatically open.
 - a. Use the drop down to change the surface conditions to their appropriate value

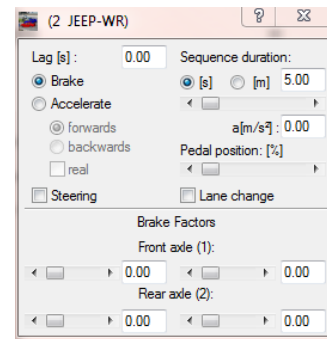
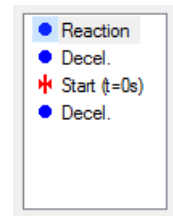


Step 7: Collision Optimization

Collision optimization is the final step in determining impact velocities. It is important to note that each crash is unique. Although the following protocol attempts to reconstruct crashes in a systematic way, there is still some “finesse” involved in properly reconstructing crashes. The following steps should be implemented for collision optimization:

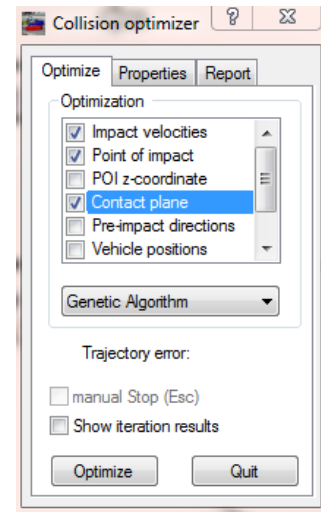
The “sequence” of events for each vehicle needs to be initialized

- 1) Select Dynamics → Sequences to open the sequences window
 - a. By default the window to the sequence depicted to the right will appear in the window for each vehicle involved.
- 2) Double click on the second decel. and a window will open for changing the decel. step in the sequence (shown to the right)
- 3) change the sequence duration to a reasonable duration.
 - a. This decel sequence duration affects the run time post impact.
 - b. A safe decel sequence duration is 15 s.
 - c. Alter the decel sequence duration for all vehicles
- 4) The presence of wheel lockup should also be added
 - a. Examine scene crash photos and the scene narrative to determine whether wheel lockup occurred. The vehicle should look bent/out-of-line
 - b. If wheel lockup occurred, change the brake factor for that wheel to 100. This indicates 100% braking on that wheel. Note that the braking can go up to 500%.
 - c. If wheel lockup occurred, add it to the results spreadsheet.



The first pass at collision optimization should be implemented. If this first pass through the optimization is “sufficient”, the results will be saved. A “sufficient” result will be one where the vehicle approximately stops at the depicted rest position.

- 1) Select Impact → collision optimizer
 - a. Two windows will open:
 - i. The collision optimizer window
 - ii. The crash simulation window
- 2) In the crash simulation window:
 - a. Select point of impact
 - b. Click a location within the two vehicles overlapping area
 - c. Unselect point of impact
- 3) Within the optimize tab in the collision optimizer window, verify that impact velocities, point of impact, and contact plane are selected, and the genetic algorithm routine has been selected. See the exemplary screen shot to the right for what this should look like.
- 4) In the crash simulation window, change the pre-impact velocities to be 30 kph each. These will serve as initial guesses.
- 5) Click Optimize in the collision optimizer window.



The results of the collision optimizer can be found by first selecting options → Values to open the values window, then within the Values window, selecting Settings → Report. The impact values should be listed under START VALUES.

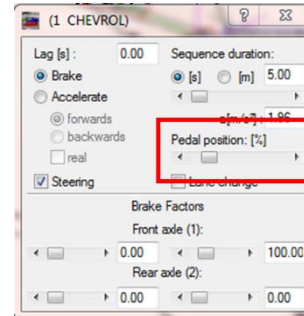
If the results of the collision optimizer seem reasonable after watching the animation, the impact velocities can be input into the results table. A reasonable result is one where the vehicles stop at their approximate rest location and rest heading.

If the results seem unreasonable, three things can be done to make the results more reasonable. **First**, if the vehicle does not come to a stop, which happens frequently for the vehicle that do not strike a roadside object(s), braking should be added. **Second**, if the trajectory indicates some

turning, steering can be added using the path following tool or manually. If lockup occurred, use the manual steering input.

If braking is required, perform the following steps:

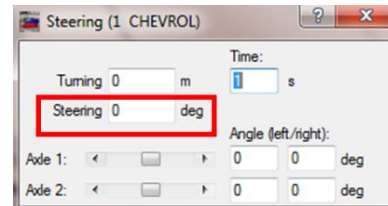
- 1) Open the sequences window by selecting Dynamics → Sequences
- 2) Under the vehicle of interest, double click the post-start decel.
- 3) Add braking using the pedal position scroll.
 - a. As a rule of thumb, it is best to start adding braking in 10 % intervals. Smaller intervals may be required for some crashes.



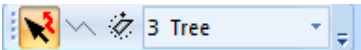
If steering is required, perform one of the following set of steps:

For manual steering input. (Note: should be used if lockup occurred)

- 1) Open the sequences window by selecting Dynamics → Sequences
- 2) Under the vehicle of interest, double click the post-start decel.
- 3) Check the steering check box to open up a steering options window (shown to right)
- 4) Change the Time to 0 s.
- 5) Steering should be added to the red boxed area
 - a. Positive steering rotates the vehicle counter-clockwise
 - b. As a rule of thumb, add steering in 15 degree increments.



For path following steering input.

- 1) Locate the following toolbar: 
- 2) Select the  button in the tool bar.
- 3) Left click to draw the vehicle path in segments
- 4) After the path has been drawn, right click to finish drawing.
- 5) The path can be deleted by clicking the trajectory line using the  then clicking delete.

A.5 Case Viewer Program

A customized case viewer was used by the reviewers for viewing case evidence.

The screenshot displays the Case Viewer Program interface for case 2006-003-027. On the left, a list of case numbers is shown, with 2006003498983 highlighted. A red box labeled "Case Search Tool" encompasses the list and a search field. The central area shows a street diagram with a crash scene, labeled "Crash Scene" and "Opens Easy Street Draw File". On the right, a "Scene Narrative" box contains a summary and detailed descriptions of the crash. At the bottom, a question "Is this a valid SCP intersection crash?:" is posed with "Yes", "No", and "Unknown" buttons.

2006-003-027

2005002585724
2006002229046
2007002229909
2005003498161
2005003498181
2005003498282
2005003498381
2005003498501
2005003588241
2005003588301
2006003498003
2006003498244
2006003498304
2006003498543
2006003498585
2006003498763
2006003498843
2006003498883
2006003498903
2006003498923
2006003498983
2006003588104
2006003588163
2006003588223
2006003588743
2006003588963
2007003498287
2007003498347
2007003498505

Search for a Case...
Search

Crash Scene

Open Scene Diagram in Easy Street Draw

2006-003-027
PSU 03
Scale: 1cm=2.5m
Speed Limit: 48kmph (30mph)
Roadway Type: Asphalt
Roadway Condition: Wet
Grade: 0/81

Scene Narrative

Summary:
The crash occurred in the evening hours of a weekend on the intersection of two two-way roadways. The intersection consisted of a north/south roadway and an east/west roadway. The intersection was controlled by a traffic control signal. Both roadways were wet, straight and level, and had a speed limit of 48kmph (30 mph).
V1, a 1999 Lincoln Town Car, was traveling northbound approaching the intersection where it intended to go straight. V2, a 1987 Toyota Camry, was traveling eastbound and approaching the same intersection. As V2 approached the intersection, it failed to stop for the traffic control signal and the front of V2 impacted the right side of V1. Both vehicles came to a final rest in the intersection near the point of impact.
V1 was driven by a 24 year-old male who sustained minor injuries and was transported to a hospital. The passengers, a 32 year-old male and a 36 year-old male also sustained minor injuries and were transported to a hospital. The Lincoln was towed due to damage.
The Critical Pre-crash Event for V1 was coded as other motor vehicle encroachment, from crossing street, across path. The Critical Reason for the Critical Event was not coded to the driver. The wet roads were coded as a roadway related factor. The other possible associated factors were coded unknown because no interview was obtained.
V2 was driven by a 66 year-old male who sustained minor injuries and was transported to a hospital. The Toyota was not towed due to damage.
The Critical Pre-crash Event for V2 was coded as this vehicle traveling, crossing over (passing through) intersection. The Critical Reason for the Critical Event was coded as an unknown reason. An associated factor coded to the driver was a Decision Factor, an illegal maneuver because he disregarded the traffic control signal. Wet roads were coded as a roadway related factor, and the other possible associated factors were coded unknown because no interview was obtained.

Picture: 1/1
Resize

1/19
Is this a valid SCP intersection crash?:
Yes No Unknown

Leave Message for Case
Done

A.6 Easy Street Draw Program

